

**PERSPECTIVES
OF ELECTROWEAK
INTERACTIONS**

XXth Rencontre de Moriond — Leptonic Session
Les Arcs - Savoie - France, March 17-23, 1985

PERSPECTIVES ⁷⁰ OF ELECTROWEAK INTERACTIONS

ISBN 2-86332-033-5

Editions Frontieres
B.P. 44
91190 GIF SUR YVETTE — France

Printed in Singapore by Kim Hup Lee
Printing Co. Pte. Ltd.

Proceedings of the Leptonic Session

TWENTIETH RENCONTRE DE MORIOND . 20.

Les Arcs - Savoie - France, March 17-23, 1985

Vol. 2

**PERSPECTIVES
IN ~~OF~~ ELECTROWEAK
INTERACTIONS**

Edited by
J. TRAN THANH VAN

éditions Frontières

M 47 1985

6892

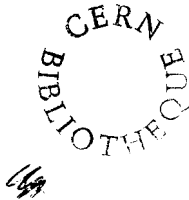
The Leptonic Session of the Twentieth Rencontre de Moriond on
IN
PERSPECTIVES OF ELECTROWEAK INTERACTIONS

was organized by

J. TRAN THANH VAN

with the active collaboration of

A. BOUQUET
J. F. GRIVAZ
F. JACQUET
G. KANE
A. MOREL
J. RANDEK
and F. VANNUCCI



Associated Editors: F. LEFEVRE
A. MOREL

FOREWORD

The XXth Rencontre de Moriond was held in 1985 in Les Arcs, Savoie (France).

The first such meeting was at Moriond in the French Alps in 1966. There experimental as well as theoretical physicists, not only shared their scientific preoccupations but also the household chores. The participants at the first meeting were mainly French physicists interested in electromagnetic interactions. In subsequent years, a session on high energy strong interactions was also added.

The main purpose of these meetings is to discuss recent developments in contemporary physics and also to promote effective collaboration between experimentalists and theorists in the field of elementary particle physics. By bringing together a relatively small number of participants, the meeting helps to develop better human relations as well as a more thorough and detailed discussion of the contributions.

This concern for research and experimentation of new channels of communication and dialogue which from the start animated the Moriond Meetings, inspired us to organize a simultaneous meeting of biologists on Cell Differentiation and to create the Moriond Astrophysics meeting. Common meetings between biologists, astrophysicists and high energy physicists are organized to study the implications of the advances in one field into the others. I hope that these conferences and lively discussions may give birth in the future to new analytical methods or new mathematical languages.

At the XXth Rencontre de Moriond, in 1985, four physics sessions and one biology session were organized :

- * January 13-19 Heavy Quarks, Flavour Mixing and CP Violation
- * March 10-17 QCD and Beyond
Cell Recognition
- * March 17-23 New Trends in Electroweak Interactions
Nucleosynthesis :
Its Implication on Nuclear and Particle Physics.

I thank the organizers of the XXth Rencontre de Moriond :

- M. GIRARD and M. FELLOUS for the Biology meeting,

- J. AUDOUZE, C. CESARSKY, Ph. CRANE, Th. GAISSER, D. HEGYI, J.W. TRURAN for the Astrophysics meeting.

- K. BERKELMAN, J.D. BJORKEN, J. DORFAN, G. KALMUS, L. MONTANET, L. OLIVER and E. PASCHOS for the Heavy Quarks, Flavour Mixing and CP Violation Session.

- A. CAPELLA, G. GOLDBABER, R. PESCHANSKI, B. PIETRZYK, F. RENARD, F. RICHARD for the QCD and BEYOND Session.

- A. BOUQUET, J.F. GRIVAZ, F. JACQUET, G. KANE, A. MOREL, J. RANDER and F. VANNUCCI for the NEW TRENDS IN ELECTROWEAK INTERACTIONS Session.

and the conference secretaries J. BORATAV, C. JOUANEN, F. LEFEVRE, N. MATHIEU, LE VAN SUU, A. POTTIER, A. RAMOS and A. SOLACARO who have devoted much of their time and energy to the success of this Rencontre.

I am also grateful to M.J. DUPUY, E. ROCCA-SERRA, D. TOURAILLE, M. VANNEAU who contributed through their hospitality and cooperation to the well-being of the participants enabling them to work in a relaxed atmosphere.

This Rencontre is sponsored by the "Centre National de la Recherche Scientifique" and by the "Commissariat à l'Energie Atomique". The Astrophysics meeting is also sponsored by NATO. I would like to express my thanks for their encouraging support.

I wish sincerely that a fruitful exchange and an efficient collaboration between the physicists, the astrophysicists and the biologists will arise from this Rencontre as in the previous ones.

J. TRAN THANH VAN

CONTENTS

I. STATUS OF THE STANDARD MODEL

HARNEW N.	"Study of w^\pm and Z^0 in UA2".	11
HOFFMANN E.	"Measurement of the ratio of neutral current to charged current cross sections of antineutrino in hydrogen".	37
LANOU R. E.	"New determination of $\text{Sin}^2 \theta_W$ from ratio of neutrino and anti-neutrino, elastic scattering by electrons".	45
KRAUS N.	"Search for the decay $\mu^+ \rightarrow e^+ e^+ e^-$, and the measurement of the decay $\mu^+ \rightarrow e^+ e^+ e^- \nu_e \nu_\mu$ with the SINDRUM spectrometer".	55
KIESLING C.	"Results from PETRA on electroweak effects and tests of QED".	65
LANG K.	"Neutrino production of like sign dimuons".	87
BLONDEL A.	"Precise measurement of $\text{Sin}^2 \theta_W$ in neutrino-iron interactions".	95

II. SUPERSYMMETRY AND SEARCH FOR NEW PARTICLES

FRERE J. M.	"Topics in supersymmetry".	107
PREPOST R.	"Particle searches at PEP".	131
BÖHM A.	"Search for new particles at PETRA".	141
BARNETT R. M.	"Limits for supersymmetry from a comprehensive study of CERN missing-energy events".	159
SCHMIDT M.G.	"SU (n,1) minimal supergravity and the SUSY particle spectrum".	169
PETCOV S. T.	"Symmetries of the cross - sections of Majorana particle production in $e^+ - e^-$ and $p - p$ collisions".	175
MOFFAT J. W.	"SU (2) x U(1) x U(1) electroweak model and the CERN monojets".	181

FRANZINI P.	"The DØ detector for the Fermilab collider".	185
-------------	--	-----

III. LIFETIME MEASUREMENTS AND FERMION PROPERTIES

GARREN L.	"A potpourri of CLEO results".	191
TUTS P. M.	"Recent results on weak interactions with CUSB".	197
MACFARLANE D. B.	"Recent results from ARGUS".	207
PREPOST R.	"Review of lifetime measurements at PEP".	219
WETTERICH C.	"Can grand unified theories predict the top quark mass?".	229
SENJANOVIC G.	"Who ordered the muon ? From families to communities".	237
PHILIPPE R.	"Theoretical ceiling in fermion masses in the standard model".	245

IV. NEUTRINO PHYSICS

MILLS G.	"Charged Kaon production in τ decays".	251
MACFARLANE D. B.	"A new limit on the mass of the Tau neutrino".	257
ZACEK V.	"Search for neutrino oscillations at the Gösigen nuclear power reactor".	265
VANNUCCI F.	"Decays and oscillations of neutrinos in the PS 191 experiment".	277
LANOU R. E.	"A brief report on a new limit on the strength of mixing between $\nu_{\mu} \rightarrow \nu_e$ ".	287
CAPONE A.	"Search for decays of heavy neutrinos in the mass range 500 - 2800 MeV".	295
POMANSKY A. A.	"Possible constraints on neutrino oscillation parameters from double beta decay experiments".	303
FACKLER O.	"An experiment to measure the electron neutrino mass using frozen tritium".	313

FELDMAN G. J.	"Search for heavy neutrinos produced in e^+e^- annihilation".	323
DAR A.	"Has a cosmological background of neutrinos from gravitational stellar collapse been detected ?".	329

V. SEARCHES FOR NUCLEON DECAYS

GERBIER G.	"Status of the Frejus nucleon decay experiment".	341
RAGAZZI S.	"Latest results from the Nussex experiment".	349
PARK H.-S.	"Experimental limits for 34 nucleon decay modes from the IMB detector".	357

VI. THEORY

PHAM QUANG HUNG	"Dynamics of strongly coupled Higgs models : vector resonances and all that".	373
DOMINICI D.	"Vector resonances from strong interacting Higgs".	379
FAYET P.	"Gauge boson/Higgs boson unification, N = 2 supersymmetry, grand unification, and new spacetime dimensions".	385
RABINOVICI E. Z.	"Introduction to superstrings".	409
PHAM QUANG HUNG	"The inflationary universe revisited".	421

VII. SUMMARY TALK

LANOU E.	"Summary talk of XXth Rencontre de Moriond".	433
----------	--	-----

STUDY OF W^{\pm} AND Z^0 IN UA2

The UA2 Collaboration

Bern - CERN - Copenhagen (NBI) - Heidelberg - Orsay (LAL) -
Pavia - Perugia - Pisa - Saclay (CEN)presented by Neville Harnew
CERN

ABSTRACT

A preliminary analysis of high p_T electrons detected in the UA2 experiment at the CERN $\bar{p}p$ Collider ($\sqrt{s} = 546$ and 630 GeV) has been done. Results on W^{\pm} and Z^0 production and properties are presented and compared to the expectations from the Standard Electroweak Model. We find good agreement between the UA2 experimental results and theoretical predictions.

1. INTRODUCTION

The UA2 collaboration has already reported experimental results on the processes

$$\bar{p} + p \rightarrow W^{\pm} + \text{anything}^{1)} \\ \quad \quad \quad \downarrow \\ \quad \quad \quad e^{\pm} + \nu(\bar{\nu})$$

and

$$\bar{p} + p \rightarrow Z^0 + \text{anything}^{2)} \\ \quad \quad \quad \downarrow \\ \quad \quad \quad e^+ + e^-$$

where W^{\pm} and Z^0 are the Intermediate Vector Bosons (IVB) of the Electroweak Theory. The data were taken at the CERN SPS $\bar{p}p$ Collider in the period 1981-1983 ($\sqrt{s} = 546$ GeV) and amounted to a total integrated luminosity $\mathcal{L} = 142$ nb $^{-1}$. Most of the UA2 results were in agreement with expectations from the Standard SU(3) \otimes SU(2) \otimes U(1) Model and with the results reported by the UA1 Collaboration on the same subject $^{4)}$.

However, the data presented also features that might have suggested the existence of unexpected phenomena. Namely :

- i) a $Z^0 \rightarrow e^+e^-\gamma$ was observed in a kinematical configuration having a low probability for internal bremsstrahlung;
- ii) 3 events, interpreted as

$$\bar{p} + p \rightarrow W + \text{hard jet(s)}, W \rightarrow e\nu$$
 were found unlikely in terms of a QCD description of the W production mechanism $^{5)}$.

These results, together with the observation of unexpected events by UA1 $^{6)}$, have been at the origin of various theoretical speculations suggesting new physics phenomena beyond the Standard Model.

The subsequent Collider running period, which took place at the end of 1984, was clearly expected to shed more light on these issues.

2. THE 1984 $\bar{p}p$ RUN

In the fall of 1984 the $\bar{p}p$ Collider ran at the higher energy of $\sqrt{s} = 630$ GeV, as a result of an improved magnet cooling system. Fig. 1 summarizes the performance of the machine during the period. The highest instantaneous luminosity was $\mathcal{L} = 3.5 \cdot 10^{29}$ cm $^{-2}$ s $^{-1}$ and the longest luminosity lifetime was ~ 24 hours $^{7)}$. The total integrated luminosity accumulated by the UA2 experiment was $\mathcal{L} = 310$ nb $^{-1}$.

The analyses described here are based on the data from the 1984 run. Cross-sections are calculated separately for the 1984 data and the previous ones, given the different centre of mass energy. For the fit of the mass of the IVB's, the measurement of the W charge asymmetry and the determination of the Z^0 width, the full data sample of the UA2 experiment is used, corresponding to an integrated luminosity $\mathcal{L} = 452 \text{ nb}^{-1}$.

All results are preliminary.

3. THE UA2 DETECTOR

The UA2 experimental apparatus has been described in detail elsewhere^(*). Fig. 2 shows a schematic view of its longitudinal cross-section in a plane containing the beam axis. There is complete cylindrical symmetry in azimuth (ϕ), while in polar angle (θ) one can distinguish two regions :

- The central region ($40^\circ < \theta < 140^\circ$) is covered by a highly segmented, tower structured electromagnetic and hadronic calorimeter. The 240 cells of the central calorimeter point to the interaction point.

- The two forward regions ($20^\circ < \theta < 37.5^\circ$ and $142.5^\circ < \theta < 160^\circ$) have been instrumented with the main aim of measuring the forward-backward charge asymmetry of W^\pm decays. They are equipped with 24 (12 on each side) identical magnetic spectrometers followed by electromagnetic calorimeters. In front of both the central and the forward calorimeters, preshower counters guarantee an accurate localization of electromagnetic showers to improve the identification of electrons against background.

4. DATA TAKING

Triggers sensitive to high p_T electrons are constructed from calorimeter phototube (PM) signals with gains proportional to transverse energy.

Electromagnetic showers may span across adjacent calorimeter cells. Trigger thresholds were therefore applied to linear sums of signals from 2×2 cell matrices. In the central calorimeter, all possible 2×2 matrices were constructed; in the forward ones only combinations in a given sector were considered.

There are two triggers sensitive to electrons in UA2 :

- The "W-trigger", for which the signal from at least one matrix must exceed a threshold set at 10 GeV
- the "Z-trigger", for which the signals from at least two matrices, separated by more than 60° in azimuth, must exceed 4.5 GeV.

To suppress background from sources other than $\bar{p}p$ collisions, a coincidence with two signals from hodoscopes at $0.47^\circ < \theta < 2.84^\circ$ on both sides of the collision point was required. These hodoscopes were part of an experiment to measure the $\bar{p}p$ total cross section⁹⁾. Their efficiency to non-diffractive $\bar{p}p$ interactions was estimated to be at least 98%.

Approximately $\sim 1.5 \cdot 10^6$ events were recorded with the W-trigger and $\sim 1.1 \cdot 10^6$ with the Z-trigger in the 1984 run. Both triggers gave a total of $\sim 2 \cdot 10^6$ events corresponding to an integrated luminosity $\mathcal{L} = 310 \text{ nb}^{-1}$.

5. THE ELECTRON ANALYSIS

Figure 3 shows a schematic representation of the signature of various particles or systems of particles in the UA2 apparatus. Shown in the figure is the transverse cross section of a quadrant of the central detector. The forward detectors present similar features with the additional measurement of the track momentum.

There are distinctive characteristics of different particles in each component of the UA2 detector :

- a) in the calorimeter, the small transverse and longitudinal extension of the electromagnetic shower distinguishes electrons from particles undergoing nuclear interactions in the calorimeter material (isolated charged hadrons or hadron jets).
- b) the presence of a track in the vertex chambers allows to recognize an electron from a photon (or a π^0) which showers electromagnetically in the calorimeter.
- c) a particularly dangerous background to electrons is given by the geometrical overlap of an energetic π^0 with a soft charged hadron. The first produces an electromagnetic shower in the calorimeter, while the latter contributes a track and may fake an electron. This background is reduced by the high resolution preshower counter, which allows the precise localisation of the showering particle.

Therefore, the identification of high p_T electrons is based on the following main criteria :

1. the presence of a localised cluster of energy deposition in the first compartment of the calorimeters, with at most a small energy leakage in the hadronic compartment;
2. the presence of a reconstructed charged particle track which points to the energy cluster. The pattern of energy deposition must agree with that expected from an isolated electron incident along the track direction;
3. the presence of a signal in the preshower counter, the amplitude of which must be larger than that of a minimum ionising particle. The geometrical matching of the preshower hit with the projection of the track must be consistent with the space resolution of the counter itself. These features are characteristic of a high energy electron starting a shower in the preshower counter.

In practice, because of the different instrumentation in the central and forward regions, these criteria are applied in different ways in the two detectors.

Details of the electron identification, together with their efficiency to detect electrons, are presented in Table Ia for the central region and Table Ib for the forward ones. An exhaustive description of the cuts is given in previous UA2 publications¹⁰⁾.

It should be noted that most of the applied selection criteria are satisfied only by isolated electrons : the detection of high p_T electrons contained in a jet of high p_T particles is excluded by the present analysis.

Electrons from photon conversions are removed by requiring a hit in at least one of the two innermost chambers of the vertex detector. Furthermore, in the forward detectors the electron candidate is rejected if it is accompanied by another track of opposite sign at an azimuthal separation smaller than 30 mr.

6. THE ELECTRON SAMPLE

In order to reduce the amount of data to be processed in the preliminary W and Z analyses presented at this Conference, a fast filter has been applied to the total event sample.

1. For the W-triggers, it required the presence in the event of an electron-like energy deposition in the calorimeter (i.e. a cluster of cells with small leakage in the hadronic compartment and small radius). The transverse energy deposited in the electromagnetic compartment E_T^{em} was required to exceed 15 GeV. In addition the event was required to have a total energy imbalance in the transverse plane of at least 13 GeV.
2. For the Z-triggers, events were accepted only if at least two electron-like clusters, with azimuthal separation of at least 60° , exceeded $E_T^{\text{em}} > 4.5$ GeV, such that their total mass was greater than $30 \text{ GeV}/c^2$.

Of the total number of $\sim 2 \cdot 10^6$ W and Z triggers, $\sim 1.2 \cdot 10^5$ remain after the filter cuts. These cuts, although very effective in reducing the data sample to be analysed, introduce biases which make the background estimate somewhat uncertain for $p_T^e < 17 \text{ GeV}/c$ or $M_{ee} < 30 \text{ GeV}/c^2$. The analysis of the total data sample is in progress, but the results presented here are only concerned with events satisfying $p_T^e > 17 \text{ GeV}/c$ or $M_{ee} > 30 \text{ GeV}/c^2$.

After applying the electron cuts we are left with a total of 290 electron candidates with $p_T^e > 17 \text{ GeV}/c$. The p_T^e distribution is shown in Fig. 4. Candidates with $p_T^e > 25 \text{ GeV}/c$ obtained by the W and Z analyses are indicated in the figure.

7. TOPOLOGY OF THE EVENTS WITH AN ELECTRON CANDIDATE

The sample of 290 electron candidates presented in Fig. 4 contains, in addition to real electrons, fake electrons coming from misidentified high p_T hadrons or jets of hadrons. Depending on whether the electron is real or fake we expect that the event contains either another high p_T lepton (e or ν) or another jet of high p_T hadrons at approximately opposite azimuth.

In order to study the topology of the events with an electron candidate we search for high p_T jets using the jet finding algorithm described in detail elsewhere¹¹⁾. We consider the jet activity at opposite azimuth to the electron candidate in a 120° wedge. We define the quantity

$$\rho_{\text{opp}} = -\vec{p}_T^e \cdot \sum \vec{p}_T^{\text{jet}} / |\vec{p}_T^e|^2$$

where the sum extends to all jets having an azimuthal separation $\Delta\phi > 120^\circ$ to the electron candidate and $p_T > 3 \text{ GeV}/c$.

We then split the sample of events with an electron candidate in :

- a) Events with $\rho_{\text{opp}} < 0.2$: this sample contains $W \rightarrow e\nu$.
The ρ_{opp} cut is estimated to be $(91 \pm 3)\%$ efficient, where the error reflects the uncertainty of the Monte Carlo simulation of low energy jets.
- b) Events with $\rho_{\text{opp}} > 0.2$: this sample includes the $Z^0 \rightarrow e^+e^-$ sample. It is dominated by two-jet background with one jet misidentified as an electron and is used to estimate the background contamination to the W-sample.

8. THE $W \rightarrow e\nu$ SAMPLE

The total number of W-triggers passing the electron filter cuts is $\sim 1.1 \cdot 10^5$. After applying the electron identification criteria the sample reduces to 257 events, 130 of which satisfy $\rho_{\text{opp}} < 0.2$.

The p_T^e distribution of these events is shown in Fig. 5. There are 87 events (71 in the central region and 16 in the forward ones) with $p_T^e > 25$ GeV/c. The background for $p_T^e > 25$ GeV/c is estimated to be 9.0 ± 0.8 events. The p_T^e distribution of Fig. 5 shows a clear Jacobian peak at $p_T^e \sim 40$ GeV/c, a distinctive feature of $W \rightarrow e\nu$ decays. Other physics processes also contribute to the electron sample. In addition to the background, shown as a dashed line in the figure, we estimate a contribution of 3.9 ± 0.9 events from $Z^0 \rightarrow e^+e^-$ decays in which one electron is not detected and 2.1 ± 0.2 events from $W \rightarrow \tau\nu$, $\tau \rightarrow e\nu\bar{\nu}$, for the event sample satisfying $p_T^e > 25$ GeV/c.

The solid curve in fig. 5 is the p_T^e distribution expected once all the contributions to the electron sample are taken into account.

8.1 Background to the W electron spectrum

Of the 257 events with an electron candidate, 124 (excluding the $Z^0 \rightarrow e^+e^-$ events) have $\rho_{\text{opp}} > 0.2$, namely some jet activity at opposite azimuth to the electron candidate itself. Their p_T^e distribution is shown in Fig. 6. The steeply falling spectrum suggests that the sample consists mostly of misidentified jets. Although the presence of real electrons with opposite jets cannot be excluded, we assume that the sample does not contain electrons from W decays. This assumption is valid to the extent that the ρ_{opp} cut does not reject W's produced at high p_T . Should the jet opposite to the electron candidate be lost outside the UA2 acceptance, these events would become W candidates. For this reason we use the sample to estimate the background to W's in the following way. From the $\sim 1.1 \cdot 10^5$ filtered W-triggers we select those events which do not contain energy clusters with $p_T > 17$ GeV/c passing the electron identification criteria described in Table I. We then apply the topology cut in the same way as was done to the electron sample. The distribution of events with $\rho_{\text{opp}} > 0.2$, normalized to 124 events, is shown as a solid line in Fig. 6.

The ratio between the two subsamples resulting from the application of the ρ_{opp} cut

$$(\text{jet} + \rho_{\text{opp}} < 0.2) / (\text{jet} + \rho_{\text{opp}} > 0.2)$$

gives the probability that in two-jet events one jet is lost outside the UA2 acceptance. This probability decreases from $\sim 10\%$ to $\sim 2\%$ when p_T increases from 15 to 25 GeV/c.

The background to the 130 W candidates is estimated from the p_T distribution of jet events with $\rho_{\text{opp}} < 0.2$ scaled by the factor

$$("e" + \rho_{\text{opp}} > 0.2) / (\text{jet} + \rho_{\text{opp}} > 0.2)$$

The resulting distribution is shown in fig. 5 as a dashed line.

8.2 Cross section for W production

The cross section for the process $\bar{p} + p \rightarrow W^\pm + \text{anything}$ followed by the decay $W \rightarrow e\nu$ is calculated as

$$\sigma_W^e = N_W^e / \varepsilon \mathcal{L} \eta$$

where N_W^e is the observed number of $W \rightarrow e\nu$ decays, ε is the overall efficiency of the electron selection criteria, \mathcal{L} is the integrated luminosity and η is the detector acceptance.

We use the 87 events with $p_T^e > 25$ GeV/c for which the acceptance is $\eta = 0.65$. The overall efficiency is $\varepsilon = \varepsilon_{\text{pop}} \cdot \varepsilon_{\text{cuts}} = 0.66 \pm 0.05$. After subtracting contributions from the background, from Z^0 decays with one electron undetected and from the decay ($W \rightarrow \tau\nu$, $\tau \rightarrow e\bar{\nu}$), we calculate

$$\sigma_W^e(630) = 540 \pm 70(\text{stat.}) \pm 90(\text{syst.}) \text{ pb}$$

for the W^\pm inclusive production of cross section at $\sqrt{s} = 630$ GeV times branching ratio into $e\nu$. The systematic error accounts for uncertainties on the luminosity \mathcal{L} (15%) and on the cut efficiencies (7%).

An independent analysis based on data from a trigger selecting events with missing transverse energy ¹²⁾ gives

$$\sigma_W^e(630) = 590 \pm 90(\text{stat.}) \text{ pb}$$

in good agreement with the result of the electron analysis.

We have recalculated the cross-section for W production at $\sqrt{s} = 546$ GeV^{1b)}, taking into account a new measurement of the total $\bar{p}p$ cross-section⁹⁾ which implies an integrated luminosity of 142 nb⁻¹ instead of 131 nb⁻¹ as used in Ref. 16.

The result is

$$\sigma_W^e(546) = 500 \pm 100 (\text{stat.}) \pm 80 (\text{syst.}) \text{ pb}$$

The cross section ratio at the two collider energies is :

$$R = \sigma(630) / \sigma(546) = 1.08 \pm 0.26$$

where most systematic errors cancel.

All the measured values are in agreement with QCD predictions¹³⁾ :

$$\sigma(546 \text{ GeV}) = 360 \begin{matrix} +110 \\ -50 \end{matrix} \text{ pb}$$

$$\sigma(630 \text{ GeV}) = 460 \begin{matrix} +140 \\ -80 \end{matrix} \text{ pb}$$

$$R = 1.26$$

8.3 The W mass

To extract the value of the W mass we combine the data collected by UA2 in 1984 ($\sqrt{s} = 630$ GeV) and in previous runs ($\sqrt{s} = 546$ GeV).

The resulting sample consists of 123 events with an electron having $p_T^e > 25$ GeV/c. The p_T^e distribution is shown in Fig. 7, together with the estimated background (dashed line) and the theoretical distribution of electrons from W decays (solid line).

The mass value is extracted from this sample by comparing the distribution $d^2n/dp_T^e d\theta_e$ with that expected from $W \rightarrow e\nu$ decays (θ_e is the measured polar angle).

To calculate $d^2n/dp_T^e d\theta_e$ we have used :

- structure functions from Glück et al.¹⁴⁾ to generate the p_L^W distribution
- the p_T^W distribution of Altarelli et al.¹⁵⁾
- fixed W width at $\Gamma_W = 3.0$ GeV/c².
- the decay angular distribution expected for the standard V-A coupling of W to fermions.

The detector energy resolution is taken into account.

The best fit to the experimental distribution is obtained with

$$M_W = 81.5 \pm 1.0 \text{ (stat.)} \pm 1.5 \text{ (syst.) GeV/c}^2$$

where the systematic error contains a contribution from the overall uncertainty on the energy calibration of the calorimeter (1.5%) and an uncertainty resulting from the p_T^W distribution used to generate the Monte Carlo data. The event with $p_T^e = 60$ GeV/c has been excluded from the mass fit.

We have also fitted the same two dimensional distribution of a sample obtained with stricter electron cuts, which has much smaller background contamination, and we find the same value for the W mass indicating, as expected, that the fit is not sensitive to the low p_T^e part of the spectrum. The fit is dominated, instead, by the high p_T^e region, which is sensitive to the topology cut ($\rho_{\text{opp}} < 0.2$).

To check that the effect of the ρ_{opp} cut is correctly taken into account in our Monte Carlo simulation, we have fitted the transverse mass distribution of the W sample, which has been shown by Monte Carlo simulation to be insensitive to the ρ_{opp} cut. We find the value

$$M_W = 81.2 \pm 0.8 \text{ (stat.)} \pm 1.5 \text{ (syst.) GeV/c}^2$$

in perfect agreement with the one obtained with the fit to the (p_T^e, θ_e) distribution.

8.4 Forward-Backward Charge Asymmetry

The helicity state of the q and \bar{q} forming the W in $\bar{p}p$ interactions is defined by the V-A coupling. As a result the W is produced with full polarisation in the direction of the \bar{p} beam. Similarly the V-A coupling determines the helicity of the decay products of the W . As a result a distinctive forward-backward asymmetry of the charge lepton must be observed in the decay $W \rightarrow e\nu$. In the W rest frame the angular distribution of the charged lepton is expected to be of the form

$$\frac{dn}{d\cos\theta^*} \propto (1 - q \cos\theta^*)^2$$

where q is the charge of the lepton and θ^* is the angle between the charged lepton and the direction of the incident proton. The UA2 experiment is equipped with magnetic spectrometers in the angular region $20^\circ < \theta < 37.5^\circ$ and $142.5^\circ < \theta < 160^\circ$, where the sensitivity to the charge asymmetry is expected to be higher.

There are 30 W candidates with $p_T^e > 20$ GeV/c in the forward spectrometers, with an estimated background of ~ 1 event. Their distribution in the (p^{-1}, E^{-1}) plane, where p is the electron momentum with the sign of $(q \cdot \cos\theta_{lab}^e)$, is shown in Fig. 8.

The measured asymmetry is

$$\alpha = [(N_p^+ + N_{\bar{p}}^-) - (N_{\bar{p}}^+ + N_p^-)]/N_{tot} = 0.47 \pm 0.16$$

where N_p^+ ($N_{\bar{p}}^-$) is the number of positrons (electrons) on the proton (antiproton) side, i.e. the right asymmetry, and equivalently for $N_{\bar{p}}^+$ (N_p^-).

The measured value of α is in good agreement with the expected asymmetry

$$\alpha = 0.54 \pm 0.04$$

where the effects of the background, of the $W \rightarrow \tau \rightarrow e$ decay chain and of the Z^0 events with only one electron detected have been taken into account.

9. THE $Z^0 \rightarrow e^+e^-$ SAMPLE

In the 1984 run $\sim 1.1 \cdot 10^6$ Z-triggers have been recorded, of which $\sim 1.5 \cdot 10^4$ passed the filter selection described in section 4.

From this sample we keep only the events which contain at least two energy clusters passing the calorimeter electron cuts described in Table I.

Although the calorimeter cuts applied are not very strict only 111 events remain with a mass of the two electron-like clusters M_{ee} greater than $30 \text{ GeV}/c^2$. The M_{ee} distribution is shown in Fig. 9a and shows that 11 events have a $M_{ee} > 80 \text{ GeV}/c^2$ with an estimated background of ~ 1 event. After requiring that at least one of the two clusters satisfies all the electron selection criteria the sample reduces to 15 events. Fig. 9b shows their M_{ee} distribution, where one can see that 8 events have $M_{ee} > 80 \text{ GeV}/c^2$ and no event is in the region $42 < M_{ee} < 80 \text{ GeV}/c^2$.

Using a sample of two-jet events, we estimate an upper limit of less than 0.15 events as a background under the Z^0 peak.

For a precise assessment of the sample of the 7 events with $M_{ee} < 42 \text{ GeV}/c^2$ it is necessary to study the spectrum at lower mass values, in order to establish the background level in this region. This study has not been performed yet, because the event distributions in this region are biased by the requirement $M_{ee} > 30 \text{ GeV}/c^2$.

9.1 The Z^0 cross-section

We use the 8 events with $M_{ee} > 80 \text{ GeV}/c^2$ to calculate the Z^0 production cross-section at $\sqrt{s} = 630 \text{ GeV}$ times branching ratio into e^+e^- . Five events have both leptons in the central region, where the efficiency to detect such a pair with the cuts described in the previous section is 86% and the acceptance is 0.34. For the remaining 3 events, in central-forward configuration, the efficiency is 89%, while the acceptance is 0.19.

For an integrated luminosity of 310 nb^{-1} we find

$$\sigma_Z^e(630) = 56 \pm 20 \text{ (stat.)} \pm 9 \text{ (syst.) pb}$$

where the systematic error has been described in section 8.2.

This result is in agreement with a theoretical expectation of 51_{-10}^{+16} pb¹³⁾.

As was done for the W, the cross section at $\sqrt{s} = 546$ GeV has been recalculated :

$$\sigma_Z^{ee}(546) = 101 \pm 37 \text{ (stat.)} \pm 15 \text{ (syst.) pb.}$$

The theoretical calculation from Ref. 13 gives 42_{-6}^{+13} pb.

9.2 The Z^0 mass and width

The total UA2 sample of events with two electrons of invariant mass $M_{ee} > 50$ GeV/c² is shown in Fig. 10. It amounts to a total of 16 events, 8 at a $\sqrt{s} = 546$ GeV²⁾ and 8 at $\sqrt{s} = 630$ GeV, corresponding to an integrated luminosity $\mathcal{L} = 452$ nb⁻¹. The masses of the events taken at $\sqrt{s} = 546$ GeV have been very slightly modified with respect to the values published in Ref. 2 after a recalibration of some calorimeter modules in a test beam.

All events have $M_{ee} > 80$ GeV/c², where the background is less than 0.2 events.

The Z^0 mass is measured to be

$$M_{Z^0} = 92.4 \pm 1.1(\text{stat.}) \pm 1.4(\text{syst.}) \text{ GeV/c}^2$$

where the systematic error accounts for the 1.5% global energy uncertainty of the calorimeter response. The masses of the individual events are distributed around M_{Z^0} as shown in Fig. 11. The 3 events indicated with an asterisk in the figure are events D, G and H of Ref. 2 which have not been used in the Z^0 mass evaluation for the reasons explained there.

The same event sample has been used to fit a value for the width of the Z^0 , Γ_Z . Given the low statistics of the sample available, several statistical estimators of a Breit-Wigner fit to the data have been studied. We quote

$$\Gamma_Z = 2.7_{-1.6}^{+2.2} \text{ GeV/c}^2 \quad (1)$$

and $\Gamma_Z < 5.6$ GeV/c² at 90% C.L.

We can obtain an independent estimate of Γ_Z within the standard model from the relation¹⁶⁾

$$\Gamma_{\bar{W}/\Gamma_Z} = (\sigma_{\bar{W}} \Gamma_{\bar{W} \rightarrow e\nu} / \sigma_Z \Gamma_{Z \rightarrow ee}) \cdot R$$

where

$$R = \sigma_Z^e / \sigma_{\bar{W}}^e = 0.137^{+0.040}_{-0.034}$$

as a weighted average of the cross sections at the two centre of mass energies. The error on R is statistical only, the systematics cancelling out.

Using the value $\Gamma_{\bar{W}} = 2.85 \text{ GeV}/c^2$ and the structure function parametrization from Ref. 16, we calculate

$$\Gamma_Z = 2.6^{+0.9}_{-0.6} \text{ GeV}/c^2 \quad (2)$$

and $\Gamma_Z < 3.8$ at 90% confidence level, in good agreement with (1).

Within the framework of the standard model, we can compare the measured value of Γ_Z to the expected one to extract the number of additional light neutrinos expected. Taking as expected $\Gamma_Z = 2.82 \text{ GeV}/c^2$ and $\Gamma_{Z \rightarrow \nu\bar{\nu}} = 180 \text{ MeV}/c^2$ we find

$$\Delta N_{\nu} < 15 \quad \text{at 90\% C.L.}$$

from (1) and

$$\Delta N_{\nu} < 5.5 \quad \text{at 90\% C.L.}$$

from (2).

10. THE $Z^0 \rightarrow ee\bar{\chi}$ DECAY MODE

As already mentioned in the Introduction, one event of the type $Z^0 \rightarrow ee\bar{\chi}$ was observed by UA2 in the data taken in 1983. The probability that internal bremsstrahlung can give rise to such, or less probable configuration is 1.4%. Therefore we expected a total of $N_{ee\bar{\chi}} = 0.11$ events of this kind in the 1983 Z^0 data sample to come from standard processes.

No such event has been observed in the 1984 data, giving a global expectation of $N_{ee\bar{\chi}} = 0.22$ events.

It should be pointed out that configurations where the opening angle between the electron and the photon is less than 20° in θ or 30° in ϕ are not detected by the UA2 apparatus.

11. CONCLUSIONS

Preliminary results on W and Z production and properties have been obtained from the data taken at the SPS Collider at $\sqrt{s} = 630$ GeV. They confirm previously published UA2 results at $\sqrt{s} = 546$ GeV. The measurement of the production cross section, the values of M_W , M_Z and Γ_Z , and the measurement of the forward-backward charge asymmetry in W decays all agree with the Standard Electroweak Model and QCD.

From the measured values $M_W = 81.2 \pm 0.8 \pm 1.5$ GeV/c² and $M_Z = 92.4 \pm 1.1 \pm 1.4$ GeV/c² we can extract a value for $\sin^2\theta_W$:

$$\sin^2\theta_W = 1 - M_W^2/M_Z^2 = 0.228 \pm 0.024.$$

We can also extract $\sin^2\theta_W$ from the relation

$$\sin^2\theta_W = (38.65/M_W)^2 = 0.227 \pm 0.004 \pm 0.009$$

which gives

$$\rho = M_W^2/(M_Z \cos\theta_W)^2 = 0.998 \pm 0.03$$

in good agreement with the minimal SU(2)⊗U(1) model.

Table I - Electron identification criteria
a) Central detector

Physical quantity	Description	Cuts	Efficiency η (isolated electron)
Calorimeter energy	Radius R_θ, R_ϕ Hadronic leakage $E_{\text{had}}/E_{\text{cl}} < H_0$	$R_\theta, R_\phi < 0.5$ cells $H_0 = 0.024 + 0.034 \ln E_{\text{cl}}$	0.96
Associated track	Track crossing energy cluster. At least one hit in chambers C_1 or C_2 .		0.90
Preshower signal ^{**)}	Signal from chamber C_5 within distance d_0 from track intercept.	$d_0 = 10$ mm	0.98
	Associated charge $Q_5 > Q_0$	$Q_0 = 3$ m.i.p.	0.96
	No additional cluster within distance d_1 of selected cluster, with charge larger than Q_5	$d_1 = 60$ mm	0.95
Track-energy cluster match	Require energy pattern to agree with that expected from electron: $P(\chi^2) > P_0$	$P_0 = 10^{-4}$	0.92
Overall efficiency			0.72 ± 0.05

b) Forward detectors

Physical quantity	Description	Cuts	Efficiency (isolated electrons)
Calorimeter energy	Cluster size ≤ 2 cells Energy fraction (charged and neutral) in adjacent cells $< f_0$	$f_0 = 0.05$	1.0
	Energy leakage $E_{\text{leak}}/E_{\text{em}} < H_0$	$H_0 = 0.02^{*})$	0.99
Associated track	Forward track crossing cluster cell. Track minimum distance t from vertex in transverse projection less than t_0	$t_0 = 50$ mm	0.98
	Associated transverse vertex track within $ \Delta\phi < \phi_0$ At least one hit in chambers C_1 or C_2 . No identified conversion	$\phi_0 = 30$ mr	0.96
Preshower signal	Signal in each MTPC plane within distance δ_0 of track intercept: $ \Delta x < \delta_x, \Delta y < \delta_y$	$\delta_x = 30$ mm $\delta_y = 20$ mm	0.99
	Associated MTPC charge $Q > Q_0$	$Q_0 \approx 6$ m.i.p.	0.93
Preshower-energy cluster match	Distance of projected MTPC position and cluster centroid as evaluated from PM ratio $ \Delta x < \Delta_0$	$\Delta_0 = 100$ mm	0.98
Momentum	Momentum p and calorimeter energy E satisfy $ p^{-1} - E^{-1} / \sigma(p^{-1} - E^{-1}) < \alpha_0$	$\alpha_0 = 2$	$0.89^{**})$
Overall efficiency			0.75 ± 0.05

*) A cut $H = 0.03$ is applied if the energy is shared between two adjacent cells.

***) This value takes into account both internal and external bremsstrahlung.

REFERENCES

1. a) Banner M. et al., Phys. Lett. 122B (1983) 476.
b) Bagnaia P. et al., Z. Phys. C Part. and Fields 24 (1984) 1.
2. Bagnaia P. et al., Phys. Lett. 129 (1983) 130.
3. For a review see Ellis J. et al., Ann. Rev. Nucl. Part. Science 32 (1982) 443.
4. Arnison G. et al., Phys. Lett. 122B (1983) 103.
Arnison G. et al., Phys. Lett. 129B (1983) 273.
5. a) Bagnaia P. et al., Phys. Lett. 139B (1984) 105.
b) For the analysis of high p_T production of W and Z and the measurement of p_T^W and p_T^Z see :
Plathow-Besch H., Associated production of W's and Z's with jets in UA2, Contribution to this Workshop.
6. Arnison G. et al., Phys. Lett. 139B (1984) 115.
7. Evans L. and Hatton V., CERN-SPS/85-3 (AOP).
8. Mansoulié B., Proc. of the 3rd Moriond Workshop on $\bar{p}p$ Physics (1983) 609.
See also Ref. 8, 9, 12, 13 of Ref. 1b).
9. Bozzo M. et al., Phys. Lett. 147B (1984) 392.
10. See for example Chapter 4 of Ref. 1b.
11. Bagnaia P. et al., Phys. Lett. 138B (1984) 430.
See also Pastore F., High p_T Jets in UA2, Contribution to this Workshop.
12. Hänni H., Search for Monojet and Multijet Events with Large Missing p_T in the UA2 Experiment, Contribution to this Workshop.
13. Altarelli G. et al., CERN-TH 4015/84 (1984).
14. Glück M. et al., Z. Phys. C Part. and Fields 13 (1982) 119.
15. Altarelli G. et al., Nucl. Phys. B246 (1984) 576.
16. Hikasa K., Phys. Rev. D 29 (1984) 1939.

FIGURE CAPTIONS

1. Integrated luminosity per fill as measured by the SPS group during the 1984 Collider period.
2. Longitudinal cross section of the UA2 detector in a plane containing the beam axis.
3. Schematic representation of particle signatures in a quadrant of the UA2 central detector.
4. The electron p_T spectrum of the 1984 data ($\sqrt{s} = 630$ GeV).
5. Electron p_T distribution of W candidates for the 1984 data sample. The dashed line is the background estimation. The solid line is the fit the distribution when electrons from all processes are taken into account (see text).
6. p_T distribution of electron candidates (histogram) and of jets (solid line) with $\rho_{\text{opp}} > 0.2$.
7. p_T distribution of electrons from $W \rightarrow e\nu$ in the entire UA2 data sample ($\mathcal{L} = 452 \text{ nb}^{-1}$). The dashed line is the background estimate, while the solid one is the expectation from $W \rightarrow e\nu$.
8. Plot of $(p^{-1} \cdot q \cdot \frac{\cos\theta}{|\cos\theta|})$ vs E^{-1} for the 30 $W \rightarrow e\nu$ candidate with $p_T^e > 20$ GeV/c detected in the forward regions θ_e is the laboratory angle of the electron with respect to the proton direction.
9. Electron pair mass spectrum of the 1984 data : a) after application of calorimeter cuts on both electron candidates, b) after requiring that at least one of the two candidates be a certified electron.
10. The Z^0 mass peak of the entire UA2 data sample.
11. Mass values and errors of the individual Z^0 candidates. The dashed vertical line corresponds to the fitted M_{Z^0} .

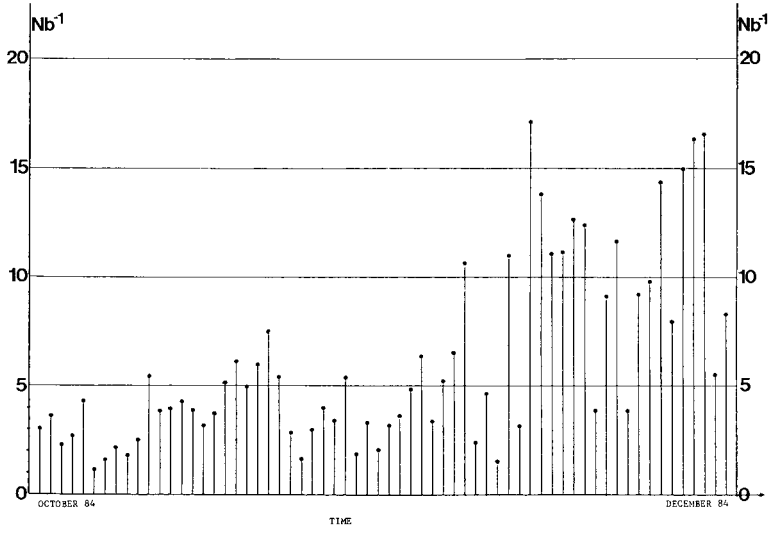


Fig. 1

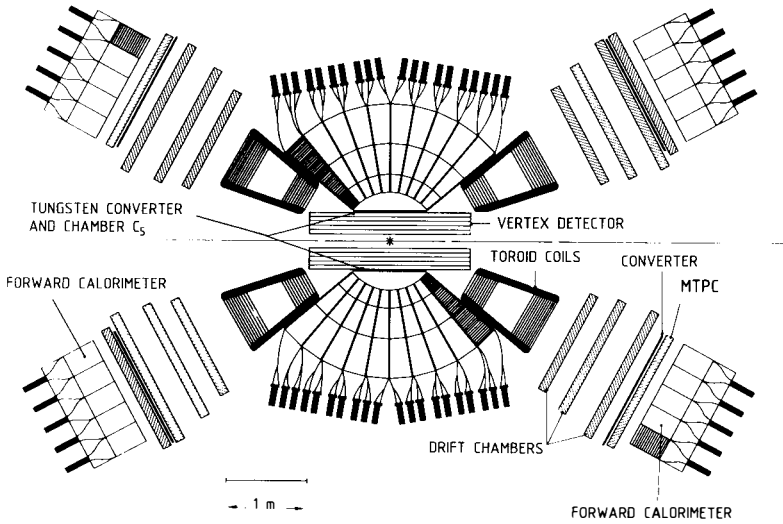


Fig. 2

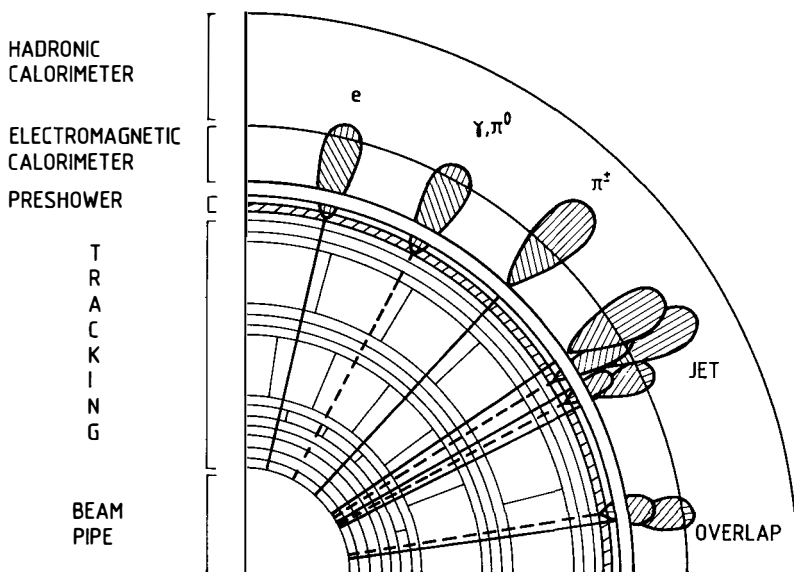


Fig. 3

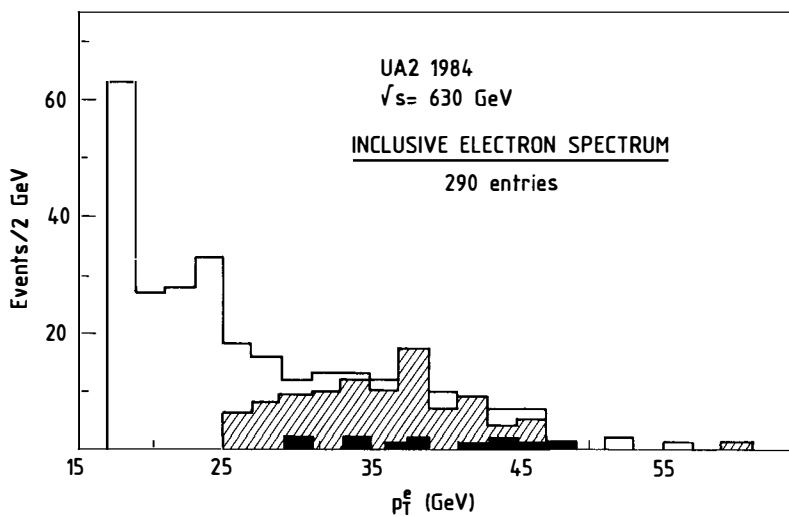


Fig. 4

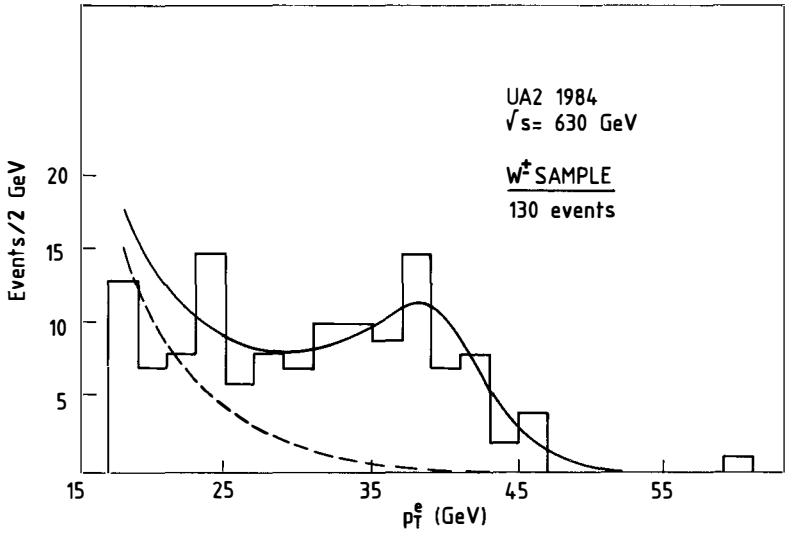


Fig. 5

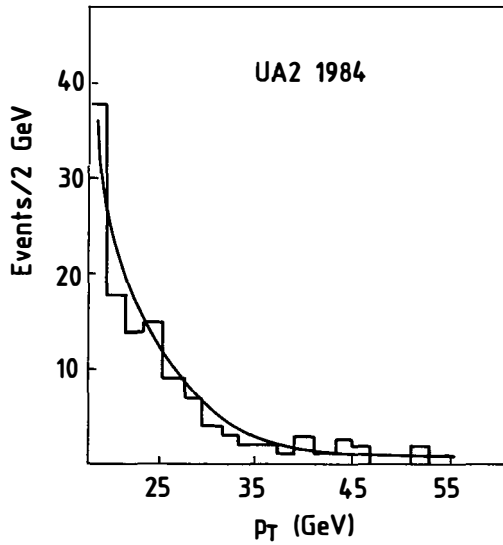


Fig. 6

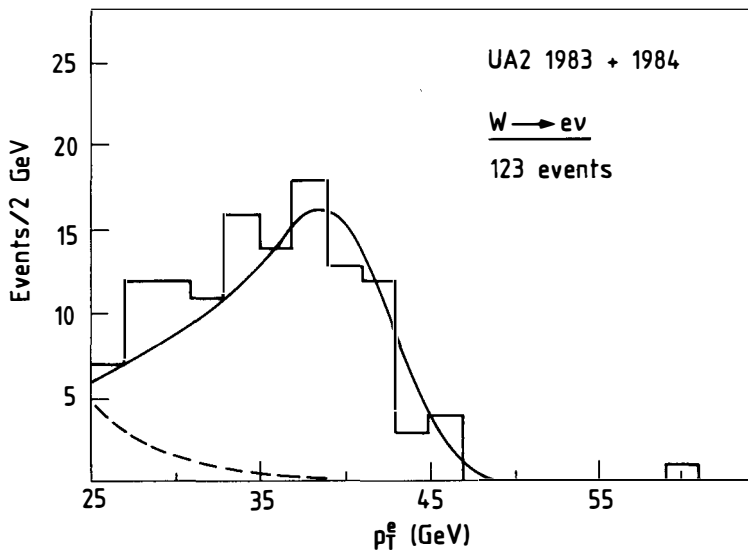


Fig. 7

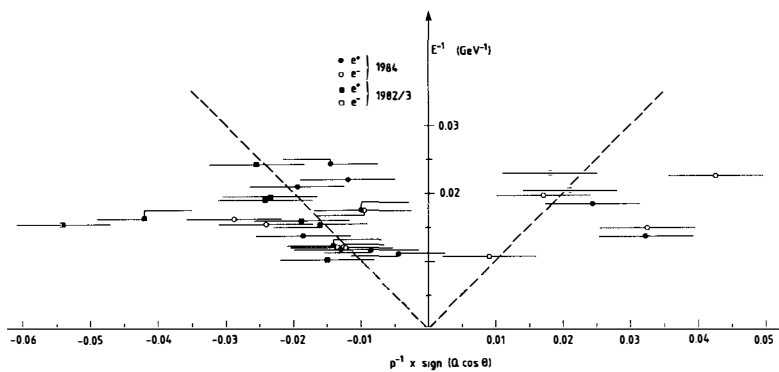


Fig. 8

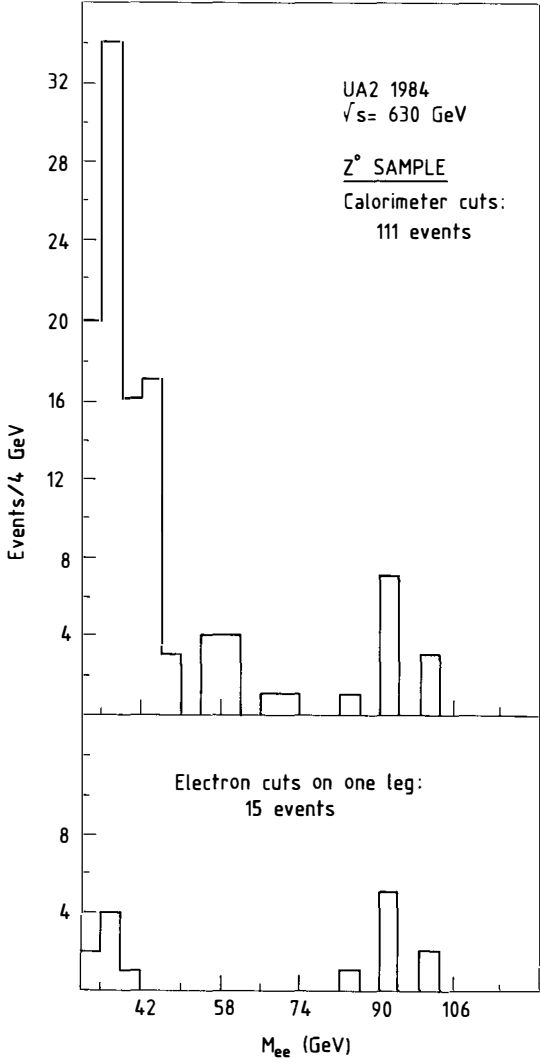


Fig. 9

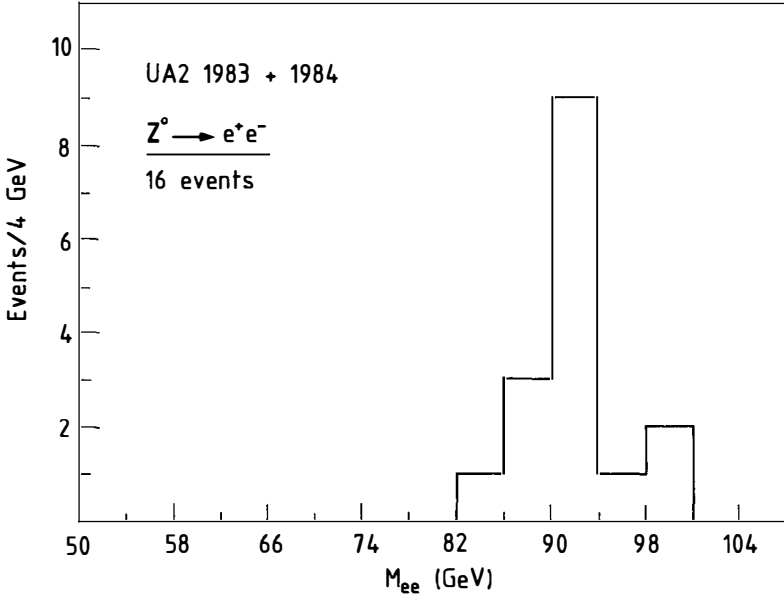


Fig. 10

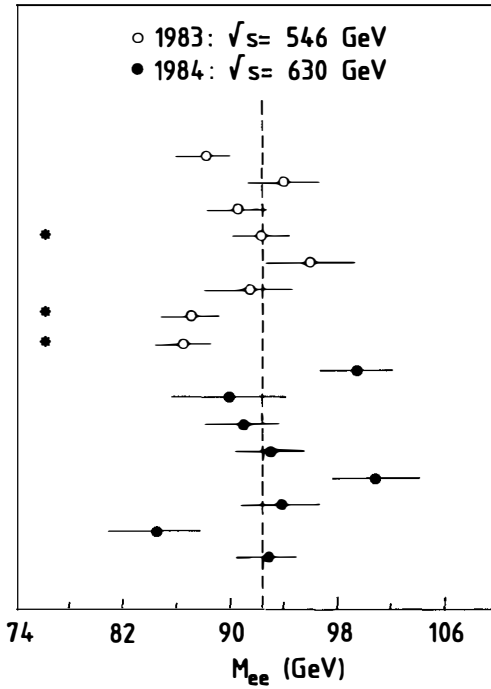


Fig. 11

MEASUREMENT OF THE RATIO OF NEUTRAL CURRENT TO CHARGED
CURRENT CROSS SECTIONS OF ANTINEUTRINO IN HYDROGEN

Birmingham-Bonn-CERN-London ICL-London UCL-Munich-Oxford Collaboration

E.Hoffmann

Physikalisches Institut der Universität Bonn



Abstract

Antineutrino-proton interactions have been studied in BEBC filled with hydrogen and equipped with the Internal Picket Fence (IPF) and the three plane External Muon Identifier (EMI). The beam was the CERN SPS wideband beam. A total of 80.000 pictures containing more than 5400 events was analysed. The IPF was used to apply a 'pattern recognition' procedure which turns out to be very effective in terms of event separation and background reduction. In the framework of the present analysis a preliminary value for the neutral to charged current cross section is found of $R_{\nu}^p = 0.332 \pm 0.032$. With the help of additional data from isoscalar targets the left and right handed quark couplings are determined. The Weinberg angle and the ρ parameter are found to be $\sin^2 \theta_w = 0.228 \pm 0.022$; $\rho = 1.01 \pm 0.06$.

1. The experiment WA21

The experimental set-up can be subdivided into three parts (fig.1):

- I. The bubble chamber BEBC filled with liquid hydrogen (H_2) at a temperature of approximately 30 K (1).

The fiducial volume was chosen to be 17 m^3 corresponding to 1t target mass. A superconduction magnet delivered inside the bubble chamber a homogenous and constant field of 3.5 T.

- II. The external muon identifier (EMI) with two downstream (inner and outer) planes and one upstream plane (2).

Between the EMI inner and outer plane an iron shield of five to ten hadronic interaction lengths is situated to separate outgoing muons from strongly interacting particles, e.g. pions. The EMI geometrical efficiency is almost 100 % for muons with momentum greater than 10 GeV/c and drops to about 50 % for muons of 3 GeV/c momentum. Muons below 3 GeV/c can not be detected.

- III. The internal picket fence IPF (3).

It consists of 2880 proportional tubes of 1.5 cm diameter and 200 cm height each, surrounding the pressure vessel of BEBC in two layers. In addition with special software (4), unique features with respect to event separation and background reduction are gained:

- a) The majority of event vertices can be reconstructed as space-time points.
- b) Almost all hadronic induced events, originating from neutrino interactions upstream the bubble chamber, can be detected on an event-by-event basis by means of their upstream(veto) picket activity (fig.2).
- c) The geometrical efficiency of the EMI is extended.
- d) Charged current events with no charged hadrons produced (one prongs) can be found with an efficiency of about 75 %.
- e) Throughgoing muons, the main systematic background for the pattern recognition to fake CC events, can be electronically measured and excluded.

The data were taken in summer 1981. On about 80.000 frames, 5437 interactions in the bubble chamber were visible. The beam was the CERN wideband beam (WBB). The SPS delivered protons with 400 GeV/c momentum on a beryllium target (10^{13} protons/spill). Parent pions and kaons were produced decaying into (anti)neutrinos with an average energy of 40 GeV. The neutrino background in the antineutrino beam was about 25 %. Contributions from $\bar{\nu}_e$ can be estimated to be less than 1.5 %.

2. Event classification and cuts

We obtain in the bubble chamber

- (i) Charged current (CC) events with an EMI identified μ^+ ,

- (ii) CC events with an EMI identified μ^- ,
- (iii) Hadronic induced (N^*) events vetoed by the IPF or in addition by through-going muons,
- (iv) all other events consisting of
 - genuine $\bar{\nu}$ - neutral current (NC) events
 - genuine ν - NC events,
 - CC events without detected muon due to geometrical and electronical losses of the EMI,
 - N^* events without specific features,
 - $\bar{\nu}$ background events (CC and NC).

In general a cut on the hadronic (visible) energy was applied at 5 GeV. In our analysis we have recalculated the true hadronic energy by means of a Monte Carlo simulation separately for NC and CC events. The results given refer to a total hadronic energy above 7.5 GeV. In addition the charged multiplicity was required to be greater/equal three.

Muons from charged current interactions were accepted down to 3 GeV/c momentum for $\bar{\nu}$ CC events and down to 5 GeV/c momentum for ν CC events.

In order to be comparable with previous calculations (5) and to minimize our systematic error we have introduced an additional cut on the hadronic transverse momentum p_t^H (fig.4).

3. Results on NC/CC calculation

	NC	CC (μ^+)
raw data	800 \pm 23	1061 \pm 33
wrong timing	3 \pm 2	
vetoed NC	60 \pm 12	
silent N^*	- 7 \pm 2	
false CC	5 \pm 3	- 1 \pm 1
Pion decay	7 \pm 3	- 4 \pm 2
EMI elec. ineff.	- 92 \pm 20	42 \pm 11
EMI geom. ineff.	- 76 \pm 5	23 \pm 2
p_μ cut	- 155 \pm 5	71 \pm 4
ν NC	- 130 \pm 14	
$\bar{\nu}_e$	- 20 \pm 3	
$E_{tot}^H \geq 7.5$	- 4 \pm 1	11 \pm 1
total	392 \pm 41	1203 \pm 35

The $\bar{\nu}$ NC background was calculated assuming $R_P^V = 0.39 \pm 0.04$ for neutrino-proton interactions (6). The contributions from $\bar{\nu}_e$ events were estimated via a WBB simulation program (7) under the assumption of muon/electron universality.

The results obtained read as follows:

$$\text{NC/CC} = 0.325 \pm 0.035 \\ 0.025 \text{ (stat)} \pm 0.024 \text{ (syst)}$$

And for $p_t^H > 0.75$:

$$\text{NC/CC} = 0.332 \pm 0.032$$

4. Interpretation of our result in terms of the Standard Model

Since we are working on a proton target it is not possible to give a model independent interpretation of the NC/CC ratio or the value of $\sin^2\theta_w$ respectively. Thus the NC/CC ratio is related to the quark couplings q_i weighted by some coefficients a_i (8):

$$\text{NC/CC} = a_1 u_L^2 + a_2 u_R^2 + a_3 d_L^2 + a_4 d_R^2$$

The coefficients a_i are sensitive to the beam and the cuts applied to the data and have been determined by Monte Carlo integration. For example:

$$a_1 = \frac{\iint \phi(E) E (1-y)^2 \{x u(x, Q^2) + x c(x, Q^2)\} + \{x \bar{u}(x, Q^2) + x \bar{c}(x, Q^2)\} dE dx dy}{\iint \phi(E) E (1-y)^2 \{x u(x, Q^2) + x c(x, Q^2)\} + \{x \bar{d}(x, Q^2) + x \bar{s}(x, Q^2)\} dE dx dy}$$

The input for a_1 is:

- $x q_i(x, Q^2)$ parametrization of the quark densities by Buras & Gaemers(9)
- $\phi(E_\nu)$ known WA21 $\bar{\nu}$ flux
- cuts on the data $E_{\text{tot}}^H > 7.5 \text{ GeV}$, p_t^H .

The remaining coefficients a_2 , a_3 and a_4 have been calculated accordingly. The dependence of the coefficients on p_t^H is given in fig.3. With the $\bar{\nu}$ beam we are especially sensitive to the right handed quark couplings. In the Standard Model without radiative corrections and neglecting heavier than charm quark contributions the NC/CC ratio without p_t^H cut has to match

$$\text{NC/CC} = 1.017u_L^2 + 0.663d_L^2 + 3.338u_R^2 + 1.83d_R^2 \\ = 0.223 \pm 0.032$$

Since we have four unknowns but only one equation we have to use boundary conditions in order to determine the quark couplings. In this analysis we have applied measurements from isoscalar targets, namely from CDHS and from the BEBC D_2 Col-

laboration (WA25).

$$u_L^2 + d_L^2 = 0.30 \pm 0.01$$

$$u_R^2 + d_R^2 = 0.03 \pm 0.01$$

$$-1.06u_L^2 + 1.06d_L^2 - 0.25u_R^2 + 0.25d_R^2 = 0.06 \pm 0.06$$

$$0.49u_L^2 - 0.49d_L^2 + 2.85u_R^2 - 2.85d_R^2 = 0.02 \pm 0.09$$

Solving the five equations simultanously one obtains:

$$u_L^2 = 0.14 \pm 0.03 \quad u_R^2 = 0.019 \pm 0.014$$

$$d_L^2 = 0.16 \pm 0.03 \quad d_R^2 = 0.011 \pm 0.017$$

The quark couplings are directly related to the weak mixing angel θ_ω (11):

$$u_L = 1/2 - 2/3 \sin^2 \theta_\omega \quad d_L = -1/2 + 1/3 \sin^2 \theta_\omega$$

$$u_R = -2/3 \sin^2 \theta_\omega \quad d_R = 1/3 \sin^2 \theta_\omega$$

Fixing $p = 1$ yields $\sin^2 \theta_\omega = 0.224 \pm 0.012$.

Leaving p as a free parameter the result is:

$$p = 1.01 \pm 0.06 \text{ and } \sin^2 \theta_\omega = 0.228 \pm 0.022.$$

5. Conclusions

We have measured the cross section for neutral to charged currents in antineutrino-proton interactions. A new technique for the event separation by means of the Internal Picket Fence leads to a considerable improvement in our analysis with respect to background reduction and systematic errors.

The obtained value of the weak missing angle $\sin^2 \theta_\omega = 0.228 \pm 0.022$ and $p = 1.01 \pm 0.06$ is in good agreement with the Standard Model. Since we have used only 1/3 of our total statistic, the errors on the right (and left) handed quark couplings are still large, compared to what we aimed for.

A complete analysis of all our statistics covering neutrino and antineutrino data is expected in the near future.

References

1. G.Harigel et al., BEBC Users Handbook
2. C.Brand et al., Nucl.Inst.& Meth. 136(1976)485
R.Beuselinck et al., Nucl.Inst.& Meth. 154(1978)445
3. H.Foeth, Nucl.Inst.& Meth. 176(1980)203
C.Brand et al., CERN/EP 81-13
4. M.L.Retter, S.Towers, Oxford Print 1985 (in prep.)
5. J.Blietschau et al., Phys.Lett.88B(1979)381
6. D.Allasia et al., Nucl.Phys. B239(1985)301
7. H.Wachsmuth, CERN/EP 78-29
8. P.C.Bosetti et al., Nucl.Phys. B142(1978)1
9. A.J.Buras, K.J.F.Gaemers, Nucl.Phys. B132(1978)249, Phys.Lett.71B(1977)106
10. C.Geweniger, Proc.of the Int.Europhys.Conf., Brighton, July83, S.216
11. C.M.Sehgal, Aachen PITHA 79/18

Figure Captions

Fig.1 : Lay-out of the system BEBC/IPF/EMI

Fig.2 : $N\bar{\nu}$ event obtained in BEBC.

ν makes a primary CC interaction in the coils upstream BEBC.

$A\mu$, charged and neutral hadrons are produced.

One neutron enters the chamber, interacts and is visible as a " $N\bar{\nu}$ " event.

The crosses are marking hits, which can be measured simultaneously by the system EMI/IPF.

Fig.3: The curves show the development of the quark coupling coefficients a_i as a function of a p_t^H cut.

Fig.4: The raw and corrected NC/CC ratio is shown in dependence of p_t^H .
The solid line represents the theoretical expectations taken from fig.3.

Schematic lay-out of EM1 picket fence in BEBC

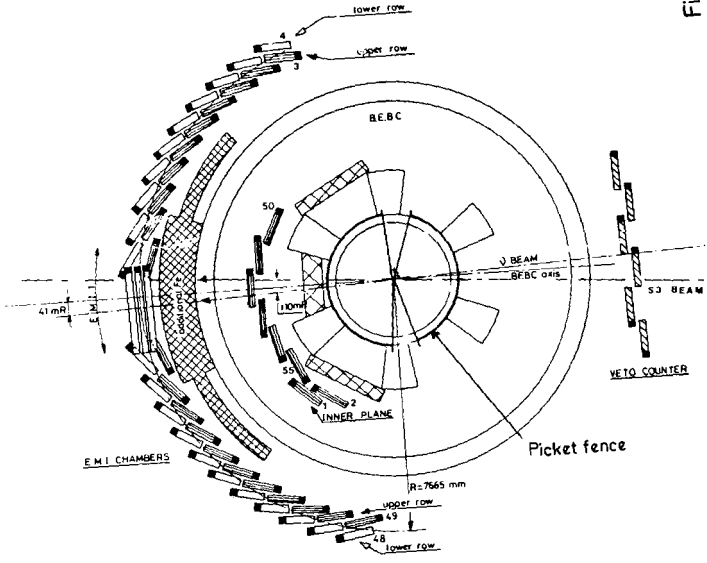


Fig.1

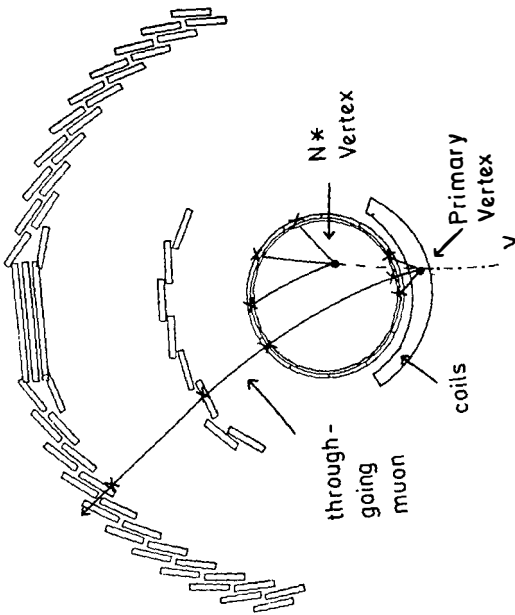


Fig.2

Evolution of Coefficients of Neutral Current Couplings
with P_t^H - cut.

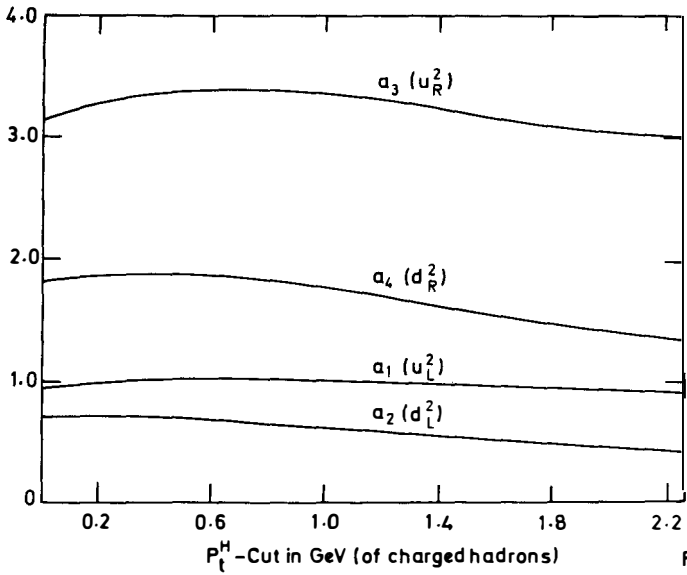


Fig. 3

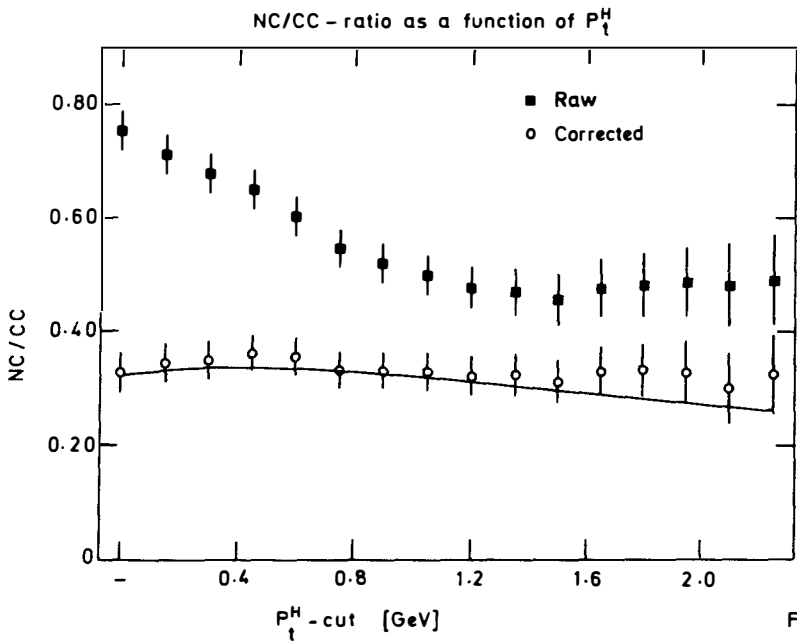


Fig. 4

**New Determination of $\sin^2\theta_W$ from
Ratio of Neutrino and Anti-Neutrino
Elastic Scattering by Electrons**

U.S.A.-JAPAN NEUTRINO COLLABORATION*

L. A. Ahrens, S. H. Aronson,
P. L. Connolly, B. G. Gibbard, M. J. Murtagh,
S. Murtagh, S. Terada, D. H. White (B.N.L.); J. L. Callas,
D. Cutts, J. S. Hoftun, R. E. Lanou, T. Shinkawa (Brown Univ.);
K. Amako, S. Kabe (K.E.K.); Y. Nagashima, Y. Suzuki, S. Tatsumi
(Osaka Univ.); K. Abe, E. W. Beier, D. C. Doughty, L. S. Durkin,
S. M. Heagy, M. Hurley, A. K. Mann, F. M. Newcomer,
H. H. Williams, T. York (Univ. of Pennsylvania);
D. Hedin, M. D. Marx, E. Stern (Stony Brook)

**Presented by R. E. Lanou
Department of Physics
Brown University
Providence, Rhode Island
02912 (USA)**

Abstract

Measurements are made of the purely leptonic weak neutral current processes $\nu_\mu + e^- \rightarrow \nu_\mu + e^-$ and $\bar{\nu}_\mu + e^- \rightarrow \bar{\nu}_\mu + e^-$. Cross sections, the vector and axial vector couplings, and the Standard Model parameters $\sin^2\theta_W$ and ρ are determined. Results are: $\sigma_0(\nu_\mu) = 1.60 \pm 0.29 \pm 0.26$, $\sigma_0(\bar{\nu}_\mu) = 1.16 \pm 0.20 \pm 0.14$ (both in units of $10^{-42} \text{cm}^2/\text{GeV}$), $g_V^e = -0.079 \pm 0.060$, $g_A^e = -0.483 \pm 0.042$, $\rho = 0.967 \pm 0.082$, $\sin^2\theta_W = 0.209 \pm 0.029 \pm 0.013$.

We report results on the weak neutral current parameters for the purely leptonic channels

$$\nu_{\mu} + e^{-} \rightarrow \nu_{\mu} + e^{-} \quad (1)$$

$$\bar{\nu}_{\mu} + e^{-} \rightarrow \bar{\nu}_{\mu} + e^{-} \quad (2)$$

The individual cross sections for these reactions are given by

$$\sigma\left(\frac{\nu}{\bar{\nu}}\right) = \frac{G_{Fm}^2}{2\pi} E_{\nu}\rho \left[(g_V^e \pm g_A^e)^2 + \frac{1}{3}(g_V^e \mp g_A^e)^2 \right] \quad (3)$$

where g_V^e and g_A^e are the vector and axial vector couplings of the electron to the neutral intermediate vector boson and ρ is a parameter expressing the neutrino coupling. In the Standard Model of Glashow-Weinberg-Salam the values are

$$g_A^e = -\frac{1}{2}; \quad g_V^e = \left(-\frac{1}{2} + 2\sin^2\theta_w\right); \quad \rho = 1$$

An important consequence of this model is the fact that the ratio of the cross sections (3) is given by

$$R = \frac{\sigma(\nu e)}{\sigma(\bar{\nu} e)} = 3 \left[\frac{1 - 4\sin^2\theta_w + \frac{16}{3}\sin^4\theta_w}{1 - 4\sin^2\theta_w + 16\sin^4\theta_w} \right] \quad (4)$$

R is thus a quantity independent of ρ , depending only upon $\sin^2\theta_w$, and free from the complications of Q.C.D.

An additional, important practical result is that the error in $\sin^2\theta_w$ is given by

$$\Delta(\sin^2\theta_w) \cong \frac{1}{8} (\Delta R/R) \quad (5)$$

when $\sin^2\theta_w$ is near 0.23. Hence, an eight percent error on $\Delta R/R$ would lead to $\Delta(\sin^2\theta_w) \cong 0.01$ and corresponds to an equivalent error in intermediate vector boson masses of about $1.2\text{GeV}/c^2$. In practice, since the absolute fluxes of neutrinos are not known, the cross sections of reactions (1) and (2) are normalized to the well measured quasi-elastic cross sections for $\nu_{\mu} + n \rightarrow \mu^{-} + p$ and $\bar{\nu}_{\mu} + p \rightarrow \mu^{+} + n$. The practical limit on the systematic error of this approach is determined by the knowledge of the inelastic subtraction for these channels.

This experiment (AGS E-734) was carried out at the alternating gradient synchrotron (A.G.S.) of the Brookhaven National Laboratory (B.N.L.). The neutrinos were obtained using a pulsed horn for focussing into a wide-band beam spectrum of average energy 1.5GeV (1.4GeV) for neutrinos (anti-neutrinos). The intensity was about 10^{10} neutrinos per GeV - m² - 10¹³ protons-on-target; this is sufficient to produce about one neutrino interaction (σ_{TOT}) per second in the 80 fiducial Mtons of our detector.

The most important requirements for achieving a good signal to noise for reactions (1) and (2) are angular resolution and a measurement of dE/dx early in the electromagnetic shower to distinguish between electron- and photon-initiated events.

From the point of view of systematic errors, the relative normalization in the flux ratio $\phi(\bar{\nu})/\phi(\nu)$ is dominant; the systematic error in the electron signal ratio, $N_e(\bar{\nu})/N_e(\nu)$, canceling almost exactly.

The detector¹¹ has been designed and constructed with the above points in mind. It is a very fine grain, fully active (liquid scintillator) electronic device of 200 Mtons (80 Mtons fiducial) with an effective radiation length of 60 cm (real space). The angular resolution (achieved with arrays of ~15,000 drift tubes) is $\Delta\theta_{x,y} = (16 \text{ mrad})/\sqrt{E(\text{GeV})}$; this is less than one half the kinematic limit for reactions (1) and (2). The energy resolution of the electromagnetic showers is determined (2000 cells of liquid scintillator) to be $\Delta E_e/E_e = (13\%)/\sqrt{E_e(\text{GeV})}$. For particle identification, dE/dx is measured in both the drift tubes and scintillators which provide six measurements in the early part of the shower on 90% of the electrons. Out-of-time background (neutrons, cosmic rays, muon decays) are discriminated against by ± 2 nsec timing and two-hit electronics. Additionally, a magnetic spectrometer at the end of the detector measures the beam composition for ν_μ and $\bar{\nu}_\mu$. The energy, angle and particle identification have been verified with appropriate test beam exposures.

The kinematics of reactions (1) and (2) is particularly distinctive; given in an obvious notation by

$$E_e \theta_e^2 = 2m_e (1 - E_e/E_\nu). \quad (6)$$

Thus there is a kinematic limit in E_e vs. θ_e^2 space of

$$E_e \theta_e^2 \leq 2m_e \quad (7)$$

At A.G.S. energies, this implies an average electron angle of roughly 40 milliradians.

The backgrounds are dominated by beam contamination of $\nu_e(\bar{\nu}_e)$ and by neutral current production of pi-zeros. There is a small contribution from very low energy mis-identified hadrons. The $\nu_e(\bar{\nu}_e)$ background occurs primarily via $\nu_e(\bar{\nu}_e) + n(p) + e^-(e^+) + p(n)$ and is suppressed by second prongs, Pauli exclusion, energy and angle cuts. The pi-zero neutral current production occurs dominantly through the $3/2 - 3/2$ isobar channel; however, at AGS energies coherent production (a severe problem at FNAL and CERN energies) is small with no forward peak. The pi-zero background is suppressed by multiple photon conversions and energy-angle cuts as well as by dE/dx discrimination. All the backgrounds are nearly flat in θ_e^2 whereas 96% of the signal is contained within $\theta_e^2 < 0.01(\text{rad})^2$.

The results reported here derive from exposures of $8.8 \times 10^{18}(\nu_\mu)$ and $3.5 \times 10^{19}(\bar{\nu}_\mu)$ protons on target. This corresponds to about one-third of our neutrino data and all of our present anti-neutrino data. The analysis procedure and data flow is illustrated in Figure 1.

Guided by the kinematic conditions stated in (6) and (7) we plot in Figure 2 the resulting θ_e^2 distributions. A clear signal peak at small θ_e^2 upon an approximately flat distribution is visible in the samples containing dominantly electrons (Fig. 2a and 2c), while the distribution of the mainly photon samples (Fig. 2b and 2d) is seen to be without significant small angle enhancement. To extract the number of events in the signal region, $\theta_e^2 < 0.01(\text{rad})^2$, we have determined the backgrounds in the region $0.01 < \theta_e^2 < 0.03(\text{rad})^2$ and extrapolated them into the signal region. The fraction of photons in the signal region (typically, 38% of the total background in that region) is calculated directly from the electron-photon selection process. The remaining background in the signal region is attributed to $\nu_e(\bar{\nu}_e)$ quasi-elastics and to low energy hadrons that scatter inelastically or are attended by small showers (typically for $\bar{\nu}_e$, 44% quasi-elastic and 18% hadrons). The electron quasi-elastic component was obtained from a Monte Carlo calculation that satisfactorily describes data used in our oscillation study.²¹ After background subtraction, which was done fitting the θ_e^2 distribution to the sum of the background components (taking the photon and low energy hadron distributions as flat) and the expected shape of reaction (2) including angular resolution, a signal of 59 ± 10 events remains. Two other independent methods were used to perform this extraction and achieved excellent consistency. Following a similar procedure a signal of 51 ± 9 events were found for reaction (1). These signals must be further corrected for acceptance, filter-scan efficiency, cuts, and "wrong sign" neutrino beam contamination -- typically, a total correction of a factor of two.

In order to normalize the fluxes and determine the cross sections we use a sample of charged current quasi-elastic $\nu_\mu(\bar{\nu}_\mu)$ events sampled uniformly throughout the running. We also measure the shape of ν_μ and $\bar{\nu}_\mu$ spectra for use in calculating appropriate averages. These samples are selected to be of low- Q^2 by requiring for the muon: $\theta_\mu < 15^\circ$, $p_\mu > 400\text{MeV}/c$, a single prong at vertex and the vertex contained in the same fiducial volume as that used for the $\nu_\mu(\bar{\nu}_\mu) - e^-$ signal. These normalization samples must also be corrected for acceptance, (0.16 ± 0.009) (ν_μ) and 0.29 ± 0.008 ($\bar{\nu}_\mu$) and backgrounds (0.31 ± 0.03) (ν_μ) and 0.28 ± 0.03 ($\bar{\nu}_\mu$).

Combining the signal and normalization data, we obtain

$$\sigma_o(\nu_\mu) = \frac{\sigma(\nu_\mu - e^-)}{E_\nu} = 1.60 \pm 0.29 \text{ Stat.} \pm 0.26 \text{ Sys.} \times 10^{-42} \frac{\text{cm}^2}{\text{GeV}}$$

$$\sigma_o(\bar{\nu}_\mu) = \frac{\sigma(\bar{\nu}_\mu - e^-)}{E_{\bar{\nu}}} = 1.16 \pm 0.20 \text{ Stat.} \pm 0.14 \text{ Sys.} \times 10^{-42} \frac{\text{cm}^2}{\text{GeV}}$$

leading to the ratio

$$R = 1.38^{+0.40}_{-0.31} \text{ Stat.} \pm 0.17 \text{ Syst.}$$

and

$$\sin^2 \theta_w = 0.209 \pm 0.029 \text{ Stat.} \pm 0.013 \text{ Sys.}$$

Figure 3 illustrates the functional relation between R and $\sin^2 \theta_w$ as well as the principal values and their errors. The best value for the parameter ρ is 0.967 ± 0.082 at this value of $\sin^2 \theta_w$.

This result for the weak mixing parameter is in good agreement with that of CHARM³¹ collaboration. Combining our result (E-734) with that of CHARM leads to $\sin^2 \theta_w$ (combined) = 0.212 ± 0.023 .

As was mentioned previously, the model independent couplings, g_V^e and g_A^e , can also be extracted from these data. Figure 4a shows the elliptic bands allowed by this experiment. The four-fold ambiguity represented by the intersection of the bands is removed by the $\bar{\nu}_e - e$ reactor data⁴¹ and the combined $e^+e^- \rightarrow \mu^+\mu^-$ asymmetry experiments.^{51e} The single resulting solution derived from this experiment is shown with 67% and 90% C.L. contours in Figure 4b; it yields the values

$$g_A^e = -0.483 \pm 0.042$$

$$g_V^e = -0.079 \pm 0.060$$

As is to be expected, these values are consistent with the G-W-S weak isospin assignments for the electron with $T_{3L} = -1/2$ and $T_{3R} = 0$.

What is the ultimate limit of this type of experiment and this one in particular? Can one hope to obtain errors on $\sin^2\theta_w$ significantly smaller than the radiative corrections? Currently, our precision is limited by the numbers of $\bar{\nu}_\mu e$ and $\nu_\mu e$ events; however, ultimately backgrounds in the normalization samples dominate.⁶¹ These backgrounds arise from the presence of charged-current soft single-pion and multipion events. Our present error on the $\nu_\mu/\bar{\nu}_\mu$ flux ratio as determined from the μ^-p/μ^+n ratio is estimated to be 9%; more than half of this arises from uncertainties in pion production cross sections and nuclear effects. Thus, while there is still room for improvement, the range is not great. The contribution to the uncertainty in R from systematic differences in the treatment of $\nu_\mu e$ and $\bar{\nu}_\mu e$ samples is 8%; improved knowledge and understanding of our filter process gained during this analysis will lead to significant reductions when the remaining data is added to these and processed in a common way.

Another, large data taking run is scheduled for autumn 1985 this should bring the total number of events to 300 (ν_μ) and 150 ($\bar{\nu}_\mu$) leading to $\Delta R/R$ of perhaps 0.08 and $\Delta(\sin^2\theta_w) \cong 0.01$. While some further improvement in normalization backgrounds is possible, this experiment with the present detector size and available running time will not reach a level of ± 0.003 without a herculean effort.

*This work was supported in part by the U.S. Department of Energy, the Japanese Ministry of Education, Science and Culture through the Japan-U.S.A. Cooperative Research Project on High Energy Physics, the U.S. National Science Foundation, and the Stony Brook Incentive Fund.

References

1. L. A. Ahrens et al, Phys. Rev. Lett. 51, 1514 (1983), G. Gidal et al (Particle Data Group), L.B.L. Report No. LBL-91, Suppl. UC-37, 1983 (unpublished), section on "Major particle detectors in elementary particle physics."
2. See L. A. Ahrens et al, "New Limit on the Strength of Mixing Between ν_μ and ν_e ," Phys. Rev. D31, 2732 (1985); and same title in Proceedings of this Conference.
3. F. Bergsma et al, Phys. Lett. 147B, 485 (1984).
4. F. Reines & H. Sobel, Phys. Rev. Lett. 37, 315 (1976).
5. See for example, A. Bohm, Proceedings of HEP83 International Europhysics Conference on High Energy Physics, Brighton, p. 686 (1983).
6. A further discussion of how the systematic errors are established is contained in L. A. Ahrens et al, Phys. Rev. Lett. 54, 18 (1985).

DATA TAKEN TO DATE:

ν	$\bar{\nu}$
2.9×10^{19}	3.5×10^{19}

Protons on Target

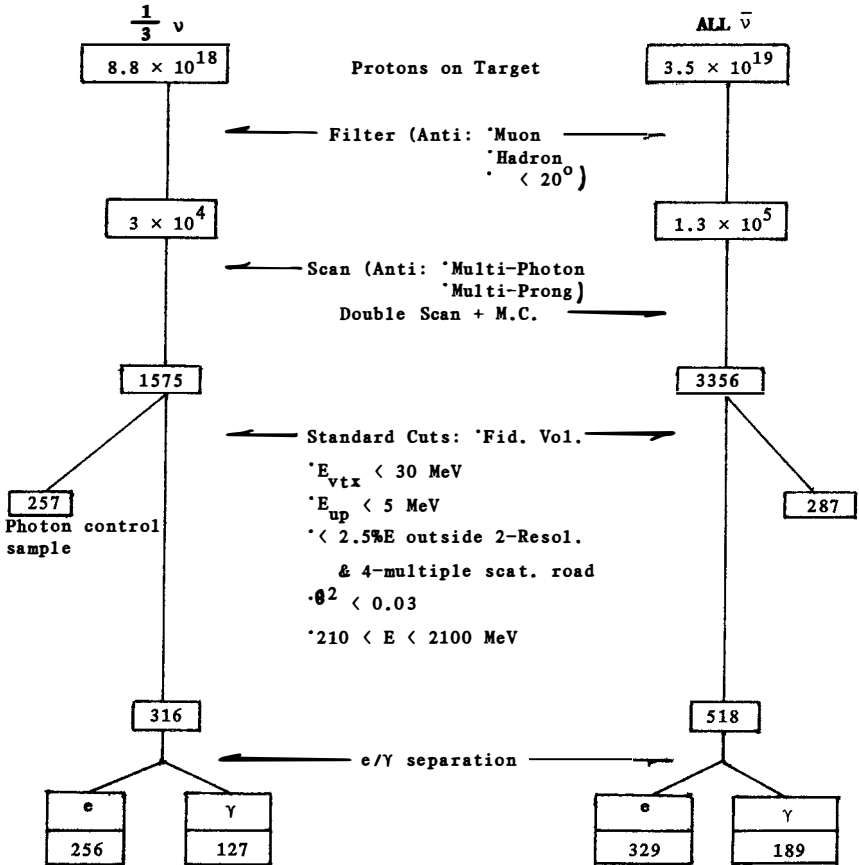
SIGNAL PROCESSED TO DATE:

Figure 1
Data Analysis Flow Diagram

(BNL E-734)
USA - JAPAN

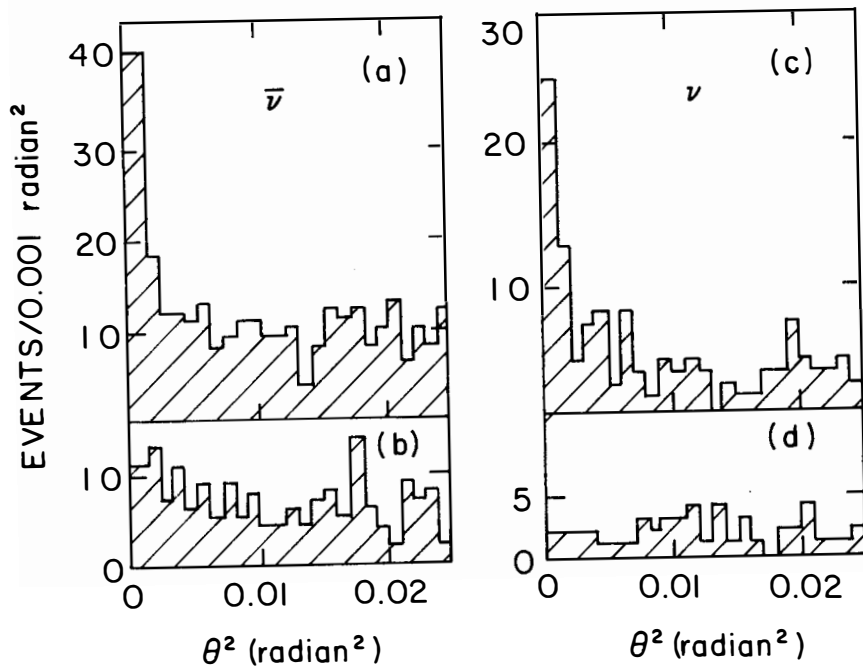


FIG. 2

Angle squared distribution of showers. dE/dx separated events are: photon candidates, (b) and (d); electron candidates, (a) and (c).

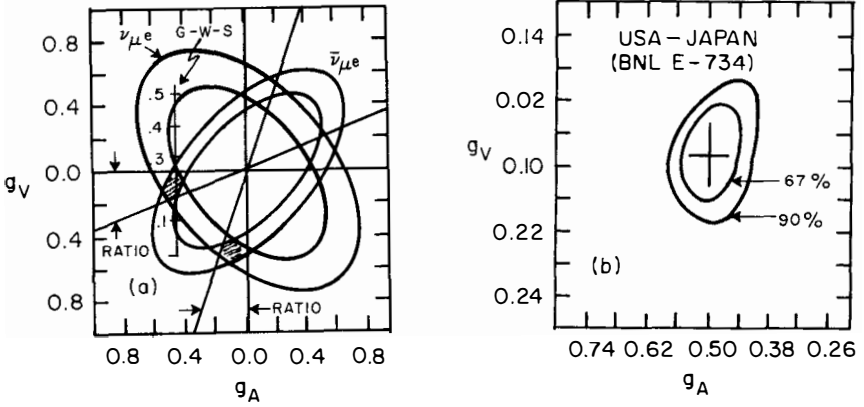
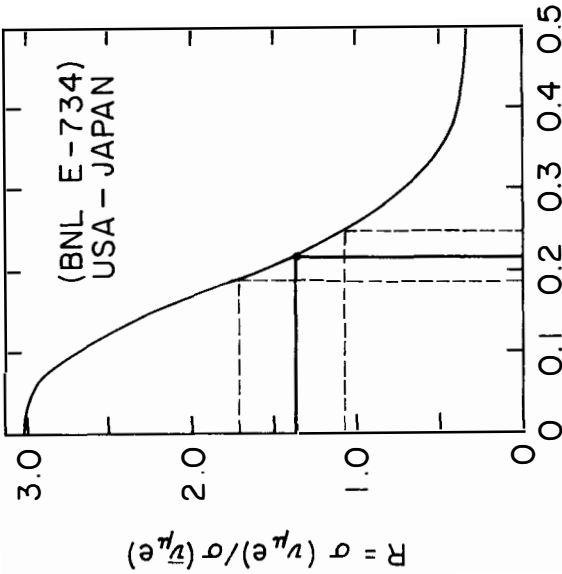


FIG. 4

a) Neutral current couplings, allowed regions (this experiment only). Cross hatched regions consistent from $\bar{\nu}_e$ -e experiments. b) Only solution allowed by this experiment consistent with $\bar{\nu}_e$ -e and e^+e^- experiments. See text for best fit values.



$\sin^2 \theta_W$
FIG. 3

R versus $\sin^2 \theta_W$, solid (light) curve; measures principal values, solid (heavy) lines; errors, dashed lines.

SEARCH FOR THE DECAY $\mu^+ \rightarrow e^+ e^+ e^-$
 AND
MEASUREMENT OF THE DECAY $\mu^+ \rightarrow e^+ e^+ e^- \nu_{e-\mu}$
WITH THE SINDRUM SPECTROMETER

SINDRUM Collaboration

Inst. f. Mittelenergiephysik der ETH Zürich,
 CH-5234 Villigen, Switzerland

* Phys. Inst. d. Univ. Zürich, CH-8001 Zürich, Switzerland
 SIN, CH-5234 Villigen, Switzerland

CEN Saclay, F-91191 Gif-sur-Yvette, France

presented by

* Norbert Kraus

Abstract

In a search for the forbidden decay $\mu^+ \rightarrow e^+ e^+ e^-$ no candidate was found, yielding a new upper limit on the branching ratio $R(\mu \rightarrow 3e) < 2.4 \cdot 10^{-12}$ (90% confidence). Implications for two models beyond the standard model of electroweak interaction are discussed. In this experiment a total number of 7443 ± 148 events was seen in agreement both in number and spectrum shape with the allowed rare decay $\mu^+ \rightarrow e^+ e^+ e^- \nu_{e-\mu}$ assuming V-A-theory. For this decay a branching ratio of $R(\mu \rightarrow 3e 2\nu) = (3.3 \pm 0.5) \cdot 10^{-5}$ was determined.

Separate lepton numbers (L_e, L_μ, L_τ) are conserved quantities in the minimal version of the standard model of the electroweak interaction. Nearly any extended model - e.g. horizontal symmetries, composite models or supersymmetric theories - does not maintain this phenomenological law and thus L_μ -violating processes such as $\mu \rightarrow e\gamma$, $\mu \rightarrow 3e$, $\mu A \rightarrow eA'$ or $K \rightarrow \pi e\mu$ are allowed. Upper limits on the branching ratios of these processes¹⁾ are experimentally known at a level of 10^{-9} or 10^{-10} and put strong constraints on the parameters of these models. Since not only the branching ratios of different L_μ -violating processes but also their relative ratios depend on the specific model, experimental limits for each of these decays are important constraints for modern theories. For the L_μ -conserving i.e. allowed, purely leptonic weak processes up to now no experimental result contradicts the V-A-structure. Nevertheless, contributions of interactions other than V-A can not be excluded at a level of up to 30%²⁾. Measurements of rare allowed μ -decays like $\mu \rightarrow 3e2\nu$ might be able to improve the situation.

The previous experimental upper limit for the forbidden decay $\mu \rightarrow 3e$ is $R(\mu \rightarrow 3e) = \Gamma(\mu \rightarrow 3e) / \Gamma(\mu \rightarrow e2\nu) < 1.3 \cdot 10^{-10}$ ³⁾ and the world sample of the rare allowed decay $\mu \rightarrow 3e2\nu$ are 25 events⁴⁾. To improve the sensitivity for the upper limit of the decay $\mu \rightarrow 3e$ to the level of 10^{-12} the magnetic spectrometer SINDRUM was built. In addition the decay $\mu \rightarrow 3e2\nu$ is measured simultaneously as an unavoidable 'background'. Last year at the rencontre de Moriond the SINDRUM-spectrometer was described and results of a test run were presented⁵⁾, final results are given in what follows.

At the SIN surface μ^+ -beam $\sim 6.5 \cdot 10^6 \mu^+$ /s are stopped in an extended target. Tracks of charged particles of μ -decays are detected by five thin ($\sim 10^{-3}$ radiation length) cylindrical multiwire proportional chambers. The charge and momentum are determined by the curvature of the track in the homogeneous magnetic field, which is parallel to the beam axis. Three of the five chambers are equipped with cathode strips to reconstruct the tracks in three dimensions. The time information is derived from a hodoscope of 64 plastic scintillators placed outside the chambers. The projections of a $\mu \rightarrow 3e 2\nu$ event are shown in figure 1.

To select $\mu \rightarrow 3e$ decays a multistage online trigger filtered out $\mu \rightarrow 3e$ candidates and $\mu \rightarrow 3e 2\nu$ events using the hodoscope information

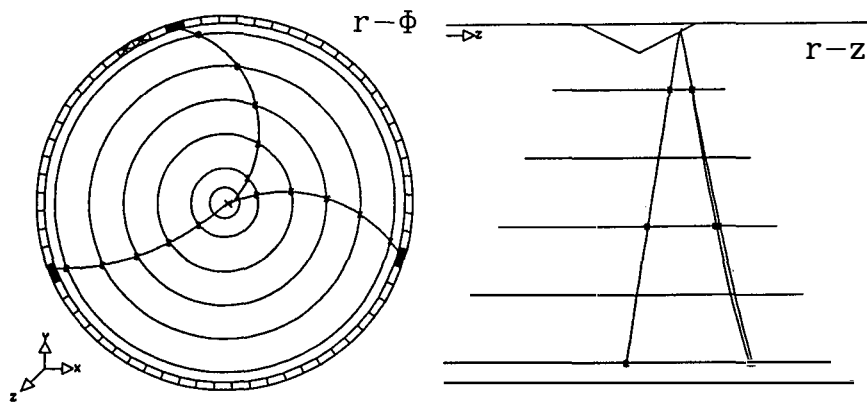


Figure 1 A $\mu \rightarrow 3e 2\nu$ event in the $r-\phi$ and $r-z$ projection. The online trigger selects the events in four stages with the following requirements: (1) the three hodoscope hits within 12 ns, (2) a negative track candidate in the outer three chambers, (3) at least one negative and two positive track candidates in all five chambers, (4) a track triple with total transverse momentum $P_T < 45 \text{ MeV}/c$.

and the wire chamber information from grouped anode hits. The stages of the hardware trigger are explained in figure caption 1. It uses the following kinematical constraints for a $\mu \rightarrow 3e$ candidate: $\sum E_i = m_\mu c^2$, $\sum \vec{p}_i = 0$, the two positrons and the electron are prompt and they have a common origin. For $\mu \rightarrow 3e2\nu$ events the first constraints are modified to $\sum E_i < m_\mu c^2$, $|\sum \vec{p}_i c| < m_\mu c^2/2$. Before being written on tape, candidates for $\mu \rightarrow 3e$ and $\mu \rightarrow 3e2\nu$ events are analyzed by a software filter searching for track triples with appropriate kinematic conditions. Loose cuts are applied on time and vertex variables. The filter output rate is typically 0.6 events/s. More details on the hardware trigger and the software filter can be found in refs.6).

The offline analysis⁷⁾ uses standard methods for event reconstruction. Accidental background to the $\mu \rightarrow 3e$ and $\mu \rightarrow 3e2\nu$ decays is reduced by requiring $e^+e^+e^-$ events to be prompt and the three tracks to have a common origin on the target. Figure 2 shows the distributions of total energy $E_{tot} = \sum E_i$ versus total momentum $P_{tot} c = |\sum \vec{p}_i c|$ ($i=1,2,3$ for the three charged particles). Figure 2a shows the final sample of 8835 events. Muon decays are kinematically forbidden in the region $K = E_{tot} + P_{tot} c > m_\mu c^2$. 8173 events lie below the line $K=112$ MeV. Figure 2b shows the same distribution for accidental events ($\Delta t > 1$ ns). The contribution of accidentals in the prompt spectrum can be extrapolated from the region $K > 112$ MeV and is estimated to be ~ 350 events in the allowed $K < 112$ MeV-region. A prompt background is induced by the bremsstrahlung decay $\mu \rightarrow e\gamma 2\nu$ with external pair production $\gamma \rightarrow e^+e^-$ in the target or in the first chamber; 380 events are expected within the acceptance of the spectrometer. The remaining 7443 ± 148 events are interpreted as $\mu^+ \rightarrow e^+e^+e^-\nu\bar{\nu}$ decays. Figure 2c shows the results of a Monte Carlo

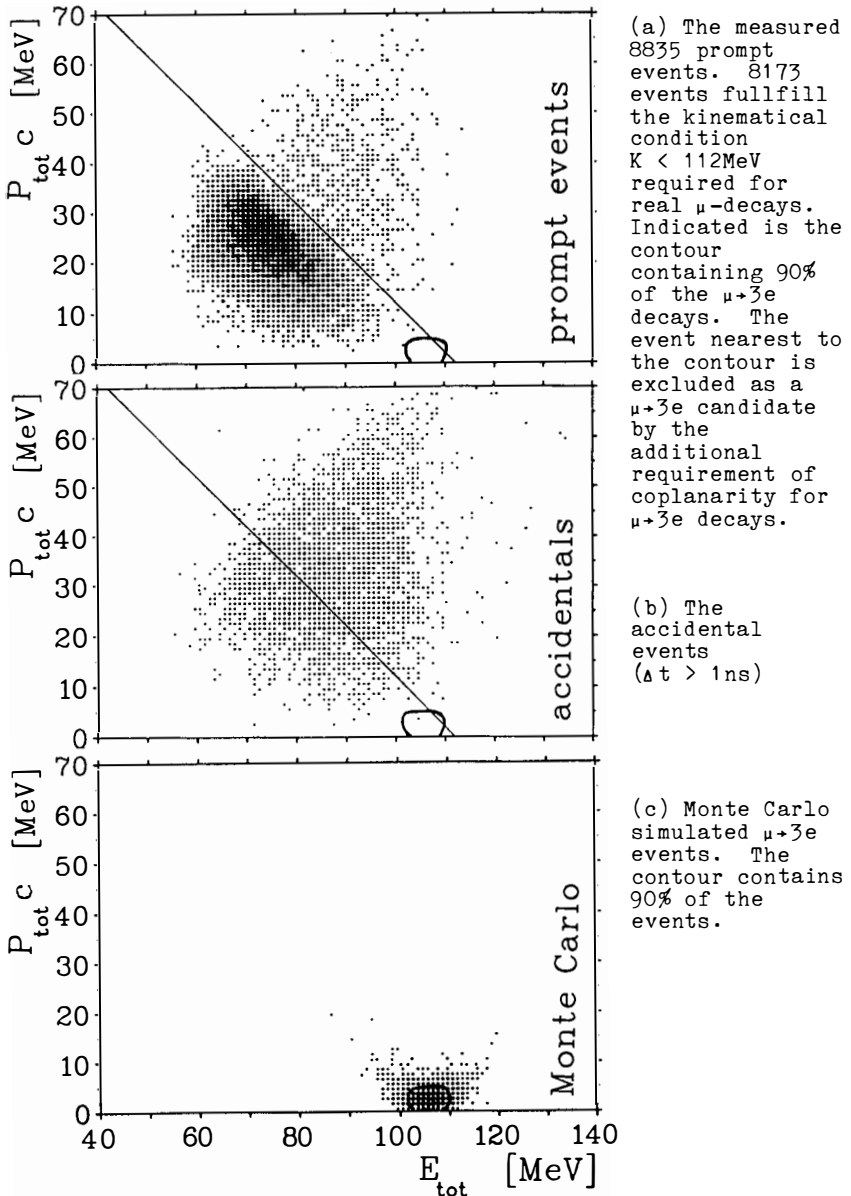


Figure 2 Total momentum $P_{\text{tot}}^c = |\sum p_i^c|$ versus total energy $E_{\text{tot}} = \sum E_i$ for e^+e^- events. The area of the dots is proportional to the intensity. Indicated are the lines $K = E_{\text{tot}} + P_{\text{tot}}^c = 112 \text{ MeV}$ ($=m_\mu c^2$ corrected for the detector resolution).

simulation for the $\mu \rightarrow 3e$ decay, assuming a constant matrix element; these events are located near $E_{\text{tot}} = m_{\mu}c^2$ and $P_{\text{tot}} = 0$. Within the contour of 90% confidence of figure 2a, no $\mu \rightarrow 3e$ candidate was found.

The total efficiency of the spectrometer is given by the solid angle, the magnetic field (which causes a transverse momentum cut on single tracks), trigger and chamber inefficiencies and inefficiencies of the analysing software. For the $\mu \rightarrow 3e$ decay the total efficiency is $\epsilon(\mu \rightarrow 3e) = 0.138 \pm 0.006$ and for the $\mu \rightarrow 3e2\nu$ decay $\epsilon(\mu \rightarrow 3e2\nu) = (3.12 \pm 0.45) \cdot 10^{-5}$.

Using the total number of muons $N = (7.3 \pm 0.5) \cdot 10^{12}$ stopped in the target during the experiment, we derive for the branching ratios:

$$R(\mu \rightarrow 3e) < 2.4 \cdot 10^{-12} \quad (90\% \text{ confidence level})$$

and

$$R(\mu \rightarrow 3e2\nu) = (3.3 \pm 0.5) \cdot 10^{-5}.$$

The $\mu \rightarrow 3e2\nu$ branching ratio is in good agreement with the V-A-prediction⁸⁾ $R(\mu \rightarrow 3e2\nu) = (3.598 \pm 0.007) \cdot 10^{-5}$.

Figures 3 and 4 show that the distribution of the measured events is well described by the V-A-prediction for the $\mu \rightarrow 3e2\nu$ decay. Figure 3 shows the $E_{\text{tot}} + P_{\text{tot}}c$ -distribution for the prompt events, the accidental background and for Monte Carlo simulated $\mu \rightarrow 3e2\nu$ decays. Measured and Monte Carlo simulated distributions are in good agreement. Figure 4 shows the distributions of the opening angle between the electron and each of the positrons. The distribution for the e^+e^- -pair with the higher invariant mass agrees well with V-A-prediction. The e^+e^- -pair with the lower invariant mass deviates slightly for angles less than 20° . This can be explained by the prompt background from the bremsstrahlung

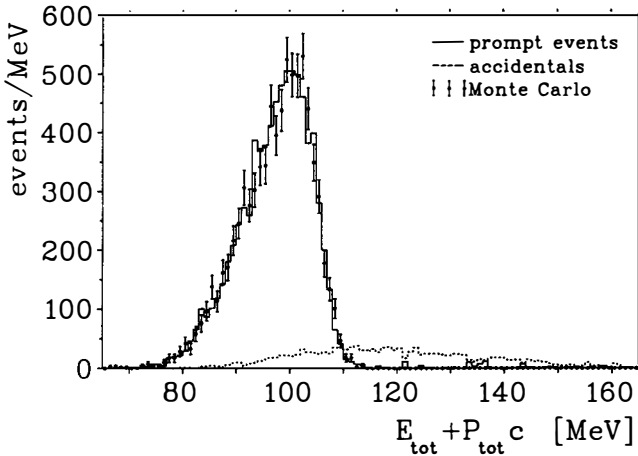


Figure 3 The $K = E_{\text{tot}} + P_{\text{tot}} c$ distribution. The full histogram represents the prompt events with accidentals subtracted, the dotted histogram the accidentals normalized in the $K > 112$ MeV region and the points with error bars are the Monte Carlo simulated $\mu \rightarrow 3e2\nu$ events.

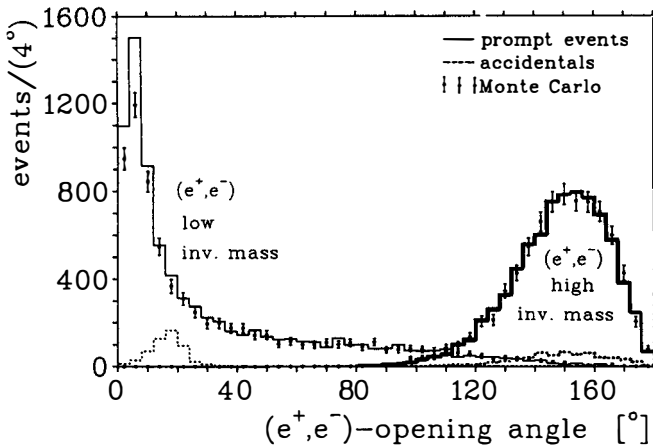
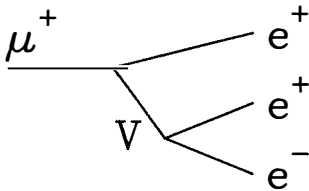


Figure 4 Distributions of (e^+e^-) -opening angles. Two opening angle distributions are shown, one for the (e^+e^-) -pairs with the lower and the other for pairs with the higher invariant mass. The full histograms are the prompt events with accidentals subtracted, the dotted histograms are the accidentals normalized in the $K > 112$ MeV region, the points with error bars are the Monte Carlo simulated $\mu \rightarrow 3e2\nu$ events.

decay $\mu \rightarrow e \gamma 2\nu$ with external pair production (380 events expected). The accidental spectrum shows a clear peak near 20° for the low invariant mass pair, as is expected for Bhabha scattering in the target and chamber 1 of positrons from normal $\mu \rightarrow e 2\nu$ decay.

The question whether the $\mu \rightarrow 3e 2\nu$ data can put more stringent limits on other interactions than V-A is still under study. In a forthcoming run we will increase the statistics by about a factor of 5, which will also increase the sensitivity for the branching ratio $R(\mu \rightarrow 3e)$.

The new upper limit on $R(\mu \rightarrow 3e)$ has implications on theoretical models which go beyond the standard model. Two specific models will be discussed in the following.



The first model assumes the $\mu \rightarrow 3e$ decay being induced by a neutral horizontal gauge boson V ⁹⁾. The decay rate is given by

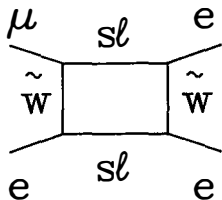
$$r(\mu \rightarrow 3e) = \left(\frac{g_{\mu e}^2}{m_V}\right) \left(\frac{g_{ee}^2}{m_V}\right) \cdot \frac{m_\mu^5}{192\pi^3}$$

where $g_{\mu e}$ and g_{ee} are the coupling constants at the μ - e - and the e - e -vertex, respectively. The prediction for $R(\mu \rightarrow 3e)$ is

$$R(\mu \rightarrow 3e) = \frac{r(\mu \rightarrow 3e)}{r(\mu \rightarrow e 2\nu)} = \frac{g_{\mu e}^2 \cdot g_{ee}^2 \cdot \frac{M_W^2}{m_V^2}}{g_{\text{weak}}^2 \cdot \frac{M_W^2}{m_V^2}}$$

with M_W being the mass of the standard vector boson and m_V the mass of the new horizontal gauge boson. With the additional assumption $g_{\mu e} = g_{ee} = g_{\text{weak}}$ one derives from the new upper limit for $R(\mu \rightarrow 3e)$:

$$m_V > 0(50 \text{ TeV}/c^2).$$



A second example is based on a supersymmetric model¹⁰⁾. The $\mu \rightarrow 3e$ decay proceeds via the box diagram shown, where $s\ell$ indicates the superpartner of the leptons and \tilde{W} the wino. For such models there exists the mass formula¹¹⁾

$$M_{s\ell} = |M_{3/2} \pm m_{\ell}|,$$

$M_{s\ell}$ is the mass for the superpartner of the lepton with mass m_{ℓ} , and $M_{3/2}$ is the gravitino mass. The branching ratio $R(\mu \rightarrow 3e)$ can be written in terms of these masses:

$$R(\mu \rightarrow 3e) \cong (2 \cdot 10^{-5} \text{GeV}^2) \frac{M_{s\mu}^2 - M_{se}^2}{M_{s\mu}^2} \cdot \frac{1}{m_{\tilde{W}}^2}$$

The new upper limit for the branching ratio yields the relation

$$\frac{M_{s\mu}^2 - M_{se}^2}{M_{s\mu}^2 \cdot m_{\tilde{W}}^2} < 0(10^{-7} \text{GeV}^{-2})$$

Assuming the s-neutrino masses much smaller than the muon mass, one gets from μ -decay experiments the limit $m_{\tilde{W}}/m_W > 4$ ¹²⁾, thus with the assumption $m_{\tilde{W}} = 320 \text{ GeV}/c^2$ one gets

$$M_{s\mu} > 20 \text{ GeV}/c^2,$$

a result comparable with results from PETRA¹³⁾.

References

- 1) Particle Data Group; Rev. Mod. Phys. 56, 2 (1984).
- 2) K.Mursula and F.Scheck; preprint MZ-TH/84-08; Mainz 1984.
- 3) S.M.Korenchenko et al.; Sov. Phys. JETP, 43, 1 (1976) 1.
R.D.Bolton et al.; Phys. Rev. Lett. 53 (1984) 1415.
W.Bertl et al.; Phys. Lett. 140B (1984) 299.
- 4) R.R.Crittenden et al.; Phys. Rev. 121 (1961) 1823.
I.I.Gurevich et al.; Sov. Phys.-JETP 10 (1960) 225.
J.Lee and N.P.Samios; Phys. Rev. Lett. 3 (1959) 55.
- 5) R.Eichler; Proceedings of the Leptonic session of the 19th
rencontre de Moriond, pg.143, 1984.
- 6) W.Bertl et al.; Nucl. Inst. and Meth. 217 (1983) 367.
A.v.d.Schaaf et al.; submitted to Nucl. Inst. and Meth.
(1985).
- 7) W.Bertl et al.; submitted to Nucl. Phys. (1985).
Ch.Grab; thesis submitted to the Philosophical Faculty II of
the University of Zürich (1985).
- 8) D.Yu.Bardin et al.; Sov. Jour. Nucl. Phys. 15 (1972) 161.
K.Gamers; privat communication, NIKHEF-H, Amsterdam, 1984.
- 9) G.L.Kane, R.Thun; Phys. Lett. 94B (1980) 512.
- 10) J.Ellis, D.V.Nanopoulos; Phys. Lett. 110B (1982) 44.
- 11) E.Cremmer et al.; Phys. Lett. 122B (1983) 41.
- 12) W.Buchmüller, F.Scheck; Phys. Lett. 145B (1984) 421.
- 13) JADE Collaboration, W.Bartel et al.; Phys. Lett. 152B (1985)
392.

RESULTS FROM PETRA ON ELECTROWEAK EFFECTS AND TESTS OF QED

Christian Kiesling

Max-Planck-Institut für Physik und Astrophysik,
Werner-Heisenberg-Institut für Physik, MünchenAbstract

Recent results from PETRA, running at its top energy, on electroweak interference and tests on QED are reviewed. The data presented, mainly from leptonic final states, are in general agreement with predictions from the standard model. From the combined PETRA data the parameters $\sin^2\theta_W$ and ρ of the standard theory have been determined in agreement with those from non- e^+e^- experiments. Higher order QED processes have been studied and confirm the validity of QED up to $s \sim 2000 \text{ GeV}^2$. No indication for excited leptons has been found.

1. Introduction

In the past year PETRA has completed its e^+e^- collider program to cover the entire center of mass energy range accessible up to a maximum \sqrt{s} of 46.79 GeV. The emphasis mainly was to search for the toponium thresholds which required a scan with energy steps $\Delta(\sqrt{s}) = 30$ MeV, well within the natural energy spread of the machine, starting at 39 GeV. As is well known, no new thresholds have materialized so far (see e.g. ref. 1)). PETRA is now running at a fixed energy of $\sqrt{s} = 44.2$ GeV, compromising between acceptable luminosity ($\geq 2 \times 10^{31} [\text{cm}^{-2}\text{sec}^{-1}]$ at the beginning of a fill) and high center of mass energy, and tries to accumulate statistics for further detailed tests of the standard theory. Note that at this energy electroweak interference effects have increased by a factor of 1.8 with respect to 34.5 GeV and by 2.7 with respect to PEP (29 GeV). In this report, recent high energy results from the installed experiments CELLO, JADE, MARKJ and TASSO are presented as well as some selected data from these experiments and the PLUTO detector, running at $\langle\sqrt{s}\rangle \approx 34.5$ GeV. The high energy data center around $\sqrt{s} \approx 44$ GeV with typical integrated luminosities of $\sim 25 [\text{pb}^{-1}]$ per experiment. This is about only 1/3 of the luminosity taken at $\sqrt{s} = 34.5$ GeV. The final states considered will be almost exclusively of leptonic nature and the physics topics include the measurement of electroweak interference effects, tests of higher order QED, and the search for excited leptons. For the many activities pursued at PETRA, or more in-depth discussion, I refer to other reviews such as refs. 2)-4).

2. "Standard" Measurements of Fermion-Pair Final States

Electroweak interference effects in e^+e^- annihilation are most directly studied in s-channel fermion-pair production where γ and Z^0 exchange contribute to the scattering amplitude to lowest order according to the diagrams and couplings depicted in fig. 1. The chiral coupling constant $c(t_3, Q)$ depends on the third component t_3 of the weak isospin and the electric charge Q of the produced fermion and is given by $c(t_3, Q) = c_{L,R} = t_3 - Q \sin^2 \theta_w$.

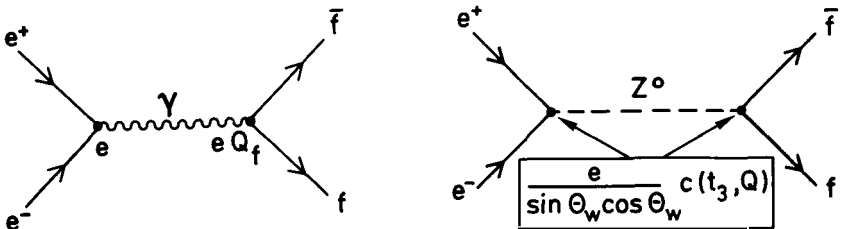


Fig. 1: Born term diagrams for γ and Z^0 exchange in $e^+e^- \rightarrow f^+f^-$.

Due to the standard weak isospin assignments, reflecting parity violation of the weak neutral current, the Z^0 couples with different strengths (c_L , c_R) to right-handed or left-handed fermions and it has become customary to define linear combinations of these couplings to describe electroweak interference effects:

$$\begin{aligned} v &= 2 (c_L + c_R) \\ a &= 2 (c_L - c_R). \end{aligned}$$

Within the framework of the standard theory the vector coupling constants v_f and the axialvector coupling constants a_f for the elementary fermions depend only on the Weinberg angle $\sin^2\theta_W$ and are given in table 1.

Table 1: Vector and axialvector couplings in the standard theory

	$v_{e,\mu,\tau}$	e,μ,τ	u,c,t	d,s,b
v	1	$-1 + 4 \sin^2\theta_W$	$1 - \frac{8}{3} \sin^2\theta_W$	$-1 + \frac{4}{3} \sin^2\theta_W$
a	1	-1	1	-1
Q_f	0	-1	$+\frac{2}{3}$	$-\frac{1}{3}$

In terms of these couplings the differential cross section for producing a fermion pair of flavor f ($f \neq e$, Bhabha scattering will be discussed separately) with unpolarized beams is given by:

$$\begin{aligned} \frac{d\sigma}{d\Omega} (e^+e^- \rightarrow f\bar{f}) &= \frac{\alpha^2}{4s} (C_s(1 + \cos^2\theta) + 2 C_a \cos\theta) \\ C_s &= Q_f^2 - Q_f v_e v_f \operatorname{Re}X(s) + \frac{1}{4} (v_e^2 + a_e^2) (v_f^2 + a_f^2) |X(s)|^2 \\ C_a &= -Q_f a_e a_f \operatorname{Re}X(s) + v_e v_f a_e a_f |X(s)|^2 \end{aligned} \quad (1)$$

The Z^0 propagator term $X(s)$ can be expressed in various ways. Using the neutral current couplings from fig. 1, $X(s)$ reads:

$$X(s) = \frac{1}{8 \sin^2\theta_W \cos^2\theta_W} \frac{s}{s - M_Z^2 + iM_Z\Gamma_Z} \quad (2)$$

* For the notation used here and details of the derivation see e.g. ref. 2).

In this parametrization $\chi(s)$ depends on $\sin^2\theta_w$ and M_Z (neglecting the small contribution of the Z^0 width far from the pole) and no connection is made with the charged current. In the following this expression for $\chi(s)$ will be referred to as parametrization A.

Alternatively, and closer to the spirit of the standard theory, the unification relation $g \sin\theta_w = e$ and the μ decay via the charged current can be used to replace the Weinberg angle by Fermi's coupling G_F :

$$\text{With } \frac{4G_F}{\sqrt{2}} = \frac{g^2}{2M_W^2} \quad \text{and} \quad \rho = \frac{M_W^2}{\cos^2\theta_w M_Z^2} \quad (3)$$

one thus obtains

$$\chi(s) = \frac{\rho G_F}{\sqrt{2}} \frac{M_Z^2}{4\pi\alpha} \frac{s}{s - M_Z^2 + iM_Z\Gamma_Z} \quad (4)$$

This expression for $\chi(s)$ will be referred to as parametrization B. It was traditionally used in describing electroweak interference as, far away from the Z^0 pole, all "unknown" parameters such as $\sin^2\theta_w$, M_Z drop out:

$$\chi(s) = -\frac{G_F}{\sqrt{2}} \frac{s}{4\pi\alpha} \quad \text{with } s \ll M_Z^2 \quad \text{and } \rho = 1.$$

Although both parametrizations seem perfectly equivalent they in fact do not lead to the same predictions at the Born level. The physical reason behind this is that the tree level definition of G_F used for parametrization B is no longer exact when M_Z and $\sin^2\theta_w$ are the renormalized physical quantities as in the case for parametrization A. One thus also expects different loop corrections for both parametrizations which then hopefully converge to a common answer. That this is indeed the case has been recently shown^{5,6)} and it has become clearer now what the experimenter has to do in order to make meaningful comparisons between his data and the theory (see below).

2.1 The Physical Observables

Given the differential cross section (1) the observables in an e^+e^- machine with unpolarized beams such as PETRA, sensitive to electroweak effects, are the total cross section σ_f , the charge asymmetry A_f and, in principle, the polarization P_f of the final state fermions. The total cross section σ_f is proportional to the symmetric coefficient C_s in (1):

$$\sigma_f(e^+e^- \rightarrow f\bar{f}) = \frac{4\alpha^2}{3s} C_s \quad (5)$$

The cross section is usually expressed in units of the point cross section σ_0

for μ pair production ($\sigma_0 = \frac{4\pi}{3s} \alpha^2$) which then reads

$$R_f = Q_f^2 - Q_f v_e v_f \operatorname{Re} X + \frac{1}{4} (v_e^2 + a_e^2) (v_f^2 + a_f^2) |\chi|^2 \quad (6)$$

At $\sqrt{s} = 44$ GeV the propagator term χ is -0.21 so that, with $\sin^2\theta_w = 0.22$ and couplings from table 1, only a very small contribution from electroweak interference (first term in (6) proportional to $v_e \cdot v_f$) and the purely weak second term is expected. The total correction thus amounts to only $+0.8\%$ for μ or τ pair production.

The differential charge asymmetry $A_f(\theta)$ is defined by

$$A_f(\theta) = \frac{d\sigma/d\Omega(\theta) - d\sigma/d\Omega(\pi-\theta)}{d\sigma/d\Omega(\theta) + d\sigma/d\Omega(\pi-\theta)} = \frac{C_a}{R_f} \cdot \frac{2 \cos\theta}{1+\cos^2\theta} \quad (7)$$

Integrating the differential cross section (1) over the forward and backward hemispheres separately yields the forward-backward charge asymmetry A_f^{FB}

$$A_f^{\text{FB}} = -\frac{3}{4} \frac{a_e a_f}{Q_f} \operatorname{Re} X \quad (8)$$

where the purely weak contribution in C_a has been safely neglected due to the smallness of the product $v_e v_f$. Since A_f^{FB} is proportional to the product of the (large) axial vector coupling constants one expects large effects, amounting to $A_\mu^{\text{FB}} = -15.5\%$ at $\sqrt{s} = 44$ GeV. Since only a limited range in $\cos\theta$ is accessible experimentally ($|\cos\theta_{\text{max}}| =:c$) some experiments prefer to present A_f^{FB} only for their acceptance range rather than to extrapolate to the full interval. In this case $A_f^{\text{FB}}(c)$ is related to (8) by

$$A_f^{\text{FB}}(c) = A_f^{\text{FB}} \frac{4c}{3+c^2} \quad (9)$$

Finally, the polarization of the final state fermion is an observable which in principle could be measured using a parity violating decay of the produced fermion, e.g. the τ lepton. The polarization is dependent on the scattering angle and is given by

$$P_f(\theta) = \frac{d\sigma/d\Omega(f_R) - d\sigma/d\Omega(f_L)}{d\sigma/d\Omega(f_R) + d\sigma/d\Omega(f_L)} = \left[v_e \frac{a_f}{Q_f} + a_e \frac{v_f}{Q_f} \frac{2\cos\theta}{1+\cos^2\theta} \right] \operatorname{Re} X \quad (10)$$

Here, the electroweak effect is proportional to $v \cdot a$ and is, contrary to the observables discussed above, truly parity-violating. In practice one may measure the polarization asymmetry $A(P_f)$, obtained analogously to the forward-

backward asymmetry, by integrating over hemispheres in $\cos\theta$:

$$A(P_f) = 2 \frac{a_e v_f}{Q_f} \operatorname{Re} x \quad (11)$$

Due to the product $v \cdot a$ in (11) the effects are expected to be very small, in fact amount to $\sim 2\%$ at $\sqrt{s} = 44$ GeV.

2.2 Radiative Corrections

When comparing measurements with predictions of the observables discussed in the preceding paragraph, radiative corrections and, in principle, higher order weak (loop) corrections have to be considered. In the following I will discuss the relevant corrections to the charge asymmetry for $\mu(\tau)$ pair production. Most important are corrections due to pure QED (α^3) including hard Bremsstrahlung which give, depending on the experimental cuts, a positive contribution of $\sim +1.5\%$ at $\sqrt{s} = 44$ GeV and are usually calculated by Monte-Carlo methods ⁷⁾ for the individual experiments. Following the nomenclature of ref. 5) these corrections are labelled "reduced QED". Beyond the reduced QED correction electroweak contributions are expected, the magnitude of which will depend on the renormalization scheme used: For parametrization A (see eq. 2) the renormalized parameters are α , M_Z and M_W or $\sin^2\theta_w$ (Glashow scheme) whereas in B (see eq. 4) α , G_F and M_Z are used (Weinberg-Salam scheme). The electroweak corrections can be divided into two groups, where a) a photon line is added in all possible ways to the Z^0 Born term (analogous to pure QED) and b) all other weak loop terms are considered. In principle, correction a) depends on the experimental cuts used to define the lepton pair final state in presence of radiative photons, as is well known both theoretically and experimentally for the pure QED radiative corrections. Correction b), on the other hand, is independent of any experimental conditions. A large amount of work has been done to calculate the electroweak radiative corrections in both schemes ^{5,6,8,9)}. For μ -pair production, a Monte-Carlo programme ¹⁰⁾ is available to determine the experiment-dependent electroweak correction a) together with pure QED (α^3) ("full QED"). Whereas in the Glashow scheme the total electroweak radiative correction (a) and b)) amounts to about 0.1% at PETRA energies ⁵⁾ and thus is entirely negligible, the corresponding correction in the Weinberg-Salam scheme is of order 1% (see ref. 6) and table 2). For both schemes the Born level values and the corresponding electroweak corrections a) and b) as defined above are shown in table 2 for the $\mu(\tau)$ charge asymmetry at two representative center of mass energies. It is stressed, however, that correction a) has been estimated theoretically by choosing "reasonable" experimental cuts: The precise

value of this correction will depend on the specific experiment.

Table 2: Weak corrections for the $\mu(\tau)$ charge asymmetry in percent for two different renormalization schemes (see text).

	Born	corr. a)	corr. b)	1 loop	renorm. scheme
$\sqrt{s} = 34.5 \text{ GeV}$	- 8.67	+ 0.59	- 0.69	- 8.77	Glashow
	- 9.25	+ 0.56	+ 0.04	- 8.65	W-S
$\sqrt{s} = 44 \text{ GeV}$	- 15.50	+ 1.11	- 1.23	- 15.62	Glashow
	- 16.60	+ 1.00	+ 0.10	- 15.50	W-S

Although differing substantially at the Born level the 1 loop corrected values agree nicely for both schemes. In addition, the loop correction to the Born term in the Glashow scheme is well below experimental accuracy so that an excellent approximation is given by just using the lowest order expression for $\chi(s)$ in the Glashow scheme (see eq. 2). Since traditionally differential cross sections are corrected for pure ("reduced") QED only, the simplest recipe for the experimenter to compare lepton charge asymmetries with theory thus seems the following: Do not apply any electroweak correction and compare to the lowest order value in the Glashow scheme. In fact, all new data on $\mu(\tau)$ asymmetries presented in this report are treated in this way. On the other hand, as data will become more accurate in the future the better way seems to apply the full QED correction to the data and only correct for loop terms (corr. b)).

3. Leptonic Final States

3.1 The Reaction $e^+e^- \rightarrow e^+e^-$

Bhabha scattering has been the classical reaction to test QED: Contributions from the weak neutral current are almost entirely swamped by the dominating photon exchange in the t-channel. The differential cross section can be written in the following way, separating the contributions from the s-channel, the t-channel and the interference of corresponding amplitudes:

$$\frac{4s}{\alpha^2} \frac{d\sigma}{d\Omega} = (1 + \cos^2\theta)F^2(s) + \frac{10+4\cos\theta+2\cos^2\theta}{(1-\cos\theta)^2} F^2(t) - \frac{2(1+\cos^2\theta)}{1-\cos\theta} F(t)F(s) \quad (12)$$

Deviations from QED have traditionally been parametrized by form factors $F(s)$, $F(t)$, defined as

$$F(s) = 1 \pm \frac{s}{s - \Lambda_{\mp}^2}, \quad F(t) = 1 \pm \frac{t}{t - \Lambda_{\mp}^2} \quad (13)$$

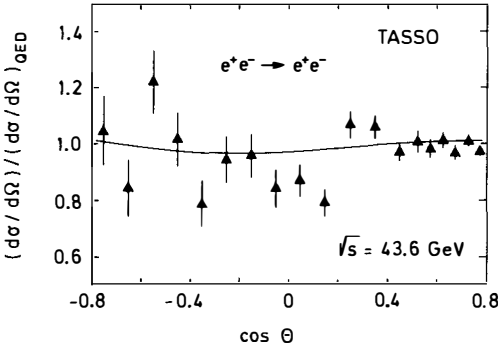


Fig. 2: Cross section for Bhabha scattering.

As for all other PETRA experiments no deviation from QED is seen within the experimental errors. Combining the available data of the PETRA experiments yields the following cut-off parameters, including the systematic errors:

$$\Lambda_- > 181 \text{ GeV} \quad 95\% \text{ C.L.}, \quad e^+e^- \rightarrow e^+e^-$$

$$\Lambda_+ > 246 \text{ GeV}$$

3.2 $e^+e^- \rightarrow \mu^+\mu^-$

Muon pair production still provides the statistically most significant test of electroweak effects in e^+e^- annihilation. The signature for this reaction is clean (two stiff, almost collinear tracks with identified muons) and backgrounds are low, typically around 2% mostly due to τ pair events. The luminosity gathered at the high energies ($\langle\sqrt{s}\rangle \sim 44 \text{ GeV}$) is about 20-30[pb^{-1}] per experiment. The total cross section normalized to the QED point cross section is shown in fig. 3. No deviation from QED is seen as expected for values of $\sin^2\theta_w$ close to 1/4 and center of mass energies well below the Z^0 pole so that the purely weak terms do not yet contribute significantly. Similar to Bhabha scattering, form factors may be introduced to parametrize a possible deviation from $R_{\mu\mu} = 1$. Including the new high energy data with their systematic errors (see fig. 3) one derives for the PETRA data

$$\Lambda_+ > 200 \text{ GeV} \quad 95\% \text{ C.L.}, \quad e^+e^- \rightarrow \mu^+\mu^-$$

$$\Lambda_- > 206 \text{ GeV}$$

Pure QED corresponds to cut-off parameters $\Lambda_{\pm} = \infty$. Roughly speaking, a non- ∞ value of $\Lambda_+(\Lambda_-)$ will indicate a smaller (larger) differential cross section with respect to the pure QED expectation, with the maximum deviation occurring around a scattering angle of 90° . As an example, preliminary data on the differential cross section for $e^+e^- \rightarrow e^+e^-$ from TASSO at $\sqrt{s} = 43.6 \text{ GeV}$ are shown in fig. 2, normalized to the lowest order QED expectation. Also drawn in the figure is the prediction from the

standard theory.

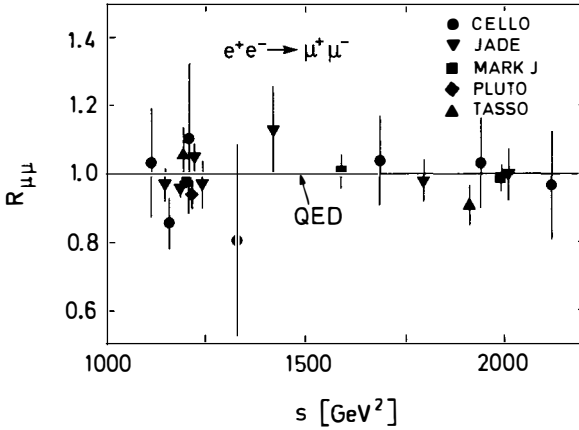


Fig. 3: Total cross section for $e^+e^- \rightarrow \mu^+\mu^-$, normalized to QED.

Electroweak interference in e^+e^- reactions is most clearly demonstrated in the muon charge asymmetry. Over the years PETRA has accumulated impressive evidence for neutral currents being at work. Preliminary data on $d\sigma/d\Omega$ from the high energy runs are shown in fig. 4. The data are corrected for pure QED contributions to order α^3 . A compilation of measurements of the charge asymmetry, extrapolated to the full angular range, is presented in table 3.

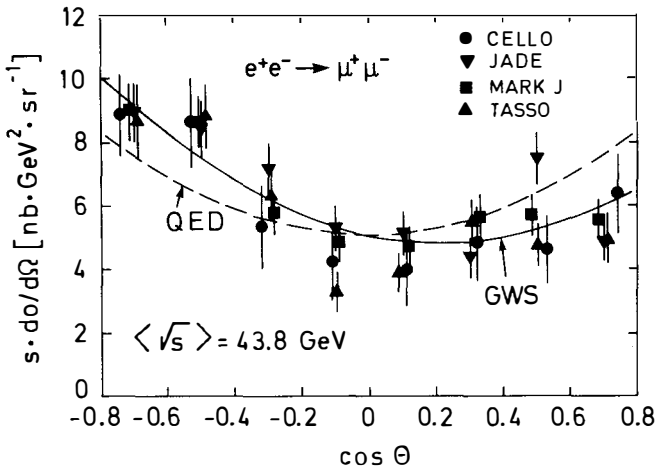


Fig. 4: Differential cross sections for $e^+e^- \rightarrow \mu^+\mu^-$.

Table 3: Measurements for the muon charge asymmetry.

Exp.	\sqrt{s}	$\int Ldt[\text{pb}^{-1}]$	# ev	$A_{\mu\mu}[\%]$	GWS (1 loop)
CELLO ¹¹⁾	34.2	11.2	387	- 6.4 \pm 6.4	- 8.5
JADE ¹²⁾	34.4	71.2	3199	- 11.7 \pm 1.8 \pm 1.0	- 8.6
MARKJ ¹³⁾	34.6	76.3	3658	- 11.7 \pm 1.7 \pm 1.0	- 8.7
PLUTO ¹⁴⁾	34.7	44.0	1553	- 14.0 \pm 3.2 \pm 1.0	- 8.8
TASSO ¹⁵⁾	34.5	74.7	2673	- 9.1 \pm 2.3 \pm 0.5	- 8.7
PETRA	34.5			- 11.2 \pm 1.1	- 8.7
CELLO	44.0	20.5	437	- 17.7 \pm 6.0	- 15.6
JADE	42.4	17.0	571	- 20.1 \pm 4.3 \pm 1.7	- 14.2
MARKJ	44.0	32.8	1014	- 14.8 \pm 3.3	- 15.6
TASSO	43.7	25.1	476	- 18.1 \pm 4.9 - 4.8	- 15.3
PETRA	43.8			- 17.0 \pm 2.2	- 15.3

Fig. 5 shows the asymmetry measurements as a function of the square of the center of mass energy. The general trend is close to the expectation of the standard theory, however, the data show a tendency towards larger asymmetries. The luminosity-weighted averages in the two energy regions are compatible with

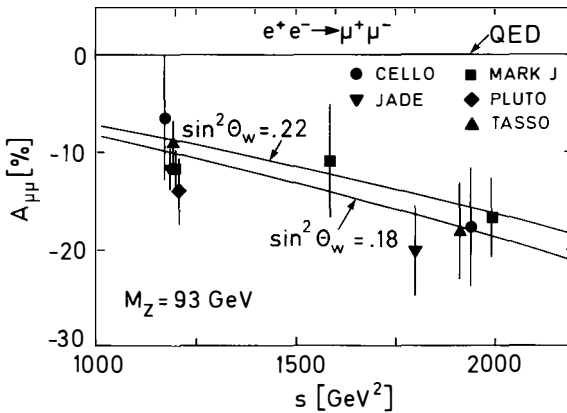


Fig. 5: Measurements of the charge asymmetry for $e^+e^- \rightarrow \mu^+\mu^-$.

the standard theory only within the $2\sigma(1\sigma)$ limit at $\sqrt{s} = 34.5$ (43.8) GeV. The error on the combined PETRA value at $\sqrt{s} = 34.5$ GeV (-11.2 ± 1.1) is close to the systematic errors of individual experiments. However, the sources of systematic error are sufficiently diverse for the various experiments so that the systematic errors may be regarded as independent, thus justifying the above estimate of the combined PETRA error.

3.3 $e^+e^- \rightarrow \tau^+\tau^-$

From the point of view of the standard theory τ pair production at high energy looks identical to μ pair production. This unfortunately is not the case for the experiments. Due to the decay of the τ , the detection and identification of τ pairs in a necessarily incomplete detector may be a subtle procedure. Furthermore, if one attempts to measure all τ decay channels, a very good understanding of the various background processes, in particular Bhabha scattering with its large positive charge asymmetry, is mandatory. The PETRA measurements of the τ pair production cross section as a function of s are shown in fig. 6, they are in good agreement with QED. In an analogous way to μ pair production cut-off parameters Λ_{\pm} can be introduced and lead to the following limits:

$$\begin{aligned} \Lambda_+ &> 192 \text{ GeV} \\ \Lambda_- &> 204 \text{ GeV} \end{aligned} \quad 95\% \text{ C.L., } e^+e^- \rightarrow \tau^+\tau^-$$

The charge asymmetry for τ pair production, although less significant statistically compared to the muons, shows a clear signal from electroweak interference. The numerical values are shown in table 4.

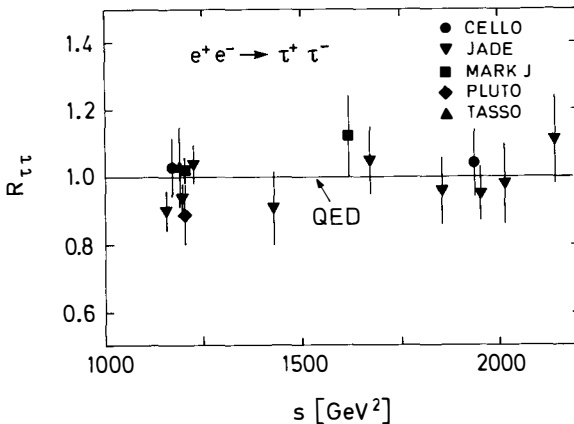
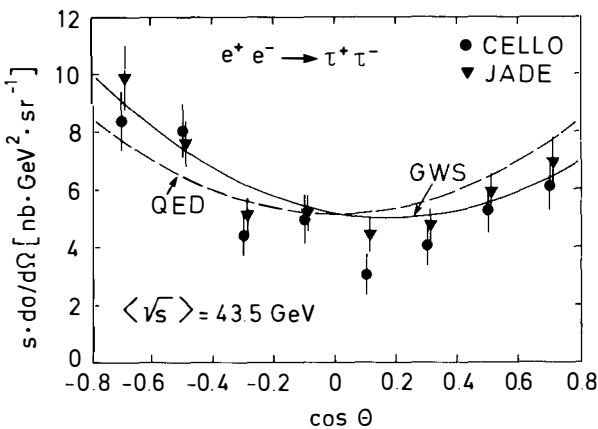


Fig. 6: Total cross section for $e^+e^- \rightarrow \tau^+\tau^-$, normalized to QED.

Table 4: Measurements for the tau charge asymmetry.

Exp.	\sqrt{s}	Ldt[pb^{-1}]	# ev	$A_{\tau\tau}$ [%]	GWS (1 loop)
CELLO ¹⁶⁾	34.2	11.0	434	- 10.3 \pm 5.2	- 8.5
JADE ¹⁷⁾	34.6	62.4	1998	- 6.2 \pm 2.5 \pm 1.5	- 8.7
MARKJ ¹³⁾	34.6	85.0	860	- 8.5 \pm 4.8	- 8.7
PLUTO ¹⁸⁾	34.6	42.3	419	- 5.9 \pm 6.8	- 8.7
TASSO ¹⁹⁾	34.5	69.4	856	- 4.9 \pm 5.3 \pm 1.3	- 8.7
PETRA	34.6			- 7.0 \pm 2.0	- 8.7
CELLO	44.0	21.0	350	- 14.4 \pm 5.3	- 15.6
JADE ¹⁷⁾	43.1	23.8	509	- 8.8 \pm 4.9 \pm <2.4	- 14.8
PETRA	43.5			- 11.7 \pm 3.8	- 15.1

The differential cross sections from CELLO and JADE (both preliminary), running at $\sqrt{s} \sim 44$ GeV, are shown in fig. 7. The data are corrected for pure QED to order α^3 . As can be seen from table 4, the τ asymmetries, except for CELLO, have a tendency towards smaller values in modulus than those expected from the standard theory. While this could be an extremely interesting physics point concerning lepton universality, I believe that the origin of the systematically

Fig. 7: Differential cross sections for $e^+e^- \rightarrow \tau^+\tau^-$.

smaller asymmetries is purely experimental: Small undetected contaminations from Bhabha scattering and other QED processes with strong positive asymmetries will generate the observed effect. CELLO with its fine grain electromagnetic calorimeter may be less susceptible to these contaminations. Alternatively, the selection of particular decay channels such as $\tau \rightarrow \mu\nu$ (MARKJ uses this concept) will also suffer less from the above-mentioned contaminations. The measured asymmetries are displayed in fig. 8. The combined PETRA values at $\sqrt{s} = 34.6$ and 43.5 show agreement with the standard theory within the 1σ limit.

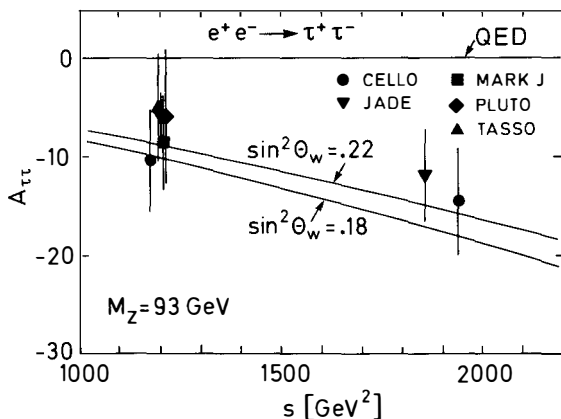


Fig. 8: Measurements of the charge asymmetry for $e^+e^- \rightarrow \tau^+\tau^-$.

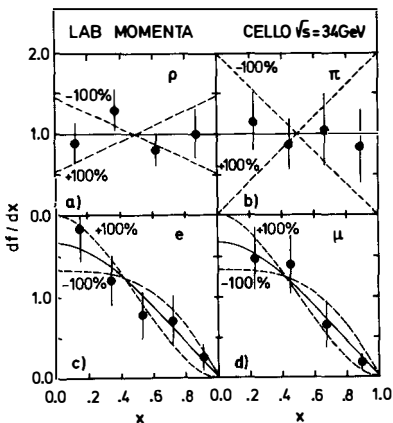


Fig. 9: τ polarization asymmetry.

At least in principle, τ pair production offers the possibility to look for parity violation in the weak neutral current via observation of a longitudinal polarization of the τ . The polarization is proportional to $v \cdot a$ (see eqs. 10,11) and thus is expected to be very small ($A(P) = +1\%$ at $\sqrt{s} = 34.5$ GeV). CELLO²⁰ have attempted to analyze their data for a possible longitudinal polarization (see fig. 9) and obtain for the polarization asymmetry

$$A(P) = (+1 \pm 22) \%$$

Since this is still the best way to obtain model-independent limits on the vector coupling constant of the τ , further improvements on this measurement are badly needed.

3.4 Analysis of Leptonic Data

The charge asymmetries from μ and τ production very directly test lepton universality: From all PETRA data presented in this report one derives

$$\begin{aligned} a_e a_\mu &= 1.21 \pm 0.10 \\ a_e a_\tau &= 0.79 \pm 0.17 \end{aligned} \tag{14}$$

With $a_e = -1.03 \pm 0.12$ from νe scattering ²¹⁾ the axial vector couplings of μ and τ are determined as

$$\begin{aligned} a_\mu &= -1.18 \pm 0.17 \\ a_\tau &= -0.77 \pm 0.19 \end{aligned} \tag{15}$$

in good agreement with the standard expectation of -1. Assuming lepton universality, all three channels (e^+e^- , $\mu^+\mu^-$, $\tau^+\tau^-$) can be combined to yield a common set of values for v and a . One obtains, including systematic errors of the data,

$$\begin{aligned} |v| &= 0.0 \pm 0.32 \\ |a| &= 1.06 \pm 0.04 \end{aligned} \tag{16}$$

where $v = -0.13$, $a = -1$ is expected in the standard theory for $\sin^2 \theta_w = 0.22$. The corresponding 95% C.L. contours in the v, a plane are shown in fig. 10 a) together with the νe results ²¹⁾. It is interesting to note that the high energy data, although representing only $\sim 25\%$ of the statistics at $\sqrt{s} = 34.5$ GeV, give very similar 95% C.L. contours compared to those obtained with the 34.5 GeV data.

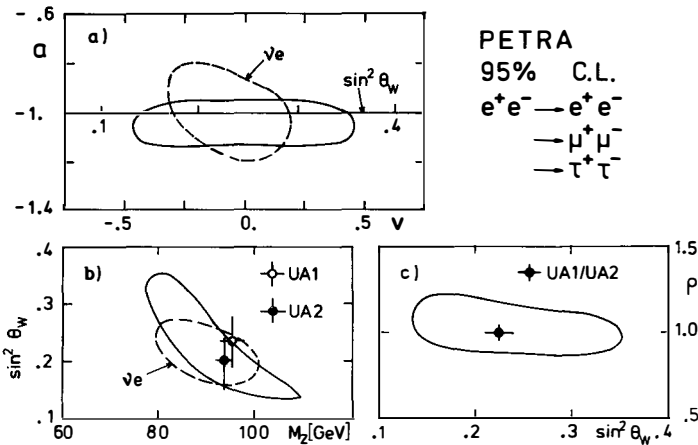


Fig. 10: 95% C.L. contours from all PETRA data, including systematic errors. Comparisons with other data are indicated.

It is obvious from (16) that the Weinberg angle is only poorly determined from the leptonic vector coupling constant. Since the mass of the Z^0 is now known ²²⁾ one may assume the standard expressions for v and a (see table 1) and use parametrization A (eq. 2) to determine the Weinberg angle. This method of extracting $\sin^2\theta_w$ from e^+e^- data, which is independent of the parameter ρ , was first employed by the MARKJ collaboration ²³⁾. With the combined PETRA data, constraining M_Z to 93 ± 2 GeV, the Weinberg angle is determined as

$$\sin^2\theta_w = 0.19 \pm 0.02 \quad (\text{all PETRA data, including systematic errors}).$$

This value is lower than any other determination from non- e^+e^- data (0.22 ± 0.01) and reflects basically the somewhat high muon charge asymmetry measurements at PETRA. Relaxing the constraint from the Z^0 mass, the corresponding 95% C.L. contour in the $(\sin^2\theta_w, M_Z)$ plane, including statistical and systematic errors, is shown in fig. 10 b).

Finally, the ρ parameter which fixes the relative strength of the neutral current to the charged current can be determined from the data, e.g. expressing M_Z via (3) in terms of G_F and $\sin^2\theta_w$. The PETRA data, including again systematic errors, yield a 95% C.L. contour in the $(\rho, \sin^2\theta_w)$ plane shown in fig. 10 c). The minimum χ^2 is obtained with

$$\begin{aligned} \rho &= 1.05 \pm 0.06 \\ \sin^2\theta_w &= 0.19 \pm 0.02 \end{aligned} \quad (\text{all PETRA data})$$

in good agreement with $\rho = 1$ as expected from the standard theory.

4. Hadronic Final States

Electroweak effects in quark pair production of a given flavour are expected to be much larger than those in leptonic final states: At $\sqrt{s} = 34.5$ GeV one expects a charge asymmetry, due to the factor $(a_e a_q)/Q_q$ in eq. (8), of -25% for b-quarks whereas only $\sim -9\%$ are expected for μ -pairs. Also the total cross section may show an effect at PETRA's top energy since the non-vanishing vector coupling constants of quarks (see table 1, with $\sin^2\theta_w = .22$) contribute substantially to the purely weak term in eq. (6). However, in order to isolate the electroweak part of the total hadronic cross section, QCD contributions have to be considered and thus necessitate an analysis over a large energy range for a reliable determination of α_s . Measurements of the total hadronic cross section and their interpretation in terms of α_s and $\sin^2\theta_w$ have been reviewed elsewhere ^{4,24)}. With the result of $\sin^2\theta_w = .23 \pm .05$, as is expected, the accuracy in the determination of $\sin^2\theta_w$ is poor in comparison to the one presented in the previous chapter.

Measurements of the charge asymmetry in quark final states require identification of both flavour and charge (Q or \bar{Q}) of the primary quarks giving rise to the observed hadron jets. Only heavy quarks have been tagged so far to some level of reliability. The method for charmed quarks has been to detect leading D and D^* mesons ($E_{D^*}/E_B > .4$) while bottom quarks are identified via large p_T leptons from semileptonic decays. While the former method suffers from statistics (efficiencies are $\sim 0.5\%$, event samples are of order 100) the latter is plagued by large backgrounds. D^* tagging, which exploits the small mass difference between D^* and D in the decay $D^* \rightarrow D \pi$, has been used by JADE²⁵⁾ and TASSO²⁶⁾, the JADE measurement at 34 GeV is shown in fig. 11. The asymmetries obtained are $(-14 \pm 9)\%$ for JADE and $(-13 \pm 10)\%$ for TASSO, in good agreement with -14% expected from the standard theory.

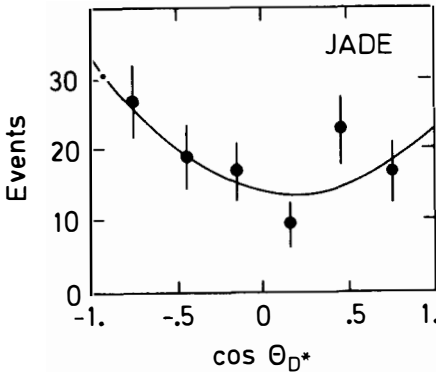


Fig. 11: Angular distribution for identified D^* mesons (JADE)

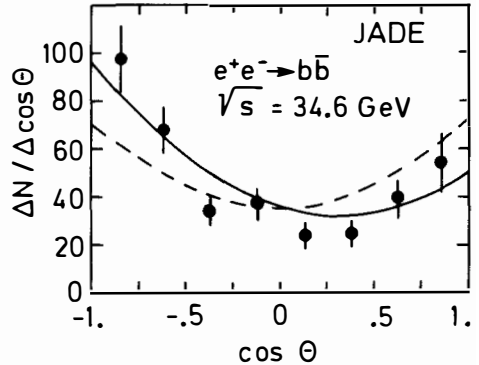


Fig. 12: Angular distribution for b quarks tagged by muons.

Bottom quark tagging via leptons has become a field of considerable ingenuity in designing cuts and fitting variables to enhance the signal over an overwhelming background. Choosing the cuts appropriately, the direct lepton tag can also be used to enhance the charmed quark and derive charge asymmetries (see table 5). Besides the positive identification of leptons (e or μ) with large transverse momentum with respect to the jet axis ($p_T \sim 0.5, 0.6, 1.3$ GeV/ c for u, d, s, c, b quarks) the different experiments use e.g. thrust (MARKJ²⁷⁾, sphericity products (TASSO²⁸⁾) and jet transverse mass (JADE²⁹⁾). The b -enriched samples contain typically 60% beauty. The JADE measurement for the differential cross section of b quarks using the lepton tag is shown in fig. 12. The corresponding charge asymmetry is $(-22.8 \pm 6)\%$ at $\sqrt{s} = 34.6$ GeV. The results from all PETRA experiments on heavy quark asymmetries are summarized in table 5. The error of the JADE measurement is remarkably small. Recently, MARKJ have

re-analyzed their complete data sample at $\sqrt{s} = 35$ GeV and find errors on the b-quark charge asymmetry in excess of 14% which is more than a factor of 2 above the JADE value. The errors found by CELLO, PLUTO and TASSO satisfy the MARKJ bound. The source of this discontinuity could either be the superior method of JADE or a somewhat different estimate of systematic errors in the various experiments.

Table 5: Measurements of the charge asymmetry for heavy quarks at $\sqrt{s} = 34.5$ GeV.

Exp.	lepton	A_{bb}^- [%]	A_{cc}^- [%]
CELLO	e	- 38 ± 21	
	μ	- 43 ± 31	
JADE	μ	- 22.8 ± 6.0	
MARKJ ³²⁾	μ	0 ± 14 ± 8	- 4 ± 9 ± 3
PLUTO ¹⁸⁾	μ	- 36 ± 25	- 16 ± 16
TASSO	e	- 25 ± 22	+ 5 ± 24
	μ	- 38 ± 28	

For the enhancement of b quarks tagged by muons a new variable Σ_μ has been proposed by the PLUTO collaboration¹⁸⁾ describing the isolation in space of a lepton by summing the normalized energies carried by other particles within a cone of opening angle Θ . A cut in Σ_μ leads to b-enriched sample with ~80% b-quarks. Fig. 13 shows the PLUTO data at 34.5 GeV together with MC estimates of the various contributions.

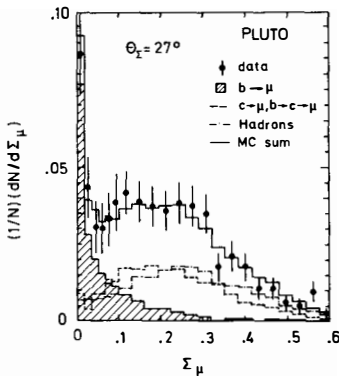


Fig. 13: Distribution of the variable Σ_μ (see text) and predictions from MC

The charge asymmetries derived for the heavy quarks, although still at a marginal statistical significance, are in good agreement with the predictions of the standard theory. Combining all measurements the following values for the axial vector coupling constants are derived (using a_e to determine the sign):

$$a_b = - 0.91 \pm 0.20$$

$$a_c = + 0.74 \pm 0.36$$

5. Tests of Higher Order QED and Search for Excited Leptons

5.1 The reaction $e^+e^- \rightarrow \gamma\gamma$

Although not a higher order QED process, this reaction provides an excellent test of QED since no electroweak contributions exist in lowest order. Preliminary data from CELLO at $\langle\sqrt{s}\rangle = 44.4$ GeV, normalized to QED, are shown in fig. 14. The 95% C.L. limits for the cut-off parameters derived from these data and those at $\sqrt{s} = 34.5$ GeV are $\Lambda_+ > 76$ GeV and $\Lambda_- > 60$ GeV.

5.2 The Reactions $e^+e^- \rightarrow 1^+1^-\gamma(\gamma)$

The reactions $e^+e^- \rightarrow e^+e^-\gamma, \mu^+\mu^-\gamma$ have been used by JADE³⁰⁾ and MARKJ³¹⁾ to confirm QED to order α^3 and have been reviewed previously^{4,24)}. New data are available from CELLO ($e^+e^-\gamma, \mu^+\mu^-\gamma$) and MARKJ³²⁾ ($\mu^+\mu^-\gamma$). The $1^+1^-\gamma$ final state is usually defined by a high energy photon ($E_\gamma > 0.1 E_B$), no other substantial neutral energy ($E < 0.5$ GeV), at least one identified lepton, large visible energy ($E_{vis} > 0.6 \sqrt{s}$) and no missing (transverse) momentum within the errors. CELLO have performed a QED analysis in the Dalitz plot where the kinematical quantities were redetermined using the precise angular measurements alone. The mass resolution obtained for the lepton-photon invariant mass is $250 \text{ MeV} \cdot E_B [\text{GeV}]/17$. Fig. 15 shows their data for three energy regimes after simple cuts to remove the bulk of "trivial" QED where the photon is close to one lepton. To compare with the QED expectation three regions have been defined in the Dalitz plot as indicated in the figure. The corresponding numbers of events from $e^+e^- \rightarrow \mu^+\mu^-\gamma$ are compared with QED (in brackets) in table 6.

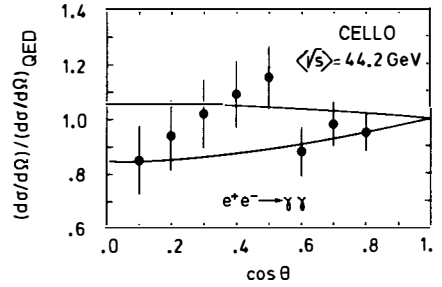


Fig. 14: Differential cross section for $e^+e^- \rightarrow \gamma\gamma$, normalized to QED. Limits from Λ_{\pm} are also drawn.

Table 6: Dalitz plot distribution for $e^+e^- \rightarrow \mu^+\mu^-\gamma$ (CELLO)

\sqrt{s} [GeV]	14 + 22	33 - 36	39.8 - 46.7
reg. I	8 (7)	7 (8.1)	12 (12.2)
reg. II	9 (7.4)	5 (8.7)	9 (12.5)
reg. III	0 (1.4)	7 (1.6)	5 (2.3)

QED seems to describe the Dalitz plot population well except for region III of the data above $\sqrt{s} = 33$ GeV where an excess of events (12, with 3.9 expected) is seen. The probability to observe such a fluctuation in QED (α^3) is about 1%.

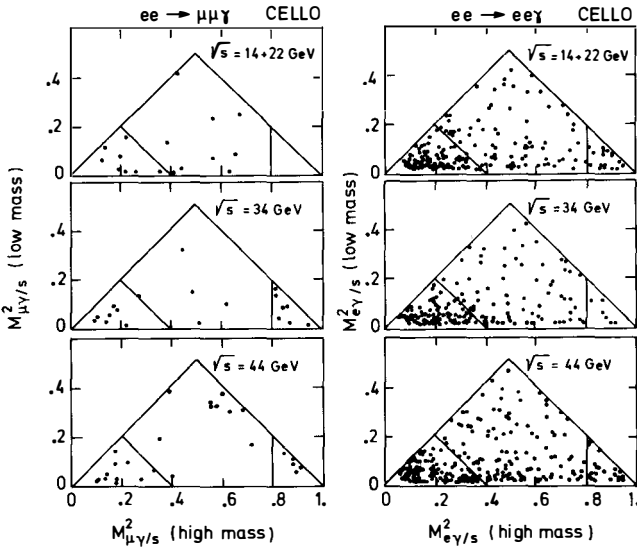


Fig. 15: Dalitz plot for $e^+e^- \rightarrow e^+e^-\gamma$ and $e^+e^- \rightarrow \mu^+\mu^-\gamma$ for three different energy intervals. Cuts were used to remove the bulk of QED.

The process $e^+e^- \rightarrow e^+e^-\gamma$ has been looked at by CELLO also in an entirely different kinematical regime where one of the leptons stays in the beam pipe and only one electron (positron) and a photon, balanced in transverse momentum, are detected. The corresponding physical process is virtual Compton Scattering. Here, 424 events have been observed from 9.5 pb^{-1} at $\sqrt{s} = 44 \text{ GeV}$, with a total visible energy distribution in excellent agreement with QED.

In models where leptons are considered composite, excited leptons of mass M_{e^*} may exist which could be detected in the above reactions. These excited leptons are expected to couple to the ground state and the photon through their anomalous magnetic moment according to the following interaction Lagrangian ³³⁾

$$L_{\text{int}} = \frac{\lambda e}{2M_{l^*}} \bar{\psi}_{l^*} \sigma_{\mu\nu} \psi_l F^{\mu\nu} + \text{h.c.} \quad (20)$$

where λ is the coupling constant of $l^*\gamma$ relative to the electric charge. No significant structure is found by any experiment in the invariant $(l\gamma)$ mass distributions. Preliminary upper limits on the mass of an excited electron as a function of $(\lambda/M_{e^*})^2$ from CELLO are shown in fig. 16, excluding such a state up to $M_{e^*} = 76 \text{ GeV}$ if $\lambda = 1$ is assumed. The corresponding plot for an excited muon is shown in fig. 17, with preliminary data from CELLO and MARKJ ³²⁾, and published values from JADE ³⁰⁾. Also shown is the preliminary τ^* limit from CELLO. Table 7 summarizes l^* mass limits obtained from the reactions $e^+e^- \rightarrow l^+l^-\gamma\gamma$ where a pointlike coupling of l^* to the photon has been assumed.

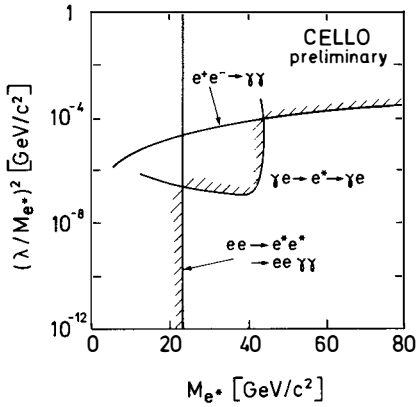


Fig. 16: Limits for excited electrons

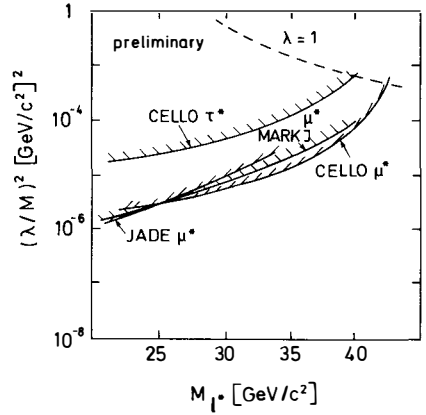


Fig. 17: Limits for μ^* and τ^*

Table 7: l^* mass limits from $e^+e^- \rightarrow l^+l^-\gamma\gamma$

Exp.	e^*	μ^*	τ^*
CELLO	23	23	22.5
JADE ^{17,31)}	23.1	22	-
MARKJ ³³⁾	22.5	19	-

5.3 The Reactions $e^+e^- \rightarrow e^+e^-l^+l^-$

The total luminosity accumulated by now at energies beyond 33 GeV ($> 90 \text{ pb}^{-1}$ per experiment, CELLO 30 pb^{-1}) allows the study of QED (α^4) processes at large Q^2 with 4 detected leptons in the final state. Preliminary data are available on the reactions $e^+e^- \rightarrow e^+e^-e^+e^-$, $e^+e^- \mu^+\mu^-$ from CELLO and JADE ¹⁷⁾ and on $e^+e^- \rightarrow e^+e^-\tau^+\tau^-$ from CELLO. The statistical significance of the data is still marginal (CELLO see 14 events, JADE 23), no event from $e^+e^- \rightarrow \mu^+\mu^-\mu^+\mu^-$ has been seen so far at PETRA. CELLO require at least 3 identified leptons with momenta $> 1.3 \text{ GeV}$ with an invariant mass $M_{l\bar{l}} > 1 \text{ GeV}/c^2$ for any l^+l^- combination. They find 7 eeee(γ), 6 ee $\mu\mu$ (γ) and 1 ee $\tau\tau$, where one of the charged particles is identified as a π due to its late shower development in the liquid argon. In 5 of their 14 events additional hard photons ($E_\gamma > 0.5 \text{ GeV}$) have been found. A distribution of the scaled invariant mass $x = M_{\text{inv}}(l^+l^-)/b$, denoting the smaller of the two lepton pair mass combinations, is shown in fig. 18 together with the QED $O(\alpha^4)$ expectation ³⁴⁾. Above $x = 0.4$, 7 events are observed whereas only 1.4 are expected. The probability that this is a fluctuation of QED amounts to only 10^{-2} . The excess events are not correlated with a threshold in center of

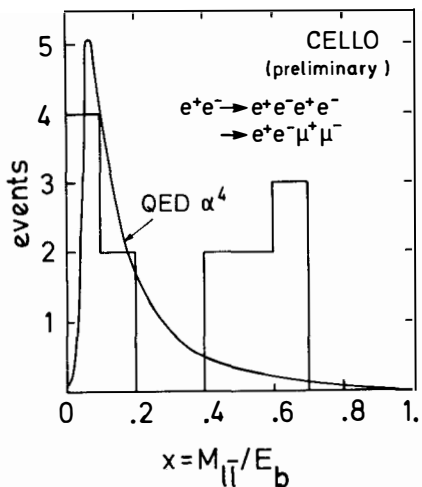


Fig. 18: Normalized lepton pair masses

estimate contributions from final state radiation to the multiperipheral diagrams, which are believed to dominate the high x (> 0.4) region: The number of events expected only rise by a fraction of an event. Clearly, more data is the only way to obtain clarification about this puzzling fluctuation.

mass energy but are evenly distributed within the data, spanning 14 to 46.8 GeV. JADE's distribution for the variable x , is shown in fig. 19. Good agreement with QED $O(\alpha^4)$ is seen in their data. As for CELLO, the JADE data contain a similar fraction of events (5 out of 23) with an additional energetic photon ($E_\gamma > 0.5$ GeV), which points towards sizeable contributions from $O(\alpha^5)$ processes, which are not taken into account in the calculations for the QED expectation. CELLO have tried to

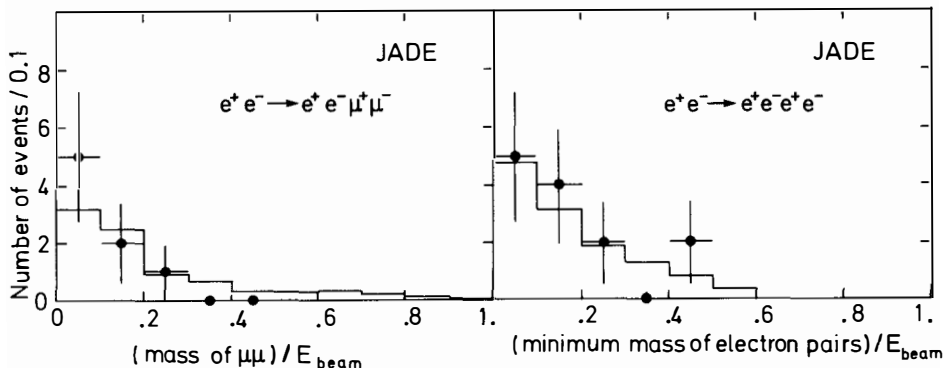


Fig. 19: Distribution of normalized lepton pair masses, separated for electron and muon pairs. The QED prediction is also shown.

Acknowledgement

I would like to thank my colleagues from the PETRA experiments for providing their new data prior to publication, especially G.Bella, C. Mana, H.-U. Martyn and B. Naroska. My thanks also go to J. Tran Thanh Van and his organizing staff for another enjoyable and stimulating meeting at Les Arcs.

References

- 1.) G. Flügge, Proc. XIX Renc. de Moriond 1984, Vol. 1, p. 341
- 2.) C. Kiesling, Recent experimental tests of the Standard Theory of Electro-weak Interaction, to appear in Springer Tracts on Modern Physics, 1985
- 3.) A. Böhm, these Proceedings
- 4.) S. Yamada, Proc. XVII Renc. de Moriond 1983, Vol. 2, p. 177
C. Youngman, Proc. XIX Ren. de Moriond 1984, Vol. 1, p. 173
- 5.) M. Böhm, W. Hollik, Phys. Lett. 139B (1984) 213
- 6.) W. Wetzel, NP B 227 (1983) 1 and Heidelberg preprint May 1983
- 7.) F.A. Berends, R. Kleiss, Nucl. Phys. B177 (1981) 237
- 8.) G. Passarino, M. Veltman, Nucl. Phys. B160 (1979) 151
- 9.) R. Brown, R. Decker, E. Pasdeos, Phys. Rev. Lett. 52 (1984) 1192
- 10.) F.A. Berends, R. Klein, S. Jadach, Nucl. Phys. B202 (1983) 63
- 11.) H.J. Behrend et al. (CELLO $\mu\mu$)
- 12.) U. Bartel et al., DESY preprint 84-078, 1984
- 13.) B. Adeva et al., Phys. Rep. 109 (1984) 133
- 14.) Ch. Berger et al., Z. Phys. C21 (1983) 53
- 15.) M. Althoff et al., Z. Phys. C22 (1984) 3
- 16.) H.J. Behrend et al., Phys. Lett. 114B (1982) 282
- 17.) B. Naroska, private communication
- 18.) G. Bella, private communication
- 19.) M. Althoff et al., Z. Phys. C26 (1985) 521
- 20.) H.J. Behrend et al., Phys. Lett. 127B (1983) 270
- 21.) W. Kreuz, PITHA 82-26 (1982)
- 22.) G. Arnison et al., Phys. Lett. B122 (1983) 103, B126 (1983) 398, B129 (1983) 273; M. Banner et al., Phys. Lett. B122 (1983) 476, P. Bagnaia et al., Phys. Lett. B129 (1983) 130
- 23.) A. Böhm, Aachen preprint PITHA 84/11 (1984)
- 24.) D. Saxon, RAL preprint 84-094 (1984)
- 25.) W. Bartel et al., DESY preprint 84-059 (1984)
- 26.) M. Althoff et al., Phys. Lett. 126B (1983) 493; 138B (1984) 317
- 27.) B. Adeva et al., Phys. Rev. Lett. 51 (1983) 443
- 28.) M. Althoff et al., DESY preprint 84-061 (1984)
- 29.) W. Bartel et al., DESY preprint 84-068 (1984)
- 30.) W. Bartel et al., Z. Phys. C19 (1983) 197 and DESY preprint 84-033 (1984)
- 31.) B. Adeva et al., Phys. Rev. Lett. 48 (1982) 967
- 32.) Results provided for this report by the MARKJ collaboration
- 33.) H. Terazawa et al., Phys. Lett. 112B (1982) 387
- 34.) F.A. Berends et al., Leiden preprint (1984).

NEUTRINO PRODUCTION OF LIKE SIGN DIMUONS*

K. Lang, A. Bodek, F. Borcharding, N. Giokaris, I.E. Stockdale;
University of Rochester, Rochester, New York, 14627
 P. Auchincloss, R. Blair, C. Haber, S. Mishra, M. Ruiz, F.J. Sciulli,
 M. Shaevitz, W.H. Smith, R. Zhu; Columbia University, New York, NY 10027
 Y.K. Chu, D.B. MacFarlane, R.L. Messner, D.B. Novikoff, M.V. Purohit,
California Institute of Technology, Pasadena, CA 91125
 D. Garfinkle, F.S. Merritt, M. Oreglia, P. Reutens;
University of Chicago, Chicago, IL 60637
 R. Coleman, H.E. Fisk, Y. Fukushima, Q. Kerns, B. Jin, D. Levinthal,
 T. Kondo, W. Marsh, P.A. Rapidis, S. Segler, R. Stefanski, D. Theriot,
 H.B. White, D. Yovanovitch; Fermi National Laboratory, Batavia, IL 60510
 O. Fackler, K. Jenkins; Rockefeller University, New York, NY 10021

*Presented by K. Lang



ABSTRACT

Neutrino interactions with two muons in the final state were studied using the Fermilab narrow band beam. A sample of 18 like sign dimuon events with momentum $p_{\mu} > 9 \text{ GeV}/c$ yields a prompt signal of 8.1 ± 4.4 events and a rate of $(1.4 \pm 0.8) \times 10^{-4}$ per single muon event. The kinematics of these events are compared with those of the non-prompt sources.

Introduction

We report on an experimental study of neutrino induced dimuon events. The dimuon data come from two runs with the same detector using the Fermilab narrow band neutrino beam as a neutrino source.^{1]} The first run (Fermilab experiment E616) took place in 1979 and 1980, with an integrated proton flux of 5.4×10^{18} on the production target. The second run took place in 1982 (Fermilab experiment E701) with a flux of 3.4×10^{18} . Data were taken at six momentum settings for π and K mesons (+100, ± 120 , ± 140 , ± 165 , ± 200 , ± 250 GeV/c), yielding neutrinos with energies between 40 and 230 GeV. The neutrino beam^{2]} was produced by decays of these sign and momentum selected ($\Delta P/P = \pm 11\%$) pions and kaons in a 352 m long evacuated decay pipe.

The neutrino detector is located in Lab E, 1292 m from the beginning of the decay pipe. The apparatus consists of a target calorimeter instrumented with scintillation counters and spark chambers followed by an iron toroidal muon spectrometer. The rms hadron energy resolution is $0.89 \sqrt{E}$ (GeV). The total transverse momentum kick of the toroids is 2.4 GeV/c and the fractional momentum resolution is $\pm 11\%$.

Dimuon Analysis

Events with two muons were selected from the sample of all charged current triggers (500K events). The computer reconstruction of the dimuon events was examined by physicists and, if necessary, the reconstruction was repeated interactively.

Events are separated into those produced by muon neutrinos from pion decay (ν_π) and from kaon decay (ν_K). The neutrino energy and decay angle (and therefore the event radius at the detector) are kinematically related. Events due to ν_K and ν_π are distinguished by examining the transverse radial position of the interaction and the measured total energy. Once this separation is made the event transverse vertex position determines the incident neutrino energy with a $\pm 10\%$ error. In order to improve the efficiency for the muon track reconstruction, at least one muon track must have a straight line extrapolation from the target that passes through the first toroid magnet, and intersects the trigger counter placed after it.

All dimuon events must pass the same analysis cuts as the single muon events. Events must have a transverse vertex within a $2.5\text{m} \times 2.5\text{m}$ square and a longitudinal vertex at least 3.8 m from the downstream end of the target, to ensure containment of the hadron shower. In addition, the vertex for ν_π events is required to have a transverse radius of less than 76 cm.

The like sign dimuon analysis requires that both muons are momentum analyzed by the toroid magnet with $P_\mu > 9$ GeV/c. Therefore each single muon

event used must have a magnetically determined momentum of $P_{\mu} > 9 \text{ GeV}/c$. A total of 116,346 charged current events pass these cuts.

The like sign dimuon sample contains 18 events in which each muon traverses one toroidal magnet and has a momentum greater than 9 GeV/c. Both muons must have angles less than 250 mrad with respect to the beam axis. In addition, both muons must have fitted tracks which originate in a common vertex consistent with counter pulse height and each track must be visible in the spark chambers after the first toroid.

The principal background sources of like sign dimuons are decays to muons of primary π 's or K's at the hadron vertex in a charged current event, and the production of prompt or non-prompt muons from the secondary interactions of the primary hadrons. The inclusive primary hadron spectra and multiplicity are obtained from BEBC ν -Ne^{3]} and EMC μ -p data.^{4]} The contribution of subsequent interactions of these hadrons is calculated using the measured prompt and non-prompt muon production by hadrons in the Fermilab experiment E379 variable density target.^{5]} This yields the probability for producing a muon, with a momentum greater than a particular cutoff value, as a function of x_{BJ} and the hadron energy E_H .

The model of the background uses the generated E_H and x_{BJ} of charged current Monte Carlo events to produce dimuon events with a particular weight and P_{μ_2} . The produced muon is given a P_{\perp} based on transverse momentum fits to hadrons from EMC μ -p data.^{6]} The Monte Carlo events are reconstructed and required to pass the dimuon analysis cuts. The background is normalized to the number of charged current data events passing the same cuts. The systematic error in the background is $\pm 17\%$.

The non-prompt background for the 18 events is calculated to be 9.2 ± 1.6 events. We have also estimated an additional background due to misclassified trimuon events (originating primarily from hadronic and electromagnetic muon pair production) for which the second muon is hidden in the shower to be 0.6 ± 0.2 events. The background from spatially and temporally coincident charged current neutrino events is calculated to be 0.1 ± 0.1 events. We therefore observe a like sign dimuon signal above background of 8.1 ± 4.4 events. CDHS reported 91 ± 9 like sign dimuons with a calculated background of 64 ± 10 events with a momentum out of 10 GeV/c from their 350 GeV wide band run,^{8]} and 47 events with a background of 30 ± 8 from their 200 GeV narrow band run.^{9]} The CHARM collaboration reported 74 ± 17 prompt ν_{μ} induced $\mu^{-}\mu^{-}$ and 52 ± 13 prompt $\bar{\nu}_{\mu}$ induced $\mu^{+}\mu^{+}$ with a 4 GeV/c momentum cut from their wide band run.^{10]} The HPWFOR collaboration reported a prompt signal of 52 ± 31 , 65 ± 15 , and 37 ± 11 from their quadrupole triplet run^{11]} with momentum cuts of 5, 10, and 15 GeV/c, respectively. The CFNRR collaboration reported 10 like sign dimuons

with a background of 4.3 events from their quadrupole triplet run.^{12]}

A calculation of the ratio of prompt like sign dimuon production to single muon production requires that the numbers of single muon and prompt like sign dimuon events be corrected for geometrical acceptance. This acceptance must rely on a specific model. In the absence of such a model for like sign dimuons, we have used a model in which the distribution of prompt dimuon events is the same as that of the non-prompt background (Model 1 - π/K). The acceptance has also been calculated using a model of gluon bremsstrahlung of charm-anticharm pairs with the anticharm decay producing the second muon^{13]} (Model 2 - $c\bar{c}$). Although the contribution to like sign dimuons from $D^0-\bar{D}^0$ mixing is negligible,^{14]} we have also calculated the acceptance using this model for completeness (Model 3 - $D^0-\bar{D}^0$). The rates calculated with the π and K decay model acceptance are presented with a comparison of acceptance correction for $c\bar{c}$ production and $D^0-\bar{D}^0$ mixing in Table 1.

TABLE 1

RAW DATA						Acceptance Corrected			Prompt
Energy Bin(GeV)	μ^- Events	$\mu^-\mu^-$ Events	Hadron Shower	Other Bkg.	Data-Bkg.	Model1 Prompt (π/K)	Model2 Prompt ($c\bar{c}$)	Model3 Prompt ($D^0-\bar{D}^0$)	Rate $\mu^-\mu^-/\mu^-$ ($\times 10^{-4}$)
30-100	106432	2	1.5	0.2	0.3	1.3	1.0	1.0	0.1 \pm 0.5
100-200	52040	11	4.7	0.4	5.9	18.8	14.5	11.9	3.6 \pm 2.1
200-250	15893	5	3.0	0.1	1.9	4.0	3.1	2.9	2.5 \pm 3.1
30-250	174365	18	9.2	0.7	8.1	24.1	18.6	15.8	1.4 \pm 0.8

A comparison with the prompt like sign and opposite sign rates from other experiments is shown in Table 2. The energy dependence of the rates of prompt like sign dimuons to charged current events is shown in Fig. 1. The line in Fig. 1 is the prompt signal calculated from the charm-anticharm production model of Ref. 13, using $\alpha_s = 0.2$ and $M_c = 1.5 \text{ GeV}/c^2$. The rate scales with α_s^2 and predicts 0.2 events for this experiment.

In addition to the overall rates, the event kinematics may be used to determine whether the π and K background can be the sole explanation of

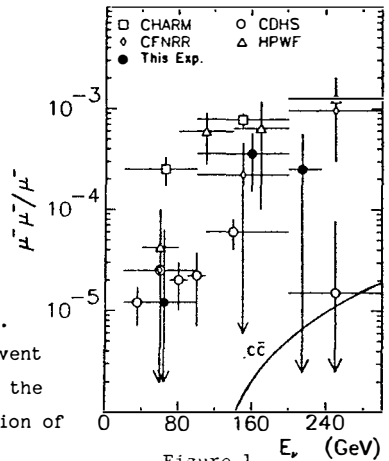


Figure 1 E_e (GeV)

the like sign dimuon signal. Distributions of several kinematic variables for the like sign dimuons and Monte Carlo events from π and K decay are shown in Fig. 2. The π and K decay shown as the dashed histogram consists of 9.2 events. The distribution of the angle between the two muon tracks projected on a plane perpendicular to the incident neutrino is shown in Fig. 2a. The peaking of this distribution near 180° indicates that the second muon is associated with the hadron shower in a large fraction of the events. This is a property expected of π and K decay.

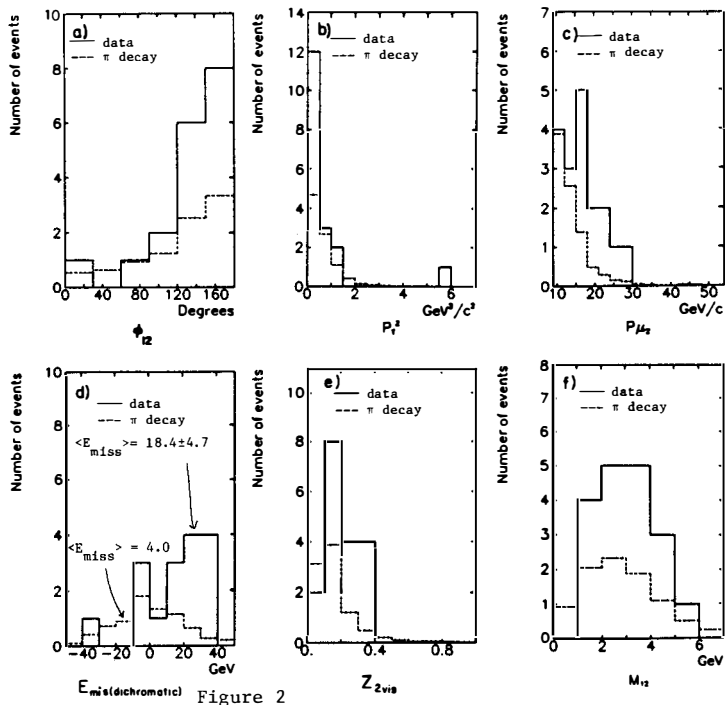


Figure 2

For further comparison with the hypothesis of π and K decay, the second muon is chosen to be the muon which has the smaller momentum in the direction perpendicular to the axis of the hadron shower ($P_{\perp 2 \min}$). The hadron shower direction is determined from the incoming ν beam properties and the chosen first muon. Figure 2b shows the $(P_{\perp 2 \min})^2$ distribution. There is one event with a $(P_{\perp 2 \min})^2$ of 5.9 (GeV/c)², which is unlikely to be from π and K decay. Figure 2c displays the momentum of the chosen second muon. The data average about 2 standard deviations greater than for π and K decay. Figure 2d shows the distribution of missing energy for all like sign ν_K dimuon events. The

missing energy is the difference between the neutrino energy determined by the transverse vertex radius and the measured energy. The determination of missing energy has been verified for single muon events where the average value for ν_K data is $0.7 \pm 0.2 \pm 1.2$ GeV where the second error is systematic. The missing energy for the like sign dimuon data is about 3 standard deviations greater than that expected for the hypothesis of π and K decay. The distribution of $Z_{\mu_2} = P_{\mu_2} / (E_H + P_{\mu_2})$ is shown in Fig. 2e and the distribution of the invariant mass of the $\mu^+ \mu^-$ pair is shown in Fig. 2f. There is no evidence of any structure in the mass distribution of the data.

TABLE 2

Experiment (Ref.)	Beam Type	p_{μ} cut (GeV/c)	$\mu^+ \mu^- / \mu^-$ prompt $\times 10^{-4}$	$\mu^+ \mu^- / \mu^- \mu^+$ prompt $\times 10^{-2}$
CCFRR (this expt)	NBB	9.	1.4 ± 0.8	5.2 ± 2.8
CDHS (8)	WBB	6.5	0.43 ± 0.23	4.2 ± 2.3
CDHS (9)	NBB	4.5	3 ± 2	5 ± 3
CHARM (10)	WBB	4.	4.5 ± 1.6	14 ± 5
HPWFOR (11)	QTB	10.	3.0 ± 0.8	7 ± 4
CFNRR (12)	QTB	9.	2.0 ± 1.1	-

It has been suggested^{15]} that enhanced $c\bar{c}$ production could account for the prompt like sign dimuon signal. Accordingly, in Figure 3 we compare the same kinematic distributions of the data in Fig. 2 with the sum of the π and K decay background (previously displayed) and the rates from the previously described $c\bar{c}$ Monte Carlo multiplied by a factor of 50 (to equal the 8.1 event prompt signal). The kinematics of $c\bar{c}$ do not differ from those of π and K decay sufficiently to attribute the prompt signal to $c\bar{c}$ production any more than to π and K decay. The mean missing energy for $c\bar{c}$ and π/K decay is about 3 standard deviations away from that of the data. The $c\bar{c}$ and π/K decay mean Z_{μ} is about 2 standard deviations away from that of the data.

Conclusions

The 18 observed like sign dimuon events with a muon momentum out of 9 GeV/c yield a prompt signal of 8.1 ± 4.4 events. This gives an average rate for prompt like sign muon production of $(1.4 \pm 0.8) \times 10^{-4}$ per single muon event. The hadron shower background and/or associated charm production with anticharm decaying into μ^- cannot explain the measured rates. In addition, although

most distributions of the data are similar to those expected from these two sources, the missing energy and p_T kinematic distributions of the data display some features which are not expected from the two models.

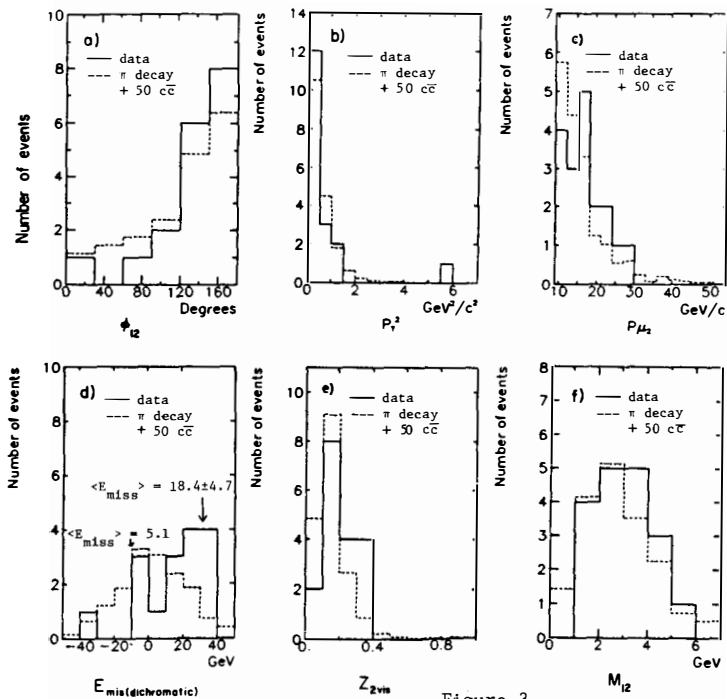


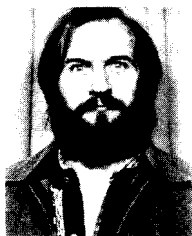
Figure 3

References

- 1) R. Blair et al, Phys. Rev. Lett. 51, 3431 (1983).
- 2) R. Blair et al, Nucl. Instr. & Meth. 226, 281 (1984).
- 3) P. C. Bosetti et al, Nucl. Phys. B149, 13 (1979); B209, 29 (1982).
- 4) J. J. Aubert et al, Phys. Lett. 114B, 373 (1982).
- 5) Fermilab E379/595. (c.f. J. Ritchie, Ph.D. thesis, University of Rochester (1983) and K. W. B. Merritt, Ph.D. thesis, Caltech 91981). Data do not exist for $E_{\pi} < 40$ GeV, where we use a M.C. calculation.
- 6) F. W. Brasse, in Proc. of XX Int. Conf., Madison, Wisc., p. 755 (1980).
- 7) K. Lang, Ph.D. thesis, University of Rochester, UR-908 (1985).
- 8) J. G. H.deGroot et al, Phys. Lett. 86B, 103 (1970).
J. Knoblock, in Proc. Neutrino '81, ed. R. J. Cence, E. Ma, A. Roberts, I:421 (1981).
- 9) M. Holder et al, Phys. Lett. 70B, 396 (1977).
- 10) M. Jonker et al, Phys. Lett. 107B, 241 (1981).
- 11) T. Trinko et al, Phys. Rev. D23, 1889 (1981).
- 12) K. Nishikawa et al, Phys. Rev. Lett 46, 1555 (1981); 54, 1336 (1985).
- 13) B. Young, T. F. Walsh, T. C. Yang, Phys. Lett. 74B, 111 (1978).
V. Barger, W. Y. Keung, R. J. N. Phillips, Phys. Rev. D25, 1803 (1982).
- 14) A. Bodek et al, Phys. Lett. 113B, 82 (1982).
- 15) R. M. Godbole, D. P. Roy, Z. Phys. C22, 39 (1984).

PRECISE MEASUREMENT OF $\sin^2\theta_w$ IN NEUTRINO-IRON INTERACTIONS

CDHSW Collaboration
Presented by A. Blondel
CERN, Geneva, Switzerland



ABSTRACT

The ratio R_ν of neutral to charged current cross-sections of neutrinos in iron is presently being measured at CERN-SPS in the upgraded CDHSW detector exposed to a dedicated version of the 160 GeV Narrow Band Beam. From the increase in statistics and the improvement of systematics we expect a final experimental precision of $\Delta\sin^2\theta_w = .005$, matching the theoretical uncertainties, allowing stringent tests of coherence of the Standard Model.

$\sin^2\theta_w$ is, in our present understanding, the only free parameter of the Glashow Salam Weinberg theory of weak and electromagnetic interactions. Knowing $\sin^2\theta_w$, one can in principle derive all weak neutral current couplings, as well as the masses of the W and Z°. The derivations however are subject to radiative corrections involving, beside the straightforward Q^2 evolution of the coupling constant, unknown quantities such as the masses of the quarks and of the Higgs boson(s).

The present measurement of M_w and M_Z from the $\bar{p}p$ collider leads to $\sin^2\theta_w = .221 \pm .007$ ¹⁾, however fully dependent on the radiative corrections. Less sensitive to these radiative corrections, and to the systematic uncertainty on the energy scale which already dominates the errors, is the quantity $\sin^2\theta_w = 1 - \frac{M_w^2}{M_Z^2}$. However it is much less precise ($\sin^2\theta_w = .220 \pm .030$ presently), and will remain limited by the statistics and systematics coming from the QCD smearing of the Jacobian peak of the W.

The mass of the Z° will be measured very precisely at SLC and LEP, but precision on M_w will certainly wait much longer.

High precision tests of the theory therefore require measurements of $\sin^2\theta_w$ from the neutral current coupling constants.

The most precise measurement so far comes from the measurement of $R_\nu = \sigma(\nu N + \nu x) / \sigma(\nu N + \mu^-x)$. Fig. 1 shows the present experimental situation²⁾.

To illustrate the need for the future precision, let us point out that the value of $\sin^2\theta_w$ extracted from R_ν at the Born approximation and the normalized value $\sin^2\theta_w (M_w^2) \frac{MS}{MS}$ (see ref. 4 for definition) differ by .013 : .239 and .226 with an error of .012.

The aim of the present experiment is to bring this error down to .005, taking profit of past experience both from the experimental and theoretical point of view.

On the theoretical side, a considerable progress has been achieved by C. Llewellyn Smith who demonstrated - without any assumption on the structure functions - that for an isoscalar target and no s or c quark involved:

$$\frac{d\sigma_{NC}^{\nu}}{dx dy} = \left(\frac{1}{2} - \sin^2\theta_w + \frac{5}{9} \sin^2\theta_w \right) \frac{d\sigma_{CC}^{\nu}}{dx dy} + \frac{5}{9} \sin^2\theta_w \frac{d\sigma_{CC}^{\nu}}{dx dy}$$

In particular, higher twist effects are shown to affect this prediction very little, especially for sufficiently high Q^2 or ν . This formula is insensitive

to assumptions about the sea content of the nucleon, longitudinal structure functions etc....

The two corrections relevant for a measurement of R_V on iron are:

- A small correction due to the non isoscalarity of the target, leading to an extra uncertainty of $\Delta \sin^2 \theta_w = .002$
- The correction for generation mixing - charm production - and the existence of strange sea quarks in the nucleus. The dominant uncertainty comes from the threshold behaviour of charm production - known as slow rescaling - which depends on the mass of the charmed quark and the shape of the strange sea distribution used in the model. Allowing these parameters to vary within the boundaries given by the measurements of dimuon production leads to an uncertainty of $\Delta \sin^2 \theta_w = .004$.

The uncertainties due to generation-mixing matrix elements have been much reduced since the measurements of the b lifetime, and are negligible if one assumes that the mixing of d and u quarks to possible higher mass generations is very small.

Altogether the theoretical uncertainty in extracting R_V from the above formula is expected to be less than .005.³⁾

Experimentally the best results so far is from the CDHS data taken in 1978-79

$$R_V = .301 \pm .007 \text{ (.005 stat. + .005 syst.)}$$

corresponding to $\sin^2 \theta_w = .226 \pm .012$.

The present experiment has been dedicated to a measurement of R_V using the same principle.

The principle of the measurement has been described in detail in ref. 2. The CDHS detector is a sandwich of magnetized iron and scintillator interspaced with drift chambers (fig. 2).

Charged Current and Neutral Current interactions are separated by the projected length, which is the distance between the first and the last scintillator hit by an event. NC events have the typical length of a hadron shower in iron, whereas in a CC event the muon generally is the most penetrating particle, according to its momentum. A small fraction of CC events (short CC) have a low momentum muon and are a background to the NC sample. This contamination is calculated by extrapolation of the CC length distribution, normalized on a monitor sample, itself constituted of events of low muon momentum (fig. 3).

This extrapolation, done by Monte Carlo, is extremely straightforward and very insensitive to the exact physics input to the Monte Carlo, or even the energy loss of the muon. It is only sensitive to a precise handling of the length measurement.

The remaining NC sample is contaminated by

- cosmics
- wide-band neutrinos
- ν_e CC interactions which cannot be distinguished from NC interactions and are subtracted on a statistical basis. Table I a and b summarize the progress made over the previous experiment.

As can be seen, the major improvement obtained concerns the statistics and the Wide Band subtraction.

The increase of statistics was obtained by using a new version of the CERN Narrow Band beam (fig. 4). An increase of acceptance of the beam line due to a wider opening of the first collimator and the use of only 4 (out of 7) of the first quadrupoles in conjunction with a better proton/hadron momentum configuration (450 GeV protons to 160 GeV hadrons instead of 400 to 200) led to an increase in event rate of 2.5 per proton. The excellent operation of the SPS permitted to increase the statistics by a factor 5.

The "Wide Bande beam" neutrinos come from the decay of anything but the 160 GeV hadrons. Since their type ($\nu_\mu, \bar{\nu}_\mu, \nu_e, \bar{\nu}_e$) is unknown, as well as their energy spectrum, they must be subtracted on a statistical basis. This was obtained in 1984 by setting a Dump in the beam just before the entrance of the decay tunnel, thus allowing the same measurement of beam intensity with the BCT for Dump in and normal runs. In addition other monitors were placed in the beam to ensure that the Dump in running was taken under the same conditions as normal running. None of these was possible in the previous data, where the wide band background was measured by closing the momentum slit of the beam, upstream of most monitoring components.

In addition, the fraction of wide band background running was optimized statistically.

The dead-time measurements, important for the subtraction of cosmics and wide band background, were performed with 3 different methods, agreeing among each other (not without some work!)

The improvement on the length measurement came from using the upgraded CDHS

detector (fig. 2). The old modules, with 45 cm wide scintillators extending horizontally over the whole width of the detector (3.85 m) had very poor lateral localisation of the showers. In the new modules, thinner scintillator strips (15 cm) are alternated horizontally and vertically, allowing a good 3-dimensional localisation of both the vertex and the end of an event.

In addition, the drift chambers were working to perfection, with a hit efficiency (2 out of the 3 planes in a chamber) of 99.95%, permitting very powerful checks on the length measurement algorithm.

The 3-dimensional structure of the new detector also helped for the subtraction of the pulse height added by the muon on top of the hadron energy in charged current events, the energy being summed over a large box, 1.5 m long, in which the muon deposits in average 3 GeV. This muon energy loss must be unfolded properly in order to compare NC events and CC events with the same E_H cut. This is being done by a semi-Monte Carlo method, folding measured showers with measured muon pulse height obtained along muons well beyond the shower end.

To conclude, after processing of the whole data sample, the sum of these improvements should permit the following result:

$$R_\nu = .xxx \pm (.002 \text{ stat.}) \pm (.002 \text{ syst.})$$

or

$$\sin^2_{\theta_w} = .xxx \pm .005 \text{ (exp.)} \pm .005 \text{ (theoretical)}$$

The data taking has been a success and the redundancy in the system permitted the discovery of many little faults and effects the understanding of which is crucial for a trust worthy result. None of these have destroyed our hope to reach the quoted precision.

We are very thankful to the SPS operation team, especially the neutrino group, who designed and ran this beautiful version of the beam. We are also indebted to the technicians and engineers, who maintained the now defunct CDHS detector in perfect condition until the last burst of neutrinos.

Table IaImprovements made to the measurement of R_ν due to statistics

	78-79 Data		84 Data ^{a)}		Comments
	NC	CC	NC	CC	
Candidates $E_H > 10$ GeV	18176±135	44274±210	92000±300	215700±460	improvement in statistics
Cosmics	-181±7	-4±1	-1020±30	18±9	
Wide-Band neutrinos	-641±119	-404±85	-2800±111	-5500±132	optimisation of Dump in running
Short CC events	-2285±78	-2299±69	-15800±126	-15830±126	same as before
Long NC events	+151	-151	+800±50	-800±50	same as before
$\nu_e + N \rightarrow e + x$	-1100±11	+940±9	-5100±70	-4350±60	same as before
Corrected events	14120±197	46957±237	68000±360	229500±500	
$R_\nu =$.301±.005		.3xxx±.0017		
$\frac{\Delta R_\nu}{R_\nu} =$	17.10 ⁻³		6.10 ⁻³		

Table Ib

Improvements due to systematics

	$\Delta R_\nu / R_\nu$		Comments
	78-79 Data	84 Data	
Cosmics	1.10 ⁻³	negligible	Dead time understanding
Wide band	12.10 ⁻³	2.10 ⁻³	Dead time + special dump situation
Short CC	9.10 ⁻³	4.10 ⁻³	3-D length measurement and momentum-range measurements
Long NC	5.10 ⁻³	2.10 ⁻³	Test beam data
$\nu_e + N \rightarrow e + x$	3.10 ⁻³	3.10 ⁻³	No change
Muon energy loss	6.10 ⁻³	3.10 ⁻³	Use directly measured pulse height, and special muon runs
	±17.10 ⁻³	±7.10 ⁻³	

a) extrapolated from 1/3 of the data analysed.

REFERENCES

- 1) UA1 collaboration, G. Arnison et al., Phys. Lett. 126B (1983) 398 and 129B (1983) 273.
 UA2 collaboration, P. Bagnaia et al., Z Phys. C - Particles and Fields 24 (1984) 1.
 See W.J. Marciano in Fourth topical workshop on proton-antiproton collider physics, CERN 1984 84-09, For a compilation of $p\bar{p}$ results on $\sin^2\theta_w$ (from 1983 data)
 Also UA2 contribution to this conference for 1984 data.
- 2) CHARM collaboration, M. Jonker et al., Phys. Lett. 99B (1981) 265.
 ABCDLOS collaboration, P.B. Bosetti et al., Nucl. Phys. B217 (1983) 1.
 CCFRR collaboration, P.G. Reutens, XIthe Int. Conf. on Neutrino Physics and Astrophysics, Nordkirchen near Dortmund 1984, eds. K. Kleinknecht and E.A. Paschos (1984, ISBN 9971-966-70-0).
 CDHS collaboration, M. Holder et al. Phys. Lett. 71B (1977) 222, and H. Abramowicz et al., IHEP-HD/84-10 submitted to Z. für Physik C.
- 3) A. Stirlin and W.J. Marciano, Nucl. Phys. B189 (1981) 442.
 J.F. Wheeler and C.H. Llewellyn Smith, Nucl. Phys. B208 (1982) 27.
 C.H. Llewellyn Smith, Nucl. Phys. B228 (1983) 205, and Workshop on field target physics, CERN 83-02 - II p. 180.
- 4) A. Sirlin, Phys. Rev. D22 (1980) 891;
 W. Marciano and A. Sirlin, Phys. Rev. D22 (1980) 2695.

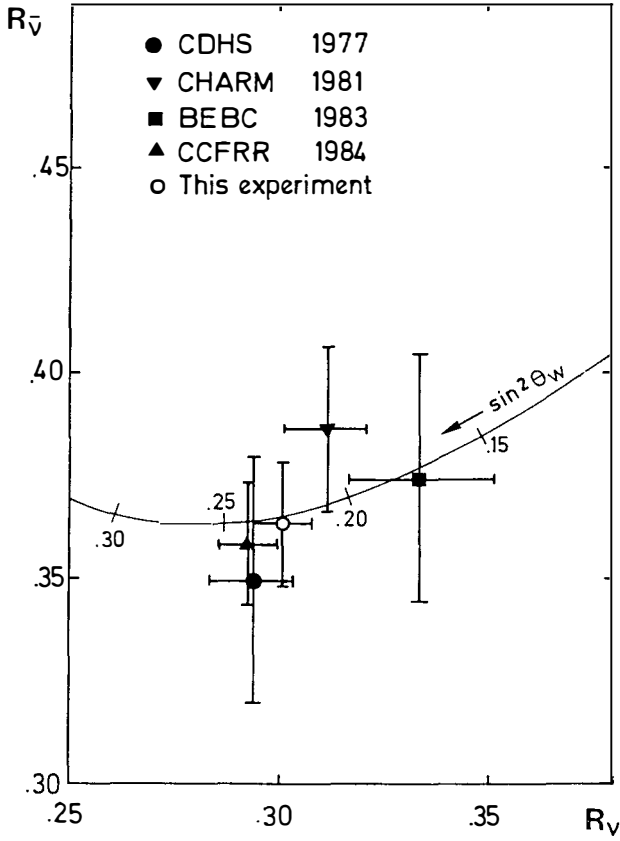


Fig. 1 - Present measurement of R_v and $R_{\bar{\nu}}$. "This experiment" is CDHS 78-79 Data.

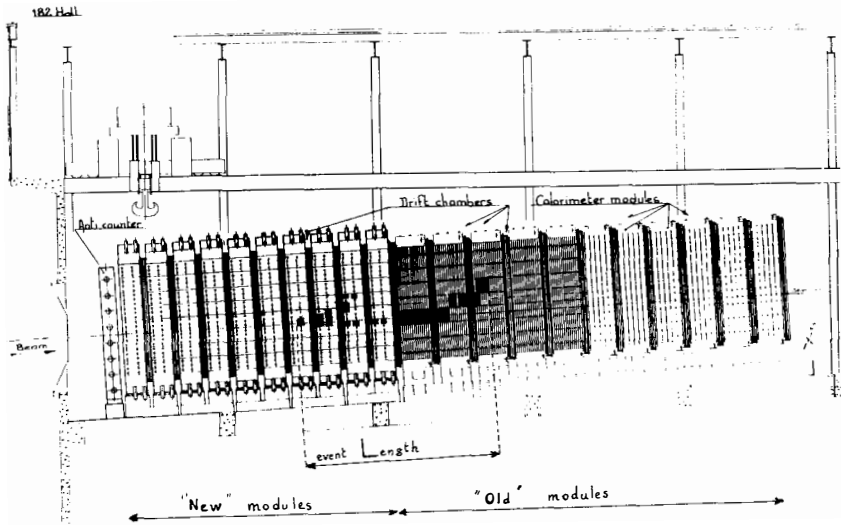


Fig. 2a - Side view of the CDHS detector displaying a neutrino event.

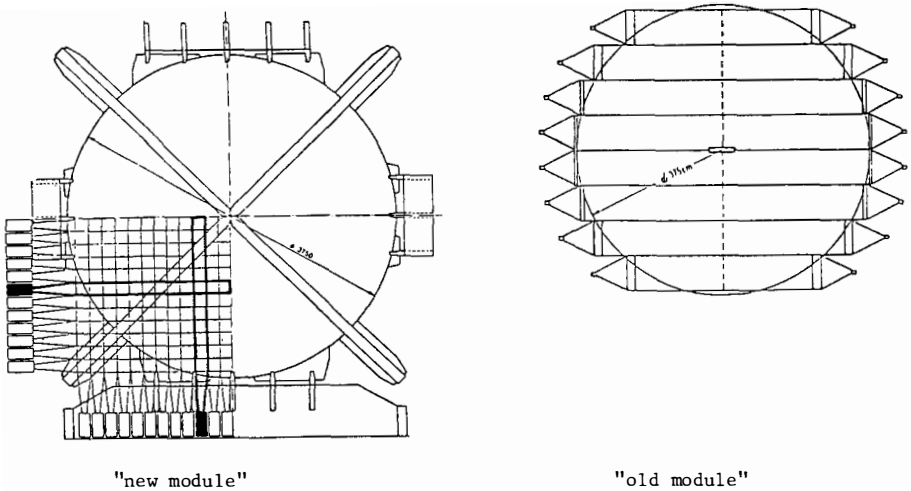


Fig. 2b - End view of the scintillator set-up in the new and old modules of the detector.

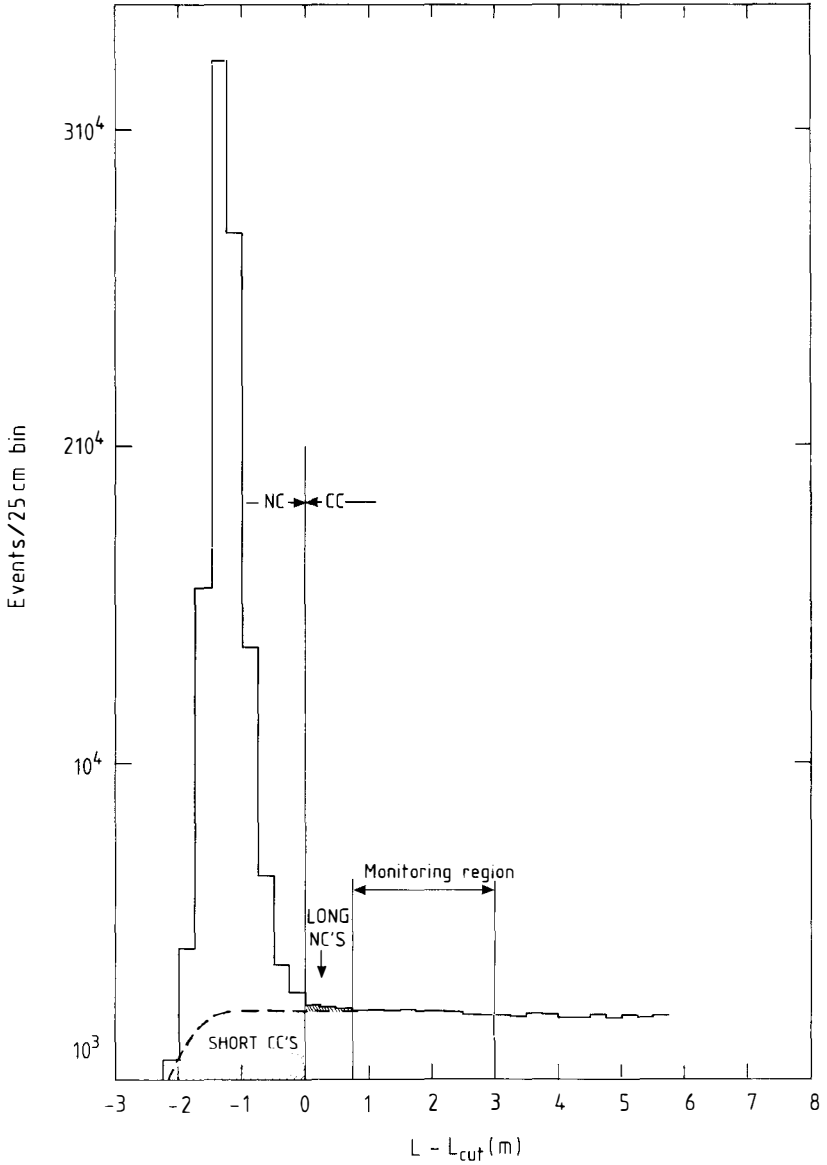


Fig. 3 - Event length distribution. L_{cut} , which is here subtracted, is an energy dependent length containing 99% of hadronic showers.

1984 NBB

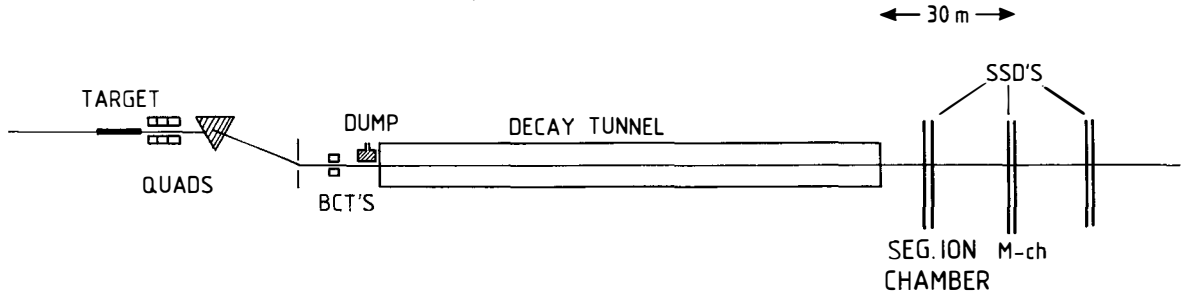


Fig. 4a - Overall view of the 1984 160 GeV Narrow Band beam.

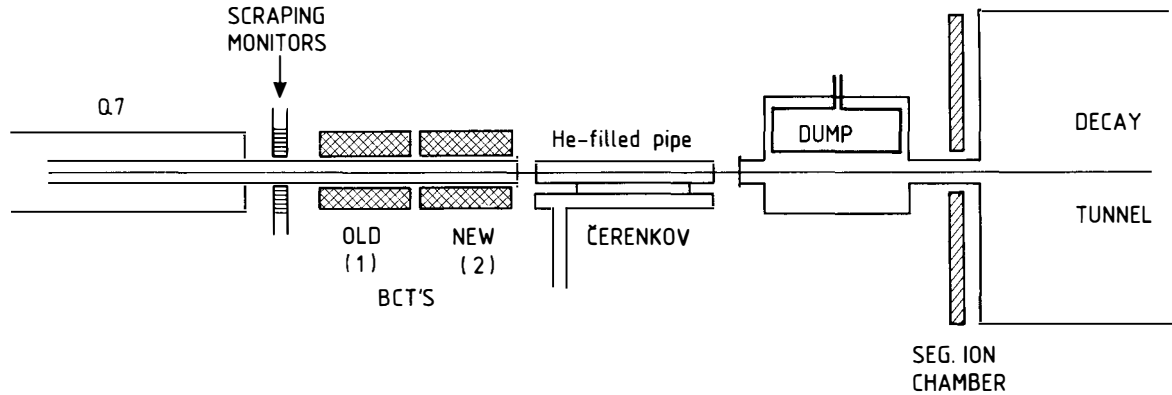


Fig. 4b - Detail of the section before the decay tunnel showing the monitors in front of the Dump.

TOPICS IN SUPERSYMMETRY

J.-M. Frère[†]
Physique Théorique CP225
Université Libre, Bruxelles

Abstract

We briefly review the most popular supersymmetric extensions of the "standard" model, insisting on the arbitrariness left in the phenomenological effective Lagrangian. We also discuss the possibility of building completely finite theories based on N=2 supersymmetry.

This work was supported in part by the U.S. Department of Energy and by NATO under contract 656/84

[†]Chercheur Qualifié du Fonds National de la Recherche Scientifique (Belgique).

1. Motivation for Supersymmetry.

The motivation for supersymmetry remains fairly theoretical. The initial image of a new symmetry relating known fermions to known bosons does not withstand the analysis.

While supersymmetry establishes some connections between gauge bosons and scalars, this connection is relatively loose and rather accidental in the $N=1$ theories. Indeed, while the masses of scalars and gauge bosons are related for unbroken SUSY¹), the choice of the group representations is left arbitrary (e.g.: in the "standard" model, supersymmetry does not explain why scalars should lie in doublets rather than triplets). Such relations become, however, much more compelling in $N>2$ supersymmetric theories.

The most economical solution would identify the scalar partners \tilde{e} , $\tilde{\nu}$ of the e and ν with the scalars* responsible for breaking $SU(2) \times U(1)$. This, however, would violate lepton number conservation. Also, another "Higgs" doublet H_1 is necessary in SUSY models to give mass to the charge $2/3$ quarks, and the cancellation of anomalies then requires a similar particle H_2 with opposite hypercharge - nothing is saved in terms of particle content! (see below for more discussion of $\langle \tilde{\nu} \rangle$).

The motivation which may be considered closest to the preoccupations of a phenomenologist is provided by an attempt at solving the "hierarchy problem." This problem arises very generally from the assumption that the presently known interactions may be unified into a single gauge group at some scale. An estimate of the scale at which this would happen is then provided by the study of the renormalization group equations, as established from the currently known particle spectrum (of from some assumed spectrum if SUSY is considered). The unification of the electromagnetic and strong coupling then suggest a very high mass scale ($> 10^{15}$ GeV).

The simultaneous presence of such a large mass scale and of fundamental

*Also known as BEGH²K bosons or "Higgs" bosons.

light scalars leads to some difficulties in perturbation theory, where quadratic divergences appear which destroy the initially assumed potential. Formally there is nothing here which cannot be blamed on the perturbation expansion or cured by an appropriate order by order renormalization.

However, the very fact that the low energy theory is so sensitive to minute fluctuations of the couplings associated with the high energy structure is disturbing in itself, and may prove a real problem when gravity is eventually coupled to the model. This is usually referred to as the "hierarchy" problem. Supersymmetry can cure this difficulty: adding up fermionic and bosonic contributions kills the troubling quadratic divergencies. If the effective breaking of SUSY appears at some scale μ , one expects then the corrections to the Higgs masses squared to be of $O(\alpha_{\mu}^2)$. Asking that such corrections be no larger than the typical v.e.v.'s then gives some estimate of the expected scale, $\mu \sim 300\text{GeV}/\sqrt{\alpha}$ -in other words, and depending upon which amount of tuning is judged acceptable, $\mu \sim$ several TeV's.

There are other, more theoretical justifications for the extension of the present models to SUSY, such as the unification of gravity in the framework of supersymmetry, or the desire to build a perturbatively finite model. These do not demand in any way that SUSY be broken at low energy, and the scale of the breaking is anybody's guess.

In practice, we must thus accept that extending the "standard model" to supersymmetry involves the association of at least one unobserved SUSY-partner to each known particle. The separation in mass between SUSY partners may be expected to be of the same order as the effective SUSY-breaking scale which is only limited in practice by our desire to avoid the "hierarchy" problem. The following abbreviations will be used.

Particle	SUSY Partner	
	<u>Scalars</u>	<u>Spinors</u>
e_L	S. electron \tilde{e}_L	
e_R		\tilde{e}_R
ν_L	S. neutrino $\tilde{\nu}_L$	
w^μ		\tilde{w} wino
B^μ		\tilde{B} bino
H		\tilde{h} higgino
g^μ		\tilde{g} gluino

Although the couplings of those SUSY partners are similar to the corresponding vertices in the standard model, they can escape detection, due to their mass and the fact that they need to be pair produced [this latter feature, while usually implemented in models suffers some exceptions, see below].

In the following sections we will

- quickly review the existing patterns of SUSY breaking, and some of their phenomenological implications.
- present the framework for finite, $N=2$, softly broken SUSY models.

2. Softly Broken SUSY.

Since the anticommutator of the SUSY charges is related to the 4-momentum the supersymmetric vacuum if it exists, has automatically the lowest possible energy:

$$\{Q_\alpha, \bar{Q}_\beta\} = 2\sigma_{\alpha\beta}^\mu p^\mu \quad (1)$$

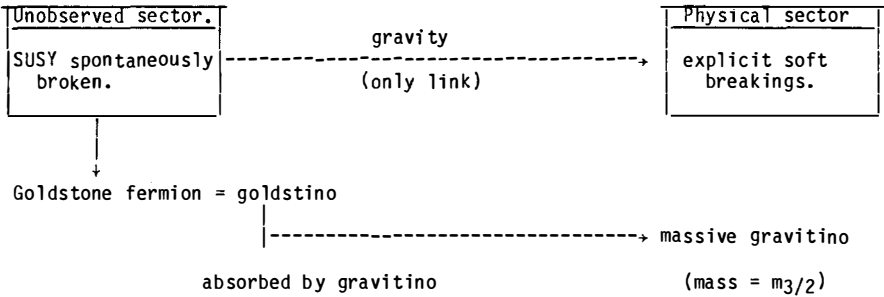
In order to break SUSY spontaneously one is led to look for situations where no possible SUSY vacuum exists. Such models, although somewhat difficult to build are possible²⁾. They require

either the introduction of extra scalar multiplets or of an extra $U(1)$ gauge group. The phenomenological consequences of earlier versions of these models have been reviewed, e.g., in ref.3; some significant progress has been made recently in models using the extra $U(1)$ ⁴⁾. The main problem of that extra gauge symmetry consisted in the presence of anomalies, which can be removed at the cost of parity doubling; it is interesting to note that this operation can lead quite naturally to $N=2$ theories.

An obviously easier solution consists in the explicit breaking of supersymmetry. Of course, introducing explicit breakings by hand cannot be a fundamental solution to the problem. A suitable set of breaking parameters which do not reintroduce quadratic divergences, could, however, constitute a technical solution to the "hierarchy" problem. Such terms, usually referred to as "soft breaking" terms have been enumerated in ref.5 -they involve mass terms for the scalar partners of quarks and leptons, or even for the fermionic partners of gauge bosons (gauginos).

This "technical" solution happily received some comfort from the consideration of local SUSY models (including gravity). These models are considered at the lowest order in the gravitational interaction, and provide an effective Lagrangian for low-energy supersymmetry⁶⁾.

Of course, even in the presence of gravity, some SUSY-breaking mechanism is still needed, and can be implemented by the use of a "hidden sector," where one of the usual²⁾ spontaneous symmetry breaking schemes is used. Since that "hidden" sector is only coupled to ordinary matter via gravity, the news of SUSY breaking is transferred to the visible sector in a perfectly universal way (irrespective of colour, flavour ...)



As a consequence of this universal character of the relations between the hidden and the observed sector, the effective SUSY breaking parameters depend only upon the spin of the particles.

As a typical example, we have:

$$\begin{aligned}
 \mathcal{L}_{\text{broken}} = & \mathcal{L}_{\text{global SUSY}} - m_{3/2}^2 A_i^+ A_i - B m_{3/2}^2 \sum m_{ij} A_i A_j \\
 & - A m_{3/2}^2 \sum g_{ijk} A_i A_j A_k
 \end{aligned}
 \tag{2}$$

where A_i are the scalar components of the various superfields (e.g., higgs scalar, scalar neutrino, scalar quarks), while m_{ij} and g_{ijk} are respectively the ordinary mass terms and Yukawa couplings. A and B are in principle calculable constants, but model dependent. This scheme, with the justification arising from Supergravity itself seems both simple and predictive, in view of the few parameters involved.

At first sight, it could be applied as such, using the bilinear coupling to induce gauge symmetry breaking without putting any mass scale by hand, $m_{3/2}$ being then the only dimensional parameter. It is not difficult however to check that such a scheme, which would indeed break the gauge symmetry is unacceptable phenomenologically, as it would lead, e.g., to the non-conservation of electric charge⁷⁾. Other less restrictive models are however possible³⁾.

Alternative mechanisms have been suggested, which assume that the

coefficient of the trilinear term is small enough that it does not play an important role in the symmetry breaking process.

While it would be impossible to give a negative mass to all the scalars without making the potential unbounded from below, it is conceivable that radiative corrections push one of these masses down, thereby allowing the familiar gauge symmetry breaking mechanism to take place. The leading logarithm corrections to the n point vertices associated to (2) can be evaluated by a renormalization group -improved calculation based on the relevant 1-loop diagrams.

When it comes to writing the corresponding renormalized Lagrangian, one is obviously free to choose the most convenient renormalization point -the one which minimizes further radiative corrections. Since we want to use a grand unified theory, it is natural to use the "grand unification scale" as a subtraction point, and to impose the values of the soft breaking terms at that scale. This defines the theory once and for all.

This choice of renormalization constants guarantees that, e.g., the 3-point function associated to $\tilde{e}_R \tilde{H}_L$ has value $m_{3/2} A.g_e$ when evaluated at a momentum transfer $-p^2 = \mu_{GUT}^2$. This, however, does not tell us directly what the value of that function is for low energy scattering! This value can be computed by summing the perturbation series, according to the renormalization procedure presented above. Alternatively, one may find it convenient to rewrite the Lagrangian in terms of another subtraction point, using the renormalization group equations, so as to minimize the value of further radiative corrections evaluated at low energy. The same is true for the coefficient of, say, H^+H in (2). While its value is fixed to $+m_{3/2}^2$ when the theory is renormalized at the GUT scale, this does not imply that the vacuum is stable. One possible test for the stability of the vacuum is the presence of Tachyons: the low-energy behavior of the 2 point function associated to H^+H must, therefore, be calculated by summing the corresponding diagrams at low energy. In other terms, the renormalized Lagrangian does not tell us the whole story without calculation, and what matters is in fact

the effective potential. While the two subtraction points lead to strictly equivalent theories, according to a re-parameterization associated to the renormalization group equations, one minimizes the radiative corrections at high energies and is, therefore, useful in establishing symmetrical boundary conditions, while the other, which minimizes the radiative corrections at low energy, is closer to the effective potential, and therefore indicative of the (in)stability of the trivial vacuum.

The renormalization group equations for the various parameters appearing in (2) are at present well-known. We list the most relevant ones, following the notations of ref.9b) (G is the Higgs doublet coupled to u_R , H is coupled to d_R)

$$4\pi^2 \frac{dM_G^2}{d\ln\Lambda} = 6[M_G^2 \text{Tr}\lambda_u\lambda_u^\dagger + \text{Tr}\lambda_u M_Q^2 \lambda_u^\dagger + \text{Tr}\lambda_u^\dagger M_u^2 \lambda_u + \text{Tr}\eta_u^\dagger \eta_u] - 8 \sum_{\alpha=1,2} C_\alpha(G) \mu_\alpha^2 g_\alpha^2 \quad (3.a)$$

$$4\pi^2 \frac{dM_Q^2}{d\ln\Lambda} = 2\left[\frac{1}{2}\{\lambda_u^\dagger \lambda_u + \lambda_D^\dagger \lambda_D, M_Q^2\} + M_G^2 \text{Tr}\lambda_u\lambda_u^\dagger + M_H^2 \text{Tr}\lambda_D\lambda_D^\dagger + \lambda_u^\dagger M_u^2 \lambda_u + \lambda_D^\dagger M_D^2 \lambda_D + \eta_u^\dagger \eta_u + \eta_D^\dagger \eta_D\right] - 8 \sum_{\alpha=1,2,3} C_\alpha(Q) \mu_\alpha^2 g_\alpha^2 \quad (3.b)$$

$$4\pi^2 \frac{dM_L^2}{d\ln\Lambda} = 2\left[\frac{1}{2}\{\lambda_L^\dagger \lambda_L, M_L^2\} + M_H^2 \text{Tr}\lambda_L\lambda_L^\dagger + \lambda_L^\dagger M_L^2 \lambda_L + \eta_L^\dagger \eta_L\right] - 8 \sum_{\alpha=1,2} C_\alpha(L) \mu_\alpha^2 g_\alpha^2 \quad (3.c)$$

$$4\pi^2 \frac{d\eta_u}{d\ln\Lambda} = \eta_u [5\lambda_u^\dagger \lambda_u + 3\text{Tr}\lambda_u\lambda_u^\dagger + \lambda_D^\dagger \lambda_D - 2C_\alpha^W g_\alpha^2] + 2\lambda_u [2\lambda_u^\dagger \eta_u + 3\text{Tr}\eta_u\lambda_u^\dagger + \lambda_D^\dagger \eta_D + 2C_\alpha^U \mu_\alpha g_\alpha^2] \quad (3.d)$$

$$4\pi^2 \frac{d\lambda}{d\ln\Lambda} = \lambda_u [3(\lambda_u^\dagger \lambda_u + \text{Tr}\lambda_u\lambda_u^\dagger) + \lambda_D^\dagger \lambda_D - 2C_\alpha^U g_\alpha^2] \quad (3.e)$$

where Q, L represent quarks and lepton doublets, λ_U, λ_D are the Yukawa couplings which provide the quark masses and mixing angles, η_U is the coefficient of the trilinear coupling $\bar{u}_R G \tilde{q}_L$, and obeys $\eta_U = A m_{3/2} \lambda_U$ at the G.U. scale. $C_\alpha(X)$ are the Casimir coefficients for the representation X of the gauge subgroup $SU(\alpha)$ (the charges squared for $\alpha=1$); G is the "Higgs" field coupled to the up quarks. [M_Q^2, λ_U, \dots are matrices in generation space]. $C_\alpha^2 = C_\alpha(Q) + C_\alpha(U) + C_\alpha(G)$; $C_\alpha^d = C_\alpha(Q) + C_\alpha(D) + C_\alpha(H)$. It is easy to check from eq.(3) that the mass of the scalar fields is "pushed" down by the Yukawa couplings when A decreases. On the other hand, gaugino masses μ seem to increase M_G^2 . As a result we expect that the particle with the largest Yukawa couplings and the smallest gauge couplings will be the first to develop a negative "mass" term. This points immediately to the Higgs field coupled to the top quark, whose Yukawa couplings are further enhanced by a color factor which the top s-quark does not enjoy. Furthermore, the top squark is protected by its gauge interaction if the gaugino masses turn out to be large.

This far the model seems to remain quite predictive, since eq.(3) only depends on the physical Yukawa couplings and on the parameters $A, B, m_{3/2}$ appearing in (2). (no gaugino mass is present in (2).) Several models have been suggested along this line, usually requesting a fairly heavy top quark.

It should be remarked, however, that the hypothesis of vanishing gaugino masses is not justified. It is indeed simple to check that (2) generates such masses at the one-loop level; furthermore, they become logarithmically divergent at the 2-loop level,⁷⁾ which imposes some renormalization. It is therefore fair to say that the gaugino masses μ_α appearing in (3) should be treated as arbitrary parameters; the number of those parameters being only reduced by the requirement of grand unification. (see ref.10)

As a consequence of this, the various models become almost unconstrained, with predicted gluino and top masses varying between 0 and 200 GeV (see e.g., ref.11). The reason why the solution of eq.(3) is so sensitive to gaugino masses (more specifically gluino masses) is somewhat indirect: while μ_3 does not appear in (3.a), it enters in (3.6) where it pushes up the s-quark masses, which in turn enter (3.a) to push down M_G^2 .

Lepton Number Violation

We will have more to extract from equations (3), specially when we will deal with quark mixings. One intriguing possibility deserves to be examined; namely, the question of lepton number conservation.

As is well-known the scalar partners of the lepton doublets have the same quantum numbers under $SU(3) \times SU(2) \times SU(1)$ or $SU(5)$ as the "higgs" bosons. For this reason, some discrete symmetry is used to avoid explicit non-conservation of lepton number at the Lagrangian level (one can e.g. require invariance under a transformation where all lepton fields change sign, while "higgses" stay unchanged). Such a symmetry is usually implemented as part of the susy R. symmetry [it is interesting to note that such precautions are unnecessary in other gauge groups, like $SO(10)$ where Higgses and leptons occur in different representations].

Even if the bare Lagrangian conserves lepton number, the possibility still exists that spontaneous symmetry breakdown violates it. This can indeed be the case in the present approach: there is a zero direction of the quadratic term of the potential corresponding to $\langle L^0 \rangle^2 = \langle G^0 \rangle^2 - \langle H^0 \rangle^2$; the issue of spontaneous lepton number violation then depends on the evolution of the scalar masses, according to eq.(3). The situation has been studied in detail in ref.12, which showed that a necessary condition would be $m_t > 5m_{\tilde{L}}$.

In view of the present limits on $m_{\tilde{L}}$ this seems unlikely; it should nevertheless, be kept in mind that most limits are still conditional, and that, on the other hand, the presence of a 4th generation could satisfy these

bounds. It is interesting to mention some of the particular consequences of such lepton number violations.

First, if the violation is indeed spontaneous, a Goldstone boson - the Majoron - is expected to appear¹³⁾. This causes some trouble with the stability of red giant stars, but can be avoided at the cost of an explicit breaking of lepton numbers, which is easily realized by introducing right-handed neutrinos and Majorana masses (the phenomenological consequences of such breaking can be minimized by the use of large Majorana masses and small couplings between left and right handed neutrinos). More interestingly, $\langle \tilde{\nu}_\tau \rangle$ would mix wino's and leptons, leading to neutrino masses, departures from lepton universality and, last but not least, production of odd numbers of supersymmetric partners¹⁴⁾.

Looking for Sypersymmetry.

With the exception of an (unlikely) violation of lepton number, the yet unseen spectrum of the above models consists at least, in heavy scalar leptons and quarks (left and right handed partners slightly mixed), heavy gluinos, two Dirac Fermions made out of the 4 Weyl spinors ($\tilde{w}^+, \tilde{w}^-, \tilde{h}^+, \tilde{h}^-$), and 4 Majorana spinors which are linear combinations of ($\tilde{w}^0, \tilde{b}^0, \tilde{h}^0, \tilde{h}^0$). We will use ($\tilde{\gamma}_1 \dots \tilde{\gamma}_4$) to label those neutral mass eigenstates. In any case, there is no fundamental reason why any of these particles should be light; their masses are related to the effective scale of SUSY breaking, which can be several TeV's. This is essential to keep in mind when experimental data are examined, as should be remembered that only correlated limits can be given (see an example below).

Not only can the masses be large, but the actual eigenstates depend strongly on the type of model chosen. For a discussion of the gaugino masses and mixing, see e.g., ref.15. In two extreme cases, we may form Dirac spinors out of (\tilde{w}^-, \tilde{w}^+) and (\tilde{h}^-, \tilde{h}^+) on one hand, or (\tilde{w}^-, \tilde{h}^+) and (\tilde{h}^-, \tilde{w}^+) on the other hand. The first case provides for a vectorlike theory (no forward-backward asymmetry in the production), with the first fermion more

strongly coupled to W and Z than the second, while the other case provides for 2 particles with similar couplings to W, Z and a forward-backward asymmetry in e^+e^- production somewhat smaller than a standard lepton pair. These particles will decay into standard leptons or quarks, plus some neutral "photino" ($\tilde{\gamma}_1, \dots, \tilde{\gamma}_4$). Since the neutral particle is massive, less energy will be available for the outgoing leptons (hadrons) than in a typical lepton sequential decay, which may hamper their detection.

Flavour Changing Transitions and CP Violation

Since susy particles are assumed to be produced in pairs, the simplest process where to look for them is where 0 pairs are produced. It is readily apparent from (2) and (3) that the scalar quarks will not be mass degenerate; therefore, they can mediate flavor changing transitions.¹⁶⁾ Contributions to the $K^0\bar{K}^0$ mass differences and CP violation parameters arise, e.g., from the graphs



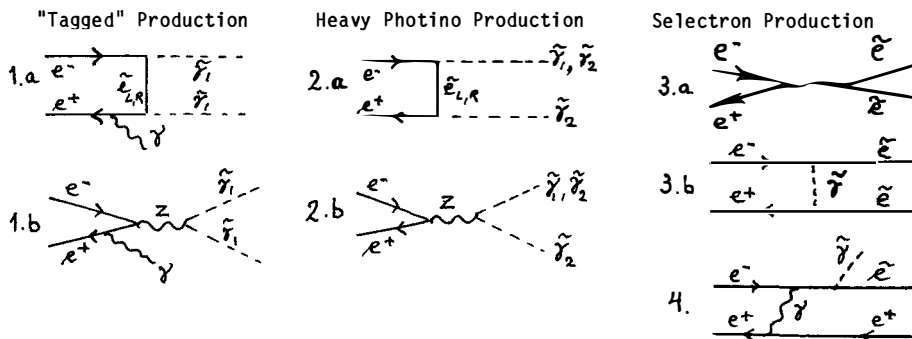
The scalar quarks and the quarks themselves cannot in general be diagonalized simultaneously, and more mixing parameters should thus be introduced. Ref.9 has shown that only mild constraints on the squark masses can be extracted from the $K\bar{K}$ mass difference.

As far as the CP violation parameters are concerned, only simplified cases have been considered so far, where the squark mixing was identified to the usual Kobayashi-Mashkawa matrix, and the extra phases associated with SUSY¹⁸⁾ have been neglected. It is noteworthy that already in this approximation¹⁹⁾²⁰⁾, the squarks/gluino contribution can flip the sign of ϵ'/ϵ with respect to the standard model; small or negative values can be fitted. The low experimental value quoted for ϵ'/ϵ (these proceedings)

could be the only experimental hint in favor of supersymmetry. However, the uncertainties associated with the prediction of ϵ'/ϵ in the standard model do not allow such a conclusion; also, several other schemes could account for the value of ϵ'/ϵ (e.g., L.R. models).

SUSY Pair Production

This has certainly been the most investigated topic in SUSY searches. For a general review, see e.g. ref.21. The associated production of gluinos and/or squarks will be dealt with in great detail by M. Barnett (these proceedings), in order to illustrate the difficulty to give model-independent limits I will focus on the simplest possible system of SUSY particles, and deal with scalar electrons \tilde{e}_L, \tilde{e}_R and neutralinos $\tilde{\gamma}_1 \dots \tilde{\gamma}_4$ (all neutral SUSY fermions are denoted $\tilde{\gamma}$ below; the index refers to the mass, $\tilde{\gamma}_1$ being the lightest; while $\tilde{\gamma}_1$ is often assumed to be "the" photino, there is no compulsory reason for this). Several processes have been suggested to observe those particles²²). The following graphs summarize them:



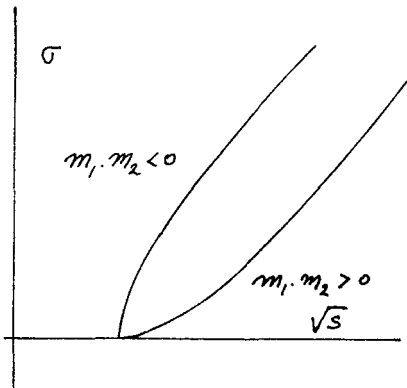
Which of these processes is most favorable for observation depends strongly on the model. In the case of photino production, \tilde{e} exchange (1, a, 2, a) is important; if $\tilde{\gamma}_1$ is a higgsino these graphs are negligible. On the other hand 1b vanishes for a pure photino but not for a higgsino. The processes described in 1 are further suppressed by the electromagnetic coupling;

therefore, the processes in (2) (where $\tilde{\gamma}_1 \rightarrow \tilde{\gamma}_2 + \text{quarks, or leptons and } \tilde{\gamma}_1$ escapes, which gives a "one sided event") can be competitive if $m_{\tilde{\gamma}_1} + m_{\tilde{\gamma}_2} < \sqrt{s}$ and the mixing is not negligible, or if $2m_{\tilde{\gamma}_2} < \sqrt{s}$. The relative interest of (3) and (4) depends upon the ratio $m_{\tilde{\gamma}}/m_{\tilde{e}}$, but also on the nature of the involved photino, since a higgsino would be very lightly coupled.

Experimental bounds will be presented by several groups at this meeting (see e.g., talks by Bohn, Hollebeek, Prepost). While the experimental results are usually formulated in terms of massless photinos, degenerate scalar electrons, and assume no mixing, this should be considered a convenient way of presenting the data rather than a real discussion of the excluded region in parameter space. Such an enterprise, as we have tried to show, would involve dealing with at least a 4 or 5 parameter space and seems somewhat premature at the present stage.

More subtle differences may arise; e.g., in the "one-sided" process (2), the threshold for $\tilde{\gamma}_2 \rightarrow \tilde{\gamma}_2 + \tilde{\gamma}_2$ is always P-wave while, if $\tilde{\gamma}_1 \rightarrow \tilde{\gamma}_2$ are produced, the nature of the threshold behavior depends upon the relative sign of their Majorana masses. Intermediary situations are possible if CP is violated²³). These peculiarities of Majorana particles, while a potential challenge for experimentalists, would be very interesting to observe.

As a conclusion for this section, possible SUSY signatures are many, but no one can be pointed at as the crucial test; due to the high value of the permitted SUSY effective breaking scale, negative searches even conducted at the next generation of accelerators would not completely exclude the existence of SUSY partners. But a positive evidence for SUSY may appear every day.



3. Finite Models[†]

The infinities related to the perturbative expansion of gauge theories are adequately dealt with by the renormalization procedure. As we have seen when dealing with the "hierarchy" problem this, however, mixes the various scales of the model and often results in the introduction of more phenomenological parameters.

It has been shown recently²⁴⁾ that a large class of finite theories could be built. They rest on the $N = 2$ extension of supersymmetry²⁵⁾ (hypersymmetry), and are fairly restrictive in terms of the particle contents and couplings. The basic structure of such a theory contains the following physical fields:

	vectors	spinors	scalars	group representation
gauge multiplet	V^μ	λ_1	M	adjoint
		λ_2		
scalar multiplet		ψ_1^i	A_1^i	r
(i)		ψ_2^i	A_2^i	\bar{r}

With respect to $N = 1$ SUSY, the number of fermions for each multiplet is doubled; for each scalar multiplet, ψ_1^i and ψ_2^i are left handed fermions transforming respectively under the representation r and \bar{r} of the gauge group \mathcal{G} . The "gauge scalar" M transforms according to the adjoint representation of \mathcal{G} . The Lagrangian of such theories is severely constrained. Let us first mention the finiteness condition which states the vanishing of the 1-loop β function:

$$\sum_i n_{R_i} C_2(R_i) = n_{\text{adj}} C_2(\text{adj}) \quad (4)$$

[†]This work was done in collaboration with Y.-P. Yao

where n and C_2 respectively stand for the dimension and Casimir coefficient of the representation. As we will see below, this condition strongly limits the number of possible matter representations for a given group (SU(5) is excluded).

The only Yukawa couplings permitted are determined by the gauge interaction²⁶⁾ and read

$$-ig\sqrt{2}(\bar{\lambda}_2\bar{\lambda}_1^M + \bar{\psi}_1^i\bar{\lambda}_1\psi_1^i + \bar{\lambda}_2^i\lambda_2\psi_1^i + \psi_2^M\psi_1^i - A_2^M\lambda_1\bar{\psi}_2^M) + \text{h.c.} \quad (5)$$

(notice that λ_1 acts diagonally on the indices 1,2, while M and λ_2 mix fermions carrying the index 1 with their "mirror partner" carrying index 2.) An explicit mass term for the matter fields is also allowed for each multiplet i :

$$+ m_i\psi_2^i\psi_1^i \quad (6)$$

This far we have only dealt with unbroken $N = 2$ SUSY. As was the case with $N = 1$, we may now ask what are this time the "soft breaking terms," which, while breaking SUSY, preserve finiteness.

This question has been dealt with for various groups^{27),28)}. Are these soft breaking terms sufficiently general to allow a realistic breaking pattern for the gauge group? Can they also help us get rid of the unobserved mirror symmetry implied by $N = 2$?

We will consider here the special case where the soft breakings are diagonal in the matter representations (full expressions can be found in ref.28). In addition to $N = 1$ terms, we may introduce:

$$\delta m_M^2 MM^+ + \delta m_{1\ell}^2 |A^1|^2 + \delta m_{2\ell}^2 (A^2)^2 \quad (7.a)$$

$$m_M^{12} M^2 + \text{h.c.} \quad (7.b)$$

$$\delta m_{ij}^2 A_m^i U A_n^j \quad (7.c)$$

$$\frac{i}{2} \delta p_{ij}^p A_m^+{}^i M A_n^j - \frac{1}{2} m_{ij}{}^\lambda A_m^i \lambda^j + \text{h.c.} \quad (7.d)$$

where $A^i U A^j$ is only permitted for real or pseudoreal representations, and U is the matrix which projects out the singlet out of $A \otimes A$ (e.g., ϵ_{kl} in the case of $SU(2)$). The Majorana-like terms (7.b) and (7.c) appear totally unrestricted by perturbative finiteness, while the terms (4.a) and (4.d) have to obey:

$$\delta m_M^2 - \frac{1}{n} [(\delta m_1^2)_{\ell}^{\ell} + (\delta m_2^2)_{\ell}^{\ell}] = m_{ij} \bar{m}^{ij} \quad (8.a)$$

$$(\delta m_1^2 + \delta m_2^2)_{\ell}^{\ell'} = \frac{1}{n} (\delta m_1^2 + \delta m_2^2)_k^k \delta_{\ell\ell'} \quad (8.b)$$

$$\delta P_{ij}^{mn} = -2\sqrt{2} m_{ij} g \delta_{mn} \quad (8.c)$$

where n is the number of matter representations. As appears readily from (7) and (8), the mirror symmetry which relates A_1 and A_2 in \mathcal{L} can be easily broken by choosing $\delta m_1^2 \neq \delta m_2^2$, since only the sum of those quantities is fixed for each matter representation by (8.a).

This breaking of the $1 \rightarrow 2$ symmetry only applies this far to the bosonic sector, and the real concern we have is about the fermionic sector. Before dealing with this we should attract attention to the fact that, while conditions (8) guarantee the perturbative finiteness of the theory, they say nothing of the stability of the vacuum. Introducing negative mass terms, as is customary in spontaneously broken gauge theories may prove dangerous. The danger is quite general in view of the existence of numerous flat directions in the quadratic part of the potential, leading to unboundedness from below. While a general study seems extremely difficult, a few interesting no-go theorems can be found in ref.28. There is, however, a breaking mechanism which is safe with respect to those flat directions. Indeed, the quartic potential has no flat direction where $\langle MA \rangle$ is vanishing, which is also the condition for a (negative) contribution to arise from the trilinear terms. It is easy to check (27) that such a breaking is indeed both safe and possible.

Which Group?

A general review of the possible grand unification groups can be found in ref.29. An interesting mechanism for the breaking of mirror symmetry has been suggested recently³⁰⁾ but unfortunately not in the framework of a grand unified theory—and such a theory is essential to ensure finiteness, since small groups and a fortiori U(1) factors cannot satisfy eq.(4), which has to be true for each factor group.

This is a biased review of groups suitable for the construction of a grand unified finite model. The bias comes from the fact that we give special importance to the breaking scheme in which the trilinear coupling plays a central role, as exemplified in the previous section. In general, both the adjoint and at least one matter representation will then develop v.e.v.'s $\langle M \rangle$ and $\langle A_1 \rangle$ respectively.

As a consequence of the presence of the only allowed Yukawa coupling, $g\psi_2^{\lambda M}\psi_1^{\lambda}$, "Dirac" mass terms will be induced, linking $\psi_1^{\lambda\alpha}$ and $\psi_2^{\lambda\alpha}$, where α is an index in group space. Since under the unbroken little group $g_1 \langle M \rangle$ necessarily transforms as a singlet while ψ_1 and ψ_2 transform under reducible conjugate representations R_1 and \bar{R}_1 we would get massive Dirac fermions interacting in a vector-like way with the gauge boson representing g_1 . (This picture would be modified for the "generation" directly linked to $\langle A_1 \rangle$, since we have the further entry $\psi_2^{\lambda\lambda_2}\langle A_1^{\lambda} \rangle + \psi_1^{\lambda}\langle A_1^{+\lambda} \rangle$, but would still obtain for most of the fermions involved).

As a typical example, let us imagine a toy model based on SU(5) [a realistic model is impossible, since all observed particles cannot be included]. The usual breaking along the adjoint (24) leaves SU(3) \times SU(2) \times U(1) invariant; however, it joins the $10 + \bar{10}$, $5 + \bar{5}$ into Dirac fermions; in the 5 representation we have:

$$\psi_2 \psi_1 \langle M \rangle \sim (d \ d \ d \ \bar{e} \ \bar{\nu}) \begin{vmatrix} 2 & & & & \\ & 2 & & & \\ & & 2 & & \\ & & & -3 & \\ & & & & -3 \end{vmatrix} \begin{vmatrix} \bar{d} \\ \bar{d} \\ \bar{d} \\ e \\ \nu \end{vmatrix}$$

This may prove a major drawback in the way to construct models. There are, of course, several ways around. We will list them briefly, and concentrate on the direction which seems most promising.

-If the group G is large enough that the physically interesting particles are not affected by $\langle M \rangle$, one may avoid the above trouble. However, the difficulty will pop up again at the level of the unbroken subgroup g_1 . The breakdown of that group will then have to proceed via the matter representation alone. Such breaking schemes are usually not very promising, however, because the defining representation above breaks $SU(5)$ into $SU(4)$, $SU(3)$, $SU(2)$... assuming that enough independent sets of scalars are available.

Notice, however, that for each matter representation, one subset of the particles appearing in (9) can be made massless by introducing suitable mass for the matter multiplet, resulting here in a cancellation between (6) and (9) for either the "quarks" or "leptons". This means that in such a scheme, physical leptons and quarks cannot be found in the same multiplet (as a very long shot, this can be seen as an argument for an extended proton lifetime). -By adjusting m_1^2 , m_2^2 , δm^2 in eq.(1.4) one can tune the ratio $\langle M \rangle / \langle A \rangle$; if $\langle M \rangle$ is made negligible, one finds directly the above situation, where the matter representations above are to be held responsible for the whole breaking pattern. We must keep in mind, however, that only a very limited set of matter representations is available due to the finiteness conditions.

-A more expedient way would consist in giving ab initio a large (Majorana) mass to the fermions corresponding to, say ψ_2^2 . The presence of $\langle M \rangle$ would then only induce a slight perturbation in the diagonalization of the mass

matrix of $(\psi_1^L, \psi_2^L, \lambda_1, \lambda_2)$, and leave a state close to ψ_1 essentially massless. Such a Majorana mass $\mu \psi_2^L \psi_2^L$ is usually forbidden, for it would break the gauge symmetry. The necessary condition to allow it is obviously that $R \times R \supset \mathbf{1}$, namely that the representation R be real or pseudoreal. Such a mass term is always allowed if included in an $N = 1$ soft term $\phi_1 \lambda U \phi_m$, where ϕ_1 stands for the superfield (A_1, ψ_1, F_1) . This solution seems to be leading from bad to worse! Instead of having a "reality" problem associated to the presence of $R + \bar{R}$ for any representation R in use, we further demand that R itself be (pseudo) real!

The advantage, however, is that such a doubling allows us to completely eliminate \bar{R} from the observable spectrum, and liberates us from the unique but unwanted Yukawa coupling $\psi_1 M \psi_2$. A corollary of this is that the light fermion masses will have to be generated beyond the tree level. The loop diagrams involved may prove considerably less transparent to evaluate; on the other hand, they constitute very "soft" effective mass terms for the fermions, which may be an interesting property.

With the above motivation in mind, we now turn to a list of the groups suitable for grand unification, paying special attention to the real or pseudoreal representations.

For each group, the tables below list the representations which are permitted by the finiteness condition (1.2), their real/complex character, their indices $(-\frac{n_R \cdot C_2(R)}{n_{\text{adj}}})$. We have examined successively the groups* $SU(N)$, $SO(2N)$, $SO(2N=1)$ and the exceptional groups E_7 , E_8 .

While $SO(9)$ comes close to the correct particle content, using the 16 representation, it is known not to have the correct charge assignments (the right-handed leptons transform like doublets under the $SU(2)_{\text{weak}}$ group). We therefore do not consider it here.

	Real Pseudo- Complex	Index	Max Number Allowed		Real Pseudo- Complex	Index	Max Number Allowed
S0(9) (B4)	16 R 9 R 36 adj	4 2 14	3 *		S0(10) (D5)	16 c 10 R 45 adj	4 2 16
S0(11) (B5)	32 P 11 R 55 adj	8 2 18	2		S0(12) (D6)	32 P 12 R 66 adj	8 2 20
S0(13) (B6)	64 P 13 R 78 adj	16 2 22	1		S0(14) (D7)	64 c 14 R 91 adj	16 2 24
S0(15) (B7)	128 R 15 R 105 adj	32 2 26	NO		S0(18) (D8)	128 R 16 R 120 adj	forbidden 2 28
E7	56 R 133 adj	12 36	3		SU(5)	5 C 10 C 24 adj	1 3 10
E8	248	60	(N=4)		SU(6) (A5)	20 R 35 adj	4 12
					SU(8) (A7)	70 R 63 adj	20 16

*wrong particle content

If we insist on having 3 equivalent "generations" included within the matter fields we see that none of the SU or S0 groups can satisfy the finiteness conditions, while retaining an acceptable particle content. (We exclude a priori the real N representations of S0(N), in view of the familiar problems associated with charge-2 exchanges and have not considered here the symplectic groups.) The only groups accepting a triplicate matter generation structure with real or pseudoreal representation are E₇ and E₈. For E₇, taking 3 times the spinorial representation 56 exactly satisfies the finiteness condition: this group, therefore, appears as a very strong candidate. E₈ is a special example; since one cannot distinguish between the gauge and matter fermions, its more natural framework is N=4 supersymmetric theory.

The constraint to have equivalent triplication of the matter generations as a unique solution is obviously very attractive. We may nonetheless think of relaxing it, and take into account the gauge fermions as was done for the

*Same additional solutions can be found in the case of pseudoreal representations for a different realization of $N = 2$ SUSY³¹.

case of E_8 . The smallest group then turns out to be given by $SO(11)$ [as the $\underline{16}$ representation of $SO(10)$ is not real]. (Of course, larger groups than $SO(11)$ may also satisfy our criteria, but we should note that the index of the spinoidal representation grows geometrically, while that of the adjoint only linearly. Therefore, groups larger than $SO(16)$ must be excluded from our analysis.) Focusing on $SO(11)$, we may satisfy the vanishing beta function criteria (1.2) by including $2(32) + 1(11)$ as matter representations. When decomposed under $SU(5)$, this gives:

$$32 = \bar{5} + 10 + 1 + 1 + \overline{10} + 5$$

$$11 = \bar{5} + 5 + 1$$

$$55 = 24 + 1 + 10 + \overline{10} + 5 + 5$$

and we, therefore, obtain the required $3(\bar{5}+10)$ fermionic content. We have checked that a satisfactory breaking pattern down to $SU(5)$ was indeed possible; in view of the many parameters still present, study of the further breaking steps proves difficult.

Acknowledgements

Except for money-related acknowledgements (see page 1), I would like to thank more specially Gordy Kane, Serguey Petcov, Michael Barnett, Charling Tao for discussions. Many thanks to Donna Macey for kindly typing an illegible manuscript.

References

1. See P. Fayet, this meeting.
2. P. Fayet, Phys. Lett. 142B (1984) 263.
3. See for instance, P. Fayet, Proc XXIst Int. High Energy Conf., Paris, July, 1982 and references therein.
4. P. Fayet, Phys. Lett. 142B (1984) 263.
5. L. Girardello and M.T. Grisaru, Nucl. Phys. B 194 (1982) 65.
6. E. Cremmer, B. Julia, J. Scherk, S. Ferrara, L. Girardello and P. Van Nieuwenhuizen, Nucl. Phys. B147 (1979) 105; R. Barbieri, S. Ferrara and C.A. Savoy, Phys. Lett. 119B (1982) 343; E. Cremmer, S. Ferrara, L. Girardello and A. Van Proeyen, Phys. Lett. 116B (1982) 231 Nucl. Phys.

- 8212 (1983) 413; A.H. Chamseddine, R. Arnowitt and Pran Nath, Phys. Rev. Lett. 49 (1982) 970, Phys. Rev. Lett. 50 (1983) 232.
7. J.-M. Frère, D.R.T. Jones and S. Raby, Nucl. Phys. B222 (1983) 11.
 8. See e.g., A.H. Chamseddine, in Proceedings, XIXth Rencontre de Moriond, 1984, p.319 (Tran Thanh Van, editor).
 - 9.a K. Inoue, A. Kakuto, H. Komatsu, S. Takeshita, Progr. Theor. Phys. 68 (1982) 927; erratum 71 (1984) 413.
L.E. Ibanez, Nucl. Phys. 8218 (1983) 514; L. Alvarez-Gaumé, J. Polchinski and M. Wise, Nucl. Phys. 8221 (1983) 495.
 - 9.b. A. Bouquet, J. Kaplan and C.A. Savoy, On Flavor Mixing... Preprint LPTHE 84.25, Paris VII.
 10. J. Ellis, A.B. Lahanas, D.V. Nanopoulos and K. Tamvakis, Phys. Lett. 134B (1984) 429; J. Ellis, C. Kounnas, D.V. Nanopoulos, Nucl. Phys. B241 (1984) 406; Nucl. Phys. 8247 (1984) 373; Phys. Lett. 1438 (1984) 410; J. Ellis, K. Enquist, D.V. Nanopoulos, Phys. Lett. 147B (1984) 99; C. Kounnas and M. Quiros, Phys. Lett. 151B (1985) 189.
 11. H.P. Nilles Proceedings XIXth Rencontre de Moriond, 1984, p. 303.
 12. B. Gato, J. Leon, J. Perez-Mercader and M. Quiros, "Is Spontaneous Breaking of R Parity Feasible...", Madrid Preprint IEM HE-5 (1984).
 13. C.S. Aulakh and R.N. Mohapatra, Phys. Lett. 1198 (1982) 136.
 14. J. Ellis, G. Gelmini, C. Jarlskog, G.G. Ross and J.W.F. Valle, Phys. Lett. 1508 (1985) 142.
 15. J.-M. Frère and G.L. Kane, Nucl. Phys. 8223 (1983) 331; J.-M. Frère, Proceedings XIXth Rencontre de Moriond, 1984, p.291.
 16. M.J. Duncan, Proceedings XIXth Rencontre de Moriond, 1984, and ref. therein; M.J. Duncan, Phys. Rev. D31 (1985) 1139.
 17. M. Dugan, B. Grinstein and L. Hall, Harvard preprint HUTP 84/A023.
 18. F. del Aguila, M.B. Gavela, J.A. Grifols, A. Mendez, Phys. Lett 1268 (1983) 71; J. Ellis, S. Ferrara and D. Nanopoulos, Phys. Lett. 114B (1982) 231; W. Buchmuller and D. Wyler, Phys. Lett. 121B (1983) 321; S.P. Chia and S. Nandi, Phys. Lett. 121B (1983) 321; J. Polchinski and M. Wise, Phys. Lett. 1258 (1983) 393.
 19. P. Langacker and B. Sathiapalan, Phys. Lett. 1448 (1984) 401.
 20. J.M. Gerard, W. Grimus, A. Raychandhuri, G. Zoupanos, Phys. Lett. 1408 (1984) 349.
 21. H. Haber and G.L. Kane, Physics Reports 117 (1983) 75.

22. M.K. Gaillard, L. Hall and I Hinchliffe, Phys. Lett. 1168 (1982) 279; F. Kobayaski and M. Kuroda, Phys. Lett. 1348 (1984) 271; P. Fayet, Phys. Lett. 1178 (1982) 460; J. A. Grifols, X. Mor-Mur and J. Sola, Phys. Lett. 1148 (1982) 35; J. Ellis, J.-M. Frère, J. Hagelin, G.L. Kane and S.T. Petcov, Phys. Lett. 1328 (1983) 436.
23. S.T. Petcov, private communication.
24. P. Howe, K. Stelle, P. West, Phys. Lett. 1248 (1983) 55; M.T. Grisaru and W. Siegel, Nucl. Phys. 8210 (1982) 292; P.S. Howe, K. S. Stelle and P.K. Townsend, Nucl. Phys. 8236 (1984) 125.
25. For more details on $N = 2$, see P. Fayet, these proceedings.
26. L. Mezincescu and Y.P. Yao, Nucl. Phys. 8241 (1984) 605; G. Sierra and P.K. Townsend, Nucl. Phys. 8233 (1984) 289.
27. A. Parkes and P. West, Phys. Lett. 1278 (1983) 353; J.-M. Frère, L. Mezincescu and Y.P. Yao, Phys. Rev. D29 (1984) 1196.
28. J.-M. Frère, L. Mezincescu and Y.P. Yao, Phys. Rev. D30 (1984) 2238.
29. S. Kalara, D. Chang, R.N. Mohapatra, A. Gangopadhyaya, Phys. Lett. 1458 (1984) 323.
30. F. del Aguila, M. Dugan, B. Grinstein, L. Hall, G.G. Ross and P. West, Harvard Preprint HUTP 84/A001.
31. J.P. Derendinger, S. Ferrara and A. Masiero, Phys. Lett. 1438 (1984) 133.

PARTICLE SEARCHES AT PEP

Richard Prepost

Department of Physics, University of Wisconsin, Madison, Wisconsin, U.S.A.



Abstract

The status of the search for new particles at the PEP storage ring is reviewed. The results of searches for supersymmetric particles by the MAC and MARK II groups are presented and mass limits are given. The HRS, MAC, and MARK II limits for monojet production are given and the results are interpreted in terms of limits on Higgs particle and heavy neutral lepton production.

INTRODUCTION

The status of particle searches at the PEP storage ring is reviewed. The searches that will be discussed are the MAC and MARK II searches for supersymmetric particles and the HRS, MAC, and MARK II searches for monojet events. The searches for supersymmetric particle production are of two kinds. Both MAC and MARK II have made a search based on single electron spectra which is a search for real selectron production. Results based on these searches have been previously published and the most recent results are presented. The MAC search for photino pair production based on single photon spectra is reviewed and the most recent results are presented. Photino pair production proceeds through selectron exchange and therefore the results are sensitive to selectron as well as photino masses.

New searches for monojet production by the HRS, MAC, and MARK II groups are then described. The wide interest in the UA1 monojet events has led to various speculations for an explanation. It has been proposed that the monojet events may arise from Z^0 decay into a pair of Higgs particles, one of which decays into a jet while the other lighter one escapes undetected. The electron positron colliders at present energies while not yet capable of making real Z^0 particles nevertheless can have reactions that are energetically allowed proceed through virtual Z^0 production. Since the CERN monojet events have a relatively light mass, the PEP and PETRA colliders are sensitive to such Z^0 processes. The PEP results of this search for monojet like events is described, and the results are interpreted in terms of limits on Higgs particle masses and also, for the MAC case, as a limit on the production of heavy neutral leptons.

SEARCHES FOR SUPERSYMMETRIC PARTICLES

1) Introduction

The searches for supersymmetric particle production at PEP which will be reported here are based on the study of single electron and single photon spectra. The reactions which have been studied are: (1) $e^+e^- \rightarrow e^\pm \tilde{e}^\mp \tilde{\gamma} \rightarrow e^\mp$ and (2) $e^+e^- \rightarrow \tilde{\gamma} \tilde{\gamma} \gamma \rightarrow \gamma$. The searches involve triggering the detector on either a single electron or a single photon. Reaction 1 is a process for the production of a real single selectron and hence is limited to $m_{\tilde{e}} \leq \sqrt{s}$. Reaction 2, on the other hand, is the radiative production of a real photino pair via selectron exchange and hence sets bounds on combinations of the selectron and photino masses. However, for the special case of massless photinos, the limit on the selectron mass is limited only by backgrounds and luminosity and not by the beam energy.

2) Single \tilde{e} Production

Limits on the selectron mass from reaction 1 result from an analysis which assumes that the $\tilde{\gamma}$ is stable and not seen in the detector. Calculations for this process¹⁾ also show that

the e^\pm which accompanies the \tilde{e} in the final state tends to escape undetected down the beam pipe. The only observed final state particle is then the e^\mp from the \tilde{e}^\mp decay. This electron has high energy $\approx m_{\tilde{e}}/2$ and an almost flat angular distribution. The reaction is sensitive to $m_{\tilde{e}} \leq 2E_{beam}$ depending on the $\tilde{\gamma}$ mass. MAC²⁾ and MARK II³⁾, using this technique, have previously reported lower limits on the \tilde{e} mass of 22.4 and 22.2 GeV/c² respectively, at the 95% confidence level. This report updates the MAC search to a data sample three times larger than previously reported.

Background single electron events can come from $ee\gamma$ final states where only one of the electrons is detected. If the detector is inefficient at detecting particles or has dead regions, this background can be several orders of magnitude larger than the expected signal. However, if the undetected particles are constrained to be at small angles relative to the beam axis then momentum conservation limits the energy distribution of the observed electron. A search region for the single electrons can then be defined so that the $ee\gamma$ background is negligible.

More serious backgrounds result from decays of $\tau\tau$, $\tau\tau\gamma$, and $e\tau\tau$ events in which most of the energy is taken by the neutrinos. If one τ decays to a visible electron and two neutrinos, and the other decays to neutrinos and a soft electron or pion which escapes down the beam pipe, then this event is indistinguishable from the SUSY process. This background has been calculated by Monte Carlo technique.

The results of these searches are interpreted as limits on the mass of the selectron assuming a massless photino, or as correlated limits on the photino and selectron masses. Fig. 1 shows the MARK II result as a contour in photino versus selectron mass for the two cases of degenerate and nondegenerate left and righthanded selectron masses. The 90% confidence level limit for the case of zero photino mass and degenerate right and left handed selectrons is 22 GeV.

The MAC updated result based on a sample of 110 pb⁻¹ gives an upper limit on the single electron cross section in the search region of <0.017 pb at the 90% confidence level. The corresponding mass limit is $m_{\tilde{e}} > 25$ GeV/c² assuming $m_{\tilde{e}_R} = m_{\tilde{e}_L}$. If $m_{\tilde{e}_L} \gg m_{\tilde{e}_R}$ then the lower limit on the lighter \tilde{e} mass is 24 GeV/c². Future increases in the MAC data sample will only marginally improve the \tilde{e} mass limit. Further improvements on the \tilde{e} mass limit will necessarily be made at higher beam energies or with different reactions.

3.) $\tilde{\gamma}$ Pair Production

Reaction 2, $e^+e^- \rightarrow \tilde{\gamma}\tilde{\gamma}\gamma$ involving the detection of a single photon,⁴⁾ requires only that the photino is non interacting in the detector. This reaction also permits $m_{\tilde{\gamma}} = 0$ as a possibility, but in general the mass limits set by the experiment will be a contour with $m_{\tilde{e}}$ and $m_{\tilde{\gamma}}$ as variables. The most recent MAC result for this process is described below.

There are potential backgrounds to the above process from radiative electromagnetic processes where charged particles are produced at angles smaller than the detector acceptance but where the photon is detected. These backgrounds include radiative Bhabha scattering and radiative tau pair production. The process $e^+e^- \rightarrow \gamma\gamma\gamma$ is a potential background if only one of the photons is emitted into the detector acceptance. There can also be single photons resulting from beam gas interactions and beam spill. Finally, the radiative neutrino pair production process $e^+e^- \rightarrow \gamma\nu\bar{\nu}$ is indistinguishable from the $\gamma\tilde{\gamma}\tilde{\gamma}$ process. However it is very desirable to also measure the cross section for this process. The cross section for radiative photino pair production has been calculated by several authors.⁵⁾ The cross section for the MAC acceptance is shown in Fig. 2 for several values of the selectron mass. The radiative neutrino pair production cross section is also shown for comparison.⁶⁾ At PEP energies, photino production is the dominant process for selectron masses less than about $50 \text{ GeV}/c^2$. The experiment is accomplished by defining acceptance criteria for the detected photon and demanding no other activity in the detector. Since the detector acceptance goes to zero below some minimum angle, this condition corresponds to setting a minimum veto angle which in turn corresponds to a minimum E_{\perp} for the detected photon.

The analysis cuts require an electromagnetic shower with $|\cos\theta| < 0.77$ and an energy greater than 1 GeV. Below about 2 GeV the trigger efficiency for single photons begins to fall off. In addition, there can be no charged tracks in the central drift chamber. Further cuts on the electromagnetic shower profile and vertex constraints are also made. These cuts are all tuned experimentally using single electrons and tagged photons from radiative Bhabha scattering.

Two data samples were used for the analysis. For the first data set of 36 pb^{-1} the luminosity and the veto conditions were the same as used for the single \tilde{e} search. The second data set of 80 pb^{-1} was taken after the installation of a special small angle tagging system which covers the region $5^\circ \leq \theta \leq 10^\circ$ with lead-proportional chamber shower counter and lead-scintillator shower counter arrays installed specifically for this experiment. The location of this veto package relative to the main detector is shown in Fig. 3, and the segmentation of the proportional chambers as well as their placement relative to the lead absorber is shown in Fig. 13. The veto calorimeter energy cut was taken to be 0.25 GeV.

The observed E_{\perp} distribution of the detected photons for the case of the larger ($\theta_{veto} \geq 5^\circ$) data sample is shown in Fig. 4 together with the calculated yield from radiative Bhabha scattering. The search regions were taken to be $E_{\perp} > 4.3 \text{ GeV}$ and $E_{\perp} > 3.0 \text{ GeV}$ for the two data samples respectively. The overall trigger and analysis efficiencies for the two samples were approximately 65%. The small angle veto inefficiency was determined to be $\approx 10^{-4}$.

The most important backgrounds were calculated to be: $\nu\bar{\nu}\gamma \approx 0.5$ event, $\tau\bar{\tau}\gamma \approx 0.05$ event, and $e\bar{e}\gamma \approx 0.1$ event. One event from the second data set is observed in the combined search regions at $E_{\perp} = 5.3$ GeV. The observed event, regardless of interpretation, limits the single photon production cross section in the detector acceptance to < 57 fb at the 90% confidence level. This corresponds to a limit of $N_{\nu} < 41$ for the reaction $e^{+}e^{-} \rightarrow \gamma\nu\bar{\nu}$. The calculated cross section for radiative photino pair production has been used to obtain limits for the \tilde{e} and $\tilde{\gamma}$ masses. The result at the 90% confidence level is shown in Fig. 5. For $m_{\tilde{\gamma}} = 0$ and $m_{\tilde{e}_L} = m_{\tilde{e}_R}$, the limit is $m_{\tilde{e}} > 37$ GeV/c². For $m_{\tilde{e}_L} \gg m_{\tilde{e}_R}$, the limit is $m_{\tilde{e}_R} > 30$ GeV/c². These limits are significantly higher than those obtained from searches for either single \tilde{e} production^{2,3)} or $\tilde{e}^{+}\tilde{e}^{-}$ pair production.⁷⁾ The calculation by Ware and Machacek⁸⁾ of the radiative supersymmetric neutrino pair production cross section is used to obtain a limit for the $\tilde{\nu}$ mass. For the range of \tilde{W} masses assumed in this calculation, $20 < m_{\tilde{W}} < 29$ GeV/c², the limit $m_{\tilde{\nu}} > 10$ GeV/c² is obtained at the 90% confidence level.

SEARCH FOR MONOJET PRODUCTION

1) Introduction

The standard electroweak theory has proven very successful in describing present high energy experiments. The discovery of the intermediate vector bosons at the CERN $\bar{p}p$ collider has placed the theory on even more solid ground. On the other hand, the collider experiments have found some classes of anomalous events⁹⁾ which may not fit in the standard model and which have stimulated considerable theoretical speculation.¹⁰⁾ Monojet events are one such class of events. There have been proposed interpretations speculating that the monojets are direct products of Z^0 decay into either new neutral lepton pairs¹¹⁾ or light Higgs particle pairs.¹²⁾ These models also predict an observable rate for monojet production in the currently operating $e^{+}e^{-}$ storage rings via virtual Z^0 production.

2) The Experimental Searches

The search for monojets as a consequence of Z^0 decays is viable at existing $e^{+}e^{-}$ energies since the branching ratio for Z^0 decay into light Higgs particles is about 3%. This implies a yield of about 40 events at $\sqrt{s}=29$ GeV for an integrated luminosity of 200 pb⁻¹. The HRS,¹³⁾ MARK II,¹⁴⁾ and MAC¹⁵⁾ groups have performed such a search. The criteria for these searches is to identify events with missing energy and momentum. This event sample is then examined to determine if conventional backgrounds can account for the events. The search criteria for the three searches are listed in the following table.

	HRS	MARK II	MAC
$\int \mathcal{L} dt$	176 pb ⁻¹	222 pb ⁻¹	238 pb ⁻¹
N _{charged}	≥ 4	≥ 2	≥ 2
p _⊥	≥ 7 GeV/c	≥ 8 GeV/c	≥ 3 GeV/c
cosθ	≤ 0.5	≤ 0.67	≤ 0.8
opposite requirement	no tracks	no tracks	no tracks
efficiency	≈ .3	≈ .3 - .4	≈ .6
Events	1	2	11

Here the quantities p_⊥ and cosθ are defined relative to the thrust axis of the jet and the selection criteria in the above table define the jet. The observed events that result from these selection criteria are then examined further. The E_⊥ of the jets must be sufficiently high to exclude jets that result from the two photon annihilation process e⁺e⁻ → e⁺e⁻X. It is still then possible to observe monojet-like events from tau pair production where one tau decays into a hard jet while the other tau decays such that the neutrino takes away almost all of the visible energy. The experiments must also correct for any lack of a hermetic seal in the direction approximately opposite the direction of the observed jet. The MAC experiment has sufficient sensitivity due to the larger p_⊥ acceptance to expect a background from tau decays. Fig. 6 shows the p_⊥ distribution of the measured events as well as the calculated distribution for tau events for two search regions corresponding to data taken with and without the small angle veto tagging system which was also used for the single photon search. The observed events are seen to be completely consistent with the tau decay hypothesis. The observed events also have the characteristic low multiplicity of tau decays, specifically no events were found with five or more charged particles.

Upper limits at the 90% confidence level for monojet production have been calculated from the combined data samples by subtracting the calculated tau backgrounds. The detection efficiencies used in the calculation were determined for the detector and trigger configurations for each data sample assuming the two different monojet production models described below. In order to combine the data samples, an effective detection efficiency was obtained by taking an average of these efficiencies weighted by the integrated luminosity of each data sample.

An interpretation of this cross section limit may be made in terms of virtual Z⁰ production and decay. The total cross section e⁺e⁻ → m₁m₂ may be written:

$$\sigma_{m_1 m_2} = \frac{G_F M_Z \Gamma_Z s}{\sqrt{2}((s - M_Z^2)^2 + M_Z^2 \Gamma_Z^2)} (1 - 4 \sin^2 \theta_W + 8 \sin^4 \theta_W) \cdot BR_{m_1 m_2}$$

where G_F is the Fermi coupling constant, M_Z=92 GeV/c² and Γ_Z=3.0 GeV are the Z⁰ mass

and width, and BR_{m_1, m_2} is the Z^0 branching ratio of the decay responsible for the monojet events.

The upper limit for the branching ratio BR_{m_1, m_2} has been calculated for two cases:

- 1) $m_1 = 0.2 \text{ GeV}/c^2$ and m_2 variable, and
- 2) $m_1 = m_2$ variable.

Case 1 has mass conditions suitable for the Glashow-Manohar model¹²⁾ as a monojet source, namely production of Higgs particles $e^+e^- \rightarrow \chi^0\lambda^0$ followed by $\chi^0 \rightarrow \tau^+\tau^-$ or $c\bar{c}$ decay. The scalar Higgs particle λ^0 has a long lifetime because of its small mass and does not interact in the detector. The mass of the λ^0 was assumed to be $0.2 \text{ GeV}/c^2$ and the mass of the χ^0 was varied from 4 to $10 \text{ GeV}/c^2$, a range compatible with the CERN monojet events. The production angular distribution for this case is $d\sigma/d\Omega \propto \sin^2\theta$ and the χ^0 was assumed to decay preferentially into $\tau^+\tau^-$ or $c\bar{c}$ giving a jet detection efficiency of about 60%. If no mixing of the Higgs particles is assumed, the Z^0 decay rate into a Higgs particle pair is well defined and the expected branching ratio for $Z^0 \rightarrow \chi^0\lambda^0$ is given by:¹⁶⁾

$$BR_{\chi^0\lambda^0} = \frac{G_F M_Z^3}{24\sqrt{2}\pi\Gamma_Z} \cdot \left[1 - \frac{2}{s}(m_\chi^2 + m_\lambda^2) + \frac{1}{s^2}(m_\chi^2 - m_\lambda^2)^2 \right]^{\frac{3}{2}}$$

where m_χ and m_λ are the χ^0 and λ^0 masses respectively.

Fig. 7 shows the measured MAC result for the 90% confidence level upper limit for the monojet cross section and Z^0 branching ratio as a function of the mass of the jet. Limits are given both for the case of the Glashow-Manohar model and for the case of neutral heavy lepton production where only one of the heavy neutral leptons gives visible energy.¹⁷⁾ It can be seen that both models predict significantly more events with jet mass above $4 \text{ GeV}/c^2$ than are observed. The Mark II and HRS experiments give a similar result with less sensitivity due to the smaller acceptance of the detectors for this type of measurement. The MARK II experiment expects 14 events based on the Glashow-Manohar model while only 2 candidate events were observed for a jet parent mass of $5 \text{ GeV}/c^2$. The HRS experiment bases their limits on no observed events with jet masses below $3.6 \text{ GeV}/c^2$ and at most one candidate at higher masses. The limits thus obtained are similar to those of the MARK II group and correspond to a monojet cross section limit varying from 50 to 120 fb over the mass range $2\text{-}10 \text{ GeV}/c^2$.

On the basis of the above limits, the hypothesis that the UA1 monojet events are due to Z^0 decays into light Higgs particles is ruled out for masses up to about $10 \text{ GeV}/c^2$. The hypothesis that the CERN events are due to Z^0 decays into heavy neutral leptons is ruled

out for a branching ratio into monojets as small as 0.5% for Z^0 decays into masses up to approximately $10 \text{ GeV}/c^2$.

The author would like to thank G. Feldman, R. Hollebeek, and M. Derrick for supplying information about their respective experiments. This work was supported in part by the Department of Energy under contract number DE-AC02-76ER00881.

REFERENCES

1. M. K. Gaillard, L. Hall, and I. Hinchliffe, *Phys. Lett.* **116B**, 279 (1982).
2. E. Fernandez et al., *Phys. Rev. Lett.* **52**, 22 (1984).
3. L. Gladney et al., *Phys. Rev. Lett.* **51**, 2253 (1983).
4. P. Fayet, *Phys. Lett.* **117B**, 460 (1982); J. Ellis and J. S. Hagelin, *Phys. Lett.* **122B**, 303 (1983).
5. K. Grassie and P. N. Pandita, *Phys. Rev.* **D30**, 22 (1984); J. Ware and M. E. Machacek, *Phys. Lett.* **142B**, 300 (1984); T. Kobayashi and M. Kuroda, *Phys. Lett.* **139B**, 208 (1984).
6. E. Ma and J. Okada, *Phys. Rev. Lett.* **41**, 287 (1978); K. J. F. Gaemers et al., *Phys. Rev.* **D19**, 1605 (1979).
7. H. J. Behrend *et al.* (CELLO Collaboration), *Phys. Lett.* **114B**, 287 (1982) excluded $2 < m_{\tilde{z}} < 16.8 \text{ GeV}/c^2$ at the 95% confidence level.
8. J. D. Ware and M. E. Machacek, *Phys. Lett.* **147B**, 415 (1984).
9. G. Arnison *et al.*, *Phys. Lett.* **139B**, 115 (1984).
10. For example some supersymmetric explanations for the CERN events are: E. Reya and D. P. Roy, *Phys. Lett.* **141B**, 442 (1984); *Phys. Rev. Lett.* **53**, 881 (1984); V. Barger, K. Hagiwara, J. Woodside, and W.-Y. Keung, *Phys. Rev. Lett.* **53**, 641 (1984); J. Ellis and H. Kowalski, *Phys. Lett.* **142B**, 441 (1984); *Nucl. Phys.* **B246**, 189 (1984).
11. L. M. Krauss, *Phys. Lett.* **143B**, 248 (1984); M. Gronau and J. L. Rosner, *Phys. Lett.* **147B**, 217 (1984).
12. S. Glashow and A. Manohar, *Phys. Rev. Lett.* **54**, 526 (1985); similar models are proposed by S. F. King, *Phys. Rev. Lett.* **54**, 528 (1985); H. Georgi, *HUTP-85/A004* (1985 unpublished).
13. C. Akerlof et al., Argonne National Laboratory report ANL-HEP-PR-85-11.
14. G. J. Feldman et al., *Phys. Rev. Lett.* **54**, 2289 (1985).
15. W. W. Ash et al., *Phys. Rev. Lett.* **54**, 2477 (1985).
16. G. Pöcsik and G. Zsigmond, *Z. Phys.* **C10**, 367 (1981); N. G. Deshpande, X. Tata, and D. A. Dicus, *Phys. Rev.* **D29**, 1527 (1984).
17. J. L. Rosner, CERN-TH. 4086/85 (January 1985, unpublished).

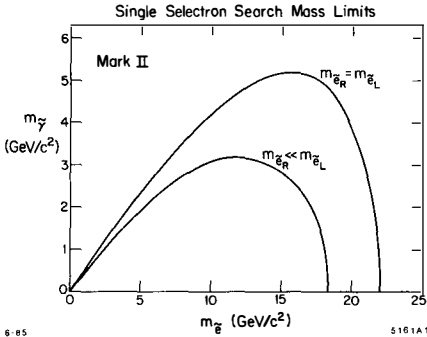


Fig. 1. The MARK II result for selectron and photino mass limits based on the single electron search described in the text. The contours represent 95% confidence level lower limits.

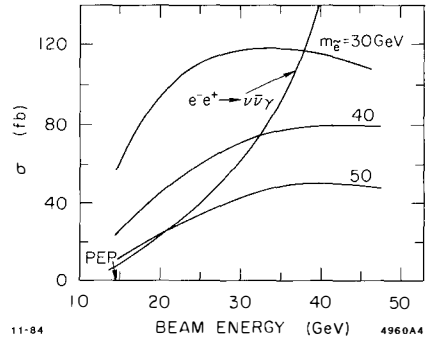


Fig. 2. The theoretical cross section for radiative photino pair production for the MAC acceptance as a function of beam energy for several values of the selectron mass. The radiative neutrino pair cross section is also shown.

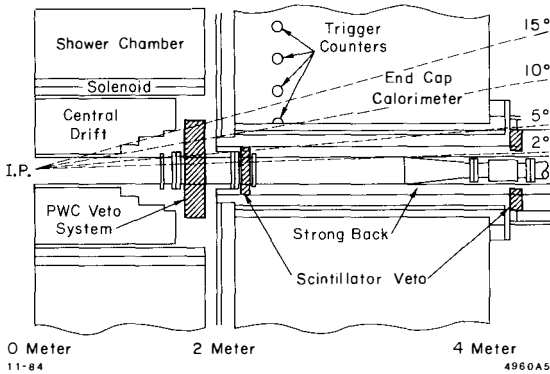


Fig. 3. A schematic drawing of the MAC small angle PWC veto system shown relative to the beam pipe and main detector.

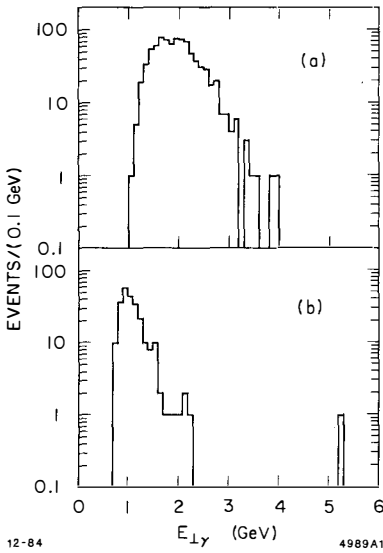


Fig. 4. The observed $E_{\perp\gamma}$ spectra for the MAC experiment for two data sets with $\theta_{veto} = 10^\circ$ and $\theta_{veto} = 5^\circ$ in a) and b) respectively.

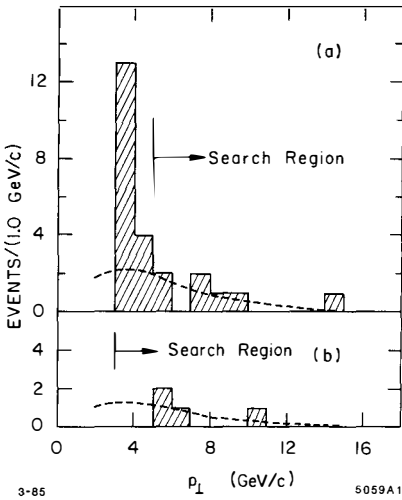


Fig. 6. The observed P_{\perp} spectra for the MAC monojet search for two data samples corresponding to 10° and 5° veto angles respectively. The calculated tau yield is also shown in the figures as a dashed line.

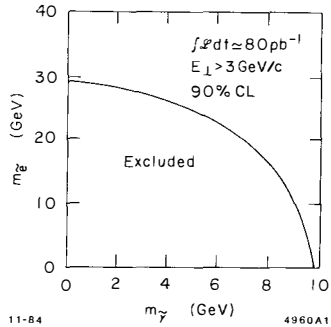


Fig. 5. The lower limit for $m_{\tilde{\tau}}$ as a function of $m_{\tilde{\gamma}}$. The solid curve is for $m_{\tilde{\tau}_L} = m_{\tilde{\tau}_R}$. The dashed curve is for $m_{\tilde{\tau}_L} \gg m_{\tilde{\tau}_R}$. The limits are at the 90% confidence level.

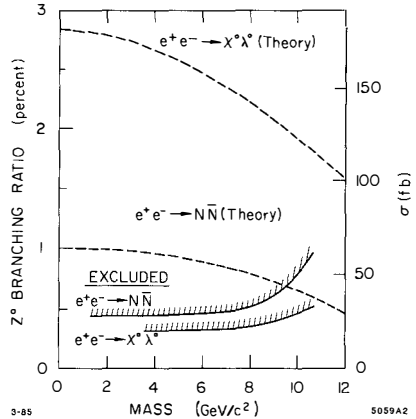


Fig. 7. The MAC upper limits at the 90% confidence level limit for the monojet production cross section and Z^0 decay branching ratio into monojets for the two case described in the text. The calculated cross sections and branching ratios for these cases are also shown as a dashed line.

SEARCH FOR NEW PARTICLES AT PETRA

Albrecht Böhm
III. Physikalisches Institut RWTH Aachen
5100 Aachen Fed.Rep. of Germany

ABSTRACT

Searches for new particles at PETRA are summarized. The study of e^+e^- reactions at energies up to 46.78 GeV leads to stringent limits on the existence of new quarks and leptons, supersymmetric particles, monojets and lepto-quarks.

1. INTRODUCTION

The e^+e^- -storage ring PETRA has reached 46.78 GeV, which is the highest possible energy at this machine. Four experiments CELLO, JADE, MARK J and TASSO have performed measurements and each of them has taken an integrated luminosity between 20 and 30 pb^{-1} at energies above 40 GeV. This data is the basis for the search of new particles since it enables us to set the highest mass limits attainable so far¹⁾.

The mass limits which can be reached are given by the highest possible c.m. energy, if the particle is produced as a resonance. If the particle is produced in pairs, the mass limit is normally half the c.m. energy, which is 23 GeV at PETRA. The existence of particles which have masses higher than the c.m. energy can be detected if cross-sections are modified by space-like exchanges of these particles.

If we search for new particles we have two signatures for their production, which are distinct from known processes. Since I am not able to describe details on the event selection, I wish to make a short comment on two very widely used variables for detecting new particles; these are the missing energy and the acoplanarity. Take the example of the pair production of supersymmetric muons, which decay into a muon and a photino.



If the photino is undetected, we observe an acollinear muon pair with missing energy. Acollinear muon pairs can also come from $e^+e^- \rightarrow \mu^+\mu^-\gamma$ or $e^+e^- \rightarrow e^+e^-\mu^+\mu^-$ if the photon or the electrons stay inside the beam pipe and remain undetected. However these muon pairs are coplanar, if viewed along the beam, because the missing momentum points along the beam. This is in contrast to reaction (1) which can lead to acoplanar muon pairs as indicated in Fig. 1.

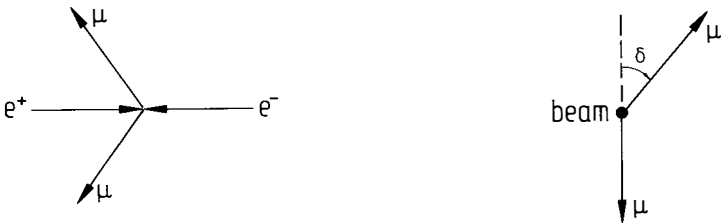


Fig. 1: Acoplanar lepton pairs from reaction (1). This example shows that the acoplanarity and the missing energy are very effective criteria searching for new particle production.

2. SEARCH FOR THE TOPONIUM AND THE TOP QUARK

The search for the toponium resonance has been performed at PETRA by scanning in steps of 30 MeV up to $\sqrt{s} = 46.78$ GeV. Fig. 2 shows the combined measurement of R , which is the cross-section $e^+e^- \rightarrow \text{hadrons}$ normalized by the pointlike cross-section. No signal of the expected size is observed. The height of the resonance depends on the partial resonance width Γ_{ee} , and on the branching ratio B_h of the resonance into hadrons. The PETRA experiments can set upper limits for $\Gamma_{ee} \cdot B_h$, if the mass of the toponium is less than 46.7 GeV (Table 1). Note that a resonance with quarks of charge $1/3$ cannot be excluded, since the expected resonance height would be a factor of 4 lower.

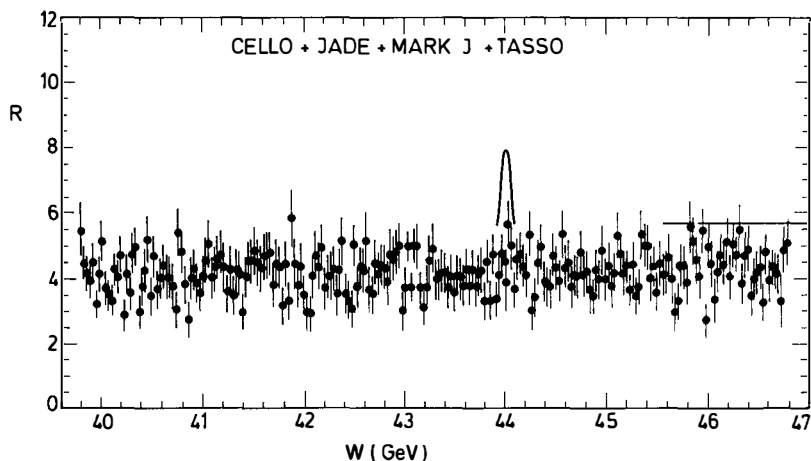


Fig. 2: Combined data from Cello, JADE, MARK J and TASSO on $R = \sigma(e^+e^- \rightarrow \text{hadrons})/\sigma_{\text{pt}}$. The expected height of a toponium resonance and the increase of R due to open top production are indicated.

Experiment	$\Gamma_{ee} \cdot B_h$ (95% C.L.)
CELLO ²⁾	< 2.9 keV
JADE ³⁾	< 1.9 keV
MARK J ⁴⁾	< 3.0 keV
TASSO ⁵⁾	< 2.5 keV
expected	3.5 keV

Table 1: Upper limits of $\Gamma_{ee} \cdot B_h$ with 95% confidence⁶⁾.

Searches for open top production are performed by three methods:

- Observing an increase of the hadronic cross-section by $\Delta R \approx 3Q^2$, where Q is the charge of the new quark.
- Observing broad hadronic jets indicating the fragmentation of a new heavy quark.
- Observing a high rate of broad hadronic events with a prompt muon, which comes from the semileptonic decay of a top quark.

The analysis of data has been done by searching for the top quark with $|Q| = \frac{2}{3}$ and for a new quark with $|Q| = \frac{1}{3}$. Experiments at PETRA exclude the existence of a new quark up to a mass of 23.3 GeV (22.7 GeV) for $|Q| = \frac{2}{3}$ ($|Q| = \frac{1}{3}$), if the new quark is produced with a cross-section of $\Delta R \approx 3Q^2$.

Experiment	$ Q = \frac{2}{3}$	$ Q = \frac{1}{3}$
CELLO ²⁾	23.3 GeV	22.7 GeV
JADE ³⁾	23.3 GeV	22.0 GeV
MARK J ⁴⁾	23.3 GeV	22.5 GeV
TASSO ⁵⁾	22.4 GeV	22.0 GeV

Table 2: Upper limits (95% C.L.)
of the mass of a new quark.

3. SEARCH FOR FREE QUARKS AND STABLE HEAVY PARTICLES

JADE has performed a simultaneous measurement of the momentum and the energy loss dE/dx of charged particles. This allows to separate particles with different charges for small momenta i.e. large masses. No candidates for unknown heavy particles have been found⁷⁾. Fig. 3 shows the upper limits for the inclusive production $e^+e^- \rightarrow q\bar{q} X$, where $q\bar{q}$ signifies a quark-antiquark pair or any other stable particle-antiparticle pair of charge Q .

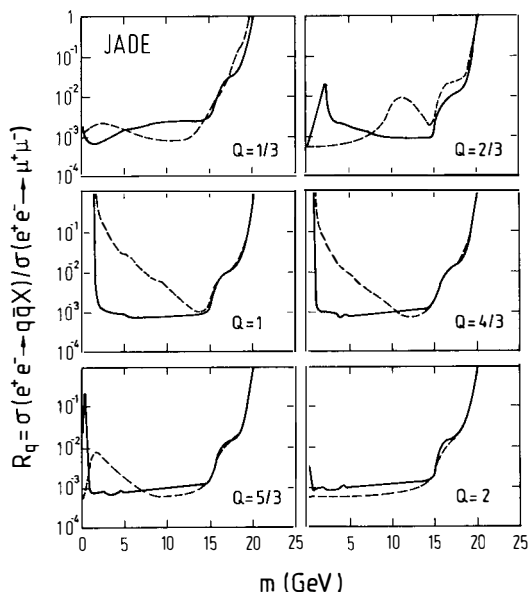


Fig. 3:
Upper limits(90% C.L.) of the inclusive production cross-section of stable particles (or free quarks) with charge Q and mass m . The momentum distribution of these particles has been assumed to be flat (dashed line) or exponentially falling (solid line) ^{7,8}

4. NEW HEAVY LEPTONS

If another charged sequential lepton exists it could well be produced below the top threshold as it has been the case for the tau and the charm threshold. Because we believe that quarks and leptons are related to each other, we would consider a new sequential lepton as an indication for the existence of a new family of leptons and quarks. A typical signature is a muon in one hemisphere, hadrons in the other hemisphere and missing energy. If the mass of the new lepton is close to the beam energy, we would expect events where the muon is acollinear to the hadron jet. Five experiments at PETRA have been searching for a new charged lepton. Since no signal has been observed, the experiments give lower limits for it's mass, which are listed in Table 3.

Experiment	$m_L \geq$
CELLO	16.3 GeV
JADE	22.7 GeV
MARK J	22.5 GeV
PLUTO	14.5 GeV
TASSO	15.5 GeV

Table 3: Lower limits (95% C.L.) of the mass m_L of a new sequential charged lepton.

5. COMPOSITE LEPTONS AND QUARKS

If leptons are composite particles, it should be possible to observe excited leptons. These leptons ℓ^* can be produced by the reactions $e^+e^- \rightarrow \ell^*\ell^*$ and $e^+e^- \rightarrow \ell^*\ell$, or modify the cross-section of $e^+e^- \rightarrow \gamma\gamma$ by a spacelike exchange of an excited electron. Since these searches are summarized at this conference by C. Kiesling, I will be very brief.

A search for the pair production of excited leptons leads to the result that these leptons must be heavier than 23 GeV. The study of $e^+e^- \rightarrow \ell^*\ell$ and $e^+e^- \rightarrow \gamma\gamma$ extends the mass limits to higher values. There is, however, an unknown parameter characterizing the coupling strenght of the $\ell^*\ell\gamma$ vertex.

If the masses of excited leptons or quarks are outside of the range of accelerators we can still detect a sign of compositeness by observing a deviation from the pointlike behaviour of known quarks and leptons. Such deviations are expressed in terms of a formfactor $F(q^2)$, which modifies the pointlike cross-section σ_{st} calculated from the standard model including QCD. The observed cross-section is given by

$$\sigma = \sigma_{st} \cdot |F(q^2)|^2 \quad . \quad (2)$$

The formfactor is usually parametrized in terms of a cut-off parameter Λ :

$$F(q^2) = 1 \mp \frac{q^2}{q^2 - \Lambda_{\pm}^2} \quad . \quad (3)$$

q^2 is the four-momentum transfer squared or the c.m. energy squared. A precise measurement of cross-sections at PETRA gives the following lower limits (95% C.L.) of the cut-off parameters Λ_{\pm} for the reactions:

$$\begin{array}{ll} e^+e^- \rightarrow e^+e^- & \Lambda_{\pm} \geq 200 \text{ GeV} \\ e^+e^- \rightarrow \mu^+\mu^- & \Lambda_{\pm} \geq 200 \text{ GeV} \\ e^+e^- \rightarrow \tau^+\tau^- & \Lambda_{\pm} \geq 150 \text{ GeV} \\ e^+e^- \rightarrow q\bar{q} \rightarrow \text{hadrons} & \Lambda_{\pm} \geq 300 \text{ GeV} \end{array}$$

If we convert these limits into a distance d by $d = \hbar c/\Lambda$, we can say that all leptons and quarks show a pointlike interaction down to distances of the order of 10^{-16} cm.

6. SEARCH FOR SPINLESS BOSONS

The observation of radiative Z^0 decays, $Z^0 \rightarrow e^+e^-\gamma$ ¹⁰⁾ and $Z^0 \rightarrow \mu^+\mu^-\gamma$ ¹¹⁾ can be explained by the existence of spinless bosons ¹²⁾. The invariant mass is close to the maximum energy of PETRA. There are two kinds of signatures of a spinless boson at PETRA ¹³⁾:

a. If the mass of a spinless boson X is less than 46.78 GeV, we expect to find a resonance in $e^+e^- \rightarrow X \rightarrow e^+e^-, \mu^+\mu^-, q\bar{q}$ or $\gamma\gamma$. Estimates of the width give $\Gamma_{ee} \approx 2$ MeV ¹³⁾. This value could be lower by more than a factor of two to three, since no new candidate for a radiative decay of the Z^0 has been observed ¹⁴⁾. From a simultaneous search for a resonance in all decay channels, as proposed by MARK J ¹⁵⁾, the PETRA experiments determine upper limits of Γ_{ee} . Table 4 displays the results deduced from a scan at c.m. energies between 39.79 and 46.78 GeV.

Experiment	$\Gamma_{ee} \leq$
CELLO ¹⁶⁾	28 keV
JADE ¹⁾	73 keV
MARK J ⁴⁾	20 keV
TASSO ⁵⁾	72 keV

Table 4: Upper limits (95% C.L.) on Γ_{ee} of a spinless boson X , if its mass is between 39.9 GeV and 46.7 GeV.

The limits on Γ_{ee} are two orders of magnitude smaller than estimated. This excludes the existence of an X-boson with a mass between 39.9 and 46.7 GeV.

b. If the spinless X-boson has a mass which is outside the PETRA energy range, we can detect its existence, since it modifies the cross-section of $e^+e^- \rightarrow e^+e^-$ and $e^+e^- \rightarrow \gamma\gamma$. MARK J ^{4,15)} rules out the existence of a scalar doublet of X-bosons up to masses of 48 GeV with the assumption that $\Gamma_X = 70$ MeV and $\Gamma_{ee} = 2$ MeV. CELLO ¹⁶⁾ and TASSO ⁵⁾ present their mass limits as a function of $\alpha_h = 2\Gamma_{ee}/m_X$ and assume $\Gamma(Z^0 \rightarrow e^+e^-\gamma)/\rho = 5$ MeV (Fig. 4). The parameter ρ characterizes the relative strenght of the couplings $XZ\gamma$ and $X\gamma\gamma$ and is estimated to be between 1 and 4, as discussed in ref. 13. If we assume $\rho = 4$ and $\Gamma(Z^0 \rightarrow e^+e^-) = 30$ MeV we see from Fig. 4 that the complete mass range up to the Z^0 mass is excluded. This is, however, not a very realistic assumption. $\Gamma(Z^0 \rightarrow e^+e^-\gamma)$ may be 10 MeV or lower, because no new radiative decays have been found. In this case one obtains only very weak limits.

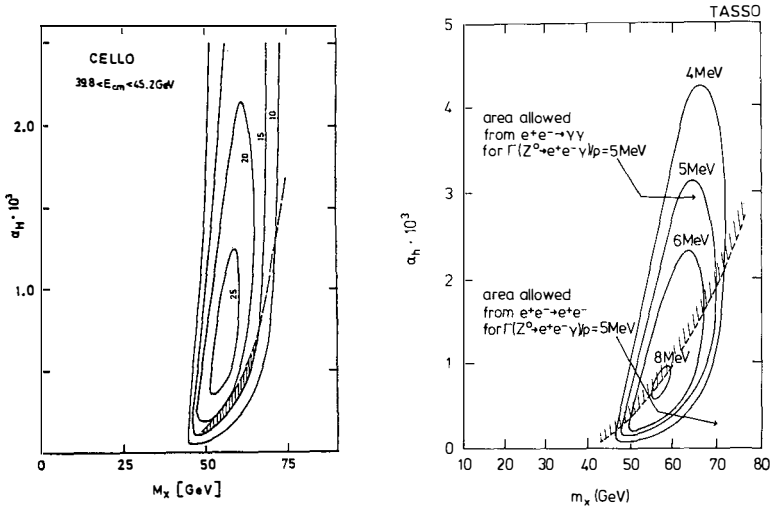


Fig. 4: The allowed region in the (α_h, m_χ) plane for different values of $\Gamma(Z^0 \rightarrow e^+e^- \gamma)/\rho$. The contours from CELLO are evaluated with $\rho = 4$ and the values of $\Gamma(Z^0 \rightarrow e^+e^- \gamma)$ are given in MeV.

7. SUPERSYMMETRIC PARTICLES

Supersymmetry¹⁷⁾ postulates that ordinary particles have partners whose spins are 1/2 unit smaller or larger. In simple versions spin-1/2 leptons and quarks have spin-0 partners and spin-0 and spin-1 bosons have spin-1/2 partners. The search for supersymmetric particles is complicated by the fact that a conserved quantum number R exists which is used to distinguish supersymmetric particles ($R = \pm 1$) and ordinary particles ($R = 0$). This has the consequence that supersymmetric particles have to be produced in pairs such as $e^+e^- \rightarrow \tilde{\mu}^+ \tilde{\mu}^-$ or $e^+e^- \rightarrow \tilde{Z} \tilde{\gamma}$. Supersymmetric particles decay into ordinary particles and at least one other SUSY-particle. This process continues until the lightest SUSY-particle is reached, which is stable. Another complication arises from the fact that neutral spin - 1/2 SUSY particles such as the photino $\tilde{\gamma}$, zino \tilde{Z} and the higgsinos $\tilde{H}_1^0, \tilde{H}_2^0$ can mix as similarly the charged spin - 1/2 SUSY particles wino \tilde{W} and higgsino \tilde{H}^+ and \tilde{H}^- . Thus we find that searches for one SUSY-particle depend on assumptions on the mass, lifetime etc. of other SUSY-particles and on the mixing between these particles.

The search for SUSY-particles is a very large field, which cannot be covered in sufficient detail. I will briefly summarize the results. For more details I refer to the publications of the experimental groups.

a. Supersymmetric partners of leptons.

The main production process for sleptons is

$$e^+e^- \rightarrow \tilde{\nu}^+\tilde{\nu}^- \rightarrow \ell^+\tilde{\gamma}\ell^-\tilde{\gamma} \quad . \quad (4)$$

The signature is a pair of acoplanar leptons, if the photino escapes undetected. These searches are limited to slepton masses below the beam energy. Higher masses of the selectron can be accessed by studying the reactions $e^+e^- \rightarrow e\tilde{e}\tilde{\gamma}$ and $e^+e^- \rightarrow \tilde{\gamma}\tilde{\gamma}$ through the exchange of a virtual selectron.

Four experiments have been searching at PETRA for the partners of the supersymmetric leptons, but no signal has been detected. Table 5 gives the mass range of \tilde{e} , $\tilde{\mu}$ and $\tilde{\tau}$, which is excluded if one assumes that the photino is very light.

	CELLO ¹⁸⁾	JADE ¹⁹⁾	MARK J ⁴⁾	TASSO ²⁰⁾
\tilde{e}	< 25	< 25.2	< 22	< 16.6
$\tilde{\mu}$	3 - 16	< 20.9	< 20	< 16.4
$\tilde{\tau}$	6 - 15.5	4 - 18	2 - 17	-

Table 5:

Range of slepton masses (in GeV) excluded with 95% C.L. by PETRA experiments.

b. Photino

The search for a stable photino is connected to the search for the selectron. The reader is referred to earlier reviews²¹⁾ and to the references in Table 5. Here we wish to discuss searches for an unstable photino, which decays into a photon and a gravitino (or goldstino). The process to be studied is

$$e^+e^- \rightarrow \tilde{\gamma}\tilde{\gamma} \rightarrow \gamma\gamma + \text{missing energy} \quad . \quad (5)$$

We would have to observe an acoplanar pair of photons, because the gravitino escapes undetected. Fig. 5 summarizes the results from CELLO²²⁾, JADE²³⁾, MARK J²⁴⁾ and TASSO²⁵⁾. A large range of photino and selectron masses is excluded. If the photino is very light, its lifetime is expected to be very long. Therefore it cannot be detected in $e^+e^- \rightarrow \tilde{\gamma}\tilde{\gamma}$. Stable photinos with very small masses are, however, excluded by a study of $e^+e^- \rightarrow \tilde{e}\tilde{e}$ or $e\tilde{e}\tilde{\gamma}$ or $\tilde{\gamma}\tilde{\gamma}\tilde{\gamma}$, if the selectron mass is less than 25 GeV as discussed previously.

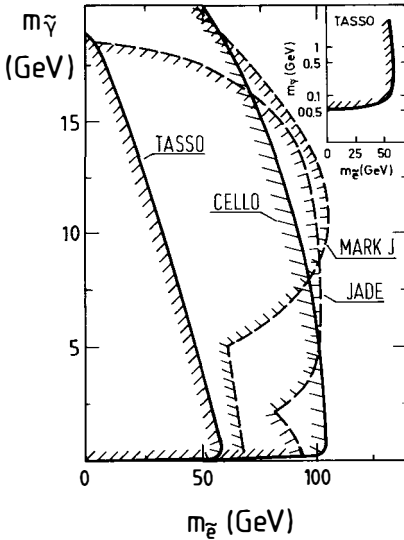


Fig. 5: Unstable photino and selectron masses excluded with 95% C.L. by different PETRA experiments. The insert shows as an example the contour from TASSO for small photino masses.²⁶⁾

c. Wino and Zino

Many models of supersymmetry predict that the spin-1/2 partner of the W^\pm and Z^0 , the wino \tilde{W} and zino \tilde{Z} are light²⁶⁾. It could be that they are lighter than the intermediate vector bosons. The wino can be produced by the reaction

$$e^+e^- \rightarrow \tilde{W} \tilde{W} \tag{6}$$

or
$$e^+e^- \rightarrow e \tilde{\nu} \tilde{W} \tag{7}$$

and decay into $\ell \nu \tilde{\gamma}$ or $\ell \tilde{\nu}$. The zino can be produced by the reaction

$$\begin{array}{c}
 e \longrightarrow \tilde{\gamma} \\
 \longrightarrow \tilde{e} \\
 e \longrightarrow \tilde{Z}
 \end{array}
 \quad
 e^+e^- \rightarrow \tilde{Z} \tilde{\gamma} \tag{8}$$

and decay into $\ell^+ \ell^- \tilde{\gamma}$, $q\bar{q}\tilde{\gamma}$ or $q\bar{q}\tilde{g}$. MARK J has searched for the leptonic decays of the wino and zino, which give acoplanar lepton pairs in reaction (6) and (8) and single leptons in reaction (7). No signal for the existence of \tilde{W} and \tilde{Z} has been observed by MARK J²⁷⁾. Fig. 6 shows the resulting mass limits.

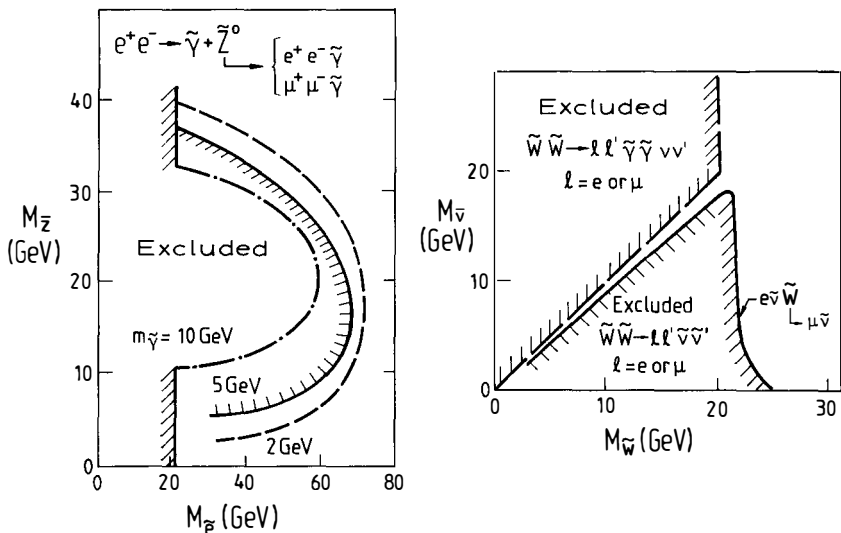


Fig. 6: Results of the search for the zino and wino by MARK J²³⁾. The zino mass limits (95% C.L.) are shown as a function of the electron mass for three different photino masses. The wino mass limits are determined as a function of the mass of the supersymmetric partner of the neutrino.

JADE²⁸⁾ has performed a search for zino production including hadronic decay modes $\tilde{Z} \rightarrow q\bar{q}\tilde{\gamma}$ and $q\bar{q}\tilde{g}$ assuming that the gluino decays via $\tilde{g} \rightarrow q\bar{q}\tilde{\gamma}$. Again no evidence for the existence of the zino has been found. Fig. 7 shows the result of JADE for two different gluino masses.

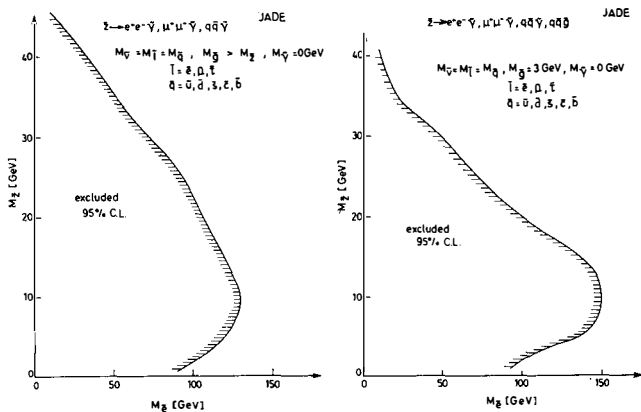
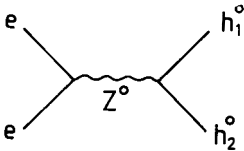


Fig. 7: Mass limits (95% C.L.) from JADE²⁴⁾ as a function of the selectron mass. The results are shown for two assumptions on the gluino mass, $M_{\tilde{g}} > M_{\tilde{Z}}$ and $M_{\tilde{g}} = 3 \text{ GeV}$.

Summarizing the search for the wino and zino, we can say that the wino mass must be larger than ≈ 20 GeV except for the case of $m_W \approx m_V$. The zino mass limit depends strongly on the selectron mass, which is larger than 25 GeV for $m_Y \leq 50$ MeV or even larger than 100 GeV for $100 \text{ MeV} < m_Y < 13 \text{ GeV}$ (see Fig. 5). From Fig. 6 and 7 we estimate $m_{Z_2} > 35$ GeV for $m_E \leq 50$ GeV and for small photino masses. The mass limit is, however, very weak if the selectron mass is above 100 GeV.

8. SEARCH FOR MONOJETETS

Motivated by the observation of UA1²⁹⁾ a search for monojets has been performed by the JADE group³⁰⁾. Glashow and Manohar³¹⁾ have proposed to explain monojets by the production of two neutral Higgs bosons, where the lighter one, h_1^0 , is stable and escapes detection while the heavier one, h_2^0 , decays into hadrons:



$$h_2^0 \rightarrow f\bar{f} \text{ or } h_1^0 + f\bar{f}$$

$$\text{and } f\bar{f} = c\bar{c}, b\bar{b}, \tau\bar{\tau}$$

Since the h_1^0 escapes undetected, we observe a monojet if the mass of the h_2^0 is relatively small. If the h_2^0 has a mass larger than the beam energy, we find two acoplanar hadron jets from $c\bar{c}$, $b\bar{b}$ or $\tau\bar{\tau}$. No evidence for such events has been found and JADE excludes the existence of h_2^0 for masses between 1 and 21 GeV with 95% C.L. JADE presents the analysis in a less model dependent form by varying the coupling constant at the $Z^0 h_1^0 h_2^0$ vertex. Fig. 8 shows the mass limits of h_2^0 as a function of the branching ratio

$$\xi = \frac{\Gamma(Z^0 \rightarrow h_1^0 h_2^0)}{\Gamma(Z^0 \rightarrow \nu_\mu \bar{\nu}_\mu)} \tag{9}$$

and for different decay branching ratios

$$r = \frac{\Sigma \Gamma(h_2^0 \rightarrow f\bar{f})}{\Sigma \Gamma(h_2^0 \rightarrow f\bar{f}) + \Sigma \Gamma(h_2^0 \rightarrow h_1^0 + f\bar{f})} \tag{10}$$

where the sum extends over the $f\bar{f}$ final states $c\bar{c}$, $b\bar{b}$ and $\tau\bar{\tau}$.

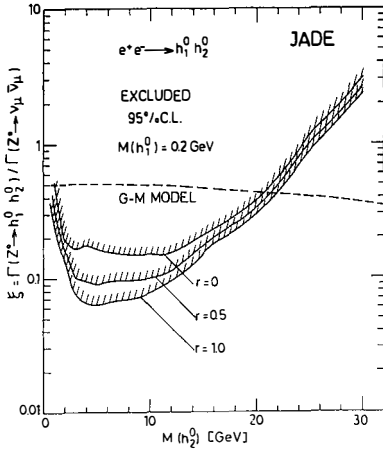


Fig. 8:
Mass limits (95% C.L.) of h_2^0 for different branching ratios ξ and r (see text). The dashed curve denotes the prediction of the Glashow-Manohar model³¹⁾.

9. SEARCH FOR LEPTOQUARKS

Light leptoquarks cannot be excluded if there is one leptoquark per lepton generation³³⁾. Flavor changing neutral currents can be avoided, if these leptoquarks do not mix. Decays of leptoquarks can give rise to monojets. Leptoquarks can be produced in e^+e^- reaction in pairs by $e^+e^- \rightarrow \lambda_2 \bar{\lambda}_2$ and decay via $\lambda_2 \rightarrow \mu s$ or $\nu_\mu c$. We have chosen the leptoquark of the second generation, since it can produce an event signature of $\mu^+ + \mu^- + 2$ jets, as observed by CELLO³⁴⁾. Other event signature would be $\nu_\mu + \mu + 2$ jets or $\nu_\mu + \nu_\mu + 2$ jets. JADE has performed a search for events with these signatures³⁵⁾. The preliminary result is one candidate with two muons and two jets at 46.57 GeV. The group does not consider this event as an evidence for a leptoquark. Using all three signatures of events JADE excludes the existence of a leptoquark of the 2nd generation for masses between 4 and 20.8 GeV.

10. OBSERVATION OF 8 EVENTS WITH A BROAD ENERGY FLOW AND AN ISOLATED MUON ABOVE 46.3 GeV BY MARK J

Up to now we have heard of many searches for particles proposed by theories. None of them has been found. There are however interesting events observed by the MARK J collaboration³⁶⁾ at $46.3 \leq \sqrt{s} \leq 46.78$ GeV, which is the upper limit of the PETRA energy. The total luminosity taken by MARK J at these energies has been 2.8 pb^{-1} .

The events appeared by selecting reactions $e^+e^- \rightarrow \mu + \text{hadrons}$. Usually a cut on thrust, $T < 0.8$, has been applied to search for events indicating open top production. No signal has been observed below 46.3 GeV. However, 8 events were observed at $46.3 \leq \sqrt{s} < 46.78$ GeV while 1.9 events were expected from the data between 37 and 46.3 GeV. The event statistics are 14 times larger at lower energies. Fig. 9 shows the thrust distribution for both data sets.

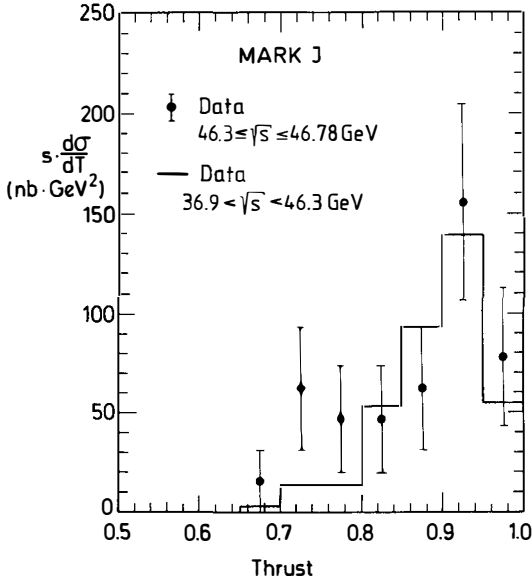


Fig. 9:
Thrust distribution of events selected as $e^+e^- \rightarrow \mu + \text{hadrons}$. The sample for $46.3 \leq \sqrt{s} \leq 46.78$ GeV shows an excess of 8 events for $T < 0.8$ in comparison to the data from lower energies (continuous line)

An inspection of these events has revealed further unusual features:

a. The muon is very isolated from the hadronic or electromagnetic energy flow. The angle of the muon with respect to the thrust axis, which is the axis of the main energy flow, is larger than 45° . Only 0.5 events with this signature are expected from low energy data, while 8 events are seen.

b. The muons have low momenta of $\approx 3 - 4$ GeV. Only one event has a muon with 16 ± 5 GeV.

c. The events have small missing energy which is in average less than 10% of \sqrt{s} .

No explanation has been found for these events. The most important question is whether this is a statistical fluctuation. This could have been answered by further measurements. Unfortunately the running at $\sqrt{s} \approx 46.6$ GeV has been stopped for two reason:

a. There has been no indication for these events from the other experiments, CELLO, JADE and TASSO.

b. Running above 46.3 GeV has been very difficult at PETRA with low luminosity (in average $50 \text{ nb}^{-1}/\text{day}$) and high background.

Since PETRA has now been modified and can no longer reach 46.6 GeV, we need to wait for future e^+e^- machines or leave it to the $p\bar{p}$ collider to clarify this signal.

11. CONCLUSIONS

Intensive searches for new particles have been made at PETRA with the following results:

1. No new quark or lepton has been detected up to $\sqrt{s} = 46.78 \text{ GeV}$.
2. Quarks and leptons show a pointlike interaction down to a distance of 10^{-16} cm .
3. No particle predicted by supersymmetry has been found and mass limits are set for most of these particles.
4. The Higgs particle h_2^0 , introduced to explain monojets, and leptoquarks of the 2nd generation are excluded for masses less than $\approx 21 \text{ GeV}$.
5. MARK J observes 8 events with a broad energy flow and an isolated muon. Further data are needed to clarify this effect.

ACKNOWLEDGEMENTS

I wish to thank the members of the CELLO, JADE, PLUTO, TASSO collaborations and my colleagues from the MARK-J group for discussion and for providing me with unpublished data. The hospitality of the organizers of the Rencontre de Moriond is gratefully acknowledged. I wish to thank Dr. R. Schulte for critical reading of the manuscript.

REFERENCES

1. Earlier reviews are
 - P. Schacht, Proc. of the XXII. Int. Conf. on High Energy Physics, ed.
 - A. Meyer and E. Wieczorek, Leipzig 1984, Vol. I, p. 196;
 - G. Flügge, Proc. of the XIXth Rencontre de Moriond, ed. J. Tran Than Van, La Plagne 1984 p. 341; For results from PEP see R. Prepost, these proceedings.

2. H.J. Behrend et al., Phys. Lett. 144B, 297 (1984).
3. W. Bartel et al., Phys. Lett. 129B, 145 (1983) and private communication.
4. B. Adeva et al., Phys. Lett. 152B, 439 (1985) and Physics Reports 109, 131 (1984).
5. M. Althoff et al., Phys. Lett. 138B, 441 (1984) and Phys. Lett. 154B, 236 (1985).
6. MARK J has obtained a weaker limit. The difference to the results of other groups seems to come from the fact that they apply radiative corrections to the data and to the theoretical cross-section for a resonance. This would be inconsistent. Further investigation is needed on this point.
7. W. Bartel et al., Z. Phys. C6, 295 (1980) and private communication.
8. For limits from experiments at lower energies see Fig. 2 in H. Albrecht et al., DESY preprint 85-037 (1985).
9. C. Kiesling, these proceedings.
10. P. Bagnaia et al., Phys. Lett. 129B, 133 (1983).
11. G. Arnison et al., Phys. Lett. 135B, 250 (1984).
12. U. Baur, H. Fritzsche and H. Faissner, Phys. Lett. 135B, 313 (1983); R.D. Peccei, Phys. Lett. 136B, 121 (1984); M.J. Duncan and M. Veltman, Phys. Lett. 139B, 310 (1984); A. de Rújula, L. Maiani and R. Petronzio, Phys. Lett. 140B, 253 (1984).
13. W. Hollik, F. Schremp and B. Schremp, Phys. Lett. 140B, 424 (1984); F. Bopp, S. Brandt, H. Dahmen and D. Wähler, Z. Phys. C24, 367 (1984).
14. N. Harney (UA2) and A. Honna (UA1), these proceedings.
15. B. Adeva et al., Phys. Rev. Lett. 53, 134 (1984).
16. H.-J. Behrend et al., Phys. Lett. 140B, 130 (1984).
17. Yu. A. Gel'fand and E.P. Likhtman, JETP Letters 13, 323 (1971); J. Wess and B. Zumino, Nucl. Phys. B70, 39 (1974); For a review article, see P. Fayet and S. Ferrara, Phys. Rep. 3C, 249 (1977).
18. H.-J. Behrend et al., Phys. Lett. 114B, 287 (1982) and private communication.
19. W. Bartel et al., Phys. Lett. 152B, 380 and 385 (1985).
20. R. Brandelik et al., Phys. Lett. 117B, 365 (1982).
21. U. Becker and S. Yamada, Proc. of the XXII. Int. Conf. on High Energy Physics, ed. A. Meyer and E. Wieczorek, Leipzig 1984, Vol. I, p. 198.
22. H.-J. Behrend et al., Phys. Lett. 123B, 127 (1983) and private communication.
23. W. Bartel et al., Phys. Lett. 139B, 327 (1984).
24. M. Chen, Proc. of the XIXth Rencontre de Moriond, ed. J. Tran Than Fan, La Plagne (1984) and ref. 4.
25. M. Althoff et al., Z. Phys. C26, 337 (1984).
26. S. Weinberg, Phys. Rev. Lett. 50, 387 (1983); P. Fayet, ENS Report No. 83/16 (1983); J. Ellis and D.V. Nanopoulos, Phys. Lett. 110B, 44 (1984); A. Arnowitt, A.H. Chamsedine and P. Nath, Phys. Rev. Lett. 50, 232 (1983); D.A. Discus, S. Nandi, W.W. Repko and X. Tata, Phys. Rev. D29, 1317 (1984); J.M. Frere and G. Kane, Nucl. Phys. B223, 331 (1983); E. Reya, Phys. Lett. 133B, 245 (1983).
27. B. Adeva et al., Phys. Rev. Lett. 53, 1806 (1984).

28. W. Bartel et al., Phys. Lett. 146B, 126 (1984).
29. G. Arnison et al., Phys. Lett. 139B, 115 (1984).
Note that there is no further evidence for monojets in the new $p\bar{p}$ data.
See ref. 14.
30. W. Bartel et al., DESY Report 85-22 (1985).
31. S.L. Glashow and A. Manohar, Phys. Rev. Lett. 54, 526 (1985).
32. H. Bare, K. Hagiwara and S. Komamiya, DESY Report DESY 85-12 (1985).
33. B. Schrempp and F. Schrempp, Phys. Lett. 153B, 101 (1985).
34. H.-J. Behrend et al., Phys. Lett. 141B, 145 (1984).
35. S. Komamiya, private communication.
36. B. Adeva et al., to be published;
F.P. Poschmann, RWTH Aachen thesis, 1985 (unpublished);
A. Böhm, Aachen preprint PITHA 85-09 (1985), to be published in the
Proc. of XXth Rencontre de Moriond on 'QCD and Beyond', La Plagne, 1985.

LIMITS FOR SUPERSYMMETRY FROM A COMPREHENSIVE STUDY
OF CERN MISSING-ENERGY EVENTS

R. Michael Barnett
Lawrence Berkeley Laboratory, University of California
Berkeley, California 94720



ABSTRACT

We have performed a comprehensive analysis of supersymmetric processes which can lead to missing-energy events such as those observed by the UA1 collaboration. Several critical aspects of the theoretical analysis are discussed here including fragmentation, backgrounds, and evolution of gluinos. When the experimentalists publish their final data, excellent limits will be set for $M_{\tilde{g}}$ and $M_{\tilde{u}}$, and it is possible that certain mass regions will not be excluded as explanations of the data. This work was in collaboration with H. Haber and G. Kane.

Any product should have a warning label for the user (reader). Here the warnings should include the limitations of perturbative QCD; K-factors, fragmentation, initial-state radiation, etc. are at best partially understood. Second, a theorist analyzing the data can only model the cuts, triggers, and jet selection criteria. Third, the current data of interest here are very limited statistically and have had only a preliminary analysis by the experimentalists and include backgrounds.

The data are from the UAL collaboration.¹⁾ Integrated luminosities of approximately 100 and 300 nb⁻¹ were collected in 1983 and 1984 at $\sqrt{s} = 540$ and 630 GeV respectively. Among the phenomena observed were a number of events which can be loosely described as having large missing transverse energy, a hadronic jet with $E_T^{\text{jet}} \geq 25$ GeV and sometimes other jets with $E_T^{\text{jet}} \geq 12$ GeV. If all secondary jets have less than 12 GeV, then the event has been labeled as a "Monojet", while events with one secondary jet greater than 12 GeV are called "Dijets". Clearly this distinction (though necessary) is a subtle one.

These data can have important consequences²⁾ for supersymmetric extensions of the Standard Model of the fundamental interactions. Since Jean-Marie Frère has given at this conference a very good introduction to the motivations for and nature of supersymmetry, I will not review those topics. The work reported here was done by H. Haber, G. Kane, and myself, and can be summarized by:

- 1) The matrix elements of all supersymmetric processes which contribute to missing-energy events were calculated; these include the decay of the final-state squarks and gluinos.
- 2) Since some processes require knowledge of the gluino structure function, we wrote a computer program to perform the QCD evolution of this function.
- 3) An efficient Monte Carlo program was written for each process to calculate rates and distributions for monojets, dijets, and multijets. Several checks were built-in to assure accuracy.
- 4) UAL cuts, triggers, and jet selection criteria were modeled as accurately as possible in this program.
- 5) Fragmentation and gluon bremsstrahlung were incorporated inherently in the program.
- 6) Initial-state p_T distribution was included when appropriate.
- 7) Experimental resolution is incorporated in new versions of our program but not in the results reported here.
- 8) Most values of $M_{\tilde{g}}$ and $M_{\tilde{q}}$ were studied for all processes.
- 9) All relevant data will be analyzed.
- 10) Many backgrounds giving missing-energy events have been calculated (rates and distributions).
- 11) Our results are given independent of supergravity models and cosmology.

The minimal extension of the Standard Model (SU(3)×SU(2)×U(1)) is used. Supersymmetry breaking is parameterized by arbitrary soft-supersymmetry-breaking terms. Predictions can then be made as a function of the masses of squarks and

gluinos. Squark masses are taken as degenerate and the photino is assumed to be the lightest supersymmetric particle ($m_{\tilde{\gamma}} = 0$ here).

We calculate the production of $\tilde{q}\tilde{q}$, $\tilde{q}\tilde{q}$ via W production, $\tilde{q}\tilde{g}$, $\tilde{q}\tilde{\gamma}$, $\tilde{g}\tilde{g}$, and $\tilde{g}\tilde{\gamma}$. Each of these typically involves the calculation of several diagrams.

An essential ingredient of our analysis is the inclusion of processes in which one of the initial partons is a gluino.^{3]} This is important because for $M_{\tilde{g}} < 25$ GeV the gluino structure is quite large. The large magnitude occurs because $\tilde{g}(x, Q^2) = 6q(x, Q^2)$ where q refers to a heavy quark of the same mass as the gluino. The dominant process with an initial-state gluino is $\tilde{g} + q \rightarrow \tilde{q}$ where one needs a heavy squark (>60 GeV) to pass the cuts.

The matrix elements we calculate also involve the decays of the squarks and gluinos. The nature of these decays depends on the relative masses of the two particles. We additionally sometimes consider decays with smaller branching ratios when the resulting processes is more likely to pass the experimental cuts. In total, we have therefore, calculated 16 independent processes each requiring a separate program because of differing kinematics.

There are a number of subtleties in handling cuts and triggers. I will mention one example here. The missing transverse energy, E_T^{miss} , is required to obey $E_T^{\text{miss}} > 4\sigma$ where $\sigma = 0.7\sqrt{E_T}$ to eliminate events which result from non-uniform calorimetry and other mismeasurements. E_T is the scalar sum of all transverse energy whether or not it is in a jet. This quantity is not calculated by theorists. We have therefore scaled the equivalent distribution for minimum-bias events up to energies appropriate for these events. A comparison of our distribution to the preliminary data is shown in Fig. 1. Our distribution is certainly plausible. A more detailed discussion of this and other cuts and triggers will appear in a long paper in preparation.^{4]}

We impose cuts of either $E_T^{\text{miss}} > 32$ GeV or $E_T^{\text{miss}} > 40$ GeV to minimize mismeasurement effects and backgrounds and to reduce dependence on the details of cuts and triggers. We also check the region $E_T^{\text{miss}} < 32$ GeV for certain processes where needed.

Gluinos (and squarks) cannot emerge as free particles; they must first hadronize. From study of quarks we know^{5]} that $E(\text{D meson}) < E(\text{c quark})$ and $E(\text{B meson}) < E(\text{b quark})$. Similarly if we define G as the resulting hadron containing the gluino, then $E(G) < E(\tilde{g})$. This implies that the photino (the source of missing-energy) from G decay has less energy than we would have calculated from the decay of the bare gluino. This means that fewer events pass the E_T^{miss} cut.

Let us define $z \equiv p_{\text{out}}/p_{\text{in}}$. There are three sources of photino energy loss. There is gluon bremsstrahlung from the gluino (large compared to that from quarks because the coupling is $\frac{9}{4}$ larger). We use the parameterization^{6]}

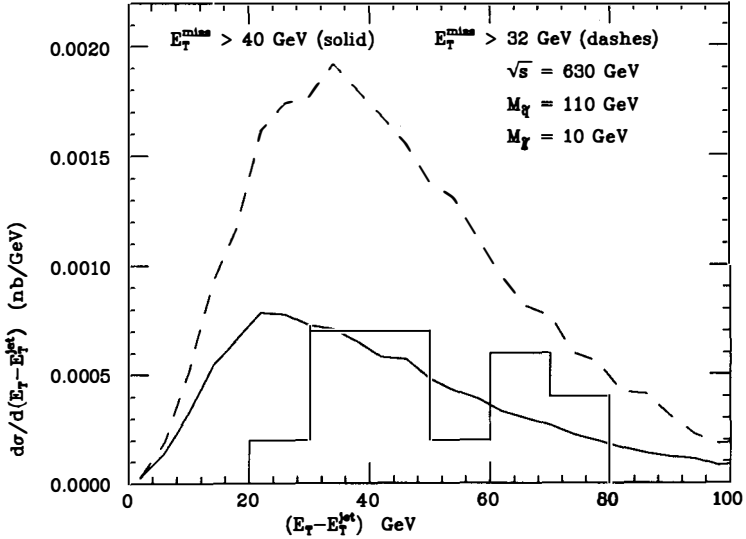


Fig. 1 - The distribution of the total scalar E_T minus E_T^{jet} in $p\bar{p}$ scattering from missing-energy events passing the UAL cuts and $E_T^{\text{miss}} > 32$ GeV (dashed) and $E_T^{\text{miss}} > 40$ GeV (solid). The curves show the sums of contributions from all supersymmetric processes when $M_{\tilde{g}} = 110$ GeV and $M_{\tilde{\tau}} = 10$ GeV. The data (Ref. 1) shown as a histogram are for $E_T^{\text{miss}} > 40$ GeV only, are preliminary, and have not had background events removed.

$D_b = A(1-z_1)^{A-1}$ with $A = \frac{36}{25} [\ln \tilde{s}/\Lambda^2 / \ln 4m^2/\Lambda^2]$. The fragmentation of heavy particles into hadrons has been parameterized^{7]} by $D_h = \frac{c(1-z_2)^2}{[(1-z_2)^2 + (\frac{0.6}{m})^2 z_1]^2}$.

And finally, though we neglect it, the photino spectrum from the decay of G is softer^{8]} than that from \tilde{g} .

We convolute the first two and place the result directly into our Monte Carlo program. We find that fragmentation effects are very important for gluinos as heavy as 20 GeV (a factor of 2 when using the $E_T^{\text{miss}} > 32$ GeV cut).

I believe it is best to study the missing-energy events by combining the data for monojets, dijets, and multijets. These events all have large total E_T and most have secondary jets of 6-15 GeV. Since nonperturbative QCD corrections, spectator activity, fragmentation effects, experimental resolution, etc. can add or subtract from a given secondary jet, the defined boundary at 12 GeV becomes very fuzzy. Clearly it is preferable to use all the data, increase the statistical significance and decrease sensitivity to theoretical and experimental limitations. However, the dijet-monojet ratio does contain important

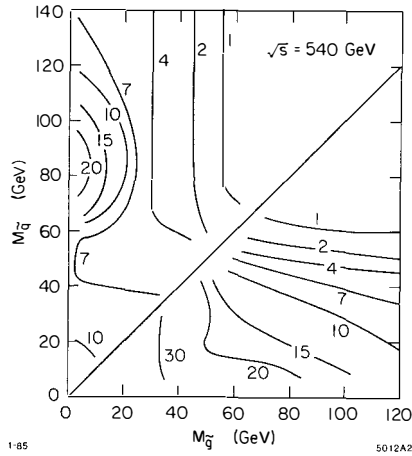


Fig. 2 - The number of monojet events at $\sqrt{s} = 540$ GeV per 100 nb^{-1} passing the UAI cuts plus the $E_T^{\text{miss}} > 32$ GeV cut are shown as a contour plot as a function of $M_{\tilde{g}}$ and $M_{\tilde{q}}$. This number is the total from all supersymmetric sources.

information which with careful study may yield further results concerning supersymmetry. Based on the observed jets accompanying W bosons, we expect that single squark production will have accompanying 12 GeV jets from gluon emission in roughly 35% of the events.

We have not quite finished updating our rate calculations for the 1984 data at $\sqrt{s} = 630$ GeV by summing all missing-energy events (not just monojets), by installing the 1984 cuts and triggers and by including fragmentation effects and resolution effects. These have only been done so far for selected mass values. Fig. 2 shows our old figure for monojet rate per 100 nb^{-1} as a simultaneous function of gluino and squark mass. For a typical choice of $M_{\tilde{g}}$ and $M_{\tilde{q}}$, the rate shown may come from:

$\tilde{g}\tilde{g}$	3.3 events / 100 nb^{-1}
$\tilde{g}\tilde{q}$ ($\tilde{q} \rightarrow q + \tilde{\gamma}$)	0.4 "
$\tilde{g}\tilde{q}$ ($\tilde{q} \rightarrow q + \tilde{g}$)	0.6 "
\tilde{q} ($\tilde{q} \rightarrow q + \tilde{\gamma}$)	1.3 "
\tilde{q} ($\tilde{q} \rightarrow q + \tilde{g}$)	4.4 "
others	negligible
Total	9.9 events / 100 nb^{-1}

When we complete the updated version of Fig. 2 and when the 1984 data are published, we will be able to set strict limits for supersymmetry from this

figure.⁴⁾ We may also be able to identify regions where the signal might have supersymmetric origins.

Fig. 2 indicates only the magnitude of event rates and not the shape of distributions. The shapes will further limit $M_{\tilde{g}}$ and $M_{\tilde{q}}$. However the data for distributions also contain backgrounds which ideally should be subtracted out. But even short of that, certain mass regions can be ruled out if supersymmetry predicts events with characteristics which are not observed.

Shapes of distributions are quite independent of \sqrt{s} , so we have combined the 1983 ($\sqrt{s} = 540$ GeV) and the preliminary 1984 ($\sqrt{s} = 630$ GeV) data. The 1984 data have not yet had backgrounds or some mismeasured events subtracted out. They are only shown to indicate that supersymmetry is a plausible source for the observed events (assuming that the rate is greater than that for backgrounds). The solid and dashed curves in Figs. 3-4 show our results for the two different E_T^{miss} cuts. I believe it may be impossible to learn the source of missing-energy events unless the events between $E_T^{\text{miss}} = 32$ and 40 GeV are also studied. Note that these curves do include fragmentation but not resolution effects.

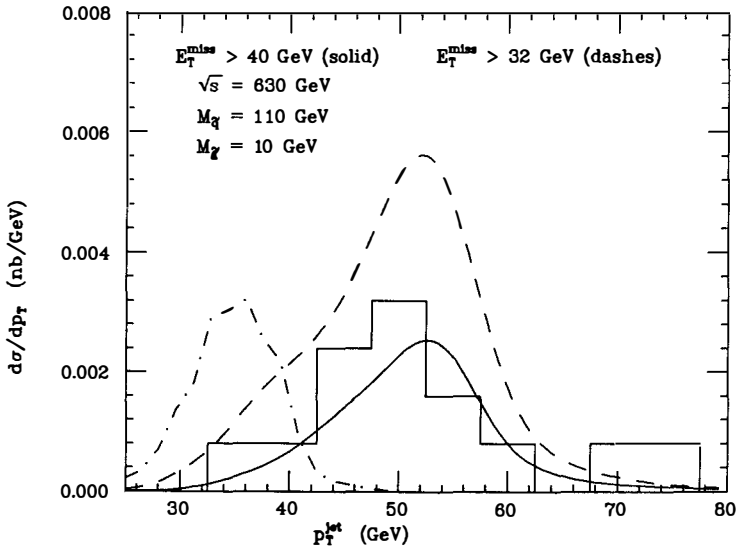


Fig. 3 - The E_T^{jet} distribution in $p\bar{p}$ scattering from missing-energy events passing the UA1 cuts and $E_T^{\text{miss}} > 32$ GeV (dashed) and $E_T^{\text{miss}} > 40$ GeV (solid). The curves show the sums of contributions from all supersymmetric processes when $M_{\tilde{q}} = 110$ GeV and $M_{\tilde{g}} = 10$ GeV. The data are for $E_T^{\text{miss}} > 40$ GeV only and see the remarks in Fig. Cap. 1. The dot-dashed curve shows the background from $W \rightarrow TV$ with $E_T^{\text{miss}} > 32$ GeV.

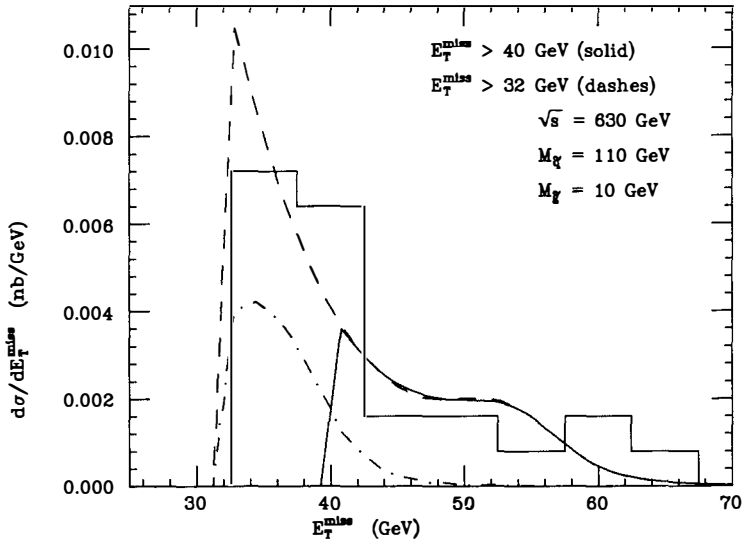


Fig. 4 - The missing-energy E_T^{miss} distribution in $p\bar{p}$ scattering from missing-energy events passing the UAl cuts and $E_T^{\text{miss}} > 32$ GeV (dashed) and $E_T^{\text{miss}} > 40$ GeV (solid). The curves show the sums of contributions from all supersymmetric processes when $M_{\tilde{g}} = 110$ GeV and $M_{\tilde{g}} = 10$ GeV. The data are for $E_T^{\text{miss}} > 32$ GeV; otherwise see the remarks in Fig. Cap. 1. The dot-dashed curve shows the background from $W \rightarrow \tau\nu$ with $E_T^{\text{miss}} > 32$ GeV.

There are a number of possible sources of backgrounds. 1) Detector limitations. 2) The process^{9]} $p\bar{p} \rightarrow W^\pm + X$ with $W^\pm \rightarrow \tau\nu$ and $\tau \rightarrow \nu + \text{jett}$. Since $W^\pm \rightarrow e\nu$ is measured one can calculate this background accurately (though experimental resolution and efficiency may affect the result). We wrote a Monte Carlo program for this process. 3) The process^{10]} $p\bar{p} \rightarrow Z^0 + \text{gluon or quark}$ with $Z^0 \rightarrow \nu\bar{\nu}$. Non-perturbative corrections make this difficult to calculate accurately. To get a rough idea of rates and distributions, we have written a Monte Carlo program for the leading-order process. 4) The process^{10]} $p\bar{p} \rightarrow W^\pm + \text{gluon or quark}$ with $W^\pm \rightarrow e\nu$ and the electron missed.

The dot-dashed curves in Figs. 3-4 show the $W \rightarrow \tau\nu$ results for $E_T^{\text{miss}} > 32$ GeV. The data in Fig. 3 are only for $E_T^{\text{miss}} > 40$ GeV. The $Z^0 \rightarrow \nu\bar{\nu}$ results which will be shown elsewhere are harder and similar to the supersymmetry curves.

The rate for $Z^0 + g$ can be estimated three ways: 1) Determine the K-factor as the ratio of the experimental to theoretical $W \rightarrow e\nu$ rates. This ratio is larger than the theoretical K-factor found by log summation techniques. 2) The

rate for $Z^0 \rightarrow \nu\bar{\nu}$ is expected to be 6 times that for $Z^0 \rightarrow e^+e^-$ which is measured. From Altarelli et al.^{11]} we can find the fraction of Z^0 with $p_T(Z^0) > p_0 = E_T^{\text{miss}}$. 3) the 1983 UAl data for W bosons with an accompanying jet with $E_T^{\text{jet}} > 25$ GeV are roughly 2% of the total. These three techniques yield:

1.2	1.3	1.	events/100 nb ⁻¹	for $E_T^{\text{miss}} > 32$ GeV
0.5	0.7	-	events/100 nb ⁻¹	for $E_T^{\text{miss}} > 40$ GeV.

These are clearly consistent. Detailed calculations for this and background (4) are being reported by Ellis, Stirling, and Kleiss.^{10]} At this time it is possible that these backgrounds are smaller than the signal.

In order to minimize backgrounds and mismeasurements, the experimentalists have sometimes applied a cut $\theta < 150^\circ$ on the angle between the large jet and either a secondary jet or the residual p_T . For $\tilde{q}\tilde{q}$ production the resulting angular distribution peaks between 80° and 150° . However, for $\tilde{g}\tilde{g}$ production with light gluinos the peak is 150° - 180° . If one assumes that the initial-state partons total p_T is the same as that seen in $\bar{p}p \rightarrow W$, the peak moves to 130° - 170° . Therefore I would like to emphasize that a $\theta < 150^\circ$ cut may throw out the baby with the bath water.

In conclusion: Fragmentation is very important for gluinos as heavy as 20 GeV. I believe it is best to combine monojet, dijet, and multijet data. Study of the region $E_T^{\text{miss}} > 32$ GeV is at least as important as that above 40 GeV. We will need all possible data fully analyzed by the experimentalists. A full theoretical-experimental calculation of backgrounds is essential. If no events above backgrounds are observed, then excellent limits on $M_{\tilde{g}}$ and $M_{\tilde{q}}$ will be obtained with our comprehensive analysis. Two regions which we will investigate thoroughly are $M_{\tilde{q}} \sim 100$ GeV with $M_{\tilde{g}} \sim 10$ GeV and $M_{\tilde{q}} \sim 65$ GeV with $M_{\tilde{g}} \sim 70$ GeV. Ultimately our ability to decide whether there is evidence for supersymmetry may rest on our ability to eliminate "Explainatons." Explainatons are particles with the characteristic that their properties change with time to explain whatever data is available today.

We would like to acknowledge recent conversations with J. Ellis, S. Ellis, J.-M. Frère, A. Honma, A. Kernan, W. Kozanecki, Z. Kunszt, F. Paige, C. Rubbia, D. Smith, W. Stirling, C. Tao, and X. Tata.

The Berkeley Particle Data Group is supported by the Director, Office of Energy Research, Office of High Energy and Nuclear Physics, Division of High Energy Physics of the U.S. Department of Energy under Contract No. DE-AC03-76SF00098, and by the U.S. National Science Foundation under Agreement No. PHY83-18358.

REFERENCES

1. G. Arnison, et al., Phys. Lett. 139B, 115 (1984); M. Mohammadi, talk at the 1st Annual Aspen Winter Physics Conference, Aspen, Colorado, Jan. 6-12, 1985; J. Rohlf, talk at the Workshop on "Experimental and Theoretical Investigations of Family Problems," Santa Barbara, Jan. 7-9, 1985.
2. P. Fayet, Phys. Rep 105C, 21 (1984); R.M. Barnett, H.E. Haber, and G.L. Kane, Phys. Rev. Lett. (to be published); P.R. Harrison and C.H. Llewellyn Smith, Nucl. Phys. B213, 223 (1983) (E: B223, 542 (1983)); I. Antoniadis, L. Baulieu, and F. Delduc, Z. Phys. C23, 119 (1984); S. Dawson, E. Eichten, and C. Quigg, Phys. Rev. D31, 1581 (1985); M.J. Herrero, L.E. Ibanez, C. Lopez, and F.J. Yndurain, Phys. Lett. 132B, 199 (1983); 145B, 430 (1984); H.E. Haber and G.L. Kane, Phys. Lett. 142B, 212 (1984); G. Altarelli and R. Ruckl, Phys. Lett. 144B, 126 (1984); N.D. Tracas and S.D.P. Vlassopoulos, Phys. Lett. 149B, 253 (1984); J. Ellis and H. Kowalski, Phys. Lett. 142B, 441 (1984); Nucl. Phys. B246, 189 (1984); preprint CERN-TH.4126/85; E. Reya and D.P. Roy, Phys. Rev. Lett. 51, 867 (1983); (E: 51, 1307 (1983)); *ibid.*, Phys. Lett. 141B, 442 (1984); Dortmund preprint, DO-TH 84/19 (1984); M. Gluck, E. Reya, and D.P. Roy, preprint DO-TH 85/1 (1985); V. Barger, K. Hagiwara, and J. Woodside, Phys. Rev. Lett. 53, 641 (1984); V. Barger, K. Hagiwara, and W.-Y.Keung, Phys. Lett. 145B, 147 (1984); V. Barger, K. Hagiwara, W.-Y.Keung, and J. Woodside, Phys. Rev. D31, 528 (1985) and preprint MAD/PH/230 (1985); A.R. Allan, E.W.N. Glover, and A.D. Martin, Phys. Lett. 146B, 247 (1984); A.R. Allan, E.W.N. Glover, and S.L. Grayson, Durham preprint DTP/84/28 (1984); A. De Rújula and R. Petronzio, preprint CERN-TH-4070/84; F.M. Renard and P. Sorba, preprint LAPP-TH-127 (1985); K. Enqvist, D.V. Nanopoulos, and A.B. Lahanas, preprint CERN-TH-4095/85.
3. M.J. Herrero, Ref. 2 and B.A. Campbell, J. Ellis, and S. Rudaz, Nucl. Phys. B198, 1 (1982); I. Antoniadis, C. Kounnas, and R. Lacaze, Nucl. Phys. B211, 216 (1983); C. Kounnas and D.A. Ross, Nucl. Phys. B214, 317 (1983); S.K. Jones and C.H. Llewellyn Smith, Nucl. Phys. B217, 145 (1983); M.J. Herrero, C. Lopez, and F.J Yndurain, Nucl. Phys. B244, 207 (1984).
4. R.M. Barnett, H.E. Haber, and G.L. Kane, paper in publication.
5. J.M. Izen, preprint DESY 84-104 (1984).
6. A. De Rújula, Ref. 2.
7. C. Peterson et al., Phys. Rev. D27, 105 (1983).
8. E. Franco, Phys. Lett. 124B, 271 (1983); G. Altarelli et al., Nucl. Phys. B208, 365 (1982).
9. M. Mohammadi, Ref. 1.
10. S.D. Ellis, R. Kleiss, and W.J. Stirling, preprint CERN-TH-4096/85.
11. G. Altarelli et al., preprint FERMILAB-PUB-84/107-T (1984); and Nucl. Phys. B246, 12 (1984).

SU(n,1) MINIMAL SUPERGRAVITY AND THE SUSY PARTICLE SPECTRUM

Michael G. Schmidt
 Institut für Theoretische Physik
 der Universität Heidelberg

ABSTRACT

SU(n,1)-Minimal SUGRA automatically leads to sliding mass scales which are fixed through radiative corrections including a gauge singlet tadpole contribution. A gauge singlet field coupled to the Higgses allows for the tadpole and also for a natural doublet-triplet Higgs splitting. The weak scale, the grand unification scale and the gravitino mass are given in terms of the Planck mass. Lower bounds on the charged SUSY partners lead to $m_{3/2} \sim O(10^4)$ GeV and to a SUSY mass spectrum including a \tilde{W} or sl_{right} with a mass below 38 GeV, and heavy \tilde{g} , sq and $\tilde{\gamma}$.

Our SU(n,1) Minimal Supergravity (SUGRA) Model^{1,2,3)} wants to explain the large hierarchy between the weak scale $M_W \sim 100$ GeV and the Planck scale $M_{Pl} \sim 2.4 \cdot 10^{18}$ GeV and gives restrictive predictions for the SUSY mass spectrum. We call it "minimal" because the transition to gauged supersymmetry, i.e. supergravity, is performed⁴⁾ by the minimal substitution procedure for gauging internal symmetries. Minimal SUGRA corresponds to a superfunction $G(Z, Z^*)$ for matter (super)fields Z_i ($i = 1, \dots, n$) leading to a noncanonical scalar kinetic energy $G_i^j \partial_\mu Z^i \partial^\mu Z_j^*$ where $G_i^j = \partial^2 G / \partial Z^i \partial Z_j^*$ represents a SU(n,1) hyperbolic metric in the field space^{5,1)}.

SU(n,1) is not a symmetry of the full theory though the superpotential $g(z)$ (contained in G as $\log |g(z)|^2$) has interesting transformation properties¹⁾. In canonical SUGRA models⁶⁾ one has $G_i^j = \delta_i^j$. They have many disadvantages⁷⁾ and seem to be less promising. In distinction from other SUGRAS SU(n,1) Minimal SUGRA has the following very important property¹⁾:

If SUSY is spontaneously broken and if the cosmological constant $V_{\min} = 0$, there exists a field direction y along which the potential V has a flat valley, i.e. calling the other fields z one has $V_{\min}(y \text{ fixed})(y, z) = 0$. The Vev $\langle y \rangle$ is related to the scale of SUSY breaking, the gravitino mass $m_{3/2}$.

This is a generalization of previous results⁸⁻¹¹⁾ on the existence of a superpotential leading to $V(y) = 0$. The SUSY breaking in the field y should be fed to the observable low energy sector through radiative corrections and its scale should be fixed minimizing the potential including these higher order contributions. Discussing the general form of the superpotential in Minimal SUGRA we found a way^{1,2,3)} to feed the SUSY breaking to a gauge non-singlet field (say A_{24} with 24 the adjoint representation of SU(5)) without losing minimality. Here we differ from no-scale models^{5,10,12)}, which introduce a non-minimal and non-canonical kinetic energy for the gauge fields and introduce SUSY breaking to the observable sector through gaugino masses. This leads to very different results.

Our effective low energy theory (below M_{Pl}) is a global SUSY theory with F-breaking in the field A_{24} . Presuming that the sliding $\langle y \rangle$ is fixed by radiative corrections near the boundary of the hyperbolic field space $\langle y \rangle = -\sqrt{3}(1-2\varepsilon^2)$ with $\varepsilon \ll 1$, we have the mass M_A and the SUSY breaking scale $\Delta M_A^2 / M_A = m$ resp. $m_{3/2} = 2m$ propor-

tional $M_{Pl} \epsilon^3$. The grand unification scale M_{GU} turns out to be ϵM_{Pl} .

Our Higgs potential^{2,3)} has the form $\langle H \rangle^T = \langle H' \rangle = (h, 0)$

$$V(h, m) = f^2 h^4 + h^2 m^2 (p + q f^2 \log \frac{m^2}{M_{Pl}^2}) \tag{1}$$

p is related to the gauge interaction of Fig. 1a and q to a tadpole graph of type Fig. 1b, where the lines inside the graph are specified in a detailed model³⁾ ("mercedes star graph"). A term dependent on the top mass should be added to (1), but it turns out that for $m_f \sim 40$ GeV its influence is not important³⁾. We found it important to introduce a gauge singlet superfield S coupling to H, H' with coupling f . This allows for the tadpole term q , introduces the term $f^2 h^4$ in (1), and also leads to an elegant explanation of heavy H_3 and light H_2 ¹³⁾ (contrary to canonical SUGRA, where the tadpole graph is lethal). It is very attractive - though speculative - that the same radiative corrections which fix the weak scale are also responsible for determining the scale m of SUSY breaking¹²⁾. Minimizing (1) with respect to h and m we obtain

$$\frac{m^2}{M_{Pl}^2} = \exp \left(\frac{-p}{f^2 q} - 1 \right); h^2 = \frac{q}{2} m^2 \tag{2}$$

leading to a hierarchy for $f^2 q < p$ (not hierarchically smaller!). Instead of the model parameters (f, q) we can take the known value of h and $m = 2m_{3/2}$ as a free parameter and calculate³⁾ the "standard SUSY" spectrum including the singlet particles S, \tilde{S} . It is plotted in Fig. 2a, b, c. We observe the following properties of the spectrum:

- (i) The lightest charged partner particle - either sl_r or \tilde{W}_{light} - has a mass below 38 GeV.
- (ii) The PETRA bound¹⁴⁾ leads to $5 \text{ TeV} < m = 2m_{3/2} < 22 \text{ TeV}$.
- (iii) Neutral partner fermions are lighter than charged ones for

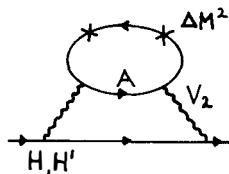


Fig. 1a

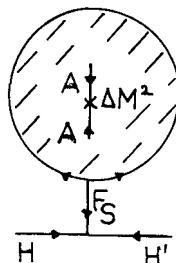


Fig. 1b

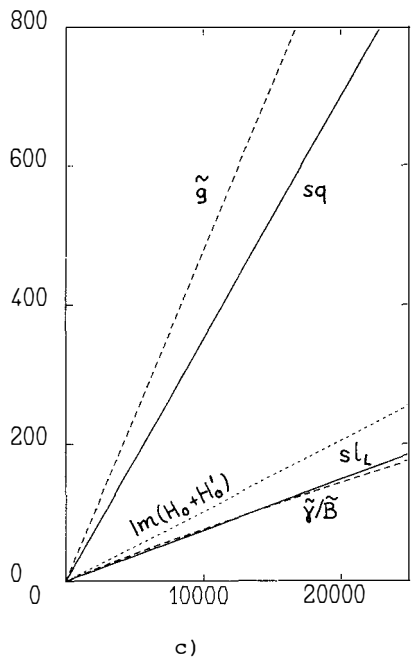
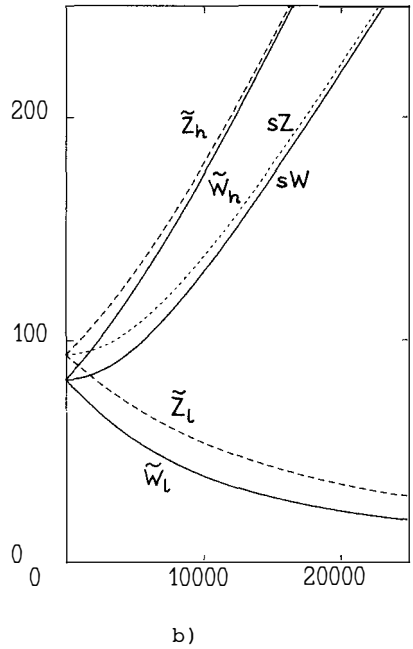
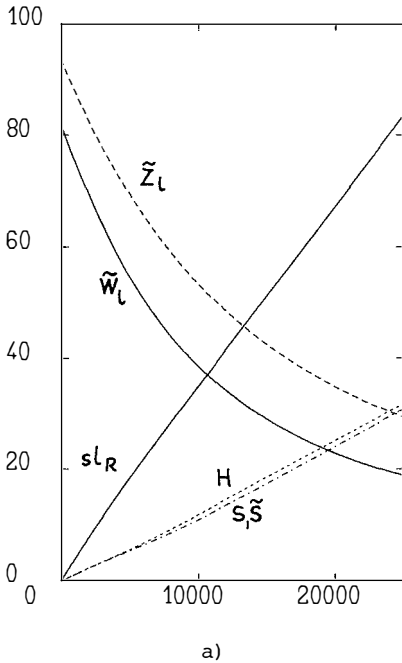


Fig. 2 Predicted masses as function of the SUSY breaking scale $m=2m_{3/2}$ (in GeV) for $m_{top} \sim 40$ GeV. The lightest neutral particles are the S-scalar, the \tilde{S}/\tilde{H} -Dirac fermion and the standard Higgs $H=Re(H_0+H'_0)$ (Fig. 2a). Without top contribution they are degenerate. For vanishing SUSY breaking the Majorana fermions \tilde{Z}_1, \tilde{Z}_2 and the real scalar $sZ \equiv Re(H_0-H'_0)$ together with the Z-boson form a SUSY multiplet as do the charged Dirac fermions \tilde{W}_1, \tilde{W}_2 , the scalar $sW = H_0 - H'_0$ and the W-boson (Fig. 2b).

$m < 19$ TeV; this avoids charged relics of the big bang.

(iv) Gauginos and squarks are heavy; there is no light photino.

(v) The influence of m_{top} is very small for $m_t \sim 40$ GeV, but it becomes rapidly important for larger m_t . $m_{\text{top}} \gtrsim 65$ GeV is excluded.

The "light" SUSY particles should show up in a detailed study of W and Z decays. However, it might be hard to reconstruct the relevant W decays (see e.g. Fig. 3) in collider experiments.

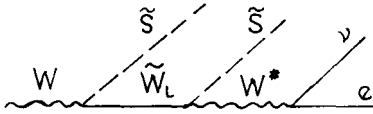


Fig. 3 $W \rightarrow e + \text{neutrals}$

References

- 1) N. Dragon, M. G. Schmidt, U. Ellwanger, Phys. Lett. 145B (1984) 192.
- 2) U. Ellwanger, N. Dragon, M. G. Schmidt, CERN TH 3974 (1984), Nucl. Phys. B, to appear.
- 3) N. Dragon, U. Ellwanger, M. G. Schmidt, HD-THEP-85-1 (1985); CERN preprint "A Grand Unified Theory...".
- 4) J. Wess, B. Zumino, Phys. Lett. 79B (1978) 394; J. Wess and J. Bagger, Supersymmetry and Supergravity, Princeton Press (1983).
- 5) J. Ellis, C. Kounnas, D. V. Nanopoulos, Nucl. Phys. B247 (1984) 373.
- 6) H. P. Nilles, Phys. Rep. 110C (1984) 2; J. Ellis, CERN TH. 3802 (1984); further references in these papers.
- 7) N. Dragon, M. G. Schmidt, Z. Phys. C (1984) 157, and ref. there.
- 8) N. Chang, S. Ouvry, X. Wu, Phys. Rev. Lett. 51 (1983) 327.
- 9) E. Cremmer, S. Ferrara, C. Kounnas, D. V. Nanopoulos, Phys. Lett. 133B (1983) 61.
- 10) J. Ellis, C. Kounnas, D. V. Nanopoulos, Nucl. Phys. B241 (1984) 406.
- 11) S. Ouvry, Phys. Lett. 136B (1984) 165; X. Wu, Phys. Rev. D30 (1984) 2462.
- 12) J. Ellis, A. B. Lahanas, D. V. Nanopoulos, K. Tamvakis, Phys. Lett. 134B (1984) 429.
- 13) E. Witten, Phys. Lett. 105B (1981) 267; L. Ibáñez, G. G. Ross, Phys. Lett. 110B (1982) 215; J. Ellis, L. Ibáñez, G. G. Ross, Nucl. Phys. B221 (1983) 29.
- 14) Jade Coll., Phys. Lett. 152 (1985) 385, 392; Pluto Coll. 84-121; Tasso Coll. 85-001, DESY preprints.

SYMMETRIES OF THE CROSS - SECTIONS OF MAJORANA
PARTICLE PRODUCTION IN $e^+ - e^-$ AND $p - \bar{p}$
COLLISIONS

S.T.Petcov

Institute of Nuclear Research, Bulgarian
Academy of Sciences, 1184 Sofia, Bulgaria

ABSTRACT

Some characteristic symmetries of the cross-sections of production of Majorana particles in $e^+ - e^-$ and $p - \bar{p}$ collisions are discussed. These symmetries are a consequence of the specific CP- and CPT- transformation properties of the Majorana fermions.

The neutral fermions can be of two varieties: they either can be assigned a conserved additive quantum number, i.e. they can be Dirac particles¹⁾, or else be absolutely neutral, i.e. Majorana particles²⁾. All known neutral fermions ($n, \Lambda, \Sigma^0, \dots$) are or behave to a very good approximation like Dirac particles and no experimental evidences for the existence of Majorana fermions have been found to date. At the same time Majorana fermions are present in many extensions of the standard $SU(3) \times SU(2) \times U(1)$ theory. They appear inevitably in the modern supersymmetric (SUSY) theories³⁾. In the minimal supersymmetric version of the standard theory these are the superpartners of the neutral gauge and Higgs bosons: the photino ($\tilde{\gamma}$), zino (\tilde{z}), two higgsinos ($\tilde{H}_{1,2}^0$) and gluinos (\tilde{g})⁴⁾. Heavy neutral Majorana leptons are often the right-handed counterparts of the ordinary neutrinos in the electroweak theories based on the group $SU_L(2) \times SU_R(2) \times U(1)$ ⁵⁾. And the ordinary neutrinos themselves might be mixtures of Majorana neutrinos possessing nonzero masses⁶⁾.

Although the properties of the Majorana and the neutral Dirac fermions are very different⁷⁾, no universal and relatively simple solution to the problem of distinguishing experimentally between them has been proposed to date. In the present talk we shall consider some characteristic features of the cross-sections of production of Majorana particles (other than light neutrinos) in $e^+ - e^-$ annihilation and $p - \bar{p}$ collisions⁸⁾. These features follow from the specific CP- and CPT- transformation properties of the Majorana particles and may be used as a possible signature for their production. The CP- and CPT- transformations leave the Majorana fermions, which do not have distinctive antiparticles, essentially unchanged. As a consequence the cross-sections of inclusive production of Majorana particles as well as of exclusive production of Majorana particles with a set of particles or their antiparticles in $e^+ - e^-$ and $p - \bar{p}$ collisions possess a certain symmetry⁸⁾, which is exact when the corresponding amplitudes are CP-symmetric and approximate if the production mechanism is perturbative and the S-matrix is CPT-invariant^{*}). In the centre of mass

* For the case of $p - \bar{p}$ collisions the second statement is valid under some additional but rather general assumptions.

system of the initial particles this symmetry corresponds to a symmetry between the particle spatial distributions in the forward and in the backward hemispheres (i.e., implies zero forward-backward (F - B) asymmetry).

We shall give below for illustration a schematic proof of one of these results for the case of the simple process of $e^+ - e^-$ annihilation into a pair of arbitrary Majorana fermions χ and χ' :

$$e^+ + e^- \longrightarrow \chi + \chi' \quad (1)$$

Processes of this type are predicted to exist at high energies ($\sqrt{s} \gtrsim 40$ GeV), e.g., by the supersymmetric theories⁹⁾, one example being the associative production of photino $\tilde{\gamma}$ and zino \tilde{z} in $e^+ - e^-$ annihilation. We shall be interested in the properties of the differential cross-section of the process (1) averaged over the spins of the initial particles and summed over the spins of the particles in the final state.

Under the CP- and CPT-transformations

$$\begin{aligned} I e^{\bar{+}}(s, p) &\xrightarrow{CP} I e^{\bar{+}}(-s, p_p) > , p_p = (-\vec{p}, ip_0), \\ I e^{\bar{+}}(s, p) &\xrightarrow{CPT} I e^{\bar{+}}(-s, p) > . \end{aligned} \quad (2)$$

Here $I e^{\bar{+}}(s, p) >$ is the state vector of a free electron (positron) with 4-momentum $p = (\vec{p}, ip_0)$ and projection s of the spin on the momentum \vec{p} . Since Majorana fermions possess no distinctive antiparticles we have:

$$\begin{aligned} I \chi^{(i)}(r, k) &\xrightarrow{CP} I \chi^{(i)}(-r, k_p) > , k_p = (-\vec{k}, ik_0), \\ I \chi^{(i)}(r, k) &\xrightarrow{CPT} I \chi^{(i)}(-r, k) > , \end{aligned} \quad (3)$$

where the notations are obvious.

Let us assume first that the couplings of χ and χ' are CP-invariant. Under the CP-transformation the configuration of particles which is shown in Fig. 1a and corresponds to the process (1) changes into the configuration depicted in Fig. 1b. This implies

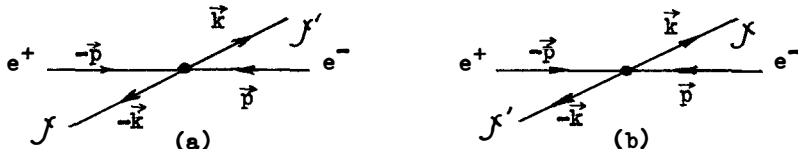


Fig. 1. Two possible configurations of χ and χ' produced in the case of CP-invariance with equal cross-sections.

that if the amplitude of the process (1) is CP-invariant, the cross-sections of production of χ and χ' with momenta correspond-

ing to the two configurations shown in Fig. 1 are equal. Thus, the (F - B) asymmetry in the distribution of χ' (or χ) is identically equal to zero.

This general conclusion is not valid if the χ and χ' couplings are not CP-symmetric. It can be shown⁸⁾, however, that it is still true to leading order of the perturbation theory if the process (1) is perturbative (i.e., if χ and χ' do not possess couplings which cannot be treated perturbatively at the energies at which the process of interest occurs^{*}) and if the S-matrix is CPT-invariant.

It is possible to derive⁸⁾ exactly the same results for the (F - B) asymmetry in the distribution of a Majorana particle χ produced in association with a Dirac particle (set of particles) N or its antiparticle (their antiparticles) \bar{N}

$$e^+ + e^- \rightarrow \chi + N \text{ or } \bar{N}, \quad (4)$$

as well as for the case of inclusive production of χ :

$$e^+ + e^- \rightarrow \chi + \text{anything} . \quad (5)$$

Further, in the case of CP-invariant χ - proton couplings χ will be produced in the reaction

$$p + \bar{p} \rightarrow \chi + \text{anything} \quad (6)$$

with equal cross-sections in the forward and in the backward hemispheres⁸⁾ (in the $p\bar{p}$ c.m.s.). Finally, if the χ - proton couplings are not CP-invariant, but the process (6) can be treated in the framework of the perturbative QCD and the relevant subprocesses involve only two particles (quarks or/and gluons) in the initial state, the (F - B) asymmetry in the distribution of χ can be shown to vanish⁸⁾ in the leading order of the perturbation theory, as in the corresponding case of $e^+ - e^-$ annihilation.

These results are relevant to a multitude of processes discussed in the literature. In particular, they are valid for the set of subprocesses considered in¹⁰⁾, wherein the production of SUSY particles in $p - \bar{p}$ collisions was studied in detail:

* For $\sqrt{s} \gg$ several GeV this requirement is supposed to be satisfied, e.g., for the particles whose strong interaction is governed or fixed (e.g., via the supersymmetry) by QCD (like gluinos).

$$q + \bar{q} \rightarrow \begin{matrix} \tilde{u} \\ \tilde{d} \\ \tilde{s} \end{matrix} + \begin{matrix} \tilde{q} \\ \tilde{q} \\ \tilde{s} \end{matrix}, \quad q + \bar{q}' \rightarrow \begin{matrix} \tilde{w}^+ \\ \tilde{w}^+ \\ \tilde{w}^+ \end{matrix} + \begin{matrix} \tilde{\gamma} \\ \tilde{g} \\ \tilde{z} \end{matrix}, \quad g + q \rightarrow \begin{matrix} \tilde{q} \\ \tilde{q} \\ \tilde{s} \end{matrix} + \begin{matrix} \tilde{q} \\ \tilde{q} \\ \tilde{s} \end{matrix}$$

$$q^{(\prime)} = u, d, \dots,$$

where \tilde{w}^+ is the supersymmetric partner of the W^+ - boson.

Let us add in conclusion that, as obviously follows from our considerations, the detection of a nonzero (F - B) asymmetry in the distribution of a Majorana particle, produced in one of the reactions (1), (4) - (6), would be an evidence for CP-nonconservation in the reaction.

Detailed proofs of the results formulated above as well as a more complete discussion of their possible applications can be found in ⁸⁾.

REFERENCES

1. P.A.M. Dirac, Proc. Roy. Soc. (London) A117 (1928) 610; *ibid.* A118 (1928) 351 and A126 (1930) 360.
2. E. Majorana, Nuovo Cimento 14 (1937) 170.
3. See, e.g.: P. Fayet, these proceedings; H.P. Nilles, Phys. Rep. 110C (1984) 1.
4. See, e.g.: J.-M. Frère, these proceedings.
5. See, e.g.: R. Mohapatra and G. Senjanovich, Phys.Rev. D23 (1981) 165.
6. V. Gribov and B. Pontecorvo, Phys.Lett. 28B (1969) 49.
7. See, e.g.: S.T. Petcov, Lecture Notes in Physics, vol. 181 (eds. R. Raitio and J. Lindfors, Springer-Verlag, 1982) p. 398. B. Kayser, Proc. of the Fourth Moriond Workshop on Massive Neutrinos in Astrophysics and in Particle Physics, La Plagne, Savoie, France, January 15-21, 1984 (ed. J. Tran Thanh Van, Editions Frontieres) p. 11.
8. S.T. Petcov, Phys.Lett. 139B (1984) 421.
9. J.-M. Frère and G. Kane, Nucl.Phys. B223 (1983) 331; J. Ellis, J.-M. Frère, J.S. Hagelin, G. Kane and S.T. Petcov, Phys.Lett. 132B (1983) 436.
10. S. Dawson, E. Eichten and C. Quigg, FERMILAB-Pub-83/82-THY, October 1983.

SU(2) X U(1) X U(1) ELECTROWEAK
MODEL AND THE CERN MONOJET

J.W. Moffat
Department of Physics
University of Toronto
Toronto, Ontario M5S 1A7
Canada



ABSTRACT

An extended electroweak model based on SU(2) X U(1) X U(1) can describe the monojet events observed at UA1, since a decay $Z^0 \rightarrow \lambda^0 h^0$ occurs where λ^0 is a pseudoscalar Higgs meson with mass $m_\lambda \sim 4$ Gev, while h^0 is a light scalar meson with mass $m_h \sim 0.2 - 0.3$ Gev that escapes the detector and describes the missing energy.

An extended model based on the continuous, local gauge symmetries of $SU(2) \times U(1) \times U(1)'$ has been proposed¹⁾ that can describe the CERN UA1 monojet events $p\bar{p} \rightarrow Z^0 \rightarrow P_{\perp} + \text{jet}$.²⁾³⁾ The minimal scheme uses the covariant derivative⁴⁾

$$D_{\nu} = \partial_{\nu} - ig_0 \vec{T} \cdot \vec{W}_{\nu} - ig_1 \frac{Y}{2} B_{\nu} - ig_2 \frac{Y'}{2} B_{\nu}' , \quad (1)$$

where we introduce the new hypercharge quantum number Y' and a new neutral gauge boson B_{ν}' . The B_{ν}' does not couple to the known fermions of the standard model.

The Higgs sector is described by

$$\Phi = \begin{pmatrix} \phi^+ \\ \phi^0 \end{pmatrix}, \chi_1^0, \chi_2^0 , \quad (2)$$

where ϕ is non-trivial under transformations of $SU(2) \times U(1)$ and trivial under $U(1)'$ transformations, while χ_1^0 and χ_2^0 are trivial under $SU(2) \times U(1)$ transformations and non-trivial under $U(1)'$ transformations. Thus χ_1^0 and χ_2^0 do not couple to the known fermions at the tree-graph level. The quantum numbers of the Higgs fields are:

$$Y = 1, T(3) = \pm \frac{1}{2}, Y' = 0 \text{ for } \phi \quad (3)$$

$$Y = y, T = 0, Y' = -y \text{ for } \chi_1^0, \chi_2^0 ,$$

where y is a real number.

There are two Z^0 bosons whose masses satisfy $m_{Z_1} < m_Z < m_{Z_2}$, where m_Z is the mass of the Z^0 in the standard model. The effective Hamiltonian for the charged fermion interactions at low energies agrees with the standard model predictions, except that there is an additional piece proportional to the square of the electromagnetic current Q :

$$H_{\text{eff}} = \frac{G_F}{\sqrt{2}} [j^+ j^- + (j_3 - \sin^2 \theta_W Q)^2 + N Q^2] . \quad (4)$$

The extra neutral current term does not contribute to parity violation and is masked by the photon contribution at $q^2 \rightarrow 0$. The $I = \frac{1}{2}$ properties of the Higgs sector give a ratio of neutral-to-charged current effective coupling strengths, which is the same as in the standard model i.e. $\rho = NC/CC = 1.00 \pm 0.02$. The predicted $\sin^2 \theta_W$ is such that $0 < \sin^2 \theta_W < 1$. A calculation yields $N = (\cos \theta_W)^4 r \sim 0.6r$ where

$$r = (m_{Z_1}^{-2} - m_Z^{-2})(m_Z^{-2} - m_{Z_2}^{-2}) m_{Z_1}^2 m_{Z_2}^2 . \quad (5)$$

The vacuum expectation values are $\langle 0 | \phi | 0 \rangle = \begin{pmatrix} 0 \\ v_0/\sqrt{2} \end{pmatrix}$, $\langle 0 | \chi_1 | 0 \rangle = v_1/\sqrt{2}$ and $\langle 0 | \chi_2 | 0 \rangle = v_2/\sqrt{2}$. The Higgs potential that is to be minimized has the form

$$\begin{aligned}
V(\Phi, \chi) &= \lambda_1 (\Phi^\dagger \Phi - v_0^2)^2 \\
&+ \lambda_2 (\chi_1^\dagger \chi_1 - v_1^2)^2 + \lambda_3 (\chi_2^\dagger \chi_2 - v_2^2)^2 \\
&+ \lambda_3 [(\Phi^\dagger \Phi - v_0^2) + (\chi_1^\dagger \chi_1 - v_1^2) \\
&+ (\chi_2^\dagger \chi_2 - v_2^2)]^2 \\
&+ \lambda_4 [(\Phi^\dagger \Phi)(\chi_1^\dagger \chi_1) + (\Phi^\dagger \Phi)(\chi_2^\dagger \chi_2) \\
&- (\Phi^\dagger \chi_1)(\chi_1^\dagger \Phi) - (\Phi^\dagger \chi_2)(\chi_2^\dagger \Phi)] \\
&- \frac{1}{4} (\Phi^\dagger \chi_1 + \Phi^\dagger \chi_2 - \chi_1^\dagger \Phi - \chi_2^\dagger \Phi)^2.
\end{aligned} \tag{6}$$

The diagonalization of the Higgs sector produces four neutral physical Higgs particles λ^0 , h_1^0 , h_2^0 and $\phi_s^{(1)}$. Here λ^0 is a pseudoscalar combination of the standard Higgs particle ϕ_s and h_1^0 and h_2^0 , while h_1^0 and h_2^0 are the physical scalar Higgs particles that can induce a coupling to the known fermions in loop graphs containing fermions and Higgses. Provided the vev for, say, the χ_1 is kept small, it will lead to a relatively small mass for the h_1^0 particle, $m_{h_1} \approx 0.3$ Gev, and then it will not decay in the hermetic detector and will produce the missing transverse energy. The h_2^0 can have arbitrarily large mass, while the pseudo-scalar λ^0 producing the jet is chosen to have a mass $m_\lambda \sim 4-6$ Gev. The diagonalization of the Higgs sector in general involves three angles α , β and γ but one of these is chosen to be zero, thus prohibiting the coupling of the χ^0 to the known fermions. An angular dependence is then left undetermined.

The Higgs-Z Lagrangian produces a trilinear coupling

$$L_{zh\lambda} = \frac{g_1 \phi}{2 \cos \theta_w} Z_\mu^i (h^0 \partial^\mu \lambda^0 - \lambda^0 \partial^\mu h^0), \tag{7}$$

where ϕ is the unknown angular dependence left over from the Higgs diagonalization.

The width for $Z^0 \rightarrow \lambda^0 h_1^0$ is given by⁵⁾

$$\begin{aligned}
\Gamma(Z_i^0 \rightarrow \lambda^0 h^0) &= \frac{\alpha \phi m_{Z_i}}{12 \sin^2 2\theta_w} \\
&\cdot \left[1 - \frac{2}{m_{Z_i}^2} (m_{\lambda^0}^2 + m_{h^0}^2) \right. \\
&+ \left. \frac{1}{m_{Z_i}^2} (m_{\lambda^0}^2 - m_{h^0}^2)^2 \right]^{3/2}.
\end{aligned} \tag{8}$$

The differential cross section for $p\bar{p} \rightarrow \mu^+ \mu^- (e^+ e^-)$ and the branching ratio $BR(Z_1^0 \rightarrow \lambda^0 h^0) + BR(Z_2^0 \rightarrow \lambda^0 h^0)$ and $[\Gamma(Z_1^0 \rightarrow \lambda^0 h^0) + \Gamma(Z_2^0 \rightarrow \lambda^0 h^0)]/\Gamma_V$ (where $\Gamma_V = \Gamma(Z_1^0 \rightarrow \nu\bar{\nu}) + \Gamma(Z_2^0 \rightarrow \nu\bar{\nu})$) have been calculated⁶⁾ and compared with the SLAC⁷⁾, DESY⁸⁾ and UA1 data. For $\phi \sim 0.1 - 0.2$ and $m_{Z_1} = 90$ Gev and $m_{Z_2} = 200$ Gev a fit to the SLAC and DESY data for $Z \rightarrow \lambda^0 h^0$ yields $\sim 4-8$ monojet events above the QCD background, produced by $W \rightarrow \tau\nu_\tau$ and $Z^0 \rightarrow \nu\bar{\nu} + \text{gluons}$. Similar results were obtained for $\phi \sim 0.1-0.2$ and $m_{Z_1} = 90$ Gev, $m_{Z_2} = 96$ Gev.

The Glashow-Manohar⁹⁾ model based on the standard model with two Higgs doublets Φ_1, Φ_2 and the discrete, global symmetry $\Phi_i \rightarrow -\Phi_i$, predicts $\phi \sim 1$ and is ruled out with a 95% confidence level by the SLAC⁷⁾ and DESY⁸⁾ data.

REFERENCES

1. J.W. Moffat, Phys. Letts. B154, 444 (1985).
2. UA1 Collaboration, G. Arnison et al., Phys. Letts. 139B (1984) 115.
3. C. Rubbia, Talk given at the Spring Meeting of the American Physical Society, Washington D.C., April 1985.
4. E.H. deGroot, G.J. Gounaris, and D. Schildknecht, Z. Phys. C5, 127 (1980).
5. G. Pócsik and G. Zsigmond, Z. Phys. C10, 367 (1981).
6. R. Campbell and J.W. Moffat, University of Toronto, preprint, May 1985.
7. W.W. Ash et al., SLAC-PUB-3581 (1985).
8. W. Bartel et al., DESY preprint 85-022, 1985.
9. S.L. Glashow and A. Manohar, Phys. Rev. Letts. 54, 526 (1985).

THE DØ DETECTOR FOR THE FERMILAB COLLIDER

Paolo Franzini[†]
Columbia University, New York, N. Y. 10027

Abstract

Some of the main features of a new detector for the 2 TeV Fermilab proton-antiproton collider are presented. The "DØ detector" is the first example of a detector relying entirely on calorimetry and hermeticity to achieve excellent energy resolution. Only muon momenta are magnetically measured in a very thick magnetized iron absorber.

INTRODUCTION

By late '86 the Fermilab superconducting ring is expected to be operating as a proton-antiproton collider, sometimes known as TEV-I, at a c.m. energy $\sqrt{s} = 2$ TeV, with a luminosity of $10^{30} \text{ cm}^{-2} \text{ s}^{-1}$. In a departure from tradition, the Fermilab Program Advisory Committee decided, in mid 83, to call for a new general purpose detector for the Fermilab collider, to be located at the DØ interaction area. The new detector is supposed to be complementary to the CDF detector, now nearing completion, with emphasis on calorimetry and lepton identification. The basic design goals were set forward by the newly formed DØ collaboration [1] in a Design Report submitted in December 1983. Following approval by the Fermilab PAC, by technical committees and by the US DOE administration, the DØ detector

is now beginning to become reality. A revised design report was prepared in November 1984 [2].

THE DØ DETECTOR

At the new energies and luminosities available at the Fermilab collider it will become feasible to study properties of the weak interactions at an unprecedented level of accuracy as well as to uncover possible new phenomena [2]. The experience of the UA1 and UA2 detectors at CERN has clearly shown the importance of very good hadronic and electromagnetic energy resolution, with 4π coverage and fine segmentation.

At $\sqrt{s} = 2$ TeV "particles" to be detected are: electrons, photons, jets, neutrinos (photinos? etc.) and muons. With the exception of muons all of the above are best detected by calorimetry. In the case of neutrinos, as well as other more exotic objects such as photinos etc., calorimetry must be hermetic. Thus insensitive regions between detector elements can severely limit the "detectability" of non interacting particles and, of course coverage down to extremely small angles is essential. The DØ detector has no central magnetic field, allowing for construction of a compact and thicker calorimeter which is of paramount importance in detecting the above "particles".

The importance of complete coverage of the full solid angle is schematically illustrated in figure 1. Figure 1a shows the frequency of measuring a missing transverse momentum p_t^M , in events where none is missing, with an ideal detector for which measurements errors are normal-distributed. If small angles are not covered and the detector has dead regions (cracks) or regions of different response, the rms error on p_t^M might hardly be affected but tails appear in the frequency distribution which might completely obscure signals of interest, as indicated in figure 1b. See also M. Barnett's talk at this Rencontre.

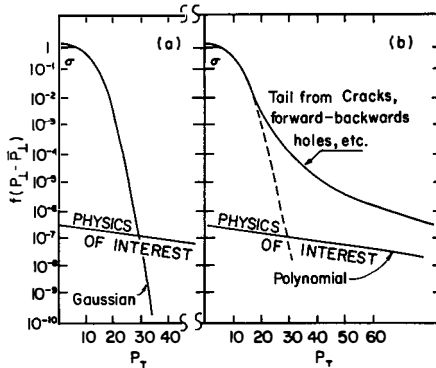


Figure 1. The distribution of the observed missing p_t^M .

Uranium-Liquid-Argon calorimetry [4] offers at present the best energy resolution and the most reliable calibration. The core of the DØ detector is a uranium-liquid-argon calorimeter surrounding the interaction region to within 1° of the two beams. Since e.m. showers develop more rapidly than hadronic ones and have considerably smaller transverse dimensions the calorimeter is subdivided longitudinally into 4 e.m. compartments for a total of ≈ 20 radiation lengths (X_0) followed by 4 hadronic compartments with total thickness from 7 nuclear absorption lengths (λ_0) at 90° to $9 \lambda_0$ at small angles. The calorimeter is subdivided into ~ 5000 e.m. 'towers' and ~ 1000 hadronic towers pointing to the interaction region, covering constant intervals in rapidity and azimuth. Table I gives some parameters of the DØ and CDF calorimeters in the central region.

TABLE I

Parameter	DØ Detector	CDF Detector
Coverage	$45-135^\circ$	$50-135^\circ$
Thickness (90°)	$7 \lambda_0$	$5.6 \lambda_0$
Resolution e.m.	$11\%/\sqrt{E} + 0.5\%$	$14\%/\sqrt{E} + 1.5\%$
Hadr.	$37\%/\sqrt{E} + 0.5\%$	$62\%/\sqrt{E} + 5.5\%$
Segmentation e.m.	3360 twrs, 4 smpls	480 twrs, 1 smpl
Hadr.	576 twrs, 4 smpls	384 twrs, 1 smpl

Tracking around the interaction region is provided by a vertex chamber and a cylindrical shell drift chamber. Small angles are covered by more drift chambers. Figure 2 is a sketch of the DØ detector in the interaction hall.

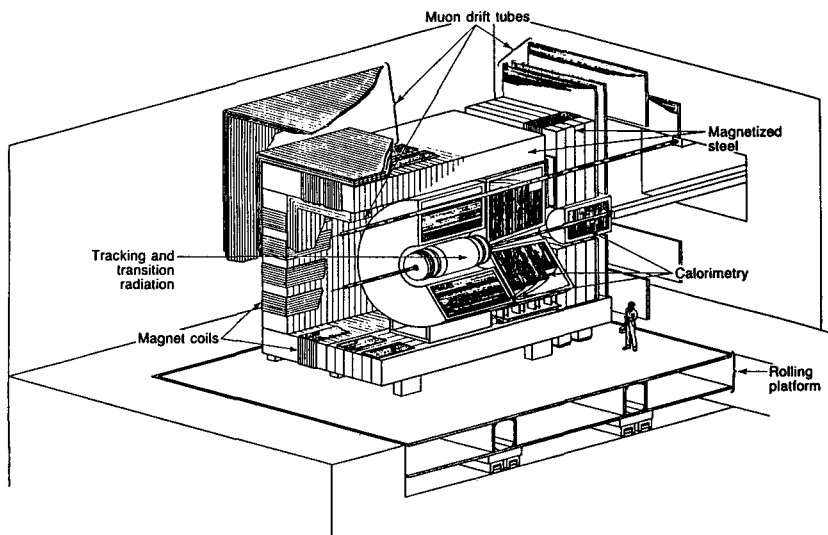


Figure 2. The DØ Detector.

The chambers provide good track pairs resolution and specific ionization measurements for rejection of electron pairs from converted photons. Stacks of transition radiation detectors (TRD) in the central region and at small angles provide electron identification. The four sampling of the e.m. shower, together with the TRD's, give superior electron-hadron separation. For isolated electrons the information from the depth segmented e.m. calorimeter and the TRD detectors results in a pion/electron confusion of less than 4×10^{-5} and, for electrons close to a jet, of less than 10^{-2} . In addition the e.m. calorimeter can distinguish γ from π^0 and other neutral particles decaying into two or more photons, both by shower shape and conversion depth, thus allowing measurements of direct photon production.

Muons are identified as particles which cross without interaction the entire calorimeter and additional magnetized iron which allows momentum analysis with an accuracy of 17% up to transverse momenta of 300 GeV. The total thickness of material that a muon must cross varies from $13 \lambda_0$ at 90° to $18 \lambda_0$ at 10° . The incident energy of a single pion, which results in average in one leakage particle is 600 GeV at 90° and 6000 GeV at 10° . Muons can therefore be identified with negligible background, even in the core of a shower over the whole energy range. The muon detector system covers 99% of 4π .

PERFORMANCE OF THE $D\bar{0}$ DETECTOR.

Figure 3 shows the expected performance of the $D\bar{0}$ detector in terms of its ability to correctly measure transverse missing momentum in $p\bar{p}$ collisions at 2 TeV. The calculation has been performed using events generated with the Isajet Monte Carlo program of F. Paige. [5]. The effect of the 1° hole is shown alone and combined with the resolution of the detector, determined from energy and angular resolutions. Both curves correspond to events in which heavy quarks decay non leptonically and there is no W or Z production. Semileptonic decays of quarks give an additional signal, as shown by the dashed line. This contribution can overwhelm other signals, as from the production of gluinos, followed by decay into a photino, which escapes the detector. Events with neutrinos from quark decays can however be removed if

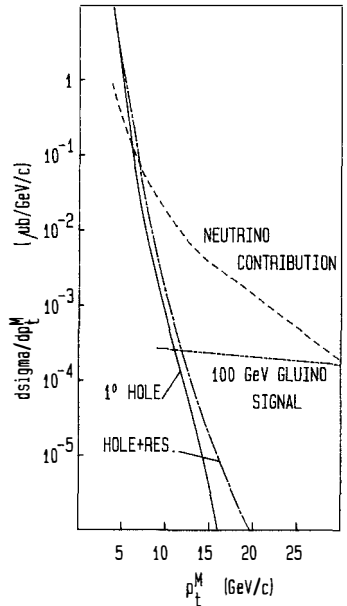


Figure 3. The $D\bar{0}$ p_t^M response.

the associated lepton can be recognized with high efficiency. Calculations show that the contribution to the p_t^M spectrum from quark decays can be reduced by at least a factor ten, thus allowing observation of a possible signal due to production of 100 GeV gluinos [6] as indicated in figure 3. The "gluino signal" in figure 3 should be understood as just an example of how a new class of phenomena might be detected in the future. The point we want to stress is the importance of lepton identification over the full solid angle, with high efficiency, in conjunction with superior calorimetry.

PHYSICS WITH THE DØ DETECTOR

The following is a list of some of the Physics for which the DØ detector is best suited.

1. The accurate simultaneous measurement of the W^\pm and Z^0 masses.
2. Measurement of W and Z width to 200 MeV accuracy.
3. Measurement of $p\bar{p} \rightarrow WYX$, to directly observe the electroweak gauge coupling.
4. Measurements of γ/π^0 , $\gamma+2\text{jets}$ vs. 3 jets to measure the strong coupling constant α_s .
5. Observe $W \rightarrow q\bar{q}$ from dijet invariant mass.
6. Searches for exotic new objects, resulting in leptons, jets or missing p_T , such as : heavy leptons, SUSY particles, heavy quarks, leptoquarks etc.

ACKNOWLEDGEMENTS

I wish to acknowledge the work of all members of the DØ Collaboration which resulted in the conception and the design of the DØ Detector.

REFERENCES

†For the DØ Collaboration.

1. The DØ collaboration consists of physicists from Brookhaven National Laboratory, Brown University, Columbia University, Fermilab, Florida State University, Berkeley Lawrence Laboratory, University of Maryland, Michigan State University, Northwestern University, University of Pennsylvania, University of Rochester, CEN Saclay, State University of New York at Stony Brook and Virginia Polytechnic Institute.
2. DØ Design Report, November 1984.
3. Proc. 1982 DPF Summer Study, etc. Ed. R. Donaldson, R. Gustafson and F. Paige. "Snowmass 1982".
4. C. W. Fabian et al., Nucl. Inst. Meth. 141 (1977) 60
5. F. Paige, BNL-27066
6. S. Aronson et al., Snowmass 1982.

A POTPOURRI OF CLEO RESULTS

Lynn Garren
 Wilson Synchrotron Laboratory
 Cornell University
 Ithaca, New York 14853, U.S.A.

Abstract

Results are presented for several decay modes observed by the CLEO detector. From the decay $\bar{B}^0 \rightarrow D^{**} + X$, we find $N(D^{**}/B) = 0.23 \pm 0.05 \pm 0.08$. From this decay and the decay $\bar{B}^0 \rightarrow D^{**} \ell \bar{\nu}$, we estimate the ratio D^{*+}/D^+ . We have measured the branching ratio $BR(\bar{B}^0 \rightarrow D^{*+} \rho^-) = 7.3 \pm 2.6 (+9.2, -2.6)\%$. We set 90% confidence level upper limits for $BR(\Upsilon(1S) \rightarrow \rho^0 \pi^0) < 0.019\%$ and $BR(\Upsilon(1S) \rightarrow \rho^+ \pi^-) < 0.025\%$.

In this report, I will discuss recent results of B meson decay into inclusive and exclusive D^* decay modes, as well as a search for the decay $\Upsilon(1S) \rightarrow \rho\pi$.

All data were collected at the Cornell Electron Storage Ring (CESR) with the CLEO detector.^{1]} B meson decay studies use 40.6 pb^{-1} on the $\Upsilon(4S)$ and 16.8 pb^{-1} on the continuum below the $\Upsilon(4S)$. We have a total of 41,600 $B\bar{B}$ events. I will also discuss results from 12.1 pb^{-1} at the $\Upsilon(1S)$ and 4.4 pb^{-1} from the nearby continuum. There are 274,000 $\Upsilon(1S)$ decays in the data sample. In all quoted results, the first error is statistical and the second systematic.

The B meson is produced copiously at the $\Upsilon(4S)$, as this is just above $B\bar{B}$ threshold. In the spectator model, the B decays via W^* into a charmed meson and a quark or lepton-neutrino pair. Hence, the D^* is a natural signal to use for studying B decays. Since the momentum carried by the B meson is only 420 MeV/c at the $\Upsilon(4S)$, we can approximate the decay kinematics by assuming that the B decays from rest.

Inclusive Decay of B mesons into Charged D^*

In a search for the inclusive decay $B \rightarrow D^{*+} X$, we look for the decay mode $D^{*+} \rightarrow D^0 \pi^+ + K^- \pi^+ \pi^+$ and its charged conjugate. We do not use particle identification, but make appropriate combinations of three charged tracks, assigning two to be pions and one to be a kaon. We then require that the mass difference between the $K\pi$ mass and the $K\pi\pi$ mass be within $2.5 \text{ MeV}/c^2$ of the mass difference between the D and D^* . To eliminate random track combinations, we require $\cos\theta > -0.8$, where θ is the angle between the K and D^0 , measured in the rest frame of the D^0 .

Figure 1 shows the $K\pi$ mass distribution for $\Upsilon(4S)$ and continuum data. Because we require the $K\pi\pi$ momentum to be between 1.0 and 2.6 GeV, we see no contribution to D^* production from the continuum. The data are binned in momentum and each mass distribution is fit to an

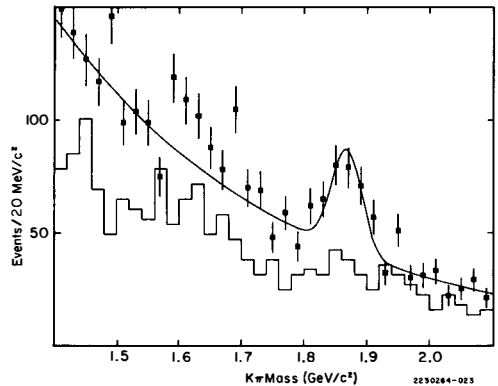


Figure 1. The $K^- \pi^+$ invariant mass spectrum, where the three-particle combination $K^- \pi^+ \pi^+$ was required to satisfy $|\mathcal{M}(K\pi\pi - K\pi) - 145.4 \text{ MeV}/c^2| < 2.5 \text{ MeV}/c^2$, $\cos\theta > -0.8$ and $1.0 \text{ GeV}/c < p_{K\pi\pi} < 2.6 \text{ GeV}/c$. The points represent $\Upsilon(4S)$ data, the solid histogram is scaled continuum and the curve is the result of a fit of the points to a Gaussian peak with free mass and an exponential background.

exponential background plus a gaussian distribution. Efficiencies and widths of the D^0 distributions are found from Monte Carlo generated $B\bar{B}$ events. Figure 2 shows the D^{**} and D^0 momentum spectra. The D^* momentum points below 1.0 GeV/c are maximum values derived from our D^0 measurement by assuming that each D^0 comes from a D^{**} decay. The curve plotted in Figure 2a is the spectrum from the V-A decay $B \rightarrow D^{**} e \bar{\nu}$. The similarity of the semileptonic momentum spectrum to both the D^* and the D momentum spectra is strong evidence for spectator dominance in B meson decay.

The number of observed charged D^* 's with momentum greater than 1.0 GeV/c is 510 ± 120 . Using $BR(D^{**} \rightarrow D^0 \pi^+) = 0.60 \pm 0.15^3]$ and $BR(D^0 \rightarrow K^- \pi^+) = 0.049 \pm 0.010,^4]$ we calculate the number of charged D^* 's above 1.0 GeV/c produced per B:

$$n_{D^{**}}(p > 1 \text{ GeV/c}) = 0.21 \pm 0.05 \pm 0.07 \text{ per B meson decay.}$$

We use the V-A momentum spectrum to extrapolate to momenta below 1 GeV/c:

$$n_{D^{**}} = 0.23 \pm 0.05 \pm 0.08 \text{ per B meson decay.}$$

To estimate total D^* production, we use the following assumptions:^{5]}

$$BR(\Upsilon(4S) \rightarrow B^0 \bar{B}^0) = 0.45 \pm 0.05 \quad \frac{BR(B^0 \rightarrow D^{*+} X)}{BR(B^0 \rightarrow D^{*+} X) + BR(B^0 \rightarrow D^{*0} X)} = 0.75 \pm 0.25$$

With these assumptions, the ratio of neutral to charged D^* 's is 1.1 ± 0.2 . Since a D^* of momentum 1.0 GeV/c will decay to a D with momentum 0.93 ± 0.05 GeV/c, we compare D^* 's of momenta greater than 1.0 GeV/c to D^0 's with momenta greater than 0.93 GeV/c. The number of D^0 's from B meson decay is $0.11 \pm 0.13 \pm 0.07$ per B.^{2]} The ratio D^*/D^* is $0.68 \pm 0.30 \pm 0.19$. The total $D+D^*$ production from B meson decay is $0.71 \pm 0.23 \pm 0.15$, which is smaller than expected.^{6]}

Observation of the Decay $\bar{B}^0 \rightarrow D^{*+} \rho^-$

We have looked for the decay $\bar{B}^0 \rightarrow D^{*+} \rho^-$ and its charged conjugate, via the decays $D^{*+} \rightarrow D^0 \pi^+$ and $\rho^- \rightarrow \pi^- \pi^0$. We search for two oppositely charge tracks and a π^0 , where the π^0 is identified by shower counters outside the magnet coil.^{1]}

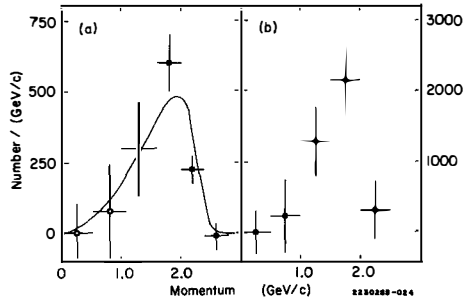


Figure 2. (a) Momentum distribution of D^{**} from B meson decay. Points above 1 GeV/c (solid squares) are direct measurements, while those below (open squares) are maximum numbers based on D^0 data. The curve is the distribution expected for the semileptonic V-A decay $B \rightarrow D^{**} e \bar{\nu}$ and is scaled to the number of D^{**} 's in the momentum range above 1 GeV/c. (b) Momentum distribution of D^0 from B decay.

Because the B meson is nearly at rest, the ρ momentum must be between 2.0 and 2.4 GeV/c. Therefore, we require the $\pi^-\pi^0$ momentum to be in this range. The π^+ emitted by the D^{*+} will have a momentum less than 0.23 GeV/c. Kinematics also require that the direction of this pion be within 26° of being backward to the ρ direction. The only unknown is the azimuthal angle of the D^{*+} about the π^+ . Since energy conservation requires that the energy of the B^0 equal the beam energy, the B mass will reconstruct to within 14 MeV of the beam energy if this is a genuine B decay. We calculate M_{\max}^0 , the maximum allowed B^0 mass.

Figure 3 shows $M_{\max}^0 - E_{\text{beam}}$ for different $\pi^-\pi^0$ mass regions. We see a clear enhancement near $M_{\max}^0 = E_{\text{beam}}$ in the ρ mass region, Figure 3b. Three background estimates are used: (1) same sign charged pions, (2) reflecting the momentum of the π^+ , and (3) a three charged pion combination. None of these background estimates show a signal in the ρ mass region. After subtracting background, we observe 12.4 ± 4.5 $D^{*+}\rho^-$ events.

Since the data are insufficient to determine the helicity state of this decay, our efficiency, $0.74 \pm 0.37\%$, is the average of Monte Carlo results for helicity-1 and helicity-0 states. Using $\text{BR}(D^{*+} \rightarrow D^0 \pi^+) = 0.60 \pm 0.15$, $\text{BR}(\Upsilon(4S) \rightarrow B^0 \bar{B}^0) = 0.40$,^[7] and $\text{BR}(\bar{B}^0 \rightarrow D^{*+} \pi^-) = 2.1 \pm 0.6 \pm 0.5\%$,^[8] we obtain:

$$\text{BR}(\bar{B}^0 \rightarrow D^{*+} \rho^-) = 7.3 \pm 2.6 \begin{matrix} +0.2\% \\ -2.6\% \end{matrix}$$

$$\frac{\text{BR}(\bar{B}^0 \rightarrow D^{*+} \rho^-)}{\text{BR}(\bar{B}^0 \rightarrow D^{*+} \pi^-)} = 4.2 \pm 2.9$$

These results are consistent with theoretical predictions.^[8,9]

Observation of the Semileptonic Decay of the B meson into D^{*+}

We have also seen the exclusive semileptonic decay $\bar{B}^0 \rightarrow D^{*+} \ell^- \bar{\nu}$, where ℓ^- is a μ^- or e^- . We have identified these events by using a tagged lepton and searching for the pion from the decay $D^{*+} \rightarrow D^0 \pi^+$. We use all charged tracks with opposite sign to the lepton as pion candidates. To reduce background, we require the lepton momentum to be between 1.2 and 2.4 GeV/c. We can approximate

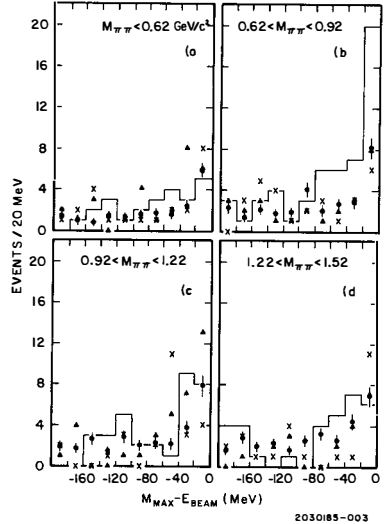


Figure 3. The distribution of $\Upsilon(4S)$ events in $M_{\max}^0 - E_{\text{beam}}$ for different regions of $M_{\pi\pi^0}$. The histogram shows the data for the channel $\bar{B}^0 \rightarrow D^{*+} \pi^- \pi^0$. The plotted points show three background estimates: (1) triangles - the same sign channel ($\bar{B}^0 \rightarrow D^{*+} X^+$, $X^+ \pi^+ \pi^0$); (2) crosses - the reflected soft pion background; (3) circles - the channel $\bar{B}^0 \rightarrow D^{*+} X^0$, $X^0 \pi^+ \pi^+$, multiplied by a normalization factor.

2030185-003

the direction of the D^* by the direction of the pion, and use this information to measure $\cos\theta$, the angle between the D^* and the lepton. In the approximation that the B meson decays at rest, the ratio:

$$r \equiv \frac{E_\pi}{E_{D^*}} \equiv \frac{m_\pi}{m_{D^*}} = 0.069$$

This ratio will be used to identify semileptonic D^* decays.

We calculate E_{D^*} from $\cos\theta$ and p_ℓ , the lepton momentum. We require that $|\cos\theta - \cos\theta^*| < 0.5$, where θ^* is the calculated angle for $r = 0.069$. To measure the background, we use the same sign pion as the lepton. The r distributions for same sign and opposite sign combinations are shown in Figure 4. They are normalized above $r = 0.13$, since 99% of the semileptonic D^* decays have $r < 0.11$. To see the signal, we subtract the same sign combinations from the opposite sign combinations, as shown in Figure 5a. The data agree well with the expected distribution as calculated from $B\bar{B}$ Monte Carlo events (see Figure 5a). We have checked our technique by doing the same analysis with the lepton from the previous event and see no signal, as shown in Figure 5b. Figure 5c shows the continuum r distribution. We see no background from the continuum.

Our signal contains 255±56 events in the mode $D^{*+}\ell^-\bar{\nu}$, $D^{*+}\rightarrow D^0\pi^+$, with an efficiency of

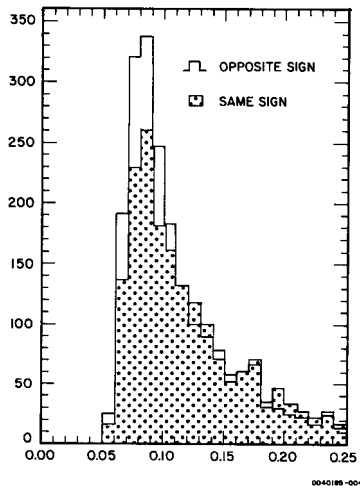


Figure 4. The r distribution for opposite and same sign pions, normalized for $r > 0.13$.

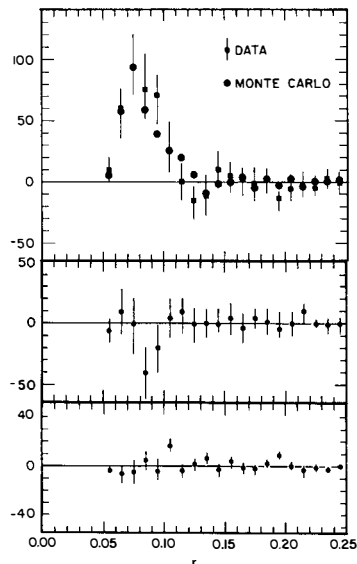


Figure 5. (a) Resultant r distribution, after subtracting same sign from opposite sign of Figure 4. The circles are Monte Carlo points. (b) Subtracted r distribution with lepton momentum of previous event. (c) Subtracted r distribution using data from the continuum region below $1(4S)$.

0.13 ± 0.01 . Using $BR(D^{*+} \rightarrow D^0 \pi^+) = 0.60 \pm 0.15$, $BR(\Upsilon(4S) \rightarrow B^0 \bar{B}^0) = 0.45 \pm 0.05$, and $BR(B^0 \rightarrow X \ell \nu) = 0.116 \pm 0.006^{10]}$ we calculate the ratio $D^*/D+D^* = 0.77 \pm 0.19 \pm 0.22$.

Upper Limit on $\Upsilon(1S) \rightarrow \rho \pi$

Using 12.1 pb^{-1} of data taken in the fall of 1984 at the $\Upsilon(1S)$, we have searched for the decay $\Upsilon \rightarrow \rho \pi$ in both charged and neutral modes. The branching ratio for $\Psi \rightarrow \rho \pi$ is 1.2% ,^{11]} and we can use a naive scaling model to predict the branching ratio of $\Upsilon \rightarrow \rho \pi$:

$$BR(\Upsilon \rightarrow \rho \pi) = \frac{m_c^2}{m_b^2} \frac{\Gamma(\Upsilon \rightarrow \text{hadrons})}{\Gamma(\Psi \rightarrow \text{hadrons})} BR(\Psi \rightarrow \rho \pi) = \frac{(1.5 \text{ GeV}/c^2)^2 (44 \text{ keV})}{(5.0 \text{ GeV}/c^2)^2 (63 \text{ keV})} (1.2\%) = 0.08\%$$

We have enough data to see a signal at this level. We look for the decays $\Upsilon \rightarrow \rho^+ \pi^- \rightarrow \pi^+ \pi^0 \pi^-$ and its charged conjugate, and $\Upsilon \rightarrow \rho^0 \pi^0 \rightarrow \pi^+ \pi^- \pi^0$.

We search for a π^0 and two charged tracks which are not lepton candidates. The pion emitted by the Υ will be in the opposite hemisphere to the pion pair produced by the ρ . We require that the mass of the two pions in the same hemisphere be within $300 \text{ MeV}/c^2$ of the ρ mass, and that the three pion mass be within $1.2 \text{ GeV}/c^2$ of the $\Upsilon(1S)$ mass. Only four events pass all cuts. When these events are scanned, we retain two as good $\rho \pi$ candidates. No events are seen in the continuum data.

Our efficiency is 0.078 ± 0.007 in the charged mode and 0.044 ± 0.010 in the neutral mode. Using 2 candidate events in the charged mode and none in the neutral mode, we set 90% confidence level upper limits for the branching ratios, $BR(\Upsilon(1S) \rightarrow \rho^+ \pi^-) < 0.025\%$ and $BR(\Upsilon(1S) \rightarrow \rho^0 \pi^0) < 0.019\%$. If we use the two events in the charged mode to compute a branching ratio, we get $BR(\Upsilon \rightarrow \rho^+ \pi^-) = 0.009 \pm 0.002\%$, an order of magnitude below our naive scaling prediction.

References

1. D. Andrews et al., Nucl. Instr. Meth. **211**, 47 (1983).
2. J. Green et al., Phys. Rev. Lett. **51**, 347 (1983).
3. G. Goldhaber et al., Phys. Lett. **69B**, 503 (1977).
4. R. H. Schindler, California Institute of Technology Report No. CALT 68-1161, 1984 (unpublished).
5. We do not have conclusive evidence to indicate if $BR(\Upsilon(4S) \rightarrow B^0 \bar{B}^0)$ is 0.40 or 0.50, and therefore choose the average of these values. We also use the average $\bar{B}^0 \rightarrow D^{*+}$ fraction. This number would be 1.0 for pure spectator decay with no fragmentation, and 0.5 for full fragmentation.
6. We expect 1.1 charmed mesons per B decay.
7. S. Behrends et al., Phys. Rev. Lett. **50**, 881 (1983).
8. R. Giles et al., Phys. Rev. D **30**, 2279 (1984).
9. A. Ali, J. G. Korner, G. Kramer and J. Willrodt, Z. Phys. C **1**, 269 (1979); F. Hussain and M. D. Scadron, Phys. Rev. D **30**, 1492 (1984).
10. A. Chen et al., Phys. Rev. Lett. **52**, 1084 (1984).
11. C. G. Wohl et al. (Particle Data Group), Rev. Mod. Phys. **56**, S20 (1984).

RECENT RESULTS ON WEAK INTERACTIONS WITH CUSB

P. M. Tuts
Columbia University
New York, NY 10027
U.S.A.



ABSTRACT

We discuss some recent results which bear on electroweak interactions using CUSB-I and a quadrant of CUSB-II. The $T(5S)$ and $T(6S)$ resonances which have recently been discovered in the context of coupled channel model calculations bear promise to be B^* and B_S factories and hence bear on $B^0\bar{B}^0$ mixing. The B^* meson has been discovered (the measured fraction of 1.4 B^* per $b\bar{b}$ event agrees with the model calculation) and thus yields an estimate of the B decay constant, f_B , of ~ 200 MeV. A brief description of the CUSB-II BGO detector and the performance of a quadrant is presented, along with the results of a recent 400,000 T event run. Preliminary results on a Higgs search in radiative T decay yield a null result; branching ratio upper limits for $2.5 \text{ GeV} < M_H < 9 \text{ GeV}$ are presented.

INTRODUCTION

The T system has proved to be a very rich testing ground for our understanding of QCD and naked beauty, and the CUSB detector has proved to be a very powerful instrument with which to study it. The QCD aspects of recent CUSB results were presented in the previous Moriond session^{1]}; here I will concentrate on our new results that are relevant to this electroweak session. In particular, I will present the results of recent analyses of data taken in the energy region above the T(4S) with the CUSB-I detector^{2]}. This region above the B threshold shows a complicated structure with evidence of both B* and higher S state resonances. I will also present preliminary results taken with the new CUSB-II detector^{3]} during a recent T(1S) run in which a search for Higgs bosons in radiative decays was made.

ABOVE THE B THRESHOLD

A high statistics run^{4]} was taken between August 1983 and June 1984, during which 120 pb^{-1} of integrated luminosity were collected in the scan energy region from 10.6 GeV to 11.25 GeV. The result of this scan is shown in figure 1(a) with the T(4S) prominently displayed on the left (note that the zero has been suppressed in the plot). Standard hadronic event criteria that require $E > 700 \text{ MeV}$ and the presence of minimum ionizing tracks were used to analyze this data. Clear structure is visible above the continuum level below the T(4S) (solid horizontal line), broad but resolved peaks are seen at $\sim 10.8 \text{ GeV}$ and $\sim 11 \text{ GeV}$. If this structure above the continuum level is resonance related, then it should remain after a thrust cut is made to reduce the continuum ($q\bar{q}$ like) events. Figure 2b shows the result of just such a thrust cut ($T < 0.8$), which the above threshold structure survives.

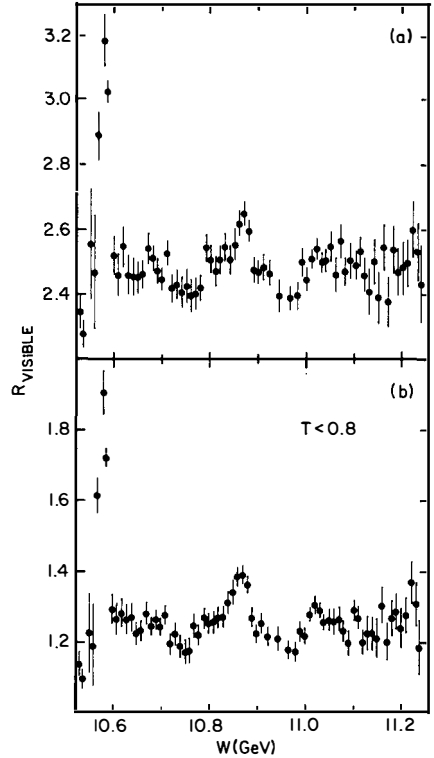


Figure 1a. R_{VISIBLE} vs E_{cm} for the region above the T(4S).

(b) the same for events with thrust < 0.8 .

Further evidence that these excess events in the region above the T(4S) form b flavored hadrons comes from a preliminary analysis of high energy electron production. Figure 2 shows the yield of high energy ($E_e > 1$ GeV) electrons from 10.6 to 11.2 GeV; the data show an excess of high energy electron events which are interpreted as electrons from the β decay of b flavored mesons ($B + e\nu_X$). In order to proceed further with unravelling the complex structure above the T(4S), we have used a coupled channel model along the lines of reference 5, where we have made some simplifying assumptions and reasonable threshold assumptions. This model was used in extracting the

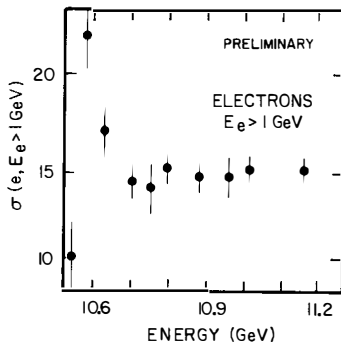


Figure 2. High energy electron cross section.

resonance parameters of the T(5S) and T(6S) resonances ($M(5S) = 10.845 \pm 0.001$, $M(6S) = 11.02 \pm 0.03$ GeV) and to predict the resonance cross section above the T(4S). The complex structure arises from the position of the zero's in the decay amplitudes of the T(4S), T(5S), T(6S), and T(7S) resonances to the two body final states $B_d(u)\bar{B}_d(u)$, $B_d(u)\bar{B}^*_d(u)$, $B^*_d(u)\bar{B}^*_d(u)$, $B_S\bar{B}_S$, $B^*_S\bar{B}_S$, $B^*_S\bar{B}^*_S$ that have been considered. The coupled channel prediction provides a remarkably good fit to the data as can be seen in figure 3 (the solid line is the prediction).

What can be learned about relative amounts of B , B^* , B_S and B^*_S produced in the region above the T(4S)? and what are the implications for $B^0\bar{B}^0$ mixing? The answer to the first question can be readily extracted from the coupled channel model calculation. Figure 4(a) shows the resonance extraction, 4(b) shows the relative amounts of B and B^* (i.e. $b\bar{u}$ and $b\bar{d}$) mesons compared to the total amounts of B_S and B^*_S (i.e. $b\bar{s}$) mesons. Barring indications that there is increased relative K production in the region of B_S production indicated by the calculation, the evidence supporting the model is provided by the

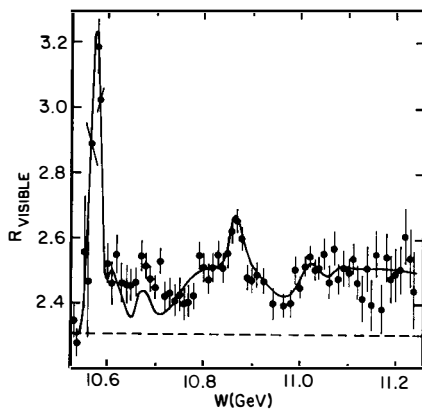


Figure 3. Coupled channel model calculation.

predicted energy dependence of the $B\bar{B}$, $B^*\bar{B} + \bar{B}^*B$, and $B^*_S\bar{B}^*_S$ cross sections as shown in figure 5. The average number of B^* produced per resonant event between 10.6 and 11.1 GeV is predicted to be 1.4 which is in good agreement observations.

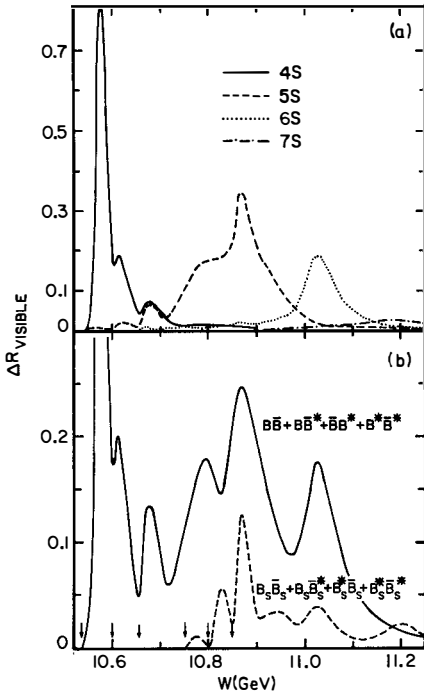


Figure 4. Coupled channel model calculation contribution from (a) T(nS) and (b) B and B_S .

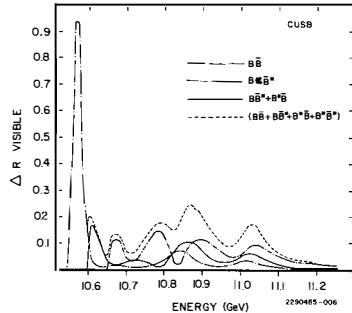


Figure 5. $\Delta R_{\text{visible}}$ for $B\bar{B}$, $B\bar{B}^* + B\bar{B}^*$, $B^* \bar{B}^*$.

OBSERVATION OF THE B^*

From scaling arguments using the measured $D^* - D$, $K^* - K$, ... splittings, it is predicted that the splitting of $B^* B$ is ≈ 50 MeV and therefore the branching ratio $BR(B^* \rightarrow B + \gamma) \sim 100\%$, with a photon energy given by $(M_{B^*}^2 - M_B^2)/2M_{B^*} = .995 \Delta M$. Initial analyses of the inclusive photon spectrum at the T(4S) energy showed that no 50 MeV photons were produced and provided the first stringent

bounds on the mass of the B meson^{6]}. The inclusive photon spectrum for hadronic events at the T(4S) energy is shown in figure 6(a) - there is no indication of any quasimonochromatic 50 MeV photon line. The difficulties in searching for photons from B^* decay above the T(4S) are (1) although the branching ratio is 100%, the cross section for producing B^* 's is small, since $\sigma(e^+e^- \rightarrow b\bar{b}) / \sigma(e^+e^- \rightarrow \text{hadrons}) \approx 8\%$, for that reason we choose to look at the region of enhanced $b\bar{b}$ production at the T(5S), and (2) the Doppler broadening of a 50 MeV photon line from the T(5S) region has a 15% Doppler broadening. Details of the B^* search are given in ref 7, a summary of the results and analysis are given here. The first indications of an excess of ≈ 50 MeV photons in the inclusive spectrum for events at the T(5S) was seen in higher efficiency, lower resolution analyses as indicated in figure 6. A clear excess at $E_\gamma = 50$ MeV is seen relative to the T(4S) spectrum, with an observed width consistent with Doppler broadening folded into the expected resolution.

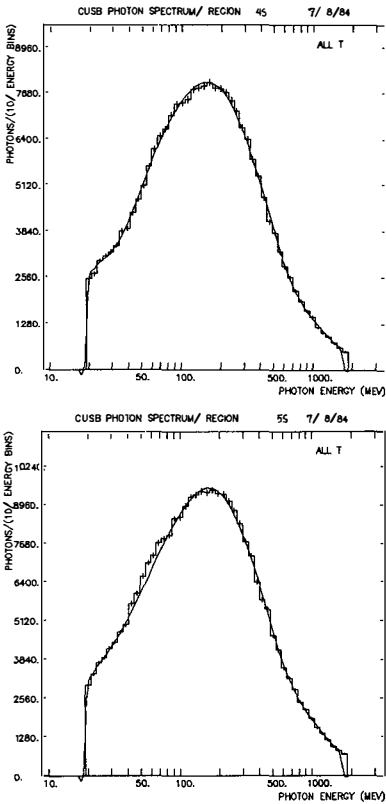


Figure 6. Inclusive photon for T(4S) (top) and T(5S) (bottom).

Further studies of this excess revealed that it was indeed resonance related since the resonance sample could be enhanced relative to continuum like events by (1) applying thrust cuts (as was done in figure 1(b) to increase the $b\bar{b}$ contribution), (2) using thrust cuts and restricting the data to regions of enhanced resonant cross section (i.e. just above the T(4S), at the T(5S) and T(6S)), and (3) selecting a sample of hadronic events with a high energy electron or muon from the β decay of the B^* mesons. Figure 7 shows the effect of the first two of these cuts. Figure 7(a) is the inclusive spectrum for hadronic events >10.62 GeV (without leptons). The fit (solid line) consists of a third order polynomial plus a gaussian of expected resolution and doppler broadening. The spectrum after subtraction of the third order polynomial is shown below in figure 7(d). This figure shows an excess of 2112 ± 424 photons centered at $E_\gamma = 51.6 \pm 1.7$ MeV. Evidence that this excess is $b\bar{b}$ related is provided by the two adjacent plots. The first (figures 7(b) and (e)) shows that after applying a thrust cut to enhance the relative $b\bar{b}$ fraction, the ratio of 50 MeV photons to resonance event remains the same at about 7%, as with 7c,f.

The second independent method involves requiring the presence of a high energy electron or muon with energy greater than 1 GeV. Figure 8 shows the inclusive photon spectrum from such lepton tagged events (solid line) superimposed on a background curve (dotted line) which is constructed from the proper admixture of $b\bar{b}$ events from the T(4S) and the continuum. Although this requirement reduces the event sample by a factor of ten, the signal to background is enhanced by a factor of four. The excess observed after the background is subtracted is 123 ± 28 photons, as shown in figure 8(b). Thus we obtain two independent measurements; a five sigma effect from the inclusive spectrum analysis and a 4.4 sigma effect from the lepton tagged analysis. The average

number of B^* per $b\bar{b}$ event is 1.4 ± 0.5 (inclusive analysis) and 1.5 ± 0.5 (lepton tagged), which is in good agreement with the earlier model calculation of 1.4. The measured mass difference is $M(B^*) - M(B) = 52 \pm 2 \pm 4$ MeV.

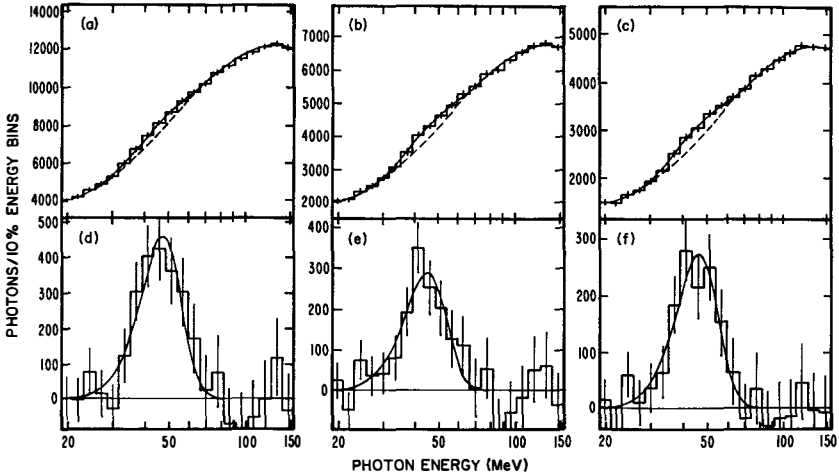


Figure 7. Photon spectra for events without a high energy lepton. a) $10.62 < E_{cm} < 11$ GeV, b) also with thrust < 0.83 , c) restricted energy region $10.62-10.72$, $10.78-10.9$, and $11-11.2$ GeV. The rest are subtracted photon spectra with d) $N_\gamma = 2112 \pm 424$ and corrected $E_\gamma = 51.6 \pm 1.7$ MeV, e) $N_\gamma = 1405 \pm 350$ and corrected $E_\gamma = 49.1 \pm 2.0$ MeV, f) $N_\gamma = 1286 \pm 272$ and corrected $E_\gamma = 50.5 \pm 1.8$ MeV.

THE B DECAY CONSTANT

The calculation of the relative contributions to the cross section and the measurement of the $B^* - B$ mass splitting has implications for the prediction of some B meson properties such as the B decay constant, f_B , and for the prediction of where to best look for $B^0 \bar{B}^0$ mixing. A full discussion of this subject is given in ref. 8. Mixing can be parametrized by the following ratio

$$r_2 = \frac{\Gamma(B^0 \rightarrow B^0) \Gamma(\bar{B}^0 \rightarrow B^0) + \Gamma(\bar{B}^0 \rightarrow \bar{B}^0) \Gamma(B^0 \rightarrow \bar{B}^0)}{\Gamma(B^0 \rightarrow B^0) \Gamma(\bar{B}^0 \rightarrow B^0) + \Gamma(B^0 \rightarrow B^0) \Gamma(\bar{B}^0 \rightarrow \bar{B}^0) + \Gamma(B^0 \rightarrow \bar{B}^0) \Gamma(\bar{B}^0 \rightarrow B^0) + \Gamma(\bar{B}^0 \rightarrow \bar{B}^0) \Gamma(B^0 \rightarrow \bar{B}^0)}$$

which can be written as
 $r_2 = [2x^2 + x^4] / [2(1 + 2x^2 + x^4)]$.

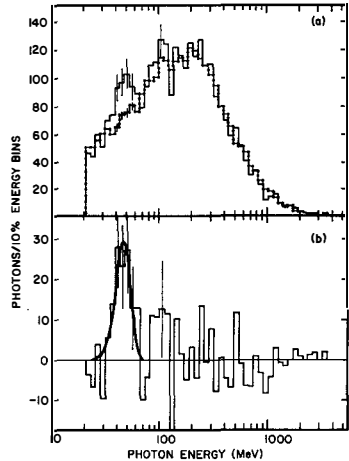


Figure 8. Lepton tagged inclusive photon spectrum.

for L odd (e.g. T(4S) decays), and as $r_2 = [3x^2+x^4]/[2+x^2+x^4]$ for L even (e.g. when one B is produced from B* decay), where $x=\Delta M\tau_B$. ΔM is the calculated mass difference and τ_B is the measured lifetime. For mixing from the various types of B mesons, we find that $r_2=.04$ (for B^0_d mixing for events from the T(4S)), $r_2=.11$ (for B^0_d mixing for events coming from the events just above the T(4S) where B* decay events produce L even $B\bar{B}$'s), and $r_2=.60$ (for B^0_s mixing for events from the T(5S) where B_s 's are produced). Note that mixing at the T(5S) may be up to 15 times greater than that at the T(4S), and therefore the T(5S) may be the optimal "factory", despite the small cross section, in which to observe mixing. One of the parameters that enters in the expression for ΔM is the B decay constant, f_B , which for the non-relativistic $b\bar{b}$ system is given by $f_B^2=[12|\psi(0)|^2]/M_b$ (i.e. the "size" of the B meson), similarly $M_B^*-M_B=[32\pi\alpha_s|\psi(0)|^2]/[9M_b m_q]$ so that $f_B^2 = 27/(8\pi\alpha_s) (M_B^*-M_B) m_q = 200 \text{ MeV}$ which is in the range of theoretical estimates⁸].

HIGGS SEARCH IN RADIATIVE T DECAY

Interest in Higgs from T and ψ decays has been motivated by supersymmetric models in which it is natural to have Higgs's with only a few GeV mass⁹]. Further interest was stimulated by reports of possible Higgs candidates by the MarkIII¹⁰] and Crystal Ball¹¹]

collaborations (christened the ξ and ζ particles respectively). The prediction for the branching ratio is given by $BR(T\rightarrow H+\gamma) = 2.5\times 10^{-4} (1-M_H^2/89.5)x^2$ where M_H is in GeV, and x is the ratio of vacuum expectation values for two Higgs fields (x=1 in the standard model). We report here on preliminary results on a large sample of data taken at the T with the new CUSB-II detector. These results improve on earlier null results obtained using the CUSB-I detector, which obtained upper limits of 0.1% for Higgs masses between 2.5 and 5 GeV.

CUSB-II DETECTOR

The CUSB-II collaboration³] has underway a program to replace the inner portion of the CUSB-I detector with a cylindrical array of bismuth germanate

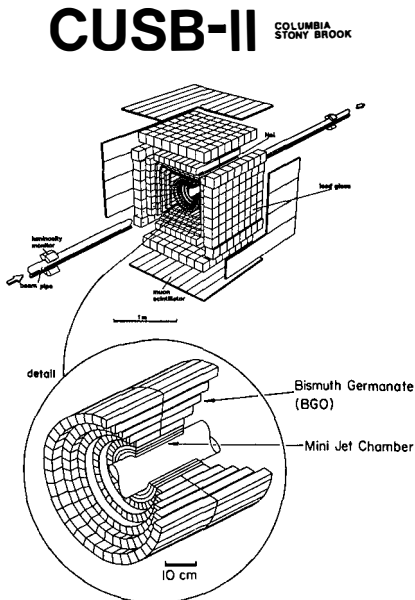


Figure 9. The CUSB-II detector.

(BGO) crystals. The detector consists of 360 BGO crystals segmented in 2 in θ , 36 in ϕ , and 5 in r , which provide a total of 12 radiation lengths. A schematic view of this detector is given in the inset in figure 9, the relation of the BGO to the rest of the detector is also shown. As a test of a BGO calorimeter, we installed an array consisting of 10 ϕ sectors and 8 radiation lengths deep (covering 110° in ϕ). In addition, thin scintillators were installed in front of all BGO and NaI sectors that were not covered by BGO to provide charged particle vetoing. This configuration was used for the data taken during the T run and provided an improvement in resolution of more than a factor of two for BGO vs NaI. Figure 10 illustrates this point; the dashed line represents the energy resolution obtained for bhabha scattering events in the NaI portion of the detector, whereas the solid line represents the resolution obtained for similar bhabha events in the BGO "quadrant". The resolution obtained in BGO at 4.7 GeV is σ_E/E of 1%. The improvement in resolution for the BGO is due in part to the much improved projective cylindrical geometry (no edges) and the improved packing (no cracks). In order to maintain this energy resolution, we have found it necessary to monitor the individual channel gains constantly, even while data taking. This calibration is achieved by placing ^{65}Zn radioactive sources on each crystal and monitoring the peak position of the source signal through a separate high gain source calibration channel. In this way we can maintain a relative crystal to crystal calibration to better than .1%. A calibration for the full detector can be completed in less than one hour.

HIGGS SEARCH RUNNING

For the T run we analyzed 400,000 T events, equivalent to 100,000 T's in the BGO and the remaining 300,000 in the NaI portion of the detector. This data was obtained from a run of 22 pb^{-1} on the T and 6 pb^{-1} on the continuum. The data were taken during the period from September to November 1984 using photon search codes that were adapted from established codes used for the NaI detector. The inclusive photon spectra obtained in this way are featureless and in agreement with expectations, namely due to photons from π^0 . We have fit these spectra using the maximum likelihood method in order to obtain upper limits on the branching ratio $\text{BR}(T \rightarrow H + \gamma)$ at the 90% confidence level. The maximum likelihood was obtained

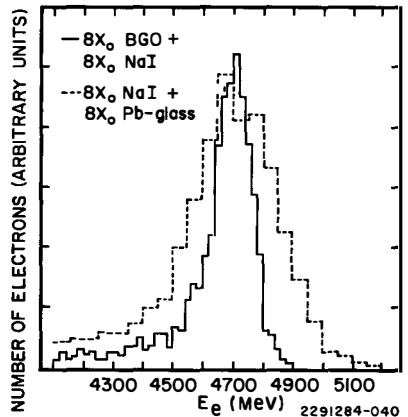


Figure 10. Energy resolution for Bhabha events in BGO (solid) and NaI (dashed).

after locally smoothing the data (since no structure was visible), and combining the NaI and BGO data sets using their respective resolutions of $\sigma_E/E=0.039/\sqrt{E}$ and $\sigma_E/E=0.018/\sqrt{E}$. The preliminary upper limit as a function of the photon energy (or equivalently the Higgs mass) is shown as the solid line in figure 11. For reference the standard model expectations for a single Higgs (i.e. $x=1$) is shown as the dashed line in the figure. Monte Carlo efficiency studies for possible Higgs decay modes are presently underway, although even at this level of uncertainty, there appears to be no possibility of anomalously high Higgs production.

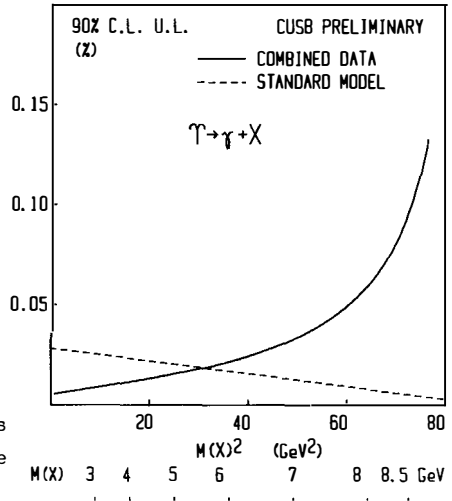


Figure 11. Preliminary $T \rightarrow \gamma X$ limit.

ACKNOWLEDGEMENTS

I wish to acknowledge all my CUSB-I and CUSB-II colleagues, especially J. Lee-Franzini and P. Franzini for invaluable discussions and help in preparation of this talk, and R. D. Schamberger and T. Zhao for their tireless efforts in bringing the BGO detector online. Finally I wish to thank the organizers for an excellent week of physics and skiing. This work was supported in part by the U.S. National Science Foundation.

REFERENCES

1. J. Lee-Franzini, in proceedings of the XXth Moriond Conference (1985).
2. CUSB-I members include: P. Franzini, D. Son, P. M. Tuts, S. Youssef and T. Zhao of Columbia University; J. Lee-Franzini, J. E. Horstkotte, C. Klopfenstein, D. M. J. Lovelock, L. Romero and R. D. Schamberger of SUNY Stony Brook; K. Han, R. Imlay, W. Metcalf and V. Sreedhar of L.S.U.; H. Dietl, G. Eigen, V. Fonseca, E. Lorenz and G. Mageras of MPI-Munich.
3. CUSB-II members include: P. Franzini, D. Son, P. M. Tuts, S. Youssef and T. Zhao of Columbia University; J. Lee-Franzini, T. M. Kaarsberg, C. Klopfenstein, D. M. J. Lovelock, S. Sontz, R. D. Schamberger, J. Willins, C. Yanagisawa and S. Yoakum of SUNY Stony Brook.
4. D. M. J. Lovelock et al., Phys. Rev. Lett. 54 (1985) 377.
5. E. Eichten et al., Phys. Rev. D22 (1980) 1819.
6. R. D. Schamberger et al., Phys. Rev. D30 (1984) 1985; 26 (1982) 720.
7. P. Franzini, in proceedings of the XXth Moriond Workshop (1985).
8. J. Lee-Franzini, in proceedings of the XXth Moriond Workshop (1985) and references therein.
9. D. Nanopolous, Cargese Summer Institute Lectures (1983).
10. D. Hitlin, in proceedings of the Int. Symp. on Leptons and Photons at High Energies, ed. by D. G. Cassel and D. L. Kreinick (Cornell, 1983).
11. C. Peck et al., DESY84-064, SLAC-PUB-3380 (1984).
12. S. Youssef et al., Phys. Lett. 139B (1984) 332.

RECENT RESULTS FROM ARGUS.

David B. MacFarlane
Department of Physics,
University of Toronto,
Toronto, Ontario, Canada

(representing the ARGUS collaboration*)



ABSTRACT. Results are reported from data accumulated by the ARGUS experiment, operating at around 10 GeV centre-of-mass energies in the DORIS II e^+e^- storage ring at DESY. An updated upper limit of 5.0% (90% confidence level) on $D^0-\bar{D}^0$ mixing is presented. The results of a search for narrow states produced in radiative T decays and coupling to $\tau^+\tau^-$ have yielded an upper limit for the product $\text{Br}(T \rightarrow \gamma X) \times \text{Br}(X \rightarrow \tau^+\tau^-)$ of less than 0.1% for $m_X < 8.4 \text{ GeV}/c^2$. A fit to the electron spectrum from semi-leptonic B meson decays provides a preliminary upper limit for the ratio of the Kobayashi-Maskawa matrix elements $|V_{bu}|/|V_{bc}|$ of 0.14 (90% confidence level).

Since early 1983, a large sample of e^+e^- annihilation events at centre-of-mass energies around $10 \text{ GeV}/c^2$ has been accumulated using the ARGUS detector, located in one of two interaction regions at the DORIS II e^+e^- storage ring at DESY. Some recent results in the area of weak interaction physics both from continuum events, and from resonance decays of various $b\bar{b}$ bound states, are presented.

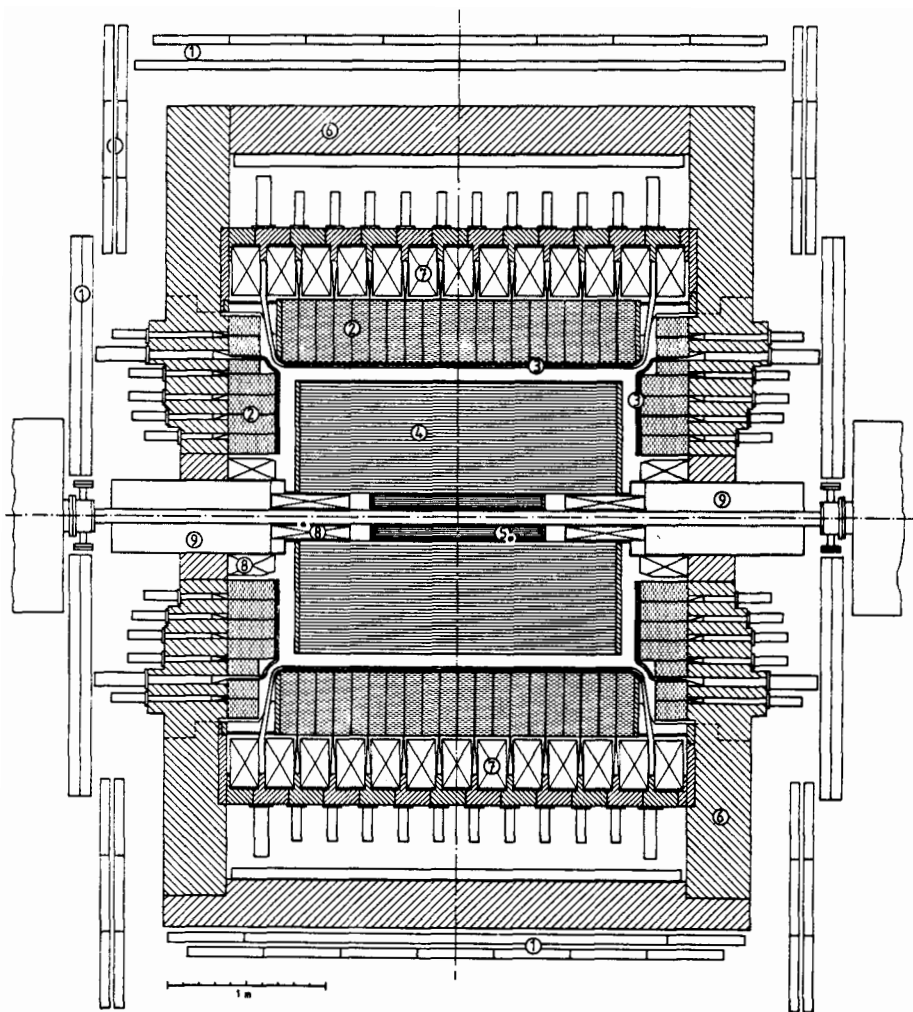
The ARGUS detector is a 4π solenoidal spectrometer, with good charged and neutral particle detection. Particle identification is made possible by both dE/dx measurements in the central drift chamber, and time-of-flight. The electromagnetic calorimeter, located inside the magnet coils, allows photon reconstruction down to energies below 50 MeV. A cross-sectional view of the detector is shown in figure 1. For a more detailed description of the experiment, the reader should consult references 1-5.

D^0 - \bar{D}^0 Mixing

Extensive results in the area of charm physics have been reported by the ARGUS collaboration. These include studies of D^{*+} fragmentation, using the decay channel $D^{*+} \rightarrow D^0\pi^+$, where the D^0 is seen in the $K^-\pi^+$ and $K^-\pi^+\pi^+\pi^-$ channels ⁶⁾, studies of F^{*+} decays into $\phi\pi^+$ and $\phi\pi^+\pi^+\pi^-$ ⁷⁾, and observation of the F^{*+} , via the single photon transition to the F , with the F decaying into $\phi\pi^+$ ⁸⁾. (The convention that charge conjugate states are implied is used in all of the following.) Here, an update is given of the limit on D^0 - \bar{D}^0 mixing, previously reported as less than 11% at the 90% confidence level ⁶⁾. The physics technique used remains the same; however, the details of the selection criteria and the size of the data set involved have changed.

From the sequence of decays $D^{*+} \rightarrow D^0\pi^+$, followed by $D^0 \rightarrow K^-\pi^+$, the expected charge combination for the final state is $K^-\pi^+\pi^+$. If, on the other hand, the D^0 changes into \bar{D}^0 , then the final state becomes $K^+\pi^-\pi^+$. The same argument holds for the $K^-\pi^+\pi^+\pi^-$ and $K^-\pi^+\pi^0$ decay channels of the D^0 . The charge conjugation state of the produced D^0 is tagged by the slow pion from the D^{*+} decay. A right sign combination has a K^- , the wrong sign a K^+ .

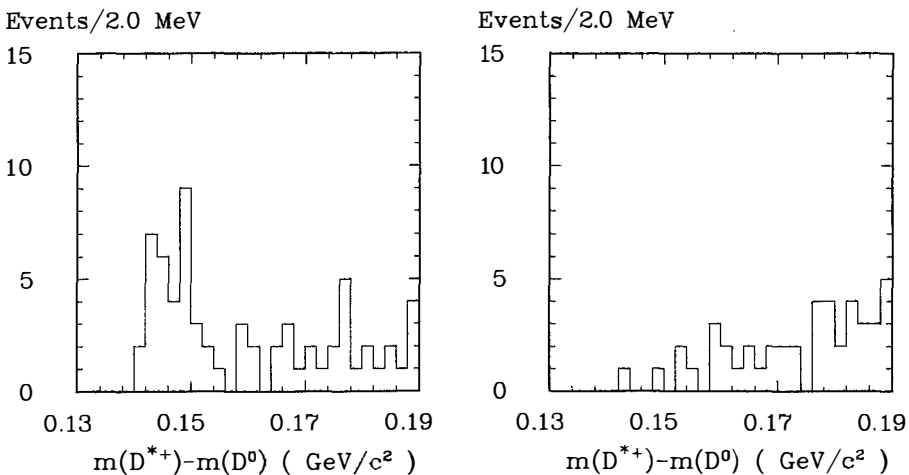
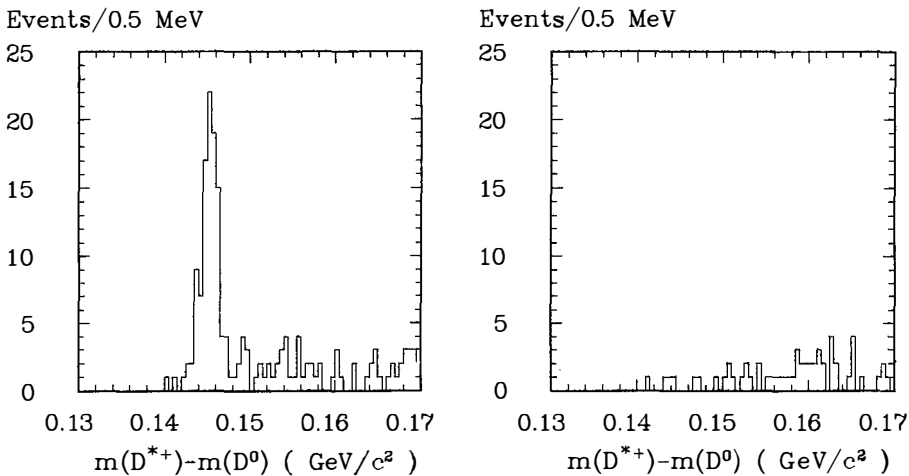
By comparing the number of events having the right sign combination with the number having the wrong sign combination, a limit on D^0 - \bar{D}^0 mixing can be found. There are two potential sources of difficulty. One is a double misidentification. For example, if in the $K^-\pi^+$ channel the particle identification assignments are reversed, the final state appears to be $K^+\pi^-$ near the correct mass, and thus represents a serious background for the mixing study. The second is doubly Cabbibo suppressed D^0 decays, which, in fact, should appear at the level of less than a percent of the allowed transitions, and represent the ultimate limit to which this method can be pushed.



1. Muon chambers
2. Shower counters
3. Time of flight counters
4. Drift chamber
5. Vertex chamber
6. Iron yoke
7. Solenoid coils
8. Compensation coils
9. Mini beta quadrupole

38269

Figure 1. Cross-sectional view of the ARGUS detector.



The data used comprises a total luminosity of 62.7 pb^{-1} , obtained on the various Υ resonances and in nearby continuum. Combinatorial background under the studied signals is minimized by the fact that D^0 decays tagged by the slow pion transition from the D^{*+} are very clean. This is a well-known ⁹⁾ result of the excellent resolution obtainable for the mass difference, $\Delta m = m(D^{*+}) - m(D^0)$, due to the low Q -value for the transition. The $K^- \pi^+$ and $K^- \pi^+ \pi^+ \pi^-$ channels are fully reconstructed from observed tracks in the detector, but the $K^- \pi^+ \pi^0$ channel is used without reconstructing the π^0 . The invariant mass distribution of $K^- \pi^+$ exhibits not only a clear D^0 signal, but also a satellite peak near $1.62 \text{ MeV}/c^2$ from the decays $D^0 \rightarrow K^{*-} \pi^+ \rightarrow K^- \pi^0 \pi^+$ and $D^0 \rightarrow K^- \rho^+ \rightarrow K^- \pi^+ \pi^0$ ¹⁰⁾, shifted from the D^0 mass because of the missing π^0 .

The problem of particle misidentification is eliminated by utilizing the dE/dx and time-of-flight measurements from the detector. For the $K^- \pi^+$ and satellite channels, either the K^- or the π^+ is required to be well identified. For the $K^- \pi^+ \pi^+ \pi^-$ channel, the K^- must be well identified. This means the particle must have momentum below $0.6 \text{ GeV}/c$, have a probability of more than 10% for the specified assignment based on the χ^2 from the dE/dx measurement, and not have this assignment vetoed by the time-of-flight measurement. Other particles in the event are identified using the standard likelihood technique ⁶⁾, which allows multiple type assignments.

The resulting distributions for the mass difference, Δm , with both the right charge and wrong charge combination, are shown in figure 2a-d. The signal is taken to lie between $\Delta m = 143 \text{ MeV}/c^2$ and $148 \text{ MeV}/c^2$ for the $K^- \pi^+$ and $K^- \pi^+ \pi^+ \pi^-$ channels, and between $141 \text{ MeV}/c^2$ and $152 \text{ MeV}/c^2$ for the satellite channel. For the fully reconstructed (satellite) channels the right sign plots show a clear signal of 88 (22) events, above a background of 12 (9), while the wrong sign has 5 (2) events, with a background of 5 (2). Using the method of maximum likelihood, the limit on the amount of D^0 - \bar{D}^0 mixing is determined to be less than 5.0% at the 90% confidence level. The DELCO collaboration has recently reported a limit of 8.1% at the 90% confidence level ¹¹⁾, using the same approach. There also exists an older, much more model-dependent measurement, from the prompt-muon experiment at Fermilab ¹²⁾, who obtained 4.4% at the 90% confidence level. However, the expected level of mixing from the standard model is less than 10^{-4} ¹³⁾, so several orders of magnitude increase in sensitivity are still needed.

Limits on Narrow States from Radiative Υ Decays

The most important, as yet, unobserved piece of the standard model is the existence of a scalar Higgs particle, by which the $SU(2) \otimes U(1)$ symmetry of the model is broken. One proposed technique of searching for the Higgs is in radiative decays of heavy vector meson

states ¹⁴⁾, such as the Υ system. Since the Higgs couples to mass, it is expected to decay predominantly into the heaviest available $q\bar{q}$ or $\ell^+\ell^-$ system. The predicted rate for such transitions is only 5×10^{-5} for the minimal Higgs model at $m_H = 8.4 \text{ GeV}/c^2$ ¹⁴⁾, but can be larger in more elaborate schemes ¹⁵⁾. For these reasons, and in the light of recent evidence claiming observation of a high-mass state in radiative Υ decays ¹⁶⁾, a search has been made in our data for such narrow states. The inclusive spectrum of photons from the calorimeter, and of photons which convert into an e^+e^- pair reconstructed from drift chamber tracks, has been studied. An upper limit of 0.15% at the 90% confidence level is derived for the branching ratio for $\Upsilon \rightarrow \gamma X$, where m_X is less than $8.4 \text{ GeV}/c^2$ ¹⁷⁾.

A search in radiative Υ decays for narrow states coupling to $\tau^+\tau^-$ also has been made ¹⁸⁾. The strategy employed in this study is to tag Υ events in the Υ' data, representing an integrated luminosity of 36.2 pb^{-1} , by means of the transition $\Upsilon' \rightarrow \pi^+\pi^-\Upsilon$. Tagging has the virtue of precluding the possibility of initial-state photon radiation, a serious background to a study of radiative Υ decays. A total of 13200 ± 300 events are observed above background in the recoil spectrum to $\pi^+\pi^-$ at the Υ mass. The transition $X \rightarrow \tau^+\tau^-$ is studied by using the substantial rate for tau leptons to decay into a single charged prong topology, $\tau^- \rightarrow e^-\bar{\nu}_e\nu_\tau$, $\mu^-\bar{\nu}_\mu\nu_\tau$, $\pi^-\nu_\tau$, or $K^-\nu_\tau$, representing $46.6 \pm 1.9\%$ ¹⁹⁾ of all tau decays. Thus, along with the recoil $\pi^+\pi^-$ pair, events must have two additional charged tracks. With no neutral energy in the calorimeter, direct decays of the Υ resonance can be studied; if one photon is allowed, a search for narrow states below the Υ , decaying into tau pairs, can be made.

First, consider the study of Υ decays to $\tau^+\tau^-$. In addition to the requirements discussed above, events were selected with (1) no more than a total of 0.3 GeV energy in the shower counters unassigned to one of the 4 charged tracks, (2) the opening angle, θ , between the 2 charged tracks from the Υ decay such that $-0.99 < \cos\theta < 0.75$, to eliminate decays into electron or muon pairs, and (3) the transverse momentum, p_T , of the charged system greater than $0.4 \text{ GeV}/c$, to eliminate 2-photon events. We observe a clean Υ peak of 60.5 ± 8.9 events in the recoil spectrum after these cuts (figure 3a). Normalizing to the number of Υ decays into e^+e^- and $\mu^+\mu^-$ observed in the same data set, correcting for the acollinearity and p_T cuts, and using the known branching ratio for the selected tau decay channels, we find:

$$\frac{\text{Br}(\Upsilon \rightarrow \tau^+\tau^-)}{\text{Br}(\Upsilon \rightarrow e^+e^- \text{ or } \mu^+\mu^-)} = 1.06 \pm 0.16 \pm 0.07 \quad (1)$$

This result, clearly consistent with e - μ - τ universality, improves the previous best measurement ²⁰⁾ considerably.

In the search for narrow radiative states, the neutral energy requirement was changed to demanding exactly 1 neutral cluster with energy more than 50 MeV. The recoil spectrum

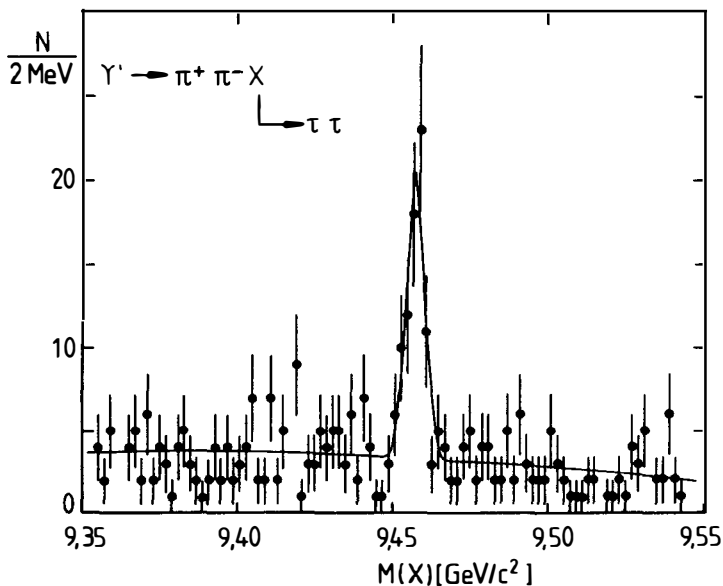


Figure 3a. Recoil mass spectrum for events with 4 charged prongs and no shower counter energy. The visible peak is due to decays $\Gamma' \rightarrow \pi^+ \pi^- X$, $T \rightarrow \tau^+ \tau^-$.

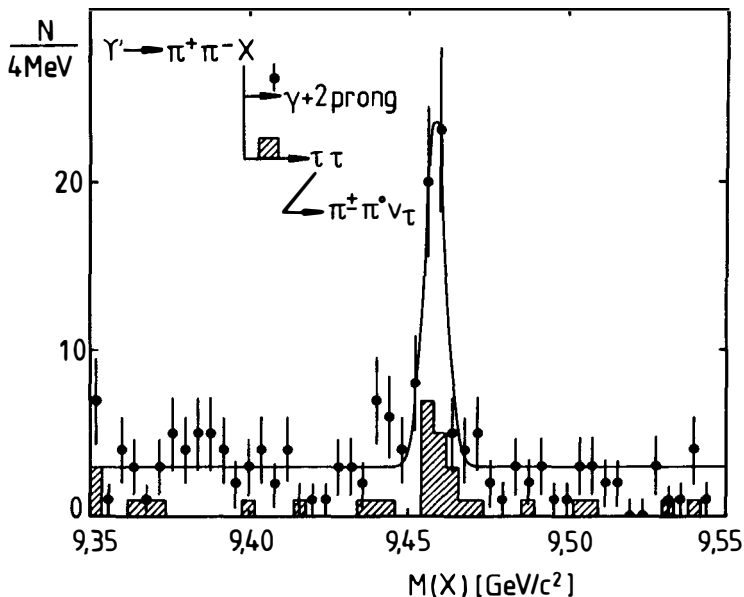


Figure 3b. Recoil mass spectrum for events with 4 charged prongs and 1 photon. The visible peak is due to feedthrough from decays $T \rightarrow \tau^+ \tau^-$ as described in the text.

still shows an excess of 45 ± 8 events at the Υ mass (figure 3b). However, both the number and the photon energy spectrum of these events is quite consistent with originating from known sources of feedthrough from resonance decays of the Υ into $\tau^+\tau^-$. One possibility is the tau leptons decay through the one-prong channel, but the event is accompanied by a fake photon. This accounts for 18 ± 4 background events, as determined from a study of the $\Upsilon \rightarrow \mu^+\mu^-$ sample. The other possibility is one of the tau leptons decays through the $\rho^+\bar{\nu}_\tau$, $\rho^+ \rightarrow \pi^+\pi^0$ channel, and either the two photons from the π^0 cannot be separated in the calorimeter, or one is lost. A further 6 ± 2 and 16 ± 4 background events originate from these cases respectively, making a total of 40 ± 6 . As can be seen from figure 3c, the observed energy spectrum is well reproduced by the predicted distribution from the described background sources.

From the photon energy spectrum for events with recoil mass between 9.45 and 9.47 GeV/c^2 , the upper limit for the branching ratio to narrow states can be determined. This limit is shown in figure 3d as a function of the mass, m_X , of such a state. In the region below $m_X = 8.4 \text{ GeV}/c^2$, the limit for the product $\text{Br}(\Upsilon \rightarrow \gamma X) \times \text{Br}(X \rightarrow \tau^+\tau^-)$ is less than 0.1%. The sum of the product of branching ratios for all states between 3.6 and 9.46 GeV/c^2 is less than 1% at the 90% confidence level. This is an order of magnitude above the predicted level for the standard Higgs, but provides some constraint for other models.

Electron Spectrum from Semi-leptonic B Decays

Much of the data so far accumulated using the ARGUS detector has been obtained on the Υ and Υ' resonances, with relatively little on the $\Upsilon(4S)$ above the open $B\bar{B}$ threshold. Of considerable interest in determining the elements of the Kobayashi-Maskawa mixing matrix ²¹⁾, is the ratio of $\text{Br}(B^- \rightarrow \ell^-\bar{\nu}_\ell X_u)/\text{Br}(B^- \rightarrow \ell^-\bar{\nu}_\ell X_c)$. Results for this ratio, from studies of semi-leptonic B decays, have been reported by both the CUSB ²²⁾ and CLEO ²³⁾ collaborations operating in the CESR e^+e^- storage ring at Cornell. The limit of less than 4% at the 90% confidence level given by CLEO, already implies that the ratio of the elements $|V_{bu}|/|V_{bc}|$ is less than 0.14. With limited statistics, but with several redundant measurements with which to distinguish electrons from hadrons, we can at present obtain a useful limit only by optimizing electron identification efficiency and geometric acceptance.

The tools available for distinguishing electrons from other particles are (1) the dE/dx information from the drift chamber, for tracks with $p_T > 0.050 \text{ GeV}/c$, (2) the time-of-flight measurement, for tracks with $p_T > 0.120 \text{ GeV}/c$, and (3) the information from the electromagnetic shower counters, including number of counters in the cluster, the energy, E_{SH} , deposited, and the shape of the distribution, as manifested in the second moment, μ_2 , of the deposition. A common approach to using such information is to make independent

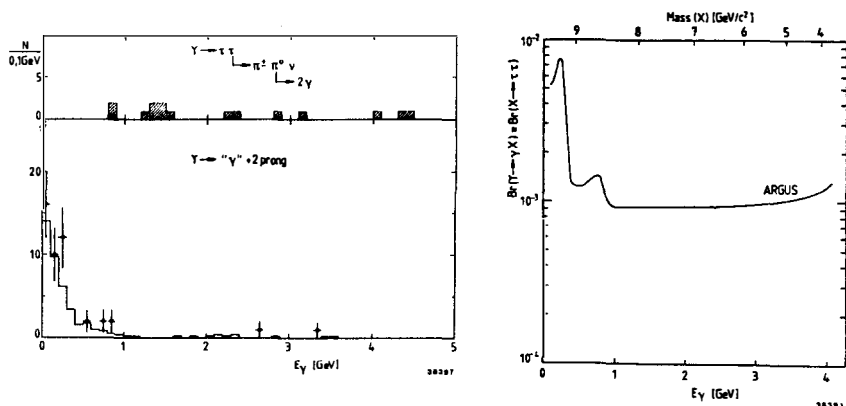


Figure 3c. Photon energy spectrum for the decay $\Upsilon \rightarrow \gamma + 2$ charged prongs. The hatched histogram shows the contribution from $\Upsilon \rightarrow \tau^+ \tau^-$, with one τ decaying into $\rho \nu$, while the open histogram shows expected backgrounds from other sources described in the text.

Figure 3d. Upper limit at the 90% confidence level for the product of branching ratios for $\Upsilon \rightarrow X$, $X \rightarrow \tau^+ \tau^-$.

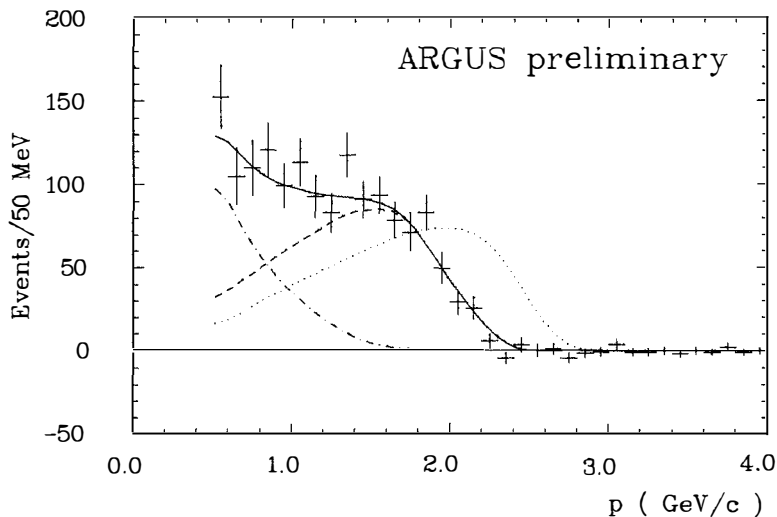


Figure 4. Continuum subtracted electron spectrum from decays of the $\Upsilon(4S)$. The solid line shows the sum of fitted contribution of $b \rightarrow c$ (dashed line) and $c \rightarrow s$ (dash-dotted line) semi-leptonic transitions. The dotted line shows the expected form of the electrons from semi-leptonic $b \rightarrow u$ decays.

cuts on each of these variables. Since the hadronic background and the electron signal are distributed differently in a given variable, cuts would be designed to remove regions where the background dominates, while retaining as much of the signal as possible. However, complete separation in any single variable is in general not possible. After making many independent cuts, the efficiency for electron identification, being the product of the efficiencies for these different cuts, would be small.

Alternatively, the information can be used in a more coherent fashion, using the likelihood ratio technique. We have already employed this idea for particle identification for charged tracks in general ⁶⁾. For electrons, with additional information available from the shower counters, the concept is merely extended. The likelihood ratio is defined as:

$$L = \frac{\prod_{i=dE/dx, TOF, SC} p_i^e(\tilde{x})}{\sum_{k=e, \mu, \pi, K, p} w^k \prod_{i=dE/dx, TOF, SC} p_i^k(\tilde{x})} \quad (2)$$

where $p_i^k(\tilde{x})$ are the probabilities for a track with measured parameters \tilde{x} to be identified as particle type k by device i , and the w^k are a priori relative production rates for the various particle types k . The electron hypothesis is accepted where L exceeds some value. A single cut in this multi-dimensional space, with all detector measurements treated in a coherent fashion, achieves high identification efficiency, with good hadronic rejection.

We have applied this technique to the study of the electron spectrum from the $\Upsilon(4S)$, a broad resonance sitting on top of a considerable background of continuum e^+e^- events. In order to suppress the latter, only events with a Fox-Wolfram ²⁴⁾ second moment less than 0.5 were studied. Nevertheless, the spectrum of electrons originating from continuum processes, such as $e^+e^- \rightarrow \tau^+\tau^-$, and $c\bar{c}$, must be determined from events recorded in nearby continuum off-resonance, and then subtracted from the spectrum on-resonance. For both $\Upsilon(4S)$ and continuum data sets, comprising integrated luminosities of 12.6 pb^{-1} and 4.7 pb^{-1} respectively, the following cuts were applied in selecting tracks: (1) momentum greater than $0.5 \text{ GeV}/c$, with a good track fit, (2) polar angle within the region, $|\cos \theta| < 0.80$, (3) number of wires used for dE/dx measurement greater than 12, with the fractional error on the measurement less than 15%, (4) number of counters in the associated shower cluster greater than 2, (5) invariant mass, when combined with other oppositely-charged electron candidates in the event, greater than $0.15 \text{ GeV}/c^2$, and (6) likelihood ratio, L , greater than 0.5. The electron identification efficiency under these conditions is $94 \pm 3\%$, an improvement of a factor of four over CUSB ²²⁾. The momentum spectrum for these tracks, after continuum subtraction, is shown in figure 4. The errors beyond $2 \text{ GeV}/c$ are dominated by the statistics of the subtraction.

The spectrum receives contributions not only from semi-leptonic decays of b-quarks, but also from c-quarks produced in b decays, which then semi-leptonically decay. In addition, the spectrum of leptons from ($b \rightarrow u$) transitions is quite dependent ²⁵⁾ on the fragmentation of the u-quark into final state hadrons, the form of which, of course, must be assumed. Using the model of Altarelli et al. ²⁶⁾ for the shapes of the electron spectra from the various contributing processes, we obtain a limit:

$$\frac{\text{Br}(B^- \rightarrow \ell^- \bar{\nu}_\ell X_u)}{\text{Br}(B^- \rightarrow \ell^- \bar{\nu}_\ell X_c)} < 4\% \quad (3)$$

at the 90% confidence level. This translates into a limit on the ratio of the relevant Kobayashi-Maskawa matrix elements of $|V_{bu}|/|V_{bc}| < 0.14$ at the 90% confidence level. From the fit, the B meson semi-leptonic branching ratio is determined to be $10.9 \pm 0.3 \pm 1.0\%$. However, we have not, as yet, made a study of the model dependence of these results. The CLEO limit ²³⁾ is based on careful study of the uncertainties so introduced. We expect to collect a large amount of $\Upsilon(4S)$ data this year, and thus improve the matrix element measurement substantially.

REFERENCES

* Current members of the ARGUS collaboration are: H.Albrecht, U.Binder, G.Harder, H.Hasemann, A.Philipp, W.Schmidt-Parzefall, H.Schröder, H.D.Schulz, R.Wurth (DESY), A.Drescher, B.Gräwe, U.Matthiesen, H.Scheck, J.Spengler, D.Wegener (Dortmund), R.Heller, K.R.Schubert, J.Stiewe, R.Waldi, S.Weseler (Heidelberg), N.N.Brown, K.W.Edwards, W.R.Frisken, Ch.Fukunaga, D.J.Gilkinson, D.M.Gingrich, M.Goddard, P.C.H.Kim, R.Kutschke, D.B.MacFarlane, J.A.McKenna, K.W.McLean, A.W.Nilsson, R.S.Orr, P.Padley, P.M.Patel, J.D.Prentice, H.C.J.Seywerd, B.J.Stacey, T.-S.Yoon, J.C.Yun (IPP Canada), R.Ammar, D.Coppage, R.Davis, S.Kanekal, N.Kwak (Kansas), G.Kernel, M.Pleško (Ljubljana), P.Böckmann, L.Jönsson, Y.Oku (Lund), A.Babaev, M.Danilov, A.Golutvin, V.Lubimov, V.Matveev, V.Nagovitsin, V.Ryltsov, A.Semenov, Yu.Semenov, V.Shevchenko, V.Soloshenko, V.Sopov, I.Tichomirov, Yu.Zaitsev (ITEP-Moscow), R.Children, C.W.Darden, and H.Gennow (South Carolina).

- 1) H.Albrecht et al. (ARGUS collaboration), Phys.Lett. **134B** (1984), 137.
- 2) M.Danilov et al., Nucl.Instr.Methods **217** (1983), 153.
- 3) R.Heller et al., Heidelberg preprint IHEP-HD/84-03, to be published in Nucl. Instr. Methods.
- 4) A.Drescher et al., Nucl.Instr.Methods **205** (1983), 125;
A.Drescher et al., Nucl.Instr.Methods **216** (1983), 35;
A.Drescher et al., DESY preprint DESY 84-106, submitted to Nucl. Instr. Methods.
- 5) A.Arefev et al., DESY preprint DESY 83-025.
- 6) H.Albrecht et al. (ARGUS collaboration), Phys.Lett. **150B** (1985), 235.

- 7) H.Albrecht et al. (ARGUS collaboration), Phys.Lett. **153B** (1985), 343.
- 8) H.Albrecht et al. (ARGUS collaboration), Phys.Lett. **146B** (1984), 111.
- 9) S.Nussinov, Phys.Rev.Lett. **35** (1976), 1672.
- 10) G.Goldhaber, Proceedings of the XVIIIth Recontre de Moriond, La Plagne (1983).
- 11) H.Yamamoto et al. (DELCO collaboration), Phys.Rev.Lett. **54** (1985), 522.
- 12) A.Bodek et al., Phys.Lett. **113B** (1982), 82.
- 13) L.-L.Chau, Phys.Rep. **95** (1983), 1.
- 14) F.Wilczek, Phys.Rev.Lett. **39** (1977), 1304.
- 15) H.L.Haber and G.L.Kane, Nucl.Phys. **B250** (1985), 716, and references therein.
- 16) C.Peck et al. (CRYSTAL BALL collaboration), DESY/SLAC preprint DESY 84-064 and SLAC-PUB-3380;
H.-J.Trost, Proceedings of the XXIIInd International Conference on High Energy Physics, Leipzig (1984) vol.I, 201
- 17) H.Albrecht et al. (ARGUS collaboration), paper in preparation.
- 18) H.Albrecht et al. (ARGUS collaboration), DESY preprint DESY 85-014, to be published in Phys.Lett. **B**.
- 19) Particle Data Group, Rev.Mod.Phys. **56** (1984), S1.
- 20) R.Giles et.al. (CLEO collaboration), Phys.Rev.Lett. **50** (1983), 877.
- 21) M.Kobayashi and K.Maskawa, Prog.Theor.Phys. **49** (1983), 652.
- 22) C.Klopfenstein et al. (CUSB collaboration), Phys.Lett. **130B** (1983), 444.
- 23) A.Chen et al. (CLEO collaboration), Phys.Rev.Lett. **52B** (1984), 1084.
- 24) G.C.Fox and S.Wolfram, Phys.Rev.Lett. **41** (1978), 1581;
G.C.Fox and S.Wolfram, Nucl.Phys. **B149** (1979), 413;
G.C.Fox and S.Wolfram, Phys.Lett. **82B** (1979), 134.
- 25) K.R.Schubert, Proceedings of the XIth International Conference on Neutrino Physics and Astrophysics, Nordkirchen (1984).
- 26) G.Altarelli et al., Nucl.Phys. **B208** (1982), 365.

REVIEW OF LIFETIME MEASUREMENTS AT PEP

Richard Prepost

Department of Physics, University of Wisconsin, Madison, Wisconsin, U.S.A.



Abstract

Recent results of lifetime measurements at PEP are reviewed. The results include new measurements from the MARK II group on the tau, charged and neutral charmed mesons, and the b quark lifetime. The MAC group new results are for the tau lepton and the b quark lifetimes. The results are discussed in the context of existing measurements.

TAU LIFETIME MEASUREMENTS

Both the MARK II and MAC groups have improved their measurements of the tau lifetime with improved statistics and in the case of the MARK II more data have been analyzed using the vertex chamber.

1) MARK II

The MARK II group uses a decay length measurement technique from $\tau \rightarrow 3\pi\nu$ decays. The event sample now contains 807 decays from an integrated luminosity of 209 pb^{-1} . The prior MARK II published result¹⁾ was based on a sample of 156 events for vertex analysis. A more recent result was presented by Jaros.²⁾

The MARK II measurement is based on a decay length analysis. A decay length and scaled resolution are determined for each event. A two parameter fit is then made to the decay length distribution. While the average standard deviation of this distribution is relatively large ($\approx 1000\mu$), the central value shift of about 400μ is determined with relatively high precision. The resultant lifetime is: $\tau_\tau = (2.86 \pm 0.16 \pm 0.25) \times 10^{-13} \text{ sec}$. This is presently the most precise determination of the tau lifetime.

2) MAC

The MAC measurement uses the full data sample of tau events that have been used for branching ratio measurements and electroweak asymmetry measurements.³⁾ The impact parameter technique is used, that is, for every track the distance of closest approach to the interaction point in the plane transverse to the beam direction is found. Since the resolution in this quantity is much larger than the expected mean due to the lifetime itself, this quantity can be negative as well as positive. The MAC analysis is based on 23584 tracks. The median value of the impact parameter $\langle\delta\rangle$ based on a $1/\sigma_\delta^2$ weighting is: $\langle\delta\rangle = 43.6 \pm 5.0 \text{ microns}$. The quantity $\langle\delta\rangle$ is related to the tau lifetime by: $\langle\delta\rangle = \alpha\tau$ where $\alpha = 0.48 \pm 0.01 \pm 0.02$ as determined from a Monte Carlo simulation. The result correcting for an estimated 3.9% background is $\tau_\tau = (3.15 \pm 0.36 \pm 0.4) \times 10^{-13} \text{ sec}$ where the first error is statistical and the second is systematic. The latter is dominated by the uncertainty in α and the possible presence of a bias in δ . These biases are checked with control samples and are estimated to be less than 6 microns.

The tau lifetime is predicted to be: $\tau_\tau = \left(\frac{m_\mu}{m_\tau}\right)^5 \cdot \tau_\mu \cdot BR(\tau \rightarrow e\nu\bar{\nu}) = (2.82 \pm 0.18) \times 10^{-13} \text{ sec}$. The theoretical uncertainty is from the BR quantity which is taken to be $BR=0.176 \pm 0.011$.⁴⁾ The tau lifetime may also be considered to depend upon a finite neutrino mass and mixing with a possible fourth generation heavy neutrino. Consequently the measurements of the tau lifetime may also be used to put limits on these parameters. The tau lifetime with parameters for a finite tau neutrino mass and mixing to a fourth generation neutrino

is: $\tau_\tau = \tau_0 \left(1 + 8 \cdot \left(\frac{m_{\nu\tau}}{m_\tau} \right)^2 \right) \cdot \frac{1}{\cos^2 \theta}$. where θ is a mixing angle in the left handed sector to a possible fourth generation neutrino.⁵⁾

The MARK II and MAC new results and a newer measurement from TASSO⁶⁾ are shown together with all prior measurements in Fig. 1. The labels IP and VC stand for impact parameter method and vertex chamber result respectively. The combined average from the MARK II, MAC, and TASSO experiments is: $\tau_\tau = 2.95 \pm 0.25$ in excellent agreement with the predictions of universality.

The measured lifetime may be used to test universality and put a limit on the tau neutrino mass. The result from the combined data is: $\frac{g_\tau}{g_\mu} \approx 1 \pm 5\%$ while the corresponding ratio for the mu-e system is $\frac{g_\mu}{g_e} \approx 1 \pm 0.8\%$. The upper limit on the tau neutrino mass is 320 MeV at the 95% confidence level. This is not the best limit on the tau neutrino mass,⁷⁾ but an interesting result nevertheless.

CHARMED PARTICLE LIFETIMES

Measurements now exist for lifetimes of D^0 , D^+ , F^+ , Λ_c^+ , and A^+ hadrons. A summary of the experiments reporting results in the following table will give some idea of the activity in this area.

Experiment type	number of groups	total number of events
D^0	8	260
D^\pm	9	248
$F^\pm, \Lambda_c^\pm, A^\pm$	2	11
Λ_c	4	22

The new results which will be discussed here are D^+ and D^0 measurements from the MARK II group and the SLAC hybrid bubble chamber facility, and preliminary results from MARK III on semileptonic branching ratios for charged and neutral D mesons. This measurement gives an independent determination of the charged to neutral lifetime ratio.

The quark lifetimes are interpreted in terms of universality and matrix elements which allow for mixing of quark states. We may therefore write an expression for the quark lifetime which in the absence of phase space and spectator quark effects is: $\frac{1}{\tau_q} = |V_{qq'}|^2 \cdot \frac{1}{BR} \cdot \frac{G_F^2 m_q^5}{192\pi^3}$.

The branching ratio factor BR is 1/5 which comes from the W decay possibilities of 2 leptons and 3 quark color states. This simple expression for the charmed case gives $\tau_c \approx 8 \times 10^{-13}$ sec and an equality of charged and neutral decays since spectator effects are explicitly absent in this simple treatment.

1) MARK II

The MARK II group has new charm lifetime results using the high resolution vertex chamber. D decays are tagged through the decay chains $D^0 \rightarrow K^- \pi^+$, $D^0 \rightarrow K^- \pi^+ \pi^0$, and $D^\pm \rightarrow K^\pm \pi^+ \pi^-$. The number of events in these samples is 39, 35, and 27 respectively. An earlier result for the D^0 lifetime has been published.⁹⁾ The limitations of space preclude anything other than quoting the results which are: $\tau(D^0) = (4.5_{-0.8}^{+0.9} \pm 0.5) \times 10^{-13}$ sec and $\tau(D^+) = (8.5_{-2.5}^{+3.4} \pm 0.5) \times 10^{-13}$ sec. The ratio of the lifetimes from this experiment alone is $\frac{\tau(D^+)}{\tau(D^0)} = 1.9_{-0.8}^{+1.0} \pm 0.5$.

2) The SLAC hybrid bubble chamber facility

The SLAC hybrid bubble chamber facility collaboration has conducted a series of experiments using photoproduction of charmed mesons with a quasi monochromatic back scattered laser photon beam. These experiments are collectively known as BC-72, BC-73, and BC-75. About 1/3 of these events are fully constrained giving a sample for lifetime analysis of 47 D^\pm , 46 D^0 , and 5 ambiguous decays. The lifetime distributions are shown in Fig. 2 giving $\tau(D^0) = (6.1 \pm 1.1 \pm 0.4) \times 10^{-13}$ sec and $\tau(D^+) = (9.2 \pm 1.5 \pm 0.5) \times 10^{-13}$ sec. The ratio of the lifetimes from this experiment alone is $\frac{\tau(D^+)}{\tau(D^0)} = 1.5_{-0.3}^{+0.6} \pm 0.1$.

BC-72/75 has 1 clean well constrained event $D^0 \rightarrow K^+ \pi^+ \pi^- \pi^-$ with a proper lifetime of 55×10^{-13} sec.⁹⁾ This event has a very long decay path of $l=9.0 \pm 0.1$ mm compared to the average value from the other events $\langle l \rangle \approx 1$ mm. This event has a very low (.1 %) a priori probability of being consistent with the current world average. The event, however, seems to be quite clean.

The results for all experiments are summarized in Fig. 3-5 for the D^0 , D^\pm , and F^\pm , A_c lifetimes respectively.¹⁰⁾

Fig. 6 shows a summary for charmed lifetime measurements with experiments combined by means of reciprocal weights. The figure shows the naive spectator model result as a guide. There is a substantially longer charged lifetime and the ratio from the combined results is $\frac{\tau(D^+)}{\tau(D^0)} = 2.4 \pm 0.3$. It is generally thought that spectator effects do not presently account for the measured charged to neutral ratio.

The MARK III group has a preliminary result for the lifetime ratio based on semi-leptonic branching ratio measurements. They have reported¹¹⁾ the result: $B_c(D^+) = 17 \pm 3 \pm 3\%$ and $B_c(D^0) = 6 \pm 3 \pm 2\%$ giving $\frac{B_c(D^+)}{B_c(D^0)} = \frac{\tau(D^+)}{\tau(D^0)} = 2.78_{-0.60-0.42}^{+0.86+0.27}$. This result is in good agreement with the measurements discussed above.

b QUARK LIFETIMES

There are new results on the b quark lifetime from the MARK II and MAC groups. The MARK II group has analyzed their data using the impact parameter distribution of the semileptonic decay muons and electrons as in their previous published result, and also with a new analysis using decay length distributions.²⁾ This method has the advantage of being less sensitive to the beam size, but does not yield as precise a result due to systematic errors relating the distribution to the tau lifetime and the fact that the primary vertices are not resolved. An analysis based on 282 events gives $\tau_b = 0.85 \pm 0.15 \pm 0.20$ psec using the impact parameter distribution, and $\tau_b = 1.25^{+0.26+0.35}_{-0.19-0.39}$ psec using the decay length distribution.

The MAC group present sample is from an integrated luminosity of 210 pb^{-1} an increase of about 40% compared to the measurement reported previously.¹²⁾ Fig. 7 shows the impact parameter distribution for the 505 events together with the distribution in errors for the events. The median value of the impact parameter distribution is $\langle \delta \rangle = 70 \pm 22 \pm 10$ microns. With an analysis similar to that used in the tau lifetime analysis described above, the result is $\tau_b = 0.81 \pm 0.28 \pm 0.17$ psec. The MAC group is currently running with a newly installed precision vertex chamber and expects to make a significant improvement in the lifetime measurement.

Fig. 8 shows the current measurements¹³⁾ of the b lifetime and an average value obtained by averaging the independent results. This combined result is $\tau_b = 1.11 \pm 0.16$ psec.

The result of these measurements in terms of K-M matrix elements combined with the Cornell result¹⁴⁾ for the upper limit of the b \rightarrow u transition gives $|V_{cb}| = 0.050 \pm 0.005$ and $|V_{ub}| \leq 0.007$.

The author would like to thank G. Feldman for discussions of the MARK II experiments and W. T. Ford for use of the lifetime summary figures. This work was supported in part by the Department of Energy under contract number DE-AC02-76ER00881.

REFERENCES

1. J. A. Jaros et al., **Phys. Rev. Lett.** **51**, 955 (1983)
2. J. A. Jaros, Talk given at the "Physics in Collision" conference, Santa Cruz, (1984).
3. E. Fernandez et al., **Phys. Rev. Lett.** **54**, 1624 (1985); **Phys. Rev. Lett.** **54**, 1620 (1985).
4. C. A. Blocker et al., **Phys. Letters** **109B**, 119 (1982).
5. F. J. Gilman and S. H. Rhie, SLAC-PUB 3657, April 1985.
6. M. Althoff et al., **Phys. Letters** **141B**, 264 (1984).
7. C. Matteruzzi et al., **Phys. Rev. Lett.** **52**, 1869 (1984).
8. J. M. Yelton et al., **Phys. Rev. Lett.** **52**, 2019 (1984).
9. K. Abe, et al., SLAC-PUB 3493.
10. The experiments not explicitly discussed here but quoted in the figures have a mix of results in journals and conference reports. NA11: R. Bailey et al., **Phys. Letters** **139B**, 320 (1984); NA16/27: M. Aguilar-Benitez et al., **Phys. Letters** **146B**, 266 (1984); WA 58: M. I. Adamovich et al., **Phys. Letters** **140B**, 119, 123 (1984); E-531: N. W. Reay in "Proceedings of the 1983 International Symposium on Lepton and Photon Interactions at High Energies", ed. by D. G. Cassel and D. L. Kreinick (1983), pp. 244-274; WA62: S. F. Biagi et al., **Phys. Letters** **150B**, 230 (1985).
11. D. Hitlin, 1984 SLAC Summer Institute and Topical Conference.
12. W. T. Ford, "Flavor mixing in Weak Interactions", edited by Ling-Lie Chau, Plenum, New York (1984), pp. 77-89.
13. DELCO: D. E. Klem et al., **Phys. Rev. Lett.** **53**, 1873 (1984); JADE: P. Steffen, talk at XXII International Conference on High Energy Physics, Leizig, July 1984; TASSO: M. Althoff et al., **Phys. Letters**, **149B**, 524 (1984).
14. J. L. Franzini in Ref. 12, pp. 217-238.

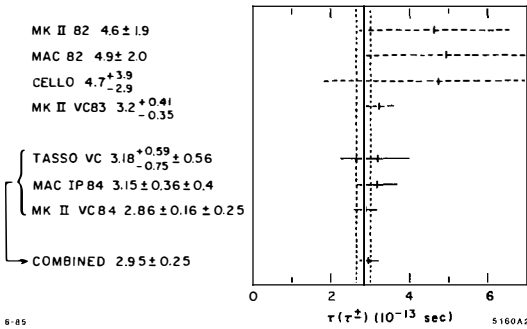


Fig. 1. A summary of results for the tau lifetime. The dotted and dashed bars denote earlier results since superseded.

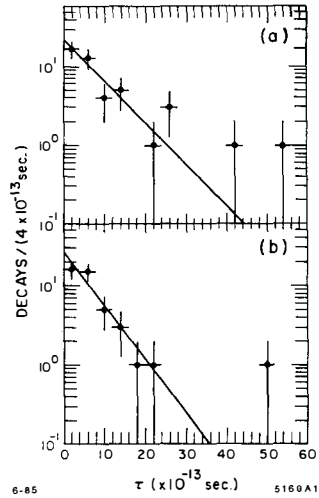


Fig. 2. Lifetime distributions for the results of the SLAC hybrid bubble chamber facility showing a) D^+ and b) D^0 decays. The lines represent best fits.

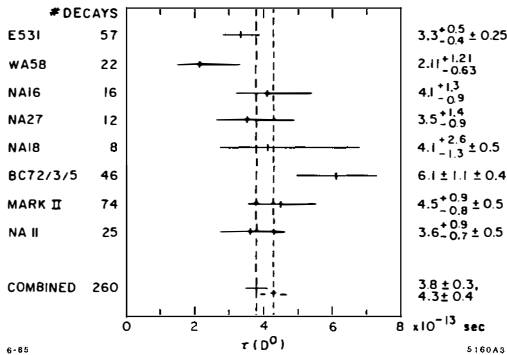


Fig. 3. Summary of results of D^0 measurements.

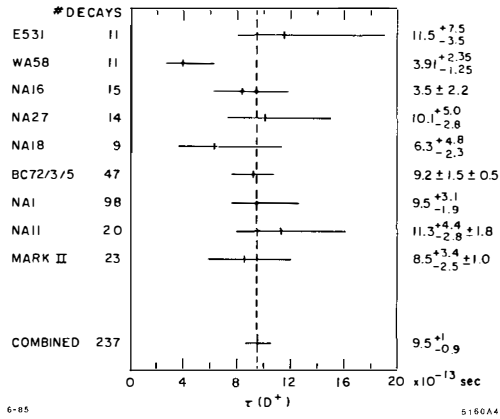


Fig. 4. Summary of results of D⁺ measurements.

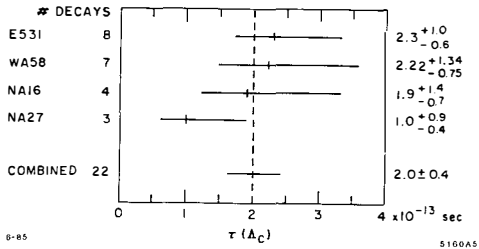
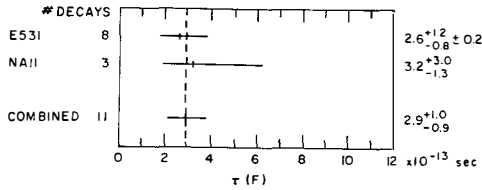


Fig. 5. Summary of results of a) F⁺ and b) Λ_c measurements.

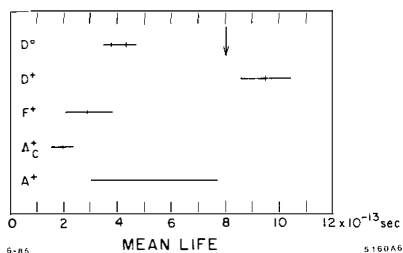


Fig. 6. Combined results for all charmed hadron decay measurements. The arrow indicates the simple non-spectator effect prediction.

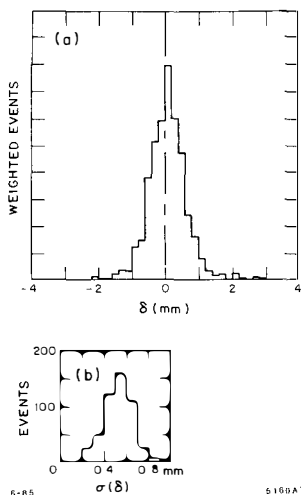


Fig. 7. a) The impact parameter distribution of b decay events from MAC, and b) the corresponding distribution of errors in δ .

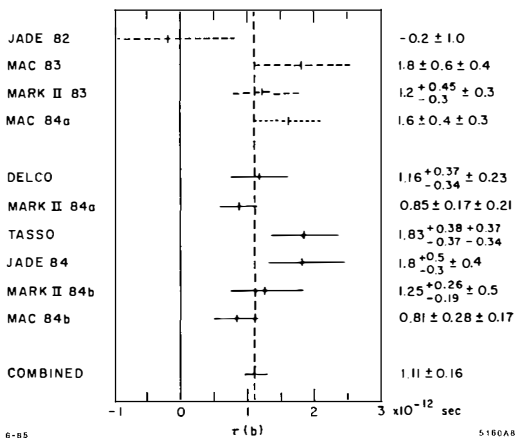


Fig. 8. Summary of results of τ_b measurements. The dotted and dashed bars are superceded measurements.

CAN GRAND UNIFIED THEORIES PREDICT THE TOP QUARK MASS?

G. Wetterich
CERN -- Geneva



ABSTRACT

We investigate the conditions for grand unified theories to predict the top quark mass relation $m_t/m_c = m_b/m_s$.

Certain models of grand unification based on $SO(10)$ or E_6 predict¹⁾⁻³⁾ at the unification scale the mass ratios

$$\frac{m_t}{m_c} = \frac{m_b}{m_s} \quad (1)$$

$$m_b = m_t \quad (2)$$

Relation (1) predicts a top quark mass of about 40 GeV, where a large uncertainty comes from the poorly known strange quark mass. Relation (2) involves only fermions of the third generation and agrees well with observation. Relation (1) involves both the third and second generation of quarks. Similar relations for the first two generations are not compatible with observation. A realistic model must be consistent with

$$m_\mu \neq m_s \quad (3)$$

$$m_e \neq m_d \quad (4)$$

$$\frac{m_c}{m_u} \neq \frac{m_s}{m_d} \quad (5)$$

It should also allow for non-zero mixing angles between different generations and CP violation.

We will see that only a very restricted class of models is consistent with realistic fermion mass matrices for the first two generations and nevertheless allows predictions of the mass relations (1) and (2). These models require

- (a) additional symmetries beyond $SU(5)$ or $SO(10)$; typical symmetry groups are $SO(10) \times U(1)_q$ or E_6 ;
- (b) appropriate scalar fields must be present;
- (c) the scales of spontaneous symmetry breaking must obey certain conditions; typically, one needs "intermediate scales" one or two orders below the unification scale for the breaking of subgroups like $SU(4)_C$ or $SU(2)_R \times U(1)_q$.

We should specify what we mean by "prediction" in the context of this investigation. Obviously, a prediction should not depend on a particular choice

of free parameters like Yukawa couplings or scalar self-interactions unless such couplings are determined by observation or symmetries. There are only very few possibilities to restrict parameters at the unification scale by observation. For the interactions of scalars only restrictions on scales of spontaneous symmetry breaking seem realistic if these fields have masses near the unification scale. In our context, a prediction of fermion mass relations should follow uniquely from symmetries and the order of magnitude of their spontaneous breaking.

Let us see how this program can be implemented for top quark predictions in grand unified theories. If the symmetry is only $SU(5)^{4)}$ the right-handed charge-2/3 and charge-1/3 quarks belong to different $SU(5)$ representations. The mass matrices M_U and M_D (for the up-type quarks and down-type quarks, respectively) are given by independent free Yukawa matrices. No top quark prediction is possible. In unification groups $SO(10)^{5)}$ or $E_6^{6)}$ all observed fermions and anti-fermions within a generation belong to only one irreducible representation. This opens the possibility that the Yukawa couplings of the top and bottom quark are related. $SO(10)$ symmetry is, however, not enough. Let us illustrate the problem by the Yukawa coupling between the fermions in a 16 representation of $SO(10)$ and a scalar in a 10 representation

$$\mathcal{L}_{\text{Yuk}} = f_{ij} 16_i 16_j 10 + \text{h.c.} \quad (6)$$

Here the index i, j labels different generations. If the 10 is a real field there is only one possible Yukawa matrix f_{ij} . In this case one has the prediction $m_t = m_b$, $m_c = m_s$, $m_u = m_d$ which is clearly unacceptable. A complex scalar 10 is needed. For a complex scalar, $SO(10)$ symmetry allows a second independent Yukawa coupling

$$\tilde{\mathcal{L}}_{\text{Yuk}} = \tilde{f}_{ij} 16_i 16_j 10^* + \text{h.c.} \quad (7)$$

For arbitrary f and \tilde{f} the mass matrices M_U and M_D are again unrelated.

One possible way to remedy this situation is to postulate an additional $U(1)_q$ symmetry so that the fermions have charge $q = -\frac{1}{2}$ and the scalar 10 has $q = 1$. Only the Yukawa coupling (7) is allowed by $U(1)_q$ symmetry. This additional Abelian symmetry can have different possible origins: in models based on the unification group E_6 it is the $U(1)$ subgroup commuting with $SO(10)$. (The scalar 10 is then embedded in a complex 27 representation of E_6 .) Otherwise, $U(1)_q$ may be a subgroup of a local generation symmetry, as for example obtained

from higher dimensional models⁷⁾. In a third scenario, $U(1)_q$ plays the role of a global Peccei-Quinn symmetry⁸⁾.

A complex 10 contains two independent electrically neutral colour singlets ϕ_1 and ϕ_2 . The Higgs doublet of the Salam-Weinberg model will be a mixture of the doublets containing ϕ_1 and ϕ_2 - we assume that only one doublet has a mass of the order of the weak breaking scale. We denote the vacuum expectation values by

$$\begin{aligned} \langle \phi_1 \rangle \\ \langle \phi_2 \rangle &= \alpha \langle \phi_1 \rangle \\ |\langle \phi_1 \rangle|^2 + |\langle \phi_2 \rangle|^2 &\approx (175 \text{ GeV})^2 \end{aligned} \quad (8)$$

The up-type quarks and down-type quarks couple to ϕ_1 and ϕ_2 respectively

$$\begin{aligned} M_U &= f \langle \phi_1 \rangle \\ M_D &= f \langle \phi_2 \rangle \end{aligned} \quad (9)$$

The charged leptons also couple to $\langle \phi_2 \rangle$. Since the Yukawa matrix f is the same for M_U , M_D and M_E , one finds the mass relations

$$M_D = \alpha M_U \quad (10)$$

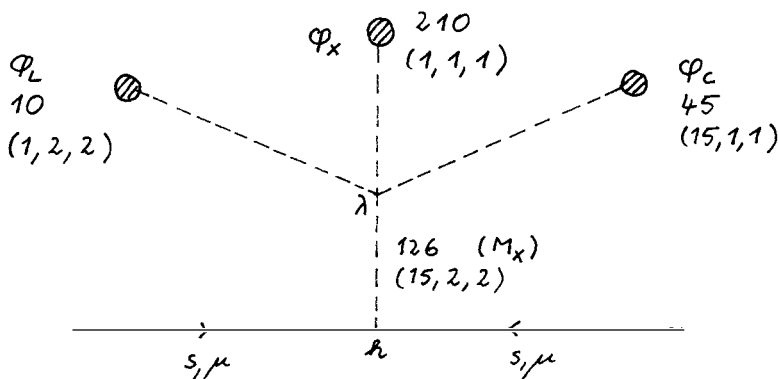
$$M_E = M_D \quad (11)$$

This leads to the relations (1) and (2), but also implies similar relations for the first two generations in contradiction with (3)-(5). In particular, all mixing angles vanish and there is no CP violation. As it stands, this model clearly is not acceptable. Other scalars with Yukawa couplings to quarks and leptons must be added. They must belong to the 126 or 120 representation of $SO(10)$.

How are relations (1) and (2) modified by these additional scalar fields? Can these relations be completely altered - in which case predictivity is lost - or are there arguments why corrections to these relations are small and controllable? Two observations are important for an answer to this question. First, the bad relations from (10) and (11) concern only the fermions with small

masses. If corrections to the mass matrices M_U , M_D and M_E are bounded by scale arguments to be smaller than a certain value, say 50 MeV at the weak interaction scale, then corrections to the masses of the third generation are small. This would imply that relation (2) is only slightly modified, but this is not enough to ensure relation (1). Second, we note that relations (10) and (11) follow already from subgroups of the unification symmetry. The relation $M_E = M_D$ is a consequence of $SU(4)_C$ symmetry and the symmetry $H_{LR} \equiv SU(2)_L \times SU(2)_R \times U(1)_q$ implies the proportionality of M_D and M_U . We therefore can refine the scale argument to contributions to the mass matrices violating $SU(4)_C$ or H_{LR} .

With respect to $SU(4)_C$, the electron is in the same four-dimensional representation as the down quark. The fact that ϕ_1 and ϕ_2 are $SU(4)_C$ singlets implies $M_E = M_D$. Corrections to this relation must come from Yukawa couplings to vacuum expectation values of scalars in non-trivial representations of $SU(4)_C$ - more precisely, this must be the 15. Assume that $SU(4)_C$ is spontaneously broken by an expectation value ϕ_C . All $SU(4)_C$ violating contributions to fermion mass matrices must then be proportional to some (positive) power of ϕ_C . Otherwise speaking, all mixings between weak doublets in the 1 and 15 of $SU(4)_C$ are suppressed²⁾ by a power of ϕ_C/ϕ_X with ϕ_X the heavy scale in the model - typically the unification scale. The vacuum expectation values of doublets in the 15 is of order $(\phi_C/\phi_X)^{\tilde{N}} \cdot \phi_1$. For small enough ϕ_C/ϕ_X the size of $SU(4)_C$ violating contributions is easily controlled and relation (2) is predicted²⁾. We have drawn a possible diagram to illustrate contributions to $m_\mu \neq m_s$ whose order of magnitude is controlled by ϕ_C/ϕ_X . [We indicate $SO(10)$ and $SU(4)_C \times SU(2)_L \times SU(2)_R$ representations of scalar fields.]



The contribution of this diagram to M_E and M_D is

$$\Delta M_E = -3\Delta M_D \sim h \frac{\lambda \phi_L \phi_C \phi_X}{M_X^2} \sim h \phi_L \frac{\phi_C}{\phi_X} \quad (12)$$

At first sight, it seems that even a moderate contribution to m_s of order 30-50 MeV would alter the top quark prediction (1) by about 30%. For the above diagram, however, relation (1) is protected by H_{LR} symmetry, if ϕ_C and ϕ_X have $q = 0$. Indeed H_{LR} symmetry implies that the vacuum expectation values in (15,2,2) coupling to charge 2/3 and -1/3 quarks - we denote them by ϕ_u^{126} and ϕ_d^{126} obey³⁾

$$\frac{\phi_d^{126}}{\phi_u^{126}} = \frac{\langle \phi_2 \rangle}{\langle \phi_1 \rangle} = \alpha \quad (13)$$

Relation (13) is easily generalized to arbitrary scalar doublets with $q = 1$ and one finds that H_{LR} symmetry guarantees $M_D = \alpha M_U$. If the $SU(4)_C$ violating expectation value ϕ_C is dominantly H_{LR} conserving, relation (1) is maintained even though m_s is strongly modified! [This motivates why we consider (1) rather than the similar relation $(m_\tau/m_c) = (m_\tau/m_\mu)$.] All corrections to (1) will be proportional to powers of ϕ_{LR}/ϕ_X , where ϕ_{LR} is the scale where H_{LR} is spontaneously broken. These H_{LR} violating contributions must be responsible for (5) and for non-vanishing mixing angles and CP violation. If ϕ_{LR}/ϕ_X is small enough, the top quark relation (1) is predicted.

It is possible to construct models with appropriate scales ϕ_C and ϕ_{LR} so that both relations (1) and (2) are predicted. Model building has to obey several constraints.

- (i) The scale ϕ_C should not be too small to allow for substantial contributions to m_s and m_μ . It must be small enough so that $SU(4)_C$ violating corrections only slightly modify (2). The leading $SU(4)_C$ violation must preserve H_{LR} in order to keep (1).
- (ii) The scale ϕ_{LR} must be small enough to keep the prediction (1). On the other hand it cannot be too small since the mixing between ϕ_1 and ϕ_2 violates H_{LR} and α is therefore of order $(\phi_{LR}/\phi_X)^{\tilde{M}}$. Also, H_{LR} violation must be large enough to allow for the observed mixing angles and CP violation.

(iii) The observed mixing angles require non-diagonal H_{LR} violating contributions to M_D of the order $\gtrsim 50$ MeV (in a basis where M_U is diagonal). If the diagonal H_{LR} violating contributions to M_D are of the same size m_S is strongly modified and prediction (1) is lost. The only way to avoid this possibility is that H_{LR} violating contributions to mixing angles are mainly induced by the Yukawa couplings of a 120 of $SO(10)$. The Yukawa couplings of 120 are antisymmetric in a basis where M_U is diagonal only if the dominant contribution to M_U comes from symmetric Yukawa couplings of the 10 (or 126) so that M_U is diagonalized by transformations leaving the symmetry type of a matrix unchanged. This requires that the mixing between the (1,2,2) in 10 and 120 must be suppressed. This would be the case if the mass of the 120 scalar is larger than the scale of $SO(10)$ breaking M_X .

In conclusion, we have found that models which predict the top quark mass relation (1) are rather constrained. Since there is no independent observational or theoretical indication for the constraints (i), (ii) and (iii) we think that grand unified models based on $SO(10) \times U(1)$ or E_6 could well explain a posteriori the relation (1), but that this relation depends on too many details to be considered as a real prediction. Relation (2), in contrast, is predicted in a much wider class of models. Probably some new ingredients - perhaps from higher dimensions⁹⁾ - are needed for a reliable top quark prediction.

ACKNOWLEDGEMENTS

The author thanks the organizers of "Rencontres de Moriond" for giving him the opportunity to attend this pleasant meeting at Les Arcs.

REFERENCES

- 1) M.S. Chanowitz, J. Ellis and M.K. Gaillard - Nucl.Phys. B128 (1977) 506;
R. Barbieri and D.V. Nanopoulos - Phys.Lett. 91B (1980) 369;
B. Stech - in "Unification of Fundamental Particle Interactions" (Plenum, New York, 1980), p. 23; Phys.Lett. 130B (1983) 189;
S.L. Glashow - Phys.Rev.Lett. 45 (1980) 1914.
- 2) G. Lazarides, Q. Shafi and C. Wetterich - Nucl.Phys. B181 (1981) 287;
C. Wetterich - Nucl.Phys. B187 (1981) 343.
- 3) C. Panagiotakopoulos, Q. Shafi and C. Wetterich - Bartol Preprint (1985).
- 4) H. Georgi and S.L. Glashow - Phys.Rev.Lett. 32 (1974) 438;
A.J. Buras, J. Ellis, M.K. Gaillard and D.V. Nanopoulos - Nucl.Phys. B135 (1978) 66.
- 5) H. Georgi - Particles and Fields (1974) (APS/DPF Williamsburg),
ed. C.E. Carlson (AIP, New York, 1975);
H. Fritzsch and P. Minkowski - Ann. Phys. (N.Y.) (1975) 193.
- 6) F. Gürsey, P. Ramond and P. Sikivie - Phys.Lett. 60B (1976) 177.
- 7) C. Wetterich - Nucl.Phys. B244 (1984) 359.
- 8) R. Peccei and H. Quinn - Phys.Rev.Lett. 38 (1977) 1440;
S. Weinberg - Phys.Rev.Lett. 40 (1978) 223;
F. Wilczek - Phys.Rev.Lett. 40 (1978) 279.
- 9) C. Wetterich - CERN Preprint TH. 4154 (1985).

WHO ORDERED THE MUON?
FROM FAMILIES TO COMMUNITIES

Goran Senjanovic¹
Physics Department
Brookhaven National Laboratory
Upton, New York 11973

ABSTRACT

I review the possibility that the underlying theory of weak interactions possesses a family symmetry, either global or local. The spontaneous symmetry breaking of this symmetry leads to important phenomenological implications: the existence of Goldstone bosons, the familons in the case of global symmetry and the existence of mirror fermions, in the case of local symmetry (in the context of grand unification). Both alternatives will soon be tested.

It has now been decades since I.I. Rabi posed his famous question pondering the existence of the muon: "Who ordered that?" And we may not be much closer to the answer today than we were then. It has become a fundamental, if not the central question in weak interaction physics. Why do fermions come in repetitive structures ("families"), with the same quantum numbers?

And if this question is too hard, then, at least, how many families are there? In which sense are they related to each other? What is responsible for the nontrivial particle mass spectrum? You will see that we still don't have an answer to any of these questions. There are, however, some important phenomenological consequences that we end up with when some of the above issues are discussed. This is the main content of this brief review of the problem of families. I will try to summarize the results of the belief that the underlying theory of weak interactions possess a family symmetry, only to be spontaneously broken. If the families form a "community", what about community and family ties. This is the central theme of my talk.

In some sense, the main message seems to be: every man for himself; and yet some beautiful things may happen from the life in a community. Since I am not here to advocate any particular lifestyle, let me just describe what happens. We know that family symmetry should either be global or local gauge symmetry. In the former case, the necessary existence of Goldstone bosons, so called familons, leads to rare decays such as $K^+ \rightarrow \pi^+ + \text{familon}$ and $\mu e + \text{familon}$, with possibly observable branching ratios. Furthermore, if the family symmetry is chiral then, except in the case of four families, one tends to end up with Peccei-Quinn symmetry needed to understand strong CP violation. The importance of this result is twofold: it may provide a rationale for otherwise ad hoc Peccei-Quinn symmetry and furthermore restrict the branching ratios of rare decays to be observed in the BNL experiment currently under way.

If the family symmetry turn out to be local, on the other hand, this would imply the existence of the so called mirror fermions, one for each ordinary fermion. These fermions look exactly like the familiar ones, except for the weak interactions beings right-handed. Truly a mirror world of our own! Furthermore, these particles should weigh less than about 200-250 GeV and so they ought to show up in supercolliders.

Now that you know the epilogue, you may or may not wish to struggle through our story. If you do, you will find the case of global symmetry discussed in the next Section and Section III then devoted to the local family symmetry and mirrors. I will restate the conclusions and offer some speculations in the last section, trying to emphasize the problems yet to be solved.

II. Global Family Symmetry

The family symmetry may or may not be gauged. Let's imagine, for the time being, it's not gauged.¹⁾ In other words, assume that the underlying theory of weak interactions, on top of the standard $SU(2) \times U(1)$ possesses also a global family symmetry G_F . We know that at low energies there is no trace of family symmetry ($m_e \neq m_\mu$): G_F must be spontaneously broken. But this leads to the existence of Goldstone bosons! These familons, as Wilczek¹⁾ coined them, are exactly massless (unlike axions), because of the absence of anomalies. But this sounds obviously crazy: massless scalars coupled to fermions! What about the Eötvoš experiment? Luckily, as you are likely to know, Goldstone bosons have only spin-dependant couplings at low energies which do not lead to coherent effects.

The couplings of familons must on purely physical grounds be inversely proportional to the scale M_F of the breaking of G_F . The nontrivial limit on M_F comes from astrophysics. Red giants being red giants tell us that familons must be weakly coupled to fermions, or they would radiate away all the star's energy.²⁾ Translated into M_F this means $M_F \gtrsim 10^9$ GeV. Is this out of the reach of Laboratory? Not necessarily! Notice that the familons change family number maximally -- this is the essence of their existence. We have flavor changing couplings such as

$$L_{\text{familon}} = \frac{\phi_F}{M_F} (m_\mu \bar{e}\mu + m_s \bar{d}s + \dots) \quad (2.1)$$

(where ϕ_F denotes familons generically), leading to rare decays

$$K^+ \rightarrow \pi^+ + \phi_F; \quad \mu^+ e + \phi_F \quad (2.2)$$

with decay rates $\sim 1/M_F^2$. You can easily show¹⁾

$$R = \frac{\Gamma(K^+ \rightarrow \pi^+ \phi_F)}{\Gamma(K^+ \rightarrow \pi^+ \pi^0)} \approx \frac{\Gamma(\mu^+ e \phi_F)}{\Gamma(\mu^+ e \nu \bar{\nu})} \approx \frac{10^{+14}}{M_F^2 (\text{GeV})^2} \quad \equiv \quad (2.3)$$

Experimental limit:³⁾ $R \lesssim 10^{-7}$ and will be pushed to about 10^{-10} by BNL experiment currently under way.⁴⁾ This will probe M_F up to 10^{12} GeV!

This tempts one to search for a rationale that could limit M_F from above. Here I'd like to report on an interesting finding my friends Darwin Chang and Palash Pal and I have arrived at.⁵⁾ If G_F is a chiral group, then the theory tends to possess accidental Peccei-Quinn symmetry,⁶⁾ leading to the well known upper limit:⁷⁾ $M_F < 10^{12}$ GeV. This in turn limits $R > 10^{-10}$, making the process $K^+ \rightarrow \pi^+ \phi_F$ soon observable. Let me describe our results in some detail. Imagine, for simplicity,⁵⁾

$$G_F = SU(N)_L \times SU(N)_\uparrow \times SU(N)_\downarrow \quad (2.4)$$

with L referring to left-handed doublets and \uparrow and \downarrow denoting up and down right handed quarks, respectively. The most general, symmetric Yukawa Lagrangian takes then the form

$$L_Y = h_u (\bar{u}\bar{d})_L^i \phi_u^* u_R^i + h_d (\bar{u}\bar{d})_L^i \phi_d^* d_R^i + \text{h.c.} \quad (2.5)$$

where $i = 1, \dots, N$ counts N different families. Notice that ϕ_u and ϕ_d are necessarily different $SU(2)_L \times U(1)$ doublets, with the transformation properties under $G_F: \phi_u(N^*, N, 1); \phi_d(N, 1, N^*)$. Hence Peccei-Quinn $U(1)_{PQ}$ symmetry in the Yukawa sector. Furthermore, the Higgs potential also respects $U(1)_{PQ}$, except for $N = 2$ when a term $(\phi_u^* \phi_d)^2$ is allowed. Is this why there are at least three families?

This, however, cannot be the whole story. Family symmetry must be broken by an additional Higgs scalar(s) H , singlet under $SU(2)_L \times U(1)$, since $M_F > 10^9$ GeV. When the dust settles, we find the following

- (i) for $N = 3$ families there is unique H which preserves $U(1)_{PQ}$
- (ii) for $N = 4$ $U(1)_{PQ}$ is always broken
- (iii) for $N > 4$ $U(1)_{PQ}$ is automatic.

If there are more than four families

$$R(K^+ \rightarrow \pi + \phi_P) > 10^{-10} \quad (2.6)$$

just to be probed!

III. Local Family Symmetry

In view of our ignorance, we must also consider the possibility that the family symmetry is gauged. If anything, the theoretical bias is more likely to go in this direction.

The first obvious observation is that we must go beyond the $SU(5)$ theory. The minimal GUT that unifies a single family of fermions in $SO(10)$. The sixteen Weyl fields of one family (include ν_R , please!) constitute a spinorial representation of $SO(10)$. Also spinorial representation of orthogonal groups are unique: when decomposed under subgroups, they contain only spinors and nothing else.

I will take this, as may other people, as the strong encouragement to pursue orthogonal groups only for family unification. We shall search for the simplest theory based on $SO(10+2n)$ ^{8,9)} (you will see why $2n$ shortly). The irreducible spinorial representation of $SO(10+2n)$ has a dimension $2n \times 16$. The minimal candidate is the $SO(14)$ ($n = 2$). However, and this is the general, remarkable feature of any $SO(10+2n)$ group: half of the families have right-handed interactions with the W -boson. In other words, for every usual fermion there must be a mirror fermion,¹⁰ with exactly the same quantum number, but $V + A$ interactions.

Before I proceed with the physics of mirrors, let me say a few words about orthogonal groups and their spinorial representations.⁹⁾ These are nothing but the Euclidian version of Dirac spinors. Imagine a Clifford algebra

$$\{\gamma_i, \gamma_j\} = 2\delta_{ij} \quad ; \quad i, j = 1, \dots, 2N. \quad (3.1)$$

You can easily convince yourselves that

$$T_{ij} = \frac{1}{4i} [\gamma_i, \gamma_j] \quad (3.2)$$

generate a complex 2^N -dimensional spinorial representation at $SO(2N)$ group. Furthermore, in complete analogy with the Lorentz groups $\gamma_{FIVE} = \gamma_1 \dots \gamma_{2N}$ ($\gamma_{FIVE}^2 = 1$) commutes with all T_{ij} . Hence "left" and "right" 2^{N-1} dimensional spinors.

Now, choose a basis in which $2T_{2k-1, 2k}$ are diagonal, with eigen value $\epsilon_k = \pm 1$. Then

$$\gamma_{FIVE} = \epsilon_1 \dots \epsilon_N \quad (3.3)$$

which we will now fix to be 1.

In the case of $SO(10+2n)$: $\epsilon_1 \dots \epsilon_5 \epsilon_6 \dots \epsilon_{5+n} = 1$, which gives two different possibilities

$$\begin{aligned} \text{(i)} \quad \epsilon_1 \dots \epsilon_5 = 1 & \quad \text{(ii)} \quad \epsilon_1 \dots \epsilon_5 = -1 \\ \epsilon_6 \dots \epsilon_{5+n} = 1 & \quad \epsilon_6 \dots \epsilon_{5+n} = -1 \end{aligned} \quad (3.4)$$

This is the remarkable fact I mentioned before: if (i) is an ordinary family (f), then (ii) is necessarily a mirror family (F). This, at the first glance at least, appears to be a curse, since we would expect that fermions and mirror fermions just pair off and go to Planck or GUT scale: a survival hypothesis,¹¹⁾ as it is usually called. Notice, however, that

$$U = e^{i(\epsilon_6 + \dots + \epsilon_{5+n})} = i^n \epsilon_6 \dots \epsilon_{5+n} \quad (3.5)$$

is a group rotation in $SO(10+2n)$. But

$$Uf = i^n f \quad ; \quad UF = -i^n F \quad (3.6)$$

For $n = 2k$ U will forbid mixings between ordinary and mirror fermions. We are forced to SO(10+4k) theories, since the others do not allow chiral fermions. The same is true of $SO(\text{odd})$ groups.

This has hopefully provided you with enough background to take a guided tour through $SO(10+4k)$ groups. The first candidate, $k = 1$ $SO(14)$, although a beautiful theory, is unfortunately ruled out since it allows only $2f + 2F$ families. Another victim of the ugly facts of the nature?

Believe it or not, the symmetry of the world is $SO(18)$. At the GUT level it contains 8 ordinary families and 8 mirror families, all massless. This is far too many: if all survived down to low energies, asymptotic freedom would be lost. Fortunately this is not what happens. Only a portion of original mirror symmetry remains unbroken down to M_W , allowing some f 's and some F 's to pair-off and decouple from physical consideration. Still, the phenomenological and comological consistency of mirror fermions is by no means obvious. Here, I'll report on the work with F. Wilczek and A. Zee,¹²⁾ addressed to this issue. Our results can be summarized as follows

- (i) Mirror symmetry must eventually be broken - we do not want stable mirror matter, since there is no trace of it on this planet or elsewhere.

- (ii) Mirror symmetry gets broken at M_W , leading to $d = 5$ effective mixing

$$L_{\text{eff}} \approx \frac{1}{M_X} \bar{f} \phi^2_F \quad (3.7)$$

where ϕ denotes generically Higgs doublets. Therefore, the f - F mixing $\theta_{fF} \approx M_W/M_X \leq 10^{-13}$ explains why mirror matter is practically decoupled for laboratory purposes.

- (iii) The f - F mixing plays a profound cosmological role, however; a typical lifetime for the decay $F \rightarrow f\bar{f}\bar{f}$ becomes

$$\tau_F \approx \theta_{fF}^{-2} G_F^{-2} M_F^5 \approx 1 \text{ sec} \quad (3.8)$$

for $M_X \approx 10^{15}$ GeV, $M_F \approx 100$ GeV. There is no mirror matter any more in the universe.

- (iv) Begger and Dimopoulos show that the number of light families must be even. Asymptotic freedom uniquely then selects $N_F = 4$ families (and 4 mirror families).

- (v) The strong CP problem unfortunately remains even in such a grand scheme. With the inclusion of Peccei-Quinn symmetry, the number of families is not fixed anymore; we have found a consistent theory with three families.

- (vi) Neutrinos. There is a danger of having far too many light neutrinos (in view of mirror families). Now, in theories with both helicity neutrinos GRS see-saw mechanism is operative: $SU(2) \times U(1)$ singlet components pick up superlarge masses (survival principle). Corresponding to each of these there is a light neutrino. Fortunately, some singlets may survive to low energies, find their opposite helicity partners and become Dirac neutral leptons with masses in the GeV region, e.g., in our case we end up with five light neutrinos.

- (vii) An important comment. In the context of GUTS, it is crucial that no coupling blows up before M_X . This implies an upper bound on fermion masses of the order of 250 GeV. You should see mirror fermions in the supercolliders.

IV. Outlook and Speculations

Why do fermions come in different families? Nobody knows. Whatever the fundamental reason, it appears sensible to believe that they are related by some symmetry. If so, the consequences, as I discussed, are well defined and testable. Either you get Goldstone bosons which induce rare decays in the global symmetry case; or if the symmetry is gauged, in the context of GUTS you end up with mirror fermions.

In either case, it appears that these "community" ties are very weak. In the global case $M_F \gtrsim 10^9$ GeV, and in the local case $K_L \rightarrow \bar{l}e$ implies $M_F \gtrsim 10^5$

GeV. And if the latter possibility is realized within GUTS, then actually $M_F = M_X \approx 10^{15}$ GeV.

Let me, for the sake of fairness, end up on a sober note, by summarizing the failure of the program. No successful computation of particle spectrum and mixings has yet emerged. It is not easy to see how GUTS per se will ever come out with the predictions for quark and lepton masses. In the global case, the nontrivial complication stems from the fact that higher dimension operators play an important role at low energies, in some sense M_F does not decouple.

I should mention that recently some attempts were made to understand the physics of SO(18) to a higher degree.¹³⁾ In particular why mirror fermions are heavier than the standard ones, and the issue of neutrinos. I feel that some work is still needed before we have a complete picture. Furthermore, the problems of both weak and strong CP violation were not yet fully addressed; it would be nice to find a solution to the strong CP problem without involving Peccei-Quinn symmetry from the outside. In any case it is good to know that the ideas I have discussed here will be tested experimentally in the near future.

Acknowledgment

My own work described here has been performed in collaboration with Darwin Chang, Palash Pal, F. Wilczek and A. Zee. Besides them, thanks are due to Pavle Senjanović, Saško Šokorac and Apo Gittis for support.

References and Footnotes

1. G. Gelmini, S. Nussinov, and T. Yangida, Nucl. Phys. B219, 31 (1983) F. Wilczek, Phys. Rev. Lett. 49, 1549 (1982).
2. D. Dicus, E. Kolb, V. Teplitz, and R. Wagoner, Phys. Rev. D18, 1829 (1978).
3. Y. Asano et al., Phys. Lett. 107B, 159 (1981).
4. I.H. Chiang et al., BNL-AGS experiment (in progress).
5. D. Chang, P. Pal, and G. Senjanović, Phys. Lett. B (to appear).
6. R. Peccei and H. Quinn, Phys. Rev. D16, 1791 (1977).
7. J. Preskill, M. Wise, and F. Wilczek, Phys. Lett. B120, 127 (1983); L. Abbot and P. Sikivie, Phys. Lett. B120, 133 (1983); M. Dine and W. Fischler, Phys. Lett. B120, 137 (1983).
8. M. Gell-Mann, P. Ramond, and R. Slansky, in Supergravity, eds. J. van Nieuwenhuizen and D. Freedman (North Holland, Amsterdam, 1979).
9. F. Wilczek and A. Zee, Phys. Rev. D25, 553 (1982). Also, R.N. Mohapatra and B. Sakita, Phys. Rev. D21, 1062 (1980).
10. Mirror fermions were first discussed by J. Pati and A. Salam, Phys. Lett. 58B, 333 (1975) and work thereafter; see for a review J.C. Pati, Proc. ICOBAN Cont. (Bombay, 1981). In their theory mirror fermions emerged for reason of anomaly cancellations in SU(N) groups. A lot of work on mirror fermions has been performed by the Helsinki group and also K. Yamamoto. See,

e.g. K. Enquist, J. Maalampi, Z. Phys. C21, 345 (1984) and K. Yamamoto, Phys. Lett. 120B, 157 (1983) and references therein. For further detail and references, see G. Senjanović, Proc. of the Inner Space/Outer Space Conf., Fermilab, 1984.

11. H. Georgi, Nucl. Phys. B156, 126 (1979).
12. G. Senjanović, F. Wilczek, and A. Zee, Phys. Lett. 141B, 389 (1984).
Similar work has been performed by J. Bagger and J. Dimopoulos, Nucl. Phys. B244, 247 (1984) and P. Ramond, CALT - 68-109 (unpublished) and also H.M. Asatryan, Yerevan preprint (1982).
13. J. Bagger, J. Dimopoulos, E. Masso, and H. Reno, SLAC preprints (1985); D. Chang and R.N. Mohapatra, Maryland preprint (1985).

THEORETICAL CEILING ON FERMION MASSES IN THE STANDARD MODEL

R. Philippe
Randall Laboratory of Physics
University of Michigan
Ann Arbor, MI 48109
U.S.A.

Abstract

The demand that our vacuum be stable against radiative corrections can be shown to impose constraints on fermion masses. A complete renormalization group analysis of the standard model scalar potential yields the stringent upper bound on quark masses $m_{\text{quark}} < 80 \text{ GeV} + .54 m_{\text{Higgs}}$.

A crucial ingredient of the standard model is the phenomenon of spontaneous symmetry breaking. This is achieved by the introduction of a scalar Higgs field acquiring a non-zero vacuum expectation value. The couplings of this field to the gauge bosons and fermions consequently result in masses for these particles. It was realized by Coleman and Weinberg¹⁾ that radiative corrections to the scalar potential can play a significant role in determining the vacuum. This led Politzer and Wolfram²⁾ and independently Hung³⁾ to derive conditions for the stability of this vacuum, which could be recast as upper bounds on fermion masses. These original studies, however, neglected the effects of the negative mass-squared term in the tree level scalar potential on the radiative corrections and took into account only the first-order leading log term in the effective potential. The desire to finally settle the question of the maximum permissible fermion masses in the standard model warrants a complete renormalization group analysis of the stability of the vacuum. We would like to emphasize that we assume here nothing but the validity of the perturbative minimal standard model of electromagnetic, weak and strong interactions.

This work⁴⁾ was done in collaboration with M.J. Duncan and M. Sher.

The tree level scalar potential is given by

$$V_0(\phi) = -\frac{1}{2} \mu^2 \phi^2 + \frac{1}{4} \lambda \phi^4 \quad (1)$$

with $\mu^2, \lambda > 0$. This potential ensures symmetry breaking. The resulting vacuum is $\langle \phi \rangle^2 = \mu^2/\lambda$. The leading log approximation to the one-loop radiative corrections to the classical potential can be calculated to read (in the Landau gauge)

$$V_1^{LL}(\phi) = \frac{1}{64\pi^2} \left\{ \left[\frac{3}{16} (g_1^4 + 3g_2^4 + 2g_1^2 g_2^2) - \Sigma g_f^4 \right] \phi^4 \ln(\phi^2/\kappa^2) \right. \\ \left. + (3\lambda\phi^2 - \mu^2)^2 \ln[(3\lambda\phi^2 - \mu^2)/\kappa^2] - \mu^4 \ln(-\mu^2/\kappa^2) \right\} \quad (2)$$

where g_1 , g_2 , g_f and κ are the hypercharge, isospin, fermion Yukawa coupling constants and the renormalization mass scale. The fermion sum runs over flavor and color. In what follows we assume that there is only one heavy quark, so we replace $\sum g_f^4$ by $3 g_q^4$. We now clearly see that for large values of g_q or for heavy quarks the coefficient of the $\phi^4 \ln \phi^2$ term, which dominates at large ϕ , becomes negative and the potential unbounded from below. Our vacuum is then unstable against radiative corrections. In order to obtain a more reliable potential we must sum all leading logs and solve the renormalization group equation for the effective potential

$$\left(\beta_{\mu^2} \frac{\partial}{\partial \mu^2} + \beta_{\lambda} \frac{\partial}{\partial \lambda} + \sum_{i=1,2,3,q} \beta_{g_i} \frac{\partial}{\partial g_i} + \kappa \frac{\partial}{\partial \kappa} - \gamma \phi \frac{\partial}{\partial \phi} \right) V_{\text{eff}}(\phi) = 0 \quad (3)$$

with γ the anomalous dimension of ϕ

$$\gamma = \frac{-3}{64\pi^2} (g_1^2 + 6g_2^2 - 4g_q^2). \quad (4)$$

The β -functions for the g_i are given by $\beta_{g_1} = 41g_1^3/96\pi^2$, $\beta_{g_2} = -19g_2^3/96\pi^2$, $\beta_{g_3} = -7g_3^3/16\pi^2$ and $\beta_{g_q} = g_q(9g_q^2/2 - 8g_3^2)/16\pi^2$. To find β_{μ^2} and β_{λ} we equate $O(\hbar)$ terms in (3)

$$\left(\beta_{\mu^2} \frac{\partial}{\partial \mu^2} + \beta_{\lambda} \frac{\partial}{\partial \lambda} - \gamma \phi \frac{\partial}{\partial \phi} \right) V_0(\phi) = -\kappa \frac{\partial}{\partial \kappa} V_1^{\text{eff}}(\phi), \quad (5)$$

from which we derive by inspecting the ϕ^2 and ϕ^4 coefficients

$$\beta_{\mu^2} = \frac{3}{8\pi^2} \lambda + 2\gamma \quad (6)$$

$$\beta_{\lambda} = \frac{1}{8\pi^2} \left[\frac{3}{16} (g_1^4 + 3g_2^4 + 2g_1^2 g_2^2) - 3g_q^4 + 9\lambda^2 \right] + 4\lambda\gamma.$$

Eq.(3) can then be solved by the method of characteristics to yield the solution

$$V_{\text{eff}}(\phi) = -\frac{1}{2} \mu^2(t) G^2(t) \phi^2 + \frac{1}{4} \lambda(t) G^4(t) \phi^4 \quad (7)$$

where the running coefficients satisfy

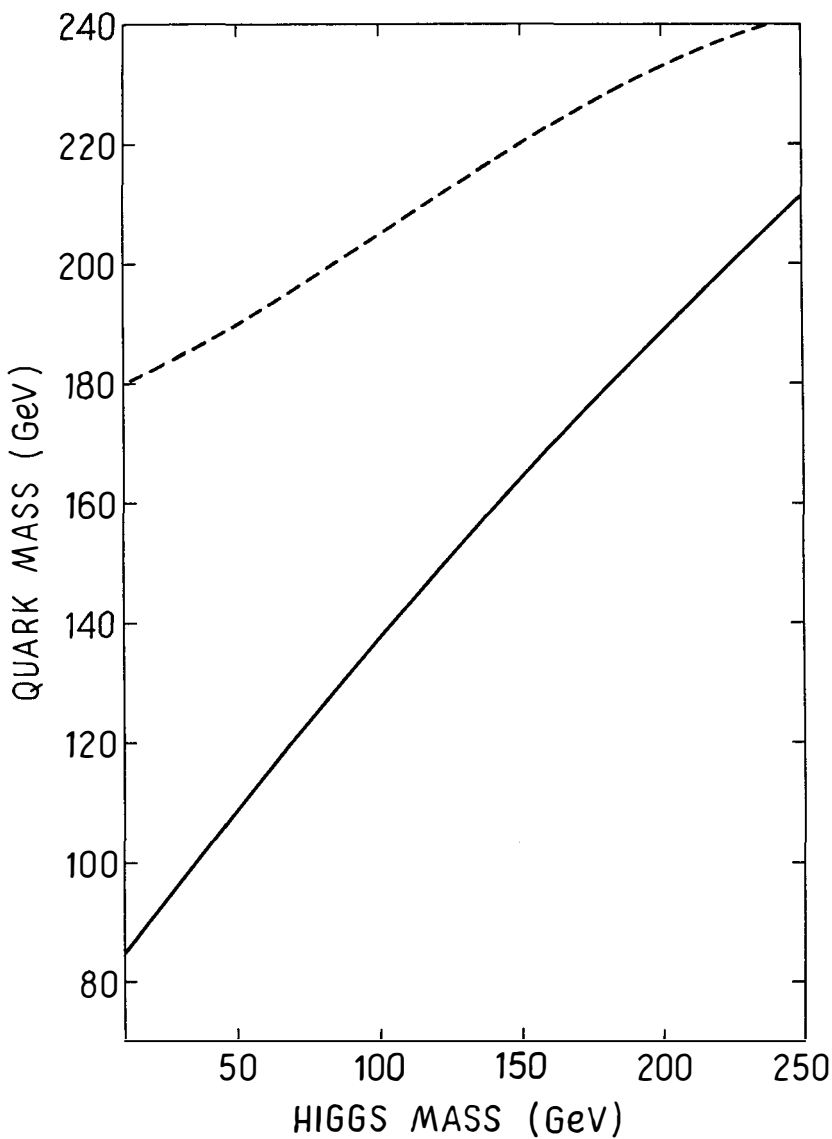
$$\begin{aligned} \frac{d\mu^2(t)}{dt} &= \mu^2(t) \beta_{\mu^2}(\lambda(t), g_i(t)) \\ \frac{d\lambda(t)}{dt} &= \beta_{\lambda}(\lambda(t), g_i(t)) \\ G(t) &= \exp\left(-\int_0^t \gamma(\lambda(t'), g_i(t')) dt'\right). \end{aligned} \quad (8)$$

The parameter t is $t = \ln(\phi/\kappa)$. Only the question of the initial values of the coupling constants remains to be addressed. The initial values of the gauge couplings are obtained from low energy experiments. Furthermore, we get relations between initial values by using

$$\left. \frac{\partial V_{\text{eff}}(\phi)}{\partial \phi} \right|_{\phi_0} = 0 \quad \text{and} \quad m_H^2 = \left. \frac{\partial^2 V_{\text{eff}}(\phi)}{\partial \phi^2} \right|_{\phi_0} \quad (9)$$

and choosing the subtraction point to be the v.e.v. of the scalar $\kappa = \phi_0 = (\sqrt{2} G_F)^{-1/2}$ with G_F the Fermi coupling constant. These running coupling constants are then put into (7). The requirement that the present vacuum be stable now leads to an upper bound on quark masses for a given Higgs mass. The result is quite stringent. It is summarized in the figure. It turns out that it can be fit rather well to a straight line

$$m_{\text{quark}} < 80 \text{ GeV} + .54 m_{\text{Higgs}} \quad (10)$$



Ceiling on quark masses as a function of the Higgs mass. The present vacuum is absolutely stable below the solid line. Between the dashed and solid curves our vacuum is unstable but with a lifetime greater than 10^{10} years.

for m_{Higgs} smaller than 250 GeV. Strictly speaking, however, we do not have to demand that our vacuum be absolutely stable, only that its lifetime be greater than 10^{10} years. The resulting limit is very insensitive to running couplings.

Finally, it is straightforward to generalize this ceiling to more complicated models. If there are many heavy leptons and quarks, then m_{quark} is replaced by $(\frac{1}{3} \sum m_{\text{lepton}}^4 + \sum m_{\text{quark}}^4)^{1/4}$ in eq.(10). The bound, however, becomes useless as the number of Higgs particles proliferates.

References

- (1) S. Coleman and E. Weinberg, Phys. Rev. D7 (1973) 1888.
- (2) H.D. Politzer and S. Wolfram, Phys. Lett. 828 (1979) 242.
- (3) P.Q. Hung, Phys. Rev. Lett. 42 (1979) 873.
- (4) M.J. Duncan and R. Philippe, University of Michigan preprint UM TH 84-22 (1984); M.J. Duncan, R. Philippe and M. Sher, Phys. Lett. 1538 (1985) 165.

Charged Kaon Production in τ Decays[†]

Geoffrey Mills*
California Institute of Technology



ABSTRACT

Measurements from the DELCO detector on charged kaon production in τ lepton decays are presented. The implications regarding $e-\mu-\tau$ universality and the τ neutrino mass are discussed.

The subject of this talk is the results from the DELCO experiment on the subject of charged kaon production in τ lepton decays. There are three separate topics included in this subject: single prong (1 charged particle) decays, multi-prong decays (3 charged particles), and a neutrino mass limit. The first is used to test $e-\mu-\tau$ universality, the second verifies CVC and SU(3) sum rule predictions, while the last represents a search for a finite mass τ neutrino.

The apparatus used in the experiment, located at the PEP e^+e^- storage ring (operated at 29 GeV/c² C.M.), is described elsewhere.¹⁾ The main feature of the detector is a large solid angle, isobutane gas, threshold Čerenkov counter with a pion threshold of 2.6 GeV/c and a kaon threshold of 9.4 GeV/c allowing for π/K separation in that range. The active solid angle of the Čerenkov counter is augmented by a magnetic spectrometer and a shower counter system.

[†]Work supported by U.S. Department of Energy Contract No. DE-AC03-81-ER40050.

*Representing the DELCO Collaboration.

1. Single Prong τ Decays

The single prong branching ratio measurements are described in detail in Ref. 2. Events from the process $e^+e^- \rightarrow \tau^+\tau^-$ are selected by requiring 2 or 4 prongs to be found in the event with 1-1 and 1-3 topologies, respectively, when the event is divided into two hemispheres along its thrust axis. Single prong hemispheres are then required to have a Čerenkov identified charged kaon. Fifty-five events remain after these and a few other minor cuts. We estimate a small (5 ± 2)% contamination from hadronic events in the final sample. The shower counter system is then used to separate the channel $\tau \rightarrow K\nu_\tau$ from $\tau \rightarrow K\nu_\tau + n\pi^0$'s ($n > 0$). The resulting branching ratios are shown in Table 1.

Recently, with the newly measured τ lifetime,³⁾ it has become possible to make quantitative tests of $e-\mu-\tau$ universality. In the standard model of the weak interactions, the decays $\tau \rightarrow \pi\nu_\tau$ and $\tau \rightarrow K\nu_\tau$ are related to the $e\nu_e$ and $\mu\nu_\mu$ decays of the π and K pseudoscalar mesons, respectively. The pseudoscalar form factor f_K (or f_π) is identical in all of the decays involving the K (or π) meson and hence there is no theoretical ambiguity in the comparison of decay rates. In order to compare the measurements in the context of universality, we first normalize all of the decay rates to the corresponding decay rate involving the muon, then we divide the measured value of this ratio by the theoretically predicted value of this ratio. This forms a quantity ρ which is unity if universality holds:

$$\rho \equiv \frac{\Gamma_{M\nu}^{\text{meas}}/\Gamma_{M\mu\nu}^{\text{meas}}}{\Gamma_{M\nu}^{\text{pred}}/\Gamma_{M\mu\nu}^{\text{pred}}} \quad \begin{array}{l} M = K \text{ or } \pi \\ l = e, \mu, \text{ or } \tau \end{array} \quad (1)$$

where $\Gamma_{M\nu}^{\text{meas}}$ corresponds to the measured decay rate and $\Gamma_{M\nu}^{\text{pred}}$ corresponds to the theoretically predicted rate for the decay involving the meson M (π or K) and the leptons $l\nu_l$ ($e\nu_e$, $\mu\nu_\mu$ or $\tau\nu_\tau$). The measured decay rates are calculated from the pion lifetime³⁾ and branching ratios,⁴⁾ the kaon lifetime⁵⁾ and branching ratios,⁶⁾ and the τ lifetime⁷⁾ and branching ratios. The result, shown in Fig. 1, verifies the lepton universality hypothesis to a level comparable to other measured decay modes of the τ .

2. Multi-prong τ Decays

Multi-prong events are selected by requiring the 1-3 topology and by demanding that there be a Čerenkov identified kaon on the 3-prong side of the event. The analysis is described in detail in Ref. 8. These events result from two types of decays, $\tau \rightarrow K\pi\pi(\pi^0)\nu_\tau$ and $\tau \rightarrow KK\pi\nu_\tau$, where the first is Cabibbo suppressed and the second is Cabibbo favored but phase space suppressed. In the Cabibbo suppressed decay, the charge of the kaon is always the same as the charge of the τ . In the Cabibbo favored case, kaons of both charges are observed. The data yield 6 same sign events, 2 opposite sign events, and one event with 2 identified kaons. A Poisson likelihood fit to these events using the branching ratios as free parameter yields the results shown in Table 1. The $\tau \rightarrow KK\pi\nu_\tau$ branching ratio can be predicted from the $e^+e^- \rightarrow KK\pi$ cross section in the isospin 1 channel using CVC. The results shown in Table 1 are in agreement with our data. The $\tau \rightarrow K\pi\pi(\pi^0)\nu_\tau$ branching can be calculated assuming $\tau \rightarrow Q(1300)\nu_\tau$ dominance in the decay and SU(3) sum rule relations⁹⁾ and are consistent with our data. This measurement provides the first observation of multi-prong τ -decays involving charged kaons.

3. Neutrino Mass Limit

The $\tau \rightarrow K^+K^-\pi$ decay channel is a good channel to use in determining a neutrino mass limit. This is because the mass of the $K^+K^-\pi$ system is constrained by the available phase space to be close to the end point, where it is sensitive to m_{ν_τ} . In order to obtain a limit on the τ neutrino mass we search for events where two kaons are identifiable. The selection criteria for kaon identification can be relaxed in this case since it is the square of the kaon misidentification probability which enters as background. The result of this selection is 4 events where a K^+K^- pair is identified on the 3-prong side of the event. Because two kaons are required to have a momentum above pion threshold, the background from hadronic events is reduced to a level of $(1.0 \pm 0.5)\%$.

The invariant mass distribution of these four events may be used to determine an upper bound on m_{ν_τ} , the mass of the τ neutrino. The invariant masses along with their associated resolution are shown in Fig. 2. A likelihood fit of the invariant masses to the expected distribution as a function of m_{ν_τ} is then performed. The fit incorporates the individual event mass resolution functions, the predicted invariant mass distribution coming from CVC, and the cross section for the reaction $e^+e^- \rightarrow K^*K^-$. The result is insensitive to reasonable variations in the widths of the resolution functions. The mass limit is found to be $m_{\nu_\tau} < 157 \text{ MeV}/c$ at 95% C.L., which is the best published limit to date.

In conclusion, the production of charged kaons in τ decays is consistent with $e-\mu-\tau$ universality and the standard model. There is no evidence for a massive τ neutrino.

I would like to thank the entire DELCO collaboration for making this work possible and especially the members from Caltech, B. Barish, T. Pal, W. Ruckstuhl, and R. Stroynowski.

TABLE 1

The branching ratios measured by DELCO. The first two are obtained from an analysis of charged kaons in single prong τ decays, while the second two are obtained from an analysis of multi-prong decays.

Branching Ratios		
Mode	Measured	Predicted
$\tau^- \rightarrow K^-\nu_\tau$	$(.59 \pm .18)\%$	$(0.71 \pm 0.10)\%$
$\tau^- \rightarrow K^-\nu_\tau + n\pi_0$ $n \geq 0$	$(1.71 \pm 0.29)\%$	$(1.51 \pm 0.14)\%$
$\tau^- \rightarrow K^-\pi^+\pi^-(\pi^0)\nu_\tau$	$(.22 \pm_{0.13}^{0.16})\%$	$(0.11 \pm .01)\%$
$\tau^- \rightarrow K^+K^-\pi^-\nu_\tau$	$(.22 \pm_{0.11}^{0.17})\%$	$(0.24 \pm .05)\%$

References

- 1) D. Koop, Ph.D. Thesis, Caltech preprint CALT-68-1149, 1984.
- 2) G. Mills *et al.*, *Phys. Rev. Lett.* **52**, 1944 (1984).
- 3) D. Ayres *et al.*, *Phys. Rev.* **D3**, 1051 (1971).
- 4) D. Bryman *et al.*, *Phys. Rev. Lett.* **50**, 7 (1983).
- 5) R. Ott *et al.*, *Phys. Rev.* **D3**, 52 (1971).
- 6) J. Heintz *et al.*, *Phys. Lett.* **60B**, 302 (1976).
- 7) J. Jaros, SLAC-PUB-3569, 1985.
- 8) G. Mills *et al.*, *Phys. Rev. Lett.* **54**, 624 (1985).
- 9) Y. S. Tsai, *Phys. Rev.* **D4**, 2821 (1971).

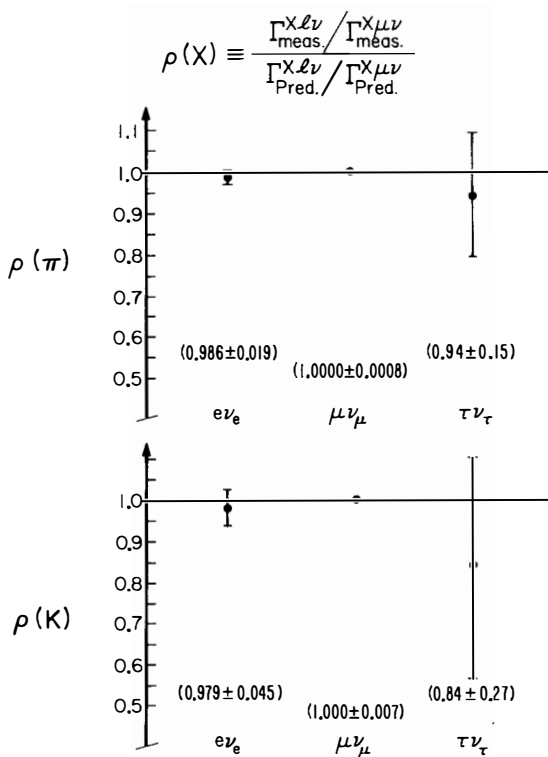


Figure 1. This figure illustrates the current knowledge of the universality of the interactions of the three leptonic currents with the pseudoscalars π and K . The value of ρ should be unity if universality holds.

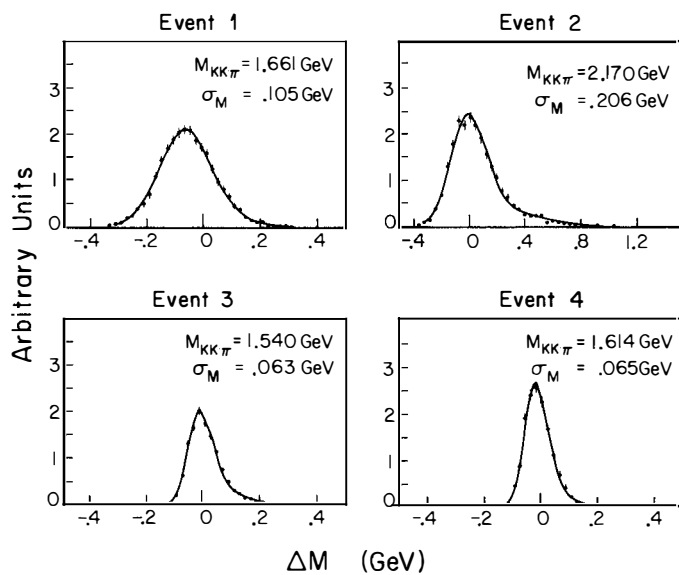


Figure 2. This figure shows the measured masses and the mass resolution function for each of the four events used in the likelihood fit to determine an upper bound on m_{ν_e} .

A NEW LIMIT ON THE MASS OF THE TAU NEUTRINO.

David B. MacFarlane
Department of Physics,
University of Toronto,
Toronto, Ontario, Canada

(representing the ARGUS collaboration*)



ABSTRACT. A high statistics sample of tau-lepton decays into $\pi^+\pi^-\pi^\pm\nu_\tau$ has been collected using the ARGUS detector, operating at around 10 GeV centre of mass energies in the DORIS II e^+e^- storage ring at DESY. From the endpoint of the tau neutrino energy spectrum, we derive a preliminary upper limit for the mass of the tau neutrino of $70 \text{ MeV}/c^2$ at the 95% confidence level.

Previous upper limits for the mass of the tau neutrino have been established from the energy spectrum of the electron ¹⁾ in three body decays of $\tau^- \rightarrow e^- \bar{\nu}_e \nu_\tau$, and from the end point of the pion energy spectrum ²⁾ in the decay $\tau^- \rightarrow \pi^- \nu_\tau$. (The convention that charge conjugate states are implied is used in all of the following.) The tau leptons were produced in e^+e^- collisions at the SPEAR storage ring, with centre-of-mass energies around $3.5 \text{ GeV}/c^2$. The mass sensitivity in the electron case is limited, since this is a three body decay. The endpoint of the pion spectrum is, in principle, a direct measure of the mass, but a substantial background from radiative Bhabhas and hadronic events had to be subtracted from the raw spectrum in the actual measurement.

More recent limits have been determined from tau decays, observed at PEP, into the $\pi^+\pi^-\pi^-\pi^0\nu_\tau$ ³⁾ and $K^+K^-\pi^-\nu_\tau$ ⁴⁾ channels. There, a different technique was used. The high mass region of the hadronic mass spectrum, sensitive to neutrino mass, was studied to obtain an improved measurement. The increased sensitivity is due to the fact that the mass spectrum for such channels peaks near the tau mass, where the effects of a finite neutrino mass are large. The data samples were, in fact, relatively small. In passing, it should be noted that such limits have some dependence on whether the three or four-body mass spectrum is phase space, or resonant. The present best limit so obtained is the mass of the tau neutrino is less than $143 \text{ MeV}/c^2$ at the 95% confidence level ³⁾.

Here, a new experimental limit for the tau neutrino mass from the ARGUS collaboration ⁵⁾ is reported, based on a study of a sample of about 1500 decays in the channel, $\tau^- \rightarrow \pi^+\pi^-\pi^-\nu_\tau$. The tau leptons were produced in e^+e^- annihilation at centre-of-mass energies around $10 \text{ GeV}/c^2$. The data were collected using the ARGUS detector, located in one of the two interaction regions at the DORIS II e^+e^- storage ring at DESY. In obtaining this new limit, we have returned to the method of studying the high-energy endpoint of the hadronic energy spectrum, or equivalently, the low energy part of the tau neutrino energy spectrum. The improvement in the limit is due to high statistics, good resolution with small systematic absolute scale error ($\pm 0.15\%$), and low backgrounds from Bhabha or hadronic events. The first is a result of the higher cross section at DORIS energies in comparison to PEP/PETRA. The second and third reflect the improvement in detector technology since the early SPEAR measurements, and the fact that the topologies for tau and multi-hadron events are more cleanly distinguishable at DORIS energies.

A short description of the ARGUS detector and trigger requirements can be found in reference 6. The event sample used in the analysis represents a total luminosity of 61.4 pb^{-1} , of which, 7.3 pb^{-1} , 36.2 pb^{-1} , 8.8 pb^{-1} and 9.0 pb^{-1} were collected on the $\Upsilon(1S)$, $\Upsilon(2S)$, $\Upsilon(4S)$ and nearby continuum, respectively. Events were selected which would satisfy the

topology of tau-pair production, where one tau (τ^+) decays into a single charged track, and the second (τ^-) into 3 charged tracks. The decay into a single isolated charged track acts as a tag, which, if the further requirement is made that no neutral energy be seen in the detector, represents $46.6 \pm 1.9\%$ ⁷⁾ of all tau decay channels.

The acceptance of the single charged track tagging has been increased by including the contribution from the decay channel $\tau^+ \rightarrow \rho^+ \nu^+$, where $\rho^+ \rightarrow \pi^+ \pi^0$, accounting for a further $22.1 \pm 2.4\%$ ⁷⁾ of tau decays. The π^0 is reconstructed from shower counter measurements: either from two observed neutral clusters, which reconstruct to within ± 20 MeV/c² of the π^0 mass, or from a single shower cluster of energy greater than 1 GeV, at which energy the two photons from the π^0 decay often coalesce into a single shower. A ρ^+ was defined by the reasonably unrestrictive requirement that the invariant mass of the tagging track and the π^0 lies between 0.57 GeV/c² and 1.07 GeV/c².

Events were required to satisfy the following specific conditions, maximizing the acceptance for the desired tau-pair decay topology, while minimizing backgrounds:

- (1) exactly four charged tracks, with charge sum zero,
- (2) momentum sum, $P_s = \sum_{i=1}^4 |p_i|$, greater than 2.7 GeV/c, to eliminate two-photon events, and less than $0.92\sqrt{s}$, to eliminate exclusive resonance decays,
- (3) a hemisphere cut, $\cos\theta_{1i} \leq 0$, where θ_{1i} is the angle between the tagging track 1 and tracks $i = 2, 4$, and $\cos\theta_{ij} > 0$, where $i = 2, 4$ and $j = 3, 4$, for the tracks on the three-prong side of the event,
- (4) for the tagging track, a polar angle cut, $|\cos\theta_1| \leq 0.75$, to ensure good momentum resolution and that trigger conditions are satisfied,
- (5) tracks on the three-prong side of the event satisfy the pion hypothesis based on dE/dx and time-of-flight measurements made by the detector,
- (6) sufficiently large opening angles between the three charged pions, with $\cos\theta_{\pi^+\pi^-} < 0.992$, to reject Bhabha and radiative $\mu^+\mu^-$ events with converted photons,
- (7) besides the 1 or 2 clusters required to reconstruct a π^0 if the ρ -channel tag is used, no additional energy in the shower counters exceeding 50 MeV and unassigned to one of the charged tracks, thereby suppressing feedthrough from tau decays into $\pi^+\pi^-\pi^-\pi^0\nu^+$,
- (8) for the case of a ρ channel tag, momentum of the ρ greater than 0.9 GeV/c, and the angle between the π^0 and π^- from the ρ of less than 90° , again suppressing contributions from four-pion tau decays,

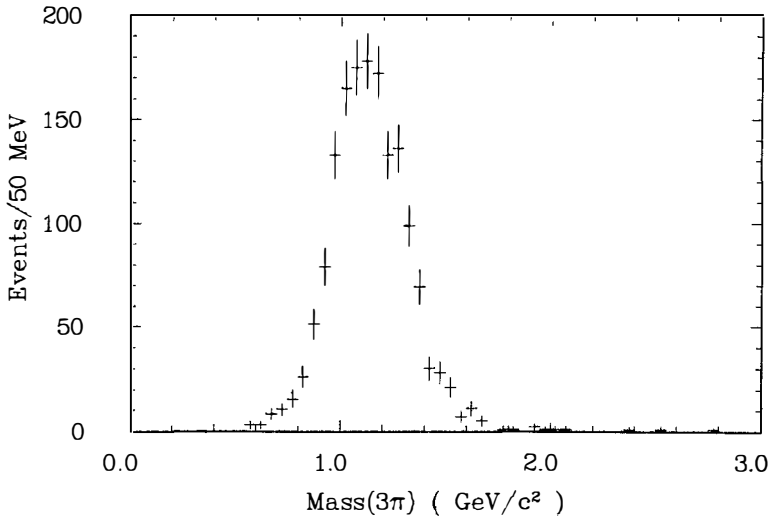


Figure 1. Invariant mass of three charged pions from the decay $\tau^- \rightarrow \pi^+\pi^-\pi^-\nu_\tau$, without acceptance corrections.

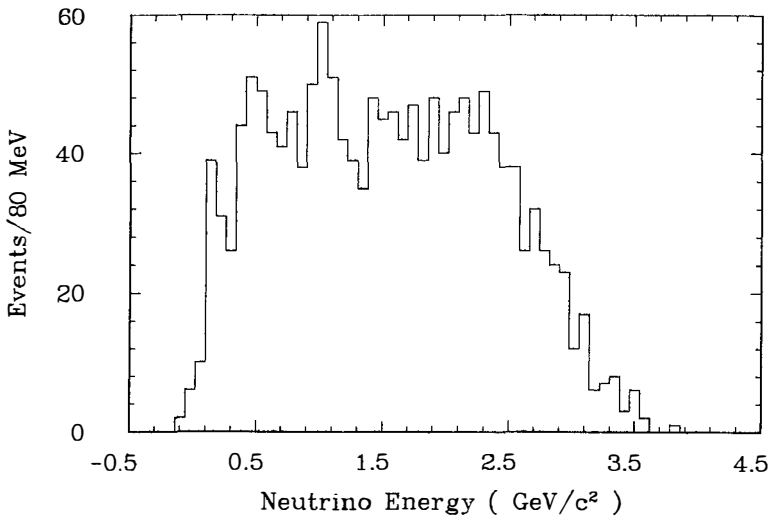


Figure 2. Tau neutrino energy spectrum determined from the energy of the three pion system in the decay $\tau^- \rightarrow \pi^+\pi^-\pi^-\nu_\tau$, without acceptance corrections.

- (9) shower counter energy for the tagging charged prong less than 3.5 GeV, in order to suppress background from Bhabha events.

The last requirement causes some loss of acceptance for the case where the tagging track is an electron. However, Bhabha events would populate the low-energy region of the neutrino energy spectrum, and thus are potentially troublesome in a study sensitive to this portion of the spectrum.

A total of 1566 events satisfy these selection criteria, and are predominantly three-prong decays of the tau lepton. The amount of background from hadronic, radiative Bhabha and muon-pair events is estimated, from the number of events beyond a three-pion mass of 1.8 GeV/c², to be less than 1%. Contributions from misidentification of tau decays into $\pi^+\pi^-\pi^-\pi^0\nu_\tau$ and $K^+K^-\pi^-\nu_\tau$ are estimated to be less than 4%, populating mostly the region of low three pion invariant mass. The invariant mass spectrum for the events, uncorrected for acceptance, is shown in figure 1, with the pion mass assumed for each of the three hadrons. The spectrum is dominated by a broad resonance, which has been shown to have the properties of the A_1 ^{8,9}. This interpretation is certainly consistent with our observation that the three-body final state is more than 90% composed of the two-body subsystem $\rho^0\pi^-$, although a definitive result awaits the completion of a full Dalitz plot analysis. However, knowledge of the resonant behaviour of this three-body tau decay channel is not an important factor in obtaining the tau neutrino mass limit.

Rather than studying the three-pion energy spectrum directly in obtaining the mass limit, we convert this to a spectrum for the tau neutrino energy, by using:

$$E_\nu = E_\tau - \sum_{i=2}^4 E_i \quad (1)$$

where E_τ is the beam energy, and the energies, E_i , of the three decay hadrons are calculated from their measured momenta, again using pion mass assignments. The resulting spectrum is shown in figure 4.

For a given three-pion invariant mass, assuming an isotropic decay of the tau, events uniformly populate the region between:

$$E_\nu^{\text{min}} = \gamma E^* (1 - \beta) \quad (2)$$

and

$$E_\nu^{\text{max}} = \gamma E^* (1 + \beta) \quad (3)$$

where $\gamma = E_\tau/m_\tau$ and $\beta = p_\tau/E_\tau$, and E^* is the energy of the tau neutrino in the tau centre-of-mass. If the tau neutrino has a finite mass, then the energy spectrum is shifted higher

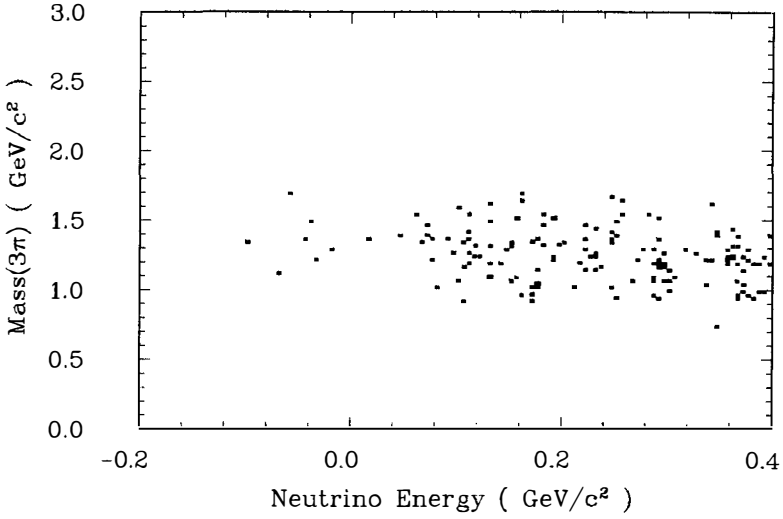


Figure 3. Plot of the low-energy end of the neutrino energy spectrum versus invariant three pion mass. The size of the squares is proportional to the number of entries in a given bin.

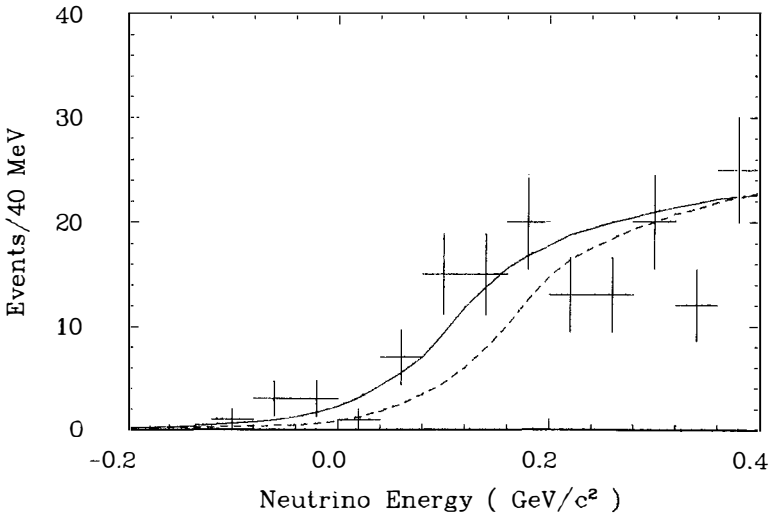


Figure 4. Mass sensitive region of the tau neutrino energy spectrum, with superimposed Monte Carlo expectations for $m(\nu_\tau)=0$ (solid line) and $140 \text{ MeV}/c^2$ (dashed line), normalized to the number of events in the complete spectrum.

by:

$$E_{\nu}^{\text{min}}(m_{\nu} \neq 0) = E_{\nu}^{\text{min}}(m_{\nu} = 0) + \frac{\gamma m_{\nu}^2}{2 E^*} \quad (4)$$

The lower limit, E_{ν}^{min} , is a slow function of the three-pion invariant mass, so that, for $m_{\nu} = 0$, the entire mass spectrum has some contribution to the region below $E_{\nu} = 300 \text{ MeV}/c^2$. The relative importance of the higher mass portion of the spectrum of course is greater, since the density of events there as a function of E_{ν} is greater. However, the mass sensitive region is dominated by the high statistics portion of the three-pion mass spectrum, as can readily be seen in figure 3.

In order to compute the limit on the tau neutrino mass, we have used a Monte Carlo to predict the shape of the spectrum in the mass sensitive region. The calculation is based on the observed mass spectrum for masses less than m_{τ} , assumes isotropic decays of the tau lepton, $\tau^{-} \rightarrow (3\pi)^{-}\nu_{\tau}$, in the tau rest frame, and includes the effects of momentum resolution, the machine energy spread, radiative corrections¹⁰⁾ and detector acceptance. The momentum resolution, which is the most important factor in determining the obtainable limit, is confirmed by two experimentally accessible measurements: muon-pair events at high momenta¹¹⁾, where $\sigma(p_{\text{T}})/p_{\text{T}} = 0.012 p_{\text{T}} \text{ GeV}/c$, and by the width of the T peak in the missing mass spectrum of $\Upsilon' \rightarrow \pi^{+}\pi^{-}\text{X}$ events⁶⁾ at lower momenta, where the average $\sigma(p_{\text{T}})/p_{\text{T}}$ is 0.009.

The low-energy endpoint of the neutrino energy spectrum is shown in figure 3, together with the calculated spectrum assuming $m_{\nu} = 0$ and $m_{\nu} = 140 \text{ MeV}/c^2$. The shift, proportional to m_{ν}^2/E^* , of the calculated spectrum toward higher energies is clearly illustrated. The maximum likelihood technique has been used in the mass sensitive region from $-100 \text{ MeV}/c^2$ to $+300 \text{ MeV}/c^2$ to obtain a limit on the tau neutrino mass. There are 90 events in the fit region.

The sensitivity of the obtained limit to sources of systematic error has been studied by varying both the upper limit of the three-pion-mass included and the limits of the interval of neutrino energy used, by changing the momentum resolution by 20%, and by varying the level of hadronic background by a factor of four. The mass limit was found to vary relatively little under such changes; the result is statistics dominated. If account is taken of all such sources of systematic error, including the amount of hadronic background and reasonable uncertainties in the momentum resolution, we obtain an upper limit on the tau neutrino mass of $70 \text{ MeV}/c^2$, at the 95% confidence level.

In summary, we have obtained a new limit for the mass of the tau neutrino. This limit is based on a study of the neutrino energy spectrum, obtained from a high statistics sample of tau decays into the channel, $\pi^{+}\pi^{-}\pi^{\pm}\nu_{\tau}$. The method used, namely a measurement of the

endpoint position of this spectrum, is quite analogous to earlier measurements in the $\pi^\pm\nu_\tau$ channel by MARK II ²⁾. High statistics, small hadronic backgrounds and good control of systematics have resulted in an improvement by a factor of two over the previous best limit ³⁾.

REFERENCES

- * Current members of the ARGUS collaboration are: H.Albrecht, U.Binder, G.Harder, H.Hasemann, A.Philipp, W.Schmidt-Parzefall, H.Schröder, H.D.Schulz, R.Wurth (DESY), A.Drescher, B.Gräwe, U.Matthiesen, H.Scheck, J.Spengler, D.Wegener (Dortmund), R.Heller, K.R.Schubert, J.Stiewe, R.Waldi, S.Weseler (Heidelberg), N.N.Brown, K.W.Edwards, W.R.Frisken, Ch.Fukunaga, D.J.Gilkinson, D.M.Gingrich, M.Goddard, P.C.H.Kim, R.Kutschke, D.B.MacFarlane, J.A.McKenna, K.W.McLean, A.W.Nilsson, R.S.Orr, P.Padley, P.M.Patel, J.D.Prentice, H.C.J.Seywerd, B.J.Stacey, T.-S.Yoon, J.C.Yun (IPP Canada), R.Ammar, D.Coppage, R.Davis, S.Kanekal, N.Kwak (Kansas), G.Kernel, M.Pleško (Ljubljana), P.Böckmann, L.Jönsson, Y.Oku (Lund), A.Babaev, M.Danilov, A.Golutvin, V.Lubimov, V.Matveev, V.Nagovitsin, V.Ryltsov, A.Semenov, Yu.Semenov, V.Shevchenko, V.Soloshenko, V.Sopov, I.Tichomirov, Yu.Zaitsev (ITEP-Moscow), R.Childers, C.W.Darden, and H.Gennow (South Carolina).
- 1) W.Bacino et al. (DELCO Collaboration), *Phys.Rev.Lett.* **42** (1979), 749.
 - 2) C.A.Blocker et al. (MARK II Collaboration), *Phys.Lett.* **109B** (1982), 119.
 - 3) C.Matteuzzi et al. (MARK II Collaboration), *Phys.Rev.Lett.* **52** (1984), 1869; W.Innes (MARK II Collaboration), *Proceedings of the XXIIInd International Conference on High Energy Physics, Leipzig (1984) vol.I*, 264.
 - 4) G.B.Mills et al. (DELCO Collaboration), *Phys.Rev.Lett.* **54** (1985), 624.
 - 5) H.Albrecht et al. (ARGUS Collaboration), *Phys.Lett.* **134B** (1984), 137.
 - 6) H.Albrecht et al. (ARGUS Collaboration), "An upper limit on the mass of the tau neutrino", to be submitted to *Phys.Lett B*.
 - 7) Particle Data Group, *Rev.Mod.Phys.* **56** (1984), S1.
 - 8) W.Wagner et al. (PLUTO collaboration), *Z.Phys.* **C3** (1980), 193.
 - 9) J.Kadyk (MARK II collaboration), *Proceedings of the XXIIInd International Conference on High Energy Physics, Leipzig (1984), vol.I*, 319.
 - 10) F.A.Berends and R.Kleis, *Nucl.Phys.* **B177** (1981), 141.
 - 11) H.Albrecht et al. (ARGUS Collaboration), DESY preprint DESY 85-021 (1985), to be published in *Z.Phys C*.

SEARCH FOR NEUTRINO OSCILLATIONS
AT THE GOESGEN NUCLEAR POWER REACTOR

Viktor Zacek
CALTECH-SIN-TUM Collaboration
Technical University Munich, FRG



Abstract:

A status report on a continued search for neutrino oscillations of the disappearance type is presented. Measurements of the $\bar{\nu}_e$ -spectrum at two distances (37.9m and 45.9m) from the core of the Gösigen power reactor (Switzerland) have been completed, using the detection reaction $\bar{\nu}_e + p \rightarrow e^+ + n$. No evidence for ν -oscillations was found. The analysis of the spectra yields limits on the oscillation parameters of $\Delta m^2 = 0.016 \text{ eV}^2$ (90 % c.l.) for full mixing and $\sin^2 2\theta = 0.16$ (90 % c.l.) for large Δm^2 . The measurements are continued in a third distance (64.7m) from the reactor core.

INTRODUCTION

The neutrino evolved within the last couple of years from an exotic particle to a powerful probe to study the physical structure of elementary particles: Neutrino beams lead to the discovery of charmed particles and neutral currents. In addition neutrinos serve to explore the inner constituents of nucleons, as well as the interior of the sun and they even may decide whether the universe is closed. However, the intrinsic properties of neutrinos remain puzzling and the question, whether the neutrino possesses a finite rest mass, remains one of the most challenging problems in today's physics. Unfortunately there is little guidance from theory itself. Although in extended versions of Grand Unified Theories the neutrino can acquire a mass, a wide range from 10^{-6} eV to 10 eV might be possible.

A finite neutrino mass, together with violation of lepton number offers the exciting possibility of neutrino oscillations. The underlying assumption for the existence of oscillations is, that the neutrinos being created and detected by weak interaction processes (ν_e, ν_μ, \dots) are a coherent superposition of neutrino states of definite masses (ν_1, ν_2, \dots), in formal analogy to the KM - mixing of hadronic charged weak currents:

$$\begin{pmatrix} \nu_e \\ \nu_\mu \\ \cdot \\ \cdot \\ \cdot \end{pmatrix} = \begin{pmatrix} U \end{pmatrix} \begin{pmatrix} \nu_1 \\ \nu_2 \\ \cdot \\ \cdot \\ \nu_n \end{pmatrix} \quad (1)$$

where U is a unitary matrix with $\frac{1}{2}(n^2-n)$ angles and $\frac{1}{2}(n-1)(n-2)$ phases. Since the propagation of a particle is determined by its mass, the interference of different mass eigenstates during evolution in space time changes the character of the ν -wave packet and a different weakly interacting neutrino-flavor can appear. In the simplest picture of ν -oscillations involving only two types of neutrinos, the probability for a neutrino with energy E_ν , emitted in a given weak interaction eigenstate, to be in the same state at a distance L from the source, is given by ¹⁾:

$$P(E_\nu, L, \Delta m^2, \theta) = 1 - \sin^2 2\theta \cdot \sin^2 \left(\frac{1.27 \Delta m^2 (\text{eV}^2) L (\text{m})}{E_\nu (\text{MeV})} \right) \quad (2)$$

The parameters characterizing the oscillations are the mixing angle θ , relating the weak interaction eigenstates to the mass eigenstates in (1) and the mass parameter $\Delta m^2 = |m_1^2 - m_2^2|$, where m_1 and m_2 are the mass eigenvalues. Thus for a monoenergetic ν -beam the mass parameter determines the frequency of the oscillation pattern, while the mixing angle governs the oscillation amplitude. With increasing distance from a neutrino source an experiment tests smaller mass parameters, e.g. in the case of 10 MeV solar neutrinos, mass parameters down to 10^{-10} eV^2 are investigated. Reactor experiments with neutrino energies between 2 and 10 MeV installed at typical detector core distances of 10 to 70 m probe mass parameters in the range from 0.01 to 10 eV^2 .

In the Gösgen oscillation experiment²⁾ flux and energy spectrum of electron antineutrinos from β -decaying fission products were monitored at three distances from the core of a 2.8 GWth power reactor (37.9m, 45.9m, 64.7m). The detector system is based on the reaction $\bar{\nu}_e + p \rightarrow n + e^+$ and an alternating array of liquid scintillation counters and ^3He wire chambers serve for positron and neutron detection. Since the neutrino energy is related to the energy of the positron by $E_\nu = E_{e^+} + 1.804 \text{ MeV}$, the measured e^+ -spectrum directly reflects the incident neutrino spectrum. Comparing the e^+ -spectra obtained at different distances enables us to set limits on the oscillation parameters without relying upon a precise knowledge of the neutrino source spectrum, detection cross section and detector efficiency. In addition the data are analyzed in terms of oscillations and checked for possible ν -disappearance by referring to the expected neutrino source spectrum.

THE REACTOR ANTINEUTRINO SPECTRUM

Most of the produced fission products in a nuclear reactor end up in an unstable, neutron rich configuration and further undergo β -decay. The great number of these decays and the thereby emitted neutrinos make a nuclear reactor an intense antineutrino source in

the energy region from 0.5 to 10 MeV, with an intensity of $1.9 \cdot 10^{17} \bar{\nu}/\text{sec MWth}$. The Gösigen 2.8 GWth reactor thus constitutes a neutrino source with a strength of $5 \cdot 10^{20} \bar{\nu}/\text{sec}$. The reactor working period is about 10 months, followed by a scheduled shut down of about 1 month to allow the replacement of one third of the fuel elements. At the beginning of a cycle the number of fissions divides up in 69 % ^{235}U , 21 % ^{239}Pu , 7 % ^{238}U , 3 % ^{241}Pu . Since the ν -spectra following the fission of the uranium and plutonium isotopes differ among each other, the time dependent fission contributions provided by the reactor staff have to be registered over the entire measuring period. The relative contributions to the number of fissions of the four dominant isotopes averaged over two measuring periods are shown in Table 1.

Table 1

^{235}U	^{239}Pu	^{238}U	^{241}Pu		
62.5 %	26.7 %	6.7 %	4.1 %	Gösigen I	(37.9 m)
59.1 %	29.3 %	6.8 %	4.8 %	Gösigen II	(45.9 m)

Other fissioning isotopes e.g. ^{236}U , ^{240}Pu , ^{242}Pu supply less than 0.1 % to the total number of fissions. For the dominant isotopes ^{235}U and ^{239}Pu neutrino yields per fission were used, which were derived from measured composite β -spectra of fission fragments³⁾. For the remaining isotopes calculated spectra were taken⁴⁾. Since the measurements in the 37.9 and 45.9m positions covered slightly different timespans of the reactor fuel cycle, differences between the corresponding $\bar{\nu}_e$ -spectra of less than 1.3 % result, which are taken into account in the data analysis.

In order to evaluate the experimental e^+ -spectrum the total cross section for the detection reaction $\bar{\nu}_e + p \rightarrow e^+ + n$ has to be determined. Including the kinematics of the scattering process, this cross section is evaluated in analogy to the decay of the free neutron; adopting as value for the neutron lifetime $\tau_n = 912 \pm 18$ sec, the cross sections is determined by:

$$\sigma(E_\nu) = (9.279 \pm 0.18) \left(1 - 4.12 \frac{E_\nu}{M_n}\right) (E_\nu - (M_n - M_p)c^2) \cdot \quad (3)$$

$$\cdot ((E_\nu - (M_n - M_p)c^2)^2 - (m_e c^2)^2)^{1/2} \cdot 10^{-44} \text{ cm}^2$$

Various refinements to (3) on the percent level have to be included, like recoil and radiative corrections. Finally the expected e^+ -spectrum at a distance L in the presence of oscillations, characterized by the parameters Δm^2 , $\sin^2 2\theta$ is expressed by

$$Y(E_{e^+}, L, \Delta m^2, \theta) = \frac{n_p \cdot \varepsilon}{4\pi L^2} S(E_\nu) \sigma(E_\nu) P(E_\nu, L, \Delta m^2, \theta) \quad (4)$$

where $S(E_\nu)$ represents the ν -source spectrum and n_p the number of target protons. ε denotes the overall detection efficiency. Figure 1 illustrates how the measured e^+ -spectrum evolves as a function of detector core distance in presence of neutrino oscillations ($\Delta m^2 = 0.2 \text{ eV}^2$, $\sin^2 2\theta = 0.4$).

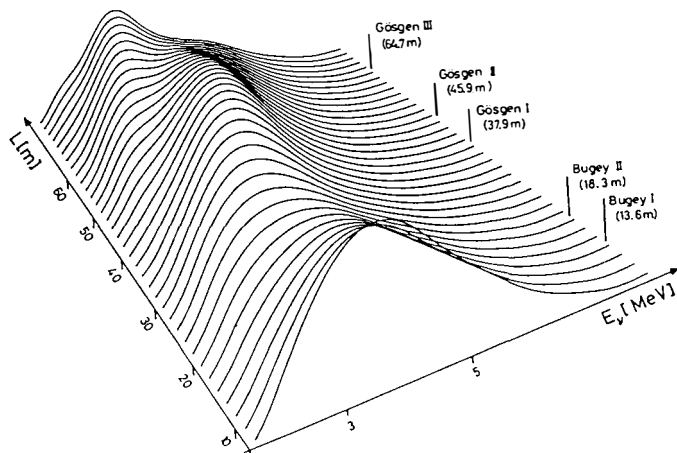
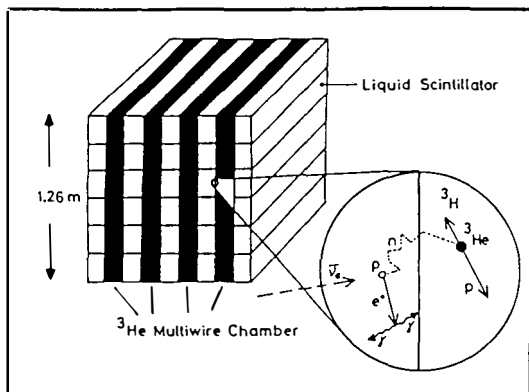


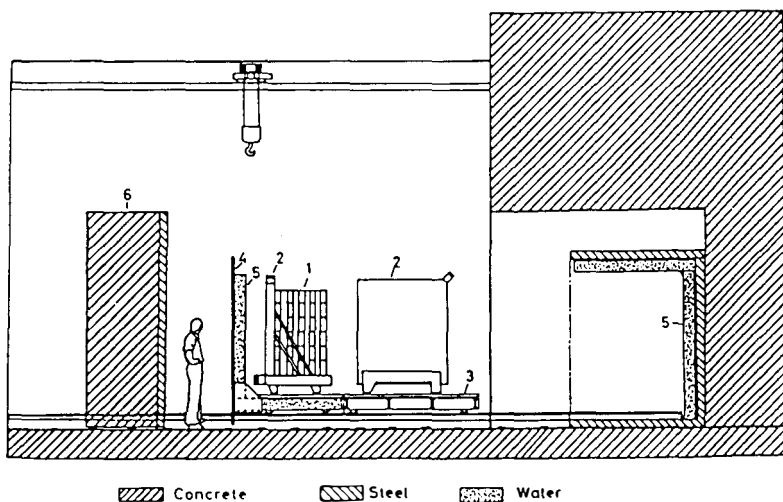
Fig. 1 Modulation of the $\bar{\nu}_e$ -spectrum as a function of distance from the reactor core in presence of $\bar{\nu}$ -oscillations described by the parameter set $\Delta m^2 = 0.2 \text{ eV}^2$ and $\sin^2 2\theta = 0.4$.

THE NEUTRINO DETECTOR

The neutrino detector consists of five planes of six liquid scintillator cells stacked on top of each other, alternating with four ^3He multiwire proportional chambers (Fig. 2a). The 377 l of liquid scintillator (NE235C) constitutes a neutrino target of $2.41 \pm 0.017 \times 10^{28}$ protons. Following an antineutrino interaction with one of the protons in the liquid scintillator, the positron is slowed down, producing a prompt light pulse in the scintillator. The neutron is thermalized within 10 μsec and diffuses within 200 μsec into one of the adjacent wire chambers filled with ^3He -gas. Capture of thermal neutrons by a ^3He -nucleus ($\sigma=5600$ b) yields a proton and a triton with a Q-value of 765 keV. A 250 μsec time coincidence between positron and neutron is required as signature for a neutrino event, as well as a 24cm position correlation between the scintillator and the wire chamber events. The position sensitivity of the detector system is achieved by charge division along the wires of the neutron counters and by time of flight technique in the scintillator cells. The requirement of position correlation between target cell and neutron counter events gives a factor seven reduction in the accidental background rate, at the modest cost of an 8 % loss in detection efficiency. As an additional feature the scintillator possesses pulse shape discrimination capability, needed to suppress background from fast cosmic ray induced neutrons: fast neutrons can generate a recoil proton in the scintillator before being thermalized and captured in a wire chamber and simulate a good neutrino event. To suppress background from cosmic ray muons the detector is completely surrounded by a 15cm thick liquid scintillator veto system. The active shielding is successively followed by layers of passive shielding materials 5mm boron carbide, 20cm water, 2m concrete with an extra 2m concrete layer overhead (Fig. 2b). Towards the reactor core the containment building provides an additional amount of 8m concrete shield. Thus the reactor itself does not constitute a source of background.



a)



b)

Fig. 2a Layout of the Gösgen neutrino detector: five liquid scintillator planes and four ^3He -wire chambers serve to detect the products of the detection reaction $\bar{\nu}_e + p \rightarrow n + e^+$.

Fig. 2b Experimental arrangement of detector system and shielding. The detector (1) is rolled out into the service hall. Part of the veto (2) is removed. After servicing the detector, the veto is closed tightly, the rails (3) are removed and the detector together with the steelwall (4) and watertanks (5) is pushed inside the concrete shield. Finally the bunker is closed by the 2m thick concrete door (6).

MEASUREMENTS AND RESULTS

In the closest position at 37.9m, 10930 ± 220 neutrinos ($3.2 \bar{\nu}/h$) were recorded in the interval of $0.7 \text{ MeV} < E_{\nu} < 5.6 \text{ MeV}$ with a signal/background ratio of 3.5. For the 45.9m position the signal to background ratio amounted to 2.2 and 10590 ± 190 neutrinos ($2.16 \bar{\nu}/h$) were observed. During the regular annual reactor shutdowns the correlated background was measured separately. Figure 3a) shows the positron yield recorded in the second 45.9m position for the reactor on and off measurements. The figure also shows the accidental background, which is constantly monitored online within a time window delayed with respect to the correlated events. Figure 3b) compares after subtraction of accidental and correlated background the 45.9m data (solid line, left scale) to the positron spectra obtained in the 37.9m position (dashed line, right scale).

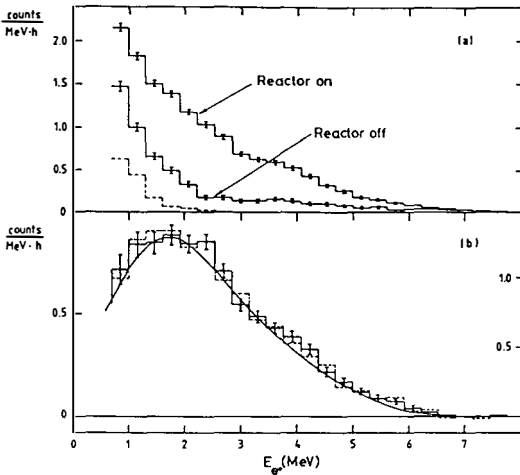


Fig. 3a Reactor-on and reactor-off spectra at 45.9m with stat. errors. Dashed curve shows accidental contribution.

Fig. 3b Experimental positron spectra (reactor-on minus reactor-off) for 45.9m (solid, left scale) and 37.9m (dashed, right scale). Left and right scales differ by the appropriate solid angle factor. The solid curve: predicted positron spectrum assuming no oscillations (normalization error 6%).

The systematic errors are highly correlated in both data sets and arise mainly from uncertainties in the reactor antineutrino spectrum (3.7 %) and the detector efficiency, which were found to be 0.1665 ± 0.0054 and 0.1652 ± 0.0054 in the 37.9m and 45.9m position respectively, with a relative uncertainty of 2 %. In dividing the 45.9m data by the 37.9m data most systematic errors drop out,

resulting in a ratio of 1.01 ± 0.03 (statistical) ± 0.02 (systematic), consistent with the absence of oscillations.

In order to compare the measured positron spectrum with the spectrum expected for a specific oscillation hypothesis, $Y(E, L, \Delta m^2, \theta)$ of eq. (4) must be folded with the energy response of the detector and averaged over the reactor core and detector volume

$$\tilde{Y}(E, L, \Delta m^2, \theta) = a_{\text{PSD}}(E) \iint Y(E') P(E', l', \Delta m^2, \theta) r(E', E) h(l', L) dE' dl' \quad (5)$$

$a_{\text{PSD}}(E)$ represents the energy dependent acceptance of the pulse shape discrimination window. The function $h(l', L)$ is the weight factor for finite core and detector size. The scintillator response function $r(E', E)$ reflects the energy resolution of the detector. It includes the effect of positron annihilation at rest and in flight, the energy deposition of positrons that finally escape and the additional contribution of positrons from neutrino interaction in the lucite walls of the scintillator cells.

One way to analyze the experiment proceeds by including the information on the reactor neutrino spectrum. Thus the best fit to the data is determined by minimizing a χ^2 -expression in which the 37.9m and 45.9m data sets are directly compared to various oscillation hypothesis given by $\tilde{Y}(E, L, \Delta m^2, \theta)$. The minimum ($\chi_{\text{min}}^2 = 28.9$ for 32 degrees of freedom) was found at $\Delta m^2 = 0.87 \text{ eV}^2$ and $\sin^2 2\theta = 0.03$. To assign a relative probability to any parameter set $(\Delta m^2, \theta)$ a likelihood ratio test was performed by comparing $\chi^2(\Delta m^2, \theta)$ to χ_{min}^2 . Figure 4 presents the 90 % confidence limit (solid line), where the region to the right of the curve is excluded. For maximum mixing we find $\Delta m^2 < 0.016 \text{ eV}^2$ and $\sin^2 2\theta < 0.16$ for large Δm^2 .

How do these limits change, when the absolute normalization is changed deliberately? Such a change could occur e.g. if the currently used neutron lifetime of $912 \pm 18 \text{ sec}$ had to be adjusted with the advent of new measurements of τ_n . Decreasing the normalization by 3 % gives the following limites: $\Delta m^2 < 0.019 \text{ eV}^2$ (full mixing) and $\sin^2 2\theta < 0.2$ (large Δm^2).

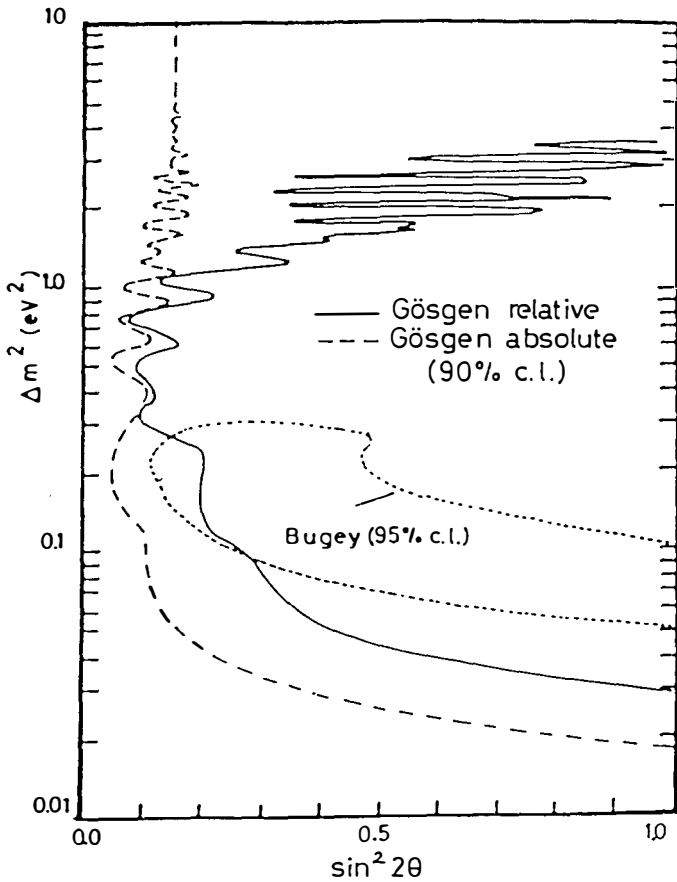


Fig. 4 Limits on the neutrino oscillation parameters Δm^2 and $\sin^2 2\theta$ (90% c.l.). The solid line is the result from the two position analysis of the 37.9m and 45.9m data alone. Limits represented by the dashed line include in addition the reactor $\bar{\nu}$ -spectrum. Parameters lying to the right of both curves are excluded. The dotted line encircles the allowed parameter region proposed by the experiment at the Bugey reactor.

An analysis independent on the precise knowledge of the reactor source spectrum, detector efficiency and cross section, although less restrictive, is obtained by comparing the two data sets to each other. Again a likelihood ratio test is performed to obtain limits for the parameters Δm^2 and $\sin^2 2\theta$. The 90 % confidence contour is displayed in Fig. 4 (dashed line). Again all oscillation hypothesis characterized by parameters lying to the right of the curve are excluded. Parameters to the left of the curve especially the no-oscillation case are supported by our data.

The dotted line in Fig. 4 shows the result of an oscillation experiment performed by the ISN-LAPP collaboration at 13.6m and 18.3m from the core of the 2.8GWth reactor in Bugey (France)⁵⁾. This experiment found an indication for neutrino oscillation described by the parameters enclosed by the contour line. Though there exists a small overlap region of the Gösigen two position contour line and the Bugey solution, where both data sets seem to be compatible, there is a serious conflict if we ask for a common neutrino source spectrum: Inferring the reference ($L=0$) neutrino spectrum from the Bugey measurement at 13.6m, the result differs at small energies ($E_\nu \approx 4$ MeV) by 20 % from all existing neutrino yield predictions, which at this particular energy only vary by 3 % among themselves (3,4,6,7). This also implies disagreement between the Bugey and the Gösigen data, since both Gösigen measurements reproduce the predicted ($L=0$) neutrino spectrum. Preliminary results in a third (64.7m) position at Gösigen underline this trend. Figure 5 demonstrates the consistency of the three Gösigen data sets, although their joint analysis in terms of oscillations has to wait for a second reactor off measurement in summer '85.

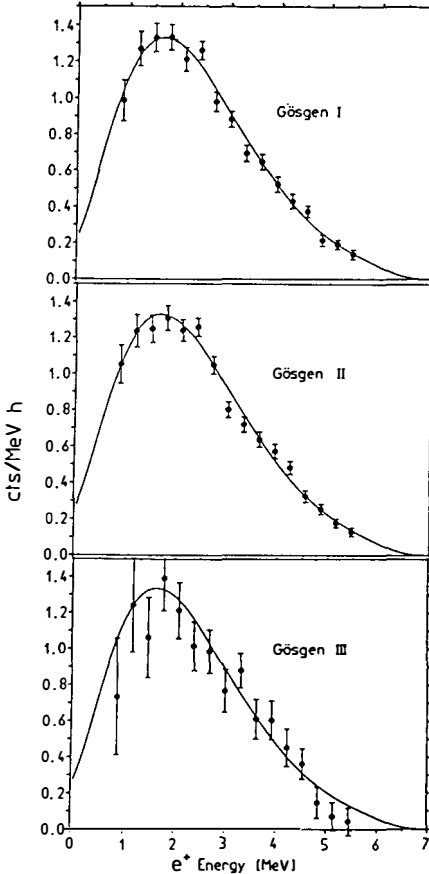


Fig. 5 Joint fit of a common ($L=0m$) neutrino source spectrum to the Gösgen measurements. The preliminary 64.7m data are included to demonstrate the consistency of the whole data set with no oscillations ($\chi^2=0.96$). All experiments were scaled to Gösgen I (37.9m).

References

- 1) S.M. Bilenki, B. Pontecorvo, Phys. Rep. 41 (1978) 225
- 2) Caltech-SIN-TUM coll.,
J.L. Vuilleumier et al., PL 114B (1982) 298
K. Gabathuler et al., PL 138B (1984) 449
- 3) F. v. Feilitzsch et al., PL 118B (1982) 162
- 4) P. Vogel et al., Phys. Rev. C24 (1981) 1543
- 5) J.F. Cavaignac et al., PL 148B (1984) 387
- 6) H.V. Klapdor et al., Phys. Rev. Lett. 48 (1982) 127
Phys. Lett. 112B (1982) 22
- 7) V.I. Kopeikin, Sov. J. Nucl. Phys. 32 (1980) 1507

Acknowledgment:

I am very grateful to Dr.K.Gabathuler and Dr.G.Zacek for valuable help and many illuminating discussions.

DECAYS AND OSCILLATIONS OF NEUTRINOS
IN THE PS 191 EXPERIMENT *

F.VANNUCCI
L.P.N.H.E.- Paris

ABSTRACT

A detector composed of a 12 m long decay volume followed by a fine-grain calorimeter, looked for heavy neutrinos' decays in the CERN-PS beam. No candidates were observed but the analysis of neutrino interactions in the calorimeter shows a possible excess of events with electrons. The interpretation by oscillations is discussed.

* Members of the Athens-CERN-Paris-Rome collaboration :

G.Bernardi, G.Carugno, F. Di Carlo, M.Dris, J.Dumarchez,
M.Ferro-Luzzi, J.M.Lévy, D.Lukas, J.M.Perreau, Y.Pons,
A.M.Touchard and F.Vannucci.

I - THE BEAM AND THE DETECTOR

We used the low-energy PS neutrino beam to search for decays of neutrinos. During 5 weeks of running time the total ν_μ flux through the detector was 2.10^{16} with a peak at ~ 600 MeV. The ν_e contamination was at the level of 0.7% with a peak at ~ 1500 MeV.

The detector was positioned 130 m from the target. It consisted of a 12 m long decay volume filled with 6 helium bags to avoid interactions. This decay part was followed by a fine grain calorimeter of the Frejus type ¹⁾ covering 6m x 3m. The structure was as follows : 3mm thick iron plates (17% rad length) sandwiched with flash-tube chambers of cell dimensions 5mm x 5mm. We had a total of 20 tons of iron and 30 000 read-out channels. Fig.1 shows a photograph of the set-up. 100 000 triggers were written on tape and all of them were scanned.

II - SEARCH FOR DECAYS OF HEAVY NEUTRINOS

The primary aim of the experiment was to look for neutrino decays ²⁾. If massive neutrinos exist they may decay, in particular if the mass is larger than 1 MeV we may have :

$$\nu_H \rightarrow e^+ e^- \nu_e$$

The lifetime of this process is :

$$\tau = 2,8 \cdot 10^4 / m^5 \nu |U_{He}|^2 \quad (\text{s})$$

where m_ν is the ν_H mass, E_ν its energy and U_{He} is the Kobayashi-Maskawa mixing matrix element between ν_H and e . In a ν_μ beam there is a ν_H component at the level of $|U_{H\mu}|^2$. The ν_e part of the beam also gives a ν_H component at the level of $|U_{He}|^3$, not negligible since $\pi, K \rightarrow \nu_H e$ is no more suppressed, with respect to $\pi, K \rightarrow \nu_\mu e$ in the m_ν range investigated here ³⁾. Being able to calculate the flux of hypothetical massive neutrinos and their decay probability, it is easy to extract a limit on mixing elements.

In the present experiment no candidates were found fulfilling the criteria of a possible $e^+ e^-$ pair arising in the helium volume, although $e^+ e^-$ pairs from the shield in front of the detector are clearly signed. This allows us to put limits which are shown on Fig.2. Two limits are extracted as a function of m_ν : $|U_{He}|^2$ or $|U_{H\mu}| \times |U_{He}|$. In both cases the experiment gives a better than 2 orders of magnitude improvement over previous results ⁴⁾ in a large range of m_ν .

III - NEUTRINO INTERACTIONS IN THE CALORIMETER

There are two classes of neutrino interactions analysed in the set-up :

1) Interactions in the Shield

The shield in front of the detector gives rise to interactions of which products can be seen through the decay volume. Most of them appear as one or several straight tracks signed as minimum ionizing in the calorimeter. But there are also 24 tracks, coming from the shield, and giving an electromagnetic shower with an energy greater than 400 MeV in the calorimeter.

These are electrons. Fig.3 shows an example. We expect only 3.2 such electrons coming from the interactions of the ν_e in the beam. But the background is large mainly from decays of μ produced by the predominant ν_μ beam. After background subtraction and contribution of the ν_e flux, one is left with a possible excess of 9.4 ± 5.1 such electrons.

2) Interactions in the calorimeter

If there is an excess of ν_e in the beam, this excess should also appear in the interactions inside the calorimeter. This calorimeter is an excellent detector for ν interactions at low energies. Fig 4 gives an example of a 3 branch event. The study of events with 2,3 or more branches gives a good confirmation of the ν_μ flux calculation. The calorimeter also allows to study events with 1 or more electromagnetic showers. During the scan we found 22 events with 2 showers accompanied by 1 or 2 minimum ionizing tracks. Fig.5 gives such an example. We also found 70 events with only 1 shower. An example is shown on Fig.6. Electromagnetic showers can come from γ or e . The calorimeter has a granularity good enough to disentangle these two sources by allowing the measurement of the distance between the vertex of the interaction and the beginning of the shower in the case of few prong events. Fig 7 proves this point for events with more than 400 MeV of electromagnetic origin. Fig 7a shows this distance in number of flash chamber planes for events with 2 showers interpreted as γ coming from π^0 . The distribution is in agreement with a Monte Carlo simulation. Fig 7b shows the same distribution for events having only one shower. Also here a comparison with Monte Carlo is done to evaluate the π^0 contribution. A clear peak of 27 showers attached to the vertex is seen : these are presumably electrons in ep or $e\pi$ events. Only 5.9 events can be understood as arising from the ν_e flux in the beam. From the Monte Carlo study 3 events are attributed to π^0 . The background from π^+ giving a charge exchange is negligible as shown by the result of a calibration in a pion test beam. Thus this analysis gives an excess of 18.1 ± 5.6 events which look like an electron accompanied by 1 or 2 minimum ionizing tracks, and which cannot be understood as either background or products of the known ν_e flux.

IV - OSCILLATIONS OF NEUTRINOS ?

It is tempting to interpret this signal as an excess of ν_e in the incoming beam. This excess could be attributed to the oscillation $\nu_\mu \rightarrow \nu_e$ detected in the appearance mode. Actually the energy distribution of the electrons in the "ep" events seems in good agreement with what is expected from the interactions of neutrinos having the energy spectrum of the ν_μ beam, not of the ν_e beam. If indeed the events come from ν_e interactions, one can measure the ν_e flux by directly comparing the number of detected events with the events having the same topology but coming from ν_μ interactions : μp , $\mu p \pi$... We find $\nu_e/\nu_\mu = (2.9 \pm 0.9)\%$ while calculations⁵⁾ give an expectation of 0.7%.

Continuing the interpretation by oscillations, we can extract the usual parameters characteristic of the phenomenon. We find (for the first solution)

$$\sin^2 2\theta \sim 2-3\% \quad \delta m^2 \sim 5 \text{ eV}^2$$

This solution is not in contradiction with previous limits on oscillations, and is at the edge of compatibility with a recently published BNL result⁶⁾. It remains to be seen if the excess is confirmed with increased statistics hoped for in a continuing run.

REFERENCES

- 1) Aachen-Orsay-Palaiseau-Saclay Wuppertal collaboration.
Talk at this conference.
- 2) M.Gronau, Preprint SLAC-PUB 2967 (1982)
F.Vannucci, Preprint LPNHE 83-01.
- 3) R.E.Schrock- Phys Rev D 24 (1981) 1232
- 4) A.M.Sarkar-Cooper Preprint CERN-EP 84-136
- 5) S.M.Bilenky and B.Pontecorvo- Phys-Report 41 (1978) 226.
- 6) L.A.Ahrens et al. BNL Preprint E-734-84-2.

FIGURE CAPTIONS

- Fig.1 View of the PS191 experiment
- Fig.2 Limits on mixings of heavy neutrinos in searches for decays
- Fig.3 An electron reconstructed over the 12m of decay volume with an electromagnetic shower in the end calorimeter.
- Fig.4 Example of a 3 branch ν_{μ} interaction in the calorimeter
- Fig.5 Example of an event with 2 disconnected showers
- Fig.6 Example of an event with 1 shower attached to the interaction vertex.
- Fig.7 Distribution of distances between the vertex of the interaction and the beginning of the shower in the case of 2γ (7a) or 1γ (7b) events. The Monte Carlo simulation for π^0 is shown by the dashed line.



Fig. 1

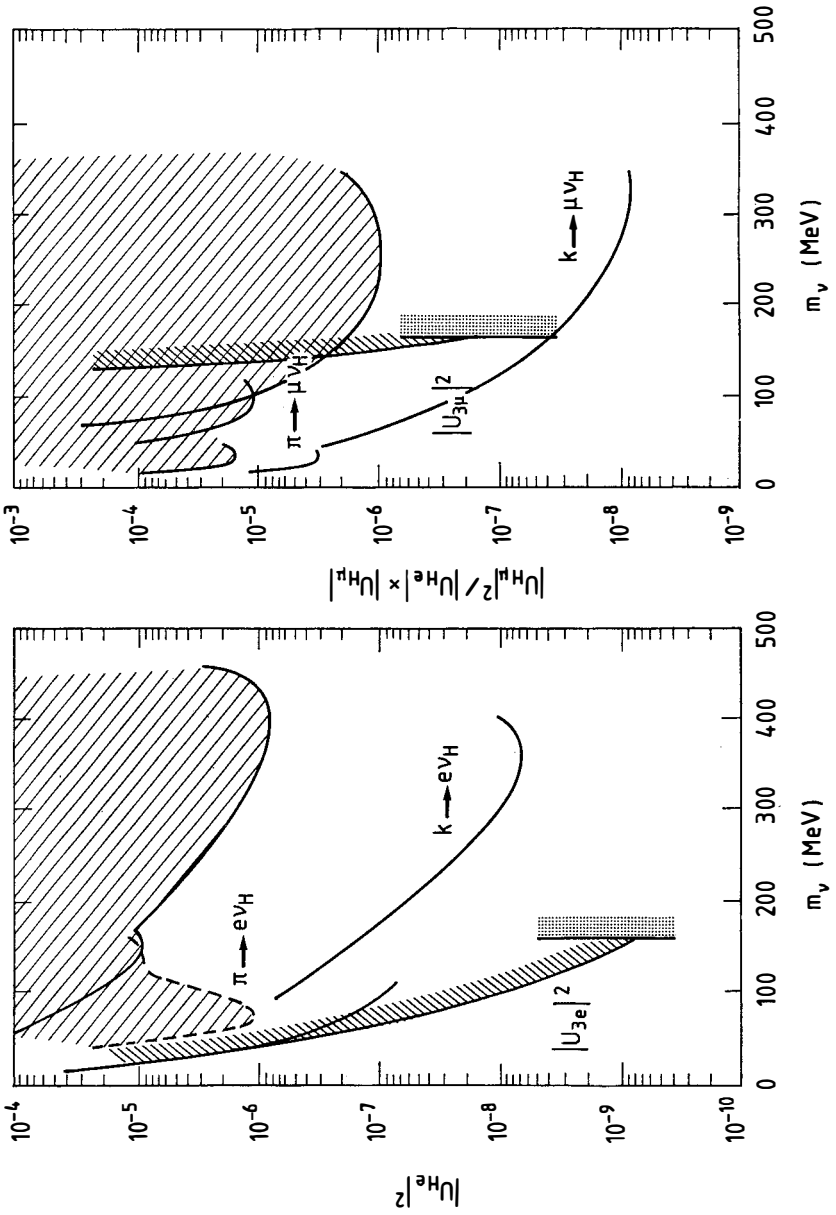


Fig. 2

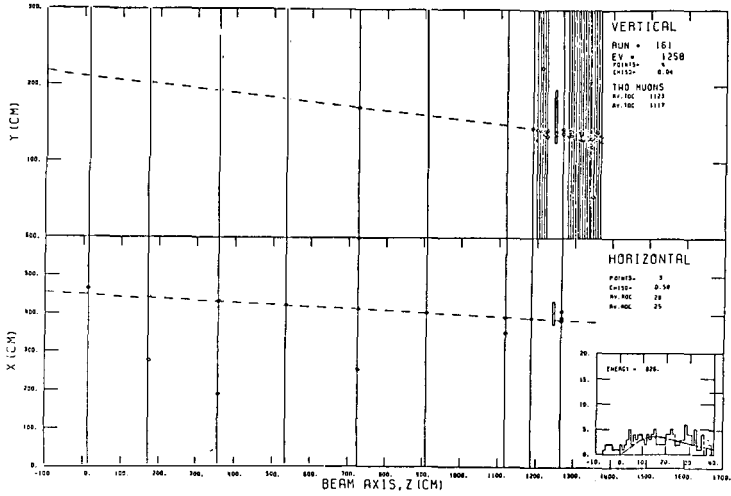


Fig. 3

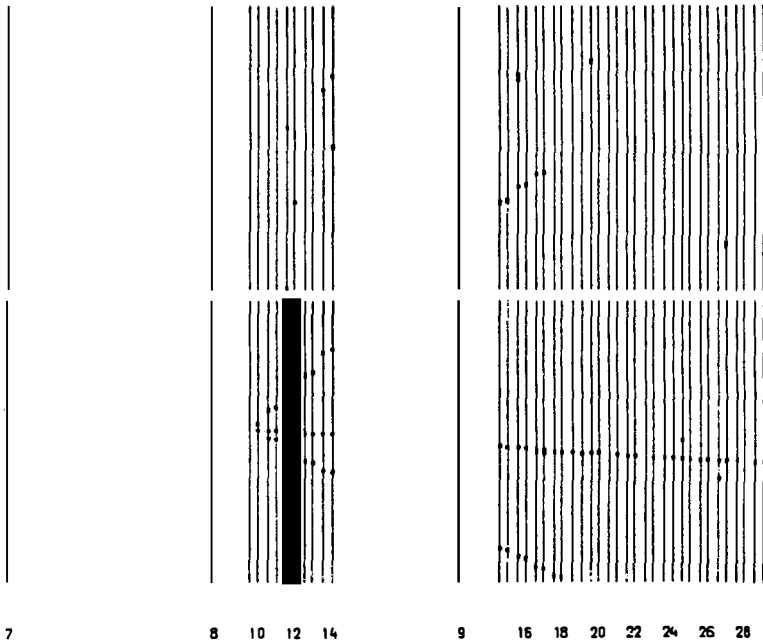


Fig. 4

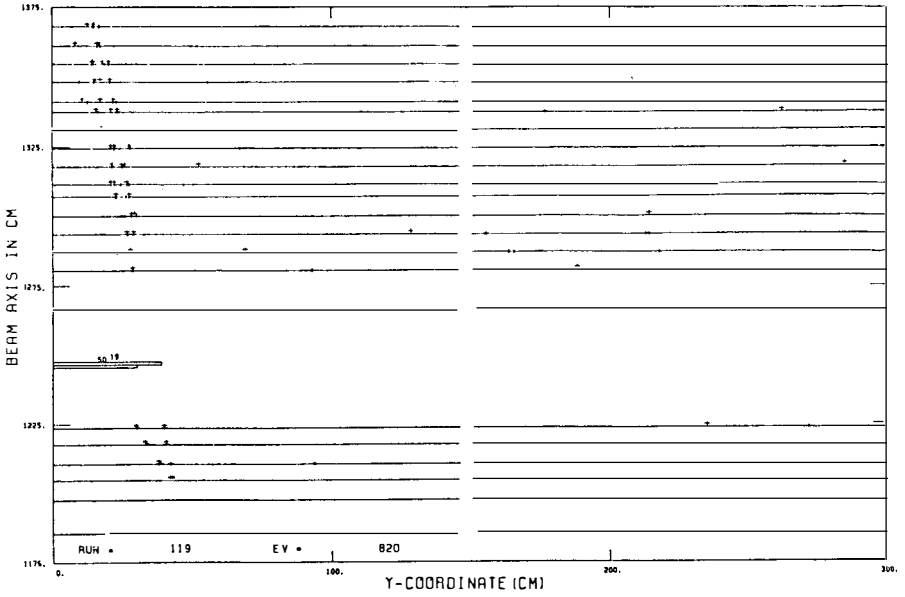


Fig. 5

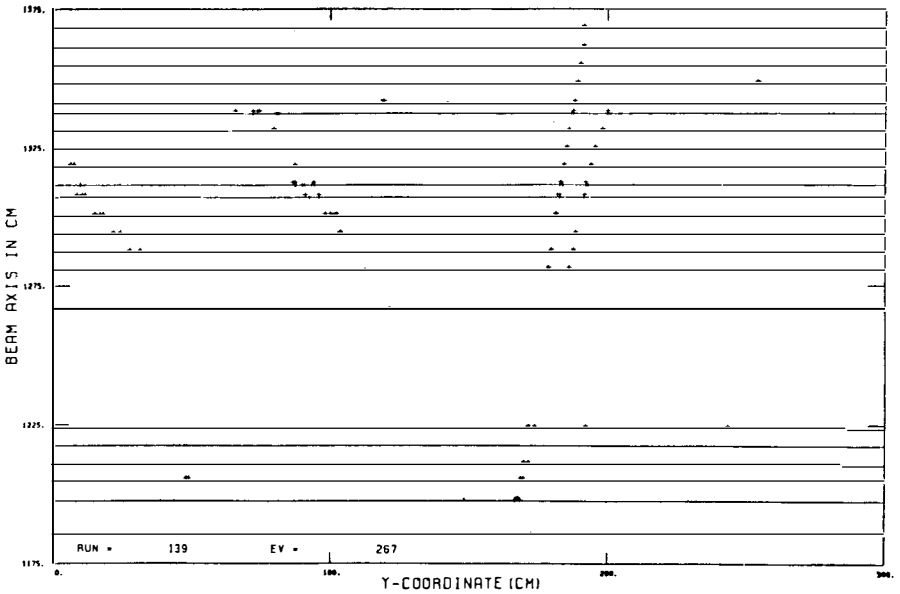


Fig. 6

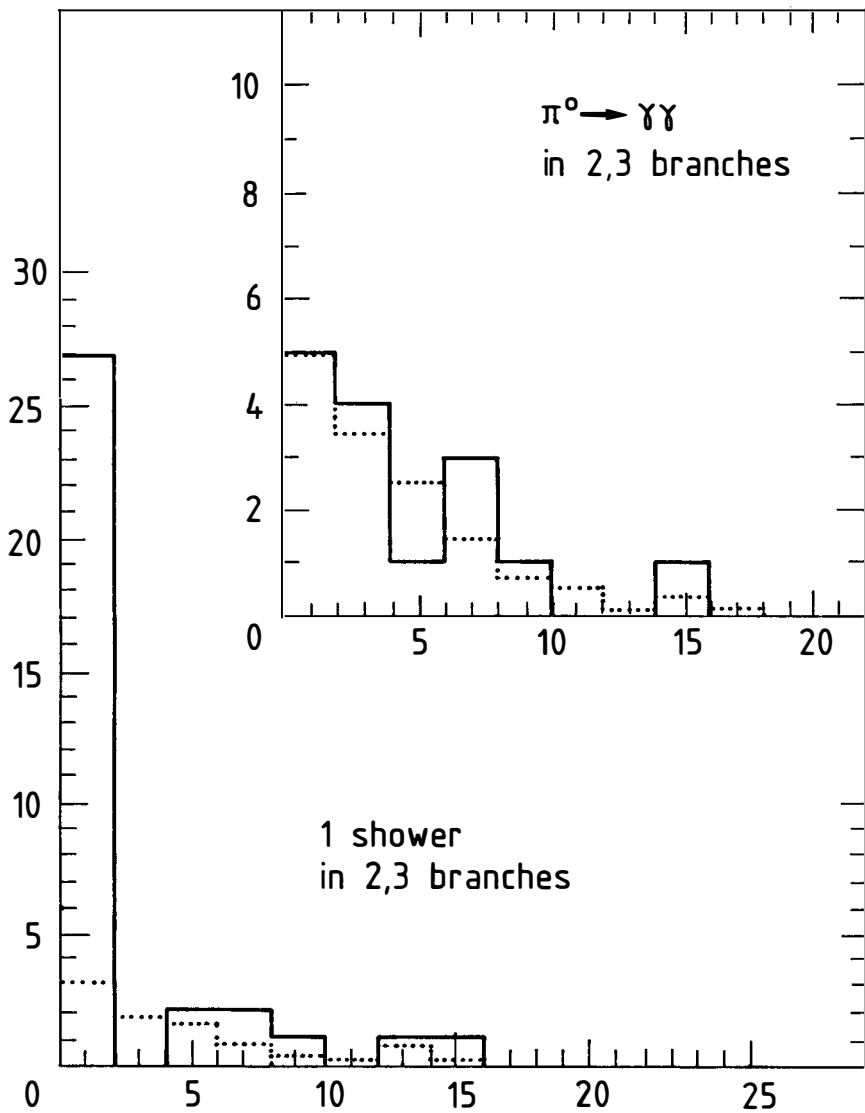


Fig. 7

**A Brief Report on a New Limit on the
Strength of Mixing Between $\nu_\mu \rightarrow \nu_e$**

JAPAN-U. S. A. NEUTRINO COLLABORATION*

L. A. Ahrens, S. H. Aronson,
P. L. Connolly, B. G. Gibbard, M. J. Murtagh,
S. Murtagh, S. Terada, D. H. White (B.N.L.); J. L. Callas,
D. Cutts, J. S. Hoftun, R. E. Lanou, T. Shinkawa (Brown Univ.);
K. Amako, S. Kabe (K.E.K.); Y. Nagashima, Y. Suzuki, S. Tatsumi
(Osaka Univ.); K. Abe, E. W. Beier, D. C. Doughty, L. S. Durkin,
S. M. Heagy, M. Hurley, A. K. Mann, F. M. Newcomer,
H. H. Williams, T. York (Univ. of Pennsylvania);
D. Hedin, M. D. Marx, E. Stern (Stony Brook)

**Presented by R. E. Lanou
Department of Physics
Brown University
Providence, Rhode Island
02912**

Abstract

Measurements have been made of the reactions $\nu_e n \rightarrow e^- p$ and $\nu_\mu n \rightarrow \mu^- p$ in a detector located 96 meters from the A.G.S. neutrino source. A direct measurement is made of the energy dependent flux ratio for the two neutrino species. After comparison to calculated energy dependence of this same ratio, an improved new limit of $\sin^2 2\alpha < 3.4 \times 10^{-3}$ (90% CL) at large Δm^2 is obtained. Possible systematic errors are estimated to be less than 20%.

The USA-JAPAN neutrino detector constructed for studies of neutral current reactions ($\bar{\nu}_\mu e^- \rightarrow \bar{\nu}_\mu e^-$ and $\bar{\nu}_\mu p \rightarrow \bar{\nu}_\mu p$) and normalization reactions ($\nu_\mu n \rightarrow \mu^- p$, $\bar{\nu}_\mu p \rightarrow \mu^+ n$) at the B.N.L.-A.G.S. has been used to search for neutrino oscillations. The detector^{1]} is a fully active one (liquid scintillator) with good angular and energy resolution --

$$\Delta\theta_{x,y}^e = \frac{16 \text{ mrad}}{\sqrt{E(\text{GeV})}} \text{ and } \frac{\Delta E_e}{E_e} = \frac{13\%}{\sqrt{E(\text{GeV})}}, \text{ respectively.}$$

The detector was placed at a mean distance of 96 meters from the effective neutrino source. The beam was a wide band, horn focussed one of most probable energy about 1GeV (see Fig. 2).

The configuration of detector elements is such that we can detect both quasi-elastic reactions:

$$\nu_e + n \rightarrow e^- + p \quad (1)$$

$$\nu_\mu + n \rightarrow \mu^- + p \quad (2)$$

These reactions are used to establish the ν_e and ν_μ relative composition of the beam at the detector position.

In a two component model the probability for ν_μ of energy E_ν (Mev) to have oscillated to ν_e at a distance L (meters) is

$$P(\nu_\mu \rightarrow \nu_e) = \sin^2 2\alpha \sin^2 \left(1.27 \frac{L}{E_\nu} \Delta m^2 \right) \quad (3)$$

where $\Delta m^2 = |m_1^2 - m_2^2|$ and $\sin^2 2\alpha$ is the mixing strength between the states of mass, m_1 and m_2 .

Note that in the limit of large Δm^2 ,

$$P(\nu_\mu \rightarrow \nu_e) \longrightarrow \frac{1}{2} \sin^2 2\alpha \quad (4)$$

and is independent of L/E_ν .

If we define $\Phi_L^e(E_\nu)$ and $\Phi_L^\mu(E_\nu)$, respectively, as the flux of ν_e and ν_μ at L, then as a function of E_ν , $\int \Phi_L^e(E_\nu) dE_\nu / \int \Phi_L^\mu(E_\nu) dE_\nu \neq 0$ even with no oscillations due to some ν_e contamination in the ν_μ beam (typically 0.5% at A.G.S. energies) due to $\pi - \mu - e$ and kaon decays. However, an important feature at these energies is that this neutrino flux ratio is particularly characteristic but not very sensitive to either the π/K production ratio or to the absolute flux.

The principle of the experiment then is to directly measure the energy dependence of $\phi_L^e(E_\nu)/\phi_L^\mu(E_\nu)$ and to test it against the neutrino oscillation hypothesis.

The procedure of the experiment is briefly as follows:

- a) First, we isolate reactions (1) (418 events) and (2) (1370 events) in the region $0.9 < E_e < 5\text{GeV}$.
- b) On an event by event basis the energy, E_ν , is solved for using θ_e and E_e for reaction (1) and θ_p and E_p for reaction (2).
- c) The acceptances (a^{eP} and $a^{\mu P}$) for reactions (1) and (2), respectively, are calculated by Monte Carlo. For a^{eP} the momentum transfer range is $0 < Q^2 < 0.4 \text{ (GeV/c)}^2$ and for $a^{\mu P}$, $0.4 < Q^2 < 1.1 \text{ (GeV/c)}^2$. The standard (V-A) form for the quasi-elastic cross section is assumed and the experimentally^{2]} determined value of the axial-vector mass is used. A contribution of 14% systematic error to $[\sigma^e(\text{Q.E.}) \times a^{eP}]/[\sigma^\mu(\text{Q.E.}) \times a^{\mu P}]$ is established from variation of these parameters.
- d) Corrections for backgrounds of 28% and 18% to reactions (1) and (2), respectively, are made. Figure 1 illustrates the nature of the bin-by-bin subtraction made for the $\nu_e + n \rightarrow e^- + p$ channel.
- e) An indirect check upon the Q^2 dependences of a^{eP} and $a^{\mu P}$ is made and, as can be seen in Figure 3, is a good representation of the data.
- f) Utilizing the data resulting from the steps (a) through (e), the experimental flux ratio, $[\phi_L^e(E_\nu)/\phi_L^\mu(E_\nu)]_{\text{OBS.}} \equiv R_{\text{OBS.}}$ is determined in seven energy bins. These are shown as the points in Figure 4a.
- g) A detailed Monte Carlo beam program^{3]} is then used to calculate the flux ratio, $R_{\text{CALC.}} = [\phi_L^e(E_\nu)/\phi_L^\mu(E_\nu)]_{\text{CALC.}}$, to be expected in the absence of neutrino oscillations. The result of this calculation is illustrated as the solid curve in Figure 4a. The comparison of calculation and measured spectrum for the separate channels (1) and (2) is shown in Figure 2. The agreement in the relevant energy ranges is seen to be quite satisfactory.

This satisfactory agreement can be used to set a limit on the oscillation mixing strength by forming the difference, $[R_{\text{CALC.}} - R_{\text{OBS.}}]$. The result of this subtraction is shown in Figure 4b. We conclude that there is no evidence for $\nu_\mu \rightarrow \nu_e$ oscillations in this kinematic range. The excluded area is shown in Figure 5. These mixing limits extend the excluded region beyond that of the previous^{4]} best search for $\nu_\mu \rightarrow \nu_e$ oscillations.

In the limits of large and small mass differences we can give results for the complementary variable both with and without flux subtraction. These are at **90% C.L.**,

- **No flux subtraction** and data in the range 0.9 - 1.5 Gev:

$$\sin^2 2\alpha \leq 1.0 \times 10^{-2} \text{ at large } \Delta m^2$$

$$\Delta m^2 \sin 2\alpha \leq 0.67 \text{eV}^2 \text{ at small } \Delta m^2$$

- **Flux subtracted** and data in the range 0.9 - 2.1GeV:

$$\sin^2 2\alpha \leq 3.4 \times 10^{-3} \text{ at large } \Delta m^2$$

$$\Delta m^2 \sin 2\alpha \leq 0.43 \text{eV}^2 \text{ at small } \Delta m^2$$

Two additional comments should be made. First, the total systematic error is estimated to be about 20% with equal contributions from uncertainties in the acceptance and flux calculations. A more detailed discussion of these effects is in reference 5. Secondly, it should be noted that since R is independent of L/E_ν , at large Δm^2 , any oscillation effect can be no greater at high E points (Figure 4b) than it is at 1GeV; consequently, these higher energy points serve as a direct test (within errors) of the flux calculation particularly as it relates to the π/K production ratio.

* This work was supported in part by the U.S. Department of Energy, the Japanese Ministry of Education, Science, and Culture through the Japan-U.S.A. Cooperative Research Project on High Energy Physics, The U.S. Natural Science Foundation, and the Stony Brook Incentive Fund.

References

1. L. A. Ahrens et al, Phys. Rev. Lett. 51, 1514 (1983); Phys. Rev. Lett. 54, 18 (1985).
2. N. J. Baker et al, Phys. Rev. D23, 2499 (1981).
3. D. H. White, Internal Report Brookhaven National Laboratory Report O.G.793; to be published.
4. N. J. Baker et al, Phys. Rev. Lett. 47, 1576 (1981).
5. L.A. Ahrens et al, Preprint E-734-84-2 and Phys. Rev. D31, 2732 (1985).

E - 734
BNL (USA - JAPAN)

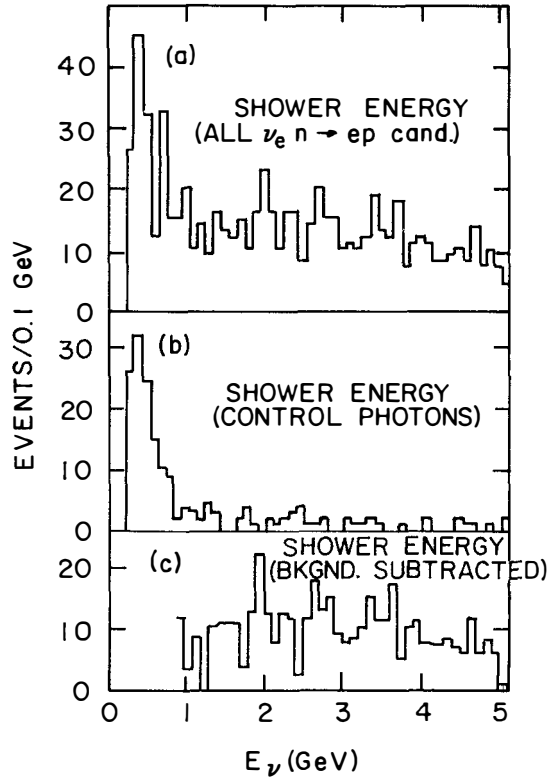


FIG. 1

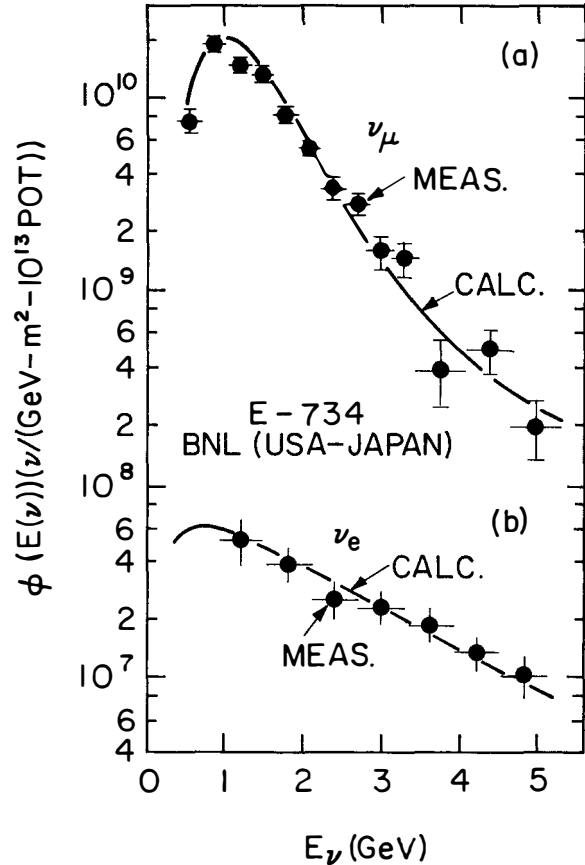


FIG. 2

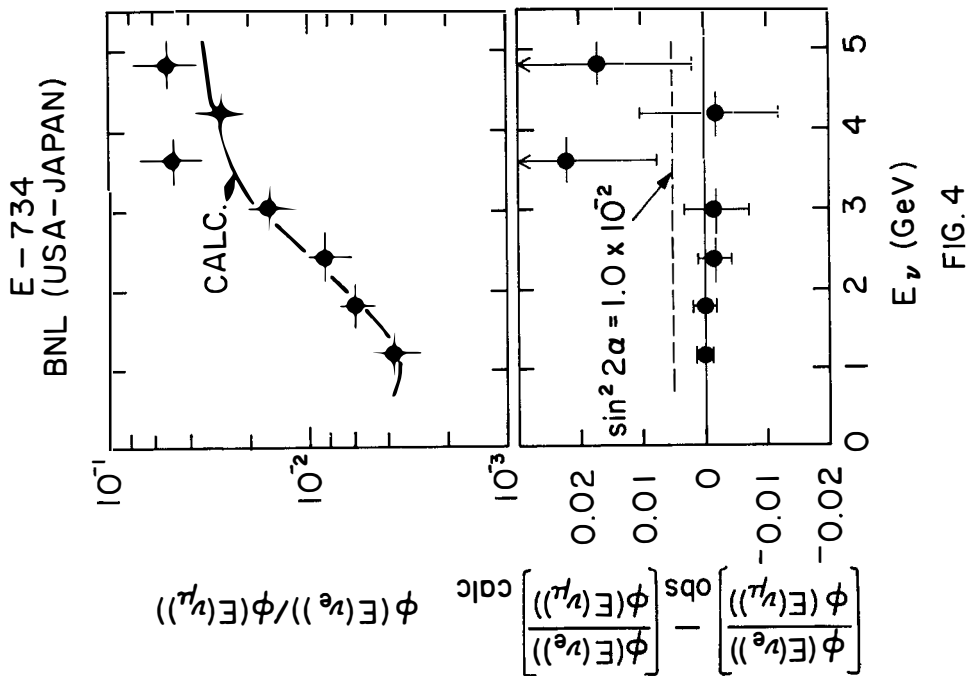


FIG. 4

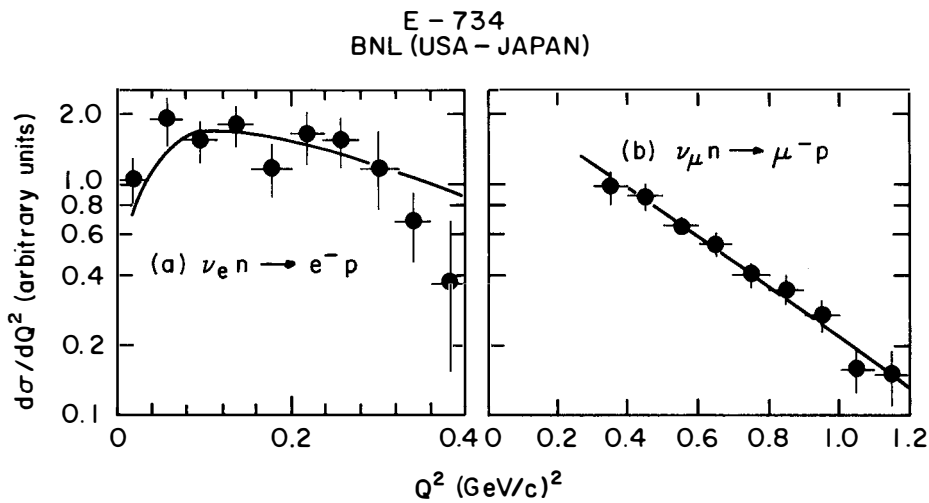


FIG. 3

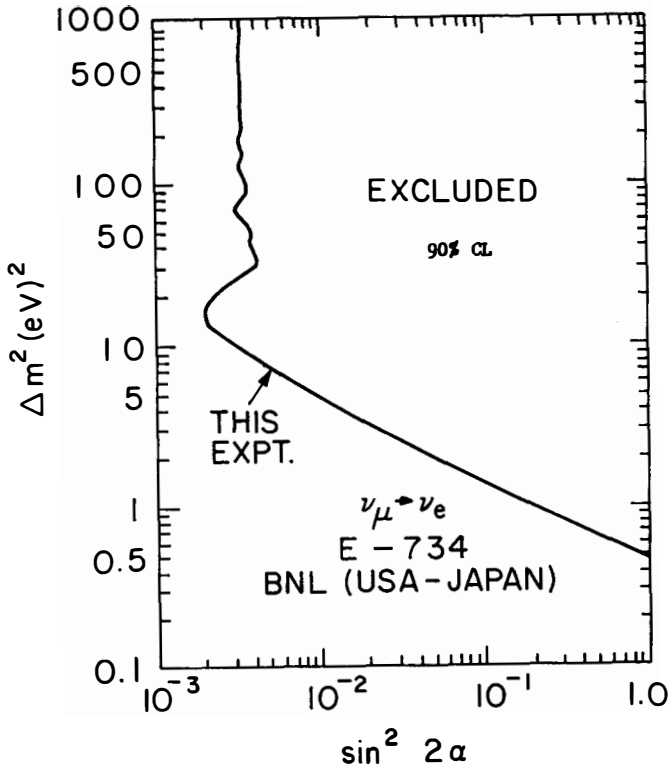


FIG.5

SEARCH FOR DECAYS OF HEAVY NEUTRINOS
IN THE MASS RANGE 500–2800 MeV

CHARM Collaboration¹⁾

presented by A. Capone²⁾

CERN Geneva, Switzerland



Abstract

A search for decays of heavy neutrinos was conducted by the CHARM Collaboration in the neutrino beam produced by dumping 400 GeV protons and in the wide band neutrino beam produced by 400 GeV primary protons. No candidate event was found. In the beam dump experiment heavy neutrinos have been assumed to be produced in the decays of the charmed mesons D. Neutrinos with mass in the range 500–1800 MeV decaying into a pair of electrons and a light neutrino were looked for. A limit at 90% c. l. equal to $\approx 10^{-7}$ was obtained for the square of the neutrino mixing angle for neutrino masses above 1000 MeV. In the wide band experiment heavy neutrinos were supposed to be produced by neutrino interactions in the CHARM calorimeter. Neutrinos decaying into a μ and hadrons were searched for. This experiment is sensitive to neutrinos with mass in the range 500–2800 MeV yields an upper limit of the square of the neutrino mixing angle of 3×10^{-3} for masses above 2000 MeV.

¹⁾ Members of the CHARM collaboration are: F.Bergsma, J.Dorenbosch (NIKHEF Amsterdam); J.V.Allaby, U.Amaldi, G.Barbiellini, C.Berger, A.Capone, W.Flegel, L.Lanceri, M.Metcalf, C.Nieuwenhuis, J.Panman, C.Santoni, K. Winter (CERN); I.Abt, J.Aspiazu, F.W.Büsser, H.Daumann, P.D.Gall, T.Hebbeker, F.Niebergall, P.Schütt, P.Stähelin (Hamburg); P.Gorbunov, E.Grigoriev, V. Kaftanov, V.Khovansky and A.Rosanov (Moscow); A.Baroncelli, L.Barone, B.Borgia, C.Bosio, M.Diemoz, U.Dore, F.Ferroni, E.Longo, L.Luminari, P.Monacelli, F.de Notaristefani, P.Pistilli, R.Santacesaria, L.Tortora, V.Valente (Rome).

²⁾ On leave of absence from Dipartimento di Fisica, Università "La Sapienza", Roma and INFN Sezione di Roma, Rome, Italy.

CHARM collaboration has already reported previously on search for decays of neutrinos in the mass range 10–400 MeV [1].

Extending the concept of flavour mixing from the quark sector of weak interactions to the lepton sector, one can, in analogy with the Kobayashi – Maskawa mixing matrix, introduce a unitary neutrino mixing matrix U_{li} and express the weak (flavour) eigenstates are linear combinations of the mass eigenstates [2,3]:

$$\nu_l = \sum U_{li} \nu_i \quad (l = e, \mu, \tau, \dots, i = 1, 2, 3, \dots) \quad (1)$$

Then a charged – current coupling of the massive neutrino ν_i to the charged lepton l is proportional to the square of the mixing angle U_{li} defined in (1) . There are models [3] in which the neutral – current interactions of the heavy neutrinos are also flavour changing. The coupling is proportional to $|U_{li}|^2$.

Two different samples of data have been analysed searching for a heavy neutrino decay signature: events collected during a proton (400 Gev) beam dump on copper and data collected during the neutrino wide band (WBB) produced by 400 Gev primary protons at the CERN SPS.

In the beam dump experiment heavy neutrinos have been supposed to be produced in the decays of the charmed mesons D. Neutrino decays into a pair of electrons [2,3] (Fig. 1a):

$$\nu_i \rightarrow e^+ e^- \nu_e, \quad (2)$$

were searched for in an empty decay region of 35 m length and $3 \times 3 \text{ m}^2$ cross section area [1] (the layout is shown in Fig.2) , parallel to the CDHS [4] and to the CHARM [5] neutrino detectors and covering a solid angle of 3.9×10^{-5} sr. The decay region, defined by two scintillator planes, SC1 and SC2, is parallel to the neutrino beam line at a mean distance of 5 m, corresponding to an angle with respect to the incident proton beam of 10 mrad. One module of the CHARM fine – grain calorimeter [5] was displaced to the end of the decay region. The decay volume is subdivided into three regions

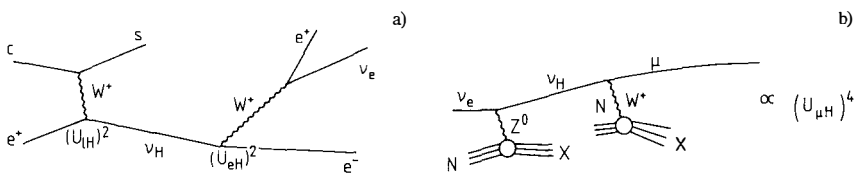


Fig. 1

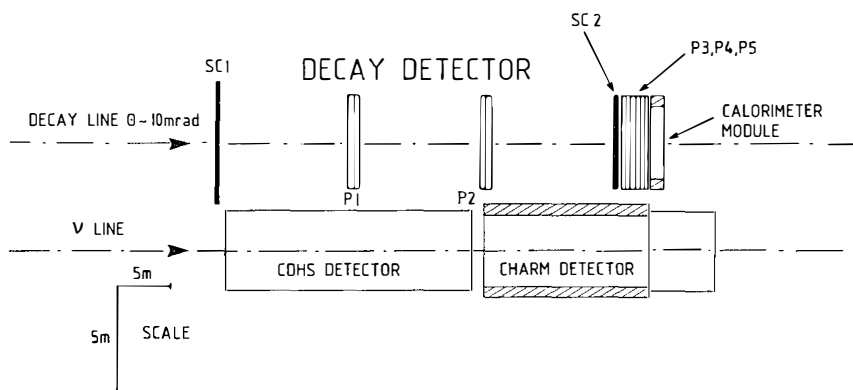


Fig. 2

using two sets of proportional tubes (P1 and P2) [6] (see Fig. 2). In order to improve the angular resolution of the shower and to better reconstruct the decay point, three sets of proportional tubes (P3, P4, and P5) were put in front of the CHARM calorimeter module.

The signature of the events induced by reaction (2) would be one or two electromagnetic showers with their origin in the decay region and a small angle with respect to the neutrino direction. The dominant background come from inelastic scattering of ν_e and ν_μ neutrinos and antineutrinos producing hadron shower.

Compared to the heavy neutrino decay events background events have a broader angular distribution. The regularity of the development of electromagnetic showers has been also used to distinguish between these events.

The detector was exposed to a neutrino flux produced by 2.4×10^{18} protons on a copper target [7]; 21,000 events were collected satisfying the trigger requirements: no hits in the scintillator plane SC1 and a hit in at least 4 scintillator planes of the calorimeter module.

Two estimators for the event separation have been evaluated [8] using a Monte Carlo simulation: 1) the deviation of the reconstructed shower axis from the incoming beam direction and 2) the fraction of the energy seen in tubes situated outside a narrow cone around the shower axis. No event compatible with the features of reaction (2) was found.

The expected number of decays of heavy neutrinos with mass m in the decay region was computed according to the expression:

$$N = N_D P[D \rightarrow \nu_1(m)] A(m) P[\nu_1(m) \rightarrow e^+ e^- \nu_e] \epsilon(m) \quad (5)$$

N_D , the number of D mesons produced by protons in the dump, was computed from the number of prompt single-muon events observed in the CHARM calorimeter (1380 ± 250) [1], during the exposure. Both neutral and charged D's semileptonic decays can produce heavy neutrinos, in our computation a ratio $\sigma(D^\pm) = \sigma(D^0)/2$ was assumed. $P[D \rightarrow \nu_1(m)]$, proportional to $|U_{1l}|^2$, is the probability of the D meson to decay into a neutrino of mass m and a lepton l ($l = e, \mu$). The acceptance factor $A(m)$ gives the fraction of heavy neutrinos that cross the decay region. In the acceptance calculation the production of D mesons was simulated by a Monte Carlo program, assuming a distribution for the Feynman variable x corresponding to $(1-x)^5$ and a transverse momentum distribution proportional to $\exp(-2 p_\perp)$ [p_\perp in GeV]. This parametrization described satisfactorily the energy spectrum of prompt $\nu_\mu, \bar{\nu}_\mu$ observed in the calorimeter. $P[\nu_1(m) \rightarrow e^+ e^- \nu_e]$, proportional to $|U_{e1}|^2$, is the probability for the heavy neutrino to decay in the fiducial decay region according to reaction (2). The factor $\epsilon(m)$ describes the efficiency of the combined estimators 1) and 2) to select $\nu_1 \rightarrow e^+ e^- \nu_e$ events.

The 90% confidence limit on the square of the mixing angle in the neutrino mass range 500–1800 MeV is shown in Fig. 3 as a function of the neutrino mass. Very similar limits were obtained for the product of the mixing angles $|U_{\mu 1} U_{e 1}|$. For large mixing angles the sensitivity of this experiment is limited to small masses (i.e for $|U_{1l}|^2 > 10^{-1}$ the experiment is sensitive to $m < 1000$

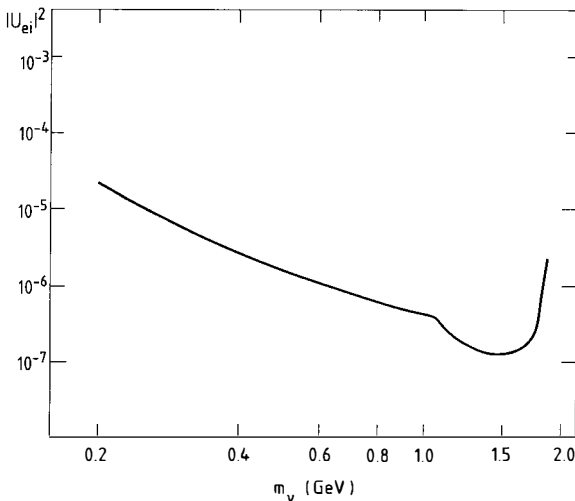


Fig. 3

MeV and for $|U_{1j}|^2 > 10^{-4}$ to $m < 1500$ MeV) because a beam of heavy neutrinos is attenuated by decay before reaching the detector which is located at a distance of 480 m from the target.

In the WBB experiment heavy neutrinos were supposed to be produced by muon neutrinos in the CHARM calorimeter [5] via a neutral - current interaction:

$$\nu_{\mu} N \rightarrow \nu_1 X. \quad (3)$$

with subsequent decays into a muon and hadrons [2,3] (Fig. 1b):

$$\nu_1 \rightarrow \mu X. \quad (4)$$

were searched for in the calorimeter itself.

We searched for decays of heavy neutrinos in a sample of 1.04×10^5 neutrino and 2.64×10^5 antineutrino interactions induced in the fine-grain CHARM calorimeter [5] by CERN wide-beam interactions. The topology of events induced by the production of heavy neutrinos according to reaction (3) and their subsequent decay in the calorimeter [reaction (4)] would show up as two showers separated by a gap in the longitudinal direction, and with a muon pointing to the vertex of the second one. In this experiment the average length of the decay region is 6 m from the production point: the sensitivity then is limited to large masses (> 500 MeV) and large mixing angles ($> 10^{-3}$). To select events we required:

1) the interaction point in a fiducial region of 240×240 cm² cross section in the transverse direction, the vertex of the first shower between plane 5 and 55 and the event had to be fully contained in the target calorimeter.

2) the visible energy was required to be larger than 0.5 GeV.

3) the event pattern in the proportional drift tubes system [9] compatible with the one in the scintillators in order to reject events due to random superpositions of two different events occurring in the gate time of the trigger.

The following topologies were searched for out of this sample of events:

1) events without μ -track candidate emerging either from the primary shower or from the secondary one;

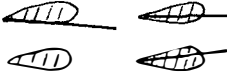
2) events with a μ -track emerging from both showers;

3) events with a μ -track emerging either from a) the primary vertex or b) the secondary vertex. The

results of this search are reported in Table 1.

Table 1

Classification of the candidate events in the WBB experiment according to the topology.

Class	Topology	Number of events	Background
1 3a		38	3.6 ± 0.7
2 3b		3	3.3 ± 0.6

Categories 1) and 3)a contain 38 events of which 3.6 ± 0.7 are estimated to be background events. The number of events left is fully compatible with the expected number of secondary showers produced by K_{0L} and neutrons induced by the first shower [10]. The number of events found in categories 2) and 3)b is 3 while the expected number of background events is 3.3 ± 0.6 . In particular one event containing a muon emerging only from the secondary shower was found. The estimated number of background events is 1.9 ± 0.4 .

The expected number of decays of heavy neutrinos with mass m in the fiducial volume of the calorimeter was computed according to the expression:

$$N = N_{\nu_1(m)} P[\nu_1(m) \rightarrow \mu X] \epsilon(m) \quad (6)$$

$N_{\nu_1(m)}$ is the number of heavy neutrinos produced in the neutral-current neutrino interaction. It was obtained from the number of neutral current events collected in the calorimeter during the exposure times the square of the mixing angle $|U_{\mu 1}|^2$ and taking into account the threshold effect due to the heavy neutrino mass. $P[\nu_1(m) \rightarrow \mu X]$ is the probability for the heavy neutrino to decay in the fiducial volume. It is proportional to $|U_{\mu 1}|^2$.

The efficiency to select heavy neutrino decay events $\epsilon(m)$ was computed in a way very similar to the one used in a previous search of fractionally charged particles [9]. Two real single-shower events with hadron energy larger than 2 GeV were selected at random from a sample of neutrino and anti-neutrino induced WBB events. These events were superimposed by placing the second one at a pre-determined position with respect to the first one; these pseudo events were then processed by the analysis program to identify events with two showers. The efficiency of this automatic selection was computed for different combinations of hadronic energies and different relative distances between the

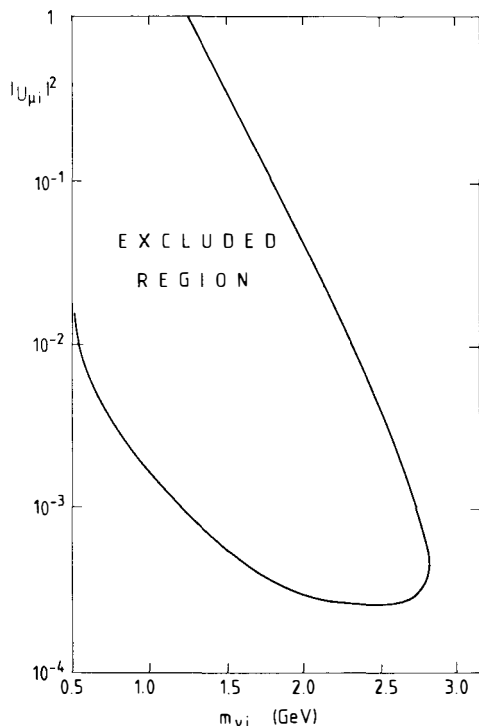


Fig. 4

two showers. The heavy neutrino production in (anti)neutrino neutral-current interaction was described by a Monte Carlo simulation assuming that the hadron energy distribution is equal to the one measured in neutral-current events [11]. Having observed 1 heavy neutrino candidate event, and expected 1.9 background events, the 90% confidence limit on $|U_{\mu i}|^2$ was computed inserting into eq. (6) $N = 3.9$. The results are shown in Fig. 4.

In conclusion we did not find evidence for the existence of neutrinos with mass in the range 500 – 1800 MeV and 500 – 2800 MeV decaying into a pair of electrons and one light neutrino or into a muon and hadrons, respectively. The first search is sensitive to values of $|U_{e i}|^2$ and $|U_{\mu i} U_{e i}|$ around 10^{-7} for neutrino masses larger than 1000 MeV. In the second search we obtained a limit of $|U_{\mu i}|^2 < 10^{-3}$ at 90% confidence level for neutrino masses around 2000 MeV.

REFERENCES

1. F. Bergsma et al. (CHARM Collab.), Phys. Lett. 128B (1983) 361.
2. R. E. Shrock, Phys. Rev. D24 (1981) 1232.
M. Gronau, SLAC-PUB-2967, August 1982.
3. M. Gronau, C. N. Leung, J. L. Rosner, Phys. Rev. D29 (1984) 2359.
4. M. Holder et al, Nucl. Instrum. Methods 148 (1978) 235.
5. A. N. Diddens et al. (CHARM Collab.), Nucl. Instrum. Methods 178 (1980) 27.
M. Jonker et al. (CHARM Collab.), Nucl. Instrum. Methods 200 (1982) 183.
6. M. Jonker et al. (CHARM Collab.), Nucl. Instrum. Methods 176 (1980) 189.
7. M. Jonker et al. (CHARM Collab.), CERN/SPSC/80-31, SPSC/P142 Add. 1, 12 March 1981.
8. F. Bergsma et al. (CHARM Collab.) Search for axion-like particle production in 400 GeV proton-copper interactions. To be published in Phys. Lett.
9. F. Bergsma et al. (CHARM Collab.), Zeits. Phys. C24 (1984) 217.
10. A. Baroncelli, Nucl. Instrum. Methods 118 (1974) 445.
11. M. Jonker et al. (CHARM Collab.), Phys. Lett. 102B (1981) 67.

POSSIBLE CONSTRAINTS ON NEUTRINO OSCILLATION
PARAMETERS FROM DOUBLE BETA DECAY EXPERIMENTS

A.A.Klimenko, A.A.Pomansky, A.A.Smolnikov
Institute for Nuclear Research
Academy of Sciences
117312 Moscow, USSR



ABSTRACT. By using the experimental data of the ^{150}Nd double beta decay experiment some constraints on Δm^2 of neutrino oscillations with the small mixing are given in the frame of the concrete model for fermion mass matrices. The comparison with some oscillation experiment results and the possible considerations following from the constraints are discussed.

There are three types of experiments giving some information about a neutrino mass: measurements of the end point of the tritium beta decay spectrum, neutrino oscillations and neutrinoless double beta decay $\beta\beta(0\nu)$. The latter is the most sensitive test to indicate the nonzero Majorana mass of electron neutrinos. There were some discussions in recent papers^{/1/} about possible relationships between this mass $\langle m_\nu \rangle_{\beta\beta}$ and the mass extracted from tritium experiment. Certainly, the real form of this relationship must be in direct dependence on the same neutrino mass matrix.^{/2/} As for the relationships among $\langle m_\nu \rangle_{\beta\beta}$ and Δm^2 and $\sin^2 2\theta$ of neutrino oscillations, they were discussed only in phenomenologi-

cal considerations without any quantitative estimations.

In this paper some results of such an estimation are discussed in the frame of the latest models proposed by Stech^{/3/} and extended by Kim and Nishiura^{/4/}.

At the beginning let us recall that $\beta\beta(0\nu)$ like the neutrino oscillations depends on both neutrino mass eigenstates and mixing angles. Actually, in the case of two generations and in the absence of right-handed currents the transition amplitude for the $\beta\beta(0\nu)$ mode should be proportional to

$$\langle m_\nu \rangle_{\beta\beta} = |m_1 \cdot \cos^2 \theta_1 + m_2 \cdot \sin^2 \theta_1| \quad (1)$$

as long as the condition $m_1, m_2 \ll E$ is satisfied. Here m_1 and m_2 are the neutrino mass eigenstates and E is the $\beta\beta$ transition energy. One can obtain some model independent constraints on $\Delta m^2 = m_2^2 - m_1^2$ via $\langle m_\nu \rangle$ and $\sin^2 2\theta_1$ from (1) directly supposing the Majorana type of electron neutrino. However, the constraints obtained in this way

$$\Delta m^2 \leq 4 \langle m_\nu \rangle^2 / (1 - \sqrt{1 - \sin^2 2\theta_1})^2 \quad (2)$$

are not so strong as the ones extracted from oscillation experiments. The stronger constraints on Δm^2 and θ_1 via $\langle m_\nu \rangle_{\beta\beta}$ may be obtained using in addition to (1) the known regularities in the charged fermion mass spectrum and some theoretical premises.

Recently Stech has proposed a simple structure of the fermion mass matrix^{/3/} motivated by assumptions on unification of all fermions of the same generation in a certain multiplet, the hermiticity of the up, down and charged lepton mass matrices and the dominance of the simplest Higgs representations. These assumptions have been realized in the frame of $SO(10)$. Essentially, the relations which have been obtained in this paper predict a B-meson life time, a range of values for the t-quark mass and a CP-violating phase angle. These predictions are in a good agreement with the measured value of τ_B ^{/5/} and do not contradict the recent reports about t-quark detection with the mass about 40 GeV^{/6/}.

In their paper^{/4/} Kim and Nishiura generalized the Stech model to include a neutrino mass matrix in order to obtain some relationships among the net lepton mixing angles and neutrino masses. There exist some modifications in this case. First of all the higher Higgs representations are taken into account that leads to additional uncertainties of predictions. Moreover, the Yukawa couplings of the fermion fields with the available Higgs fields generate both Dirac neutrino masses M_D and Majorana masses - left-

handed M_L and right-handed M_R . Nevertheless, they assume that after diagonalizing these neutrino mass matrices light left-handed Majorana neutrinos are decoupled from the M_R and M_D under the assumption that the condition $M_D^2 \ll M_L \cdot M_R$ is satisfied. Thus M_L represents the light left-handed Majorana neutrino and one can claim that the observable neutrino is a pure Majorana particle in this case. In paper /4/ they deal with the case of the first two generations for the case of three generations there exist too many unknown parameters. It is probable the extension to three generations doesn't influence the predictions to a marked degree.

It is interesting that the charged lepton mixing angle Θ_E in the case of two generations can be calculated using the known quark and charged lepton masses, but as the authors emphasize this angle is not the observable one in the lepton sector unless the neutrinos remain unmixed. Instead they obtained the net lepton mixing angle $\Theta_1 = (\Theta_E - \Theta_\nu)$ as a function of m_1/m_2 , Cabibbo angle Θ_c and the known quark and charged lepton masses:

$$\cos 2\Theta_1 = x \cdot (1 + m_1/m_2) / (1 - m_1/m_2) + y \cdot (1 - m_1/m_2) / (1 + m_1/m_2) \quad (3)$$

where x and y denote the simple algebraic functions of the quark and charged lepton masses and the Cabibbo angle. There are some uncertainties here because of the masses can be either positive or negative for the procedure of diagonalizing mass matrices phases are not properly absorbed into fermion fields. Therefore, there exist four independent mass ratios m_d/m_s , m_s/m_μ , m_e/m_μ and m_u/m_c . From the 16 possible sign combinations only 9 yield physical solutions for the charged lepton mixing angle: $-1 \leq \cos 2\Theta_E \leq 1$. These combinations can be divided into three classes: (a) $m_d/m_s > 0$ and $m_s/m_\mu < 0$; (b) $m_d/m_s < 0$ and $m_s/m_\mu < 0$; (c) $m_d/m_s < 0$ and $m_s/m_\mu > 0$. From the additional physical constraints $-1 \leq \cos 2\Theta_1 \leq 1$ and $-1 \leq \cos 2\Theta_\nu \leq 1$ one can find the limits on m_1/m_2

$$\begin{aligned} 2.0 \times 10^{-2} &\leq m_1/m_2 \leq 1.7 \times 10^{-1} & (a) \\ 8.6 \times 10^{-4} &\leq m_1/m_2 \leq 7.6 \times 10^{-3} & (b) \\ -3.0 \times 10^{-3} &\leq m_1/m_2 \leq -1.5 \times 10^{-1} & (c) \end{aligned} \quad (4)$$

for the above-mentioned classes respectively. One can see that $(m_1/m_2) > 0$ for classes (a) and (b) which means that both neutrino mass eigenstates have the same CP eigenvalues. In class (c) $(m_1/m_2) < 0$ and the situation is opposite.

From the constraints on m_1/m_2 one can obtain the available limits on Θ_1 , which are fixed in the model and don't depend on $\langle m_\nu \rangle_{\beta\beta}$. These limits are:

(a) $0 \leq \theta_1 \leq 24^\circ$; (b) $0 \leq \theta_1 \leq 5.4^\circ$; (c) $0 \leq \theta_1 \leq 9.3$; (5)

As a result, from (1) and (3) they obtain Δm^2 as a function of $\langle m_\nu \rangle_{\beta\beta}$, $\sin^2 2\theta_1$, x and y :

$$\Delta m^2 = 8x \cdot \langle m_\nu \rangle^2 \cdot \left[(1 - \sin^2 2\theta_1)^{1/2} - (1 - \sin^2 2\theta_1 - 4xy)^{1/2} \right] \cdot \left[(1 - 2x) \cdot (1 - \sin^2 2\theta_1)^{1/2} - (1 - \sin^2 2\theta_1 - 4xy)^{1/2} \right]^{-2} \quad (6)$$

By using this relationship we obtain the allowed area for Δm^2 and $\sin^2 2\theta_1$ in neutrino oscillations by taking the limit on the $\langle m_\nu \rangle$ from our results of the experiment searching for $\beta\beta$ decay of ^{150}Nd ^{7/} which is one of the most promising isotopes for decay searches. Its decay energy (3.37 MeV) is exceeded only by ^{48}Ca

The measurements with 50g of ^{150}Nd are being carried out in the low-background underground laboratory of the Baksan Neutrino Observatory. In the experiment we use a method based on multidimensional analysis of $\beta\beta$ -events. It allows us to search different modes and mechanisms of $\beta\beta$ -processes. In fact, the event distribution in the two-dimensional matrix for a given $\beta\beta$ decay mode is well separated from the distributions characterizing other modes ^{7/}. Thus we have a chance to extract the individual limits on the $\langle m_\nu \rangle_{\beta\beta}$ and the admixture of right-handed currents λ_{RHC} from our experimental data concerning both " m_ν " and " λ_{RHC} " mechanisms separately in contrast to the experiments where only a peak corresponding to the $\beta\beta(0\nu)$ transition energy is detected. So, one can substitute the obtained limit on the $\langle m_\nu \rangle_{\beta\beta}$ in (6) directly. Moreover, the two-neutrino mode of the ^{150}Nd $\beta\beta$ decay is being measured simultaneously. It helps us to extract more reliable limits on $\langle m_\nu \rangle_{\beta\beta}$ and other parameters because the main uncertainty in evaluation of those is associated with the values of nuclear matrix elements. In the case of 2ν mode direct determination of the value $|M_{\text{GT}}|$ is possible because if $|M_{\text{F}}|$ is negligible one can write ^{8/}:

$$T_{1/2}(2\nu) = 3.3 \times 10^{21} y \cdot \mathcal{M}_0^2 / f_{2\nu}(\mathcal{E}_0) \cdot \chi(Z, \mathcal{E}_0) \cdot |M_{\text{GT}}|^2 \quad (7)$$

where $\mathcal{M}_0 = [\langle E_1 \rangle - (M_A + M_B)/2] / m_e$, $\langle E_1 \rangle$ is the average energy of the intermediate nucleus, $f_{2\nu}(\mathcal{E}_0)$ is the phase space factor depending on kinetic energy \mathcal{E}_0 and $\chi(Z, \mathcal{E}_0)$ is the Coulomb correction with relativistic enhancement ^{9/}. Although there is some uncertainty in the \mathcal{E}_0 estimation this uncertainty is likely much smaller than that for $|M_{\text{GT}}|$.

It is necessary to emphasize that in our experiment $2\nu, 0\nu\chi^0$ and 0ν modes are measured with the same isotope. It gives us a

chance to connect $|M_{0\nu}|$ and $|M_{GT}|$ because the rate of the 0ν process mediated by Majorana neutrino is proportional to $\langle f | \langle m_\nu \rangle \Omega_\nu | i \rangle^2$ and $|\Omega_\nu| = |M_{GT}| \cdot f(r_{ij})^{8/}$ where $f(r_{ij})$ is approximated roughly by $(\tilde{f} \cdot r_0 \cdot A^{1/3})^{-1}$ and $\tilde{f} = 0.58^{9/}$.

For 1000 h measuring live time with 50 g of the ^{150}Nd sample and the same time without it we obtained the limit $T_{1/2}(2\nu, 0^+ \rightarrow 0^+) \geq 1.3 \times 10^{19} \text{y}$ at 95% c.l. By using (7) and taking $\mathcal{M}_0(^{150}\text{Nd}) \approx 20^{9/}$ one can obtain the limit $|M_{GT}| \leq 0.5^{7/}$. From this result we can calculate that the actual value of $|M_{GT}|$ for ^{150}Nd is smaller than those calculated by Haxton and Stephenson for ^{76}Ge , ^{82}Se , $^{128,130}\text{Te}$ ^{9/}. Nevertheless our limit is in good agreement with the geochemical results for ^{82}Se and $^{128,130}\text{Te}$ and with the latest direct measurements for ^{82}Se by Moe et al.^{10/} ($T_{1/2}(2\nu, 0^+ \rightarrow 0^+) \geq 4.1 \times 10^{19} \text{y}$).

Moreover, following Morales et al.^{11/} and Klapdor et al.^{12/} we will try here to make a rough evaluation $|M_{GT}|$ for ^{150}Nd . In the paper /11/ they computed the absolute rates for the $\beta\beta(2\nu)$ in the cases where the simple $\beta^-(1^+ \rightarrow 0^+)$ and $\beta^+(1^+ \rightarrow 0^+)$ decays are experimentally known by assuming the dominance of the lowest 1^+ state of the intermediate nucleus. In this assumption they express the nuclear matrix elements in terms of the single decay matrix elements of both branches computing those through the experimental values of $\lg(ft)_1$ for $(\beta^+, 1^+ \rightarrow 0^+)$ and $\lg(ft)_2$ for $(\beta^-, 1^+ \rightarrow 0^+)$:

$$|\tilde{M}_{GT}|^2 = 1.44 \times 10^8 / 10^{\lg(ft)_1 + \lg(ft)_2} \quad (8)$$

Naturally, the value of \mathcal{M}_0 is connected with the $A, Z+1(1^+) \rightarrow A, Z(0^+)$ transition energy in this case. Since both $^{82}\text{Se} \rightarrow ^{82}\text{Kr}$ and $^{130}\text{Te} \rightarrow ^{130}\text{Xe}$ $\beta\beta$ transitions have no 1^+ intermediate states, Morales et al. have applied the Pontecorvo hypothesis about approximately equal matrix elements for neighbouring even-even nuclei to the ^{80}Se and ^{82}Se , ^{128}Te and ^{130}Te pairs. As a result they obtained the half lives for some isotopes. In particular, their prediction for ^{82}Se and ^{130}Te are in a good agreement with the corresponding experimental values.

Unfortunately, three possible $\beta\beta$ transitions of $\text{Nd}(^{146,148,150}\text{Nd} \rightarrow ^{146,148,150}\text{Sm})$ have no 1^+ ground state of the intermediate nucleus. However, by using the same assumption as in /11/ we modify their method taking into consideration the decay chain of the neighbouring isotope ^{152}Nd . In our opinion the experimental values of $\lg(ft)_{1,2}$ for this chain may be applied to estimate $|M_{GT}|$ of ^{150}Nd in the same way as in the Morales scheme. Moreover, in this case

we deal with two single β^- transitions ($0^+ \rightarrow 1^+$, $1^+ \rightarrow 0^+$) occurring one after the other instead of the intermediate nucleus in 1^+ ground state emitting both e^+ and e^- .

So, taking $\lg(ft)_1 \approx 4.6$ for $^{152}\text{Nd} \rightarrow ^{152}\text{Pm} + e^- + \nu$ and $\lg(ft)_2 \approx 6.4$ for $^{152}\text{Pm} \rightarrow ^{152}\text{Sm} + e^- + \nu$ and putting those into the ^{150}Nd case we have $|\tilde{M}_{GT}| = 0.038$ or $|\tilde{M}_{GT}|/\tilde{M}_0 = 1.07 \times 10^{-2}$. Whence substituting the suitable quantities one can obtain $T_{1/2}(2\nu, 0^+ \rightarrow 0^+) \approx 6 \times 10^{19} \text{y}$. It is interesting that in one of their previous papers and in the recent one^{/11/} Doi et al. cite the estimations of $\beta\beta(2\nu)$ half life for ^{150}Nd being equal to $3.9 \times 10^{19} \text{y}$ and $7 \times 10^{19} \text{y}$ which are educated guesses only.

Thus proceeding from the above considerations we can suppose that our experimental limit on $T_{1/2}(2\nu, 0^+ \rightarrow 0^+)$ for ^{150}Nd is close to the real half life. It permits us to use the upper value of the corresponding limit $|M_{GT}| \approx 0.5$ as a bare value.

Then according to /8/ and using our experimental limit $T_{1/2}(0\nu; m_\nu \neq 0, \lambda_{\text{RHC}} = 0) \geq 1.2 \times 10^{21} \text{y}$ we find^{/7/} $\langle m_\nu \rangle \leq 25 \text{eV}$ at 90% c.l. By using this value and (6) we calculate the allowed areas for Δm^2 versus $\sin^2 2\theta_1$ for (a), (b) and (c) classes. These areas are shown in fig.1a,b,c respectively. In the same figures the dashed curves represent results from neutrino oscillation accelerator^{/13/} experiments.; the region to the right of the solid curve represents the possible indication for $\bar{\nu}_e \rightarrow \bar{\nu}_x$ oscillations from the experiment at the Bugey reactor^{/14/}. For comparison include the bound on $\langle m_\nu \rangle_{\beta\beta}$ obtained from our experiment if one uses the $|M_{GT}|$ value of the same order as Haxton's predictions for ^{76}Ge , ^{82}Se and ^{128}Te and ^{130}Te , e.g. taking $|M_{GT}| \approx 2.8$. Then we find $\langle m_\nu \rangle_{\beta\beta} \leq 5 \text{eV}$ if $\chi(Z, \xi_0)$, the Coulomb correction with relativistic enhancements, is included. It is seen that this limit is approximately the same as the ones for ^{76}Ge extracted from the recent direct experiment. So we don't plot these values here. However, as a minimal possible constraint on Δm^2 we give in fig.1 the interpretation of geochemical measurements of ^{128}Te ^{/15/} deduced by Klapdor and Grotz^{/12/} (dash-dotted curve).

Concluding we would like to emphasize some features of the constraints obtained:

1) In the frame of the discussed theoretical assumptions decay experimental results give new nontrivial constraints on the parameters of neutrino oscillations.

2) All solutions (a,b,c) give the upper boundary of Δm^2 at

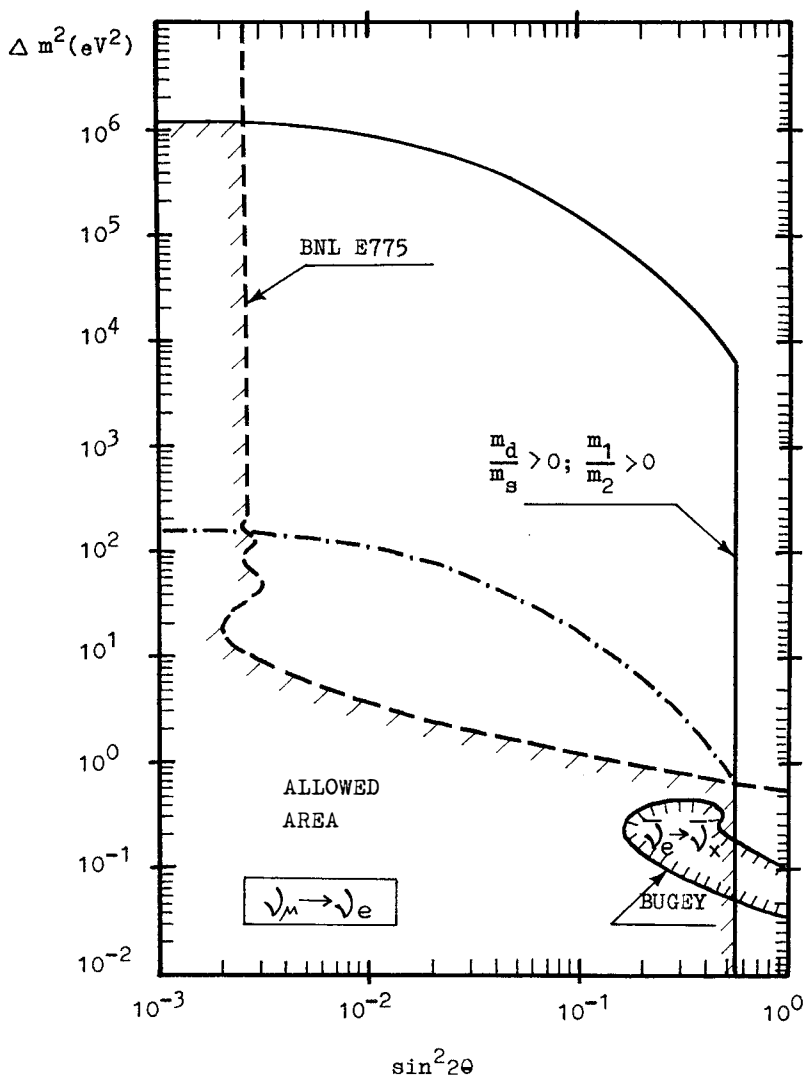


Fig.1a

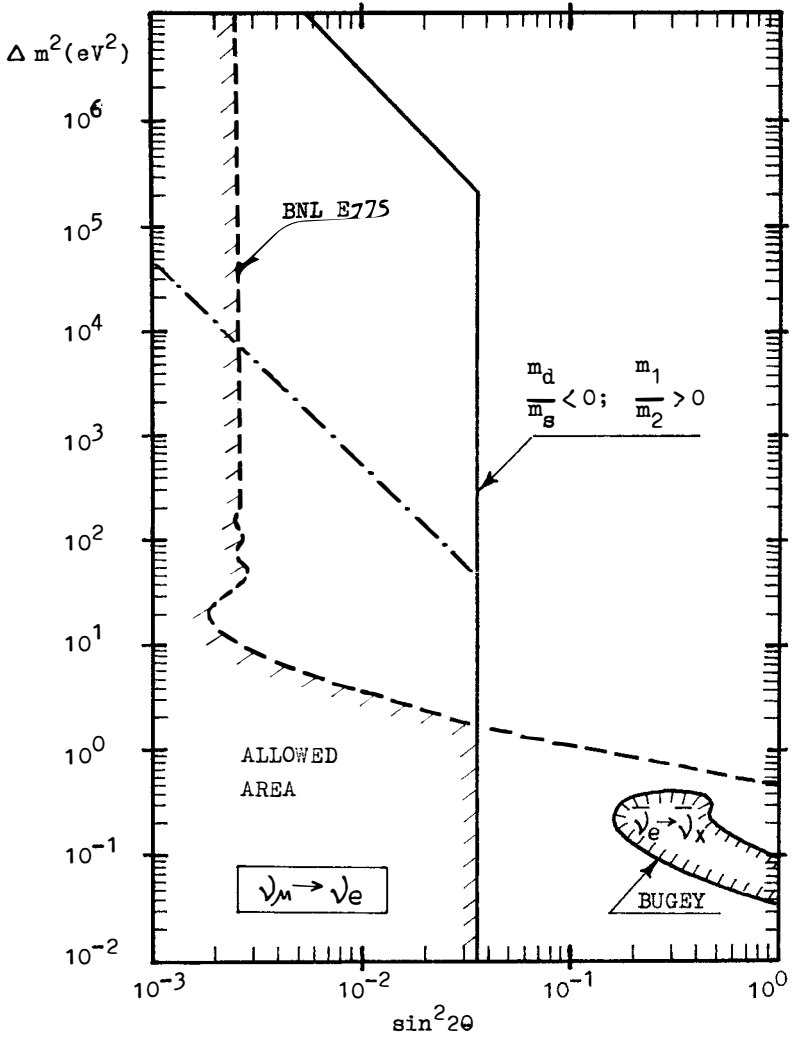


Fig.1b

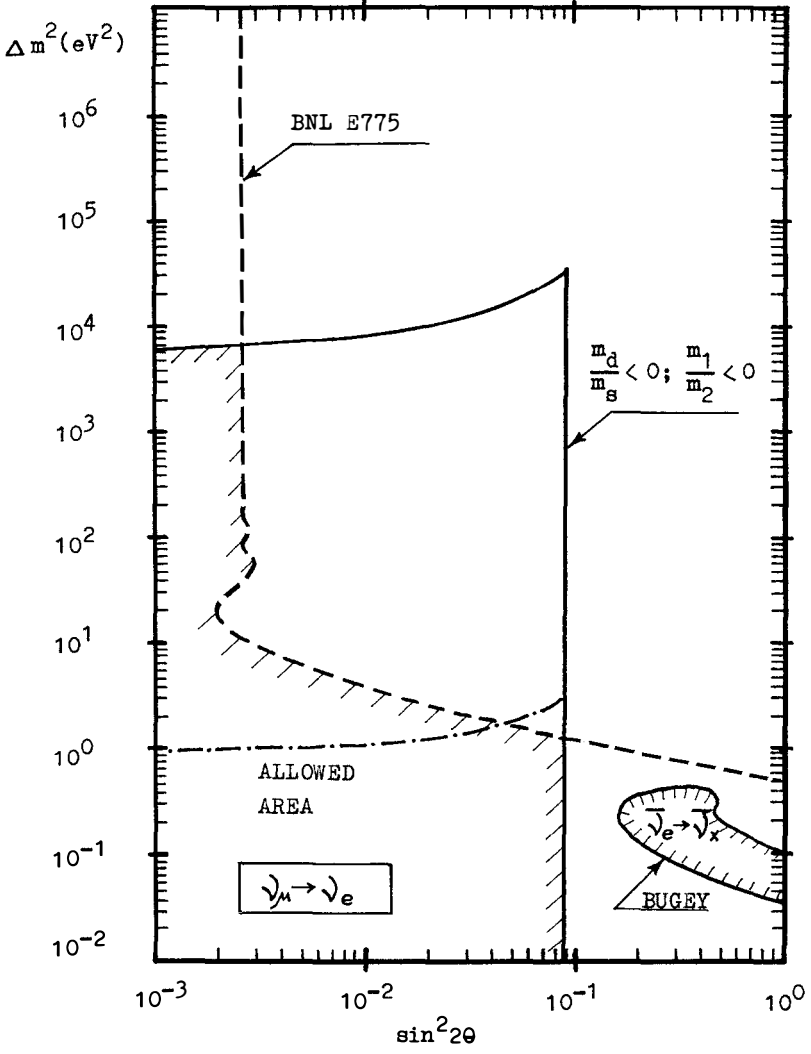


Fig.1c

the small $\sin^2 2\theta_1$ where there are no constraints from oscillation experiments.

3) There exists a maximal mixing angle independent of m for each solution.

Some words about the reliability of the obtained constraints. It is not excluded that results such as (6) or something similar may be a correct model even if the SO(10) model is wrong. In any case we would like to pay attention to the importance of investigations where data of neutrino oscillations and that of $\beta\beta$ decay are compared. In particular, if (6) is really right and the positive Bugey result will be confirmed one can conclude from fig.1 that only the model with $m_d/m_s > 0$ and $m_1/m_2 > 0$ is in agreement with the experiment. In this case, there is no cancellation of $\langle m_\nu \rangle_{\beta\beta}$ generated by opposite signs of m_1 and m_2 .

Acknowledgement. It is a pleasure for the authors to acknowledge fruitful discussions with A.Yu.Smirnov.

REFERENCES

1. M.DoI et al., Neutrino mass conference, Telemark, Wisconsin, October 1984, and references therein.
2. V.A.Lubimov et al., XXII International conference on High Energy Physics, Leipzig, July 1984.
3. B.Stech, Phys.Lett.130B(1983) 189.
4. C.W.Kim, H.Nishiura, Phys.Lett.139B (1984) 53
5. G.Goldhaber, QCD and beyond, Rencontres de Moriond, March 1985 κ.Krepost, this conference.
6. C.Rubbia, Proceedings of "Neutrino-84"Conference, Dortmund, June 1984, p.1.
7. A.A.Klimenko et al., Proceedings of "Neutrino-84" Conference, Dortmund, June 1984, p.161.
8. J.D.Vergados, Nucl.Phys. B218 (1983) 109
9. W.Haxton et al., Los Alamos Preprint LA-UR-83-417
10. M.K.Moe et al., Preprint UCI-Neutrino N133, 1984
11. J.Abad et al., Anales de Fisica, Serie A, 80 (1984) 9
12. H.V.Klapdor, K.Grotz, MPI H-1984-V 29
13. R.Lanou, this conference
14. H.Pessard, this conference
15. T.Kirsten et al., Phys.Rev.Lett.50 (1983) 474

AN EXPERIMENT TO MEASURE THE ELECTRON
NEUTRINO MASS USING FROZEN TRITIUM

O. Fackler^{‡,*}, B. Jeziorski^{!,"}, W. Kolos^{!,+},
H. Monkhorst[†], M. Mugge^{†,‡}, H. Sticker^{*},
K. Szalewicz^{!,+}, R. M. White[‡], R. Woerner[‡]

‡ Lawrence Livermore National Laboratory
Livermore, CA 94550

* Rockefeller University
New York, NY 10021

! University of Warsaw, Warsaw, Poland

" University of Waterloo, Waterloo, Ontario, Canada

+ University of Florida, Gainesville, Florida 32611

† Fermilab, Batavia, IL 60510

ABSTRACT

We are performing an experiment to determine the electron neutrino mass with the precision of a few eV by measuring the tritium beta decay energy distribution near the endpoint. Key features of the experiment are a 2 eV resolution electrostatic spectrometer and a high-activity frozen tritium source. It is important that the source have electronic wavefunctions which can be accurately calculated. These calculations have been made for tritium and the HeT⁺ daughter ion and allow determination of branching fractions to 0.1% and energy of the excited states to 0.1 eV. We discuss the excited final molecular state calculations and describe the experimental apparatus.

The goal of our experiment is to measure the neutrino mass to better than 2 eV. If the neutrino mass is finite, the tritium beta decay energy distribution changes appreciably only within a few neutrino masses from the endpoint (see Fig. 1). For a zero neutrino mass, the fraction of decays within 2 eV of the endpoint is only 2.6×10^{-12} . This small fraction dictates a low-background, high-resolution spectrometer with large acceptance. After beta decay, the resulting atom or molecule can be left in one of many excited states. These excited states take energy from the emerging beta and give rise to a number of branches, each with a different endpoint energy, in the beta energy distribution. The sum of these branches results in the observed Kurie plot. An accurate physics result emerges only if one knows the occupation fractions and energies of these final excited states and hence, the expected shape of the measured distribution. In addition, the spectrometer resolution function must be well understood. A wide resolution function or long tails in this function can introduce a significant smearing in the tritium beta decay spectrum. Such effects greatly complicate the interpretation of the data. Finally, the emerging electrons undergo a dE/dx loss in the source itself. Ideally, a measurement of the dE/dx loss is made and a consistent neutrino mass is determined in sources of different thicknesses.

For complex molecules or tritium binding processes, the final state effects are not calculable with sufficient precision for a high accuracy measurement. However, molecular tritium (T_2) at liquid helium temperatures is ideal because the low intermolecular binding energy (on the order of 1/400 eV) means it essentially has the electronic wavefunction of the free T_2 molecule.

We have calculated the β -decay energy spectrum which results from the decay of one of the nuclei in the T_2 molecule^{1,2}. An accurate, explicitly correlated basis set was used to describe the electronic states of both the parent and daughter molecules. All channels which meaningfully effect the spectrum have been incorporated in the calculation including the resonance and scattering channels.

Unlike the atom, the HeT^+ ion in its ground state has both vibrational and rotational degrees of freedom which can absorb energy from the decay beta. At the liquid helium temperature of our source, only the lowest vibrational and rotational states are populated. However, after the decay, when one of the atoms has been given an impulse from the decay beta, most of the possible vibrational and rotational states will be populated for transitions to bound states. The details of these calculations will be presented in Ref. 3.

These calculations have been performed independently by another group⁴ using totally different techniques. In particular, the electronic wavefunctions were

determined using a complete configuration interaction calculation. In all cases the agreement between these approaches was exceedingly good.

The HeT^+ is primarily excited to a high vibrational state when, near the endpoint of the beta decay distribution, the decay beta is emitted nearly aligned with the internuclear axis. Conversely, the HeT^+ ion is left in a highly excited rotational state when the decay beta is emitted nearly perpendicular to the internuclear axis. This coupling between the beta decay and the vibrational and rotational states gives a high density of states near the top of the potential well (see Fig. 2). The full width at half height of this distribution is about 0.7 eV. As a consequence of this small spread, the ground state branch in the Kurie plot is smeared by only an average of 1 eV. This additional spread is a small penalty to pay for the ease of using molecular rather than atomic tritium.

We present the results of our calculations in the form of a Kurie Plot. These plots have been generated using the formula

$$K(\epsilon; m_\nu) = \sum_n \left[P_n K^2(\epsilon; E_n, m_\nu) \right]^{1/2}$$

where ϵ is the energy measured relative to the endpoint of the spectrum, m_ν is the neutrino mass, E_n is the energy level, and P_n is the transition probability to this level. The energy E_n is measured with respect to the lowest energy value in a given treatment of nuclear motion. If the electronic spectrum of the daughter ion is used, this lowest energy value is its ground state energy for the T_2 equilibrium nuclear distance, ($R = 1.4$ bohr), or its ground state energy averaged over the ground vibration of the initial T_2 system. If the nuclear-motion-resolved calculations are used, E_n is relative to the ground rovibronic level of ${}^3\text{HeT}^+$. $K(\epsilon; E_n, m_\nu)$ is a single branch of the Kurie plot defined as

$$K(\epsilon; E_n, m_\nu) = (m_\nu + \epsilon - E_n)^{1/2} [(m_\nu + \epsilon - E_n)^2 - m_\nu^2]^{1/4}$$

for $\epsilon \geq E_n$, and $K(\epsilon; E_n, m_\nu) = 0$ for $\epsilon < E_n$. For the continuous part of the spectrum, the summation is changed to an integration.

In Fig. 3 we compare Kurie plots obtained for pure nuclear, atomic, and molecular (T_2) tritium decay processes for an assumed 30 eV neutrino mass. The molecular plots are presented for three cases: (1) constructed for a fixed internuclear distance ($R = 1.4$ bohr); (2) obtained for R averaged over the ground state vibration of the T_2 molecule; (3) same as (2) except for a complete treatment of the final state nuclear motion for

the most significantly contributing ${}^3\text{HeT}^+$ electronic states. The final result of this work is presented in plot (3).

Fig. 3 clearly shows that the Kurie plot is comparably effected far from the endpoint by final state effects in both the atom and the molecule. However within about 3 eV from the endpoint the molecular rovibrational effects are much more important than the atomic effects. This distortion is only about 3 eV and is accurately calculated.

The Kurie plots resulting from this calculation are presented for neutrino masses between 0 and 50 eV in Fig. 1. The plots become practically linear above 100 eV and are very close to linear for $\epsilon > 75$ eV.

Strictly speaking, these results only apply to gaseous T_2 . Our source is actually solid tritium rather than a free molecule. Nevertheless, the tritium molecular wavefunction in the frozen solid is very close to the molecular wavefunction of the free molecule. We can understand this qualitatively by noting that the tritium melting temperature implies that the intermolecular binding energy is very much less than the orbital electron binding energy. Consequently we can expect a very small perturbation on the molecular wavefunction because of intermolecular binding forces. Quantitatively, the electron probability density halfway to the nearest molecular neighbor is approximately 2×10^{-4} of the maximum. This small electronic overlap gives rise to a negligible distortion of the molecular wavefunction. The depth of the internuclear potential well is approximately 1,600 times that of the intermolecular potential well. This difference in binding energies also indicates a very small perturbation of the molecular wavefunction in the solid.

The experimental evidence for a very small change in the electronic wavefunction resulting from the binding in the solid comes from Raman spectra in gaseous and solid hydrogen. The vibrational energy levels are determined by the shape of the internuclear potential well and the shape of this well is determined by the electronic wavefunction. The typical measured shift in the vibrational energy levels resulting from the binding in solid hydrogen is about 1/2000 eV. Since this energy shift is very small compared with the typical vibrational energy level spacing of about 0.1 eV, this is evidence for a very small perturbation in the molecular wavefunctions resulting from the intermolecular binding in the solid. Furthermore, the molecular binding forces are so weak that the rotational states are hardly perturbed and the molecules can rotate as though they were nearly free. We conclude that the fractional change in the wavefunction due to intermolecular binding in the solid is less than 0.1%. Hence our results apply to both gaseous and frozen T_2 .

The experimental apparatus is shown in Figure 4. It is contained in a vacuum tank 0.9 m in diameter and 7 m long. The tank is passively shielded by 2 concentric

magnetic shields giving a residual field of less than 2 milligauss in the active region. The source is a liquid helium cooled plate on which tritium is frozen. Varying the amount of tritium gas introduced allows source thickness variation from a few monolayers up to any thickness. The source points upstream allowing the decay electrons to enter a region which is the electrostatic analog of a parabola with the source at its focus. Hence, electrons emerging from the source are mapped into a larger essentially parallel beam traveling downstream.

Following the electrostatic parabola, a variable-length collimator defines the angular acceptance of the electrons and limits the maximum angle which the electrons can make with the axis of the electrostatic spectrometer. The spectrometer consists of three equally spaced grid planes with field shaping electrodes around the axis. We measure the integral number of electrons within the passband of the electrostatic parabola whose energies are higher than the center grid potential. Electrons leaving the spectrometer pass through an electrostatic lens which focusses them onto a solid state detector. This detector simply counts the electrons but does not have an energy resolution of approximately 1.5 keV which aids in rejecting low energy electrons and photons.

The experimental apparatus was tested by looking at the 7.3 keV electron conversion electrons from ^{57}Co . This line has an intrinsic HWHM of 0.6 eV. Our measurement of this line showed a HWHM of 2 eV. This measured distribution is shown in Figure 5. The tail on the low energy side is due to the occurrence of close-lying satellites of the conversion lines produced by accompanying shake-off excitations.

In conclusion, we have discussed why frozen tritium is an ideal source offering the highest activity per dE/dx of any material and offering fully calculable final state effects. These final state effects contribute less than 0.2 eV of uncertainty to the final possible determination of the neutrino mass. In addition, we have built a spectrometer with a measured resolution of better than 2 eV. Monte Carlo studies indicate that by using a frozen source our apparatus will be able to determine the neutrino mass to better than 2 eV.

- 1) W. Kolos, B. Jeziorski, K. Szalewicz, and H. J. Monkhorst, Phys. Rev. A31, 551 (1985).
- 2) W. Kolos, B. Jeziorski, H. J. Monkhorst, and K. Szalewicz, Intern. J. Quantum Chem. S19, 000 (1985).
- 3) B. Jeziorski, W. Kolos, K. Szalewicz, O. Fackler, and H. J. Monkhorst, Phys. Rev. A, submitted.
- 4) N. Winter and O. Fackler, Lawrence Livermore National Laboratory, unpublished.

Work performed under the auspices of the U.S. Department of Energy by the Lawrence Livermore National Laboratory under contract No. W-7405-ENG-48, by FermiLab and by Rockefeller University.

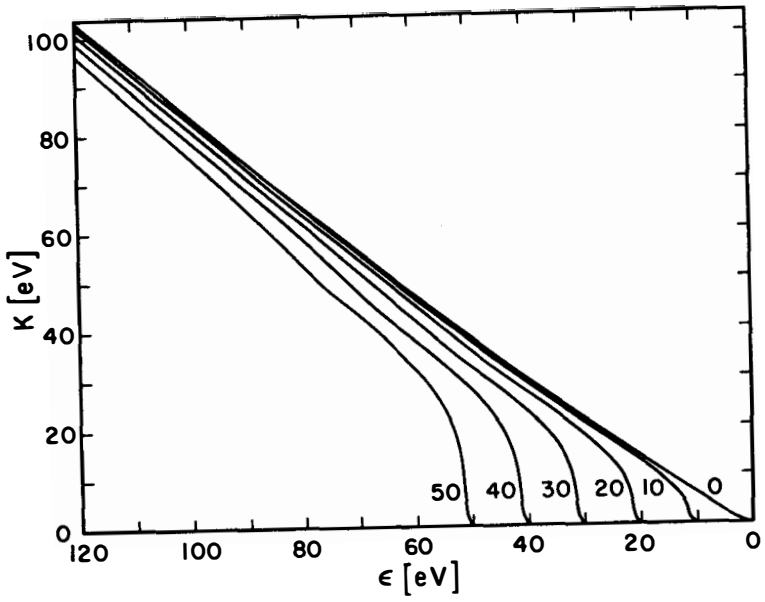


Fig. 1. Kurie plots for $m_\nu = 0$ (10) 50 eV

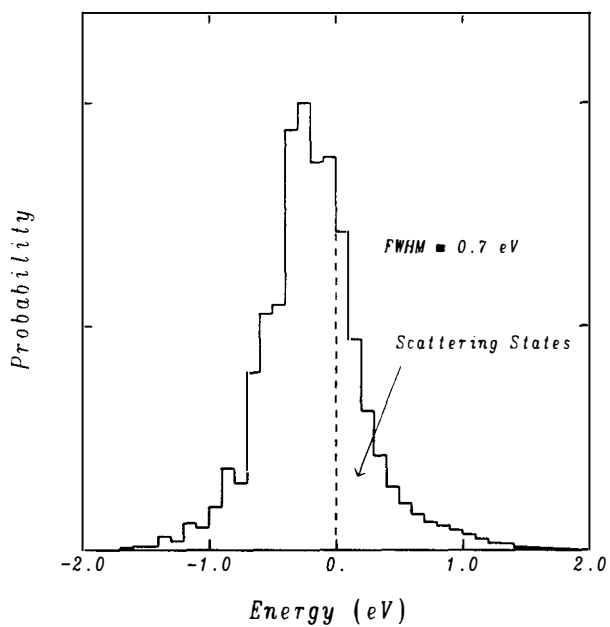


Fig. 2. Energy Spread Introduced by Molecular Vibration and Rotation

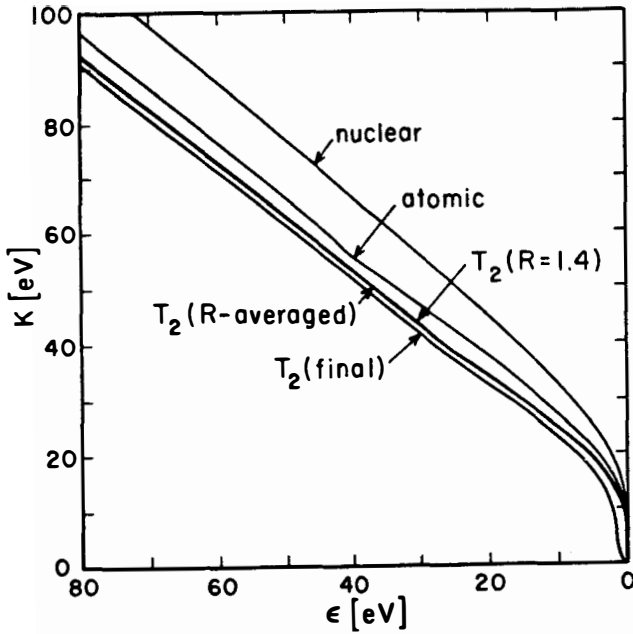


Fig. 3. Kurie Plots Assuming $m = 30$ eV

- For 1) Nuclear decay
 2) Atomic decay
 3) T_2 decay with $R_i = 1.4$ Bohr
 4) T_2 decay averaged over initial molecular vibration
 5) Same as 4) but including final state vibration and rotation

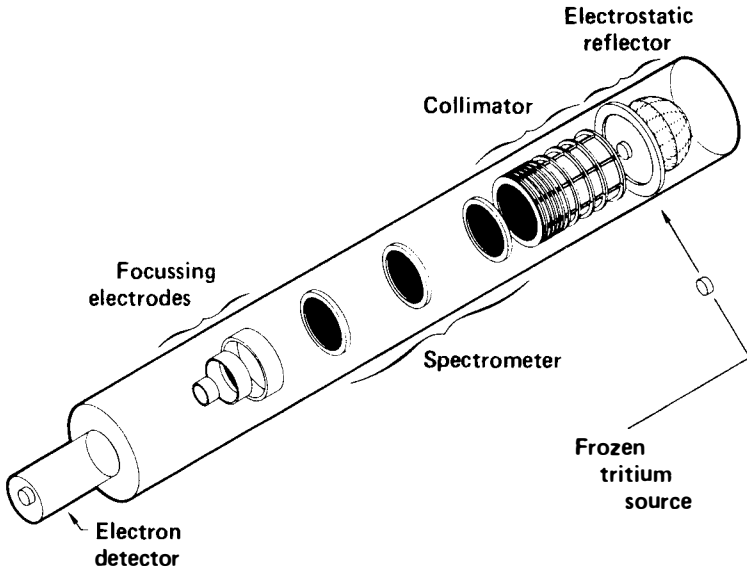


Fig. 4. Schematic Diagram of the Experimental Apparatus

- Measurements using ^{57}Co - source of monoenergetic electrons ($E = 7.302 \text{ keV}$)
- Natural width of 7.302 keV line $\approx 1.2 \text{ eV}$

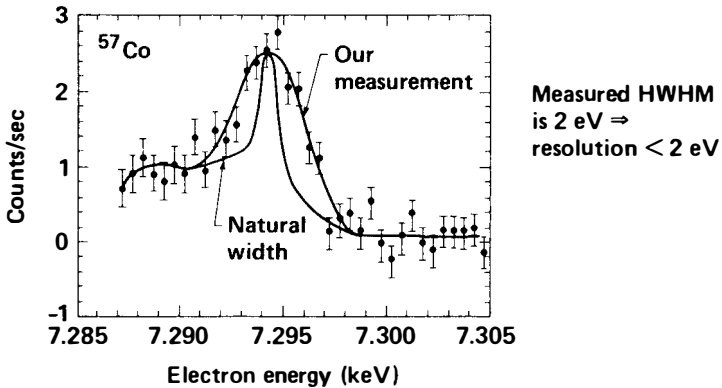


Figure 5 Measured Spectrometer Resolution. The Low Energy Tail is Due to "Shake Off" Effects

SEARCH FOR HEAVY NEUTRINOS
PRODUCED IN e^+e^- ANNIHILATION

Gary J. Feldman *

Stanford Linear Accelerator Center

Stanford University, Stanford, California 94305, U.S.A.



Abstract

We report a search for long-lived heavy neutrinos produced by the neutral weak current in e^+e^- annihilation at 29 GeV at PEP. Data from the Mark II detector are examined for evidence of events with one or more separated vertices in the radial range of 2 mm to 10 cm. No events were found that were consistent with the hypothesis of heavy neutrino production, eliminating the possibility of heavy neutrinos with decay lengths of 1 to 20 cm in mass range 1 to 13 GeV/ c^2 .

* This work was supported in part by the Department of Energy, contract DE-AC03-76SF00515.

In e^+e^- annihilation at PEP and PETRA energies the dominant reaction is the production of a pair of fundamental particles from a single virtual photon. All fundamental particles can be produced copiously in this way, provided enough energy is available to form their mass and provided that they couple to the photon, that is, that they have electric charge. One of the compelling reasons for studying e^+e^- annihilation at the Z pole at SLC and LEP is that the dominant reaction will be the formation of pair of fundamental particles from a Z, rather than a photon. Thus all fundamental particles which have weak charge will be copiously produced, including, for the first time, electrically neutral particles.¹⁾

The point of this talk is that one does not necessarily have to wait for SLC turn-on to search for new neutral particles, because even at PEP energies there is a significant coupling to a virtual Z. One example of such a particle could be a heavy neutrino, either from a fourth generation, or from a more exotic source. The cross section for producing a pair of neutrinos is²⁾

$$\sigma = \frac{G_F^2 E^2}{192\pi} \left(\frac{(1 - 4 \sin^2 \theta_W)^2 + 1}{\left(1 - \frac{E^2}{m_Z^2}\right)^2 + \frac{\Gamma_Z^2}{m_Z^2}} \right) \beta(3 + \beta^2), \tag{1}$$

where E is the center of mass energy. At the PEP energy of 29 GeV, this cross section is only 0.34 pb,³⁾ but the accumulated Mark II data of 208 pb⁻¹ yields 71 produced events and thus allows a reasonable search.

If we assume that the GIM mechanism⁴⁾ is valid for a heavy neutrino, then it will only be able to decay into one of the known charged leptons ($e, \mu, \text{ or } \tau$) and a virtual W via a (small) mixing angle ϵ .⁵⁾ This decay is illustrated in Fig. 1.

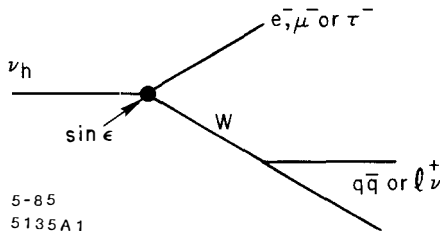


Figure 1. General diagram for heavy neutrino decay.

In this (standard) model, the lifetime of a heavy neutrino is completely calculable given the mixing angle ϵ . It can be expressed in terms of the muon lifetime as

$$\tau(\nu_h \rightarrow \ell^- X^+) = \left(\frac{m_\mu}{m_{\nu_h}} \right)^5 \frac{\tau(\mu \rightarrow e \nu \bar{\nu}) B(\nu_h \rightarrow \ell^- e^+ \nu)}{f(m_{\nu_h}, \ell) \sin^2 \epsilon}, \quad (2)$$

where ℓ represents the lepton to which ν_h primarily couples, and f is a phase space correction which is significant for our application only when $\ell = \tau$ and m_{ν_h} is at most a few times m_τ . The branching fraction B can be calculated in much the same way as in τ decay.⁹⁾ Depending on m_{ν_h} and $\sin^2 \epsilon$, the decay lengths of a heavy neutrino can be appreciable. Figure 2 shows the contours of constant decay length as a function of these two variables.

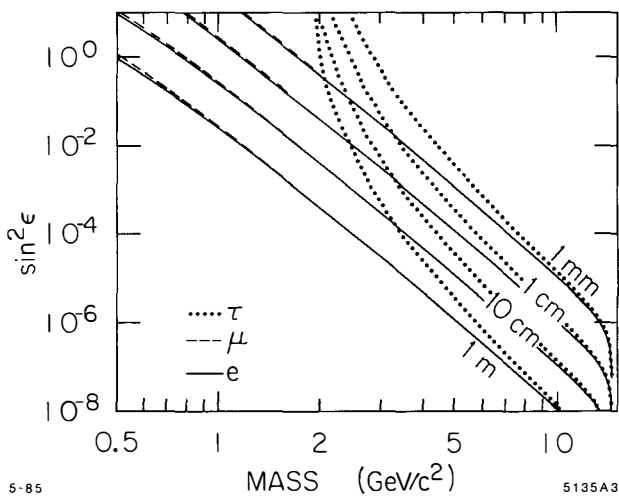


Figure 2. Contours of constant ν_h decay length.

The search was conducted with the Mark II detector at PEP.^{7,8)} The basic strategy was to look for events with two vertices that are separated from the interaction point and with no tracks coming from the interaction point. Even the observation of a single such event could be a spectacular signal. The main event requirements were

1. Four or more charged tracks. (From Fig. 1, it is clear that each ν_h must decay into at least two charged particles.)

2. One vertex with $2 \text{ mm} < r_1 < 10 \text{ cm}$, where r_1 is the radial distance between the first vertex and the interaction point. If $r_1 < 3 \text{ mm}$ or there were only four charged tracks in the event, then there must have been another vertex with $r_2 > 2 \text{ mm}$. Otherwise, a second vertex was not required.
3. No vertex within 1 mm of the interaction point.
4. The stability of the interaction point was monitored with beam position monitors. For each run that was used in this analysis, the rms beam position had to be less than $250 \mu\text{m}$ horizontally and $150 \mu\text{m}$ vertically.
5. Tracks from identified K_S^0 's and Λ 's were removed from consideration in finding vertices.
6. Events were rejected if $7.4 \text{ cm} < r_1 < 8.0 \text{ cm}$, since this was the region of the vacuum pipe.

After applying these cuts, only three events remained. (A Monte Carlo simulation predicted that we would see two events from known sources of background at this point in the analysis.) On further examination of these events, we found that they were all incompatible with the hypothesis of ν_h pair production. In one event the position of the interaction point had moved 3 mm from its assumed position. This was determined by examining the vertex of the events immediately preceding and following the candidate event. A second event had only three charged particles present. The remaining tracks were from two independent photon conversions in the chamber. The final event was kinematically incompatible with the ν_h pair hypothesis because it had a backward-going 8 GeV/c track.

Figure 3 shows the contour of excluded region at the 90% confidence level in the space of decay length and m_{ν_h} . The decay length region between 1 and 20 cm is excluded for $1 < m_{\nu_h} < 13 \text{ GeV}/c^2$. Figure 4 shows the same contour as a function of $\sin^2 \epsilon$ and m_{ν_h} .

Two other searches for ν_h have been reported at this meeting.⁹⁾ These searches exclude regions of combined lower mass and $\sin^2 \epsilon$ than this experiment. It has also been recently pointed out by Gilman and Rhie¹⁰⁾ that the monojet search data reviewed here by Prepost¹¹⁾ can be used to eliminate the possibility of a ν_h which couples primarily to electrons and has m_{ν_h} less than 12 GeV and $\sin^2 \epsilon$ greater than about 5×10^{-3} .

In conclusion, there is presently no evidence for the existence of long-lived heavy neutrinos and large regions of decay length and mixing angles have been eliminated. We look forward to experiments at the SLC and LEP, where these searches can be conducted with much more sensitivity and generality.

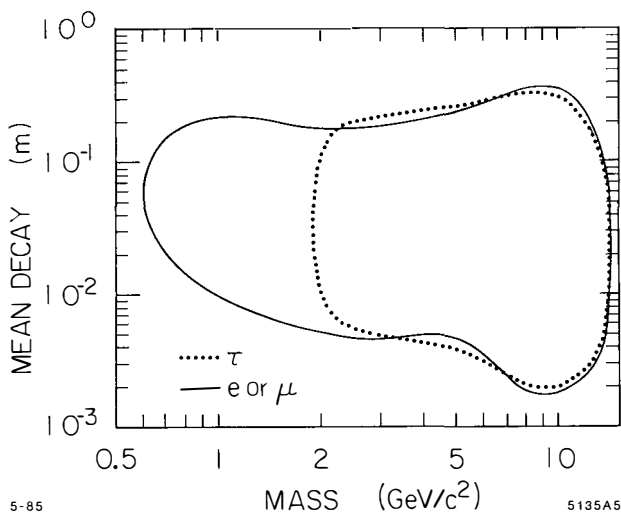


Figure 3. Excluded region for ν_h at the 90% confidence region as a function of decay length and m_{ν_h} .

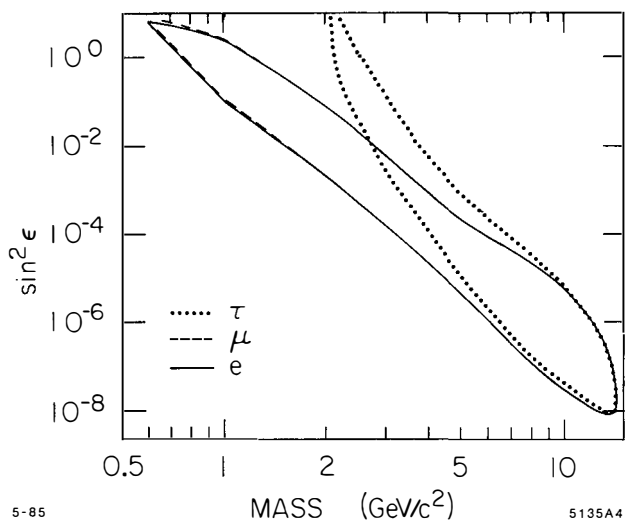


Figure 4. Excluded region for ν_h at the 90% confidence region as a function of $\sin^2 \epsilon$ and m_{ν_h} .

References

1. One exception is the production of pairs of identical self-conjugate spinless bosons, which is forbidden by symmetry considerations.
2. See, for example, F. M. Renard, *Basics of Electron Positron Collisions*, (Editions Frontières, Dreux, 1981).
3. This value includes a -5% radiative correction.
4. S. L. Glashow, J. Iliopoulos, and L. Maiani, *Phys. Rev. D* **2**, 1285 (1970).
5. For simplicity, we have assumed here that ν_h mixes primarily with a single lepton species; however, the extension to the general case is obvious.
6. H. B. Thacker and J. J. Sakurai, *Phys. Lett.* **36B**, 103 (1971); Y. S. Tsai, *Phys. Rev. D* **4**, 2821 (1971) and *Phys. Rev. D* **19**, 2809 (1979); J. D. Bjorken and C. H. Llewellyn-Smith, *Phys. Rev. D* **7**, 887 (1973); F. J. Gilman and D. H. Miller, *Phys. Rev. D* **17**, 1846 (1978).
7. The individual who did most of the work on this analysis is Chris Wendt. The other members of the Mark II collaboration at PEP are T. Barklow, A. M. Boyarski, M. Breidenbach, P. Burchat, D. L. Burke, J. M. Dorfan, G. J. Feldman, L. Gladney, G. Hanson, K. Hayes, R. J. Hollebeek, W. R. Innes, J. A. Jaros, D. Karlen, A. J. Lankford, R. R. Larsen, B. W. LeClaire, N. S. Lockyer, V. Lüth, C. Matteuzzi, R. A. Ong, M. L. Perl, B. Richter, K. Riles, M. C. Ross, D. Schlatter, A. R. Baden, J. Boyer, F. Butler, G. Gidal, M. S. Gold, G. Goldhaber, L. Golding, J. Haggerty, D. Herrup, I. Juricic, J. A. Kadyk, M. E. Nelson, P. C. Rowson, H. Schellman, W. B. Schmidke, P. D. Sheldon, G. H. Trilling, C. de la Vaissiere, and D. Wood from LBL, and M. Levi and T. Schaad from Harvard.
8. The Mark II detector has been previously described. See, for example, R. H. Schindler *et al.*, *Phys. Rev. D* **24**, 78 (1981).
9. F. Vannucci, these proceedings; A. Capone, these proceedings.
10. F. J. Gilman and S. H. Rhie, SLAC report number SLAC-PUB-3657 (1985).
11. R. Prepost, these proceedings.

HAS A COSMOLOGICAL BACKGROUND OF NEUTRINOS FROM GRAVITATIONAL
STELLAR COLLAPSE BEEN DETECTED?

Arnon Dar

Department of Physics and Space Research Institute
Technion-Israel Institute of Technology, Haifa, Israel



ABSTRACT

The rate of neutrino induced events with observed energy below 100 MeV in the KAMIOKANDE proton decay detector is much higher than expected from atmospheric neutrinos. However, it is shown here that this rate is consistent with a cosmological background of relic neutrinos that was formed by gravitational stellar collapses that have been taking place since galaxy and star formation.

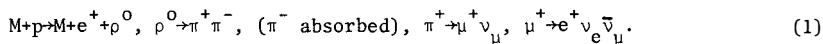
The KAMIOKANDE group which operates a massive proton decay detector deep underground at a depth of 2700 mwe in the Kamioka metal mine in Japan (25.8°N geomagnetic latitude) has recently reported¹ the observation of 80 contained events with event vertices inside a fiducial volume of 880 tons of water during 201 days of live time (0.485 kiloton-years of water exposure). Among these 80 events 22 events were identified as "single ring events" rising from either quasielastic neutrino scattering off free protons and bound nucleons ($\bar{\nu}_e + p \rightarrow n + e^+$, $\nu_e + n \rightarrow e^- + p$), or from elastic scattering off electrons ($\nu + e^- \rightarrow \nu + e^-$, where $\nu = \nu_e, \bar{\nu}_e, \nu_\mu, \bar{\nu}_\mu, \nu_\tau, \bar{\nu}_\tau$). The energy distribution of these outgoing electrons is compared in Fig. 1 with the distribution expected from atmospheric neutrinos (neutrinos which are produced by cosmic ray collisions in the atmosphere). The theoretical distribution is based on (i) the flux of atmospheric neutrinos at Kamioka which is shown in Fig. 2, and which was calculated as described in Ref. 2 utilizing the geomagnetic cutoffs that were calculated by Cooke³; (ii) the cross sections for neutrino interactions below 100 MeV which follow from the Glashow-Salam-Weinberg standard model of electroweak interactions⁴ and are summarized in Table II (and which have been verified experimentally⁵). Figure 1 shows that while the theoretical expectation is less than 1 event below 100 MeV the observed rate is 8 events for 0.485 kiloton-years water exposure. This discrepancy has been noticed independently, by Gaisser⁶. If the discrepancy between the expected rate of events due to atmospheric neutrinos and the observed rate of neutrino interactions with $E_e \leq 100$ MeV is a genuine one, then what could be the origin of these neutrinos?

The nearest astronomical source of low energy ($E_\nu < 100$ MeV) neutrinos is the sun. Three major sources of solar neutrinos have been proposed so far: (i) thermonuclear reactions that take place at its center⁷ (ii) production and decay of π 's and μ 's in the sun's atmosphere during solar flares⁸ (iii) proton decays in the sun catalyzed by magnetic monopoles.⁹

In the nuclear reactions that presumably take place at the center of the sun¹⁰ only ν_e 's from ${}^8\text{B} \rightarrow {}^8\text{Be} + e^+ + \nu_e$ have sufficient energy ($E_{\text{max}} = 14.06$) to produce electrons with $E_e > 6$ MeV that can emit Cerenkov light in water, but their energy is below the present energy threshold employed by the Kamiokande detector.

The flux of solar flare neutrinos has been estimated recently.⁸ The estimated flux when integrated over periods much longer than solar flares duration (a few hours) is much smaller than the flux atmospheric neutrinos, and thus cannot explain the observation of the KAMIOKANDE group.

Magnetic monopoles whose existence was predicted by grand unified theories¹¹ may catalyze proton decay with a cross section typical of strong interactions¹². Magnetic monopoles that impinge on the sun with typical galactic velocities lose sufficient energy via collisions with electrons and ions and fall to its center where they can induce proton decays. In minimal SU(5) neutrinos are produced only indirectly in the catalysis in sequences such as^{13,14}



The spectrum of ν_e 's from stopped muons is given by

$$\frac{dn_\nu}{dx} \cong 12 x^2 (1-x), \quad x \equiv 2E_\nu/m_\mu \quad (2)$$

Fig. 3 shows the neutrino cross section for the capture $\nu_e + {}^{16}\text{O} \rightarrow e^- + {}^{16}\text{F}^*$ weighted by the spectrum of ν_e 's from the decays of stopped muons.¹⁵ If the monopole flux in the solar system is smaller than the Parker bound¹⁶ $\phi_M < 10^{-16} \text{ cm}^{-2} \text{ sec}^{-1} \text{ sr}^{-1}$ then monopole catalysis of proton decays at the center of the sun could produce the excess events in the Kamiokande detector, only if⁰

$$B_\nu \bar{\sigma}_c \gtrsim 10^{-32} \text{ cm}^2 \quad (3)$$

where $\bar{\sigma}_c/\beta$ is the catalysis cross section ($\beta \equiv v/c$) and B_ν is the branching ratio for the ν_e producing channels. Thus at present the observations are not inconsistent with monopole catalysis of proton decays in the sun.¹⁴ This possibility however, will be ruled out if experiments will show that the excess events are not due to neutrinos which arrive from the direction of the sun, (utilizing the fact that the electrons in the reaction $\nu_e + {}^{16}\text{O} \rightarrow e^- + {}^{16}\text{F}^*$ which are produced by ν_e 's from stopped muons are peaked around 180° , as can be seen from Fig. 4)

We shall now examine whether more conventional sources of low energy neutrinos can explain the KAMIOKANDE results. Perhaps the brightest source of neutrinos with $10 \text{ MeV} \leq E_\nu \leq 100 \text{ MeV}$ is a gravitational stellar collapse. Neutrinos from a gravitational stellar collapse (GSC) are believed to be produced as follows¹⁷: In the final stages of the evolution of massive stars ($M \geq 8M_\odot$) when the heavy nuclear fuels have been exhausted, the gravitational pressure compresses the star and raises its temperature to such an extent that the iron nuclei in the core start to photodisintegrate into α particles. This nuclear disintegration of iron to helium costs a lot of internal energy causing further collapse and a large increase in the temperature. The temperature eventually reaches a point where electron capture (neutronization) occurs, i.e. $e^- + p \rightarrow n + \nu_e$. Consequently

the electron degeneracy pressure supporting the stellar core drops suddenly, the star becomes unstable, collapses to nuclear density and forms a hot neutron star (or a black hole). In the collapse to nuclear densities the gravitational energy that is liberated is about 10^{53} ergs. Most of this energy is radiated in the form of thermal $\nu\bar{\nu}$ pairs (produced by processes like $e^+e^- \rightarrow \nu+\bar{\nu}$) with energies in the range 10 to 100 MeV, corresponding to nearly 10^{58} neutrinos. This thermal neutrino pulse has a rise time of the order of a few milliseconds and a decay time of a few seconds, depending on details of the different collapse models.

The excess events in the KAMIOKANDE detector could not be due to a single burst in our galaxy since the duration of a neutrino burst from a GSC is a few seconds while the KAMIOKANDE events were distributed over 201 days. These events could rise however from a cosmological neutrino background that could have been formed by the gravitational stellar collapses that took place in galaxies which are within the horizon. A first estimate of this background can be obtained as follows:¹⁸

Let us denote by ρ_G the present density of galaxies in the universe, by r_{GSC} the average rate of GSC per galaxy, and by t_H the age of the universe. If we assume that r_{GSC} did not change significantly with time since galaxy formation then we obtain the following integral flux of cosmological neutrinos from gravitational stellar collapse

$$j_{\nu}(GSC) \sim n_{\nu}c \sim 10^{58} \cdot \rho_G \cdot r_{GSC} \cdot t_H \cdot c \quad . \quad (4)$$

From astronomical observations $\rho_G \sim 0.1xMpc^{-3}h_0^3$ and $t \sim 10^{10}h_0^{-1}$ years, where $0.5 \leq h_0 \leq 1$ is the present value of the Hubble parameter in units of $100 \text{ km} \cdot \text{sec}^{-1}/\text{Mpc}$. The rate of GSC per galaxy, r_{GSC} , is highly uncertain but rates of once every 10 to 40 years have been suggested¹⁹ based on optical and radio survey of supernovae in external galaxies and supernovae remnants in our galaxy. Pulsar birth rates have indicated collapse rates as high as once every 4 to 6 years. If one uses a "canonical" value, $r_{GSC}^{-1} \sim 10$ years, one obtains the estimate

$$j_{\nu}(GSC) \sim 10^{3\pm 1} h_0^2 \text{ cm}^{-2} \cdot \text{sec}^{-1}. \quad (5)$$

The energy of the GSC neutrinos is red-shifted during the expansion of the universe. If one introduces the red shift parameter $z(t) \equiv R_0/R(t)-1$ to describe the cosmological expansion of the scale parameter R from time t to the present time (subscripts 0) then for a Robertson-Walker metric, a zero cosmological constant and a matter dominated universe, the Hubble parameter $H \equiv \dot{R}/R$ satisfies

$H = H_0 \sqrt{1 + \Omega_0 z}$, where Ω_0 is the present energy density of the universe in units of the critical density for closure $\rho = \Omega_0 \rho_c$ where $\rho_c = 3H_0^2 (8\pi G)^{-1}$. Consequently

$$dz = -(1+z)^2 \sqrt{1 + \Omega_0 z} dt \quad (6)$$

and the present neutrino flux is given by

$$\frac{d^2 j_\nu}{dE_0 d\Omega} = \frac{c}{4\pi H_0} \int_0^\infty \frac{n_{\text{GSC}}(z) \mathcal{L}_\nu((1+z)E_0)}{(1+z)^4 \sqrt{1 + \Omega_0 z}} dz \quad (7)$$

where \mathcal{L}_ν is the differential luminosity of the collapsing star (neutrinos per unit energy at energy $(1+z)E_0$) and $n_{\text{GSC}}(z)$ is the number of GSC per unit volume per unit time at red shift z . The rate $n_{\text{GSC}}(z)$ is different from zero only for times later than galaxy formation ($z \ll 20$?) and it is highly model dependent. Also \mathcal{L}_ν the neutrino luminosity from a single GSC is highly model dependent¹⁷. Thus at present Eq. (7) cannot be used to obtain reliable estimates of the spectrum of the cosmological GSC neutrinos.

Nevertheless, let us derive an estimate of the number of events in a water detector due to the cosmological GSC neutrino background. The coupling rate in neutrino detector is proportional to $\int (dj_\nu/dE) \sigma_\nu(E) dE$. For the neutral current reactions, $\sigma_\nu \sim \alpha E$, while for the charged current reaction $\sigma_\nu \sim \beta E^2$. Therefore the counting rate is proportional to $\alpha j_{\alpha \langle E \rangle_{\text{RS}}}$ and $\beta j_{\nu \langle E^2 \rangle_{\text{RS}}}$, respectively, where j_ν is the integrated neutrino flux and the brackets indicate averaging with the red shifted distributions. If the rate of GSC per co-expanding unit volume has been constant since galaxy formation, i.e. if $(1+z)^{-3} n_{\text{GSC}}(z) = n_{\text{GSC}}(0)$ then it follows from Eq. (7) that

$$\langle E^k \rangle_{\text{RS}} \cong \langle E^k \rangle \int_{t_1}^{t_0} [R(t)/R(t_0)]^k dt/t_0 \quad (8)$$

where t_1 is the initial time of GSC, which can be taken to be zero without affecting the numerical result. For the recent era of matter dominated universe, $R(t) \sim t^{2/3}$ and consequently

$$\langle E^k \rangle_{\text{RS}} \cong \frac{3}{3+2k} \langle E^k \rangle \quad (9)$$

Thus the net effect of expansion is to reduce $\langle E \rangle$ and $\langle E^2 \rangle$ by the factors 3/5 and 3/7, respectively. In Table II we list typical neutrino luminosities for type II supernovae that were obtained by J.R. Wilson for a GSC of a massive star

with $M = 25M_{\odot}$.

TABLE II

Neutrino Luminosities from a GSC, $M = 25M_{\odot}$

	ν_e	$\bar{\nu}_e$	ν_{μ}	$\bar{\nu}_{\mu}$	ν_{τ}	$\bar{\nu}_{\tau}$	$\Sigma\nu$
n_{ν}	4.5×10^{57}	3.1×10^{57}	2.3×10^{57}	2.3×10^{57}	2.3×10^{57}	2.3×10^{57}	1.7×10^{58}
$\langle E_{\nu} \rangle$	14 MeV	15 MeV	32 MeV	32 MeV	32 MeV	32 MeV	26 MeV
$\langle E_{\nu}^2 \rangle$	16^2 MeV^2	17^2 MeV^2	36^2 MeV^2	36^2 MeV^2	36^2 MeV^2	36^2 MeV^2	30^2 MeV^2

Using these values one obtains event rates in the Kamiokande water detector that are listed in Table I.

TABLE I

Cross sections and event rates for elastic and quasielastic neutrino interactions in 0.88 kiloton water detector.

Reaction	Cross Section ($\times 10^{-44} \text{ cm}^2$) $E_{\nu} < 100 \text{ MeV}$	No. of Events in 0.88 Kt Water		
		Atmospheric $\nu_e + \bar{\nu}_e$ at Kamioka with $E_{\nu} < 100 \text{ MeV}$ (201 days)	GSC at 10 Kpc	GSC Background (201 days)
$\bar{\nu}_e + {}^{16}\text{O} \rightarrow {}^{16}\text{N}^* + e^+$ $\nu_e + {}^{16}\text{O} \rightarrow {}^{16}\text{F}^* + e^-$	Ref. 15	0.12	214	2
$\bar{\nu}_e + p \rightarrow n + e^+$	$7.5 \times E_{\nu}^2$	0.2	382	3
$\nu_e + e^- \rightarrow \nu_e + e^-$	$1.0 \times E_{\nu}$	0.002	18	0.2
$\bar{\nu}_e + e^- \rightarrow \bar{\nu}_e + e^-$	$0.30 \times E_{\nu}$	0.001	4	0.1
$\nu_{\mu} + e^- \rightarrow \nu_{\mu} + e^-$	$0.15 \times E_{\nu}$	0.0003	3	0.04
$\bar{\nu}_{\mu} + e^- \rightarrow \bar{\nu}_{\mu} + e^-$	$0.15 \times E_{\nu}$	0.0003	3	0.04
$\nu_{\tau} + e^- \rightarrow \nu_{\tau} + e^-$	$0.15 \times E_{\nu}$	0.0003	3	0.04
$\bar{\nu}_{\tau} + e^- \rightarrow \bar{\nu}_{\tau} + e^-$	$0.15 \times E_{\nu}$	0.0003	3	0.04
Sum		0.32	630	5.5

In a 0.485 kiloton-year water exposure the total number of events that are expected to be induced by the cosmological background of GSC neutrinos is therefore $5.5 \times 10^{0 \pm 1}$, consistent with the experimental results of the Kamiokande group. However, the theoretical estimate is uncertain by more than an order of magnitude. Therefore at present no definite conclusion can be drawn. In particular the efficiency of the neutrino detector decreases dramatically below 30 MeV. The rate, therefore, becomes a sensitive function of the neutrino spectrum from GSC. To produce a realistic neutrino spectrum one must use a GSC numerical code with a realistic neutrino transport code. Such a code must modify the charged current and the neutral current cross sections on isolated stationary electrons, positrons, nucleons and nuclei, and take into account the thermal motion of the "target" particles, the excitation of target nuclei and in particular the Fermi blocking due to the high degeneracy of electrons, positrons, neutrinos, etc. Consequently the effective neutrino cross sections become very complicated functions of the thermodynamic and chemical conditions which are changing rapidly as function of position and time. Generally, the effective cross sections become smaller than their values on free particles and may thus produce harder neutrino spectra than those which are currently produced by the numerical GSC codes.

FIGURE CAPTIONS

- Fig. 1. Comparison between the energy distribution of single electrons due to elastic and quasielastic ν -interactions in 0.485 kiloton-year water exposure at Kamioka and the theoretical expectation due to atmospheric neutrinos.
- Fig. 2. The flux of atmospheric ν_e 's and $\bar{\nu}_e$'s at Kamioka.
- Fig. 3. Calculated cross section¹⁵ for the reaction $\nu_e + {}^{16}_0\text{e}^- + {}^{16}_F^*$ as function of energy weighted by the spectrum of neutrinos of stopped muons.
- Fig. 4. Calculated cross section¹⁵ for the reaction $\nu_e + {}^{16}_0\text{e}^- + {}^{16}_F^*$ as function of the electron angle summed over all levels of ${}^{16}_F$ and weighted by the neutrino spectrum of stopped muons.

REFERENCES AND FOOTNOTES

1. Y. Totsuka, Proceedings of the XIXth Rencontre De Moriond La Plagne France, Vol. 1, 625 (1984) (Ed. J. Tran Thanh Van).
T. Suda, Talk presented at "Neutrino 84" Int. Conf., Dortmund, Germany 1984 (unpublished).
2. A. Dar, Phys. Rev. Lett. 51, 227 (1983).
3. D. Cooke, Phys. Rev. Lett. 51, 320 (1983).
4. S.L. Glashow, Nucl. Phys. 22, 579 (1961).
A. Salam in "Elementary Particle Theory" ed. N. Svartholm, p. 367, Stockholm 1968 (Almquist and Wiksell Pub.).
S. Weinberg, Phys. Rev. Lett. 19, 1264 (1967).
5. See for instance, P.Q. Hung and J.J. Sakurai, Ann. Rev. Nucl. Part. Sci. 31, 375 (1981) and references therein.
6. T.K. Gaisser, Proc. of "Neutrino 84" Int. Conf., Dortmund, Germany 1984 (to be published).
7. See for instance J.N. Bachall et al., Rev. Mod. Phys. 54, 787 (1982) and references therein.
8. A. Dar and S.P. Rosen, "High Energy Solar Neutrinos and Proton Decay Detectors", submitted for publication in Phys. Rev. Lett. (Preprint LA-UR. 84-).
9. J. Arafune and M. Fukugita, Phys. Lett. 133B, 380 (1983).
M. Fukugita, "Monopoles in the Solar System, Proc. Int. Conf. Symposium on Cosmic Rays and Particle Physics, Tokyo 1984.
10. M. Koshiha, Proc. XXII Int. Conf. on High Energy Physics, Leipzig, Germany 1984.
11. G. 't Hooft, Nucl. Phys. B79, 276 (1974),
A.M. Polyakov, JETP Lett. 20, 194 (1974).
12. V.A. Rubakov, JETP Lett. 33, 645 (1981); Nucl. Phys. B203, 311 (1982).
C.G. Callan, Phys. Rev. D26, 2058 (1982),
F. Wilczek, Phys. Rev. Lett. 48, 1146 (1982).
13. J. Ellis et al., Phys. Lett. 116B, 127 (1982).
F.A. Bais et al., Nucl. Phys. B219, 189 (1983).
14. J. Arafune and M. Fukugita, Phys. Rev. Lett. 50, 1901 (1983).
15. J.B. Langworthy et al., Nucl. Phys. A280, 35 (1977);
E. Bugaev et al., Nucl. Phys. A324, 350 (1979).
16. E.N. Parker, A. J. 160, 383 (1970),
M.S. Turner et al., Phys. Rev. D26, 1296 (1982).
17. See for instance, J.C. Wheeler, Reports on Progress in Physics 44, 85 (1981), and references therein.

18. Earlier estimates of the cosmological neutrino background generated by gravitational stellar collapse include:
 - A. Dar, "High Energy Neutrino Astronomy" a lecture at the XVIII Rencontre De Moriond, La Plaigne, France, March 1983.
 - S. Bludman, private communication, 1983.
 - L.M. Krauss, S.L. Glashow and D.N. Schramm, Nature 310, 191 (July 1984).
19. See for instance S. Weinberg, Gravitation and Cosmology" (Wiley, N.Y. 1972)
 - A. Sandage and G.A. Tammann, Ap. J. 196, 313 (1975); 197, 266 (1975).
20. See for instance K. Lande, Ann. Rev. Nucl. Part. Sc. 29, 395 (1979);
 - V. Trimble, Rev. Mod. Phys. 54, 1183 (1983) and references therein.

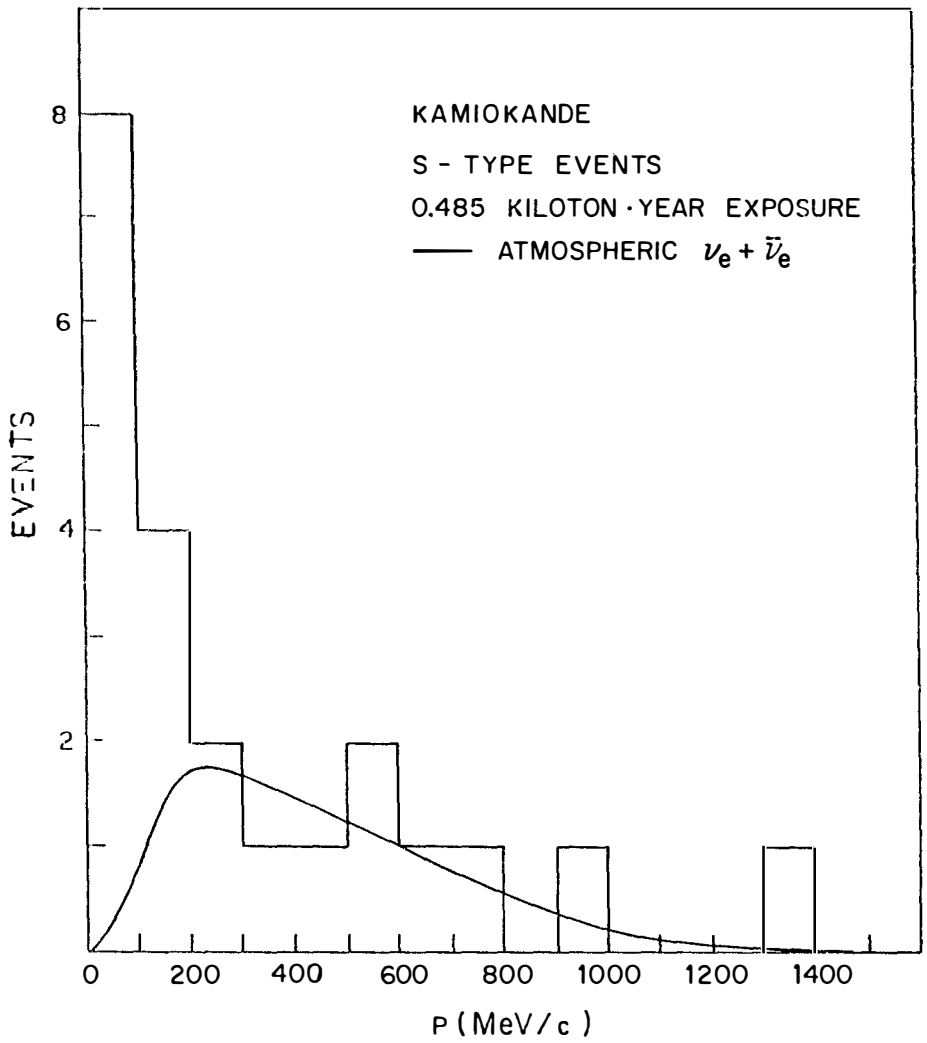


Fig. 1

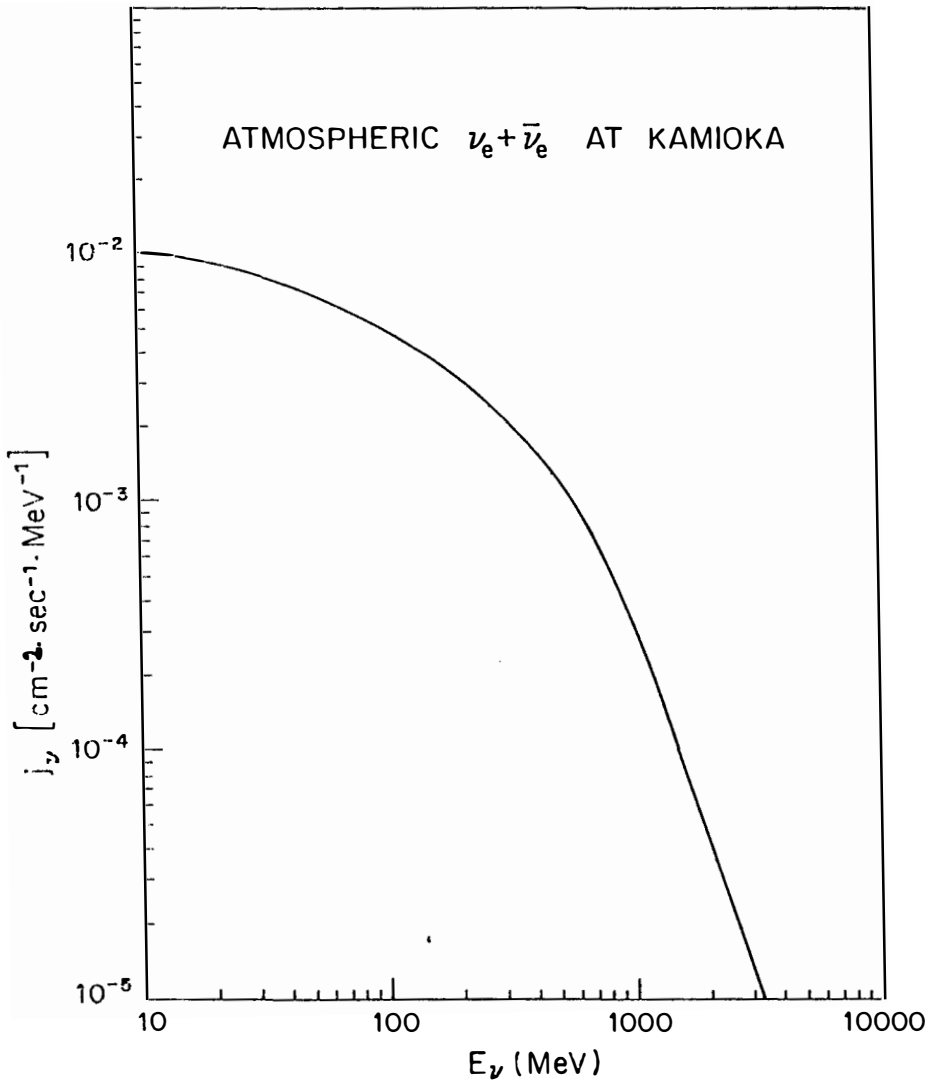
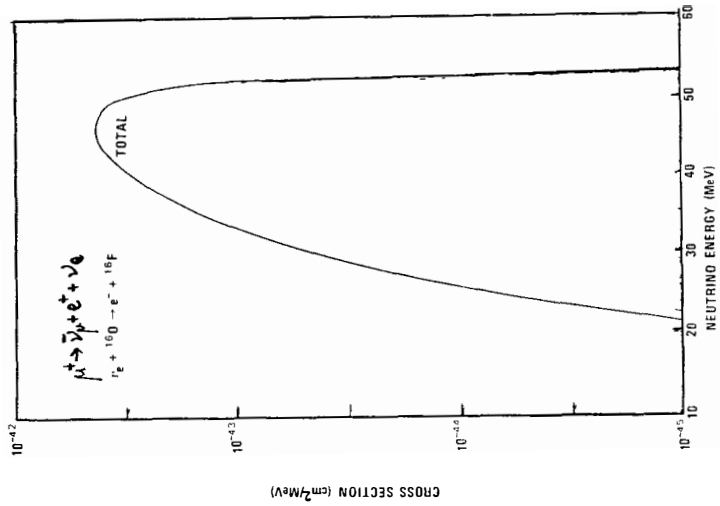
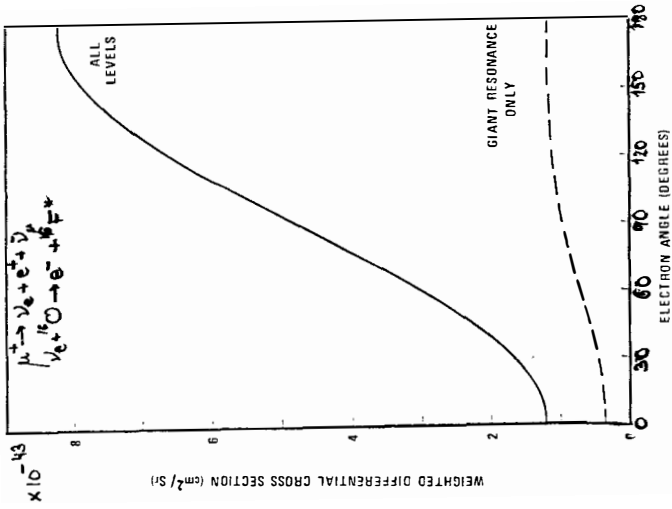


Fig. 2



STATUS OF THE FREJUS NUCLEON DECAY EXPERIMENT
 Aachen-Orsay-Palaiseau-Saclay-Wuppertal collaboration

G. GERBIER
 DPhPE, CEN SACLAY, 91191 Gif sur Yvette, Cedex, France



ABSTRACT

The Fréjus proton lifetime detector is a 904 ton fine grain calorimeter located in the Fréjus tunnel in the Alps, at the French Italian border, at a depth of 4800 MWE. Its mounting has just been completed (March 1985) and part of the detector has been operated for about 1 year.

Fourteen contained events (corresponding to a fiducial tonnage of 200 ton year) have been observed among which no candidates for nucleon decay in the modes $e^+ \pi^0$, $\mu^+ K^0$. Samples of 71 000 single mu and of 2000 multimuons have been reconstructed; they are currently analysed in view of determining the primary cosmic ray composition at energies around 10^5 to 10^6 GeV and for point source origin effects.

1 - Introduction

The Fréjus detector is a track visualising type detector with a very fine grain (5*5 mm cell), designed to study the nucleon decay. It is also well suited for cosmic ray physics through the analysis of the muon and multimMuon events.

After a brief description, the main properties of the detector and its working conditions will be presented; then, some results will be given about the contained events and the multimMuon events.

2 - Brief description

The laboratory is located in a gallery inside the highway Fréjus tunnel between Modane-France and Bardonecchia-Italy (Fig 1) ; the mean thickness of rock which is traversed by muons coming from the atmosphere above is about 1800 meters which corresponds to 4800 MWE. The measured muon flux is 4.2 muon/m²/day (horizontal surface).

The detector has a modular structure ; it is composed of sandwiches of iron plates which provide the mass, of geiger tubes which provide the trigger, and of flash chambers which give the fine resolution ; these planes of 6*6 meters are mounted vertically with the cell direction alternatively in the horizontal and vertical direction (Fig 2). This provides two orthogonal "views" of the detector, called "side" view and "top" view hereafter. The main characteristics of the detector are summarized in Table 1.

Table I
Main characteristics of the Fréjus detector

Total mass	904 tons
Fiducial mass	575 tons
Dimensions	6 x 6 x 12 meter 3
Average density	2 g/cm ³
Flash Chambers (Polypropylène)	
Size of a cell	0.5 x 0.5 cm ²
Sampling	3mm of iron
Gaz composition	He-Ne (30-70)
High voltage	8 KV
Total number of cells	900 000
Geiger planes	
Size of a cell	1.7 * 1.7 cm ²
Sampling	24 mm of iron
Gaz composition	Ar-C ₂ H ₅ OH (98-2) + Freon 70 ppm
Total number of cells	40 000
Resolution time	200 ns

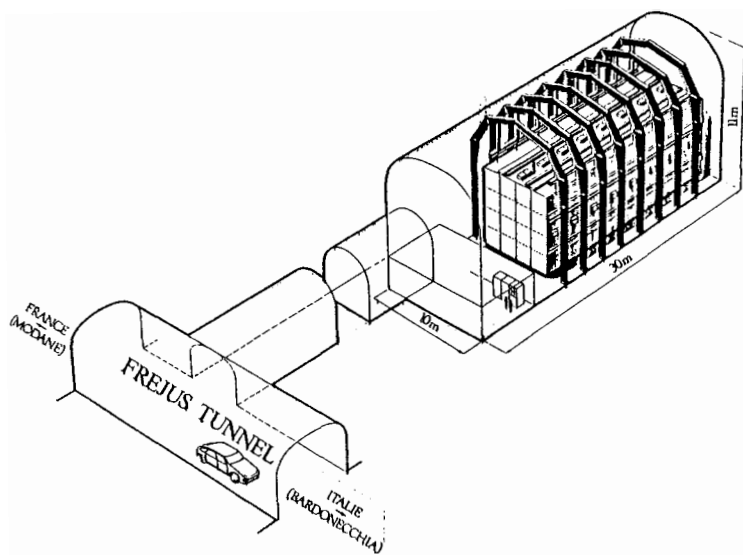


Fig. 1 - Overview of the gallery

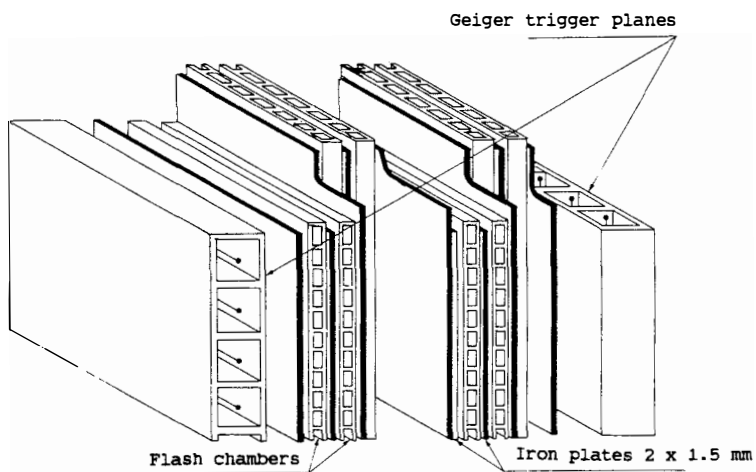


Fig. 2 - Structure of a basic module

The flash chambers are triggered by the Geiger system : when a trigger occurs, a high voltage pulse is applied to each flash element through a spark gap which discharges a distributed delay line. The induced electric field is 8 KV/cm : if the passage of a particle has produced ionisation in a cell, a plasma forms and propagates over the full length of the cell. For more details, see the references [1].

The mounting has begun in September 1983 and has been completed in March 1985.

3 - Working conditions of the detector

The trigger conditions which have been required until now, are the following: 5 Geiger tubes should be hit in 5 consecutive planes with at most 3 tubes per plane. The total trigger rate (for a 800 Tons detector) is 38 per hour, which splits in 18 physical events (mainly muons) and 20 background events. This rate induces a dead time of 3 % due to the flash chambers.

The efficiency to detect a nucleon decay for which all the energy is deposited in the detector is very high, from 85 to 90 %, depending on the decay mode.

The energy threshold is about 250 MeV for a muon, and 150 MeV for an electron. To get a lower energy threshold, one could lower the required total number of tubes, but then the background rate due to radioactivity gets higher and the total dead time due to the flash chambers increases. The actual trigger conditions are a compromise between these requirements. The situation cannot be much improved without changing the electronics.

The flash chambers are working well; their efficiency is nearly constant and has been determined to be of the order of 80 %. This value corresponds to a minimum delay between the time at which the trigger arrives and the time at which the high tension is discharged in the flash chambers of about 1.2 μ s. Increasing this time delay allows to detect more electrons from muon decays but induces a decrease of the efficiency of about 5 % per microsecond added delay. This parameter has to be tuned.

The efficiency for the detection of $\mu \rightarrow e$ decay, combining the topological information from Geiger and flash tubes, for the above quoted time delay, is about 65 %.

The noise in the flash chambers is due to radioactivity and noisy cells ; it is very low, of $6 \cdot 10^{-5}$ per cell, with equal contributions from both sources. This corresponds to less than 1 background cell in the volume occupied by a typical nucleon decay.

4 - Data acquisition

Thanks to its modular structure, part of the detector could be operated during the period of mounting; the data taking started in march 1984 and the mass in acquisition was increased by megamodules of 80 tons. Now (March 1985) the detector is completed (904 Tons).

The corresponding integrated luminosity is 345 ton year for the whole mass, and 200 t.y for a fiducial volume defined by taking off a veto region of 50 cm.

As the trigger rate is low, the events are scanned and identified nearly on-line. So far, 71 000 single muons, 2000 multimuons, 470 "exotic" events (big hadronic or electromagnetic showers) and 30 events possibly produced in the detector have been observed.

5 - The contained events

An event is said to be "contained" if its vertex is inside the fiducial volume defined above; its tracks may leave the fiducial volume or even the detector itself.

Among the 30 above quoted events, 14 events fulfill the containment criterium. Some of them are shown on Fig 3 and 4. The fine granularity allows to well separate the tracks (Fig 3) and the electrons are well identified by their showering (Fig 4). The events have then been split in 7 ν_μ , 5 ν_e induced charged current interactions and 1 probable neutral current event with neither obvious muon candidate nor showering track.

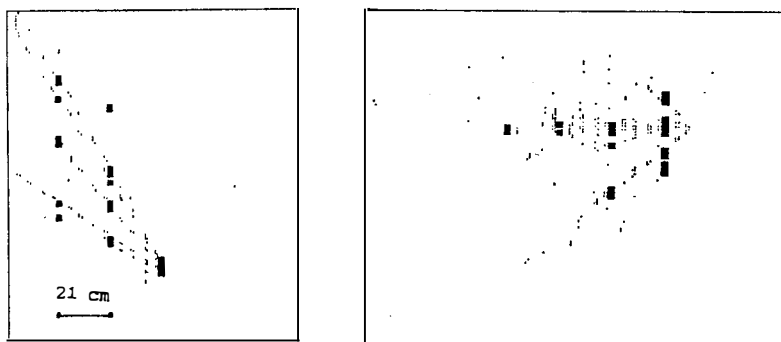


Fig. 3,4 - Neutrino interactions (zoom)
Big squares are the geiger tubes, dots are the flash cells

There is no event compatible with a nucleon decay with a charged lepton in the final state, more precisely with the total energy deposited in the detector. The events which could be interpreted as nucleon decay with a neutral lepton in the final state are under study.

The energy calibration for electrons has been done with a test module at DESY. It has been found that the energy is approximately proportional to the number of hit flash cells till 1 GeV (140 cells per GeV), with a resolution of 12 % at 1 GeV. The energy of the muons is obtained from their range with a resolution of 70 MeV at 500 MeV. This module has also been put in a pion beam at Bonn; the data are currently analysed.

It should be noticed that these events include one single track interaction which has been interpreted as an upgoing muon stopping in the detector. However, the track direction is not always possible to determine and some more work is needed to know our ability to do it from the multiple scattering analysis for particles of momenta lower than 500 MeV/c.

Another important point, for the rejection of neutrino background, is a good knowledge of the atmospheric neutrino interactions in the detector ; for that purpose, we are analysing the films of the Aachen-Padova experiment using streamer chambers exposed in the PS neutrino beam [2]. The sampling and mean density are quite similar to those of the Fréjus detector.

6 - Muon and multimuon events

Its large acceptance ($500 \text{ m}^2 \cdot \text{sr}$), good spatial resolution (separation of 2 tracks down to 1 cm in space), good angular resolution (a few mrad), make this detector well adapted to multimuon and muon events study.

About 71000 single and 2000 multimuon events have been reconstructed ; their multiplicity distribution is shown on Fig 5: multiplicities as high as 15 have been observed (Fig 6).

Two main topics are under study : the primary cosmic ray composition and the point source hunting. There are not yet definitive results concerning these analyses, but the main motivations will be shortly presented.

a) Primary composition

Let us recall that the muon multiplicity and the spatial separation between the muons of multimuon events are variables which are sensitive to the primary cosmic ray composition and especially to the presence of high mass elements [3]. This composition is well known at low energies (up to 10^4 GeV) from the emulsion chamber experiments and at high energies (greater than 10^7 GeV) from the large air shower array detectors [4]. However, at the intermediate energies, the data seem contradictory and difficult to interpret.

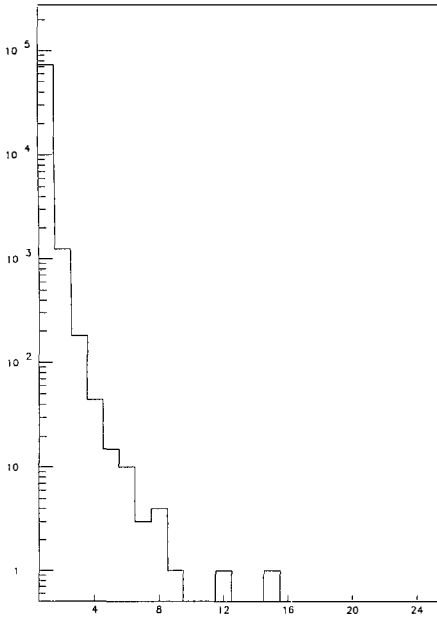


Fig. 5 - Muon multiplicity distribution

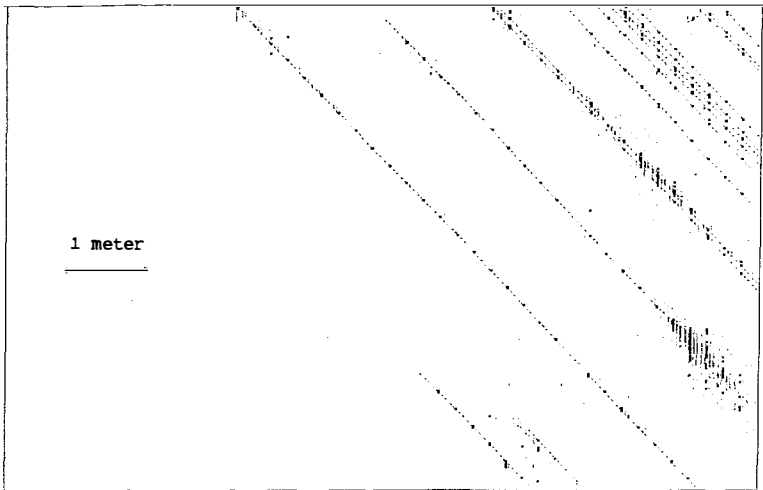


Fig. 6 - Multimuon event (15 muons) . Side view

By chance, the depth of the Fréjus detector is such that the energy of the primary particles giving rise to the muon and multimMuon events observed in the detector spans the region 10^4 to $5 \cdot 10^6$ GeV.

The data, however, have to be interpreted via a Monte Carlo simulation of the chain primary interaction-cascade-propagation, which is being developed.

b) Point source hunting.

Great attention has been paid to this subject at these Rencontres, especially to the production of high energy neutrinos from binary systems like Cygnus X3 (A. Dar communication). The Fréjus detector is not in good position for that search because of the difficulty to separate upgoing crossing muons induced by neutrino interactions in the rock from normal downgoing muons.

Nevertheless, two underground experiments have already reported an observation of an excess of normal downgoing muons pointing towards a region around Cygnus X3 [5]. We focus the analysis in that direction.

7 - Conclusion

The detector, which has just been completed, works well. No event compatible with a nucleon decay with all the energy deposited inside the detector have been observed so far. Within one year, the luminosity will have been increased by a factor three. So, there is still room for surprises.

References

- [1] J. Ernwein, XVII th Rencontres de Moriond (1982)
- [2] H. Faissner et al., Phys. Rev. Letters 41 (1978) 213
- [3] T.K. Gaisser, Science Underground, (Los Alamos, 1982)
AIP Conference Proceedings N° 96.
- [4] J. Linsley, XVIII th International Conference on Cosmic Ray,
Bangalore, 1983
- [5] SOUDAN 1 experiment
J. Bartelt et al., preprint ANL-HEP-PR-84-80
M.L. Marshak et al., preprint ANL-HEP-PR-85-19
NUSEX communication, Saint Vincent Conference (Aoste 1985)

LATEST RESULTS FROM THE NUSEX EXPERIMENT

NUSEX Collaboration: LNF-Milano-Torino-CERN[†]

Presented by Stefano Ragazzi

I.N.F.N. Milano

ABSTRACT

27 fully contained events have been observed in 2.4 years of operation of the 150 tons detector installed in the Mt. Blanc Laboratory. Data concerning nucleon lifetime and neutrino interaction rate are presented in this paper.

[†] G. Battistoni, E. Bellotti, G. Bologna, P. Campana, C. Castagnoli, V. Chiarella, A. Ciocio, D.C. Cundy, B. D'Ettorre Piazzoli, E. Fiorini, P. Galeotti, E. Iarocci, C. Liguori, G. Mannocchi, G.P. Murtas, P. Negri, G. Nicoletti, P. Picchi, M. Price, A. Pullia, S. Ragazzi, M. Rollier, O. Saavedra, L. Satta, L. Trasatti, L. Zanotti.

I. THE SITE

The detector is installed in a garage beside the road tunnel under the Mont Blanc at 45.8° N latitude and 6.9° E longitude, 42.7° geomagnetic latitude. The slant depth is greater than 4800 hg/cm^2 standard rock in every direction (Fig. 1).

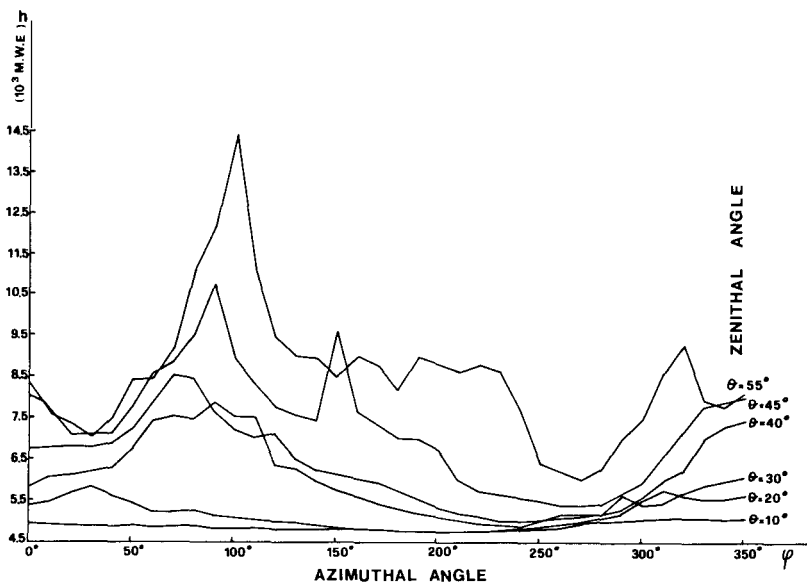


Fig. 1. Laboratory overburden (hg/cm^2 s.r.) as a function of azimuth and zenith angles.

II. THE DETECTOR

The detector is a digital tracking calorimeter. It consists of a sandwich of 136 iron plates $1 \text{ cm} \times 3.5 \times 3.5 \text{ m}^2$ interleaved with plastic streamer tubes 3.5 m long $9 \times 9 \text{ mm}^2$ cell size. Total mass is 150 tons, the average density is 3.5 gr/cm^3 . The tubes are made of extruded PVC coated with high resistivity varnish acting as cathode. Anode wires diameter is $100 \mu\text{m}$. Tubes are operated at 3.9 kV with an $\text{Ar-CO}_2\text{-Pentane}$ (1+2+1) gas mixture. Bidimensional read out is obtained for each plane by means of longitudinal (X) and transversal (Y) strips. X strips, parallel to wires, are 4 mm wide and 6 mm spaced, Y strips are 10 mm wide and 2 mm spaced. The total number of read out elements is 81472. The streamer induced pulses ($>2 \text{ mV}/50 \Omega$) from the strips are discriminated and shaped to $7 \mu\text{s}$, in case of trigger they are read out through a shift register chain. A single readout bus is used for 1 plane, (608 strips). A fast OR signal, available for each plane, is used for trigger logic and timing information. Trigger logic is based on coincidences, within $1 \mu\text{s}$, of contiguous planes. Minimum trigger requirements

are 4 contiguous planes hit, or 1 triple plus 1 double, or 3 doubles. A TDC with 100 ns resolution is available in order to register hit time for each plane. Delayed positrons from stopping μ^+ can thus be detected with 35% efficiency. An independent system (monopole trigger) based on a 9-fold delayed coincidence between groups of planes has also been installed in order to trigger on slowly moving low ionizing penetrating particles. It is estimated to be sensitive to particles with $\beta > 2 \times 10^{-4}$ and ionizing at least 2×10^{-2} of a minimum ionizing particle. A detailed description of the apparatus is given in ref. 1.

III. DETECTOR CALIBRATION

During 1981 a test module reproducing in structure the Mt. Blanc detector was exposed at CERN to e , π and ν beams²⁾.

Runs with electrons and pions were carried out at beam momenta ranging from 0.15 to 1.5 GeV/c, and at various angles of incidence. Data from these runs were used to obtain energy calibration curves and to develop algorithms for e/π separation and shower direction recognition^{1,2)}.

The neutrino run²⁾ was specifically carried out to obtain an estimate of the neutrino background to proton decay with a detector of the same structure (same systematics) as the nucleon decay detector. Great care was also devoted to reproducing the atmospheric neutrino spectrum in the 1 GeV region. A total of 403 neutrino events, corresponding to ~ 35 years of running at Mt. Blanc, were obtained in two runs with detector axis at 0° and 45° with respect to the beam. The background estimates quoted in next section rely on direct calibration, not on simulation or extrapolation of data taken with different detectors and different systematics.

IV. RESULTS

Data were collected during 21229 hours live time, from June '82 to March '85, with live time/solar time = 0.87. The corresponding sensitivity is 2.19×10^{32} nucleons \times year. We searched for fully contained events according to the following criteria:

- a) event vertex must be inside the detector volume;
- b) tracks coming from vertex must stop inside the detector;
- c) no incoming track must be associated to the event.

In this way we guarantee to collect only events due to ν interaction in the detector, and possibly nucleon decay, being the neutron background negligible.

27 events were observed satisfying these requirements.

i) Neutrino rates.

The visible energy spectrum of the 27 contained events is shown in Fig. 2. Due to uncertainties in trigger and scanning efficiency at very low energy we applied a further cut requiring $E_{vis} > 250$ MeV. We are thus left with 26 events. Considering all these events as due to ν interactions, we can identify 18 of them as due to ν_μ interactions, 7 as ν_e interactions, while 1 is ambiguous $\nu_\mu - \nu_e$. I would like to remark that in Fig. 2 is shown the visible energy spectrum not corrected for losses due to unseen

neutrals, soft protons, π absorption and fast protons identified as pions.

Correcting for overall detection efficiency on an event by event basis we obtain for the ν interaction rate in our laboratory:

$$\nu_{\text{rate}} = 136 \pm 28 \nu / (\text{kton} \cdot \text{year})$$

and for the ratio of ν_e to ν_μ interactions:

$$\nu_e / \nu_\mu = 0.34 \pm 0.14$$

It has to be noted that these rates, though independent on assumptions on atmospheric neutrino spectrum, are slightly biased because the containment efficiency for muon neutrinos is near to zero for energies above 2 GeV. A more detailed analysis of atmospheric neutrinos is under way in our collaboration; we hope to present soon more complete results.

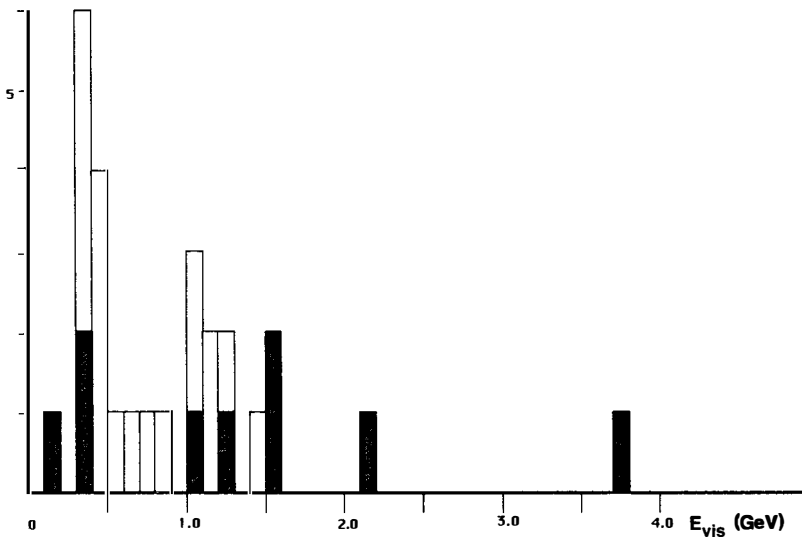


Fig. 2. Visible energy spectrum of contained events. Shaded areas represent ν_e .

ii) Nucleon decay.

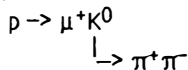
In order to obtain a better event reconstruction, therefore a higher discrimination against neutrino interactions, we applied further cuts in nucleon decay analysis:

- in 1 prong/shower final states the angle with the normal to iron plates is required to be less than 60° ;
- for $e\pi$, $\mu\pi$ candidates the lepton angle with the normal to plates must be less than 60° ;
- in events candidates for decay channels with ≤ 3 prongs in the final state each particle must hit at least two planes.

Applying these cuts and requiring kinematical fit to a possible nucleon decay channel we find 7 candidates in the $\nu\pi\pi^+$ channel, 1 in the μ^+K^0 , 1 in the $e^+\pi^0$.

The seven candidates for the $\nu\pi\pi^+$ channel are well consistent with the estimated background of six events from elastic ν_μ interactions. The limit to decay rate in this channel is obtained after background subtraction.

The candidate in the μ^+K^0 channel (event 1) has been extensively discussed in previous papers^{3,4,5}. As reported there it fits the hypothesis:



with:

$$p_\mu = 0.38 \pm 0.15 \text{ GeV}/c, M_{\pi\pi} = 0.55 \pm 0.08 \text{ GeV}/c, p_K = 0.3 \pm 0.1 \text{ GeV}/c, E = 1.0 \pm 0.2 \text{ GeV}, p = 0.4 \pm 0.2 \text{ GeV}/c.$$

This event also fits the hypothesis $p \rightarrow \nu K^*$ and $p \rightarrow 3\mu^3$. From the analysis of ν test data we find 2 events, out of 403, simulating the decay $p \rightarrow \mu^+ K^0$ (or the decay in any 3 prong final state with no missing energetic neutral). Normalizing to the total number of ν_μ interactions in the Mt. Blanc detector we estimate a background of 0.1 ± 0.07 events for this channel.

Event 22 (Fig. 3) is a candidate for the $e^+\pi^0$ channel. It is identified by our shower reconstruction algorithm as 22 showers back to back. The best hypothesis is 3 showers with:

$$\begin{aligned} E_1 &= 370 \pm 110 \text{ MeV}, E_2 = 550 \pm 140 \text{ MeV}, E_3 = 140 \pm 80 \text{ MeV}, \theta_{12} = 160^\circ, \theta_{13} = 140^\circ, \theta_{23} = 50^\circ, \\ E_{\text{tot}} &= 1060 \pm 200 \text{ MeV}, p = 250 \pm 150 \text{ MeV}. \text{ With } \pi^0 \text{ mass constraint on showers 2 and 3 we obtain:} \\ E_2 &= 525 \text{ MeV}, E_3 = 50 \text{ MeV}, E_{\text{tot}} = 945 \pm 170 \text{ MeV}, p_{\text{tot}} = 230 \pm 150 \text{ MeV}. \end{aligned}$$

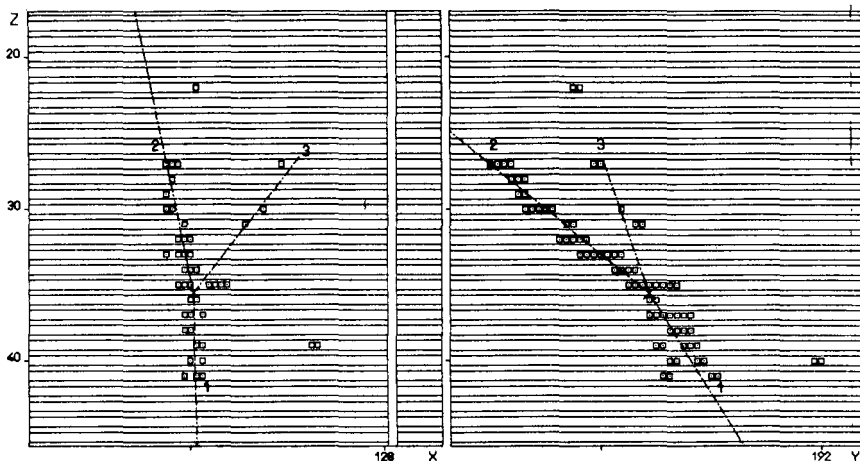


Fig. 3. Event 22.

There are 2 sources of background for this topology:

- a) $\nu_e + N \rightarrow e + \pi^0 + \text{unseen hadrons}$

Background from this source is evaluated from the rate of $\mu\pi\pi$ events with $\theta_{\mu\pi} > 120^\circ$ in our neutrino test. Then multiplying by the relative frequency of $\mu\pi^0$ events with respect to total of $\mu\pi\pi$ we find that $0.5 \pm 0.3\%$ of ν_e interactions are expected to produce the $e^+\pi^0$ topology with an opening angle between e and π^0 greater than 120° . Normalizing to 7 ν_e events, observed in Mt. Blanc, with shower axis at less than 60° to the normal to iron plates, we expect a background of 0.04 ± 0.02 events from this source.

b) $\nu_e + N \rightarrow e +$ unseen hadrons, with the single shower misidentified as ≥ 2 showers

If event 22 is reconstructed under the single shower hypothesis we obtain: $E = 1.5 + 0.35 / -0.30$ GeV. From our calibration data with electron beams we find that 9% of the 1.5 GeV electrons, incident at an angle nearly equal to the one reconstructed for event 22, are reconstructed as ≥ 2 showers back to back. Normalizing to 2 elastic ν_e events (including event 22) in the energy range 1. – 1.5 GeV and shower axis at less than 60° to normal we estimate a background of 0.18 ± 0.06 events from this source.

Total background to the $e^+\pi^0$ channel is then 0.22 ± 0.07 events.

However I would like to point out that if we consider together the four decay channels of nucleon into charged lepton plus pion, the total background is ~ 1 event; i.e., with the present exposure, we expect about one background event in one of the four channels.

Limits on nucleon lifetime divided by branching ratio for different nucleon decay channels are summarized in Table 1.

TABLE 1. NUCLEON LIFETIME LIMITS

DECAY MODE	CANDIDATES	BACKGROUND	τ /B.R. YEARS (90% C.L. limit)
$p \rightarrow e^+\pi^0$	1	0.22	$> 0.6 \times 10^{31}$
$n \rightarrow e^+\pi^-$	0		$> 0.8 \times 10^{31}$
$N \rightarrow e^+\pi$			$> 1.0 \times 10^{31}$
$p \rightarrow \mu^+\pi^0$	0		$> 0.7 \times 10^{31}$
$n \rightarrow \mu^+\pi^-$	0		$> 0.4 \times 10^{31}$
$N \rightarrow \mu^+\pi$			$> 1.1 \times 10^{31}$
$p \rightarrow \nu\pi^+$	7	6	$> 0.2 \times 10^{31}$
$n \rightarrow \nu\pi^0$	0		$> 1.1 \times 10^{31}$
$p \rightarrow \nu K^+$	0		$> 0.8 \times 10^{31}$
$n \rightarrow \nu K^0$	0		$> 0.9 \times 10^{31}$
$p \rightarrow \mu^+K^0$	1	0.1	$> 0.7 \times 10^{31}$

iii) Search for point-like sources of cosmic rays.

As reported elsewhere ⁶⁾ the Nusex detector is crossed by ~ 27 cosmic muons per day. The structure of our detector allows reconstruction with an error of 0.5° of the muon direction.

An analysis of single muons is presently performed searching for point-like cosmic rays sources. By now we have an indication of a signal coming from the direction of Cygnus x-3, an X-ray and high energy γ -ray source, correlated in time with the 4.8 hours period observed both in X ^{7,8)} and γ rays⁹⁻¹²⁾. As this signal shows the unpleasant feature of a dispersion around the source inconsistent with what expected from multiple scattering, geomagnetic field and measurement errors, we are presently checking for detector misalignment and other sources of errors which could lead to this effect.

REFERENCES

- 1) G. Battistoni et al., " *The Nusex Detector* "; submitted to Nucl. Instr. Meth.
- 2) G. Battistoni et al., Nucl. Instr. Meth. **219** (1984), 300.
- 3) G. Battistoni et al., Phys Lett. **118B** (1982), 461.
- 4) G. Battistoni et al., Phys Lett. **133B** (1983), 454.
- 5) G. Battistoni et al. in " *Proceedings of the Leptonic Session of the Nineteenth Rencontre de Moriond - Vol 1 - Phenomenology of the Gauge Theories* " edited by J. Tran Thanh Van (Editions Frontières 1984), presented by S. Ragazzi.
- 6) G. Battistoni et al., " *Primary cosmic ray spectrum at energies $\approx 10^{13} - 10^{16}$ eV from multiple muons in NUSEX experiment* "; submitted to Nuovo Cimento C.
- 7) R.F. Elsner et al. Astrophys. J. **239** (1980), 335.
- 8) M. Van der Klis and M. Bonnet-Bidaud Astronom. Astrophys. **95** (1981), L5.
- 9) M. Samorsky and W. Stamm Astrophys. J., **268** (1983), L17.
- 10) J. Lloyd-Evans et al., Nature **305** (1983), 784.
- 11) R.C. Lamb, C.P. Godfrey, W.A. Wheaton and T. Tümer, Nature **296** (1982), 543.
- 12) S. Danaher, D.J. Fegan and N.A. Porter, Nature **289** (1981), 568.

EXPERIMENTAL LIMITS FOR 34 NUCLEON DECAY MODES FROM THE IMB DETECTOR*

R.M. Bionta, G. Blewitt, C.B. Bratton, D. Casper, B.G. Cortez,
P. Chrysicopoulou, R. Claus, M. Crouch, S.T. Dye, S. Errede,
G.W. Foster, W. Gajewski, K.S. Ganezer, M. Goldhaber, T.J. Haines,
T.W. Jones, D. Kielczewska, W.R. Kropp, J.G. Learned, E. Lehmann,
J.M. LoSecco, H.S. Park, L. Price, F. Reines, J. Schultz, S. Seidel,
E. Shumard, D. Sinclair, H.W. Sobel, J.L. Stone, L.R. Sulak,
R.C. Svoboda, G. Thornton, J.C. van der Velde, and C. Wuest.

*Presented by Hye-Sook Park
University of Michigan
Ann Arbor, MI 48109

ABSTRACT

We observe 401 events originating inside the fiducial volume during 417 live days exposure of the IMB detector. Partial lifetime limits for 34 nucleon decay modes are obtained in the range of $10^{30} \sim 10^{32}$ years. Twenty one of the contained events are consistent with either ν interactions or nucleon decay into modes without a neutrino in their final state.

IMB DETECTOR

The Irvine-Michigan-Brookhaven (IMB) detector is described in previous papers¹. It is located in the Morton-Thiokol salt mine near Fairport Harbor, Ohio. The mine is situated 600 m underground providing the detector with 1570 meters of water equivalent (mwe) overburden. The detector consists of a $22.5 \times 17 \times 18 \text{ m}^3$ rectangular tank filled with 8000 tonnes of ultra purified water. There are 2048 EMI 5" diameter photomultiplier tubes (PMT's) deployed on all six surfaces with $\sim 1 \text{ m}$ spacing. The fiducial volume is set 2 m inside the PMT planes yielding a 3300 tonne fiducial mass.

Charged particles above the critical velocity ($0.75c$) are detected by their Cherenkov radiation which impinges on the PMT wall producing ring images. The particles μ^\pm , π^\pm , and K^\pm are visible above total energy thresholds of 160, 215, and 750 MeV respectively. However, e^\pm , γ , and π^0 's yield electromagnetic showers in which essentially all of their energy is deposited in the detector.

Each PMT records the photon arrival time, with a resolution of 5.5 nsec HWHM, and the pulse height allowing the reconstruction of event vertex and track direction. The visible energy of an event (E_C , the Cherenkov equivalent energy) is calculated by summing of the pulse heights after correcting for light attenuation in water, PMT angular efficiency, and PMT pulse height non-linearity. The absolute energy level is determined by throughgoing cosmic ray muons with known energy deposition. In addition, we can identify the electron signal from muon decay using the second timing scale which records subsequent PMT firings up to 7.5 μsec after the main trigger. The detection efficiency for muon decay is $\sim 60\%$.

DATA ANALYSIS

Data reduction procedures have been described elsewhere¹. Basically we search for any event originating inside the fiducial volume (contained events) among the events recorded in the mine. The first stage is a simple energy cut. We require that the number of illuminated PMT's (NPT) be in the range of $40 < \text{NPT} < 300$, which is equivalent to an energy between 150 \sim 1700 MeV. The mean NPT is ~ 180 for nucleon decay modes with maximal Cherenkov light yields (e.g. $p \rightarrow e^+e^+e^-$). This requirement retains 30% of the total triggers. Subsequent computer analysis makes use of the timing and topological characteristics of Cherenkov radiation to isolate events with vertices inside the fiducial volume. The 2 \sim 3 events/live day passing the above procedures are scanned by physicists on a color graphics display.

For atmospheric ν interactions that pass the NPT requirement, the efficiency of the data analysis for saving events originating within the fiducial volume is $\sim 80\%$. The nucleon decay modes have a survival probability

> 80% if the secondary products from a nucleon decay do not interact inside the oxygen nucleus. The mean vertex error varies between 40 ~ 100 cm depending on the light yield.

CONTAINED EVENTS

A total of 401 events are observed to originate inside the fiducial volume during 417 days of live time. Figure 1 shows the vertices and direction of these events projected onto different walls. Note that there is no obvious excess near the edge of the fiducial volume (an indication of contamination by entering neutral particles) and near top (contamination by cosmic rays). The events are uniformly distributed throughout the fiducial volume and isotropic in track direction. For low energy ν interactions the final state particles can be emitted at large angles with respect to the direction of the parent ν . This washes out the small angular anisotropy expected in the atmospheric ν angular distribution.

The visible energy spectrum for the contained data events and simulated background events are given in Figure 2. The total number of background events are normalized to the number of data events. There is no significant excess around 1 GeV and furthermore the observed energy spectrum agrees with the simulation.

BACKGROUND

The most important background to nucleon decay comes from atmospheric neutrino interactions within the detector. The ν 's arise from the decays of hadrons produced through primary cosmic ray interactions in the atmosphere. We use a detailed simulation to estimate the level of background in our detector.

• ν Flux and Angular Distribution

There is no direct measurements of the atmospheric ν flux at low energies. We use the theoretical calculation by T.K. Gaisser and T. Stanev². Their calculation begins with the primary proton flux and generates the atmospheric cascade induced by the primaries. Included are the effects of the earth's magnetic field and the modulation of the solar field at our experimental site. A comparison of this flux with that of different authors is given in various papers (e.g. see Ref. 3). A survey of those calculations suggests a $\pm 20\%$ systematic error.

The calculation by Gaisser and Stanev also provides the zenith angular distribution of neutrinos and the ratio of neutrinos to antineutrinos. The ratio of $\nu_e/\bar{\nu}_e$ is approximately 1.3, and $\nu_\mu/\bar{\nu}_\mu \sim 1$ for most of energy and angular range.

- Cross Sections

The neutrino cross section at low energies and the ratio of neutral current to charged current cross sections are measured principally in bubble chambers. We take the average of the experimental measurements at $E_\nu < 10$ GeV for our background simulation. They are:

$$\sigma_{\nu}^{CC} = 0.72 \times 10^{-38} \text{ (cm}^2/\text{GeV)}$$

$$\sigma_{\bar{\nu}}^{CC} = 0.29 \times 10^{-38} \text{ (cm}^2/\text{GeV)}$$

$$R = \frac{\sigma_{\nu}^{NC}}{\sigma_{\nu}^{CC}} = 0.30$$

$$\bar{R} = \frac{\sigma_{\bar{\nu}}^{NC}}{\sigma_{\bar{\nu}}^{CC}} = 0.37$$

- Interaction Configuration

The topology of the simulated final state particles in ν interactions are taken from individual events measured in the bubble chambers. We use freon bubble chamber data provided by the Gargamelle collaboration and neon bubble chamber data taken from Brookhaven. These data give a rather complete picture of the number, type, and momenta of the final state particles compared to other types of neutrino detectors. Measured charged current bubble chamber events are selected according to their energy. For charged current ν_μ and $\bar{\nu}_\mu$ interactions we simply use the final state particle types and momenta given by the bubble chamber reconstruction. For charged current interactions of ν_e and $\bar{\nu}_e$, we replace the μ^+ or μ^- of the charged current interactions by an e^+ or e^- of the same momentum. For neutral current interactions we substitute the charged lepton in the final state with a neutrino; and replace of a charged pion by another pion of lower or higher charge state.

- PMT Simulation

Once the type and 4 momentum of the final state particles are determined, the particles are propagated through the detector medium and undergo energy loss and nuclear interactions while generating Cherenkov radiation. The program determines the PMT response to the simulated Cherenkov radiation and creates a simulated data tape for analysis.

- Uncertainties in Background Simulation

Difficulties in the estimation of the background arise from the uncertainties in (a) the ν flux calculations; (b) the charged and neutral current cross sections at low energies; (c) the bubble chamber detection efficiency due to scanning bias and for neutral particles;(d) nuclear

effects from π absorption in the parent nucleus which may differ significantly between water and the bubble chamber liquids and uncertainties in the secondary nuclear interactions; (e) the ambiguity between π^+ and p in the bubble chamber data; (f) the amount contamination of the bubble chamber data by entering particles. Uncertainties (a) and (b) are partly addressed by the fact that the number of contained events agree well with the predicted rate (within 5%). To investigate (c) and (d), we have processed bubble chamber data from two different experiments using two different liquids (CF_3Br , and Ne). Concerning the difficulty (e), we simulated the background using different assumptions regarding the π^+/p identification ambiguity. On the basis of these considerations we assign an overall uncertainty of (-50%, +100%) to the background estimation for any given mode.

- Analysis of Simulated Background Events

We have simulated 10 years of ν interactions which are processed through the same analyses routines as the data.

ISOLATION OF NUCLEON DECAY SIGNAL

In order to isolate the nucleon decay signal from the background, we make use of four physical parameters:

(1) Total visible energy, E_C : This is ideally ~ 940 MeV, but modified for a given decay mode by the effects of Cherenkov thresholds, π absorption, and missing ν 's. Typical errors in E_C are $\pm 100\%/\sqrt{\text{NPT}} \pm 15\%$ (systematic), with $\text{NPT} = 50\sim 200$.

(2) Anisotropy, A: The total momentum imbalance in the nucleon decays is ideally 0 for decays originating in hydrogen and ≤ 225 MeV/c for decays in oxygen due to Fermi motion. A measure of the visible momentum imbalance is the anisotropy (A) which is defined as the magnitude of the vector sum of the unit vectors from the fitted vertex to each lit PMT, normalized by the total number of lit PMT's. For events with a single short track A is ~ 0.7 which is the cosine of the Cherenkov angle. For isotropic or wide angle two body decay modes $A < 0.3$. By comparing the A's calculated from the fitted vertex and the true vertex for the simulated background events, we assign an anisotropy error of ± 0.05 .

(3) Muon Decay Signature: We require the presence or the absence of the muon decay signature as appropriate for the mode under consideration.

(4) Back-to-Back Signature: For most modes it is difficult to reconstruct all of the individual tracks because we collect only $\sim 1\%$ of the total Cherenkov light. However, some two body proton decay modes produce events with two clearly visible tracks, especially when the opening angle is $> 150^\circ$

(back-to-back signature). This is rarely mimicked by the background. We require this back-to-back signature for four modes, $p \rightarrow e^+\gamma$, $e^+\pi^0$, $\mu^+\gamma$, and $\mu^+\pi^0$, by scanning the events on the color graphics. An efficiency of 90% is estimated for the back-to-back requirement by scanning the simulated background events.

Candidates for individual nucleon decay modes are selected by making appropriate cuts on these four parameters. Figure 3(a) shows a scatterplot of E_C vs A for the 401 contained events from 417 live days. As an example, the E_C vs A plot for a nucleon decay mode $p \rightarrow \mu^+\pi^0$ is given in Figure 3(b). The large spread at lower energy and higher A are mainly due to π^0 interactions in oxygen. The E_C vs A plot for 401 simulated ν background events is shown in Figure 3(c). By comparing these scatterplots the requirements on the nucleon decay candidates are determined to maximize the detection efficiency and to minimize the background. The enclosed box in Figure 3(b) shows the E_C vs A requirement for $p \rightarrow \mu^+\pi^0$. Furthermore, for this mode we require that the events should possess one identified muon decay and appear as two back-to-back tracks on the color plotter.

The requirements for various modes are listed in Table I column 2 through 5. All of the nucleon decay simulations have been filtered through the same analyses as the data to estimate the detection efficiencies which are presented in two forms: (a) with all nuclear effects included (column 6) and (b) with only Fermi motion and π^\pm interactions in the surrounding water taken into account (column 7). We use the former efficiency to derive our results. The efficiency without nuclear correction is useful to compare our efficiencies with those from other experiments which use different materials for the nucleon source and different nuclear interaction models.

Events passing all of the requirements are called "candidates" for that mode and the numbers are listed in column 8. Since the requirement region can overlap for various modes one event may be a candidate for many modes. Table II lists the candidate events for the nucleon decay modes which do not have a neutrino in the final state. The last column of Table II presents the modes for which the event is a candidate. Considering all of the candidate events as nucleon decays (the most conservative interpretation) we derive 90% CL lifetime limits given in column 10 of Table I which are in the range of $10^{30} \sim 10^{32}$ years.

The number of backgrounds expected for an individual nucleon decay mode is estimated by applying exactly the same requirements to the ν simulation. These results are given in column 9 of Table I.

SOME CANDIDATES

Some two-track events with wide opening angle are displayed in Figures 4

and 5. In these figures, the lit PMT's are projected onto a sphere and unfolded into a Mercator projection. The number of slashes associated with a tube indicates the recorded light level. In each figure, (a) is an actual data event which is candidate for a non-neutrino nucleon decay mode from Table II; (b) is a simulated nucleon decay event of the same mode; and (c) is a simulated neutrino interaction which has a similar event configuration. Notice that it is difficult to distinguish between the real event, the simulated nucleon decay event, and the simulated background event. In general, the candidate events are consistent with both being nucleon decays and atmospheric ν interactions.

CONCLUSION

In conclusion, we have found 401 events originating inside the 3300 tonne fiducial volume during 417 live days. The overall rate and characteristics are compatible with atmospheric ν interactions. Among them 21 events are observed to be consistent either a ν interaction or nucleon decay into a number of non- ν modes.

A survey of Table I shows that the most of the modes have signals at the same level as the background. Our lifetime limits for the modes favored by simple Grand Unified Theories are a few $\times 10^{32}$ years. Our lifetime limits for the modes with charged hadrons are a few $\times 10^{31}$ years; and for the modes with neutrinos in their final state, our limits are of the order of a few $\times 10^{30}$ years.

Recently the IMB detector has been upgraded to increase the light collection by a factor of two by installing wave shifters around the PMT's. Another factor of two will be obtained by the end of 1985 by replacing the 5" PMT's with 8" PMT's. We expect that further analysis of the energy and topology will reduce the ambiguity between the signal and background and thus increase the sensitivity for many modes.

ACKNOWLEDGEMENT

I would like to thank to all of the organizers of XXth Rencontre de Moriond. It was a very enjoyable meeting in many respects. This work was supported in part by the U.S. Department of Energy.

REFERENCES

1. H.S. Park, G. Blewitt et al., Phys Rev. Lett. 54, 22 (1985);
B.G. Cortez et al., Phys Rev. Lett. 52, 1092 (1984);
R.M. Bionta et al., Phys Rev. Lett. 51, 27 (1983).
2. T.K. Gaisser and T. Stanev, in Proceedings of the International Colloquium on Baryon Nonconservation, Salt Lake City, January, 1984, edited by D. Cline (University of Wisconsin Press, Madison, 1984) p. 61; T.K. Gaisser in Proceedings of the Eleventh International Conference on Neutrino and Astrophysics, edited by K. Kleinknecht and E.A. Paschos (World Scientific, Singapore, 1984), p. 372; also private communication.
3. B.G. Cortez, Ph.D. thesis, Harvard University, 1983 (unpublished).

Table I - IMB Nucleon Decay Partial Lifetime Limits (417 Days)

1 Mode	2 Requirements				5 Back to Back	6 Effic. with Nuclear Corr.	7 Effic. without Nuclear Corr.	8 Candi- dates Observed	9 No. of Bkgnd. Est. -50%, +100%	10 Limit on τ/B ($\times 10^{31}$ yr) 90% C.L.
	E_C (MeV)	A	# μ							
$p \rightarrow e^+ \gamma$	750-1100	< 0.3	0	0	0	0.66	0.66	0	0.2	36.
$p \rightarrow e^+ \pi^0$	750-1100	< 0.3	0	0	0	0.46	0.75	0	0.2	25.
$p \rightarrow e^+ K^0$	300-500	< 0.5	1			0.12	0.12	i, k, m, n, s	4	
	750-1100	< 0.3	0			0.14	0.14	0	0.7	7.7
$p \rightarrow e^+ \eta^0$	750-1100	< 0.3	0			0.37	0.54	0	0.7	
	400-650	< 0.5	1			0.07	0.15	k, n, p, s, t	4	20.
$p \rightarrow e^+ \rho^0$	200-600	0.1-0.5	1			0.16	0.30	i, j, k, m, n, p, s	7	1.7
$p \rightarrow e^+ \omega^0$	300-600	0.1-0.5	1			0.19	0.39	i, k, m, n, p, s	5	
	750-1100	< 0.3	0			0.05	0.06	0	0.7	3.7
$p \rightarrow \mu^+ \gamma$	550-900	< 0.5	1	3		0.52	0.52	0	0.6	28.
$p \rightarrow \mu^+ \pi^0$	550-900	< 0.4	1	0		0.32	0.44	c, t	0.4	7.6
$p \rightarrow \mu^+ K^0$	150-400	0.1-0.5	1, 2			0.19	0.20	g, i, j, m	5	
	550-900	< 0.5	1			0.14	0.14	a, c, t	3	4.0
$p \rightarrow \mu^+ \eta^0$	550-900	< 0.5	1			0.23	0.44	a, c, t	3	
	200-400	< 0.5	1, 2			0.12	0.22	g, i, j, m	5	4.6
$p \rightarrow \mu^+ \rho^0$	150-400	0.1-0.5	1, 2			0.10	0.16	g, i, j, m	5	1.6
$p \rightarrow \mu^+ \omega^0$	200-450	0.1-0.5	1, 2			0.18	0.32	g, i, j, k, m, n	6	
	650-900	< 0.5	1			0.03	0.05	a, c	1	2.3
$p \rightarrow \nu K^+$	150-375	0.3-0.6	1			0.08	0.08	6	5	1.0
$p \rightarrow \nu \rho^+$	300-600	0.2-0.5	1			0.07	0.19	6	5	0.8
$p \rightarrow \nu K^{*+}$	250-500	0.3-0.6	1			0.09	0.19	7	6	1.0
$p \rightarrow e^+ e^-$	750-1100	< 0.3	0			0.93	0.93	0	0.7	51.
$p \rightarrow \mu^+ \mu^-$	200-425	< 0.5	2, 3			0.58	0.58	g	0.9	19.
$n \rightarrow e^- \pi^+$	450-950	< 0.5	0			0.40	0.55	b, d, f, h, l, o, r, u	8	3.1
$n \rightarrow e^- \pi^0$	400-700	< 0.5	1			0.10	0.24	k, n, p, s, t	4	
	700-950	< 0.5	0			0.10	0.07	b, d, f, u	3	1.6
$n \rightarrow e^- \rho^-$	400-800	< 0.4	0			0.20	0.42	d, e, f, h, l, o, q r, u	2	1.4
$n \rightarrow e^- \rho^+$	400-800	< 0.4	0, 1			0.22	0.57	d, e, f, h, k, l, n, o, q, r, s, t, u	5	1.2
$n \rightarrow \mu^+ \pi^-$	200-700	< 0.5	1			0.30	0.43	i, j, k, m, n, p, s, t	8	2.3
$n \rightarrow \mu^- \pi^+$	200-500	< 0.5	1, 2			0.29	0.45	g, i, j, k, m, n, s	7	2.5
$n \rightarrow \mu^+ \rho^-$	300-550	< 0.5	1			0.07	0.29	i, k, m, n, p, s	5	0.7
$n \rightarrow \mu^- \rho^+$	300-550	< 0.5	1, 2			0.10	0.41	g, i, k, m, n, p, s	5	0.9
$n \rightarrow \nu \gamma$	350-600	0.5-1.0	0			0.77	0.77	73	56	0.9
$n \rightarrow \nu \pi^0$	350-600	0.5-1.0	0			0.51	0.82	73	56	0.6
$n \rightarrow \nu K^0$	450-700	0.2-0.5	0			0.10	0.11	3	4	1.5
$n \rightarrow \nu \eta^0$	450-800	0.1-0.5	0			0.29	0.56	7	6	2.5
$n \rightarrow \nu \rho^0$	150-500	0.1-0.4	0, 1			0.05	0.11	15	9	0.2
$n \rightarrow \nu \omega^0$	200-450	0.2-0.5	1			0.08	0.24	5	5	
	650-950	< 0.3	0			0.03	0.06	1	0.7	1.2
$n \rightarrow \nu K^{*0}$	200-700	0.15-0.5	1			0.06	0.11	8	8	0.5
$n \rightarrow e^+ e^- \nu$	500-850	< 0.5	0			0.41	0.41	5	5	4.5
$n \rightarrow \mu^+ \mu^- \nu$	150-375	0.2-0.65	1, 2			0.31	0.31	14	11	1.6

Table Captions

Column 1. For three-body decay modes flat phase space was assumed.

Columns 2-4. Different requirement regions correspond to different meson decay modes.

Column 4. Number of Muon Decay Signals required.

Column 5. Number of events rejected by requiring two clear tracks with opening angle $> 150^\circ$. Efficiencies of columns 6 and 7 include a 90% scanning efficiency for this requirement.

Column 8. Some events are candidates for more than one mode. The letters a through u represent the candidate events listed in Table II.

Column 10. Lifetime limits quoted are at 90% C.L. for 417 live days and do not include background subtraction.

Table II. Events Passing All the Requirements for Non- ν Modes

Event No.	E_C (MeV)	Anisotropy A	No. of u Decay	Possible Nucleon Decay Mode	
a	143-21939	724	0.41	1	$\mu^+ K^0 (K^0 \rightarrow \pi^0 \pi^0), \mu^+ \eta (\eta \rightarrow \text{neutrals}), \mu^+ \omega (\omega \rightarrow \pi^0 \gamma)$
b	167-24827	901	0.40	0	$e^+ \pi^-, e^- \pi^+$
c	225-7794	864	0.25	1	$\mu^+ \pi^0, \mu^+ K^0 (K^0 \rightarrow \pi^0 \pi^0), \mu^+ \omega (\omega \rightarrow \pi^0 \gamma), \mu^+ \eta (\eta \rightarrow \text{neutrals})$
d	299-72044	714	0.34	0	$e^+ \pi^-, e^- \pi^+, e^+ \rho^-, e^- \rho^+$
e	420-34248	407	0.05	0	$e^+ \rho^-, e^- \rho^+$
f	510-54208	716	0.36	0	$e^+ \pi^-, e^- \pi^+, e^+ \rho^-, e^- \rho^+$
g	588-8320	369	0.47	2	$\mu^+ K^0 (K^0 \rightarrow \pi^+ \pi^-), \mu^+ \eta (\eta \rightarrow \pi^+ \pi^- \pi^0), \mu^+ \rho^0, \mu^+ \omega (\omega \rightarrow \pi^+ \pi^- \pi^0), \mu^- \pi^+, \mu^- \rho^+, \mu^- \rho^+$
h	656-11673	496	0.36	0	$e^+ \pi^-, e^+ \rho^-, e^- \rho^+$
i	747-44203	336	0.44	1	$e^+ K^0 (K^0 \rightarrow \pi^+ \pi^-), e^+ \rho^0, e^+ \omega (\omega \rightarrow \pi^+ \pi^- \pi^0), \mu^+ K^0 (K^0 \rightarrow \pi^+ \pi^-), \mu^+ \eta (\eta \rightarrow \pi^+ \pi^- \pi^0), \mu^+ \pi^-, \mu^+ \rho^0, \mu^+ \omega (\omega \rightarrow \pi^+ \pi^- \pi^0), \mu^- \pi^+, \mu^+ \rho^-, \mu^- \rho^+$
j	889-10424	292	0.32	1	$e^+ \rho^0, \mu^+ K^0 (K^0 \rightarrow \pi^+ \pi^-), \mu^+ \eta (\eta \rightarrow \pi^+ \pi^- \pi^0), \mu^+ \rho^0, \mu^+ \omega (\omega \rightarrow \pi^+ \pi^- \pi^0), \mu^- \pi^-, \mu^- \pi^+$
k	1047-13889	416	0.24	1	$e^+ K^0 (K^0 \rightarrow \pi^+ \pi^-), e^+ \eta (\eta \rightarrow \pi^+ \pi^- \pi^0), e^+ \rho^0, e^+ \omega (\omega \rightarrow \pi^+ \pi^- \pi^0), \mu^+ \eta (\eta \rightarrow \pi^+ \pi^- \pi^0), e^- \pi^+, e^- \rho^+, \mu^+ \pi^-, \mu^- \pi^+, \mu^+ \rho^-, \mu^- \rho^+$
l	1062-13889	489	0.26	0	$e^+ \pi^-, e^+ \rho^-, e^- \rho^+$
m	1238-48756	328	0.29	1	$e^+ K^0 (K^0 \rightarrow \pi^+ \pi^-), e^+ \rho^0, e^+ \omega (\omega \rightarrow \pi^+ \pi^- \pi^0), \mu^+ K^0 (K^0 \rightarrow \pi^+ \pi^-), \mu^+ \eta (\eta \rightarrow \pi^+ \pi^- \pi^0), \mu^+ \rho^0, \mu^+ \omega (\omega \rightarrow \pi^+ \pi^- \pi^0), \mu^- \pi^-, \mu^- \pi^+, \mu^+ \rho^-, \mu^- \rho^+$
n	1238-67704	422	0.26	1	$e^+ K^0 (K^0 \rightarrow \pi^+ \pi^-), e^+ \eta (\eta \rightarrow \pi^+ \pi^- \pi^0), e^+ \rho^0, e^+ \omega (\omega \rightarrow \pi^+ \pi^- \pi^0), \mu^+ \eta (\eta \rightarrow \pi^+ \pi^- \pi^0), e^- \pi^+, e^- \rho^+, \mu^+ \pi^-, \mu^- \pi^+, \mu^+ \rho^-, \mu^- \rho^+$
o	1268-63668	516	0.30	0	$e^+ \pi^-, e^+ \rho^-, e^- \rho^+$
p	1270-31957	541	0.48	1	$e^+ \eta (\eta \rightarrow \pi^+ \pi^- \pi^0), e^+ \rho^0, e^+ \omega (\omega \rightarrow \pi^+ \pi^- \pi^0), e^- \pi^+, \mu^+ \pi^-, \mu^+ \rho^-, \mu^- \rho^+$
q	1328-24903	419	0.29	0	$e^+ \rho^-, e^- \rho^+$
r	1349-17473	608	0.19	0	$e^+ \pi^-, e^+ \rho^-, e^- \rho^+$
s	1486-42698	454	0.33	1	$e^+ K^0 (K^0 \rightarrow \pi^+ \pi^-), e^+ \eta (\eta \rightarrow \pi^+ \pi^- \pi^0), e^+ \rho^0, e^+ \omega (\omega \rightarrow \pi^+ \pi^- \pi^0), e^- \pi^+, e^- \rho^+, \mu^+ \pi^-, \mu^- \pi^+, \mu^+ \rho^-, \mu^- \rho^+$
t	1513-31678	609	0.30	1	$e^+ \eta (\eta \rightarrow \pi^+ \pi^- \pi^0), \mu^+ \pi^0, \mu^+ K^0 (K^0 \rightarrow \pi^0 \pi^0), \mu^+ \eta (\eta \rightarrow \text{neutrals}), e^- \pi^-, e^- \rho^+, \mu^+ \pi^-, \mu^+ \pi^+$
u	1528-42652	722	0.14	0	$e^+ \pi^-, e^- \pi^+, e^+ \rho^-, e^- \rho^+$

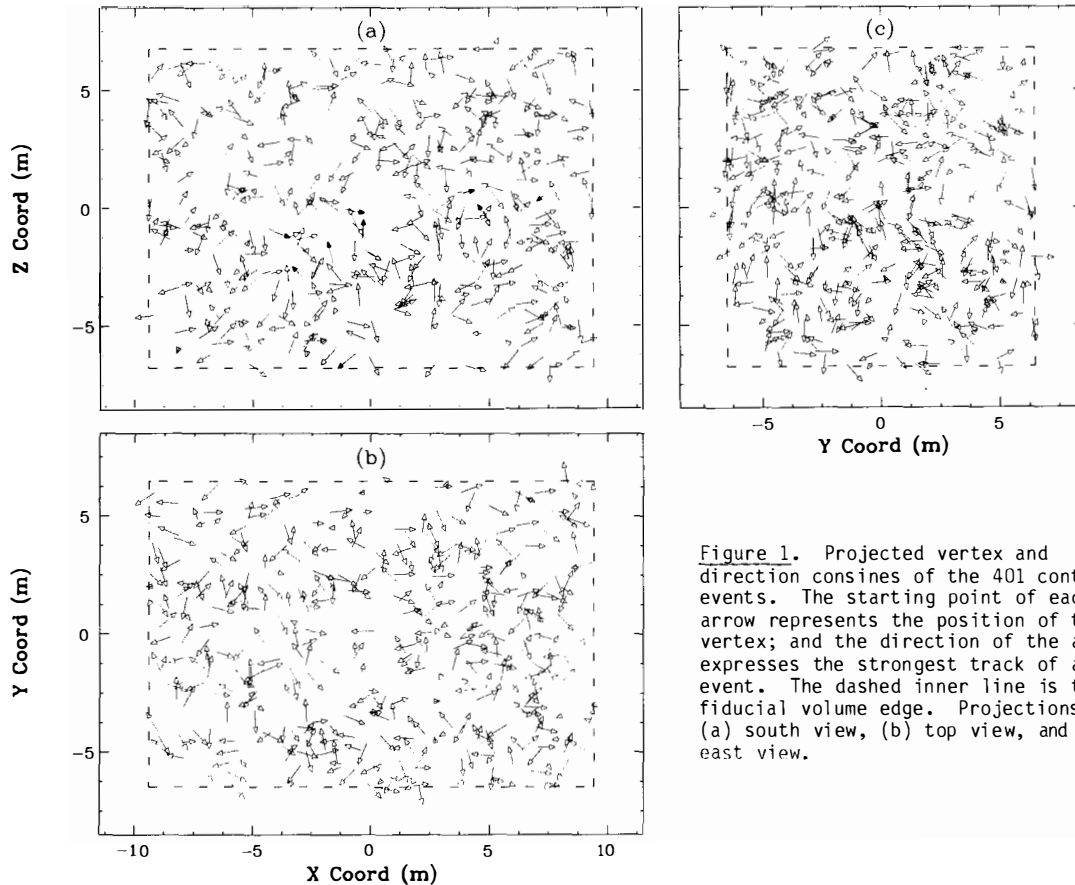


Figure 1. Projected vertex and direction cosines of the 401 contained events. The starting point of each arrow represents the position of the vertex; and the direction of the arrow expresses the strongest track of an event. The dashed inner line is the fiducial volume edge. Projections are (a) south view, (b) top view, and (c) east view.

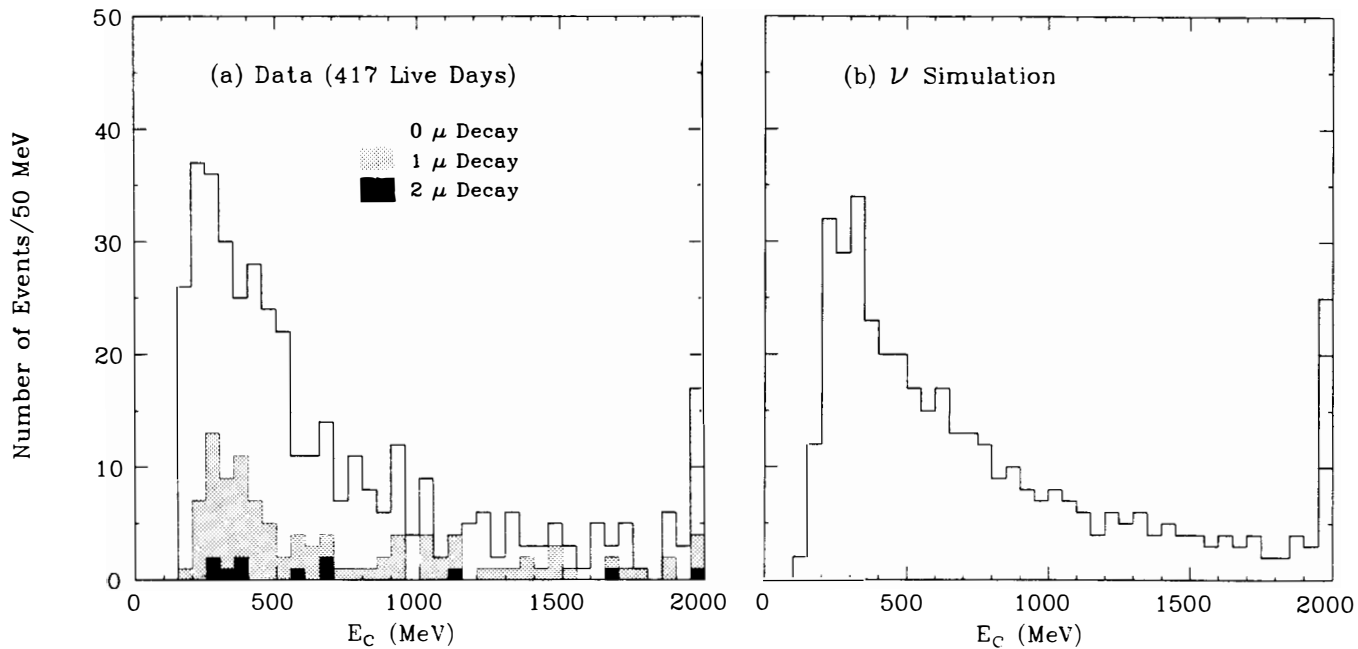


Figure 2. The visible energy distribution (a) for the contained real data events; and (b) for a background simulation of the atmospheric ν interactions. The events with one or two muon decay signatures are distinguished by the shadowed and dark area, respectively (real data events only). The number of simulated ν events is normalized to that of the contained data events.

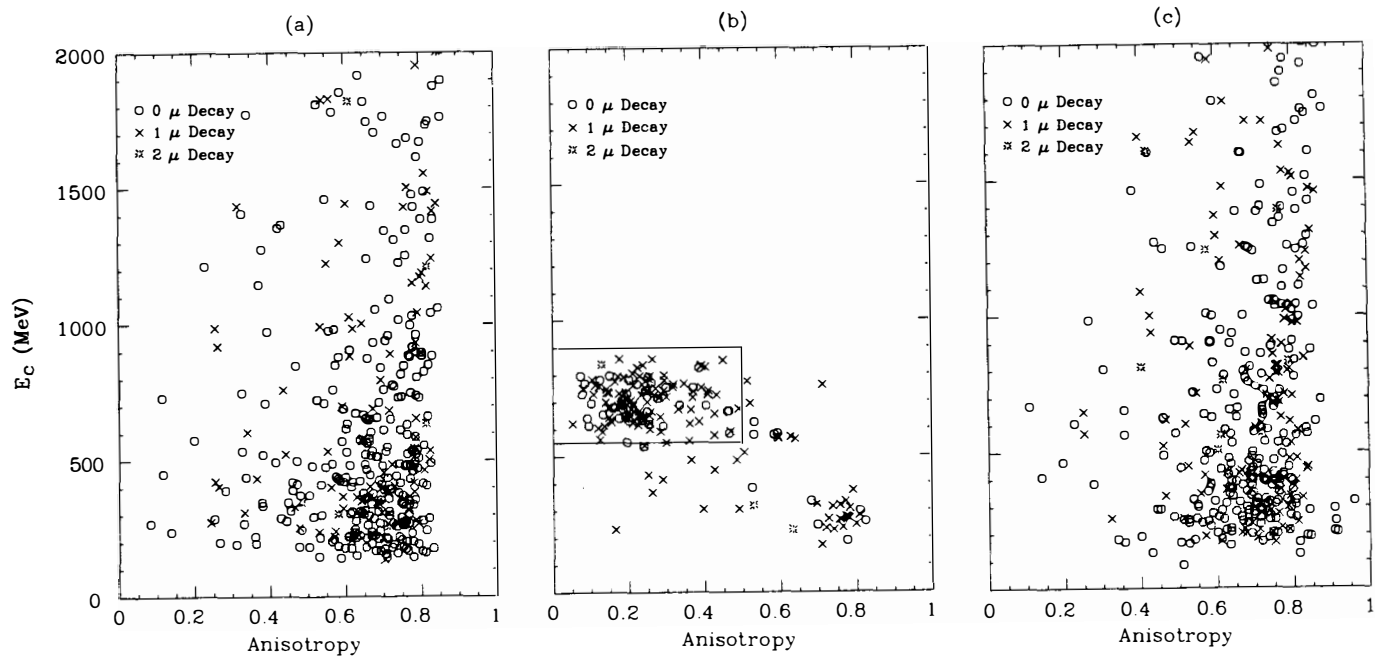


Figure 3. A scatterplot of E_c vs A for (a) the 401 contained events, (b) a simulation of the nucleon decay mode $p + \mu + \pi^0$, and (c) the simulated ν interactions. Here 'o' denotes events without muon decay; 'x' is for the events with one muon decay; and '*' expresses the events with two identified muon decay signatures.

17:08:26 2/ 2/84 Pattern Unit 63 Tape # 1238 MBD Event # 48756

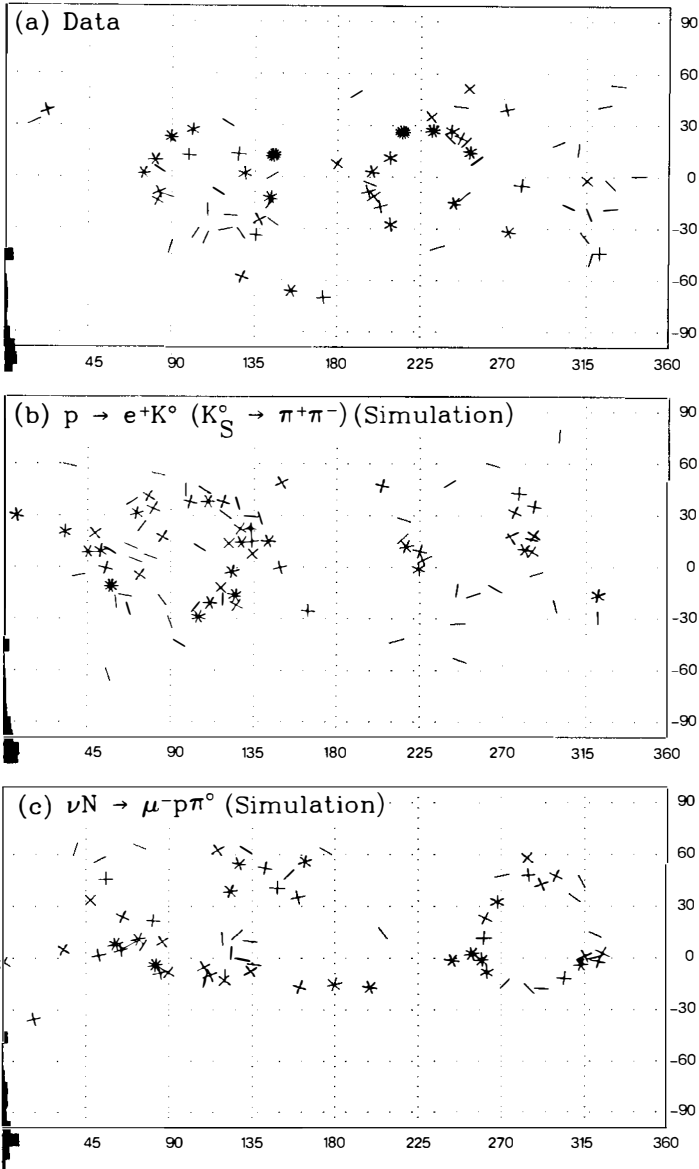


Figure 4. Mercator projection of (a) an observed event which is a candidate for the nucleon decay mode $p \rightarrow e^+K^0$; (b) a simulated nucleon decay event into e^+K^0 ; (c) a simulated background ν interaction with similar characteristics.

10:15:18 3/19/84 Pattern Unit 3 Tape # 1349 MBD Event # 17473

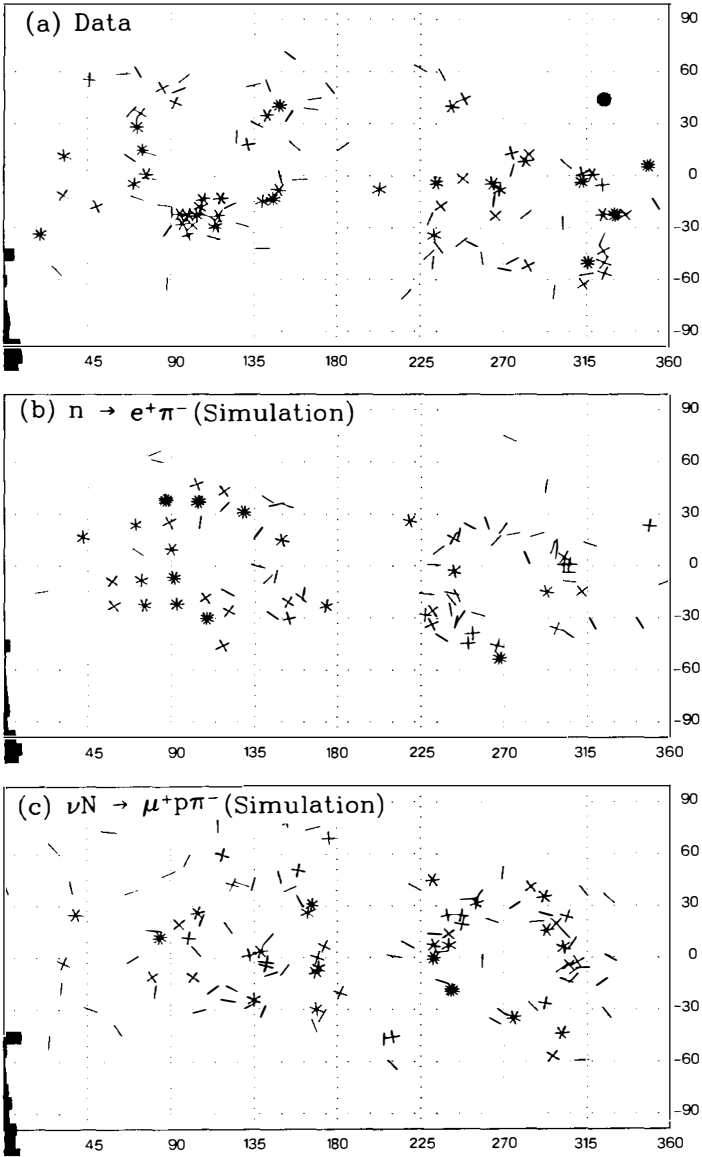


Figure 5. Mercator projections of (a) an observed event which is a candidate for the nucleon decay mode $n \rightarrow e^+\pi^-$; (b) a simulated nucleon decay event into $e^+\pi^-$; (c) a simulated background ν interaction with similar characteristics.

DYNAMICS OF STRONGLY COUPLED HIGGS MODELS: VECTOR RESONANCES AND ALL THAT

Pham Quang Hung
Department of Physics
University of Virginia
Charlottesville, VA 22901

Abstract

Heavy dynamical vector resonances are studied in the context of strongly coupled Higgs models. The production and experimental implications of these vector resonances are also briefly discussed.

I would like to report in this talk some work¹ done last summer with Hank Thacker on the question of whether or not the Higgs fields interact strongly with each other, and if they do,² what the consequences would be. We studied this question within the framework of the standard electroweak model with doublets of Higgs scalars, that is to say we tried to see how far one can push the standard model and still obtain interesting physics.

Our analysis suggested that there are $I=J=1$ dynamical resonances in a strongly coupled Higgs sector which are very much like the ρ 's of ordinary hadronic physics or the speculated technirho of technicolor models. These dynamical resonances whose masses are discussed below may prove to be very relevant to (present and future) collider experiments.

There are also many theoretical reasons for considering strongly coupled Higgs models, one of which is the possibility that the Higgs field is composite (e.g. in Technicolor models). This scenario circumvents many of the problems facing theories with elementary scalars among which are the naturalness and triviality problems.³

If the Higgs boson is heavy and possibly composite, the spin-0 fields of the standard model interact strongly with each other. To deal with such strong interaction dynamics, one can go back to the well-known σ -model whose physics has been investigated so extensively in the 60's. In fact, the standard model Higgs doublet ϕ has an $O(4)$ symmetry and can be written as $\phi = (\sigma, \vec{\pi})$ where σ is the surviving Higgs scalar and $\vec{\pi}$ are the Goldstone bosons.

The physical Higgs field has a mass $m_H = \sqrt{2\lambda} v$, where λ is the Higgs self-coupling and v is the V.E.V. of σ . To have an idea of the mass scale(s) involved in a strongly coupled Higgs sector of the standard model, let us go back to the old σ -model. There, $\langle\sigma\rangle = f_\pi \approx 93$ MeV. The ratio of the electroweak Higgs mass to the σ -mass is $m_H/m_\sigma = \sqrt{\lambda_H/\lambda_\sigma} (v/f_\pi)$, where $v \approx 250$ GeV for the standard model. Naively assuming that $\sqrt{\lambda_H/\lambda_\sigma} \approx O(1)$ and using $m_\sigma \approx 700$ MeV, one obtains $m_H \approx 1.9$ TeV. This value is only about a factor of two higher than a more rigorous bound obtained by Lee, Quigg and Thacker² which is $m_H \lesssim 1$ TeV. This latter bound was obtained by requiring tree unitarity of the scattering amplitudes for longitudinal gauge bosons. In any case, for the minimal standard model with one Higgs doublet, one should expect a strongly coupled system when the Higgs mass exceeds 1 TeV. For a multi-Higgs case, because of the constraint $\sum_i v_i^2 \approx (250 \text{ GeV})^2$ (the W-mass is $m_W^2 = \frac{1}{4} g^2 \sum_i v_i^2$), strongly coupled Higgs phenomenon could occur at lower mass values.

One can now expect dynamical resonances to be formed in such a system. Once again, an analogy with π - π scattering serves as a guidance for our study of strongly coupled Higgs models.⁴ Of special interest are the $I=J=1$ resonances such as the ρ -mesons. As demonstrated below, such ρ -like resonances

are also expected to arise in the strongly coupled Higgs scenario and, having the same quantum numbers as W and Z, can be produced via mixing with the weak gauge bosons.¹

The main ingredients in this discussion are low energy theorem, analyticity, unitarity, and crossing symmetry. It is not hard to obtain from the standard model Lagrangian the low energy theorem (neglecting pseudo-Goldstone boson masses)

$$\hat{T} = \frac{1}{v^2} [\delta_{ij} \delta_{kl} s + \delta_{ik} \delta_{jl} t + \delta_{il} \delta_{jk} u] \quad , \quad (1)$$

which obeys Bose statistics and crossing symmetry for the reaction $w_i + w_j \rightarrow w_k + w_l$, where w_i 's are (pseudo) Goldstone bosons and v is the V.E.V. ($= f_\pi$ for ordinary quark chiral symmetry breaking and 250 GeV for the standard model breaking). We took the standard steps to study the behaviour of each partial wave. I shall try to describe them in words (quantitative details could be found in our paper).

From Eq. (1), one can construct the partial wave amplitudes for the channels: $(I=J=0)$, $(I=2, J=0)$, $(I=J=1)$ which are denoted by \hat{t}_{00} , \hat{t}_{20} and \hat{t}_{11} respectively. The next step is to construct unitary amplitudes which reduce to these \hat{t} 's at low energies, e.g. $t_{00}(s) = \hat{t}_{00}(s)/(1+h(s)\hat{t}_{00}(s))$, with $h(s)$ determined from a spectral function integral with the property $1+h(s)\hat{t}_{00}(s) \cong 1$ for small s . Also, $t_{IJ} = (\sqrt{s}/k) e^{i\delta_{IJ}} \sin\delta_{IJ}$, where δ_{IJ} is the phase shift. The following features emerge.

- 1) For t_{00} , the phase shift is positive and rises close to 90° (after being Padé-improved) in the 1-2 TeV region for the one Higgs-doublet model. The width, however, is comparable to the mass, so it is not a well-defined resonance. The same feature occurs in the σ -model.
- 2) The phase shift for the $I=2, J=0$ channel is negative and we expect no resonance.
- 3) The $I=J=1$ channel is the most interesting one since earlier calculations by Basdevant and Lee⁵ have indicated that resonances can be produced in the σ -model (albeit with the wrong-width). However, as Brown and Goble⁶ has shown using the unitarized amplitude for that channel, if one requires that there is a resonance at $s = m_{\rho}^2$ (the mass squared of the vector meson), the width can be determined in terms of f_ρ , m_ρ and m_π (mass of pseudo-Goldstone bosons). Specifically $\Gamma_{\rho} = (3\pi v^2 m_\rho^2)^{-1} k_\rho^5$, where $k_\rho^2 = \frac{1}{4} (m_\rho^2 - m_\pi^2)$. For the ordinary π - π scattering, the analysis of Brown and Goble gave $\Gamma_\rho \cong 130$ MeV for $m_\rho = 775$ MeV which is quite an acceptable value. These vector mesons are indeed prominent resonances in π - π scattering. One can expect similar

situations to arise in strongly coupled Higgs models. Indeed, our calculations did support such an expectation.

The V - π - π coupling can be obtained by comparing the above width with the standard one $\Gamma_V = f_{V\pi\pi}^2 k^3 / 6\pi m_V^2$, giving $f_{V\pi\pi} = \sqrt{2} (k/v)$. Neglecting the pseudo-Goldstone mass m_π , one obtains the KSRF relation $f_{V\pi\pi} = m_V / \sqrt{2} v$. Naively assuming that $f_{V\omega\omega} = f_{\rho\pi\pi} \approx 6$ and using $v \approx 250$ GeV, the $I=J=1$ dynamical resonance in the strongly coupled minimal standard model is seen to have an estimated mass around 2 TeV, a value not unlike that predicted for the technirho in Technicolor models. Of course, it is possible that, for unknown dynamical reasons, $f_{V\omega\omega} \ll f_{\rho\pi\pi}$ so that $m_V \ll 2$ TeV. Can one get $m_V \ll 2$ TeV from some other means?

As we have detailed in our analysis, an easier way to get "low" mass vector mesons is to extend the minimal standard model to a two (or more) Higgs doublet case since then one can have Higgs V.E.V.'s which are much lower than 250 GeV. With a two-Higgs doublet model, the spontaneous breakdown of $SU(2)_L \times U(1)_Y$ produces three Goldstone bosons (w^\pm, z) which are absorbed by W^\pm and Z , three pseudo-Goldstone bosons (ζ^\pm, η) with arbitrary masses (assumed to be low, i.e. less than m_w), and two neutral Higgs scalars (H_1, H_2) which are heavy (in the framework of strongly coupled Higgs models). Notice that the V.E.V.'s are constrained by $v_1^2 + v_2^2 \approx (250 \text{ GeV})^2$. As an example, let us take $v_1 \approx 50$ GeV and $v_2 \approx 245$ GeV, and it is found that the unitarity limit is reached when $m_{H_1} \approx 170$ GeV and $m_{H_2} \approx 1$ TeV.

There are now two sets of $I=J=1$ resonances denoted by V and V' (corresponding to v_1 and v_2). They couple to ζ^\pm, ζ and w^\pm, z respectively. Since there is no reason for $f_{V\zeta\zeta}$ and $f_{V'\omega\omega}$ to have the same magnitude as $f_{\rho\pi\pi}$, the vector meson masses, $m_V = \sqrt{2} f_{V\zeta\zeta} v_1$ and $m_{V'} = \sqrt{2} f_{V'\omega\omega} v_2$ could have values of $O(170 \text{ GeV})$ and $O(1-2 \text{ TeV})$ respectively.

The easiest way to produce the above resonances is through the mixing with W^\pm and Z because of the likeness in quantum numbers. A combination of vector meson dominance and KSRF relation gives the mixing between V' and $W^{\pm,0}$, namely $\gamma_{W-V'} = g v_1 / 2 m_{V'}$. The $p\bar{p}$ and pp colliders are most suited (as far as energies are concerned, for the production of V and V' through the Drell-Yan mechanism. An important quantity is the variable $\tau = m_V^2 / s$. Cross-sections for W and Z productions decrease rapidly with increasing τ . Present (CERN) and near-future (Fermilab) colliders with energies $\sqrt{s} = 630$ GeV and 2 TeV respectively can only produce V (~ 170 GeV). As for V' (~ 2 TeV), they would be produced copiously at the yet-to-be built SSC ($\sqrt{s} \approx 40$ TeV).

With the present integrated luminosity of $\int \mathcal{L} dt \approx 413 \text{ nb}^{-1}$, and, as an example, take $v_1 \approx 50$ GeV we get ~ 20 charged V' , and ~ 4 neutral V' 's. The V' 's decay predominantly into two ζ 's. The ζ 's subsequently decay into quarks and also leptons. We gave an interpretation of the UAL monojet events⁸ based on this scenario. The experimental situation is at the present time uncertain. We

await eagerly for the confirmation or rebuttal of these monojet events as genuine new physics and not just background.

Nevertheless, based on our analysis, we are led to conclude that an important consequence of a strongly coupled Higgs sector is the appearance of dynamical resonances, and that the existence of such resonances may have significant implications for future collider experiments.

Acknowledgements

I would like to thank the organizers of the Rencontre de Moriond for the warm hospitality at Les Arcs. This work was supported in part by the National Science Foundation under Grant No. PHY-83-01186.

References (an incomplete list)

1. P. Q. Hung and H. B. Thacker, Fermilab-Pub-84/104-T preprint (to appear in Phys. Rev. D). For an earlier and related work see M. Veltman, Univ. of Michigan preprint UMHE83-22.
2. M. Veltman, Acta Phys. Pol. B8, 475 (1977); Phys. Lett. 70B, 254 (1977); B. W. Lee, C. Quigg, and H. B. Thacker, Phys. Rev. D16, 1519 (1977).
3. For a review see R. D. Peccei, "The scalar sector", MPI-PAE/PTH 65/84 preprint.
4. For a review see B. W. Lee, Chiral Dynamics, Gordon and Breach, N.Y. 1972.
5. J. L. Basdevant and B. W. Lee, Phys. Rev. D2, 1680 (1970).
6. L. S. Brown and R. L. Goble, Phys. Rev. Lett. 20, 346 (1968); Phys. Rev. D4, 723 (1971).
7. K. Kawarabayashi and M. Suzuki, Phys. Rev. Lett. 16, 255 (1966); Riazuddin and Fayyazuddin, Phys. Rev. 147, 1071 (1966).
8. G. Arnison et al., Phys. Lett. B139, 115 (1984).

VECTOR RESONANCES FROM STRONG INTERACTING HIGGS

D. Dominici^{*}
Département de Physique Théorique
Université de Genève
1211 Genève 4, Switzerland

ABSTRACT

An effective lagrangian for electroweak interactions in the limit of large Higgs mass is considered. Vector boson resonances are described by assuming the $SU(2)_V$ hidden local symmetry is dynamically realized. The low energy phenomenology of weak interactions can be rather closely reproduced even for relatively low masses of the new vector bosons.

^{*} On leave from : Dipartimento Fisica, Università di Firenze, Italy.

Recently considerable effort has been devoted to investigate the consequences of a large Higgs mass in the Standard Model. It is known^{1,2)} from long time that if M_H is sufficiently large, then $W - W$ scattering saturates unitarity for $s \geq 1.8\text{TeV}$ and weak interactions become strong. A $J = 0$ bound state is then expected to exist^{2,3)} with a width which is comparable to its mass.

We expect also $J = 1$ bound states, which could be relevant for their low energy effects^{4,5)}.

A convenient tool to investigate the formation of vector bound states is the linear formulation of the non-linear σ -model. It is known that when $M_H \rightarrow \infty$ the Higgs lagrangian is replaced by the $SU(2) \times SU(2)$ non-linear σ -model lagrangian⁶⁾. It is possible to reformulate this non-linear σ -model in a linear way by introducing vector fields of a hidden local symmetry^{7,8)}. Such composite vector fields are, at the classical level, auxiliary fields and can be eliminated by recovering the usual non-linear σ -model. However, in two dimensions, one loop computations⁹⁾ show that these vector fields become dynamical. Such a possibility, even if not proved in four dimensions, has been used in supergravity¹⁰⁾. We therefore assume that such composite vector fields become dynamical.

The Higgs sector of the Weinberg-Salam model can be formulated as a $SU(2)_L \times SU(2)_R$ gauged σ -model in terms of a 2×2 matrix M .

A formal way to investigate the consequences of a large Higgs mass is to take the limit $M_H \rightarrow \infty$. Then we get $M^+ M = f^2$, and we pass from the linear to the non-linear σ -model⁶⁾:

$$L = \frac{f^2}{4} \text{Tr} D_\mu U (D_\mu U)^\dagger + \text{gauge terms} \quad (1)$$

where we introduce the dimensionless field $U = M/f$ and

$$D_\mu U = \partial_\mu U + i(g/2) \vec{W}_\mu \cdot \vec{\tau} U + i(g'/2) U \vec{B}_\mu \tau_3.$$

If we denote by $g_{L,R}$ a group element of $SU(2)_{L,R}$, and by $v_\mu^{(0)}$ a vector field of $SU(2)_V$ we consider the following effective lagrangian (see Ref. (5) for the derivation)

$$L = -\frac{f^2}{4} [\text{Tr}(g_{L\mu}^+ g_L - g_{R\mu}^+ g_R)^2 + \alpha \text{Tr}(g_{L\mu}^+ g_L + g_{R\mu}^+ g_R)^2] \quad (2)$$

where $D_{\mu}^L g_L = \partial_{\mu} g_L + W_{\mu}^{(0)} g_L - g_L v_{\mu}^{(0)}$, $D_{\mu}^R g_R = \partial_{\mu} g_R + Y_{\mu} g_R - g_R v_{\mu}^{(0)}$, $Y_{\mu} = Y_{\mu} \tau_3 / 2$, $W_{\mu}^{(0)} = \vec{W}_{\mu} \cdot \vec{\tau} / 2$, and α is an arbitrary parameter.

If the vector field $v_{\mu}^{(0)}$ has no kinetic term, it can be eliminated and (2) becomes equivalent to (1) by identifying $U = g_L^+ g_R$.

Assuming that such a kinetic term is generated by quantum corrections, and performing the transformation $W_{\mu}^{(0)} = g_L g_R^+ \tilde{W}_{\mu} g_R + g_L g_R^+ \partial_{\mu} (g_R g_L^+)$, $v_{\mu}^{(0)} = g_R^+ \tilde{V}_{\mu} g_R + g_R^+ \partial_{\mu} g_R$ we get

$$L = -\frac{f^2}{4} \{ \text{Tr} [\tilde{W}_{\mu} - Y_{\mu}]^2 + \alpha \text{Tr} [\tilde{W}_{\mu} + Y_{\mu} - 2\tilde{V}_{\mu}]^2 \} + \text{kin. terms} . \quad (3)$$

Therefore the phenomenological lagrangian becomes equivalent (in this gauge) to a non renormalizable massive Yang-Mills theory. Then we expect again a violation of the unitarity in the W - W scattering for sufficiently large s .

After a rescaling $\tilde{W} \rightarrow g\tilde{W}$, $Y \rightarrow g'Y$, $2\tilde{V} \rightarrow g''\tilde{V}$ and a diagonalization we get the mass eigenvalues and eigenvectors. Here for simplicity we report the expression for the masses in the limit of large g'' . Notice that for $g'' \rightarrow \infty$, the vector bosons of the hidden symmetry decouple and we recover the standard mass formulae for W^{\pm} , Z^0 :

Charged sector :

$$\begin{aligned} W_i &= \tilde{W}_i \cos \varphi - \tilde{V}_i \sin \varphi \\ V_i &= \tilde{W}_i \sin \varphi + \tilde{V}_i \cos \varphi \\ M_W^2 &\sim \frac{f^2}{4} g^2 (1 - (g/g'')^2) & M_V^2 &\sim \frac{f^2}{4} \alpha g''^2 \\ \varphi &\sim -g/g'' \end{aligned} \quad i = 1, 2 \quad (4)$$

Neutral sector :

$$\begin{aligned} A &= A_2 \cos \psi + \tilde{V}_3 \sin \psi \\ Z^0 &= A_1 \cos \xi + A_2 \sin \xi \sin \psi - \tilde{V}_3 \sin \xi \cos \psi \end{aligned}$$

$$V^0 = \bar{A}_1 \sin \xi - \bar{A}_2 \cos \xi \sin \psi + \bar{V}_3 \cos \xi \sin \psi$$

where $A_1 = (g\tilde{W}_3 - g'Y)/G$, $A_2 = (g'\tilde{W}_3 + gY)/G$, $G = (g^2 + g'^2)^{1/2}$

$$M_A^2 = 0 \quad M_{Z^0}^2 \sim \frac{f^2}{4} (g^2 + g'^2) \left[1 - \frac{(g^2 - g'^2)^2}{G^2 g'^2} \right] \quad (5)$$

$$M_{V^0}^2 \sim \frac{f^2}{4} \alpha g'^2$$

$$\xi \sim \frac{1}{g''} \frac{g^2 - g'^2}{G}, \quad \psi \sim \frac{1}{g''} \frac{2gg'}{G}$$

In order to examine the low energy effects we consider the coupling to the fermions (for sake of simplicity we limit ourselves to the case where $b = 0$ of Ref. (5)) :

Charged couplings :

$$(h_W W_\mu^{(i)} + h_V V_\mu^{(i)}) T_{iL} \quad i = 1, 2$$

$$h_W = g \cos \varphi$$

$$h_V = g \sin \varphi$$

Neutral couplings :

$$Z_\mu^0 [AT_{3L} + BQ_{em}] + A_\mu eQ_{em} + V_\mu^0 [CT_{3L} + DQ_{em}]$$

$$e = \frac{gg'}{G} \cos \psi$$

$$A = G \cos \xi \quad B = -g'^2/G \cos \xi (1 - g/g' \operatorname{tg} \xi \sin \psi)$$

$$C = G \sin \xi \quad D = -g'^2/G \sin \xi (1 + g/g' \operatorname{ctg} \xi \sin \psi) .$$

The effective low energy hamiltonian for neutral current can be written as

$$H_I^{NC} = \frac{a}{4} \{ [T_{3L} + XQ_{em}]^2 + cQ_{em}^2 \}$$

where a, X, c can be expressed in terms of A, B, C, D . The measured ρ param-

eter can be obtained from the neutral to charged current hamiltonian ratio, $\rho = \frac{\sqrt{2}}{8} a/G_F$. We determine g, g' and f by fitting G_F, e, X . Then we check that even for relatively small values of M_V one obtains only small deviations from the predictions of the standard model. For instance even if we take $M_V = 150\text{GeV}$, then for $g'^2 = 20g^2$ we find

$$\rho - 1 = -.007 \quad \Delta M_W^2/M_W^2 = .04 \quad \Delta M_{Z^0}^2/M_{Z^0}^2 = .06 \quad c = .003$$

In addition to the coupling of the V to the fermions via the mixing with the W we expect also direct couplings.

If we introduce, in correspondence of each fermion doublet ψ_L , the new fermion field $\chi_L = g_L^+ \psi_L$ which is a singlet under the $SU(2)_L \times SU(2)_R$ and doublet under the local $SU(2)_V$, then we have the direct coupling

$$b \bar{\chi}_L i \gamma^\mu (\partial_\mu + \vec{V}_\mu^{(0)} \cdot \tau/2 + \frac{1}{2} (B-L) Y_\mu) \chi_L$$

where b is a new constant of the effective lagrangian and $B(L)$ is the baryon (lepton) number.

By repeating the fit using the new couplings and $b = .1$ we get now even smaller deviations from the predictions of the standard model :

$$\rho - 1 = .001 \quad \Delta M_W^2/M_W^2 = .004 \quad \Delta M_{Z^0}^2/M_{Z^0}^2 = .003 \quad c = .0007$$

The fermion decays of these new vector bosons would give rise to events of the same topology of W and Z .

Furthermore trilinear couplings can give $V^\pm \rightarrow W^\pm Z^0$ and $V^0 \rightarrow W^+ W^-$, whenever kinematically allowed.

ACKNOWLEDGEMENTS

I wish to thank R. Casalbuoni, S. De Curtis and R. Gatto for the enjoyable collaboration and interesting discussions on the work on which this talk is based.

REFERENCES

- 1) M. Veltman, Acta Physica Polonica B8, 475 (1977).
M. Chanowitz and M.K. Gaillard, Phys. Lett. 142B, 85 (1984).
M.K. Gaillard, Berkeley preprint UCB PTH 84/2 (1984).
- 2) B.W. Lee, C. Quigg and H.B. Thacker, Phys. Rev. D16, 1519 (1979).
- 3) M.R. Einhorn, Nucl. Phys. 246B, 75 (1984).
R. Casalbuoni, D. Dominici and R. Gatto, Phys. Lett. 147B, 419 (1984).
- 4) P.Q. Hung and H.B. Thacker, Fermilab-Pub 84/104 (1984).
P.Q. Hung, these Proceedings.
- 5) R. Casalbuoni, S. De Curtis, D. Dominici and R. Gatto, UGVA-DPT 1985/02-456.
- 6) T. Appelquist and C. Bernard, Phys. Rev. 22D, 200 (1980).
A.C. Longhitano, Phys. Rev. 22D, 1166 (1980).
- 7) See for example : A.P. Balachandran, A. Stern and G. Trahern, Phys. Rev. 19D, 2416 (1979).
- 8) For recent application to QCD see M. Bando, T. Kugo, S. Uehara, K. Yamawaki and T. Yanagida, RRK 84-22.
M. Bando, T. Kugo and K. Yamawaki, DPNU-38-84, DPNU-45-84.
- 9) A. D'Adda, P. Di Vecchia and M. Lüscher, Nucl. Phys. B146, 73 (1978);
ibidem B152, 125 (1979).
- 10) E. Cremmer and B. Julia, Phys. Lett. 80B, 48 (1978); Nucl. Phys. B159, 141 (1979).

GAUGE BOSON/HIGGS BOSON UNIFICATION,
 N = 2 SUPERSYMMETRY,
 GRAND UNIFICATION,
 AND NEW SPACETIME DIMENSIONS

Pierre FAYET

Laboratoire de Physique Théorique de l'Ecole Normale Supérieure
 24, rue Lhomond, 75231 PARIS CEDEX 05 - FRANCE



ABSTRACT

We discuss the physical consequences of simple ($N = 1$) and extended ($N = 2$) supersymmetries, in particular the new relations they provide between massive spin-1 gauge bosons and spin-0 Higgs bosons.

Extended supersymmetric theories predict the existence of spin-0 photons and gluons coupling leptons and quarks to their mirror partners. The anticommutator of the two supersymmetry generators includes a term proportional to the weak hypercharge, and determines the value of the grand-unification mass m_X . In minimal $N = 2$ supersymmetric GUTs, the proton is expected to be stable.

Such theories may be formulated in a 6-dimensional spacetime. The GUT mass m_X is generated by the additional components of the momentum along the extra compact dimensions. This leads to the possibility of computing m_X proportionately to $\frac{M}{L_c}$, L_c being the size of an extra dimension.

1. MOTIVATIONS FOR SUPERSYMMETRY AND EXTENDED SUPERSYMMETRY.

Supersymmetric theories associate bosons with fermions in multiplets ¹⁾. Supersymmetry was originally considered, most of the time, as an interesting structure for quantum field theory, without, unfortunately, any application to the description of the physical world. Nevertheless it is possible to make supersymmetry a physically meaningful invariance. This requires the introduction of a whole set of new particles: photinos and gluinos, Winos and Zinos, spin-0 leptons and quarks, etc., which have not been observed yet.

There is, presently, no convincing experimental evidence in favor of supersymmetry. The reasons for considering this new invariance are, still, purely theoretical:

i) better understanding of the Higgs sector of gauge theories, owing to the unification provided by supersymmetry between massive gauge bosons and Higgs bosons: spin-0 Higgs bosons now appear as the superpartners of massive spin-1 gauge bosons ²⁾;

ii) connection with gravitation, which is automatically present as soon as the supersymmetry algebra is realized locally (supergravity) ³⁾;

iii) and, as an additional motivation in the framework of grand-unification, hope of a solution to the hierarchy problem.

Gauge boson / Higgs boson unification in N=2 extended supersymmetry.

Grand-unified theories, however, require the existence of a rather large number of Higgs bosons. In a grand-unified theory with only a simple (N=1) supersymmetry most spin-0 Higgs bosons would remain unmatched with massive spin-1 gauge bosons. In order to get a better understanding of the Higgs sector of GUTs and supersymmetric GUTs we are led to use a more powerful symmetry, N=2 extended supersymmetry, also called hypersymmetry. In such theories, which are invariant under a set of N=2 supersymmetry generators Q^1 and Q^2 , every massive spin-1 gauge boson may be associated with either one or five spin-0 Higgs bosons ⁴⁾:

$$1 \text{ massive spin-1 gauge boson} \longleftrightarrow 1 \text{ spin-0 Higgs boson} \quad (1)$$

(e.g. $X^{\pm 4/3}$)

or

$$1 \text{ massive spin-1 gauge boson} \longleftrightarrow 5 \text{ spin-0 Higgs bosons} \quad (2)$$

(e.g. W^{\pm} , Z , or $\gamma^{\pm 1/3}$)

This leads to an interesting structure for the gauge and Higgs sectors of $N=2$ supersymmetric GUTs (cf. Table 2 in Section IV). In an $SU(5)$ theory, each of the W^{\pm} , Z and $\gamma^{\pm 1/3}$'s is associated with 4 spin-1/2 inos and 5 spin-0 Higgs bosons, while the $X^{\pm 4/3}$ is associated with only 2 spin-1/2 Xinos and 1 spin-0 Higgs boson⁵⁾.

The GUT mass originates from the extended SUSY algebra.

In $N=2$ supersymmetry the grand-unification mass appears in an algebraic way, in the anticommutation relations of the two supersymmetry generators. Next to the usual anticommutation relations of one supersymmetry generator with itself:

$$\{Q^1, \bar{Q}^1\} = \{Q^2, \bar{Q}^2\} = -2\mathcal{H} \quad (3)$$

there is another anticommutation relation, which reads:

$$\{Q^1, \bar{Q}^2\} = -\{Q^2, \bar{Q}^1\} = 2Z \quad (4)$$

Z is a spin-0 symmetry generator called a central charge. It has the dimension of a mass and reads⁵⁾:

$$Z = \begin{array}{l} \text{Global symmetry} \\ \text{generator} \end{array} + \begin{array}{l} \text{Spontaneously-generated term,} \\ \text{proportional to the weak hypercharge} \\ Y = 2 \cdot (Q - T_3) \\ \text{(with a coefficient } \sim m_X) \end{array} \quad (5)$$

The eigenvalues of Z for the GUT bosons $X^{\pm 4/3}$ and $\gamma^{\pm 1/3}$ are precisely equal to \mp the value of the grand-unification mass m_X !

Mirror particles, and spin-0 photons and gluons.

$N=2$ supersymmetry predicts the existence of mirror leptons and quarks (a source of serious difficulties!) and of spin-0 photons and gluons⁴⁾. The latter are related to the spin-1 photon and gluons, and to pairs of spin-1/2

photinos and gluinos. They are described by the same adjoint Higgs field (e.g. a 24 of SU(5)) which is also responsible for the spontaneous breaking of the grand-unification symmetry.

Proton stability.

In an N=2 supersymmetric GUT the mass splittings in the grand-unification multiplets turn out to be of order m_χ for the fermions (including leptons and quarks) as well as for the gauge bosons and Higgs bosons. This is a consequence of the N=2 supersymmetry algebra itself (eqs. (4,5)). As a result grand-unification provides us with the following associations:

$$\begin{array}{ll}
 \left. \begin{array}{l} \curvearrowright \text{ Light leptons} \\ \curvearrowleft \text{ Heavy quarks of mass } \simeq m_\chi \end{array} \right\} &
 \left. \begin{array}{l} \curvearrowright \text{ Light quarks} \\ \curvearrowleft \text{ Heavy leptons of mass } \simeq m_\chi \end{array} \right\} \quad (6)
 \end{array}$$

It follows that, in minimal N=2 SUSY GUTs, the proton tends to be absolutely stable ! 6)

6-dimensional theories.

Moreover, N=2 supersymmetric theories in 4 dimensions may be obtained from a N=1 theory in a 6-dimensional spacetime, the 5th and 6th dimensions being compact. One can then rewrite formulas (3,4) as a single anticommutation relation in the 6d spacetime, and establish a relation between the grand unification mass and the extra components of the (covariant) momentum along the compact dimensions. The spin-0 symmetry operator Z appears as the 5th component of the covariant 6-momentum $\mathcal{P}^{\hat{u}} = -i \mathcal{D}^{\hat{u}}$:

$$Z \rightsquigarrow \mathcal{P}^5 = -i \mathcal{D}^5 \quad (7)$$

While the W^\pm and Z masses are already present in the 6-dimensional theory, the grand-unification mass m_χ is associated with the large values of the covariant momenta carried by the $\chi^{\pm 4/3}$ or $\gamma^{\pm 1/3}$ along the extra compact dimensions 5). This leads to the possibility of computing m_χ in terms of the lengths of these dimensions:

$$m_\chi \sim \frac{\hbar}{L_c} \quad (8)$$

2. N=1 SUPERSYMMETRY AND GAUGE BOSON / HIGGS BOSON UNIFICATION.

a) The supersymmetry algebra

Supersymmetric theories are invariant under a self-conjugate spin-1/2 supersymmetry generator Q which changes the spin of particles by 1/2 unit, transforming bosons into fermions and conversely ¹⁾ :

$$\begin{aligned} Q | \text{boson} \rangle &= | \text{fermion} \rangle \\ Q | \text{fermion} \rangle &= | \text{boson} \rangle \end{aligned} \quad (9)$$

Q satisfies commutation relations with boson fields and anticommutation relations with fermion fields:

$$\begin{aligned} [Q, \text{boson field}] &= \text{fermion field} \\ \{Q, \text{fermion field}\} &= \text{boson field} \end{aligned} \quad (10)$$

By iterating (10), one finds the equations:

$$[\{Q, \bar{Q}\}, \text{field}] = 2i \gamma^\mu \partial_\mu (\text{field}) \quad (11)$$

where ∂_μ (field) is the 4-derivative of the original (bosonic or fermionic) field considered. This can be rewritten as follows:

$$\{Q, \bar{Q}\} = -2 \not{P} \quad (12)$$

Equation (12), together with

$$[Q, P^\mu] = 0 \quad (13)$$

(which expresses that the result of a supersymmetry transformation does not depend on the space-time point where it is performed), defines the supersymmetry algebra. The appearance of the generator of translations P^μ in the right-hand side of equation (12) indicates a connection between supersymmetry and space-time. This is at the origin of the relation between supersymmetry and gravitation ³⁾.

b) Minimal content of a N=1 supersymmetric gauge theory

Any (linear) representation of supersymmetry describes equal numbers of bosonic and fermionic states. They would all have the same masses if supersymmetry remained unbroken. Supersymmetry can only be, at best, a spontaneously broken symmetry.

Spontaneous breaking of global supersymmetry is made difficult by the presence of the hamiltonian in the algebra (cf. formula (12)). It has the consequence that, whenever a supersymmetric vacuum state exists, it must be stable. This is in sharp contrast with what happens for an ordinary gauge symmetry: the gauge symmetric state can easily be made unstable, gauge invariance being then spontaneously broken.

Remarkably enough, a spontaneous breaking of global supersymmetry, although hard to obtain, is still possible. It generates a massless neutral spin-1/2 Goldstone fermion called a goldstino. This one, however, cannot be identified with a neutrino.

Even if supersymmetry is spontaneously broken, we still need to introduce a rather large number of new particles into the theory. The superpartners of the photon and the W^- should not be interpreted as the neutrino and the electron, but as new particles called photino and Winos. In a similar way the octet of gluons is associated with an octet of spin-1/2 self-conjugate fermions called gluinos. Leptons and quarks are associated with spin-0 leptons and quarks (two of them for every Dirac fermion) ¹⁾.

Let us consider the massive gauge bosons W^\pm and Z. They are, in fact, associated with two (Dirac) Winos, and two (self-conjugate) Zinos, together with spin-0 particles. The last ones are precisely charged and neutral spin-0 Higgs bosons denoted by w^\pm and z, respectively.

Remarkably enough supersymmetry allows one to obtain relations between particles having, not only different spins (1, 1/2 or 0) but also ²⁾ :

- different electroweak properties: the W^\pm and Z belong to an electroweak triplet and a singlet; the Higgs bosons w^\pm and z to electroweak doublets; and the Winos and Zinos are mixings of triplet, singlet and doublet components;
- couplings of very different strengths: the gauge bosons couple proportionately to g or g', the Higgs bosons proportionately to (g or g') $\frac{m(\text{fermions})}{(m_W \text{ or } m_Z)}$.

The spontaneous breaking of the $SU(2) \times U(1)$ electroweak gauge symmetry makes use of two doublet Higgs superfields instead of only one, and this, for two reasons: i) to have the required degrees of freedom for constructing 2 massive charged Dirac fermions, which will be the two Winos associated with the W^\pm under supersymmetry; and ii) to generate masses for both charge $+2/3$ quarks on one hand, charge $-1/3$ quarks and charged leptons, on the other hand. Then one gets the following minimal scheme, common to all supersymmetric theories irrespectively of the supersymmetry breaking mechanism one considers ^{1,2} :

TABLE 1

Minimal content of a supersymmetric gauge theory

Spin 1	Spin 1/2	Spin 0
Gluons Photon	Gluinos Photino	
W^\pm Z	2 (Dirac) Winos 2 (Majorana) Zinos	w^\pm z
-----	-----	-----
	1 (Majorana) higgsino	standard h^0 pseudoscalar h'^0 } Higgs bosons
	Leptons Quarks	Spin-0 leptons Spin-0 quarks
+ Gravitation multiplet : Spin 2 graviton, and spin -3/2 gravitino		

The spin-2 graviton and its superpartner, the spin-3/2 gravitino, are present as soon as the supersymmetry algebra is realized locally. (Moreover, if an extra $U(1)$ group is gauged, there is also a second neutral massive gauge boson, U , which acquires a mass while the pseudoscalar h^0 is eliminated; then one has a perfect association between the four massive spin-1 gauge bosons W^\pm , Z and U , and the four spin-0 Higgs bosons w^\pm , z and h^0 .)

c) Supersymmetry breaking and mass spectrum

Supersymmetry is not an apparent symmetry of the physical world, otherwise bosons and fermions would be degenerate in mass, which obviously is not the case.

As we have already said, spontaneous breaking of global supersymmetry generates a massless neutral spin-1/2 particle named a goldstino; it couples leptons and quarks to spin-0 leptons and spin-0 quarks, etc.

In global supersymmetry, one can generate large masses for spin-0 leptons and quarks, at the tree approximation, if and only if the gauge group is extended to include an extra $U(1)$ factor: i.e. it can be $SU(3) \times SU(2) \times U(1) \times U(1)$, or $SU(5) \times U(1)$, etc.. (The additional neutral gauge boson, U , might possibly be responsible for the somewhat too large value of the asymmetry observed in $e^+e^- \rightarrow \mu^+\mu^-$ scatterings at PETRA.)

In locally supersymmetric theories however, there is no goldstino: it is eliminated by the super-Higgs mechanism while the superpartner of the graviton, the spin-3/2 gravitino, acquires a mass. If the gravitino mass $m_{3/2}$ is large, this parameter may be responsible for large mass splittings between ordinary particles and their superpartners: cf. the spectrum represented in Fig. 1.

d) Winos and Zinos : light or heavy ?

Winos and Zinos are a model-independent prediction of the supersymmetric electroweak theory ¹⁾ (cf. Table 1), irrespectively of either grand-unification, or supergravity.

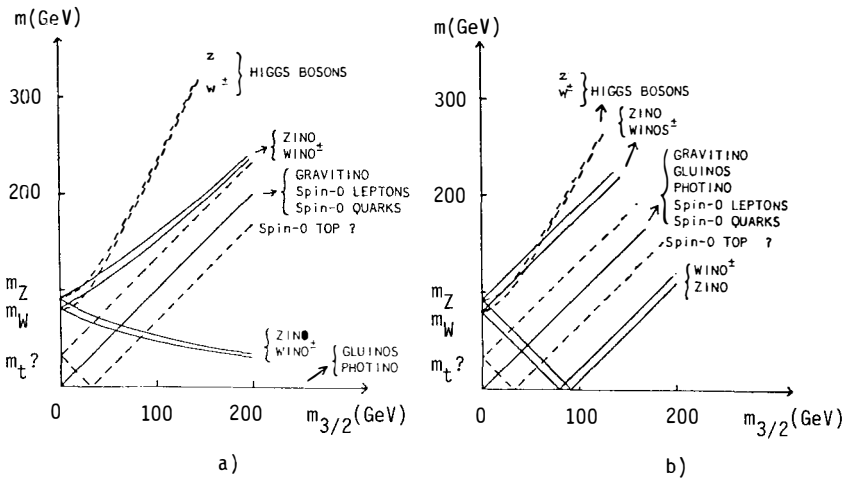


Fig. 1 : Examples of mass spectra for the superpartners of leptons and quarks, photon, gluons, W^\pm and Z , in a class of models with gravity-induced supersymmetry breaking⁷⁾, as a function of the gravitino mass $m_{3/2}$. Spin-0 leptons and quarks have masses: $|m_{3/2} \pm m_{L(Q)}|$; and the spin-0 Higgs bosons w^\pm and z associated with the W^\pm and Z :

$$\sqrt{m_{W,Z}^2 + 4m_{3/2}^2}$$

In a) there is no gravitation-induced direct mass term for gauginos, so that the photino and gluinos may be relatively light. The Wino and Zino masses are then given by

$$\sqrt{m_{W,Z}^2 + \frac{1}{4}m_{3/2}^2} \quad \pm \frac{1}{2}m_{3/2}$$

In b) the photino and gluinos have the same masses as the gravitino, and the Wino and Zino masses are $|m_{W,Z} \pm m_{3/2}|$. The lightest superpartner could be either the photino (case a), or a Wino or a Zino, a spin-0 t or b quark, or a higgsino, ... (case b). If $m_{3/2}$ becomes relatively large, we lose the hope of observing spin-0 leptons and quarks very soon, but one of the Winos and one of the Zinos may then be accessible.

The two charged Dirac Winos are always built from

- a gaugino field λ^- (a member of an electroweak triplet)
 - a higgsino field Ψ^- (a member of an electroweak doublet)
- (14)

The way the two Winos mix and the masses they acquire are, however, model-dependent: they depend, in particular, on the supersymmetry breaking mechanism considered.

i) Extra U(1) breaking.

In theories in which the supersymmetry breaking is triggered by an extra U(1) factor in the gauge group, the two Wino mass eigenstates usually are the R-eigenstates ⁸⁾

$$\begin{cases} \text{Wino}_1 = \text{gaugino}_L + \text{higgsino}_R & (R = +1) \\ \text{Wino}_2 = \text{higgsino}_L + \text{gaugino}_R & (R = -1) \end{cases} \quad (15)$$

Their masses verify ⁸⁾

$$m^2(\text{Wino}_1) + m^2(\text{Wino}_2) = 2 m_W^2 \quad (16)$$

which implies:

$$m(\text{Wino}_{1(2)}) \leq m_W \leq m(\text{Wino}_{2(1)}) \quad (17)$$

At the same time the two Majorana Zinos combine (in a R-invariant theory) to form a single Dirac Zino of mass m_2 , carrying $R = +1$.

Formulas (16,17) allow for the existence of a relatively light Wino. Indeed we suggested in 1976 that the newly-discovered τ lepton might be identified with a charged Wino ⁸⁾. Although this is no longer an acceptable possibility, a relatively light Wino might still exist, provided it is heavier than about $20 \text{ GeV}/c^2$.

ii) Gravity-induced breaking.

In a similar way, a relatively light Wino may also exist if one makes use of gravity-induced supersymmetry breaking. In that case, however, the existence of a Wino lighter than the W is no longer a necessity. We still have two Dirac

Winos (cf. formula (14)) but now they mix differently. If the two Higgs doublets responsible for the electroweak symmetry breaking acquire equal vacuum expectation values the mixing preserves parity and we get:

$$\begin{cases} \text{Wino}_1 = \cos \omega \text{ (higgsino)} + \sin \omega \text{ (gaugino)} \\ \text{Wino}_2 = -\sin \omega \text{ (higgsino)} + \cos \omega \text{ (gaugino)} \end{cases} \quad (18)$$

The Wino and Zino masses may be given by formulae such as, for example ⁷⁾ :

i) in the absence of direct gaugino mass terms

$$m \begin{pmatrix} \text{Winos} \\ \text{Zinos} \end{pmatrix} = \sqrt{m_{W(Z)}^2 + \frac{1}{4} m_{3/2}^2} \pm \frac{1}{2} m_{3/2} \quad (19)$$

ii) in the presence of direct gaugino mass terms equal to $\pm m_{3/2}$, (which make the photino and gluinos heavy at the tree approximation)

$$m \begin{pmatrix} \text{Winos} \\ \text{Zinos} \end{pmatrix} = \left| m_{W(Z)} \pm m_{3/2} \right| \quad (20)$$

or, alternately:

$$m \begin{pmatrix} \text{Winos} \\ \text{Zinos} \end{pmatrix} = \sqrt{m_{W(Z)}^2 + m_{3/2}^2} \quad (21)$$

Formulas (19,20) allow for the existence of a relatively light Wino (or Zino), the other one being heavy. Formulas (21), however, (which also give the mass spectrum of Winos and Zinos in a N=2 supersymmetric GUT ⁵⁾) require all Winos and Zinos to be heavier than m_W and m_Z , respectively.

3. CONSEQUENCES OF SUPERSYMMETRY

a) R-parity and the interactions of the new particles

Ordinary particles can be distinguished from their superpartners by means of a new quantum number, R, associated with a continuous or discrete invariance. In the latter case one talks about R-parity, $(-1)^R$. Ordinary particles all have $R = 0$, while their superpartners, gravitinos, gluinos and photinos, Winos and Zinos, spin-0 leptons and quarks... all have $R = \pm 1$.

R-parity ⁹⁾ may be defined as

$$(-1)^R = (-1)^{2S} (-1)^{3(B-L)} \quad (22)$$

and usually does remain unbroken. This is essential in the study of the production and decay of the new particles predicted by supersymmetry. The new particles can only be pair-produced. The decay of an R-odd particle will, ultimately, lead to the lightest R-odd particle. This could be the photino, but it is not necessary (cf. Fig. 1).

As an example one may have, in agreement with R-parity conservation, the following decays, which are represented in Fig. 2:

spin-0 electron \rightarrow electron + photino (or goldstino)

spin-0 quark \rightarrow quark + gluino (photino, or goldstino)

gluino \rightarrow quark + antiquark + photino (or goldstino)

$W^\pm, Z \rightarrow$ pair of spin-0 leptons, or quarks

Wino $^\pm \rightarrow$ photino (...) + $q\bar{q}'$ (or $1^\pm \nu'$) (23)

b) Searching for the new particles

Much work has been done in order to search for the new particles predicted by supersymmetry ^{1,10}).

The first particles one became interested in were those which might have been relatively light, and manifest themselves at not-too-high energies: namely gluinos (and the R-hadrons they could form by combining with quarks, antiquarks and gluons), photinos and goldstinos (or gravitinos), and spin-0 leptons.

The standard signal for gluino production is that gluinos should decay emitting a (light) neutral spin-1/2 particle (photino or goldstino) which would carry away part of the energy-momentum ⁹). The present experimental limits indicate that gluinos should be heavier than a few GeV/c^2 ¹¹). The exact value of the limit depends on the spin-0 quark masses: in beam dump experiments one searches for gluinos by looking at the reinteraction with matter of the photinos emitted in gluino decays (cf. Fig. 2c); but photino interactions depend on the spin-0 quark masses $m_{\tilde{q}}$ as follows:

$$\sigma(\text{photino} + \text{nucleon} \rightarrow \text{gluino} + \text{hadrons}) \approx \frac{32\pi\alpha_s}{9m_{\tilde{q}}^4} \langle \sum_i Q_i^2 x_i \rangle_s \quad (24)$$

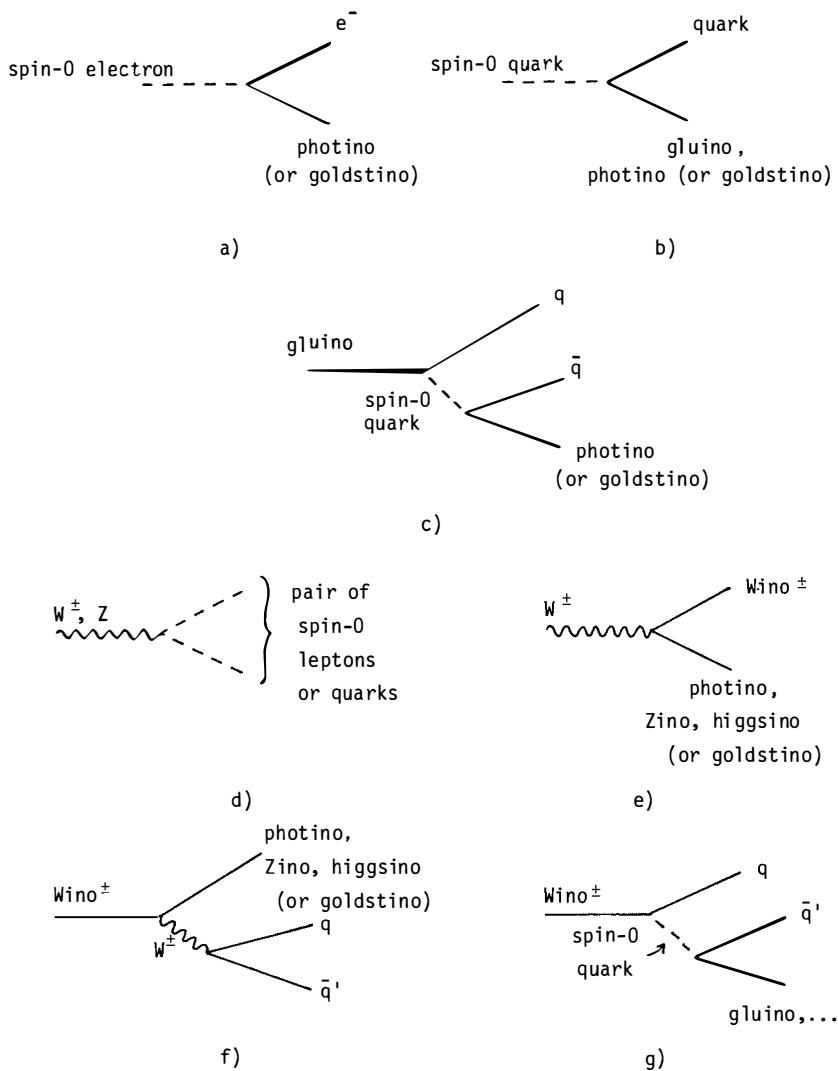


Fig. 2 : Possible decay modes involving the new R -odd particles : spin-0 leptons and quarks, Winos and Zinos, photinos, higgsinos, goldstinos.

By looking at the production of unstable spin-0 leptons in e^+e^- annihilation one gets the following limits ^{12,13}):

$$\begin{cases} m(\text{spin-0 electrons}) > 22 \text{ GeV}/c^2 \\ m(\text{spin-0 muons}) > 20 \text{ GeV}/c^2 \\ m(\text{spin-0 taus}) > 18 \text{ GeV}/c^2 \end{cases} \quad (25)$$

For spin-0 electrons the limit can be increased to 25 GeV/c^2 by searching for the production of a single spin-0 electron in association with a photino. A better limit can be obtained by searching for the process ^{14,15})

$$e^+e^- \rightarrow \gamma + 2 \text{ photinos} \quad (26)$$

induced by the exchanges of spin-0 electrons (see Fig. 3).

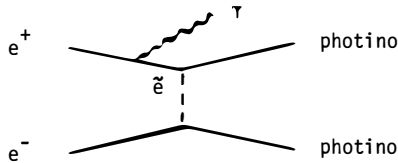


Fig. 3 : Radiative production of a photino pair in e^+e^- annihilation. \tilde{e} denotes a spin-0 electron.

Present experimental results indicate that

$$m(\text{spin-0 electrons}) > 37 \text{ GeV}/c^2 \quad (27)$$

if the two spin-0 electrons are mass-degenerate; if one of them were very heavy, the second could be as light as $30 \text{ GeV}/c^2$ ^{16,17}). (To obtain these limits one assumes that the photino is lighter than a few GeV/c^2). This reaction could allow one to detect the effects of spin-0 electrons lighter than 40 or maybe 50 GeV/c^2 . Beyond the signal gets rather small and there is a competing background (!) from $e^+e^- \rightarrow \gamma \nu \bar{\nu}$.

Moreover, the search for single γ 's in e^+e^- annihilations, produced by the reaction

$$e^+e^- \rightarrow \gamma + \text{photino} + \text{gravitino} \quad (28)$$

also leads to a lower limit on the mass of a spin-3/2 gravitino ¹⁴⁾. From the results of Ref. 16) we infer

$$m_{3/2} > 10^{-6} \text{ eV}/c^2 \quad (29)$$

After the discovery of the W^\pm and Z bosons one can also search for the production of spin-0 leptons and quarks, Winos and Zinos, photinos and higgsinos in W^\pm and Z decays, provided of course these particles are not too heavy. More generally a systematic search for the effects of the new particles, specially spin-0 quarks, gluinos and photinos, is presently in progress at the CERN $p\bar{p}$ collider.

4. EXTENDED SUPERSYMMETRY AND EXTRA SPACETIME DIMENSIONS

a) General features of N=2 supersymmetry

As discussed in section 1, one is led to contemplate the possibility for Nature to be invariant, not only under a simple supersymmetry algebra involving a single (N=1) spinorial generator Q, but under an extended supersymmetry algebra involving N=2 spinorial generators Q^i : (i=1,2).

From the theoretical point of view such theories are much more constrained, and do not present yet enough flexibility to be completely realistic. Nevertheless, we can already discuss their main physical properties ⁴⁻⁶⁾:

i) existence of larger multiplets and therefore of a new set of gravitinos, photinos, gluinos, Winos and Zinos, etc.;

ii) existence of spin-0 photons and spin-0 gluons;

iii) existence of mirror leptons and quarks having V+A charged current weak interactions;

iv) existence of additional relations between massive spin-1 gauge bosons and spin-0 Higgs bosons.

The motivation for extended supersymmetry is not apparent at this stage; indeed N=1 supersymmetric theories of weak, electromagnetic and strong interactions, whose minimal content is given in Table 1, are quite appealing.

The situation, however, changes when one considers grand-unification also:

supersymmetric grand-unified theories require a rather large number of spin-0 Higgs bosons, and we no longer have a simple classification, as in Table 1. The Higgs sector gets quite complicated, and we do not know how many Higgses should be there, and to which representations they belong. This is precisely where extended supersymmetry will help.

The reader is probably getting tired of seeing again new unobserved particles show up in the theory, and will wonder why we need to introduce a second octet of gluinos, a second photino, etc. These particles, actually, are already present, although in a hidden way, in a grand-unified theory with only a simple (N=1) supersymmetry. The complex spin-0 Higgs field (such as the 24 of SU(5)) which breaks spontaneously the GUT symmetry describes an octet and a singlet of spin-0 particles which will be interpreted later as spin-0 gluons and spin-0 photons, respectively. Their fermionic partners are a second octet of Majorana fermions ("paragluinos"), similar to the gluinos, and a singlet one ("paraphotino") similar to the photino.

Requiring N=2 extended supersymmetry means, in particular, that there is no essential difference between the by-now familiar octet of gluinos, and the second octet of colored fermions which appears as a consequence of grand-unification. Altogether we get two octets of gluinos, two photinos, as well as a complex octet of spin-0 gluons, and a complex spin-0 photon. This is summarized in Fig. 4.

b) Massless and massive gauge hypermultiplets of N=2 supersymmetry

The extended supersymmetry algebra reads:

$$\{Q^1, \bar{Q}^1\} = \{Q^2, \bar{Q}^2\} = -2\mathcal{P} \quad (30)$$

as in formula (12). In addition, the two supersymmetry generators Q^1 and Q^2 also satisfy, together, an anticommutation relation

$$\{Q^1, \bar{Q}^2\} = - \{Q^2, \bar{Q}^1\} = 2Z \quad (31)$$

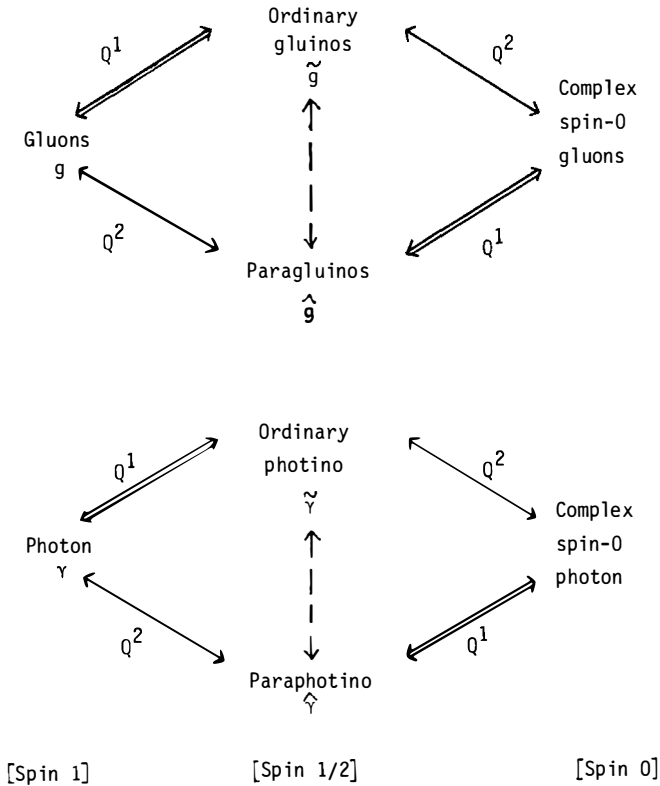


Fig. 4 : Relations between the gluons, the photon, and their spin-1/2 and spin-0 partners, in an $N=2$ extended supersymmetric theory. Q^1 denotes the action of the first supersymmetry generator, Q^2 the action of the second one. Spin-0 gluons and spin-0 photons are described by the adjoint Higgs field (e.g. a 24 of $SU(5)$) which breaks spontaneously the GUT symmetry. (They will appear, subsequently, as the 5th and 6th components of the gluon and photon 6-vector fields, in a 6-dimensional spacetime.)

Z is a spin-0 symmetry generator called a central charge, which has the dimension of a mass. Its explicit expression ⁵⁾ involves, in particular, neutral uncolored grand-unification symmetry generators, such as the weak hypercharge $Y = 2(Q - T_3)$.

With $SU(5)$ as the grand-unification gauge group we find:

$$\{Q^1, \bar{Q}^2\} = -\{Q^2, \bar{Q}^1\} = 2 \left[\begin{array}{c} \text{Global symmetry} \\ \text{generator} \end{array} - \frac{3}{5} m_X Y \right] \quad (32)$$

The central charge Z vanishes for the W^\pm and Z , γ and gluons, but equals

$$Z = \mp m_X \quad (33)$$

for the GUT bosons $X^{\pm 4/3}$ and $Y^{\pm 1/3}$ (which have weak hypercharge $Y = \pm \frac{5}{3}$).

We also find the mass relation

$$m_Y^2 = m_X^2 + m_W^2 \quad (34)$$

In $N=2$ extended supersymmetry the minimal particle content gets increased compared with that given in Table 1. It is illustrated in Table 2. As a consequence of extended supersymmetry, almost every Higgs boson now appears as the superpartner of a gauge boson. This association becomes complete if an extra $U(1)$ is gauged.

Note the existence of 3 different types of massive gauge hypermultiplets, with different field contents ⁴⁾:

- type I (like the W^\pm and Z): they describe 1 massive gauge boson, 4 spin-1/2 inos and 5 spin-0 Higgs bosons; and carry no central charge:

$$\mathcal{M} > |Z| = 0 \quad (35)$$

- type II (like the $X^{\pm 4/3}$): they describe 1 massive gauge boson, 2 spin-1/2 inos and 1 spin-0 Higgs boson, all complex; they carry a non-vanishing value of the central charge Z , and verify:

$$\mathcal{M} = |Z| > 0 \quad (36)$$

- type III (like the $Y^{\pm 1/3}$): they describe 1 massive gauge boson, 4 spin-1/2 inos and 5 spin-0 Higgs bosons, all complex; they carry a non-vanishing value of the central charge Z and verify:

$$\mathcal{M} > |Z| > 0 \quad (37)$$

TABLE 2

Minimal content of a $N=2$ supersymmetric theory, assuming $SU(5)$ as the gauge group ⁵⁾.

If an extra $U(1)$ is gauged, the higgsino multiplet is replaced by a neutral massive gauge multiplet describing the new neutral gauge boson U , 4 Majorana Uinos and 5 neutral Higgs bosons. Every spin-0 Higgs boson appears then as the superpartner of a spin-1 gauge boson.

Spin 1	Spin 1/2	Spin 0
$\chi^{\pm 4/3}$	2 charged color-triplet Dirac Xinos	1 charged color-triplet Higgs boson
$\gamma^{\pm 1/3}$	4 charged color-triplet Dirac Yinos	5 charged color-triplet Higgs bosons
W^{\pm}	4 charged Dirac Winos	5 charged Higgs bosons
Z	4 Majorana Zinos	5 neutral Higgs bosons
γ	2 Majorana photinos	2 spin-0 photons
gluons	2 color-octet Majorana gluinos	2 color-octet spin-0 gluons
	2 neutral Majorana higgsinos	4 neutral Higgs bosons
	Leptons and quarks + mirror partners	Spin-0 leptons and quarks + Mirrors
+ Gravitation multiplet : Spin-2 graviton, 2 spin-3/2 Majorana gravitinos, 1 spin-1 "graviphoton"		

Up to this point, the analysis is essentially model-independent, as was Table 1 for simple supersymmetric theories. The actual mass spectrum of the new particles, however, will depend on the way in which the supersymmetry breaking is performed. If it is induced by gravitation or by dimensional reduction, one tends to get, at the tree approximation

$$m_{\text{gluinos}} = m_{\text{photino}} = m_{3/2} \quad (38)$$

and

$$\begin{cases} m(\text{Winos}) = (m_W^2 + m_{3/2}^2)^{1/2} \\ m(\text{Zinos}) = (m_Z^2 + m_{3/2}^2)^{1/2} \end{cases} \quad (39)$$

up to radiative correction effects.

c) Replication of lepton and quark fields and proton stability in N=2 SUSY GUTs

A consequence of the appearance of the weak hypercharge operator Y in the anticommutation relation of two different supersymmetry generators (eq. (32)) is the existence of mass splittings $\sim m_\chi$ in all multiplets of the grand-unification group, i.e. in lepton and quark multiplets as well as in the gauge boson multiplet.

As a result the grand-unification symmetry associates light leptons with heavy quarks of mass $\simeq m_\chi$, and conversely, as indicated in section 1 (eq. (6)). It is therefore necessary to perform a replication of representations, in order to describe every single family of quarks and leptons ⁶⁾.

It follows that the $\chi^{\pm 4/3}$ and $\gamma^{\pm 1/3}$ gauge bosons (as well as their Higgs superpartners) do not couple directly light quarks to light leptons. The usual diagram responsible for the standard proton decay mode $p \rightarrow \pi^0 e^+$ does not exist! (cf. Fig. 5). A more refined analysis indicates that, in minimal N=2 SUSY GUTs, the proton is expected to be totally stable ⁶⁾.

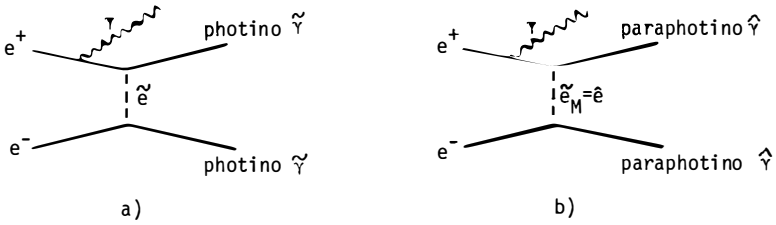


Fig. 7 : Production of photinos ($\tilde{\gamma}$) and paraphotinos ($\hat{\gamma}$) in e^+e^- annihilations. \tilde{e} denotes the two ordinary spin-0 electrons, $\tilde{e}_M = \hat{e}$ the two spin-0 partners of mirror electrons. The paraphotino couples electrons to mirror spin-0 electrons, and conversely.

e) Supersymmetric GUTS in a 5-or-6 dimensional spacetime

An additional interest of extended supersymmetric theories is that they can be formulated in a 6-dimensional spacetime ^{5,19}). The two photinos appearing in Fig. 4, or Table 2, originate from a single Weyl (chiral) spinor in 6 dimensions:

$$\begin{array}{ll}
 1 \text{ Weyl photino} & \longrightarrow & 2 \text{ Majorana photinos} \\
 \text{in 6 dim} & & \text{in 4 dim}
 \end{array} \tag{41}$$

$$\begin{array}{ll}
 1 \text{ Octet Weyl gluinos} & \longrightarrow & 2 \text{ Octet Majorana gluinos} \\
 \text{in 6 dim} & & \text{in 4 dim}
 \end{array} \tag{42}$$

Weyl spinors in 6 dimensions also describe, at the same time, ordinary leptons and quarks as well as their mirror partners.

The W^\pm and Z masses are already present in the 6-dimensional spacetime (i.e., they can be generated in a 6 d Poincaré invariant way). The grand-unification mass m_χ , on the other hand, only appears in the 4-dimensional theory: it is associated with the large values of the covariant momenta carried by the grand-unification gauge bosons (e.g. $\chi^\pm 4/3$, $\gamma^\pm 1/3$, in a $SU(5)$ theory) along the extra fifth or sixth dimension ⁵).

These two extra space dimensions are taken to form a compact space such as a torus or a 2-sphere. This leads to the possibility of computing the grand-unification mass in terms of the lengths of the extra dimensions. In the simplest case, we find:

$$m_X = \frac{10 \pi}{3} \frac{\hbar}{L_{5(6)} c} \quad (43)$$

If we are very naïve and assume $m_X \gtrsim 10^{15} \text{ GeV}/c^2$, we get from formula (43)

$$L \lesssim 2 \cdot 10^{-28} \text{ cm} \quad (44)$$

This is to be compared with the Planck length:

$$L_P = \frac{\hbar}{m_p c} = \sqrt{\frac{G_{\text{Newton}} \hbar}{c^3}} \approx 1.6 \cdot 10^{-33} \text{ cm} \quad (45)$$

at which quantum gravity effects become essential.

In any case, the extra dimensions, whatever their shapes and sizes, are likely to play an essential role in the determination of the grand-unification mass.

REFERENCES

- 1) P. Fayet and S. Ferrara, Phys.Reports 32 (1977) 249;
P. Fayet, Phys.Letters 69B (1977) 489; Proc. Europhysics Study Conf. on the Unification of the Fundamental Particle Interactions (Erice, Italy), ed. Plenum (1980), p.587; Proc. XXIst Int. Conf. on High Energy Physics (Paris), Journal de Physique C3 (1982) p.673;
S. Ferrara, Proc. Int. Conf. on High Energy Physics (Brighton, U.K.,1983), p.522;
J. Ellis, Proc. Int. Symposium on Lepton and Photon Interactions at High Energies (Cornell, U.S.A., 1983) p.439;
H.P. Nilles, Phys. Reports 110 (1984) 1;
H.E. Haber and G. Kane, Phys. Reports 117 (1985) 75;
S. Dawson, E. Eichten and C. Quigg, Phys. Rev. D 31 (1985) 1581; and references therein.
- 2) P. Fayet, Nucl.Phys. B 237 (1984) 367.
- 3) S. Ferrara, D.Z. Freedman and P. van Nieuwenhuizen, Phys.Rev. D 13 (1976) 3214;
S. Deser and B. Zumino, Phys. Letters 62 B (1976) 335;
P. van Nieuwenhuizen, Phys. Reports 68 (1981) 189.
- 4) P. Fayet, Nucl.Phys. B 149 (1979) 137; Proc. of the XVIIth Winter School of Theoretical Physics at Karpacz (Poland, 1980), Studies in High Energy Physics, Vol. 3, eds. L. Turko and A. Pękaliski (Harwood Acad.Pub., 1981), p.115.
- 5) P. Fayet, Nucl.Phys. B 246 (1984) 89; Phys.Letters 146 B (1984) 41.
- 6) P. Fayet, Phys.Letters 153 B (1985) 397.
- 7) E. Cremmer, P. Fayet and L. Girardello, Phys.Letters 122 B (1983) 41;
P. Fayet, Phys.Letters 125 B (1983) 178; 133 B (1983) 363.
- 8) P. Fayet, Phys.Letters 64 B (1976) 159.
- 9) G.R. Farrar and P. Fayet, Phys.Letters 76 B (1978) 575.
- 10) Contributions to these Proceedings.
- 11) G.R. Farrar and P. Fayet, Phys.Letters 79 B (1978) 442;
J.P. Dishaw et al., Phys.Letters 85 B (1979) 142;
G. Kane and J. Léveillé, Phys.Letters 112 B (1982) 227;
R.C. Ball et al., Contribution to the XXIst Int. Conf. on High Energy Physics (Paris, 1982); and Phys.Rev.Lett. 53 (1984) 1314;
CHARM collaboration, Phys.Letters 121 B (1983) 429.
- 12) G.R. Farrar and P. Fayet, Phys.Letters 89 B (1980) 191.
- 13) A. Böhm, R. Prepost, contributions to these Proceedings.
- 14) P. Fayet, Phys.Letters 117 B (1982) 460.
- 15) J.Ellis and J.S.Hagelin, Phys.Letters 122 B (1983) 303;
K. Grassie and P.N. Pandita, Phys.Rev. D 30 (1984) 22;
T. Kobayashi and M. Kuroda, Phys.Letters 139 B (1984) 208;
J. Ware and M.E. Machacek, Phys.Letters 142 B (1984) 300.
- 16) E. Fernandez et al., Phys.Rev.Lett. 54 (1985) 1118.
- 17) R. Prepost, H. Hollebeck, contributions to these Proceedings.
- 18) P. Fayet, Phys.Letters 142 B (1984) 263.
- 19) F. Gliozzi, J. Scherk and D. Olive, Nucl.Phys. B 122 (1977) 253;
L. Brink, J. Scherk and J.H. Schwarz, Nucl.Phys. B 121 (1977) 77.

INTRODUCTION TO SUPERSTRINGS

Eliezer Z. Rabinovici
Racah Institute of Physics
Hebrew University, Jerusalem

ABSTRACT

An elementary introduction to superstring theory in light of recent progress in the field.

During the last months there has been a tremendous burst of theoretical activity in superstring theory. In this talk I would like to convey to this general audience the reasons for the renewed interest in strings. I will attempt to consider the main points; this will be at the expense of glossing over many subtle facets, string theory thrives on subtleties. These and much more can be found in very good reviews of the subject.⁽¹⁾

Historically the string theory has arisen as a response to experimental data, the observation of novel properties of hadrons and hadronic scattering, in particular - finite energy sum rules, duality and Regge trajectories. S matrix elements in which duality was encoded were discovered by Veneziano. It was observed that such a spectrum and such scattering amplitudes occur in a theory of strings.

It was expected, in that period, that a radical departure from conventional field theory was necessary to explain the strong interactions, string theory offered such an avenue. This turned out not to be the case, strong interactions can be a manifestation of a field theory - QCD. In some limit (such as large number of colors) QCD can be described by an effective string theory, just as in another limit (small momenta) it can be described by a σ model of pions. But the fundamental description of strong interactions is by a field theory. String theory remained a departure from field theory, looking for a phenomenon of which it would be a fundamental description; a theory with a very interesting and not fully explored structure. To describe in which way string theory is a novel theoretical structure we review conventional-field theory; this leads us back to quantum mechanics. Very simple quantum mechanical systems are the bosonic and fermionic harmonic oscillators. A single bosonic (fermionic) harmonic oscillator, $a_B(a_F)$, is described by the Hamiltonian

$$H = a_B^+ a_B - \frac{1}{2} \qquad H = a_F^+ a_F - \frac{1}{2} \qquad (1)$$

where:

$$[a_B^+, a_B]_- = 1 \qquad [a_F^+, a_F]_+ = 1$$

A complete set of operators can be x , p or the bosonic (fermionic) occupation number $N_B(N_F)$. The wave function describing the system is $\psi(x)$, $\psi(p)$ or $\psi(N_B)$ for bosons and $\psi(N_F)$ for fermions. The eigenfunction and eigenvalues of the harmonic oscillators are well known. In general one can amuse oneself with studying other quantum mechanical systems described by Hamiltonians: $H_B(a_B, a_B^+)$, $H_F(a_F, a_F^+)$, $H(a_B, a_B^+, a_F, a_F^+)$ (which could be arranged to be supersymmetrical). The choice of studying a particle moving in a square well potential or a $\frac{1}{r}$ potential is dictated

by the system under consideration. The discovery of the spectrum of the hydrogen spectrum singled out in importance the $\frac{1}{r}$ case. One can study next systems with a number of oscillators a_B^i, a_F^i ($i = 1, \dots, N_d$); they are described by Hamiltonians $H(a_B^{i+}, a_B^i, a_F^{i+}, a_F^i)$ and wave functions $\psi(N_B^i, N_F^i)$ or $\psi(x^i, N_F^i)$.

Field theory described systems of an infinite number of such coupled oscillators, $H(a_B^{i+}, a_B^i, a_F^{i+}, a_F^i)$ states are described by wave functionals $\psi(N_B^i, N_F^i)$ or $\psi(\phi(x), N_F)$, where $\phi(x)$ has replaced $x(i)$ in the limit $N_d \rightarrow \infty$. Electroweak and colored interactions are well described at present energies by field theories which are Poincare invariant and possesses in addition some global and local symmetries.

String theory of one string is analogous to quantum mechanics. It describes the excitations of a single basic entity - one string. It may be called quantum mechanical string theory. It turns out that the quantum mechanics of a single string is equivalent to a two-dimensional field theory of particles. To appreciate how that may come about, consider a lattice, on each point of which is defined an oscillator, fermionic, bosonic or both. Draw next all possible lines through the lattice points. There are many more lines than points. Each single line is considered as a basic entity, it consists of the infinite number of bosonic and fermionic oscillators it connects. The actual connection is much more subtle.

The motion of a single string in D-dimensional space time traces a two dimensional world sheet. This motion is characterized by a mapping from a two dimensional parameter space (σ, τ) into D dimensional space time $X_\mu(\sigma, \tau)$ ($\mu = 1, \dots, D$). A two dimensional field theory is suitable to describe the propagation of the string.

What is the law governing the motion of this extended object? one could search for the analogs of the square well, the delta function potential etc. However one starts by studying the "Harmonic" string, it contains in it rather unexpected constraints.

In analogy to quantum mechanics the probability to propagate from some initial one string configuration to some final one string configuration is given by the sum over all surfaces with the initial and final prescribed boundaries. The weight associated with each such surface is $\exp(iS)$ where the action S is decreed to be the area of the surface

$$S = \int d\sigma d\tau g_{\alpha\beta} \eta_{\mu\nu} \partial_\alpha X^\mu \partial_\beta X^\nu \sqrt{-g} \quad (2)$$

$g_{\alpha\beta}$ ($\alpha, \beta = 1, 2$) is the metric on the parameter space and $\eta_{\mu\nu}$ the metric of the space in which the string propagates.

This action has a very large symmetry group. It consists of global Poincare invariance, local reparametrization invariance in two dimensions and Weyl invariance. This large symmetry group poses a difficulty in counting the real number of degrees of freedom associated with the string. A photon, A_μ , is found to describe, two and not four degrees of freedom, by appropriately fixing a gauge. A gauge must also be fixed to appreciate the physical degrees of freedom of the single string. In such a physical gauge the Hamiltonian is indeed given by a sum over an infinite number of harmonic oscillators.

$$H = \sum_{i,n} n a_n^{i+} a_n^i - 1 + \quad (\text{center of Mass motion of the string}). \quad (3)$$

(i = 1, ..., D-2)

The wave functional of the system is $\Psi(N_n^i)$ or $\Psi(\text{shape of the string})$. The energy levels of the systems have a $(\text{mass})^2$ proportional to their angular momentum J^2 (they occur on Regge trajectories), as well as many other interesting properties. One such property is that the theory is Lorentz invariant only in twenty six dimensions*. Another, was that the spectrum contains a tachyon. A theory describing the propagation of one "Harmonic" superstring was also constructed. In a suitable gauge it was found to contain an infinite bunch of both bosonic and fermionic harmonic oscillators. The Hamiltonian in that gauge is given by:

$$H = \sum_{i,n} a_{n,F}^{i+} a_{n,F}^i + \sum_{i,n} n a_{n,B}^{i+} a_{n,B}^i + (C.M.) \quad (4)$$

This system is free of tachyons, it is Lorentz invariant only for $D = 10$ and has a supersymmetric spectrum.

The next conceptual stage is to construct a theory of many strings, in particular a field theory of strings which would describe the local interactions of an infinite number of coupled strings. Green and Schwarz⁽³⁾ have struggled with this issue for some time; it has now become one of the central problems in research to identify the symmetry structure (analogous to Poincare plus global and local symmetries of particle field theory) of string field theory. Whatever the lagrangian turns out to be, the wave functional describing the system will be $\Psi(N_{n,B}^i, N_{n,F}^i)$ or $\Psi(\phi(\text{strings}))$, where $\phi(\text{strings})$ is a function which obtains values on the space of all possible number of strings and their shapes. This is clearly a demanding task. The challenge of understanding this new structure goes beyond its relevance to any present day phenomenology; however, why the revived

* Polyakov⁽²⁾ has shown that quantum mechanical string theories exist for $D < 26$.

interest in the subject? Let us return to the single Harmonic superstring. Strings come in several varieties, in particular strings are different if they are open or closed.

The string mass spectrum extends to infinitely high masses, if one, however, considers only the zero mass sector of the open string it turns out to have the same particle content as $N = 1$ Super Yang Milies theory in $D = 10$, (with a $SO(N)$ of $USp(N)$ internal symmetry). The massless sector of the closed string contains $N = 1$ or $N = 2$ (depending on the orientation properties of the string) supergravity in $D = 10$. The emergence of these vast symmetries in the massless sector renders the construction of the string field theory even more exciting. While $D = 10$ looked removed from our world ten years ago, we have learned in this meeting, from C. Weittrich⁽⁴⁾, why it is worthwhile to consider theories in higher dimensions. The Kaluza-Klein approach may turn yet another defeat into a victory.

It has been shown that one may obtain the Yang-Mills theory, the supergravity theory and even a combination of both as limits of various interacting strings field theories⁽³⁾. The low energy string theory could thus join various other theories as a springboard for compactification.

There were a few obstacles for doing so, the first was that the theories suffered anomalies in $D = 10$. The theories had gravitational,⁽⁵⁾ gauge and mixed anomalies which all seemed incurable. One's first reaction might be, who is afraid of anomalies in general and in ten dimensions in particular? It has been shown⁽⁶⁾ that anomalies at $D = 10$, will haunt the compactified theory all the way down to $D = 4$, so the issue is why should a theory be anomaly free in general. In short an answer is, Lorentz invariance, the standard model without quarks is not Lorentz invariant. We have no experimental evidence for the failure of Lorentz invariance. More details and references can be found in the lectures of Adler and Caneschi in a companion meeting⁽⁷⁾. There actually exists an anomaly free string theory; it is $N = 2$ supergravity. There even are signs that such a string theory is finite. This is an extremely exciting situation; one may have at hand a finite, well defined and generalized theory of some quantum gravity. The new structures embodied in the string field theories may offer a solution. The rejection of the study of $N = 2$ model as an active line of research points to a dichotomy in our attitudes. The main fault of $N = 2$ is that it can't lead to a theory consisting of chiral fermions in $D = 4$. This fault seemed to have outweighed its promise as a structure containing a finite gravity⁽⁸⁾. It may be that our insistence on having a clear view of a bridge between the deep problem of quantum gravity and present day phenomenology is too strict. In any case, Green and Schwarz⁽⁹⁾ have circumvented this dilemma by showing that one can construct anomaly free theories in

$D = 10$ which may lead to chiral fermions in $D = 4$ upon compactification. The low energy particle field theory and the string field theory are anomaly free, incorporate gravity, which may turn out to be finite and have a potential to produce upon compactification a realistic four dimensional theory. What more can one ask for? Well, one thing which comes to mind is uniqueness. Green and Schwarz have come near to that, finding that the string theory can have only one of two internal symmetry groups; $E_8 \times E_8$ and $SO(32)$. (It has since been shown that two variations of $SO(32)$ are possible.) This accumulation of good omens has brought about the feeling that one may be on the verge of very important progress. Green and Schwarz have calculated the gravitational, gauge and mixed anomalies in both the $D = 10$ string field theory and the massless particle sector^(9,10). In the particle field theory the anomalies are calculated out of various hexagon diagrams which play the role the triangle diagrams do in $D = 4$. One such diagram is the hexagon connecting six gravitons.

The value of that anomalous term is given by:

$$\frac{n-496}{7560} \text{tr}R^6 + a_1(n)\text{tr}R^2 \text{tr}R^4 + a_2(n) (\text{tr}R^2)^3 \quad (5)$$

R is the scalar curvature. n is the number of generators of the internal symmetry group, $a_1(n)$ and $a_2(n)$ are known functions of n . All anomalies have a similar structure, a leading term such as $\text{tr}R^6$ or $\text{tr}F^6$ and non leading terms. If the leading term is not zero the Green-Schwarz medicine will not work. As we see for eq. (5) that constrains n to be 496. It turns out that for this value of n the leading terms in all anomalies vanishes. The fact the overconstrained set of equations has a solution is highly non-trivial and probably will be better understood in the future. The groups $E_8 \times E_8$ $SO(32)$ are singled out in this process. (Both groups also pass the test of being anomaly free with regard to discrete gravitational anomalies⁽⁶⁾).

The next to leading terms can be eliminated by the following conspiracy: the anomaly indicates that the theory is not invariant on the quantum level under local classical symmetries. One thus adds terms on the classical level tuned in such a way that the theory is not gauge invariant classically but that gauge invariances are actually restored by the anomalies. (This trick can't be used in $D = 4$). These terms have a definite mathematical significance, something which is always reassuring. They also come out directly from the string field theory. Some formulas concerning these terms are relegated to a short appendix, however a very interesting lesson can be drawn from the details of these cancellations: In the particle field theory they don't quite work, the terms

seem to break supersymmetry, it has not yet been demonstrated that new action does not create new, non-leading anomalies which should be cancelled by an iteration process. One is beginning to feel the details of the string field theory, the massless particle sector can't explain everything on its own. This occurs again in other recent developments, results which seem reasonable cannot be completely proven in the context of truncated massless particle field theory but are very natural in a string context.

At this junction one has at least three cross-roads:

1. One may use the new opening to examine the new generalized quantum gravity; this is to my mind the most exciting and lasting aspect of the recent progress. This will demand a better understanding of the field theory of strings.
2. One may examine in more detail the results obtained by Green and Schwarz. In particular prior to their work a model in which the string carries $E_8 \times E_8$ quantum number was unknown. Such a model was recently built⁽¹¹⁾, the details of the construction offered hope to solve a problem which we have ignored.

The price of having no anomalies and a model which may lead to chiral fermions in $D = 4$ was to introduce elementary gauge bosons in $D = 10$. This is not in the Kaluza-Klein spirit in which $D = 4$ gauge symmetries are a reflection of the isometries of $D > 4$ space-time symmetries.

The closed string which carried $E_8 \times E_8$ (and also a different $SO(32)$) quantum numbers is built in such a way that the gauge symmetry may be considered as a result of a pre-compactification from $D = 26$ dimensions. This may point to a direction which restores the Kaluza-Klein spirit, without which all the motivation to study higher dimensions is to understand quantum gravity.

3. The most tempting avenue of research is to try one's luck and form the connection between $D = 10$ and present day phenomenology. I will describe now some results in that direction. I feel it would be great to see this bridge in our lifetime, but some difficulties in that direction will not diminish the importance of this new structure.

The route from $D = 10$ to $D = 4$ was described in detail by C. Wetterich⁽⁴⁾. One searches for solutions of the equations of motion in which six dimensions are compactified and one then proceeds to identify the massless excitations on that background. The particle field theory has no static solutions⁽¹²⁾ and once again string theory arguments are used to justify various compactifications.

It has been shown that if monopoles reside in the compact dimensions chiral fermions emerge in $D = 4$ ⁽¹³⁾. These monopoles are the modern Atlases which hold down the mass of the fermions, would they unwrap, all matter masses would be of the plank scale! In the presence of these monopoles the group $SO(32)$ for example, can break down to several generations of $SU(5)$.

Requiring a four-dimensional $N = 1$ supersymmetry to survive at the compactification scale one can motivate (again the strength of the arguments lies in string theory) that the compactified manifold is a very interesting mathematical structure (called a Calabi Yau space). These spaces have an anti Kaluza-Klein structure, they have no isometries and thus they do not enrich the $D = 4$ local symmetries. Quite a few of these are known by now⁽¹⁴⁾ and they lead to many possible number of generations. At this stage the uniqueness is not established, it may be that it will emerge once string theory is better understood.

Testing a $E_8 \times E_8$ string, it has been shown⁽¹⁴⁾ that on compactification to a Calabi-Yau space it reduces to a $D = 4$ $E_6 \times E_8$ model, the E_6 further breaking down to the standard model. At this stage one should go to J.M. Frere's lecture⁽¹⁵⁾ in which no-scale supergravity models are described.

Very recently (after the meeting took place) more work was done on the compatibility of the model with phenomenology and mechanisms in which the surviving supersymmetry is broken and the hierarchy problem resolved⁽¹⁶⁾. If the string theory is indeed finite there is a possibility that a zero cosmological constant results. It would definitely result in a theory with global scale invariance⁽¹⁷⁾.

While attempting to describe the universe as the infra red ripples of a string, one should mention that string models are studied also in solid state physics. The dynamics of interfaces are described by the fluctuations of surfaces⁽¹⁸⁾. Solid state physicists actually try to isolate the infra-red behaviour of a d dimensional object propagating in a D dimensional space. String theories are well defined when they are conformally invariant. The classification of all two-dimensional conformally invariant theories is also very useful in statistical mechanics⁽¹⁹⁾. In Astrophysics one even searches for cosmic string⁽²⁰⁾.

Appendix

One was accustomed to accept that gauge particles can only obtain a mass through the Higgs mechanism. An explicit mass term $m^2 A_\mu^2$, would render the system non renormalizable. While this remains true in four dimensions, it was shown⁽²¹⁾ that, at the expense of parity, one can have a gauge invariant mass term for the gauge particle in three dimensions. For an abelian gauge group the mass term is given by:

$$L_{\text{mass}} = C \epsilon^{\mu\nu\rho} A_\mu F_{\nu\rho} \quad (\text{A-1})$$

In the non-abelian case

$$L_{\text{mass}} = m \text{Trace} \left[AF - \frac{1}{3} A^3 \right] \quad (\text{A-2})$$

where the mass has to be quantized to ensure gauge invariance. Such terms (called Chern-Simons terms) appear also in higher dimensions, although their interpretation is slightly different. In particular, in three dimensions, the anti-symmetric spin one particle belonging to the graviton multiplet gives rise to a field strength H given by⁽⁹⁾

$$H = dB - \chi_3^0 \quad (\text{A-3})$$

where d is essentially a rotor and χ_3^0 is

$$\chi_3^0 = \frac{1}{30} \omega_{3Y}^0 - \omega_{3L}^0$$

$$\omega_{3Y}^0 = \text{Tr} \left[AF - \frac{1}{3} A^3 \right]$$

$$\omega_{3L}^0 = \text{tr} \left[\omega R - \frac{1}{3} \omega^3 \right]$$

A is the gauge vector potential, F the field strength associated with it. ω is the spin connection and R the curvature. Tr, indicates a trace in the adjoint representation, while tr is taken in the fundamental representation. In the absence of $\text{tr}R^6$ and $\text{Tr}F^6$ terms, appending terms such as

$$\chi_3^0 (a_4 \text{Tr}F^4 + b_4 \text{tr}R^4 + \dots)$$

to form the classical action which is not gauge invariant, one obtains gauge invariance at the quantum level, for more details consult⁽²²⁾.

References

1. V. Allesandrini, D. Amati, M. Le Bellac and D.I. Olive, Phys. Reports 1C(19H), 269.
 J. Schwarz, Phys. Reports 8C (1973) 269.
 G. Veneziano, Phys. Reports 9C (1974) 199
 C. Rebbi, Phys. Reports 13 (1974) 259
 S. Mandelstam, Phys. Rep. 13C (1974) 261.
 M. Jacob (editor), Dual theory (North-Holland, Amsterdam) 1974.
 J.H. Schwarz, Phys. Rep. 89 (1982) 223.
 M.B. Green, Surveys in High Energy Physics 3 (1983) 127.
 L. Brink, Lectures delivered at Nato Advanced Study Institute, Bonn, CERN preprint 1984.
2. A.M. Polyakov, Phys. Lett. 103B (1981) 207.
3. H. Green and J. Schwarz, Phys. Lett. 136B (1984), 367, Nucl. Phys. B243 (1984) 285.
4. C. Wetterich- these proceedings.
5. L. Alvarez-Gaume and E. Witten, Nucl. Phys. B234 (1984) 269.
6. E. Witten - Princeton University preprint (1985).
7. S. Adler - Moriond 1985 proceedings (to be published)
 L. Caneschi - Moriond 1985 proceedings (to be published)
8. See however:
 J. Schwarz - Cal Tech preprint C8-1131 (1984)
 D. Friedan and S. Shenker - to appear in the Proceeding of the Santa Fe meeting of the APS.
9. M. Green and J. Schwarz - Phys. Lett. 149B (1984) 117.
10. M. Green and J. Schwarz - Caltech preprint, CALT-68-1194 (1984).
 D. Friedan and J. Shenker - unpublished.
11. D.J. Gross, J.A. Harrey, E. Martinec and R. Rohm, Phys. Rev. Lett. 54 (1985) 502.
 P. Freund - Santa Barbara preprint (1984) USF-ITP-84-157.
12. D. Freedman, G. Gibbons and P. West, Phys. Lett., 124B, (1983) 491.
 P. Freund and P. Oh - Santa Barbara preprint NSF-ITP-84-168.
13. E. Witten - Phys. Lett. 149 B (1984) 351.
14. P. Candelas, G. Horwitz, A. Strominger and E. Witten - Santa Barbara preprint 1984, ITP-170.
 A. Strominger and E. Witten - Princeton 1985.
 R. Nepomichie, Wu Yong-Si and A. Zee, University of Washington preprint.
15. J.M. Frere - these proceedings
16. M. Dine, V. Kaplunovsky, C. Nappi, M. Mangano and N. Seiberg, Princeton preprint (1985)
 M. Dine, R. Rohm, N. Seiberg, E. Witten, Princeton preprint (1985).
 J.P. Derendinger, L.E. Ibanez, CERN preprint (1985).

S. Ceccoti, J. Derendinger, S. Ferrara, L. Girardello, M. Roncadelli, CERN preprint TH. 4103/85.

17. D. Amit and E. Rabinovici, Nucl. Phys. B (to be published)
G. Goldberg, M. Einhorn and E. Rabinovici, Nucl. Phys. B (to be published)
18. See e.g.: D. Wallace in Recent Advances in Field Theory and Statistical Mechanics (edited by J.B. Zuber and R. Storar), 1984.
19. A.A. Belavin, A.M. Polyakov and A.B. Zamolodchikov, J. Stat. Phys. 34 (1984) 763; Nucl. Phys. B 241 (1984) 333.
D. Frieden, Z. Qiu and S.H. Shenker, Phys. Rev. Lett. 52 (1984) 1575,
Fermi Institute preprints EFI 83-66 (1983), EFI 84-35 (1985).
20. Y.B. Zeldovich, Mon. Not. Roy. Astr. Soc. 192, 663 (1980)
A. Vilenkin, Phys. Rev. Lett. 46 (1983) 1169.
E. Witten - Princeton preprints 1984, 1985.
A. Vilenkin and A. Shafi, Phys. Rev. Lett. 51 (1983) 1716.
21. S. Deser, R. Jackiw and S. Tempelton, Ann. Phys. 140 (1982) 97.
22. M. Green - Caltech preprint, CALT-68-1219 (1984).

THE INFLATIONARY UNIVERSE REVISITED

Pham Quang Hung
Department of Physics
University of Virginia
Charlottesville, VA 22901

Abstract

A pedagogical review of the standard Big Bang and the new inflationary universe is presented in a way which is as model-independent as possible. Recipes for a successful inflationary model are also outlined.

I. Introduction

This talk was meant to be a pedagogical introduction for non-experts to the ideas, achievements, and future of the inflationary universe.¹⁻³ Consequently, the emphasis will be placed more on the "model-independent" aspects of the inflationary scenario, with a brief description of different models being proposed given at the end of the talk. For the sake of clarity, chronological development of the ideas will not be attempted.

It is by now a conventional wisdom that the standard Big Bang model despite its successes in describing the Hubble flow, the 2.7°K microwave background and the Helium abundance suffers from conceptual difficulties which turn it into an incomplete theory. The purpose of the inflationary scenario is to resolve these fundamental problems and, as a consequence, new lights can be shed on the structure of the very early universe ($\sim 10^{-35}$ sec). This is a domain where particle physics enters and plays a significant role. On the other hand, the very early universe can serve as a guiding light for model building enthusiasts to toy around with the most recent particle physics ideas. It is more in the latter sense that I intend to describe the working of the inflationary scenario without reference to a particular model.

The organization of this review is as follows. A brief review of the standard Big Bang model is given, followed by a description of its problems. The inflationary universe's ideas are then exposed along with its resolution of the afore mentioned problems. The review ends with some perspectives on future prospects.

II. The Standard Big Bang

On distance scales larger than 100 Mpc (1 pc = 3.2615 light-year), the observed universe appears homogeneous and isotropic. The 2.7°K cosmic background radiation appears uniform with $\Delta T/T \lesssim 10^{-3}$. The geometry used to describe such an observation is characterized by the Robertson-Walker metric

$$ds^2 = - dt^2 + R(t)^2 \left[\frac{dr^2}{1-kr^2} + r^2 d\Omega^2 \right], \quad (1)$$

where $k = -1, 0, +1$ corresponds to an open, flat and closed universe respectively.

The expansion of the universe is described by the evolution of the scale factor $R(t)$ which is in turn determined by the following equations ($m_{pl} = 1.2 \times 10^{19}$ Gev)

$$H(t)^2 = \frac{8\pi}{3m_{pl}^2} \rho - \frac{k}{R^2}, \quad (2)$$

$$\frac{d}{dR} (\rho R^3) = -3pR^2, \quad (3)$$

$$P = p(\rho), \quad (4)$$

where $H = \dot{R}/R$, ρ the energy density and p the pressure. Equations (2)-(4) are Einstein's equation, the energy conservation equation, and the equation of state respectively. The above set of equations forms the basis of the so-called Friedmann-Robertson-Walker universe.

Let us look at a solution to these equations for the very early universe. To be more specific, let us investigate the situation when the energy density is dominated by that of relativistic particles, i.e. $p = \frac{1}{3}\rho$. This is the so-called radiation-dominated universe (RDU). From (3), one finds that $\rho \propto R^{-4}$. Since, $\rho = (\frac{\pi^2}{30} g_*) T^4$, where g_* is the effective number of degrees of freedom, it follows that

$$RT = \text{constant}. \quad (5)$$

From (5), one can transform Eq. (2) into an equation for T , namely

$$\left(\frac{\dot{T}}{T}\right)^2 = \left(\frac{8\pi a}{3}\right) \left(\frac{T}{m_{pl}}\right)^2 T^2 - \epsilon(T) T^2, \quad (6)$$

where $a = \frac{\pi^2}{30} g_*$ and $\epsilon(T) = \frac{k}{R^2 T^2} = k \left[\frac{2\pi^2 g_*}{45 S} \right]^{2/3}$ with $S = R^3 \left(\frac{2\pi^2}{45} g_* T^3 \right)$ being the total entropy. If the expansion is adiabatic, S is a conserved quantity with a value $\sim 10^{87}$ ($S_Y \sim 10^{87}$). Even if $k \neq 0$, one gets $|\epsilon(T)| \sim 10^{-58}$. For temperatures a few order of magnitude below m_{pl} , one can thus neglect the curvature term $\epsilon(T) T^2$ in Eq. (6). One can immediately solve Eq. (6) giving

$$T = \left(\frac{3}{32\pi a}\right)^{1/4} \frac{m_{pl}^{1/2}}{\sqrt{t}}, \quad (7)$$

$$R \propto \sqrt{t}, \quad (8)$$

For completeness, I should mention that if the mass density is dominated by non-relativistic particles, it is easy to show that, in such a case, $T \propto t^{-2/3}$ and $R \propto t^{2/3}$.

A rough estimate of relevant numbers which arise in the very early universe can be gotten from Eqs. (7) and (8). For example, at $T \simeq 10^{14}$ Gev, we obtain $t \simeq 10^{-35}$ sec. The physical size of the present universe is of order 10^{10} years. At $t \simeq 10^{-35}$ sec, it is of order 10 cm.

The F-R-W universe described in this section suffers, however, from conceptual difficulties⁴ preventing it from becoming a complete theory extending from the present time back to the Planck time ($\sim 10^{-43}$ sec). What are these difficulties? A hint of what is waiting in store is to notice that the horizon size

at $t = 10^{-35}$ sec is approximately 10^{-25} cm.

III. Problems with the Standard Big Bang

1) The Horizon (or homogeneity and isotropy) problem.

A particle horizon is defined as the maximum distance light can travel since the initial singularity and is given by

$$d_H(t) = R(t) \int_0^t \frac{dt'}{R(t')} \quad (9)$$

For a radiation-dominated universe, $d_H(t) = 2t$.

What is the ratio of the horizon volume $d_H^3(t)$ to the physical volume $L^3(t)$? Now, if the universe expands adiabatically it follows that the total entropy $L^3 s$ is conserved (s being the entropy density), i.e. $L^3(t) s(t) = L_0^3 s_0$, where L_0 and s_0 are the present size and entropy density. Using $s = \frac{2\pi^2}{45} g_* T^3$, it is not hard to derive

$$r_H \equiv \frac{d_H^3(t)}{L^3(t)} \approx 10^{-88} g_*^{-1/2}(t) (m_{pl}/T)^3 \quad (10)$$

Typically (e.g. in SU(5)), $g_* \approx 100$ at $T \approx 10^{14}$ Gev giving $r_H \approx (d_H^3/L^3)_t \approx 10^{-35} \text{ sec} \approx 10^{-74}$. It means that there are 10^{74} causally disconnected regions at $t \approx 10^{-35}$ sec! Things do not get much better at later times; in fact at $T \approx 1$ eV (decoupling temperature), $r_H \approx 10^{-6}$.

Particles in different causal domains are not in contact with each other. In fact, in the standard Big Bang picture, a large fraction of particles were never in causal contact at a time close to the Planck time. Homogeneity and isotropy of the present universe would be an ad hoc initial condition. This is the so-called horizon problem. We now come to a different kind of problem which is no less serious.

2) The flatness problem

Is the universe open, flat or closed? An open or flat universe would expand forever while a closed universe would reach a maximum radius and recontracts again. To see how it goes, let us rewrite Eq. (2) as follows

$$\Omega(t) - 1 = \frac{k}{R^2 H^2(t)} \quad (11)$$

where $\Omega(t) \equiv \rho/\rho_c$ and the critical density $\rho_c = 3H^2 m_{pl}^2 / 8\pi$. From Eq. (11), it is easy to see that $\Omega < 1, = 1, > 1$ corresponds to $k = -1$ (open), 0 (flat), $+1$ (closed) respectively.

Observation⁵ gives the present density parameter Ω in the range

$$0.1 \lesssim \Omega_{\text{NOW}} \lesssim 2 \quad (12)$$

Why would such a range become a problem? First of all, Ω_{NOW} is not too different from 1 and $\Omega = 1$ is an unstable equilibrium point. To see this, let us use Eq. (11) once more and write it in the following form

$$\Omega(t) = 1 + (\Omega_i - 1)(t/t_i)^\alpha, \quad (13)$$

where $\alpha = 1$ or $\frac{2}{3}$ for a radiation-dominated ($R \propto \sqrt{t}$) and matter-dominated ($R \propto t^{2/3}$) universe respectively. Here, Ω_i and t_i are some initial values.

As an illustration, take $t_i \approx 10^{-43}$ sec and $t_{\text{now}} \approx 10^{17}$ sec ($\sim 10^{10}$ years) so that $t/t_i \approx 10^{60}$. Even though the universe may have gone through several alternating periods of radiation-dominated and matter-dominated phases, for simplicity let us take $\alpha = 1$ in Eq. (13). It follows that $\Omega_{\text{NOW}} = 1 + (\Omega_i - 1) \times 10^{60}$. In order for $0.1 \leq \Omega_{\text{NOW}} \leq 2$, the initial Ω_i would have to be extremely close to 1, namely $\Omega_i = 1 \pm 0$ ($\lesssim 10^{-60}$). One would have to fine tune Ω_i to at least 60 decimal places to be consistent with observation. The fact that the initial density parameter Ω has to be so extraordinarily close to one is what is referred to as the flatness problem.

It turns out that the inflationary scenario resolves both of these problems at the same time.

3) Galaxy formation problem

On a scale $d < 100$ Mpc, the universe appears inhomogeneous: planets, stars, galaxies, clusters of galaxies, etc... What is the origin of that inhomogeneity in an otherwise homogeneous universe?

4) Baryon asymmetry problem

What is the origin of n_B/n_γ ($\approx 10^{-10}$)?

5) Monopole problem

This problem only occurs in the context of Grand Unified Theories (GUTs). In the conventional GUT scenario, there are far too many monopoles produced at the GUT phase transition giving a mass density $\Omega_M \gtrsim 5 \times 10^{-18} \text{ g/cm}^3$ at the present time (i.e. $\Omega \gtrsim 10^{11}$, a grossly incorrect value). The trick is to inhibit the production of these monopoles during the phase transition and it can be seen below that the inflationary scenario does just that.

It will be discussed below how the new inflationary universe solves problems (1), (2), and (3), and possibly (4). Problem 5 depends on the details of GUT models.

IV. The New Inflationary Universe

What usually is referred to as the inflationary universe is a flat ($k=0$), exponentially expanding ($R \propto e^{Ht}$) universe characterized by the de Sitter metric

$$ds^2 = -dt^2 + e^{2Ht} dx^2, \quad (14)$$

and a cosmological constant $\Lambda (H = \sqrt{\frac{\Lambda}{3}})$. It is shown below how this de Sitter universe alone (wherever it comes from) can solve the horizon and flatness problems discussed above. The main characteristic of this de Sitter universe is the behaviour of the scale factor, namely $R(t) = e^{Ht}$ (with the normalization $R(0) = 1$). How does one arrive at this universe? What is the origin of the cosmological constant Λ ? There is no doubt that there could be many answers to these questions. I shall concentrate, however, on a particularly elegant realization of the de Sitter universe proposed by Guth and cast in a new form by Linde, and, independently, by Albrecht and Steinhardt. This scenario is now referred to as the new inflationary universe.

To understand the above scenario, it helps to get an idea on how temperature affects the symmetry properties of underlying theories. One assumes that there is a grand unified gauge group G which is spontaneously broken to G' , a subgroup of G . An example is $SU(5) \rightarrow SU(3) \times SU(2) \times U(1)$. The details of the breaking are contained in the Higgs potential $V(\phi)$. To illustrate the above ideas, I will use the following toy model for $V(\phi)$, namely

$$V(\phi) = \frac{\lambda}{4} (\phi^2 - v^2)^2 \quad (15)$$

One readily sees that this potential has a minimum at $\langle \phi \rangle = v$ and the symmetry $(\phi \rightarrow -\phi)$ is spontaneously broken. The above potential is for $T=0$ though. The inclusion of finite temperature gives

$$V(\phi, T) = \frac{\lambda'}{4} (\phi^2 - v^2 + aT^2)^2, \quad (16)$$

where a and λ' are parameters obtained from the one-loop effective potential. From (16), it is easy to see that for $T > T_c = v/\sqrt{a}$, the minimum is no longer at $\langle \phi \rangle = v$ but at $\langle \phi \rangle = 0$. The symmetry is restored at high temperatures.

Similar features appear in grand unified theories. The finite temperature potential is, of course, much more complicated than (6). With the choice of an appropriate model-dependent potential at $T=0$, it is possible to have two local minima, one at $\langle \phi \rangle = 0$ and the other one at $\langle \phi \rangle = v$. As $T \approx T_c$, these two minima are degenerate. For $T < T_c$, the minimum at $\langle \phi \rangle = v$ is lower in energy than that at $\langle \phi \rangle = 0$ and becomes the time ground state. The minimum at $\langle \phi \rangle = 0$ is now the false vacuum. If, for $T \gg T_c$, the universe is trapped in the false vacuum ($\langle \phi \rangle = 0$), it has to make a first-order phase transition to the true vacuum at some temperature $T < T_c$. The energy density of the false vacuum ($\phi = 0$) in the above toy model is $V_0 = \frac{\lambda}{4} v^4$ while that of the true vacuum ($\phi = 0$) is zero. This picture forms, in a rough sense, the impetus for the New Inflationary Universe (NIU).

The following prescriptions are made for a successful NIU:

- a) Initially, we have a hot ($T > T_c$) expanding universe.
- b) As the temperature drops, the universe finds itself trapped in a false vacuum.
- c) This false vacuum has a constant energy density $\rho_0 \equiv V_0$ which, as we will see below, translates into the existence of a cosmological constant term in Einstein's equation.
- d) The transition from false to true vacuum is first-order and is slow enough to have sufficient inflation (this statement is made more precise below). This is the so-called "slow roll-over" picture of the Higgs field.
- e) The shape of the potential is such that density fluctuations (shown below to depend on the parameters of the theory) are calculably small (i.e. $\delta\rho/\rho \lesssim 10^{-4}$), such as required by conventional wisdom.
- f) The Higgs field(s) which drives inflation (the one whose value goes from zero to v) couples strongly enough to lighter particles for the damping of the Higgs oscillatory motion about the true vacuum ($\langle\phi\rangle = v$) to be effective (by decay processes) and for particle creation to occur. This point will be made clearer below.

Let me now go over, point by point, the above prescriptions.

1) Hot initial state

One usually assumes that there are at least some patches in the early universe which are hot and in which there is thermal equilibrium. The Gibbs average of ϕ (the V.E.V. at $T=0$) is zero for $T > T_c$. This is the statement made about the assumption that the universe is trapped initially in the false vacuum. This point is a tricky one. Can one really assume that $\phi \approx 0$ for $T > T_c$? It has been shown that there are large fluctuations in ϕ at high temperatures and the statement $\phi \approx 0$ can be taken only in the (spatial or time) average sense. This fact has repercussions on the dynamics of the "slow roll-over" mechanism. Detailed studies of this question have been made and there are indications that it is all right to proceed with the above assumption.

2) The vacuum energy density and the cosmological constant

As we have discussed earlier, if the universe is trapped in the false vacuum, it has a constant energy density $\rho_0 \equiv V_0$, the value of which depends on the model considered. This constant vacuum energy density reflects itself in a cosmological constant Λ in Einstein's equation.

The cosmological constant enters Einstein's equation in the following way:

$$R_{\mu\nu} - \frac{1}{2} g_{\mu\nu} R - \Lambda g_{\mu\nu} = - \frac{8\pi}{2 m_{pl}^2} T_{\mu\nu}$$
, where Λ is positive. With the Robertson-Walker metric, one obtains instead of Eq. (2), the following equation

$$\left(\frac{\dot{R}}{R}\right)^2 = \frac{8\pi}{3m_{pl}^2} \left(\rho + \frac{\Lambda m_{pl}^2}{8\pi}\right) - \frac{k}{R^2}, \quad (17)$$

where ρ is the matter energy density. We can readily identify $\rho_0 = \Lambda m_{pl}^2/8\pi$ giving

$$\Lambda = 8\pi\rho_0/m_{pl}^2. \quad (18)$$

This is the connection between the cosmological constant and the vacuum energy density.

In a radiation-dominated universe, the total energy density ρ_{tot} is given

$$\rho_{tot} = \left(\frac{\pi}{30} g_* T^4\right) + \rho_0. \quad (19)$$

As $T < (30\rho_0/\pi^2 g_*)^{1/4} \simeq 0(v)$, the energy density is dominated by that of the vacuum and

$$\rho_{tot} \simeq \rho_0. \quad (20)$$

Also, as we have shown earlier, the curvature term k/R^2 can be ignored in the very early universe. Equation (17) becomes

$$\left(\frac{\dot{R}}{R}\right)^2 \simeq \frac{8\pi\rho_0}{3m_{pl}^2}. \quad (21)$$

With $H = (8\pi\rho_0/3m_{pl}^2)^{1/2}$, the solution to (21) takes the form

$$R(t) = e^{Ht}, \quad (22)$$

where we have normalized $R(0) = 1$. This is the de Sitter universe or inflationary universe.

Since $RT = \text{constant}$, we obtained the so-called supercooling stage

$$T(t) = T(0)e^{-Ht}, \quad (23)$$

where $T(0)$ is some arbitrary temperature at $t=0$. Because of the existence of an event horizon $d_H(t) = R(t) \int_t^\infty \frac{dt'}{R(t')} = \text{finite}$, it was shown by Gibbons and Hawking that there is a limiting (lower bound) temperature, $T_H = H/2\pi$.

3) Phase transition and the rebirth of the universe

From the false vacuum, a transition will have to be made to the true vacuum. It is accomplished by the formation of "bubbles" or fluctuation regions. The remarkable thing about the new inflationary scenario is the realization that our present universe evolved from one such fluctuation region.

Each fluctuation region is causal and within it the Higgs field at each space-time point has the same orientation in group space (they are correlated). This latter point is particularly relevant for the monopole problem (to which we will come back below). Let me first describe how this scenario is able to solve

the horizon and flatness problems.

a) The Horizon problem and the shape of the potential.

Before inflation the size of the fluctuation or causal region is $\sim H^{-1}$ (H is the only scale available). Typically, $H^{-1} \approx (10^{19} \text{ GeV})^{-1} \approx 10^{-24} \text{ cm}$ ($H = (8\pi\rho/3m_{\text{pl}}^2)^{1/2}$, $\rho_0 \sim v^4 \sim (10^{15} \text{ GeV})^4$). Inflation takes place during an interval Δt and the fluctuation region has inflated by a factor $e^{H\Delta t}$ giving a final size

$$L_f = e^{H\Delta t}/H \quad . \quad (24)$$

Notice that $d_H = R(t) \int_0^{\Delta t} \frac{dt'}{R(t')} \approx e^{H\Delta t}/H$ if $e^{H\Delta t} \gg 1$.

How much inflation is needed? To see this, notice that just at the beginning of inflation, $d_H^3/L_i^3 = 1$. The initial size being $\sim H^{-1} \approx 10^{-24} \text{ cm}$ would have to be inflated by at least a factor $10^{25} \approx e^{58}$ for $L_f \approx 10 \text{ cm}$, (the observed universe at $t \approx 10^{-35} \text{ sec}$). It means that $H\Delta t \gtrsim 58$. This is the required minimum amount of inflation. In many models proposed so far, $H t$ is much larger than 58 (in fact $H\Delta t \sim 10^6$ in some models), making an observed universe a small factor of the physical universe.

What mechanism is responsible for such a large inflation? It has to do with the growth of the Higgs field inside the fluctuation region. When ϕ reaches its final value v , the part of the universe contained inside that fluctuation region makes a transition to the Friedmann-Robertson-Walker universe, ending the inflationary stage. The classical equation in de Sitter space governing the growth of $\phi_0(t)$ is

$$\ddot{\phi}_0 + 3H\dot{\phi}_0 = - \frac{\partial V}{\partial \phi_0} \quad , \quad (25)$$

where the second term on the left-hand-side of (25) represents damping due to the expansion of the universe. It is easy to see that the growth is fastest when $\frac{\partial V}{\partial \phi}$ (the slope of the potential) is largest. It then makes sense to have $V(\phi)$ as flat as possible. One of such potential is the following Coleman-Weinberg potential $V(\phi) = \frac{25}{16} \alpha^2 [\phi^4 \ln(\phi^2/\sigma^2) + \frac{1}{2} (\sigma^4 - \phi^4)]$ where $\langle \phi \rangle = \sigma$. This potential has been abandoned because the calculation of $\delta\rho/\rho$ (to which we shall come back below) gives $\delta\rho/\rho \approx 50$, a value far too large (the requirement is $\delta\rho/\rho \lesssim 10^{-4}$). A variety of models have been proposed with a flat potential as a characteristic.

Let me now return to the flatness problem

b) The flatness problem.

At the start of inflation, $\Omega(o) = 1 + k/R(o)^2 H(o)^2$. Right after inflation, $\Omega(\Delta t) = 1 + k/R(\Delta t)^2 H(\Delta t)^2$. Since $R(\Delta t) = e^{H\Delta t} R(o)$ and $H(o) = H(\Delta t) = H$, it is easy to see that $(k/R(\Delta t)^2 H(\Delta t)^2) \div (k/R(o)^2 H(o)^2) = e^{-2H\Delta t}$. If $H\Delta t \gtrsim 58$ as required by the solution to the horizon problem, the previous ratio is $\lesssim 10^{-51}$ and hence $k/R(o)^2 H(o)^2$ can be of order unity. The flatness problem disappears.

Ω does not have to be close to unity before the inflationary period. After inflation, Ω automatically becomes $\Omega = 1 \pm 0 (\leq 10^{-51})$ which is extraordinary because at $t = 10^{-35}$ sec $\Omega_i \approx 1 \pm 0 (10^{-52})$ when we use Eq. (13). There is no need for fine tuning.

In some models, $H\Delta t \gg 58$ and in consequence $\Omega_i \approx 1 \pm 0 (\ll 10^{-52})$. So, practically $\Omega_{\text{now}} \approx 1$. Evidently, $H\Delta t \approx 58-60$ (in order for $0.1 \leq \Omega_{\text{now}} \leq 2$) seems to be a fine-tuning problem, but is it really? It now seems that $\Omega_{\text{now}} = 1$ may run into difficulty with observation. In any case, $\Omega_{\text{now}} = 1$ is a model-dependent prediction of the inflationary universe.

c) The monopole problem.

A monopole can be thought of as a topological knot which gets formed when different causally disconnected domains with the Higgs fields pointing in different directions in group space come together. In the new inflationary scenario, our universe is contained within one causal domain inside which the Higgs fields are correlated and point in the same direction in group space. There simply is little chance for one monopole to be found in such a situation, let alone many. In short, there is no monopole problem!

d) The origin of density fluctuation.

The equation governing $\phi(\vec{x}, t)$ in de Sitter space is

$$\ddot{\phi} + 3H\dot{\phi} - e^{-2Ht} v^2 \phi = - \frac{\partial V}{\partial \phi} \quad . \quad (26)$$

Now, $\phi(\vec{x}, t)$ has, in addition to the homogeneous solution $\phi_0(t)$ which obeys Eq. (25), quantum fluctuations $\delta\phi(\vec{x}, t)$, i.e.

$$\phi(\vec{x}, t) = \phi_0(t) + \delta\phi(\vec{x}, t) \quad . \quad (27)$$

If we assume that $|\delta\phi| \ll \phi_0$ then $\delta\phi$ behave like a free quantum field obeying the linearized equation

$$\delta\ddot{\phi} + 3H\delta\dot{\phi} - e^{-2Ht} v^2 \delta\phi = - \frac{\partial^2 V}{\partial \phi^2} (\phi_0) \delta\phi \quad . \quad (28)$$

From the solution for $\delta\phi$, it has been shown that these quantum fluctuations produce a position-dependent time evolution of ϕ , in the form $\phi_0(t + \delta\tau(\vec{x}))$. The Higgs field reaches its true vacuum value v at different times for different positions inside the fluctuation region. This behaviour produces a perturbation in the metric $g_{\mu\nu}$ which translates into a perturbation on the average energy density of the universe, $\delta\rho/\rho$, using Olson's formalism.

The amplitude of density fluctuation can be calculated to be

$$\delta\rho/\rho|_H = 2\sqrt{2} H\Delta\tau \quad , \quad (29)$$

where the subscript H refers to the value that $\delta\rho/\rho$ takes as a certain length scale (galaxies, clusters of galaxies, etc...) enters the horizon. The Harrison-Zeldovich spectrum for galaxy formation is scalefree and obeys $\delta\rho/\rho|_H \leq 10^{-4}$.

This serves as a constraint for model building.

In the new inflationary scenario, $\Delta\tau \propto \frac{\Delta\phi}{\dot{\phi}_0}$ and $\Delta\phi$, which is the quantum fluctuation of ϕ , is calculated from a quantum theory of free massless scalar field in de Sitter space giving $\Delta\phi \sim H/(16\pi^3)^{1/2}$. In consequence $\delta\rho/\rho|_H \propto H^2/\dot{\phi}_0$ where $\dot{\phi}_0$ is evaluated at a time $t_* \ll \Delta t$ (inflation time). Small $\dot{\phi}_0(t_*)$ means large $\delta\rho/\rho|_H$ and vice versa. Also, $\dot{\phi}_0(t_*)$ was shown to be scale-free or almost so in most models and hence $\delta\rho/\rho|_H$ obeys the Harrison-Zeldovich spectrum.

The trick now is to find a potential for which $\dot{\phi}_0(t_*) \gg H^2$. From Eq. (25), one can see that $3H\dot{\phi}_0 \cong -\frac{\partial V}{\partial\phi}(\phi_0)$ if $\ddot{\phi}_0$ can be neglected. In consequence large $\dot{\phi}_0(t_*)$ means that the potential is very steep for small value of ϕ (large $\partial V/\partial\phi$). In order to insure that there is enough inflation, the potential will have to flatten out again and for a large range of values for ϕ . Once the choice can be made, it is possible to obtain both $\delta\rho/\rho|_H \lesssim 10^{-4}$ and $H\Delta t > 58-60$. There are now a variety of models (with very different structures) which have the right shape for the Higgs potential and are acceptable as far as $\delta\rho/\rho|_H$ and $H\Delta t$ are concerned. It remains to be seen which, if any, of these models will be the correct choice.

e) The rebirth of the universe.

Because of the exponential expansion during the inflationary stage, any initial particle concentration would be greatly diluted ($e^{-4H\Delta t}$ for relativistic particles and $e^{-3H\Delta t}$ for non-relativistic ones). The universe would have to replenish itself. A particularly nice feature of the new inflationary scenario is the existence of a mechanism for particle creation. In fact, after the phase transition occurs, the Higgs field oscillates about the true minimum. This oscillation is damped by the decay of the Higgs field into lighter particles. The universe is reheated again (from a supercooled state). This reheating is effective if the ϕ -lifetime is short compared with the expansion time i.e. $\Gamma^{-1} \ll H^{-1}$. In fact, in some models, it is possible to reheat the universe to a temperature of $0(10^{14} \text{ GeV})$. The de Sitter universe is reborn as a F-R-W universe.

V. Outlook

The inflationary universe has provided us with a new way to look at the problems which plagued the standard Big Bang. There is now a set of well-defined criteria for the construction of a successful inflationary model. In addition, detailed studies have been performed with the purpose of understanding the quantum mechanical behaviour of the Higgs field in the inflationary universe for they are extremely relevant to the knowledge of the phase transition. Armed with all those ammunitions, it is probably a matter of time before a realistic model is constructed (unless we miss the boat somewhere).

Acknowledgements

I would like to thank the organizers of the Rencontre de Moriond for the warm hospitality at Les Arcs. This work was supported in part by the National Science Foundation under Grant No. PHY-83-01186.

References (an incomplete list)

1. A. H. Guth, Phys. Rev. D23, 347 (1981).
2. A. D. Linde, Phys. Lett. 108B, 389 (1982).
3. A. Albrecht and P. J. Steinhardt, Phys. Rev. Lett. 48, 1220 (1982).
4. See for example Ref. (1).
5. See for example the lectures presented by J. R. Primack, SLAC-PUB-3387 preprint (1984).
6. G. F. Mazenko, W. G. Unruh, and R. M. Wald, Phys. Rev. D31, 273 (1985).
7. G. W. Gibbons and S. W. Hawking, Phys. Rev. D15, 2738 (1977).
8. S. Coleman and E. Weinberg, Phys. Rev. D7, 1888 (1973).
9. J. Ellis, D. V. Nanopoulos, K. A. Olive, and K. Tamvakis, Nucl. Phys. B221, 524 (1983); D. V. Nanopoulos, K. A. Olive, M. Srednicki, and K. Tamvakis, Phys. Lett. 123B, 41 (1983); D. V. Nanopoulos, K. A. Olive, and M. Srednicki, Phys. Lett. 127B, 30 (1983); G. B. Gelmini, D. V. Nanopoulos, and K. A. Olive, Phys. Lett. 131B, 53 (1983); D. V. Nanopoulos and M. Srednicki, Phys. Lett. 133B, 287 (1983); B. A. Ovrut and P. J. Steinhardt, Phys. Lett. 133B, 161 (1983), Phys. Rev. Lett. 53, 732 (1984), and Phys. Lett. 147B, 263 (1984); B. A. Ovrut and S. Raby, Phys. Lett. 134B, 51 (1984); Q. Shafi and A. Vilenkin, Phys. Rev. Lett. 52, 691 (1984); P. Q. Hung, Phys. Rev. D30, 1637 (1984); S. Gupta and H. R. Quinn, Phys. Rev. D29, 2791 (1984); R. Holman, P. Ramond, and G. G. Ross, Phys. Lett. 137B, 343 (1984); S.-Y. Pi, Phys. Rev. Lett. 52, 1725 (1984); Q. Shafi and F. W. Stecker, Phys. Rev. Lett. 53, 1292 (1984).
10. A. A. Starobinsky, Phys. Lett. 117B, 175 (1982); A. H. Guth and S.-Y. Pi, Phys. Rev. Lett. 49, 1110 (1982); S. W. Hawking, Phys. Lett. 115B, 295 (1982); J. M. Bardeen, P. J. Steinhardt, and M. S. Turner, Phys. Rev. D28, 679 (1983); R. Brandenberger, R. Kahn, and W. H. Press, Phys. Rev. D28, 1809 (1983); R. Brandenberger and R. Kahn, Phys. Rev. D29, 2172 (1984).
11. D. W. Olson, Phys. Rev. D14, 327 (1976); also S. W. Hawking, Astrophys. J. 145, 544 (1966).
12. E. R. Harrison, Phys. Rev. D1, 2726 (1970); Ya. B. Zeldovich, Mon. Not. Roy. Astron. Soc. 160, 1 P (1972).
13. A. Albrecht, P. J. Steinhardt, M. S. Turner, and F. Wilczek, Phys. Rev. Lett. 48, 1437 (1982); L. F. Abbott, E. Farhi, and M. B. Wise, Phys. Lett. 117B, 29 (1982); A. D. Dolgov and A. D. Linde, Phys. Lett. 116B, 329 (1982).
14. A. H. Guth and S.-Y. Pi, MIT preprint CTP #1246 (1985) and references to related works therein.

SUMMARY TALK OF XIXTH RECONTRE DE MORIOND**"ON NEW TRENDS IN ELECTROWEAK INTERACTIONS"**

Robert E. Lanou*
Department of Physics
Brown University
Providence, Rhode Island
02912 (USA)



Abstract: This year's Recontre de Moriond was devoted once again to the present status and possible new directions in the area of electroweak interactions. This summary talk attempts to pull together and highlight those many contributions to the conference which stimulate and guide us toward the future.

* Work supported in part by U.S. Department of Energy under contract DE-AC02-76ER03130

Introduction.

Conference summary talks always seem to begin by offering an apology for not including everything. This one is no different. While the volume of new results, interpretations, and ideas is part of the standard plea, to this I will add that this summary talk is being given less than three hours from the last presentation of new results to us and working with only one eye has not only slowed me down a bit but literally forced on me to take a different point of view. Hopefully, the lack of binocular vision has not reduced to zero the depth of that view!

The point of view I have taken is what might be described a "differential" one. By that I mean to imply that I will concentrate most of our time upon those effects for which we have (or hoped we would have) seen a significant change in the slope of our knowledge at this Moriond Conference where the topics have been discussed. In Figure 1, I have illustrated the range of possibilities we seem to have encountered. Figure 1A and 1B are the "crisp" type of discontinuities we all love but unfortunately life seems to be less obliging and more often than not we have Figure 1C or 1D.

Everyone will have their own candidates for topics to include either because of the magnitude of the first or second derivative or by the significance of the topic. My list for Moriond '85 will include the following inquiries into whether there is a significant slope:

- * Changes in measured parameters of the Standard Model?
- * Monojets in $\bar{p}p$ and e^+e^- experiments?
- * Evidence for top-quark?
- * Is jet activity accompanying Z^0 's significantly different from that with W^\pm 's?
- * Are there $Z^0 \rightarrow e^+e^-\gamma$?
- * Is there high M_T structure in jet plus IVB?
- * Is there neutrino mass evidence by oscillation?
- * Prizes for elegance and youthful enterprise?

Additionally, as time permits, I would like to remind you of other topics with significant quantitative content but without significant derivative (or otherwise do not fit this scheme). These will include:

- * Negative searches for SUSY particles at e^+e^- machines.
- * Negative searches for neutrino mass by other methods.
- * Negative searches for nucleon decay.
- * Theory lessons and reviews.
- * Negative searches for lepton number violation.
- * Same sign di-lepton experiments.
- * Lifetime measurements, charm and beauty studies, and ϵ'/ϵ .
- * Future projects.

I. Changes in the measured parameters of the Standard Electroweak Model.

Here we have seen what is largely a story of continually improving errors as well as results from new reactions. Among these are new measurements^{1]} on the weak isospin assignments of all the known (including b and τ) quarks and sequential leptons from PEP, PETRA, BNL and BEBC. These beautifully confirm (at the approximately ten percent level) the Glashow-Weinberg-Salam assignments. (see also Section XIIa).

We also heard of new measurements by UA-1 and UA-2^{2]} on (V-A), masses and widths of IVB's, $\sin^2\theta_w$, and ρ . From PETRA, we also have a new extraction of $\sin^2\theta_w$ versus M_Z ^{1]}. Also on the topics of $\sin^2\theta_w$ and ρ we heard new results from the ratio of $\nu_\mu-e/\bar{\nu}_\mu-e$ elastic scattering (USA-Japan at BNL) and from a new experiment on ν_e-e at Los Alamos^{3]}. Additionally, we learned of impending (and progress toward) much improved errors on the weak neutral current mixing parameters as determined in the inelastic neutrino experiments at CERN^{4]}.

As a start, we have new values for the direct measurement of the intermediate vector boson masses from the UA-1 and UA-2 experiments. These result from the addition of more than twice the previously accumulated luminosity and, additionally, at $\sqrt{s} = 630\text{GeV}$ rather than earlier 540GeV . Additionally, there is more control and understanding on energy resolution as well as other experimental improvements. Both groups emphasize that their results are preliminary and, on some of the parameters and errors, still in progress. Table I contains these preliminary values.

TABLE I
(GeV)

	UA-1	UA-2
$M_Z(ee)$	$96.5 \pm 1.2 (\pm 3\%)$ (22 events)	$92.4 \pm 1.1 \pm 1.4$ (16 events)
$M_Z(\mu\mu)$	$88.8 \pm 5.5 - 4.6$ (9 events)	
Γ_Z	In progress	$2.7^{+2.2}_{-1.6}$ (Peak) 2.46 ± 0.71 ($\frac{\text{Ratio}}{\sigma_B}$)
$M_W(e\nu)$	In progress (201 events)	$81.2 \pm 0.8 \pm 1.5$ (123 events)
$M_W(\mu\nu)$	In progress (42 events)	
$\sin^2 \theta_W = 1 - \frac{M_W^2}{M_Z^2}$		0.228 ± 0.024
$\sin^2 \theta_W = \frac{(38.65)^2}{M_W^2}$		$0.227 \pm 0.004 \pm 0.009$

Of particular interest, are the new measurements of $\Gamma_Z(ee)$ which are new values instead of limits. Two methods were used: one based upon a fit to the mass peak, the other on the $\sigma \cdot B$ ratio for the electron modes of Z and W. The former suggests that the number of neutrino generations is <20 while the latter, $<3.3(+1.3)$.

With these new data in hand it is appropriate to ask how close is our present knowledge of $\sin^2 \theta_W$ to establishing it as a universal parameter for all electroweak phenomena when the data are suitably corrected radiatively? To $O(\alpha)$ correction on first Born term we can express^{5]} the effect of radiative corrections, Δr , as

$$M_W = \frac{37.28 \text{ GeV}/c^2}{\sin \theta_W (1 - \Delta r)^{1/2}} = M_Z \cos \theta_W$$

where Δr is estimated theoretically to be 0.0696 ± 0.003 . These theoretical uncertainties lead to uncertainties in M_Z and M_W of about $\pm 3 \text{ GeV}$ and in $\sin^2 \theta_W$ of about ± 0.003 . The correction Δr has three principal contributions: gauge bosons, leptonic and hadronic effects. A full understanding of the radiative effects and the hoped for universality of $\sin^2 \theta_W$ is then expected to come from

measurements in as many diverse processes as possible. To do this, experimental results must be compared with equivalent, suitable radiative corrections having been made or conversely used to check the different contributions to the radiative corrections.

The current procedure for the experiments which concern us here is to radiatively correct the deep inelastic neutrino-nucleon and the e^+e^- experiments in the renormalization scheme where $\sin^2\theta_W = (1 - M_W^2/M_Z^2)$, determine $\sin^2\theta_W$ from the $\bar{p}p$ collider experiments from this expression and leave the neutrino-electron scattering experiments uncorrected since the latter are free from direct hadronic involvement and serve as a check on the remaining corrections.

While the individual values for $\sin^2\theta_W$, (and ρ , M_Z) determined from these experiments are available in the individual contributions^{1-4]} they can be categorized as typically 0.23 ± 0.01 from the deep inelastic neutron-nucleon experiments, $0.14 < \sin^2\theta_W < 0.21$ at the 90% confidence level if $M_Z = 93 \text{ GeV}/c^2$ for the e^+e^- experiments, 0.22 ± 0.02 from the $\bar{p}p$ collider experiments, and typically 0.21 ± 0.02 from the cross section ratios of the neutrino-electron scattering experiments.

It is clear that we are not yet at the level of ± 0.003 error on experimental determinations of $\sin^2\theta_W$ although that possibility is held out to us in the near future by proponents of elastic neutrino-electron experiments and at the ± 0.005 level this summer from the deep inelastic experiments. Improvements in $\bar{p}p$ luminosity also hold great promise.

Figure 2 and Figure 3 illustrate (in different ways) the importance of reduction of errors. In Figure 2 we see the likelihood contours of the Bohm "banana" plot for the e^+e^- determinations of $\sin^2\theta_W$ versus M_Z . Superimposed are new (Moriond '85) and old (Leipzig)^{6]} values from UA-2 and UA-1 (M_Z only given). It is tantalizing to see as the errors improve whether these trends are toward incompatibility. In Figure 3, (the values are taken from Ref. 5) we see in a specimen GUT (SU5, for example) how tightly various parameters are coupled. The bands bracketing values in each column illustrate our present limits on each. Clearly, if we are to uncover hints as to the best direction to go for finding new physics then we have a ways to go in every parameter.

I would conclude however that we are close to being able to uncover a possible pattern of inconsistency and that from the point of view of derivatives we are in the upper half of Fig. 1C.

On a final note, the large number of $W \rightarrow e\nu$ available from the $S\bar{p}p$ s collider have shown (see Figure 4) in a beautiful, direct way (from the electron asymmetry) the (V-A) nature of the interaction.

II. Monojets and Unusual Jet Activity at $\bar{p}p$ and e^+e^- Machines?

With the increased data from the $\bar{p}p$ experiments it is appropriate to ask whether or not some of the possible "new physics" effects suggested by the earlier data have persisted or been confirmed. Additionally, inspired by these possibilities, we have heard new data and analyses from e^+e^- experiments which bear upon the possibilities raised. Taking some of these effects in turn we ask:

a) Is there more jet activity accompanying the Z than the W?

The answer from UA-1 is "apparently, no". They find Z(with jet/no jet)/W(with jet/no jet) = $(0.7 \pm 0.2)/(0.54 \pm 0.06) = 1.3 \pm .4 \pm .2$. Additionally, the p_T^W and jet angular distributions appear to be consistent with QCD^{2]}.

b) Is there significant structure at high M_T for the IVB plus jet?

The UA-1 data (53 events with W+1 jet, 12 with W+2 jets, and 6 with W+3 jets) show no structure inconsistent with a QCD ISAJET-generated tail. They indicate a limit for $X+W+jets$ at $\sigma_B < 12\text{pb}$ at the 90% C.L. if $M_X > 170\text{GeV}/c^2$.^{2]}

From their 1983 data, UA-2 had four events (A,B,C,D) with electron plus hard jet plus missing p_T . Three with masses $56 < M_T(\text{ev}) < 86\text{GeV}/c^2$ suggested involvement of the W with the jet. Background from QCD processes was expected to be only 0.5 event. Now, in 1985 at Moriond, they have added more than twice the luminosity and while they find three more new events consistent with inclusion of a W, these events are all at low $E_T(\text{jet})$ and $p_T(\text{miss})$; consequently, they are not in the "interesting region" of the previous four. The invariant mass of the W-jet system is, so far, featureless with a high mass tail as in Figure 5.^{2]}

c) Are there monojets?

First indications that there might be a distinctly new class of events outside the "Standard Model" came^{6]} from the UA-1 data of 1983. These indications (consisting of $\bar{p}p$ collisions resulting in a single hard jet with large missing p_T) have stimulated new theoretical speculations (notably those of Glashow-Manohar and Rosner) and additional searches in the new 1984 data by UA-1 and UA-2 as well as entirely new searches at e^+e^- machines.

Unfortunately for us, the UA-1 study is still in progress and there is nothing new to report. However, UA-2 in their preliminary study still has no definitive candidates. We should mention in

passing that in their studies of possible backgrounds, UA-1 has identified events with $Z^0 \rightarrow \tau^+\tau^-$ (as well as $W \rightarrow \tau\nu$) so we are well on the way to additional checks of $e-\mu-\tau$ universality.

Glashow and Manohar have suggested a process accessible at present e^+e^- machines which should result in a single jet. The process would involve decay of the virtual Z^0 to a heavy and a light scalar with the former materializing as $q\bar{q}$ (low mass, low multiplicity jets) and the latter escaping without interaction. Rosner suggests a virtual Z^0 going to a pair of neutral leptons with one producing a low multiplicity jet and the other three neutrinos. Both PEP (MAC, HRS, Mark II) and PETRA (JADE, CELLO) have reported^{8]} negative results in searches for such events. These studies are best presented as excluded-allowed contours in a width (or branching ratio) versus mass plot, and I refer you to the original papers for the various possible channels; however, Figure 6 gives the flavor of the present limits of these searches. Typically, at 95% C.L. masses of 1 to 20GeV are excluded at PEP with minimal assumptions. In terms of expectations of the model, 440 events would have been implied for 200 pb^{-1} (ignoring mixing effects) this magnitude is excluded at the 0.3% branching level.

In summary then concerning exceptional activity involving jets which might herald new physics I am afraid, that while the verdict is not yet in, we must accept a "differential" assignment of the lower-half of Figure 1C. A somewhat feeble glide toward "no", with a worry that it is perhaps more accurately described by Fig. 1B.

III. Has "top" been seen?

This difficult search is still intensively underway, stimulated again by early results from UA-1.^{9]} No formal analysis for $W \rightarrow t\bar{b}$ results from the new (1984) data were presented; however, on response to intense questioning from the audience UA-1 indicated work was still in progress while at UA-2 they have made a study applying the UA-1 cuts. This study has so far resulted in two events consistent in p_{out}^T , $\cos\theta_{j2}^*$, $M(\text{ev}j_1)$ and $M(\text{ev}j_2)$ with "top"; however, they are also completely consistent with expected background.

It is surely too early to award a "differential" classification here on the data, but it certainly deserves a four-star Figure 1A on community interest!

IV. Are there radiative ($Z^0 \rightarrow e^+e^-\gamma$) of the Z^0 ?

With now more than twice the luminosity reported previously, neither UA-1 nor UA-2 have any new candidates for such a non-"standard model" mode. For UA-2, in $16Z^0 \rightarrow e^+e^-$ they have 1 such event with 0.22 events expected from internal bremsstrahlung.

It thus looks quite unlikely that we have a significant new effect and we must reluctantly award a lower-half of Figure 1C for magnitude & sign of slope on this previously hopeful anomaly.

V. Is there neutrino mass evidence from oscillation experiments?

At this meeting we have heard new results and/or presentations from four oscillation experiments: two at reactors (Gosgen and Bugey) and two at accelerators (BNL and CERN). I believe, no matter what your prejudices, everyone will find both good news and bad news from these results -- in both reactor and accelerator experiments we have one each with a positive and one each with a negative result in similar regions of parameter space.

The reactor experiments are both of the single detector, multiple position, disappearance type. The detectors are very similar and both of course search for the disappearance of $\bar{\nu}_e$. Because at these energies oscillations resulting in other neutrino weak eigenstates will be sterile to observation via charged-current interactions and because the neutron is also detected, these experiments should be sensitive to any oscillations coupled to the electron anti-neutrino through common mass eigenstates. Such experiments are typically sensitive up to limits of 0.02eV^2 and 0.15 in the mass-difference-squared and mixing parameter squared, respectively. While there are systematic uncertainties associated with reactor source size and composition, data taking at multiple (although not simultaneous) positions tends to reduce them.

The Bugey group, who claim a positive result^{10]}, have taken data at two positions: 13.6 and 18.3 meters. No new data were presented here (but further checks and analysis were) however, new measurements at other distances are under consideration. They have calculated the no oscillation hypothesis expected spectra at the two positions in a Monte Carlo containing models of core spectrum and detector response. A systematic error of 6.9% is estimated for the ratio of data to Monte Carlo and 2.8% for ratio of position #1 data to position #2 data. The latter ratio is found to be $1.102 \pm 0.014 \pm 0.028$ for the integrated spectra -- a ten percent effect. The differential spectrum does not show any distinctive features. Extensive further checks have been made in relation to reactor burn-up, detector response background, statistical analysis, effective solid angle. They conclude that their published result

(Phys. Lett. 148B (1984) 387) still stands. The allowed area is shown in Figure 7 and the preferred single solution region is $\delta m^2 = 0.02\text{eV}^2$ and $\sin^2 2\alpha = 0.12\text{--}0.25$. Further plans include, besides a new distance, the possibility of a new detector.

The Gosgen group^{10]}, who interpret their results as not supporting an oscillation, have taken data at three positions: 37.9, 45.9 and 64.7 meters. The 64.7m data are new at this conference. Additionally, they have made a direct measurement of a reference $\bar{\nu}_e$ spectrum using the magnetic spectrometer (BILL) at the Institut Laue-Langevin. The significantly greater position distances in this experiment give quantitatively different ranges of L/E (see Figure 8). The data from the 64.7 meter position is preliminary but it permits them to make a variety of combinations of data sets to search for oscillations. Briefly, the conclusions are as follows:

- a) the spectra at all three positions are consistent with no oscillations (see Figure 9),
- b) the two position analysis (37.9, 45.9m) without use of reference spectrum cannot exclude the Bugey solution,
- c) however, the three position analysis leaves only a very small space for coexistence and
- d) the two position analysis (37.9, 45.9m) including the reference spectrum completely excludes the Bugey solution at 90% C.L. This group as well has conducted further tests on fuel burn-up, statistical analysis, etc. Their limits on oscillation are stated as $\delta m^2 < 0.016$ at full mixing and $\sin^2 2\alpha < 0.16$ for $\delta m^2 > 4\text{eV}^2$, both at 90% C.L. Further work is continuing in data collection and analysis at the 64.7 meter position.

A comparison of the allowed and excluded regions for these two groups can be seen in Figure 7.

These experiments have both reached a critical stage. I do not believe we are yet at a complete impasse, but since both are now mature experiments we do not have a great deal of freedom to maneuver -- great care is being taken and loopholes are being closed. Is the end near? Is a simultaneous two detector experiment desirable? out of the question?

Turning to the accelerator experiments presented here^{11]} on searches for $\nu_\mu \rightarrow \nu_e$ oscillations we again have a possible inconsistency.

In an experiment recently performed at the CERN P.S. (P.S.191) a suggestion of a positive result has been seen. The experiment was designed to search for decays of possible heavy neutrinos (see Section VIII, below); however, as a by-product during that run, charge-current interactions of neutrinos were also seen in the 5 ton (fiducial) volume of the calorimeter. Analysis of these

interactions has left them with an excess of 18.8 ± 5.4 events attributed to charge-current interaction of ν_e compared to a reference sample of 650 ± 65 events assigned (by observation and calculation) to ν_μ charge-current interactions. The ν_e excess is found by subtracting 3.0 ± 0.5 events for π^0 (measured and normalized) and 5.2 ± 1.5 events due to contaminating ν_e 's (beam flux calculation). The ratio of excess ν_e to ν_μ is thus $2.9 \pm 0.9\%$ (or $\sin^2 2\alpha \approx \sin^2(1.27(L/E)\delta m^2) = 0.029 \pm 0.009$). The average beam momentum is about 1 GeV and the distance from target to detector about 140 meters. The cross hatched region of Figure 10 illustrates the allowed oscillation region suggested by the experiments.

Also reported^{11]} at this meeting were results by a USA-Japan group working at the BNL-A.G.S. in a wide band beam. The experiment was designed to set a new limit on the mixing parameter ($\sin^2 2\alpha$) for $\nu_\mu \rightarrow \nu_e$ at high mass. The detector used 70 fiducial tons of liquid scintillator and proportional drift tubes. A unique feature of this experiment is that only quasi-elastic ν_e (418 events) and ν_μ charge-current events are isolated and therefore the E_ν for each event is determined. Backgrounds of approximately 20% in each channel are subtracted by measurement and normalization. Acceptances are calculated by Monte Carlo. The measurement of E_ν allows seven energy bins to be made of the data between 1-4.5 GeV, thus permitting the energy dependence of the flux to be seen. This dependence is compared to that expected by beam calculation (20% systematic error expected). At the 90% C.L. no oscillations are seen and the limits are shown by the solid line in Figure 10. At large mass this limit corresponds to $\sin^2 2\alpha < 3.4 \times 10^{-3}$.

On comparing the results from these two experiments, as shown in Figure 10, it can be seen that the allowed region of the CERN experiment is excluded by the USA-Japan result. What can we conclude at this point? The CERN experiment was designed for another purpose and did not have a very high flux of neutrinos -- one might say it is in its infancy. The CERN experimenters intend to extend this latter work with increased flux and controls. We will have to wait to see if a positive result is sustained.

Before leaving oscillations I should mention an analysis^{12]} of double beta experiments in the light of possible neutrino oscillations. Limits of $\langle m_\nu \rangle$ of < 0.35 or < 25 eV, depending upon assumptions, were suggested; however, it is difficult to use this conclusion to shed any light on the above mentioned conflicts.

In conclusion, I am afraid we must award a definitive Fig. 1D to this field in its present state. The question of neutrino mass is a serious one and deserves to be pressed to a definitive conclusion by all concerned.

VI. Prizes for Elegance and Youthful Enterprise.

A part of the Moriond tradition has always been the spirit of mutual instruction. A second part has been the encouragement of developing physicists. It seems to me appropriate to acknowledge when particular work and individuals on the youthful side give us something special which permit us to tie these traditions together. I admit we all have our own tastes, but I will risk mine this time.

I would suggest we award a prize (maybe one of Tran's T-shirts!) for elegance and youthful enterprise to two very nice pieces of work which were presented to us here in lucid talks by M. Tuts^{13]} and N. Krauss^{14]}.

In the former, we learned of a beautiful measurement and his analysis using the new BGO (CUSB-II) array at CESR to search for low mass Higgs via radiative decays of the upsilon. [$\Upsilon(1s) \rightarrow \Upsilon + H^0$]. In the important region of the reported^{15]} zeta (8.3GeV), an upper limit on the branching ratio of $<0.09\%$ is set -- a full factor five below the level of reported discovery in Reference 15. His analysis is based on a 400,000 event sample of upsilons and additionally sets a branching ratio limit of 0.025 for upsilon (1s) radiatively decaying to chi (2,2). The full range of limits is shown in Figure 11. All at the 90% C.L. limit.

From N. Kraus, we learned of a new more sensitive and elegant search for lepton number violation in muon decay. The search centers on the reaction $\mu^+ \rightarrow e^+e^+e^-$ utilizing the SINDRUM magnetic detector at SIN. The very convincing and impressive upper limit of $<2.4 \times 10^{-12}$ at 90% C.L. This is an improvement of nearly two orders of magnitude on their own previous limit. Interpreting this result through theoretical models, mass limits of $>50\text{TeV}$ and $>17\text{GeV}$ are placed on the existence of neutral horizontal gauge bosons and SUSY leptons, respectively. They simultaneously set a limit of another lepton family number violating reaction ($\mu^+ \rightarrow e^+e^+e^-2\nu$) of $3.3 \pm 0.5 \times 10^{-5}$.

In the time remaining I would like to remind us of the other important aspects of Moriond '85 which did not qualify for significant "differential" by my rules but none the less are significant and perhaps even more important for just that reason.

VII. Neutrino mass determinations by other means.

Besides oscillations, there are three other principal areas of effort on neutrino mass: (a) kinematic, that is detailed study of end points in the decay spectra or searches for sub-dominant kinks, (b) searches for decays of massive neutrinos and (c) searches for neutrinoless double beta decay.

No new data were presented here on double beta decay nor on the kinematics of tritium beta decay (either the endpoint or sub-dominant kinks) however, we had a very comprehensive review talk on the latter outlining the present status and exciting future prospects.

The tau neutrino, however, did receive new limits on its mass from studies of tau decay channels by both ARGUS and DELCO.^{17]} The DELCO results are based on the mode $\tau \rightarrow KK\pi\nu$ and they find $m(\nu_\tau) < 157\text{MeV}$ at 95% C.L. ARGUS quotes a limit $m(\nu_\tau) < 70\text{MeV}$ at 95% C.L. from the sequence $\tau \rightarrow A_1\nu_\tau, A_1 \rightarrow \rho\pi, \rho \rightarrow \pi\pi$.

There were also new limits on possible heavy neutrino decays from three experiments: PS191(CERN), CHARM(CERN), and Mark II(SLAC).^{18]}

In the P.S.191 experiment the heavy neutrino was presumed to have been produced and observed by the sequence of charged-current vertices illustrated in Figure 12a. The two-charged final state leptons to be detected in this experiment were both electrons. Consequently in the unitary matrix linking the weak and mass eigenstates for neutrinos: $\nu_i = \sum_{1h} U_{ih} \nu_h$ (where i and h are the weak and mass indices, respectively) non-zero values of $|U_{he}|^4$ and $|U_{he}|^2|U_{h\mu}|^2$ are sought.

In the experiment reported by CHARM evidence for both the mechanisms of Fig. 12a and of Fig. 12b were sought. In the latter, flavor changing neutral currents would be involved at the production vertex and for these events evidence for production and decay vertices both within the detector are looked for when exposed to a wide band beam. In a separate beam dump run, events from the topology of Figure 12a were looked for.

Mark II operating at PEP, with \sqrt{s} up to 28 GeV and making use of a vertex chamber looked for events with two, separated vertices which might arise from the diagrams of Figure 12c. All masses up to $\sqrt{s}/2$ are allowed via this neutral current production.

All three of these experiments have a negative result and the combined upper limits for the respective measures of $|U_{ih}|^2$ are shown in Figure 13.

VIII. Negative Searches for SUSY Particles, Heavy Leptons, etc. at e^+e^- Accelerators.

As the above sub-title indicates, within the kinematic limits of the machines, no positive evidence has been seen for these "beyond the Standard Model" objects. Such a bold statement masks an enormous amount of sophisticated, clever work -- so extensive in fact that I cannot do anymore than try to convey to you the flavor, range, and orders-of-magnitude by example of a single illustration and a list and refer you to the detailed write-ups^{19]} of the involved groups in these Proceedings.

At PEP, we heard results and progress from Mark II, MAC and ASP setting limits on SUSY leptons \tilde{e} and $\tilde{\nu}$ as well as photinos. These limits are typically in the range of greater than 25-37GeV depending upon mass degeneracy.

From PETRA, for CELLO, TASSO, JADE and MARK-J, with an integrated luminosity of 100pb^{-1} and $35 < \sqrt{s} < 46.8\text{GeV}$. Limits have been set on the following processes:

- * $M(t\bar{t}) > 46.7\text{GeV}/c^2$ ($B\Gamma(ee) < 2.3\text{keV}$)
- * Open top
- * New quarks ($Q=1/3, 2/3$)
- * Fractionally charged free particles
- * Heavy leptons [$\Lambda_{\pm} < 150-300\text{GeV}$ where

$$F(q^2) = 1 \pm [q^2/(q^2 - \Lambda_{\pm}^2)]$$
- * Spinless bosons ($Z \rightarrow \gamma X, X \rightarrow e^+e^-$)
- * Charged Higgs or technipions
- * SUSY leptons, photinos, zinos, winos
- * Monojets (see Section II)
- * Leptoquarks

As an illustration of the parametrization of limits, I refer you to Figure 14 where the search for photinos by several groups are shown.

No desert, no matter how barren is without at least some animals in its zoo. MARK-J presented to us eight events in the energy range $46.3 < \sqrt{s} < 46.8\text{GeV}$ each involving an isolated meson accompanied by jets of low thrust. From a lower control energy they estimate an expected background of about two events. If real, the effect is certainly worthy of a zoo.

IX. Theory Talks and Reviews.

In the excellent Moriond didactic tradition we had several very nice educational^{20]} talks. From them we heard about the wonders of: Kaluza-Klein ("there must be a desert somewhere"--is it precocious or late?) supersymmetry, superstrings, inflation, neutrino astrophysics, compositeness, and exotic extensions and variations. From them, however, we learned some sobering things, among them:

- (a) it is not so easy for them to predict unique, striking, quantitative signatures in the "low mass" (Tevatron, LEP, LHC, SSC!) regime for SUSY in 1985,
- (b) we should be careful with our model dependent cuts on data so that we do not throw out the baby (signal) with the bathwater(background).

But as experimentalists we should not despair; recall that the signature for charm was not so explicitly predicted.

I commend a reading of many of these theory review papers now that we have them in print.

X. Proton Decay

We heard of the progress being made by four of the major proton decay detectors^{21]}. On this topic it would appear that we are making a steady, gradual, careful but asymptotic approach to the background neutrino limit. Some would even say the end is near. It seems fair to characterize the present overall conclusion we can make at present as saying: the nucleon lifetime is not less than 10^{31} years (see Section I and Figure 3). More specifically we heard from the individual experiments some detailed limits by mode which I will try to briefly summarize.

From IMB, we heard that in the mode $P \rightarrow e^+ \pi^0$ the limit is $>2.5 \times 10^{32}$ years and greater than a few $\times 10^{31}$ years for those with a neutrino in the final state. They indicate a signal level equal to neutrino background in some modes.

From HPW, we were given $>5.2 \times 10^{31}$ and $>7 \times 10^{31}$ years for two and three muons respectively in the Pati-Salam model.

We also learned that after a productive and pioneering life in which it will have set a limit of $>5 \times 10^{32}$, the NUSEX detector will have reached the end of its utility. Thus, we have our first example of a "decay" -- unfortunately, of the detector and not the proton!

The FREJUS detector, which appears to be a worthy, larger successor to NUSEX (it is fine grain, solid, and with more tonnage) is now on-line and will soon be up to its full tonnage. They reported on their preliminary operations and showed us 18 events well contained in the fiducial volume but not yet analyzed.

We are all hoping for a breakthrough in this generation of detectors and their upgrades. What will the future be beyond these? Will we be able to blend smoothly from neutrino background into neutrino astronomy? Will they also be the ultimate monopole detectors?

XI. Other topics.

As I mentioned, there were several important topics which I could only list in the time available for this talk. The choice was dictated principally by the fact that most of them we had heard presented only a few hours before this talk and/or no major "differential" had occurred. For completeness, I will repeat the list with some more detail and comments.

a) Lifetimes, b and c phenomena, ϵ'/ϵ .

In principal most of these items should appear under "Parameters of the Standard Model" (Section I) only subject to the above disclaimer.

The lifetime of the τ lepton has two new measurements with much improved errors both statistically (200 pb^{-1}) and systematically (vertex chambers). The results are $2.86 \pm 0.16 \pm 0.25$ ($\times 10^{-13}$ sec) from Mark-II and $3.15 \pm 0.36 \pm 0.4$ ($\times 10^{13}$) from MAC. These values are in excellent agreement with the theoretical expectation of $2.82 \pm 0.18 \times 10^{-13}$ seconds using lepton universality and the Standard Model. Conversely, the data can be used to find $g(\tau)/g(\mu) = 1 \pm (5\%)$ and $m(\nu_\tau) < 320 \text{ MeV}$ and mixing angle $\sin\theta < 0.46$. Also in the area of lepton universality ARGUS^{24]} presented new confirming evidence via the unity branching ratio of e, μ and τ from upsilon decays.

In the quark sector, we learned of improved measurements on lifetimes and branching ratios involving the b-quark. These new data came from ARGUS^{24]}, JADE, TASSO^{25]}, Mark-II, MAC, DELCO^{23]}, CUSB^{13]} and CLEO^{26]}. The lifetimes are given in Table II.

TABLE II

	$\tau_b (\times 10^{-12} \text{ sec})$	$ V_{cb} $
JADE	$1.78 \pm 0.4 \pm 0.4$	$0.042 \pm .005 \pm .006$
TASSO	$1.57 \pm 0.32 \pm 0.4$	$0.039 \pm .005 \pm .005$
Mark II	$0.85 \pm 0.15 \pm 0.20$	
"	$1.25^{+0.26+0.35}_{-0.19-0.39}$	$0.05^{+0.004}_{-0.005}$
MAC	$0.81 \pm 0.28 \pm 0.17$	
DELCO	$1.16^{+.37}_{-.34} \pm .23$	

Using these values and minimal assumptions, a value for the Kobayashi-Maskawa mixing parameter ($|V_{cb}|$) can be extracted (see also Table II). (The ratio of $|V_{ub}|/|V_{cb}|$ has been established and shown here by CUSB, CLEO, ARGUS to be $< 0.05-0.11$). There is excellent agreement among the experiments.

Also in the area of decays involving b-quarks we have from ARGUS^{24]} and CUSB^{13]} new limits on possible narrow states appearing in radiative decays of upsilon (1s) over a wide range of masses which includes the mass of $8.2\text{GeV}/c^2$. No structure was found; thus ruling out the zeta (8.2) at a level 0.09%.

With the new CLEO^{26]} and CUSB data from the region above the upsilon (4s) we saw a very rich field of b-physics opening up. The discovery of the upsilon (5s) and (6s) is now confirmed. Coupled channel analyses reveal as probable at least six channels involving B , B^* , B_s , B_s^* in the range up to $\sqrt{s} = 11.25\text{GeV}$. Perhaps information on possibilities of B^0 - \bar{B}^0 mixing will be forthcoming. From CUSB, we saw evidence for the $B^* \rightarrow B + \gamma$ transition; yielding a measure of the B - B^* mass difference of $52 \pm 2 \pm 4 \text{MeV}/c^2$ in good agreement with the model.

In the area of decays containing c-quarks we learned of lifetime and mixing limits from SLAC^{23]} and DESY^{24]} respectively. There are new measurements of D^0 and D^\pm from Mark II and the rapid cycling bubble chamber (lifetimes) and Mark III (semi-leptonic branching ratios). These results are tabulated in Table III.

TABLE III

	$\tau(D^0)$ ($\times 10^{-13}$ sec)	$\tau(D^\pm)$ ($\times 10^{-13}$ sec)	$\frac{\tau(D^\pm)}{\tau(D^0)}$
Mark II	$4.5^{+0.9}_{-0.8}$	$8.5^{+3.4}_{-2.5} \pm 1.0$	$1.9^{+1.0}_{-0.8} \pm .5$
B.C.	$6.1 \pm 1.1 \pm 0.4$	$9.2 \pm 1.5 \pm .5$	not given
Mark III	(From branch ratio: 2.78 ± 0.86)		

A world average for the $\tau(D^\pm)/\tau(D^0)$ was presented^{23]} as 2.50 ± 0.33 , thus the conclusion seems to be inescapable that we must go beyond the spectator models for these heavy quark decays. As to which of the many suggested, with significant samples of F^+ , Λ_c^+ , A^+ coming along from the several active detectors we may not have to wait long. And finally in this area we come to the crucial related question of neutral kaon decay parameter ratio, ϵ'/ϵ . An exhaustive review of the recent published

results, present status, and future plans was presented in an earlier session^{27]}. The results are still consistent with zero: -0.0046 ± 0.0058 from the Chicago-Saclay group at FNAL and 0.0017 ± 0.0082 from BNL-Yale at the AGS -- yielding a combined result from the two experiments of -0.0026 ± 0.0048 . Thus impressive progress has been made and constraints are tightened for possible consistency with the other Standard Model parameters ($m(\text{top})$, $\Gamma(b \rightarrow u) / \Gamma(b \rightarrow c)$, Higgs sector). Work is continuing and we were brought up to date on additional experiments to be carried out at CERN (NA31, LEAR) and FNAL but the final answer on problems for the Standard Model is still a year or two off.

b) **Same-sign di-leptons.**

This is an intriguing topic of long standing. Are there same sign di-leptons produced in excess of known processes in neutrino interactions? (There were no data presented here on $p\bar{p}$ interactions with like-sign leptons). The analyses including corrections and comparison to models is complicated and somewhat experiment dependent. There have been inconsistencies among experiments. It is an active field still very much in flux; in that spirit we heard of two new results using different techniques and different channels. In one, a neon-fill bubble chamber experiment^{28]}, searching for $e^- \mu^-$ and $e^+ \mu^-$ events induced in neutrino interactions 9 events were expected (based upon $\mu^- \mu^-$ counter experiments) where only 1 was found -- thus at the 90% C.L., $e^- \mu^- / e^+ \mu^- < 6\%$ and $e^- \mu^- / \mu^- \mu^- < 8 \times 10^{-5}$.

Also reported^{29]} were new results from a counter experiment at FNAL for the channels $\mu^- \mu^-$ and $\mu^+ \mu^-$. A total of $8.8 \pm 4.4 \mu^- \mu^-$ were found giving $\mu^- \mu^- / \mu^- \mu^- = (1.5 \pm 0.8) \times 10^{-4}$ for $p_\mu > 9\text{GeV}$ and $30 < E(\nu) < 250\text{GeV}$ and $\mu^- \mu^- / \mu^- \mu^- = 4.9 \pm 2.5\%$.

We were told of additional data still to come from these and other experiments. There still remains a possibility that there is new physics here.

XII. **Future.**

In practically every topic and area we heard of new plans for the future. There is no question that ours is a vital field full of ideas. Just to remind ourselves I will list some of them.

- * New accelerators and detectors at new multi-TeV or Q^2 ranges (HERA, SLC, DØ, CDF, UA-1, UA-2 upgrades, SSC^{30]})
- * Astronomy with proton decay detectors^{22]}

- New devices and new levels of searches ASP, SINDRUM, PEP, PETRA, CUSB-II, CLEO-II, ARGUS)
- Neutrino masses (double beta decay, tritium beta decay, oscillations)
- Improvements in Standard Model Parameters (ν_N --CDHS, CHARM; ν_μ -e USA-Japan, CHARM-II; ν_e -e--LASL; e^+e^- ; UA-1, UA-2; ϵ'/ϵ --FNAL, CERN, BNL; c and b-physics--CESR, SLAC, DESY)

XIII. Conclusion.

As is the tradition here, we have had a week packed with stimulating discussion and we have all learned many new things. The field is vibrant and productive. The Standard Model looks healthier than ever; however, we still have no Higgs nor top nor are all the great hopes for "new physics" we thought we might be seeing last year (see our tally of negative differentials) turning out to be realized.

As the summary above shows, we are making good progress in all the now traditional areas and with the burgeoning range of projects under way for the near and further future we should be prepared for some exciting surprises. (see Figure 15)

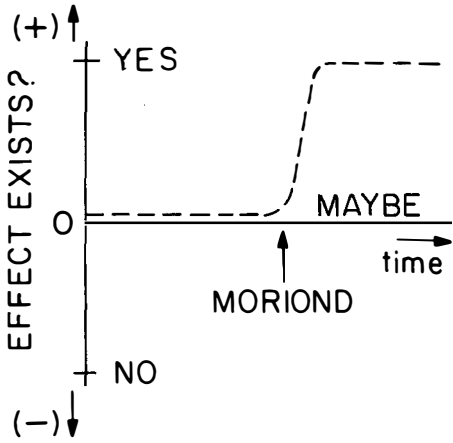
XIV. Thanks.

On this special occasion of the twentieth anniversary of the creation of Recontre de Moriond by Tran Thahn Van we all owe him first, our congratulations on such a beneficial feat and secondly, thanks for this one in particular. Additionally, all the attendees wish to thank Ms. Tran Kim, the organizers, and the tireless staff for their help and hospitality. I would like to add personal thanks to Ms. Tran Kim, Ms. Norry, Ms. Lefevre, Dr. Pastorino, Kate, Juliet Lee-Frazini, and the many notetakers who were so helpful to me.

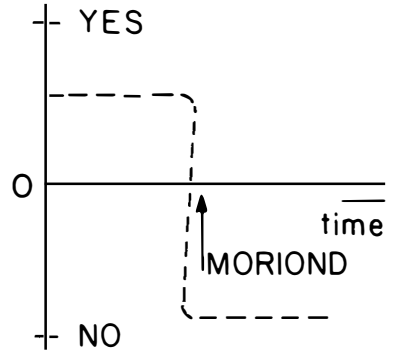
References

1. See for example, results reported from PETRA (C. Kiesling), PEP (R. Prepost), BNL-Brown-Osaka-Penn-SUNY (R. Lanou), BEBC (E. Hoffman). Proceeding of this Conference.
2. A. Honma (UA-1) and N. Harnew (UA-2), these Proceedings.
3. U.C. (Irvine)-Los Alamos-Maryland (R. Allen), these Proceedings.
4. CDHS (A. Blondel) and CHARM (M. Baubillier), these Proceedings.
5. W. J. Marciano, "Electroweak Interactions" in Proceedings of 1983 International Symposium on Lepton and Photon Interactions at High Energies, Cornell University, Ithaca, N.Y. 1983; A. Sirlin, Phys. Rev. D22, 971 (1980); W. Marciano and A. Sirlin, *ibid* D22, 2695 (1980); W. Marciano, *ibid* D20, 274 (1979).
6. Proceedings of XXII International Conference on High Energy Physics (Leipzig) Volume II, p. 12, J. Rohlf and p. 32, P. Bagnaia and J. P. Repellin (1984).
7. S. Glashow, M. Manohar, Harvard Pre-print HUTP-84/A020; J. Rosner and M. Gronau, CERN-TH.3911 (1984).
8. See Proceedings of this Conference: "Searches for SUSY Particles at PEP" (R. Prepost) and "New Particle Searches at PETRA" (A. Bohm).
9. Proceedings of XXII International Conference in High Energy Physics (Leipzig) Volume II, p. 2, R. Bock (1984).
10. See Proceedings this Conference: Bugey (H. Pessard) and Gosgen (V. Zacek).
11. See Proceedings this Conference: USA-Japan at BNL (R. Lanou) and CERN at P.S. (F. Vannucci).
12. See A. Pomansky, these Proceedings.
13. See M. Tuts, these Proceedings.
14. See N. Kraus, these Proceedings.
15. Proceedings of XXII International Conference in High Energy Physics (Leipzig), Volume I, p. 201, H. Trost (1984).
16. See O. Fackler, these Proceedings.
17. See DELCO (G. Mills) and ARGUS (D. Macfarlane), Proceedings of this Conference.
18. See Proceedings of this Conference: P.S. 191 (CERN, F. Vannucci also Ref. 11), CHARM (A. Capone), Mark II (G. Feldman).
19. See talks of A. Bohm and C. Kiesling (PETRA) and R. Prepost and R. Hollebeek (PEP) in these Proceedings.
20. See reports in these Proceedings of S. Raggazi (NUSEX), H-S Park (IMB), FREJUS, D. Cline (HPW).

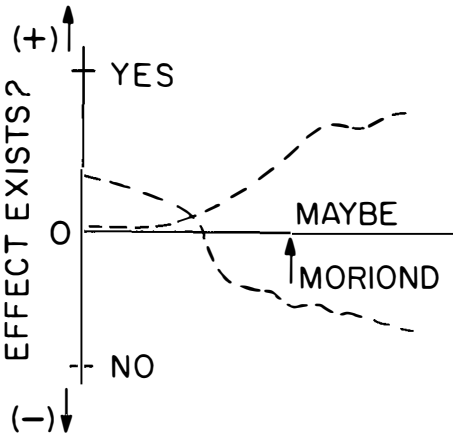
21. See reports in these Proceedings of, for example: M. Barnett, A. Dar, D. Domenici, P. Fayet, J-M. Frere, P. Hung, J. Moffat, S. Petcov, E. Rabinovici, M. Schmidt, C. Wetterich.
22. R. Bionta (IMB), see talk in these Proceedings.
23. See these Proceedings (R. Prepost for MAC and Mark II and DELCO).
24. See these Proceedings (D. Macfarlane, ARGUS).
25. See these Proceedings (H. Venkataramania for JADE and TASSO).
26. See these Proceedings (L. Garren for CLEO).
27. See these Proceedings (B. Peyaud for BNL-Yale and Chicago-Saclay).
28. See these Proceedings (A. Schaffer for BNL-Columbia-Rutgers).
29. See these Proceedings (K. Lang for Rochester-Chicago-Columbia-Cal Tech-FNAL-Rockefeller; CCFRR).
30. See these Proceedings, D. Cline (for SSC), P. Franzini (for DØ), F. Eisele (for HERA).



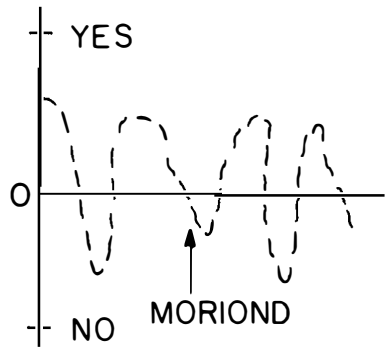
(A)



(B)



(C)



(D)

FIG. 1

Differential Measures

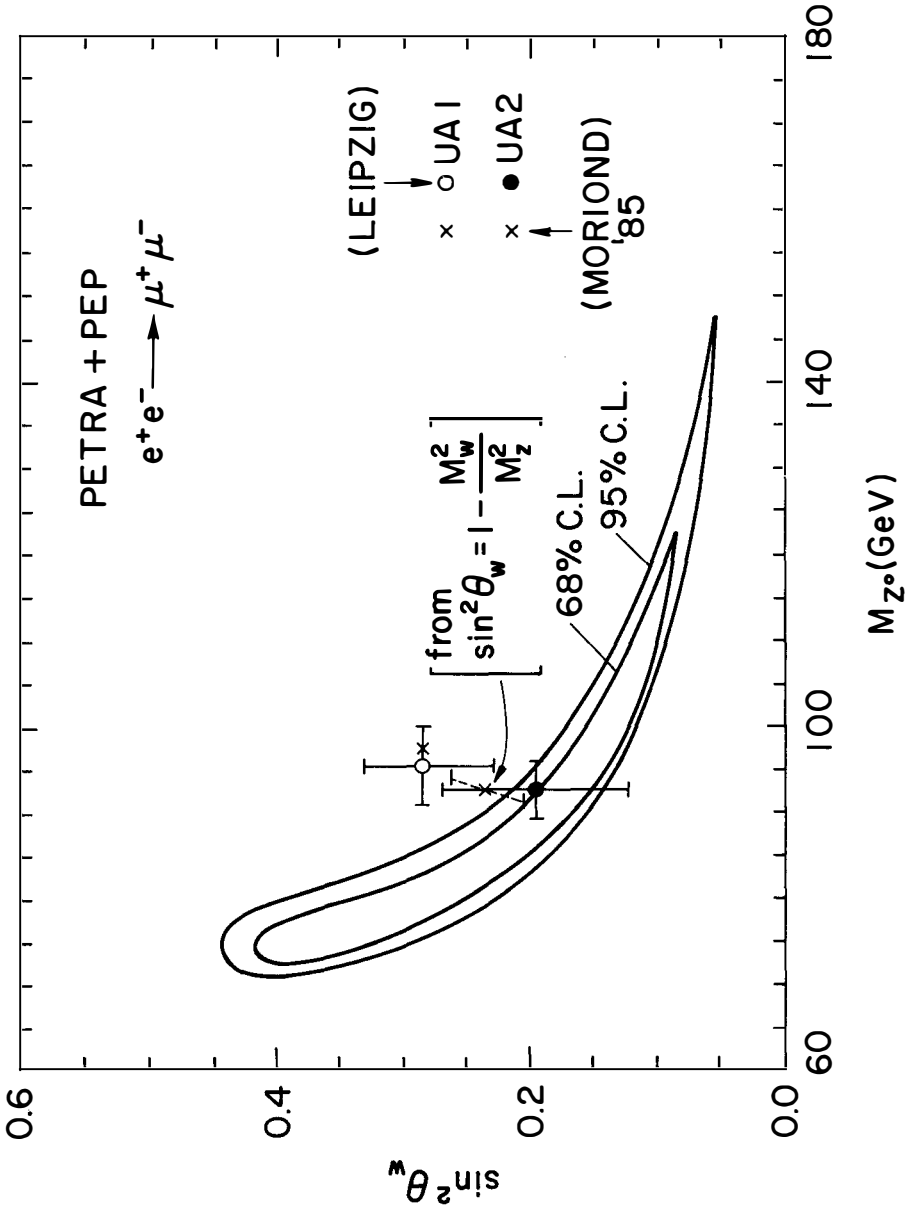


Figure 2 Comparison of e^+e^- and $p\bar{p}$

Minimal SU(5) predictions for a given $\Lambda_{\overline{MS}}$.

$\Lambda_{\overline{MS}}$ (GeV)	$\sin^2 \theta_W$	m_W (GeV)	m_Z (GeV)	m_X (GeV)	τ_P (yr)
0.025	0.226	81.3	92.3	3×10^{13}	$3 \times 10^{26 \pm 1}$
0.050	0.222	82.0	92.8	6.2×10^{13}	$3 \times 10^{27 \pm 1}$
0.10	0.218	82.8	93.6	1.3×10^{14}	$5 \times 10^{28 \pm 1}$
0.20	0.214	83.5	94.3	2.7×10^{14}	$5 \times 10^{29 \pm 1}$
0.40	0.210	84.3	94.9	5.5×10^{14}	$1 \times 10^{31 \pm 1}$

Figure 3

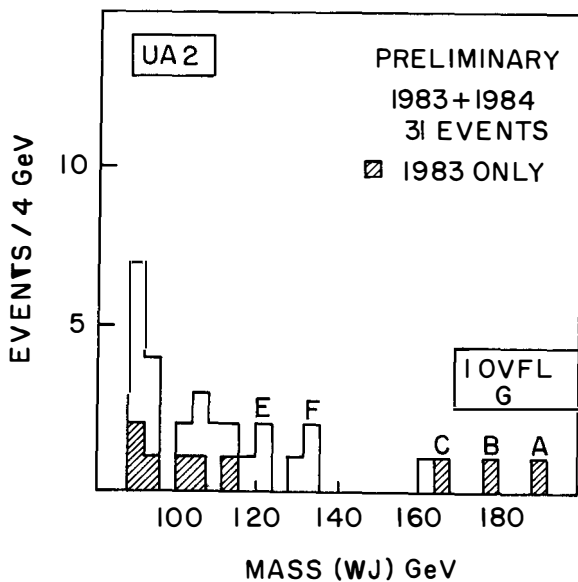
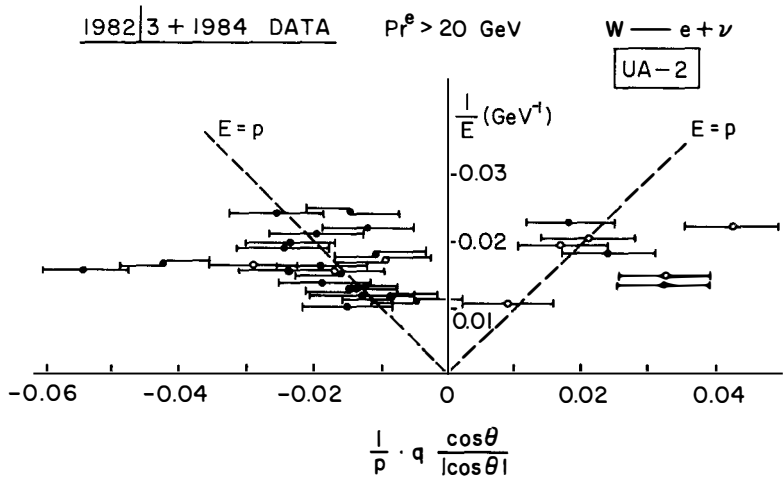
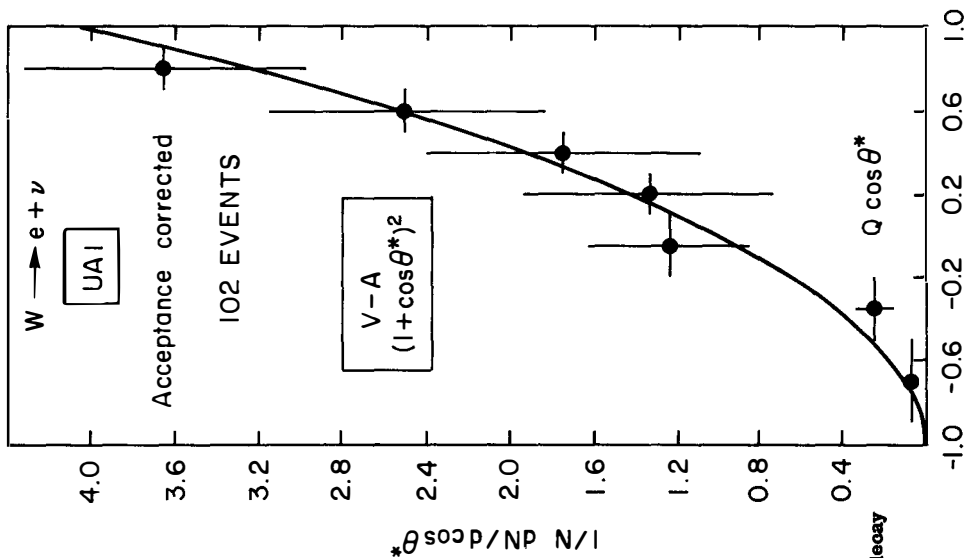


Figure 5 M_T of W+Jet System



Asymmetry $\alpha = \frac{22-8}{30} = 0.47 \pm 0.16$

$\alpha_{\text{expected}} = 0.54 \pm 0.04$

Figure 4 Angular asymmetry in w-decay

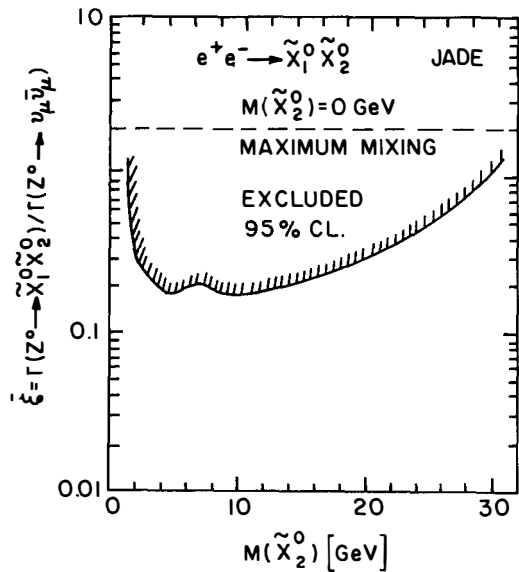
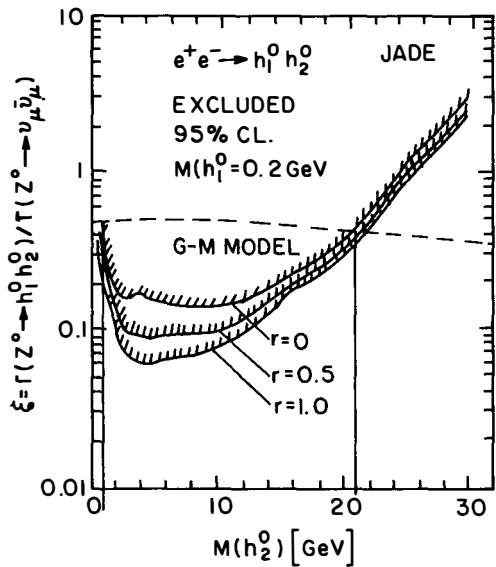


Figure 6 Search limits for massive neutrals

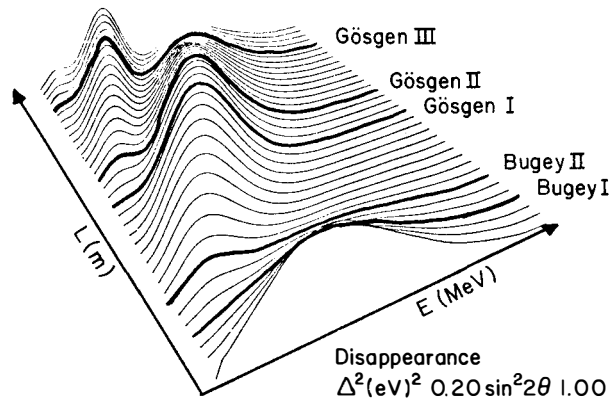


Figure 8 Reactor oscillation sensitivity

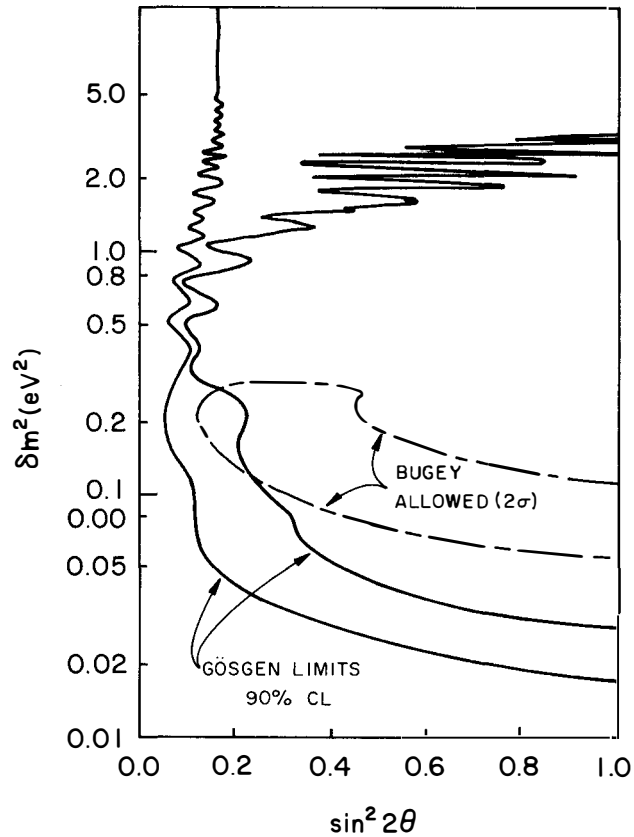
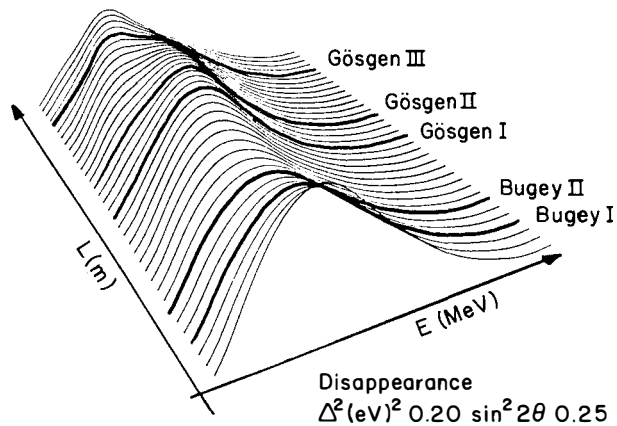


Figure 7 Reactor oscillation results

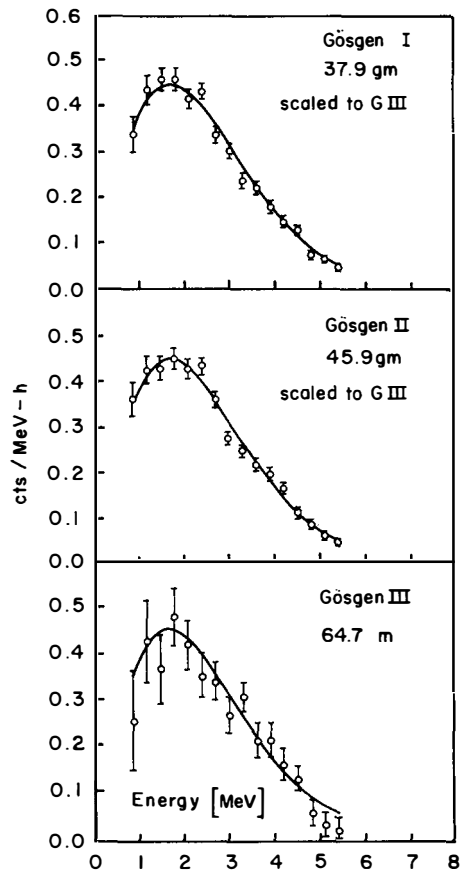
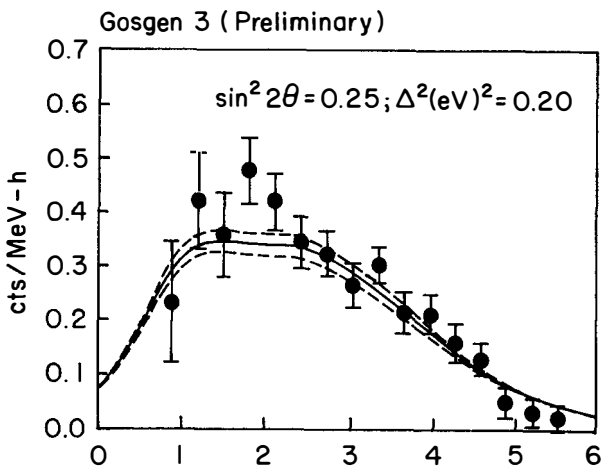
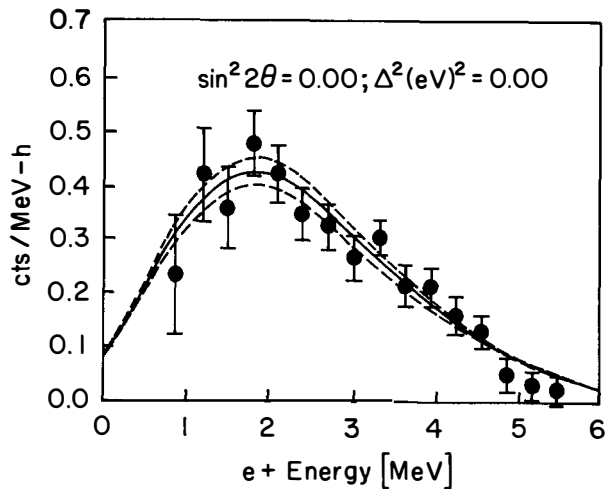


Figure 9 Gosgen Preliminary 64.7 meter results

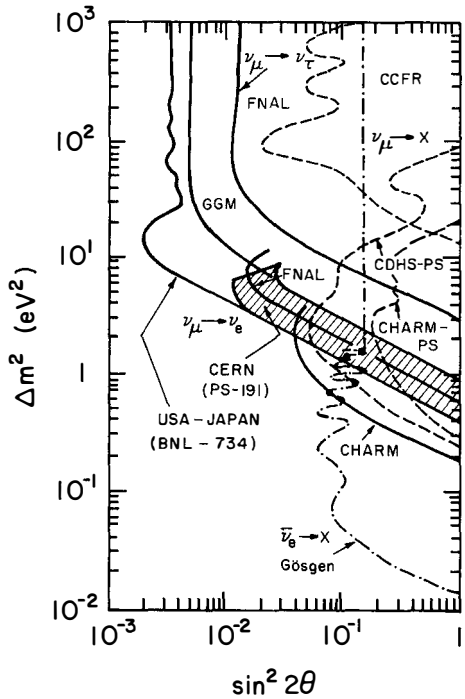
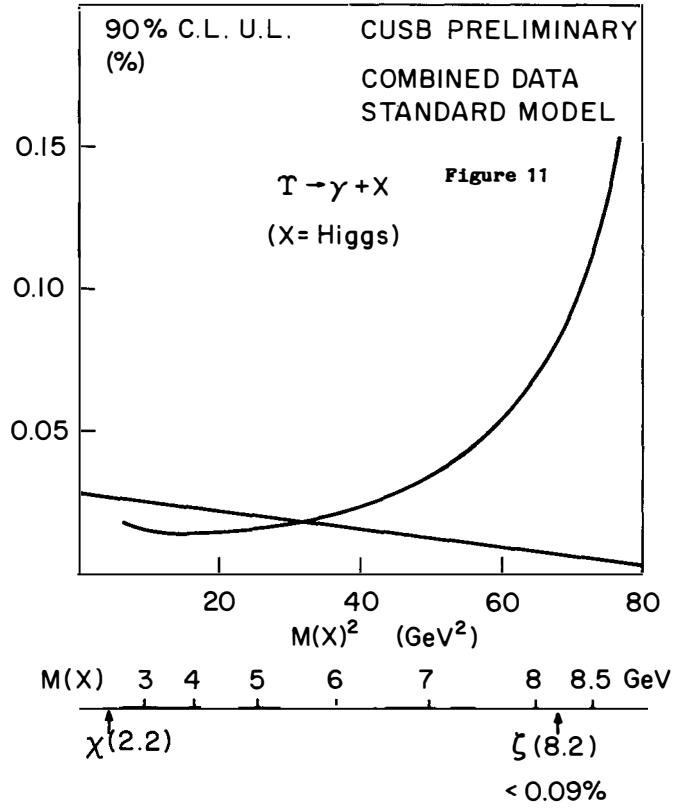


Figure 10 Accelerator oscillation results



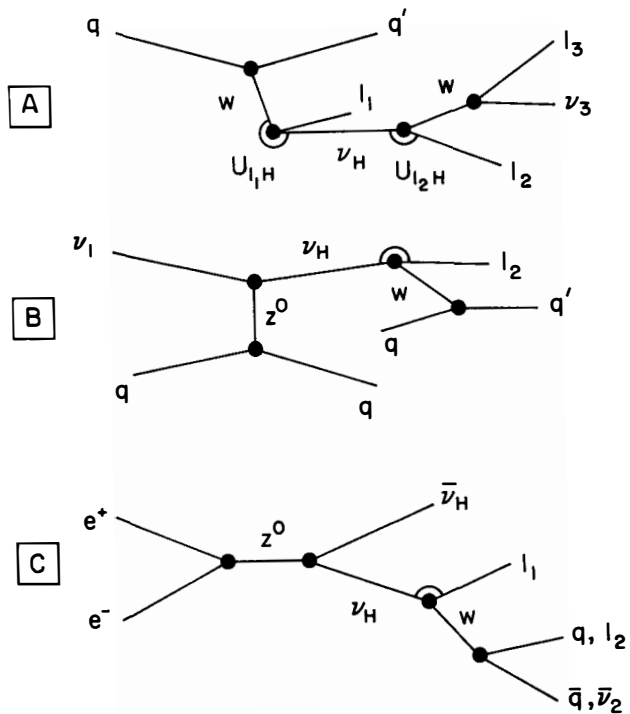


Figure 12 Massive neutrino decays

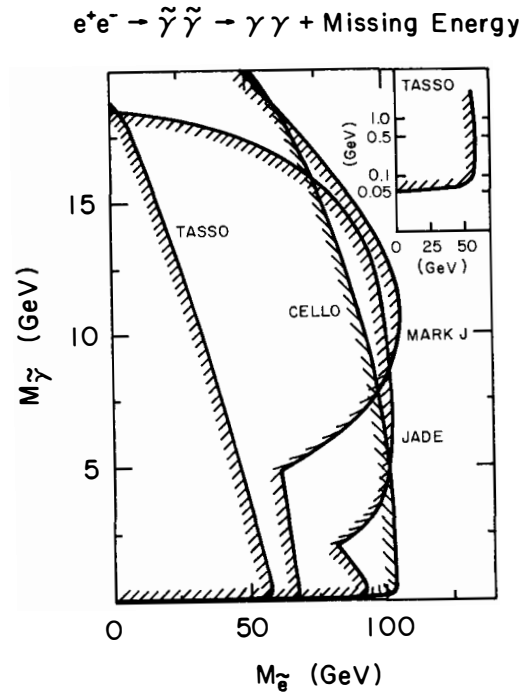


Figure 14 Photino Search limits

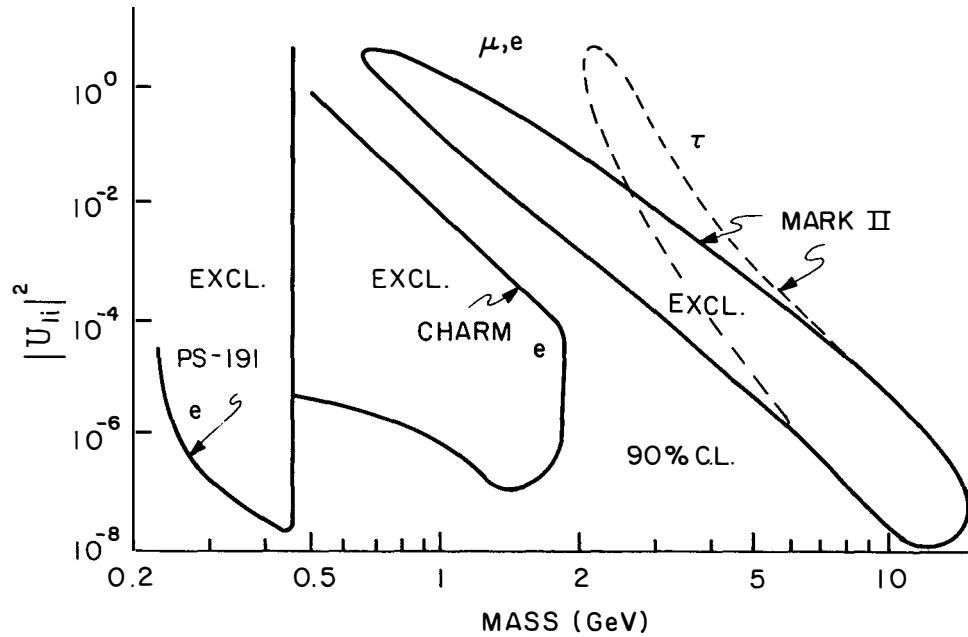


Figure 13 Massive neutrino decay limits

① LAST YEAR'S QUOTE:

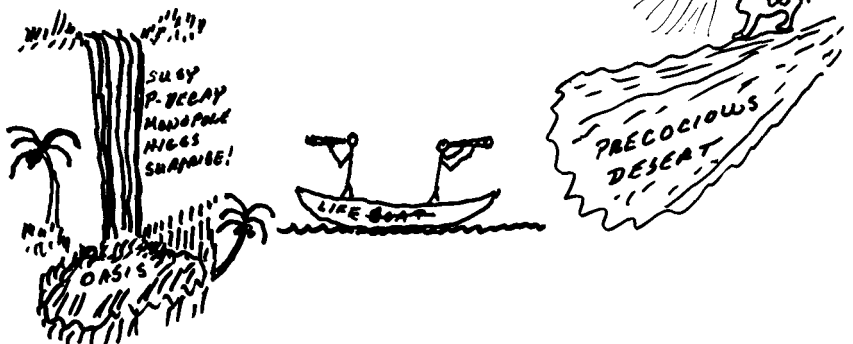
WE ARE LOOKING FOR PROTON DECAY AND
NEUTRON OSCILLATIONS.

WHAT WE KNOW FOR SURE IS THAT THE
NEUTRON DECAYS & THE PROTON DOES NOT
OSCILLATE. (M. GOLDHABER)

② WELL, THIS YEAR IT IS STILL TRUE

BUT WE HAVE MADE SOME GOOD PROGRESS
ON DETAILS BUT WE'VE PROBABLY LOST
ALL LAST YEAR'S WONDERFUL SURPRISES.

③ PERHAPS WE ARE LIKE A SAILOR AT SEA
WHO SEES MIRAGES:



④ MOTHER NATURE IS WHISPERING TO
US THESE DAYS AND WE ONLY WISH
SHE WOULD SPEAK-UP!

Figure 15

LIST OF PARTICIPANTS

ALEKSAN Roy	D.Ph.P.E / S.E.P.h CEN Saclay 91191 GIF/YVETTE Cedex FRANCE
ALLEN Richard	Physics Dept. Univ. of California 92717 IRVINE CA USA
BARATE Robert	C.E.R.N. EP Division 1211 GENEVA 23 SWITZERLAND
BARNETT Michael	Lawrence Berkeley Lab./50-308 1 Cyclotron Road 94720 BERKELEY CA USA
BARRELET Etienne	LPNHE - Ecole Polytechnique Route de Saclay 91128 PALAISEAU Cedex FRANCE
BAUBILLIER Michel	LPNHE - Univ. P. & M. Curie Tour 32,4 Place Jussieu 75230 PARIS cedex 05 FRANCE
BILLOIRE Alain	SPHT - Orme les Merisiers CEN Saclay 91191 GIF/YVETTE Cedex FRANCE
BIONTA Richard M.	Physics Dept. University of Michigan 48109 ANN ARBOR MI USA
BLONDEL Alain	C.E.R.N. EP Division 1211 GENEVA 23 SWITZERLAND
BLUEMER Hans	Inst for Physics University of Dortmund 4600 DORTMUND 50 FEDERAL REP. GERMANY
BODEK Arie	Dept of Physics & Astronomy University of Rochester 14627 ROCHESTER NY USA

- BOHM Albrecht
 III. Inst f. Physik
 RWTH Aachen, Sommerfeldstr
 5100 AACHEN
 FEDERAL REP. GERMANY
- BOUQUET Alain
 L.P.T.H.E, Univ. Paris 6 & 7
 Tour 14, 2 Place Jussieu
 75251 PARIS Cedex 05
 FRANCE
- BRAUNSCHWEIG Wolfgang
 I. Inst. f. Physik
 RWTH Aachen, Sommerfeldstr
 5100 AACHEN
 FEDERAL REP. GERMANY
- BURCKHART Helfried J.
 C.E.R.N.
 EF Division
 1211 GENEVA 23
 SWITZERLAND
- BURCKHART Helmut
 C.E.R.N.
 TH Division
 1211 GENEVA 23
 SWITZERLAND
- CAPONE Antonio
 Dipt di Fisica - Univ. di Roma
 Piazzale Aldo Moro
 00100 ROMA
 ITALIE
- CLINE Dave
 Dept of Physics (& CERN EP)
 Univ. of Wisconsin Madison
 53706 MADISON WI
 USA
- COSTA Giovanni
 Dipt di Fis.- Univ. di Padova
 Via Marzolo 8
 35100 PADOVA
 ITALY
- DAR Arnon
 Dept of Physics - Technion
 Israel Institut Techn.
 32000 TECHNION CITY Haifa
 ISRAEL
- DE LOTTO Barbara
 L.A.L.
 Bat. 200, Univ. Paris Sud
 91405 ORSAY Cedex
 FRANCE
- DELPIERRE Pierre
 L.P.C.- Collège de France
 11 Place M. Berthelot
 75231 PARIS Cedex 05
 FRANCE
- DOMINICI Daniele
 Dept de Phys. Theorique
 Univ de Geneve, 32 Bd Yvoy
 1211 GENEVE 4
 SWITZERLAND

EISELE Franz
D.E.S.Y - F11
Notkestr 85
2000 HAMBURG 52
FEDERAL REP. GERMANY

ETIENNE François
C.E.R.N.
EP Division
1211 GENEVA 23
SWITZERLAND

FACKLER Orrin
Physics Dept./Rockefeller Univ
1230 York Ave
10021 NEW YORK NY
USA

FAYET Pierre
Lab. de Physique Théorique-ENS
24 Rue Lhomond
75231 PARIS Cedex 05
FRANCE

FELDMAN Gary
S.L.A.C.
P.O. Box 4349
94305 STANFORD CA
USA

FLEURY Patrick
Ecole Polytechnique-LPNHE
Route de Saclay
91128 PALAISEAU Cedex
FRANCE

FOGLI Gianluigi
Dipt di Fisica
Via Amendola 173
70126 BARI
ITALY

FRANZINI Paolo
Columbia University
Pupin Lab.
10027 NEW YORK NY
USA

FRERE Jean Marie
Serv Phys Theorique - ULB
Bd du Triomphe , C.P. 225
1050 BRUXELLES
BELGIUM

GARREN Lynn
Dept of Physics - Wilson Lab.
Vanderbilt Univ.
14853 ITHACA NY
USA

GEORGES Antoine
Lab. de Phys. Théor., ENS
24 Rue Lhomond
75231 PARIS Cedex 05
FRANCE

GONZALEZ-MESTRES Luis
L.A.P.P.
Boite Postale 909
74019 ANNECY LE VIEUX Cedex
FRANCE

- GRARD Fernand
Univ. de l'Etat - Fac. de Scie
Ave Maistriau 19
7000 MONS
BELGIUM
- GRIVAZ Jean François
L.A.L.
Bat. 200, Univ. Paris Sud
91405 ORSAY Cedex
FRANCE
- HALPRIN Arthur
Physics Dept
Univ. of Delaware
19716 NEWARK DE
USA
- HARNEW Neville
C.E.R.N.
EP Division
1211 GENEVA 23
SWITZERLAND
- HOFFMANN Erwin
Physikalisches Inst.-& CERN EP
Univ. Bonn, Nussallee 12
5300 BONN 1
REP. FEDERAL GERMANY
- HOLLEBEEK Robert
S.L.A.C. Bin 95
P.O. Box 4349
94305 STANFORD CA
USA
- HONMA Alan
C.E.R.N.
EP Division
1211 GENEVA 23
SWITZERLAND
- JACQUET François
LPNHE - Ecole Polytechnique
Route de Saclay
91128 PALAISEAU Cedex
FRANCE
- JOLICOEUR Thierry
DPHT/Orme les Merisiers
CEN Saclay /B.P. 2
91191 GIF/YVETTE Cedex
FRANCE
- KIESLING Christian
MPI f. Phys. & Astrophys.
Fohringer Ring6/PO.401212
8000 MUNCHEN 40
REP. FED. GERMANY
- KIM Jae Kwan
K.A.I.S.
Cheongryang - Box 131
SEOUL
KOREA
- KOVACS Francis
LPNHE - Univ. P. & M. Curie
Tour 32 - 4 Place Jussieu
75230 PARIS Cedex 05
FRANCE

- KRAUS Norbert
Physik Inst der Universitat
Schonberggasse 9
8001 ZURICH
SWITZERLAND
- LANG Karol
Phys. & Astronomy Dept.
University of Rochester
14627 ROCHESTER NY
USA
- LANOU Robert
Physics Dept.
Brown University
02912 PROVIDENCE RI
USA
- LAVAGNE Yves
D.Ph.P.E
CEN Saclay
91191 GIF/YVETTE Cedex
FRANCE
- LE DOUSSAL Pierre
Lab. de Phys. Théor., ENS
24 Rue Lhomond
75231 PARIS Cedex 05
FRANCE
- LEE-FRANZINI Juliet
Physics Dept
SUNY at Stony Brook
11794 STONY BROOK LI NY
USA
- LELLOUCH Daniel
LPNHE - Ecole Polytechnique
Route de Saclay
91128 PALAISEAU Cedex
FRANCE
- LEVY Jean Michel
LPNHE-Univ. P & M Curie
Tour 12 3étage
75230 PARIS CEDEX 05
FRANCE
- LIPKIN H.
Dept of Nucl. Phys./P.O. Box26
Weizmann Inst. of Science
76100 REHOVOT
ISRAEL
- LUTH Vera
S.L.A.C. - Bin 95
P.O. Box 4349
94305 STANFORD CA
USA
- MAcFARLANE David
Dept of Physics
Univ. of Toronto
M5S 1A7 TORONTO ONTARIO
CANADA
- MAINA Ezio
Ist.di Fisica/Univ. di Torino
Corso M. D'azeglio 46
10125 TORINO
ITALIE

- MILLS Geoffrey
CALIFORNIA INST. OF TECHN.
256-48
91125 PASADENA CA
USA
- MOFFAT John
Dept of Physics
Univ. of Toronto
MS5 1A7 TORONTO ONTARIO
CANADA
- MOREL André
Dept. de Phys. Théorique
CEN Saclay
91191 GIF/YVETTE Cedex
FRANCE
- NUYTS Jean
Université de l'Etat
19 Ave Maistriau
7000 MONS
BELGIUM
- OUVRY Stephane
IPN - Div. de Phys. Théorique
Univ. Paris Sud/BP 1
91406 ORSAY Cedex
FRANCE
- PARK Hye-Sook
Physics Dept - Michigan Univ.
Randall Laboratory
48104 ANN ARBOR MI
USA
- PESSARD Henri
L.A.P.P.
Boite Postale 909
74019 ANNECY LE VIEUX Cedex
FRANCE
- PETCOV Sergey
Elem Part Theor Group
Scie Acad. - Bd Lenin 72
1184 SOFIA
BULGARIA
- PEYAUD Bernard
D.Ph.P.E
CEN Saclay
91191 GIF/YVETTE Cedex
FRANCE
- PHAM QUANG HUNG
Dept of Physics /Virginia Univ
McCormick Road
22901 CHARLOTTESVILLE VA
USA
- PHILIPPE Roeland
Randall Lab. of Physics
University of Michigan
48109 ANN ARBOR MI 1120
USA
- POGGIOLI Luc
LPNHE /Univ. P. & M. Curie
Tour 32, 4 Place Jussieu
75230 PARIS CEDEX 5
FRANCE

- POMANSKY Alexander
Nuclear Res. Inst./URSS Acad.
60th Oct. Anniv. Prospect 7a
117312 MOSCOW
USSR
- PREPOST Richard
Physics Dept. - Wiconsin Univ
1150 University Ave
53706 MADISON WI
USA
- PRIEELS René
Inst. de Phys. Nucléaire - UCL
2 Chemin du Cyclotron
1348 LOUVAIN LA NEUVE
BELGIUM
- PRIMOUT Michel
D. Ph. P. E
CEN Saclay
91191 GIF/YVETTE Cedex
FRANCE
- RABINOVICI Eliezer
Racah Institut of Physics
Hebrew University
91 904 JERUSALEM
ISRAEL
- RAGAZZI Stefano
INFN - Sezione di Milano
Via Celoria 16
20133 MILANO
ITALY
- RANDER John
D. Ph. P. E
CEN Saclay
91191 GIF/YVETTE Cedex
FRANCE
- RAU R. Ronald
Physics Dept.
Brookhaven Nat. Lab.
11973 UPTON NY
USA
- ROSIER Nadine
Inst. de Phys. Nucléaire -UCL
2 Chemin du Cyclotron
1348 LOUVAIN LA NEUVE
BELGIUM
- RYKACZEWSKI Hans
Nuclear Scie. Lab. (& CERN EP)
Massachusetts Inst. Techn
02139 CAMBRIDGE MA
USA
- SADOFF Ahren
Lab. of Nuclear Studies
Ithaca College-Cornell
14850 ITHACA NY
USA
- SCHAFFER Arthur
C. E. R. N.
EP Division
1211 GENEVA 23
SWITZERLAND

- SCHMIDT Michael G. Philosophenweg 16
6900 HEIDELBERG
FEDERAL REP. GERMANY
- SCHNEEKLOTH Uwe II. Inst. f. Experimentalphys.
Univ. Hamburg, Luruper 149
2000 HAMBURG 50
FEDERAL REP. GERMANY
- SENJANOVIC Goran Physics Dept.
Brookhaven Nat. Lab.
11973 UPTON NY
USA
- SMITH Wesley H. Columbia Univ.- Nevis Labs
P.O. Box 137
10533 IRVINGTON NY
USA
- STAUDE Arnold Sektion Physik der LMU Munchen
Schellingstr 4
8000 MUNCHEN 40
FEDERAL REP. GERMANY
- STEFFEN Peter C.E.R.N.
EP Division
1211 GENEVA 23
SWITZERLAND
- STELLA Bruno Ist. di Fisica, Univ. di Roma
Pzale A. Moro, Roma I
00185 ROMA
ITALY
- TALBY Mossadek Centre de Phys. des Particules
CNRS Luminy - Case 907
13288 MARSEILLE Cedex 9
FRANCE
- TAO Charling L.P.C. - Collège de France
11 Place M. Berthelot
75231 PARIS Cedex 05
FRANCE
- TRAN THANH VAN Jean L.P.T.H.E.
Bat 211, Univ. Paris Sud
91405 ORSAY Cedex
FRANCE
- TUNG Kuoliang CERN
EP DIVISION
1211 GENEVA 23
SWITZERLAND
- TUTS P. Michael Physics Dept. - Columbia Univ.
P.O. Box 32
10027 NEW YORK NY
USA

- VANNUCCI François
LPNHE - Univ. Paris VI & VII
Tour 32, 4 Place Jussieu
75231 PARIS Cedex 05
FRANCE
- VENKATARAMANIA Harsh
Physics Dept. - Wisconsin Univ.
1150 University Ave.
53706 MADISON WI
USA
- WEISZ Sylvain
C.E.R.N.
EP Division
1211 GENEVA 23
SWITZERLAND
- WETTERICH Christof
C.E.R.N.
TH Division
1211 GENEVA 23
SWITZERLAND
- ZACEK Viktor
Physik Dept
Technische Univ. Munchen
8046 GARCHING BEI MUNCHEN
FEDERAL REP. GERMANY
- ZINN-JUSTIN Jean
Service de Physique Théorique
CEN Saclay
91191 GIF/YVETTE Cedex
FRANCE
- ZYLBERAJCH Sylvain
D.Ph.P.E.
CEN Saclay
91191 GIF/YVETTE Cedex
FRANCE

